NASA CONTRACTOR REPORT

NASA CR-66897-2

NASA CR-66897-2

SUBSTANTIATION DATA FOR

HYPERSONIC CRUISE VEHICLE WING STRUCTURE EVALUATION

Volume 2, Sections 11 through 22

by P. P. Plank, I. F. Sakata, G. W. Davis, and C. C. Richie

Prepared by
LOCKHEED MISSILES & SPACE COMPANY
Sunnyvale, California
for Langley Research Center

NATIONAL AERONAUTICS AND SPACE ADMINISTRATION · WASHINGTON, D.C.
FEBRUARY 1970

NASA CONTRACTOR REPORT

NASA CR-66897-2

NASA CR-66897-2

SUBSTANTIATION DATA FOR

HYPERSONIC CRUISE VEHICLE WING STRUCTURE EVALUATION

Volume 2, Sections 11 through 22

by P. P. Plank, I. F. Sakata, G. W. Davis, and C. C. Richie

Prepared by
LOCKHEED MISSILES & SPACE COMPANY
Sunnyvale, California
for Langley Research Center

NATIONAL AERONAUTICS AND SPACE ADMINISTRATION • WASHINGTON, D.C.
FEBRUARY 1970

NASA CR-66897-2

SUBSTANTIATION DATA FOR

HYPERSONIC CRUISE VEHICLE

WING STRUCTURE EVALUATION

Volume 2, Sections 11 through 22

15 February 1970

by

P. P. Plank, I. F. Sakata, G. W. Davis, and C. C. Richie

Prepared under Contract No. NAS 1-7573
Lockheed Missiles & Space Company
Sunnyvale, California

for Langley Research Center

NATIONAL AERONAUTICS AND SPACE ADMINISTRATION

CONTENTS

SUMMARY

An analytical and experimental evaluation was performed for several promising structural concepts to provide the basis of minimum total-system-cost for selection of the best concepts for the design of a hypersonic vehicle wing.

Results, procedures, and principal justification of results are presented in reference 1. Detailed substantiation data are given herein. Each major analysis is presented in a separate section. Vehicle loads and temperatures are given with each structural analysis that influences weight. In addition to the weight analysis, fabrication cost, performance penalties (surface roughness drag), reliability, and total-system-cost analyses are presented.

Reference 1. Plank, P. P.; Sakata, I. F.; Davis, G. W.; and Richie, C. C.: Hypersonic Cruise Vehicle Wing Structure Evaluation, NASA CR-1568, 1970.

INTRODUCTION

The utility of a hypersonic cruise vehicle depends upon a low structural mass fraction in a high-temperature environment. Unfortunately, this requirement exceeds the limits of state-of-the-art structures. The only hypersonic structures flown to date have been the X-15 research airplane and the ASSET unmanned lifting reentry test vehicle, both of which are unsuitable for cruising flight.

For the past several years, the NASA Langley Research Center and other agencies have been investigating promising structural concepts, such as those discussed in references 2, 3, and 4, and the 1967 Conference on Hypersonic Aircraft Technology (ref. 5) was devoted to the subject.

An evaluation was performed of promising wing structure concepts to the same in-depth analyses, including all known environmental structural considerations that could affect the four evaluation factors: weight, cost, performance, and reliability. These factors were then interacted in a total-system-cost study for a system range-payload capability of 205 billion ton-miles to provide the basis for selecting the best structural concept for the wing structure of minimum total-system-cost.

Results of this structural evaluation are reported in reference 1. This reference also includes the procedures and principal justification of results, whereas this report gives detailed substantiation of the results in reference 1. Principal analytical and test efforts are presented in separate sections. This report is bound as three separate volumes.

REFERENCES

2. Heldenfels, R. R.: Structural Prospects for Hypersonic Air Vehicle ICAS paper, 1966.

3. Plank, P. P.; and MacMiller, C. I.: Analytical Investigation of Candidate Thermal-Structural Concepts Applicable to Wing, Fuselage, and Inlet Structure of a Manned Hypersonic Vehicle. AFFDL-TR-66-15, 1966 (conf).

4. Plank, P. P.: Hypersonic Thermal-Structural Concept Trends. SAE paper 660678, 1966.

5. NASA-SP-148 (Conf). Conference on Hypersonic Technology, Ames Research Center, 1967.

ACKNOWLEDGEMENT

This investigation was conducted under NASA Contract No. NAS1-7573, Research and Development Program for Development and Validation of Structural Concepts for a Hypersonic Cruise Vehicle Wing Structure. The study was originated at the Lockheed-California Company, Burbank, California and completed at Lockheed Missiles & Space Company, Sunnyvale, California. P. P. Plank was the Program Technical Manager, I. F. Sakata and G. W. Davis the Project Engineers, and C. C. Richie was head of structural concept optimization. The other contributors to the program are acknowledge at each section.

Four Lockheed-California Company personnel acted in an advisory capacity. They are L. W. Nelson, Structure Division Engineer, Structures Division; E. J. Himmel, Department Manager, Stress Analysis; W. J. Crichlow, Department Manager, Advanced Materials and Structural Mechanics; and M. G. Childers, Manager, Physical Sciences Laboratory Development Engineer.

Dr. M. S. Anderson, L. R. Jackson, and J. C. Robinson of the Structures Research Division, NASA Langley Research Center, Hampton, Virginia, were the Program Manager, Technical Representative of the Contracting Officer (TRCO), and Assistant TRCO, respectively, for the project.

Section 11

OPTIMIZATION PROCEDURE FOR PANELS OF CIRCULAR-ARC CORRUGATION SHEAR WEBS

by

G. W. Davis

SYMBOLS

b	Width of panel
D_1, D_2	Stiffness coefficients of governing differential equation of plate
E	Modulus of elasticity
E_{el}	Elastic modulus of elasticity
k, k_s	Buckling coefficients in analyses of shear buckling
$N_{xy,cr}$	Shear buckling force in xy coordinate system per unit length of section
R	Radius
t	Thickness
t_{min}	Minimum thickness
$\bar{t}$	Equivalent panel thickness
β_s	Effective aspect ratio
ϵ	Efficiency factor
η	Plasticity reduction factor
η_{sec}	E_{sec}/E , secant plasticity reduction factor
η_{tan}	E_{tan}/E , tangent plasticity reduction factor
	Stiffness parameter

Section 11

OPTIMIZATION PROCEDURE FOR PANELS OF CIRCULAR-ARC CORRUGATION SHEAR WEBS

To minimize thermal stresses, webs of circular-arc corrugation (fig. 11-1) are used for the ribs and spars. The intensity of the buckling force of a corrugated panel is expressed with equation (10-36) of Section 10 as

$$N_{xy,cr} = k\pi^2 \left(D_1 D_2^3\right)^{1/4} \Big/ b^2 \tag{11-1}$$

where

$$D_1 = \frac{\eta_1 E_{el} t^3}{12 (1-\nu^2)} \frac{\sin \phi}{\phi} \tag{11-2a}$$

$$D_2 = \eta_1 E_{el} t \frac{R^2}{2} \left(1 - \frac{3}{2} \frac{\sin 2\phi}{\phi} + 2 \cos^2 \phi \right) \frac{\phi}{\sin \phi} \tag{11-2b}$$

in which

$$\eta_1 = 0.83 \eta_{sec} + 0.17 \eta_{tan} \tag{11-3}$$

Substituting equations (11-2) into equation (11-1), neglecting the small effect of Poisson's ratio, and then dividing by the thickness t gives the following expression of the buckling stress:

$$f_{s,cr} = 5.29 k \eta_1 E_{el} \left(\frac{t}{b}\right)^2 \left(\frac{R}{t}\right)^{3/2} f(\phi) \tag{11-4}$$

where

$$f(\phi) = \left[\left(\frac{\phi}{\sin \phi}\right)^{2/3} \left(\frac{1}{2} - \frac{3}{4} \frac{\sin 2\phi}{\phi} + \cos^2 \phi \right) \right]^{3/4} \tag{11-5}$$

The local buckling stress is (ref. 11-1)

$$f_{s,cr} = 0.55\ \eta_{tan}^{1/2}\ E_{el}\left(\frac{t}{R}\right)^{3/2} \tag{11-6}$$

Multiplying equations (11-4) and (11-6) by t and then using the second resulting expression to eliminate R in the first expression yields

$$\frac{N_{xy,cr}}{\bar{\eta}\ E_{el}b} = \left\{1.71\ k^{1/2}\left(\frac{\sin\phi}{\phi}\right)^2\left[f(\phi)\right]^{1/2}\right\}\left(\frac{\bar{t}}{b}\right)^2 \tag{11-7a}$$

or

$$\frac{N_{xy,cr}}{\bar{\eta}\ E_{el}b} = \epsilon\left(\frac{\bar{t}}{b}\right)^2 \tag{11-7b}$$

in which ϵ is an efficiency coefficient and

$$\bar{\eta} = \eta_l^{1/2}\ \eta_{tan}^{1/4} \tag{11-8a}$$

$$\bar{t} = \frac{\phi}{\sin\phi}\ t \tag{11-8b}$$

From equations (11-6), (11-7b) and (11-8b),

$$\frac{R}{b} = 0.67\ \eta_{tan}^{1/3}\ \bar{\eta}^{-5/6}\left(\frac{\sin\phi}{\phi\ \epsilon^{1/2}}\right)^{5/3}\left(\frac{N_{xy,cr}}{E_{el}\ b}\right)^{1/6} \tag{11-9}$$

The optimum corrugation angle is obtained by maximizing the efficiency factor. The radius and thickness are then determined with Equation (11-7b) (11-8b) and (11-9).

For problems in which the thickness is constrained, equation (11-7a) becomes

$$\frac{N_{xy,cr}}{\bar{\eta}\, E_{el}\, b} = \left\{ 1.71\, k^{1/2} \left[f(\phi)\right]^{1/2} \right\} \left(\frac{t_{min}}{b}\right)^2 \qquad (11\text{-}10)$$

from which

$$\left[f(\phi)\right]^{1/2} = 0.58 \left(\frac{N_{xy,cr}}{\bar{\eta}\, E_{el}\, b}\right) \Bigg/ \left[k^{1/2} \left(\frac{t_{min}}{b}\right)^2\right] \qquad (11\text{-}11)$$

In reference 11-1, the optimum angle for a design with an unrestrained thickness is shown to be 80°. Because of manufacturing limitations, an angle of 60° was used for all corrugation panels of the present investigation. Noting that $\beta_s \approx 0$ and $\kappa \approx 0$, a value of 3.3 from fig. 10-8 of Section 10 was used for the buckling coefficient $k \equiv k_s$.

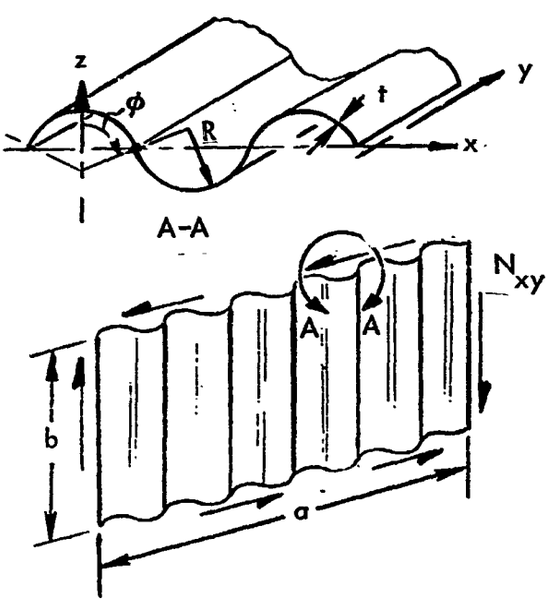

Figure 1. Corrugated shear web

REFERENCE

1-1. Emero, Donald H.; Spunt, Leonard: Optimization of Multirib and Multiweb Wing Box Structures Under Shear and Moment Loads. AIAA 6th Structures and Materials Conference, American Institute of Aeronautics and Astronautics (New York, New York), 1965, P. 346.

Section 12

OPTIMIZATION PROCEDURE FOR PANELS OF SEMIMONOCOQUE STRUCTURE

by

R. E. Hubka

CONTENTS

ILLUSTRATIONS

SYMBOLS

A	Mean area enclosed by outer and inner boundaries
a,b	x and y distances between simply supported edges of plate
D_1,D_2,D_3	Stiffness coefficients of governing differential equation of plate
d	Width of diagonal element of trapezoidal corrugation
E_{el}	Elastic modulus of elasticity
e_t,e_y	Eccentricity (deflection) of center of panel due to thermal bowing (subscript t) and difference between end shear axis and centroidal distance (subscript y)
f_b,f_c,f_s	Bending, compressive, and shear stress
$f_{b,cr},f_{c,cr},f_{s,cr}$	Bending, compressive, and shear buckling stress
G_{el}	Elastic shear modulus
h	Depth of cross section
$\bar{I}$	Moment of inertia per unit length of section
$\bar{I}_x,\bar{I}_y$	Moments of inertia per unit length of sections associated with x and y bending of orthotropic plate
$\bar{J}$	Torsional stiffness per unit length of section
k_c,k_s	Buckling coefficients in analysis of compressive and shear buckling
L	Length
M_x,M_y,M_{xy}	Bending moments and twisting moments in xy coordinate system per unit length of section

m	Number of half waves in plate buckling equations
N_x, N_y, N_{xy}	Extensional forces and shear forces in xy coordinates per unit length of section
q	Pressure
R	Radius
R_c, R_s	Stress ratios for compression and shear
t	Thickness
$\bar{t}$	Equivalent extensional thickness
$\bar{t}_s$	Equivalent shear thickness
U	Utilization factor
$\bar{\zeta}$	Location of neutral surface of panel
α	Mean coefficient of thermal expansion
β_c	Effective aspect ratio
$\bar{\gamma}_T, \epsilon_T$	Shear and compressive strains corresponding to thermal loads
η_{ST}	Stowell's plasticity reduction factor
η_{sec}	Secant plasticity reduction factor
η_{ton}	Tangent plasticity reduction factor
ν	Poisson's ratio
τ_{cr}	Shear buckling stress as defined in reference 12-3

Section 12

OPTIMIZATION PROCEDURE FOR PANELS OF SEMIMONOCOQUE STRUCTURE

Equations of the Fortran computer programs which were used to determine the minimum weight designs in the detail analysis of the four panel concepts of the semimonocoque structure are presented in this section. The analyses, formulated for the direct search method, are discussed in the following paragraphs: (1) panel loading, (2) stress analysis, (3) analysis of local buckling, (4) optimization procedure, and (5) section properties and stiffnesses.

PANEL LOADING

The total inplane stress resultants acting on the stiffened panels (fig. 12-1) are

$$N_y = N_y' + \bar{\epsilon}_{y,T} E_{el} \bar{t}$$

$$N_{xy} = N_{xy}' + \bar{\gamma}_{xy,T} G_{el} \bar{t}_s \qquad (12\text{-}1)$$

where N_y' and N_{xy}' are loading components in which thermal effects are excluded, $\bar{\epsilon}_T$ and $\bar{\gamma}_T$ are the compressive and shear strains corresponding to thermal loads of the structural model, and $E_{el}\bar{t}$ and $G_{el}\bar{t}_s$ are the elastic stiffness coefficients which are defined at the end of this section. The procedure for calculating the thermal portion of the inplane loading is consistent with the redundant-force used for calculating the internal loads of the aircraft.

A conservative approximation of the bending moment at the center of the panel in the zy plane is

$$M_y = M_y^*/(1 - U_{GI}) \qquad (12\text{-}2)$$

where M_y^* is the moment based on small deflection theory. For Panels No. 1, 2, and 3

$$M_y^* = \frac{qL^2}{8} + (e_y + |e_T| + 0.001\ L)\ N_y \qquad (12\text{-}3)$$

where q denotes uniform pressure which is always specified with a positive sign, 0.001 L is the initial deflection,

$$e_y = \begin{cases} 1.5\ t & \text{for Panel No. 1} \\ 0 & \text{for Panel No. 2} \\ 2\ t & \text{for Panel No. 3} \end{cases}$$

and e_T is the deflection due to thermal bowing. Assuming a linear temperature gradient through the thickness, which is considered to be adequate for the present investigation, the deflection at the center of a simply supported panel due to the thermal bowing can be approximated as

$$e_T = \frac{L^2 \alpha \Delta T}{8h} \tag{12-4}$$

where α is the mean coefficient of thermal expansion and ΔT is the change in temperature through the cross section of depth h. The temperature increment is positive when the temperature of the outer surface of the panel is larger than that of the inner surface.

For Panel No. 4

$$M^*_{y,O} = \frac{qL^2}{8} + \left[\max\left(-e_T, 0\right) - \left(\bar{z} + t_I\right) + 0.001\ L\right] N_y \tag{12-5a}$$

and

$$M^*_{y,I} = -\frac{qL^2}{8} + \left[\min\left(e_T, 0\right) - 0.001\ L\right] N_y \tag{12-5b}$$

in which the subscripts O and I denote moments for designing the outer and inner portions of the panel. Note that the pressure is always specified with a positive sign. The dimension $\bar{z}$, which is expressed in the last paragraph of this section, is measured from the interface of the two portions of the panel. Hence, it is a negative quantity.

Using the interaction equation

$$R_c + R_s^2 = 1$$

in which

$$R_c = N_y/N_{y,cr}$$

$$R_s = N_{xy}/N_{xy,cr} \tag{12-6}$$

the utilization factor of equation (12-2) for combined compressive and shear loading is

$$U_{GI} = \frac{R_c + \left(R_c^2 + 4R_s^2\right)^{1/2}}{2} \tag{12-7}$$

Considering simply supported, wide column theory for compressive buckling,

$$N_{y,cr} = \frac{\pi^2 D_2}{L^2} \tag{12-8a}$$

It is to be noted that the above equation significantly underestimates the buckling loads of Panels No. 3 and 4, because of their relatively large twisting stiffnesses. The shear buckling load intensity is expressed with simply supported, orthotropic plate theory as (ref. 12-1)

$$N_{xy,cr} = 46.8 \left(D_2 D_3\right)^{1/2} / L^2 \tag{12-9a}$$

for the tubular concepts. The expression, for the corrugation concepts from Section 10, is

$$N_{xy,cr} = 32.6 \left(D_1 D_2^3\right)^{1/4} / L^2 \tag{12-9b}$$

STRESS ANALYSIS

The stress at the centroid of the cross section

$$f_c = N_y/\bar{t} \tag{12-10}$$

The bending stress for Panels No. 1, 2 and 3 is

$$f_b = M_y z/\bar{I}_x \tag{12-11a}$$

and for Panel No. 4,

$$f_{b,\ell} = M_{y,\ell} z_\ell/\bar{I}_x \qquad (\ell = 0,I) \tag{12-11b}$$

Neglecting twisting due to edge eccentricities, the shear stresses of the panels are as follows:

For Panels No. 1 and 2,

$$f_s = N_{xy}/t \tag{12-12a}$$

For Panel No. 3,

$$f_s = N_{xy}/2t \tag{12-12b}$$

For Panel No. 4,

$$f_{s,\ell} = N_{xy} p/s_\ell \bar{t}_s \qquad (\ell = 0,I) \tag{12-12c}$$

ANALYSIS OF LOCAL BUCKLING

Panel No. 1, Beaded

Five modes of buckling of the beaded configuration (Fig. 12-1) are considered as follows: (1) buckling of most or all of the portion of the panel between centerlines of continuous arcs due to a uniform compressive stress, (2) buckling of the circular arc due to bending, (3) buckling of the circular arc due to shear, (4) buckling of the flat segment due to compression, and (5) buckling of flat segment due to shear. Appropriate interaction equations are used for combined loading.

Simply supported, orthotropic plate theory is used to analyze the panel for the first mode of initial buckling. Using the notation of figure 12-1 and the compressive buckling theory of Section 10, the buckling stress can be expressed as

$$f_{c,cr} = k_c \frac{\pi^2 D_I}{x_{II}^2 \bar{t}_L} \tag{12-13a}$$

where

$$k_c = \left(2 \frac{x_I^2}{x_{II}^2} \frac{D_3}{D_I} + m^2 + \frac{\beta_c^4}{m^2} \right) \frac{x_{II}^2}{x_I^2} \tag{12-13b}$$

in which

$$\beta_c = \frac{x_I}{x_{II}} \left(\frac{D_{II}}{D_I} \right)^{1/4} \tag{12-13c}$$

x_I is the bead (circular-arc) length. The stiffnesses and the average thickness, $\bar{t}_L$, of equations (12-13) are defined in the last paragraphs of this section. The buckling stress is the minimum value of $f_{c,cr}$ with respect to positive integers of m and the angle θ_2 (fig. 12-1).

In the analysis of a test specimen, $\theta_2 = 0$ and $m = 2$ gave the minimum stress. However, $\theta = 13^\circ$ and $m = 3$ gave essentially the same results. The theoretical buckling stress was in reasonably good agreement with the initial buckling stress of the test panel. It is to be noted that $\theta_2 = 0$ was used for the design of the beaded panels.

The initial buckling stress due to bending is approximated with an expression that was suggested by NASA for compressive buckling of long cylinders with an R/t range which is consistent with those of the circular arcs of Panels No. 1, 3 and 4. The buckling stress expression is

$$f_{b,cr} = 1.75 \left(\eta_{sec} \eta_{tan} \right)^{1/2} E_{el} \left(\frac{t}{R} \right)^{1.35} \tag{12-14}$$

where the plasticity coefficients, η_{sec} and η_{tan}, are based on the stresses f_c, f_b, and f_s, which are given by equations (12-10), (12-11) and (12-12). The equivalent stress for evaluating the plasticity coefficients is determined with the octahedral shear stress theory of reference 12-2.

The circular arc of the cross section was considered critical with respect to shear buckling, an assumption which needs to be verified by test. Using buckling theory for curved plates of large aspect ratios, the initial shear buckling stress is (ref. 12-3)

$$f_{s,cr} = 0.37 \, (Z_b)^{1/2} \, \tau_{cr} \tag{12-15}$$

where

$$Z_b = \frac{\ell^2}{Rt} \, (1 - \nu_{el}^2)^{1/2} \tag{12-16}$$

and from Section 10

$$\tau_{cr} = 4.40 \, \frac{\eta_{sec} E_{el}}{1 - \nu_{el}^2} \left(\frac{t}{S}\right)^2 \tag{12-17}$$

in which S is the developed length of the arc. The plasticity coefficient is evaluated the same as those of equation (12-14).

Using the interaction equation

$$r_{c,b} + r_s^n = 1$$

in which

$$r_{c,b} = f_c/f_{c,cr} + f_b/f_{b,cr}$$

$$r_s = f_s/f_{s,cr}$$

the utilization factor for combined stresses due to compression, bending, and shear can be expressed as

$$U_{L,1}^{n} - r_{c,b} U_{L,1}^{n-1} - r_s^n = 0 \qquad (12\text{-}18)$$

Since no test data were available to evaluate the exponent n of equation (12-18), a value of 1.75, which is considered to be conservative, was used for the design of the panels.

The flat segment of the beaded configuration is analyzed for buckling with long, simply supported, isotropic plate theory. The expression of the utilization factor is

$$U_{L,2} = \frac{r_c + \left(r_c^2 + 4r_s^2\right)^{1/2}}{2} \qquad (12\text{-}19)$$

Using equations of Section 10, the stress ratios can be expressed as

$$r_c = f_c \left[3.29 \frac{\eta_{ST} E_{el}}{1 - \nu_{el}^2} \left(\frac{t}{b}\right)^2 \right]^{-1} \qquad (12\text{-}20a)$$

$$r_s = f_s \left[4.40 \frac{\eta_{ST} E_{el}}{1 - \nu_{el}^2} \left(\frac{t}{b}\right)^2 \right]^{-1} \qquad (12\text{-}20b)$$

where η_{ST} is evaluated with equation (10-12a) of Section 10. η_{tan} and η_{sec} of the equation are based on the stresses f_c and f_s, which are given by equations (12-10) and (12-12a). The equivalent stress is determined with the octahedral shear stress theory of reference 12-2. It is to be noted that this mode of buckling was not encountered in the design of the beaded skin panels, since b was fixed at 0.5 inch.

Panel No. 2, Trapezoidal Corrugation

The trapezoidal corrugation (fig. 12-1) is analyzed for: (1) simultaneous buckling of the horizontal and diagonal elements due to compression, (2) simultaneous buckling of the elements due to shear, (3) compressive buckling of the horizontal element due to bending of the panel, and (4) buckling of the diagonal element due to bending of the panel. Appropriate interaction equations are used for combined loading of the corrugation elements.

The compressive and shearing buckling stresses which produce the first two modes of buckling are (ref. 12-4)

$$f_{c,d,cr} = k_{c,d} \frac{\pi^2 \eta_{ST} E_{el}}{12 (1 - \nu_{el}^2)} \left(\frac{t}{d}\right)^2 \qquad (12\text{-}21a)$$

$$f_{s,d,cr} = k_{s,d} \frac{\pi^2 \eta_{ST} E_{el}}{12 (1 - \nu_{el}^2)} \left(\frac{t}{d}\right)^2 \qquad (12\text{-}21b)$$

where the buckling coefficients, which pertain to the diagonal element of the corrugation, are given in table 12-1.

TABLE 12-1

COMPRESSIVE AND SHEAR BUCKLING COEFFICIENTS

b/d	0.2	0.3	0.4	0.5	0.6	0.7	0.8	0.9	1.0
$k_{c,d}$	5.65	5.45	5.30	5.17	5.04	4.86	4.67	4.40	4.00
$k_{s,d}$	7.17	6.86	6.65	6.56	6.45	6.32	6.11	5.82	5.35

Treating the diagonal element as a long, simply supported isotropic plate and using the elastic theory of reference 12-1, the buckling stress due to bending is approximated as

$$f_{b,d,cr} = 19.74 \frac{\eta_{ST} E_{el}}{1 - \nu_{el}^2} \left(\frac{t}{d}\right)^2 \qquad (12\text{-}21c)$$

The plasticity coefficient of equations (12-21) is evaluated with equation (10-12) of Section 10, η_{tan} and η_{sec} of which are then conservatively determined with the same procedure as the plasticity coefficients of equation (12-14) for the beaded skin panel.

Using the interaction equation

$$r_{c,d} + r_{b,d}^{1.75} + r_{s,d}^{2} = 1 \qquad (12$$

where

$$r_{c,d} = f_c/f_{c,d,cr}$$

$$r_{b,d} = f_b/f_{b,d,cr} \qquad (12\text{-}23)$$

$$r_{s,d} = f_s/f_{s,d,cr}$$

the utilization factor for combined loading of the diagonal element can be written as

$$U_{L,d}^{2} - r_c U_{L,d} - r_b^{1.75} U_{L,d}^{0.25} - r_s^{2} = 0 \qquad (12\text{-}24)$$

When $r_b = 0$, the above equation is equivalent to equation (12-19). Also, when $r_s = 0$, the equation correlates well with the buckling theory of reference 12-1 for long, simply supported isotropic plates subjected to combined compression and bending. Compared to the theory of reference 12-1 for buckling of plates due to combined bending and shear, the equation is conservative when $r_c = 0$. It is considered to be adequate for the present investigation.

Treating the horizontal element of the trapezoidal corrugation as a long, simply supported plate, the ratio of the compressive stress due to bending divided by the initial buckling stress is

$$r_{b,h} = f_b \left[3.29 \frac{\eta_{ST} E_{el}}{1 - \nu_{el}^{2}} \left(\frac{t}{b}\right)^{2} \right]^{-1} \qquad (12\text{-}25)$$

Note that the plasticity coefficient is again based on the combined stress state. Since the horizontal and diagonal elements buckle at the same compressive stress and shear stress,

$$r_{c,h} \equiv r_{c,d}$$

$$r_{s,h} \equiv r_{s,d}$$

and the utilization factor for combined loading of the horizontal element is

$$U_{I,h} = \frac{r_{c,b,h} + \left(r_{c,b,h}^2 + 4r_{s,h}^2\right)^{1/2}}{2} \qquad (12\text{-}26)$$

where

$$r_{c,b,h} = r_{c,h} + r_{b,h}$$

Panels No. 3, Tubular, and No. 4, Convex-Beaded

The system of equations is formulated for the local buckling analyses of Panels No. 3 and 4 (fig. 12-1). Using compressive buckling theory for bending,

$$r_{c,\ell} = \left(f_c + f_{b,\ell}\right)\left[1.75\left(\eta_{sec,\ell}\,\eta_{tan,\ell}\right)^{1/2} E_{el}\left(\frac{t_\ell}{R_\ell}\right)^{1.35}\right]^{-1}$$

$$(\ell = 0,I) \qquad (12\text{-}27a)$$

where f_c and $f_{b,\ell}$ are given by equations (12-10) and (12-11b).

Curved plate theory, as used for the beaded configuration, is used to determine the shear initial buckling stress of the circular arcs of Panels No. 3 and 4. Hence, the shear stress ratio can be expressed as

$$r_{s,\ell} = f_{s,\ell}\left[0.37\left(Z_{b,\ell}\right)^{1/2} \tau_{cr,\ell}\right]^{-1} \qquad (\ell = 0,I) \qquad (12\text{-}27b)$$

where

$$Z_{b,\ell} = \frac{s_\ell^2}{R_\ell t_\ell}\left(1 - \nu_{el}^2\right)^{1/2} \qquad (\ell = 0,I)$$

$$\tau_{cr,\ell} = 4.40\,\frac{\eta_{sec,\ell} E_{el}}{1 - \nu_{el}^2}\left(\frac{t_\ell}{s_\ell}\right)^2 \qquad (\ell = 0,I) \tag{12-28}$$

and f_s is given by equation (12-12c). The plasticity coefficients of equations (12-27) are based on the combined stress state.

The expression of the utilization factor is

$$U_{L,\ell} = \frac{r_{c,\ell} + \left(r_{c,\ell}^2 + 4r_{s,\ell}^2\right)^{1/2}}{2} \qquad (\ell = 0,I) \tag{12-29}$$

Equations (12-27) through (12-29) are formulated for Panel No. 4. With the subscript ℓ removed, the equations apply to Panel No. 3, the application for which the stresses are given by equations (12-10), (12-11a) and (12-12b).

OPTIMIZATION PROCEDURE

Equations for the stress and local buckling analyses of the Fortran optimization programs which were used to determine the final minimum weight panels of the semimonocoque structure have been presented. Variables of the programs are as follows:

b, R, t, θ_1	(Panel No. 1)
$b/d, h, t, \theta$	(Panel No. 2)
b, R, t, θ	(Panel No. 3)
$b, R_I, t_I, t_0, \theta_I$	(Panel No. 4)

Note that the height/chord ratio of the outer arc of Panel No. 4 is fixed at a specified value.

In the input data of the programs, upper and lower limits of the variables and the increment for varying each variable between limits are specified, together with the panel loading, thermal strains, material properties, a minimum η_{tan}, and other problem constants. The programs analyze all possible designs from the matrix of dimensions they generate and select those that have utilization factors U_I near one, which corresponds to a zero margin of safety. Note that the scanning process involves two utilization factors in the design of Panels No. 1, 2, and 4 and only one factor in the design of Panel No. 3. The programs have provisions for rejecting unacceptable designs before the analysis is completed; for example, when $U_G > U_{G,max}$ and $\eta_{tan} < 0.1$.

For the present investigation of Panels No. 1, 3 and 4, b was fixed at 0.5 inch because of practical considerations. The height/chord ratio of the outer arc of Panel No. 4 was fixed at an upper limit of 0.2 because of aerodynamic requirements. In addition, θ_1 of Panel No. 1, θ of Panel No.3, and θ_I of Panel No. 4 were fixed at an upper limit of 77.5^o because of manufacturing limitations.

SECTION PROPERTIES AND STIFFNESSES

All section properties and stiffnesses which are used in the loads, stress, and local buckling analysis of the panels of the semimonocoque structure are presented in this section.

Panel No. 1, Beaded

The bending stiffness coefficients of the beaded skin panel

$$D_1 = \frac{\eta_{sec} E_{el}}{1 - \nu_{el}^2} \bar{I}_{yy}$$

$$D_2 = \bar{\eta} E_{el} \bar{I}_{xx} \qquad (12\text{-}30)$$

where

$$\bar{I}_{yy} = \frac{a}{s} \frac{t^3}{12}$$

$$\bar{I}_{xx} = \frac{tR^3}{a} \left[\left(0.5 + \cos^2 \theta_1\right)\theta_1 - 0.75 \sin 2\theta_1 \right] \qquad (12\text{-}31)$$

in which

$$a = R \sin \theta_1 + 0.5b$$

$$s = 0.5b + \theta_1 R \tag{12-32}$$

and where

$$\bar{\eta} = \frac{\left(\eta_{tan}^2 f_c^2 + \eta_{sec}^2 f_b^2\right)^{1/2}}{\left(f_c^2 + f_b^2\right)^{1/2}} \tag{12-33a}$$

or

$$\bar{\eta} = \eta_{sec} \tag{12-33b}$$

Equation (12-33a) is used for computing the stress ratio R_c and equation (12-33b), for computing R_s. The plasticity coefficients η_{tan} and η_{sec} are based on the stresses f_c, f_b and f_s, the equivalent stress of which is determined with octahedral shear stress theory.

Additional properties which are required for the analyses of panel loading and stresses are

$$\bar{t} = st/a$$

$$\bar{t}_s = at/s \tag{12-34}$$

$$z = 0.5h = R(1 - \cos \theta_1)$$

Stiffness coefficients which are required for the first mode of local buckling are

$$D_I = \eta_{tan,L} E_{el} \bar{I}_{\xi\xi,L}$$

$$D_{II} = \frac{\eta_{sec,L} E_{el}}{1 - \nu_{el}^2} \bar{I}_{yy,L} \qquad (12\text{-}35)$$

$$D_3 = \frac{\eta_{sec,L} E_{el}}{(1 + \nu_{el})} \bar{I}_{\xi y,L}$$

in which

$$\bar{I}_{\xi\xi,L} = \frac{1}{\xi_2} \left(I_{xx,L} \cos^2 \theta_\xi + I_{zz,L} \sin^2 \theta_\xi - I_{xy,L} \sin 2\theta_\xi \right)$$

$$\bar{I}_{yy,L} = \frac{\xi_2}{s_2} \frac{t^3}{12} \qquad (12\text{-}36)$$

$$\bar{I}_{\xi y,L} = \frac{s_2}{\xi_2} \frac{t^3}{12}$$

where

$$I_{xx,L} = a\bar{I}_{xx} - tR^3\left[\left(0.5 + \cos^2\theta_1\right)\theta_2 - \sin\theta_2(2\cos\theta_1 - 0.5\cos\theta_2)\right]$$

$$I_{xy,L} = tR^2\left[a(\sin\theta_1 - \sin\theta_2) - 0.5R\left(\sin^2\theta_1 - \sin^2\theta_2\right)\right.$$

$$\left. - R\cos\theta_1(\cos\theta_1 - \cos\theta_2) - (\theta_1 - \theta_2)\, a\cos\theta_1\right] \qquad (12\text{-}37)$$

$$I_{zz,L} = tR\left[(0.5R^2 + a^2)(\theta_1 - \theta_2) - 0.25R^2(\sin 2\theta_1 - \sin 2\theta_2)\right.$$

$$\left. + 2aR(\cos\theta_1 - \cos\theta_2)\right] + tb^3/24$$

and

$$\xi_2 = \left(x_2^2 + z_2^2\right)^{1/2}$$

$$\theta_\xi = \tan^{-1}\left(\frac{z_2}{x_2}\right) \qquad (12\text{-}38)$$

$$s_2 = 0.5b + R(\theta_1 - \theta_2)$$

Expressions of the dimensions x_2 and z_2 are

$$x_2 = a - R\sin\theta_2$$

$$z_2 = R(\cos\theta_2 - \cos\theta_1)$$

Plasticity coefficients of equation (12-35) are based on the stresses f_L and f_s, the equivalent stress of which is determined with octahedral shear stress theory.

The effective thickness $\bar{t}_L$ of equation (12-13a) is expressed as

$$\bar{t}_L = ts_2 / \xi_2 \tag{12-39}$$

Panel No. 2, Trapezoidal Corrugation

The bending stiffness coefficients of the trapezoidal corrugation are given by equation (12-30) where

$$\bar{I}_{yy} = \frac{p}{2s} \frac{t^3}{12}$$

$$\bar{I}_{xx} = \frac{2}{p}\left[bt(0.5h)^2 + \frac{tdh^2}{12} \right] \tag{12-40}$$

in which

$$d = h/\sin\theta$$

$$p = 2(b + d\cos\theta) \tag{12-41}$$

$$s = b + d$$

The plasticity coefficients are evaluated the same as those of Panel No. 1.

Additional properties which are required for the analyses of panel loading and stresses are

$$\bar{t} = 2st/p$$

$$\bar{t}_s = pt/2s \tag{12-42}$$

$$z = 0.5h$$

Panel No. 3, Tubular

Stiffness coefficients of the tubular panel of symmetric cross section are

$$D_1 \approx 0$$

$$D_2 = \bar{\eta} E_{el} \bar{I}_{xx} \tag{12-43}$$

$$D_3 = 0.25 \frac{\eta_{sec} E_{el}}{1 + \nu_{el}} \bar{J}$$

where

$$\bar{I}_{xx} = \frac{4tR^3}{p} \left[(0.5 + \cos^2 \theta)\theta - 0.75 \sin 2\theta \right]$$

$$\bar{J} = 4A^2 \Big/ p\left(\frac{4R\theta}{t}\right)$$

in which

$$p = b + 2R \sin \theta$$

$$A = R^2(2\theta - \sin 2\theta)$$

The procedure for evaluating the plasticity coefficients of equation (12-43) is the same as that for equation (12-30).

Additional properties which are required for the analysis of the panel are

$$\bar{t} = 2st/p$$

$$\bar{t}_s = 2pt/s \tag{12-44}$$

$$z = R(1 - \cos \theta)$$

where

$$s = b + 2R\theta$$

Panel No. 4, Convex Beaded

Stiffness coefficients of the tubular panel of unsymmetric cross section are given by equation (12-43) in which (ref. 12-5)

$$\bar{I}_{xx} = \frac{1}{p}\left(I_{O,arc} + I_{I,arc} + A_{O,arc}\bar{z}_{O,arc}^2 + A_{I,arc}\bar{z}_{I,arc}^2 - A_y\bar{z}^2\right) \qquad (12\text{-}45)$$

$$\bar{J} = 4A^2 \Big/ 2p\left(\frac{R_O\theta_O}{t_O} + \frac{R_I\theta_I}{t_I}\right)$$

where

$$p = b + 2R_I \sin\theta_I$$

$$A_{\ell,arc} = 2R_\ell\theta_\ell t_\ell \qquad (\ell = O,I)$$

$$A_y = A_{O,arc} + A_{I,arc} + (t_O + t_I)b$$

$$\bar{z}_{O,arc} = R_O\left(\frac{\sin\theta_O}{\theta_O} - \cos\theta_O\right) \qquad (12\text{-}46)$$

$$\bar{z}_{I,arc} = -R_I\left(\frac{\sin\theta_I}{\theta_I} - \cos\theta_I\right)$$

$$\bar{z} = \left(A_{O,arc}\bar{z}_{O,arc} + A_{I,arc}\bar{z}_{I,arc}\right)\Big/A_y$$

$$I_{\ell,arc} = R_\ell^3 t_\ell\left(\theta_\ell + \sin\theta_\ell\cos\theta_\ell - \frac{2\sin^2\theta_\ell}{\theta_\ell}\right) \qquad (\ell = O,I)$$

$$A = R_O^2(\theta_O - 0.5\sin 2\theta_O) + R_I^2(\theta_I - 0.5\sin 2\theta_I)$$

and

$$R_0 = \left(h_0^2 + 0.25c^2\right)\Big/2h_0$$
$$\theta_0 = \sin^{-1}\left(\frac{0.5c}{R_0}\right) \qquad (12\text{-}47)$$

The expression of the chord dimension of equation (12-47) is

$$c = 2R_I \sin\theta_I \qquad (12\text{-}48)$$

The plasticity coefficients are evaluated the same as those of Panel No. 3.

Additional properties which are required for the analysis of the panel are

$$\bar{t} = A_y\Big/p$$
$$\bar{t}_s = \frac{p}{s_0}\left(1 + \frac{s_0}{s_I}\frac{t_I}{t_0}\right)t_0 \qquad (12\text{-}49)$$
$$z_0 = h_0 - \bar{z}$$
$$z_I = -R_I(1 - \cos\theta_I) - \bar{z}$$

where

$$s_\ell = b + 2R_\ell\theta_\ell \qquad (\ell = 0,I)$$

REFERENCES

12-1 Timoshenko, Stephen P.; and Gere, James M.: Theory of Elastic Stability. Second ed., McGraw-Hill Book Co., Inc., 1961.

12-2 Nadai, A.: Theory of Flow and Fracture of Solids. Vol. I, Second ed., McGraw-Hill Book Company, Inc., 1950.

12-3 Gerard, George; and Becker, Herbert: Handbook of Structural Stability. Part III - Buckling of Curved Plates and Shells. NASA TN 3783, 1957.

12-4 Ellison, A. M.: Optimum Open Corrugation Wing Covers (Initial Buckling). LMSC/HREC A782409 (Also, HREC/7796-1), Lockheed Missiles and Space Company, 1966.

12-5 Roark, Raymond J.: Formulas for Stress and Strain, Third ed., McGraw-Hill Book Company, Inc., 1954.

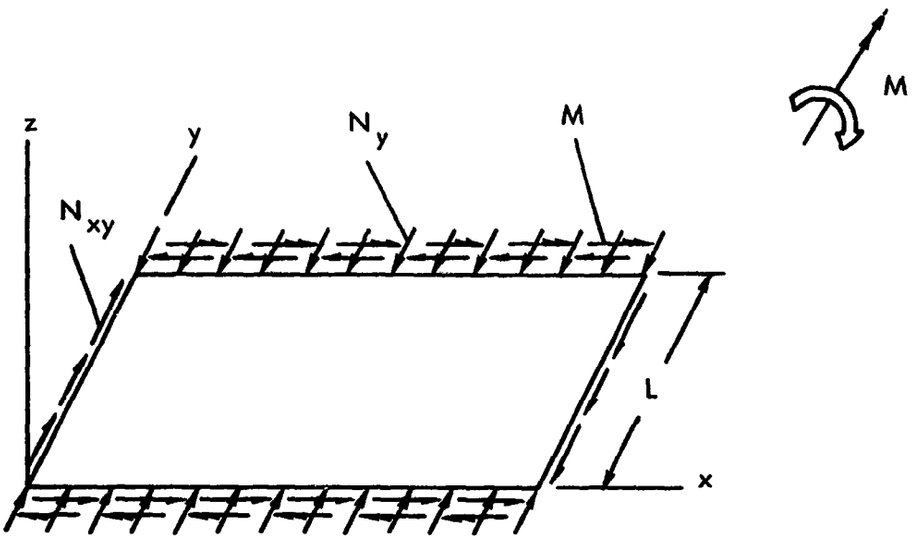

Notation of panel length and stress resultants

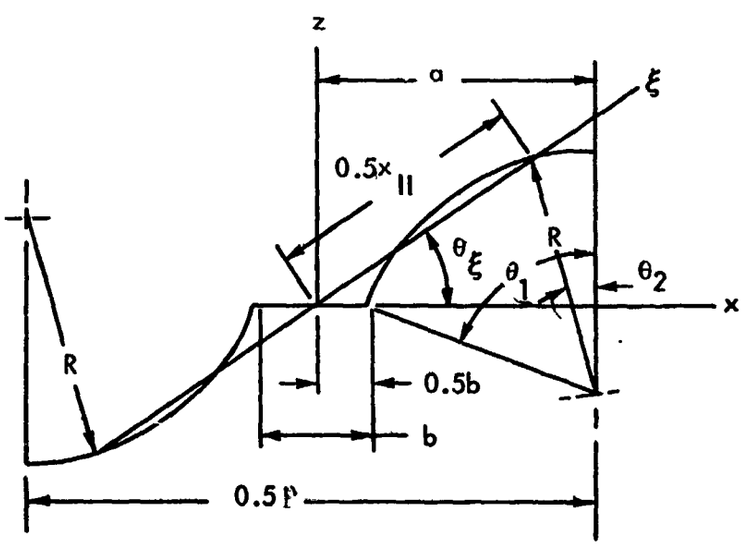

Cross section of panel No. 1, beaded

Figure 12-1. Geometry and loading of panels of semimonocoque structure

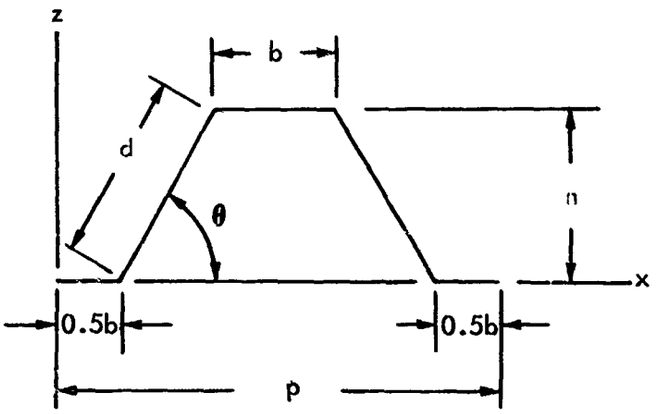

Cross section of panel No. 2, trapezoidal corrugation

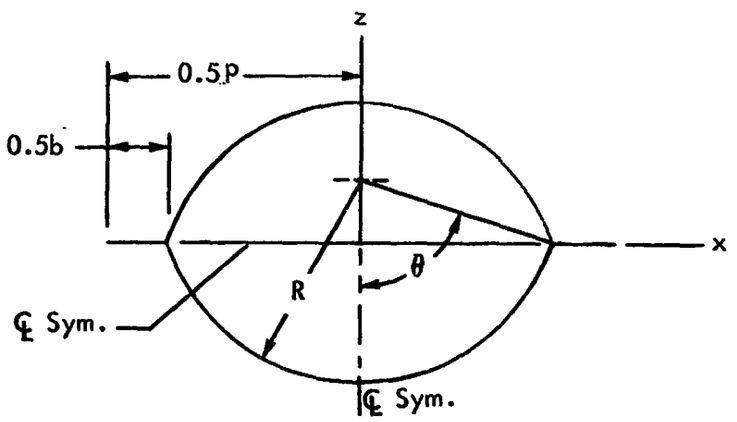

Cross section of panel No. 3, tubular

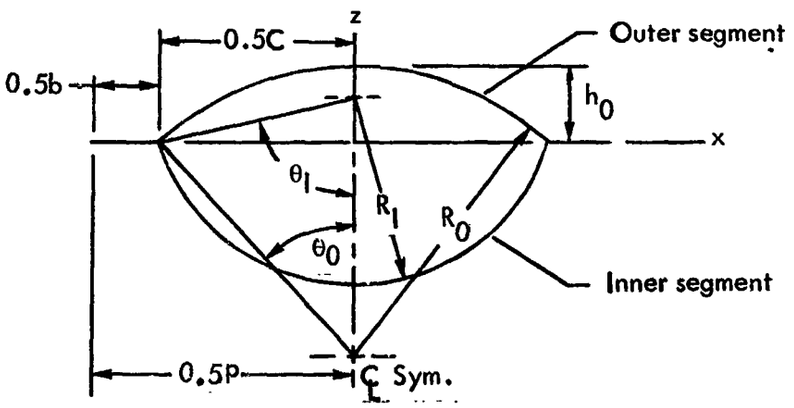

Cross section of panel No. 4, convex beaded

Figure 12-1 (Concluded)

SECTION 13

PRIMARY-STRUCTURE WEIGHT ANALYSIS

by

C. C. Richie, G. W. Davis, W. A. Claus, D. G. Watson,
F. T. Bevan

CONTENTS

TABLES

ILLUSTRATIONS

SYMBOLS

a, b	x and y distance between simply supported edges of panel; b is also trapezoidal corrugation crest width and width of flats of panels.
A	Area
A_n	Area of n^{th} element of a cross section
Area A	Area between $\mathcal{L}$ and BL 120 of wing investigation area
Area B	Area between BL 120 and BL 212 of wing investigation area
Area C	Area between BL 212 and BL 350 of wing investigatiion area
BL	Butt line
b_f	Width of flange of flanged waffle
b_s	Pitch
b_w	Distance from crest-to-crest of circular-arc, corrugated shear webs
b_n	Width of n^{th} element used in determining compression allowable
a/b	Panel aspect ratio
C	Geometric chord
D	Hole diameter
d	Width of diagonal element of trapezoidal corrugation
dB	decibels
E	Modulus of elasticity
e	Panel edge eccentricity; elongation
e_{11}	Extensional eccentricity of waffle
e_{33}	Shear eccentricity of waffle

F_{cc}	Allowable crippling stress
$F_{s,cr}$	Allowable shear stress
g	Gravitational acceleration
Hz	Hertz
h	Height
hw	Stiffener height of waffle
K	Buckling coefficient
L	Length
N	Force per unit length
N_x, N_y, N_{xy}	Extensional forces and shear force in xy coordinate system per unit length of section
n	Exponent of weight index used in wide-column curve
P	Pitch
p	Pressure
q	Dynamic pressure
R	Radius
R_ℓ	Radius of internal arc of convex-beaded configuration
R_u	Radius of external arc of convex-beaded configuration
S	Cell size of honeycomb-core
S_{max}	Maximum cell size
S_{min}	Minimum cell size
T	Temperature
t	Thickness
t_a	$1/2\ (t_s + t_c)$ for waffle single shear joint
	$1/2\ (t_s + t_b + t_c)$ for waffle double shear joint

t_b	Cap thickness
t_c	$1/2\ t_s + e_{11}$; corrugation thickness; cap thickness; core foil thickness for honeycomb- and truss-core panels
t_s	Skin thickness
t_w	Stiffener thickness for waffle configuration
t_ℓ	Thickness of internal arc of convex-beaded configuration
t_u	Thickness of external arc of convex-beaded configuration
t_1	Skin thickness of internal face sheet of honeycomb- and truss-core sandwich
t_2	Skin thickness of external face sheet of honeycomb- and truss-core sandwich
$\bar{t}$	Equivalent thickness
$\bar{t}_{Basic}$	Equivalent thickness of panel without nonoptimum factor
$\bar{t}_{Heat\ Shield}$	Equivalent thickness of heat shield
$\bar{t}_{panel}$	Equivalent thickness of panel with nonoptimum factor included
$\bar{t}_{Total}$	Total equivalent thickness
W	Unit weight
w_o	Maximum panel deflection
$\bar{Z}$	Location of neutral surface from extreme fiber
α	Semi-apex angle of beaded concepts
ΔT	Temperature difference
$\Delta\bar{t}$	Equivalent thickness difference
S	Deflection
E	Efficiency factor used in wide-column equation
$\bar{\eta}$	Plasticity factor

λ	Ratio of pitch to radius
ρ_c	Density of honeycomb-core
Σ	Summation
ϕ	Semi-apex angle of circular-ar · corrugation

Section 13

PRIMARY-STRUCTURE WEIGHT ANALYSIS

Data obtained from the analysis of trajectory, vehicle loads, aerodynamic heating, and candidate materials were applied to a detailed weight analysis of the primary structure (initial screening, intermediate screening, and final structural sizing).

INITIAL WEIGHT SCREENING

Loads are shown in Table 8-1 and the design temperatures for the monocoque, semimonocoque spanwise, and semimonocoque chordwise concepts used for the initial panel-weight screening are shown in tables 13-1, 13-2, and 13-3. Selected-size panels were designed and optimized.

Initial panel-screening results are shown for monocoque and semimonocoque primary structures, (spanwise and chordwise-stiffened) using Rene'41 and Haynes 25 materials. Following this, certain panel configurations and the use of Haynes 25 materials were eliminated because of their weight.

Monocoque

Initial screening of leading candidate panel configurations for the monocoque primary structure concept was accomplished using the structural synthesis optimization procedure presented in section 10. Optimum structural configurations, within prescribed constraints and for multiple design conditions, were determined for six different types of simply supported rectangular panels as presented in table 13-1.

Constraints on minimum gages for the leading candidate panel configurations were as follows:

1. Waffle grid (-45° x 45° and 0° x 90°)
   skin thickness, t_s = 0.020 in.
   stiffener thickness, t_w = 0.020 in.
2. Honeycomb sandwich
   internal skin thickness, t_1 = 0.010 in.
   external skin thickness (exposed), t_2 = 0.015 in.
   core foil thickness, t_c = 0.002 in.
3. Truss-core sandwich
   internal skin thickness, t_1 = 0.010 in.
   external skin thickness (exposed), t_2 = 0.015 in.
   core web thickness, t_c = 0.010 in.

Additional constraints for the honeycomb-core sandwich were:

1. Maximum (square) cell size, $S_{max} = 0.375$ in.
2. Minimum (square) cell size, $S_{min} = 0.125$ in.

Additional constraints for the waffle grid (-45° x 45° and 0° x 90°) were:

1. Maximum stiffener height/thickness ratio, $\left(\frac{h_w}{t_w}\right)_{max} = 25$
2. Maximum flange width/stiffener pitch ratio (flanged waffle grid only), $\left(\frac{b_f}{p}\right)_{max} = 0.5$
3. Maximum stiffener spacing aspect ratio (0° x 90° waffle only) $\left(\frac{P_{max}}{P_{min}}\right)_{max} = 3.0$

Typical spar caps and edge closeouts, shown in figure 13-1, were used to determine nonoptimum weight factors for the candidate panel concepts. Manufacturing processes used for the weight analysis of panel concepts are shown in table 13-4.

Weight data presented in table 13-1 indicate that the least-weight panel concept on the upper wing surface is the -45° x 45° unflanged waffle grid. On the lower wing surface, the least-weight panel concept is the 0° x 90° flanged waffle grid, with the 0° x 90° unflanged and 45° x 45° flanged and unflanged waffle grids being slightly heavier. Based on the combined weight of the upper and lower surfaces the two lower weight configurations, -45° x 45° (4.37 lb/ft^2) and 0° x 90° unflanged (4.56 lb/ft^2) waffle grids were selected for further screening. Also, since panel weights for Rene' 41 are less than those for Haynes 25 on both the upper and lower surface, Rene' 41 was selected as the primary structural panel material.

Initially, only the waffle panel was retained for further analysis. However, at the end of the final analysis, the waffle weight was found to have increased significantly, primarily as a result of pressure loads and the fact that the waffle panel is less efficient when applied to the complete wing structure than other concept Thus, the final results did not present the best choice for a monocoque concept, and the initial screening results were reconsidered. Consequently, honeycomb sandwich was chosen as the panel exhibiting the greatest potential for support of pressure and inplane loadings for monocoque studies. The honeycomb sandwich was then selected for final detailed analysis.

Semimonocoque

Panel weight, closeout weight, minimum gages, and typical heat-shield weight were considered in the initial screening of all candidate semimonocoque spanwise- and chordwise-stiffened panels. Nonoptimum factors were based on the weight of panel-edge closeout designs in which the fastener shear force and panel centroidal axis are aligned. The typical heat-shield weight was based on a refurbishable corrugated skin with two transverse hat-section stiffeners and four post supports. Table 4-5 of section 4 contains the manufacturable minimum gage constraints imposed on the concepts.

The panels were analyzed using the general and local structural stability procedures as derived in section 12. Written in the general form, the wide-column equation is

$$\frac{N}{LE\bar{\eta}} = \epsilon\left(\frac{\bar{t}}{L}\right)^n$$

A plot of weight index (t/L) versus load index ($N/LE\bar{\eta}$) is shown in figure 13-2; this figure also contains the efficiency factors (ϵ) and weight index exponents (n) for the candidate concepts considered. Curves 1, 2, 4, 6, and 9 were used for the initial panel-weight screening. Later, it was found that the corrugation-stiffened configuration was limited by fabrication, as represented by curve 3 of figure 13-2. The corrugation-stiffened configuration had a 60-deg interior angle and a flat/slant height ratio of 0.80, which is nonoptimum, as a result of the fabrication stretch-forming limitations. The trapezoidal corrugation was analyzed for the optimum 60-deg interior angle and a flat/slant height ratio of 0.85. Also, later in the study, the beaded and tubular panel concepts were based on a constant semiapex angle of 77.5 deg, reduced from the earlier 90-deg arc because of the elongation limitations of fabricating these configurations by stretch-forming. During the intermediate screening, the room-temperature beaded-panel column test (presented in section 27) resulted in a failure at a lower stress than anticipated. The local instability allowable for the beaded panel was initially assumed to depend on the radius-to-thickness ratio (R/t) of the arc; this was substantiated by local buckling tests. However, on the basis of orthotropic plate theory, the column panel test failure corresponded to an upper bound stress. Therefore, a new optimization procedure (see section 12) was developed for the final structural sizing of the beaded concept, as represented by curve 8 of figure 13-2.

Spanwise concepts. The results of the initial spanwise-stiffened panel screening given in table 13-4 indicate that all of the spanwise panel configurations are of approximately the same efficiency. The heaviest is indicated to be the tubular panel however, this panel showed the potential for much greater efficiency at longer lengths than used. Therefore, all four configurations were subjected to an additional detailed panel evaluation during the intermediate screening in which total wing cross-section weights were considered. Results showed that the Haynes 25 alloy panels were not competitive with the Rene' 41 panels.

Chordwise concepts. - The results of the initial chordwise panel screening presented in table 13-5 show that the convex beaded version (unshielded design) has the lowest weight, 3.20 lb/ft^2 for combined upper and lower surfaces. However, selection was not made until results of the intermediate analyses of the spanwise concepts were known. This delay was to allow a better evaluation of the weight of these primary-structure concepts as a function of panel size and to allow selection of a concept identical to one of the spanwise concepts in order to make a direct comparison of panel orientation.

Statically Determinate

The statically determinate structure is spanwise stiffened. The minimum-weight panel concept for the spanwise semimonocoque structure would also be very efficient for the statically determinate panels, since the loading conditions are similar. Thus, no screening was done for the statically determinate structure, and the panel selection for final weight analysis of this type of structure was the least-weight spanwise semimonocoque panel.

INTERMEDIATE WEIGHT SCREENING

The intermediate screening considered normal pressure as well as inplane loadings for total wing cross-section optimization; rib and spar spacing were varied. Preliminary considerations for thermal protection (heat shield) were included to keep the primary structure below 1600°F. Calculated weights were based on Rene'41 material and included the following items: primary structure, typical heat shields, spars and ribs, and panel closeouts. Heat-shield weight was based on a refurbishable corrugated skin with two transverse hat-section stiffeners and four post supports. In addition to the elimination of certain panel constructions, the results of the intermediate screening provided the necessary structural data for input into the final redundant-model loads analysis. For this intermediate screening analysis, the preliminary redundant-model internal loads shown in table 8-2 of section 8 were used.

A survey of the preliminary transient-temperature data for the three flight conditions (-0.5-g, +2.0-g, and cruise) and the loads of table 8-2 led to the choice of the +2.0-g maneuver condition as the controlling design for the intermediate screening. The thermal strains, rather than the thermal loads of table 8-2, were combined with the air loads and the temperatures of the preliminary transient analysis for each concept. The semimonocoque arrangements were optimized for bending and compression. The waffle and honeycomb optimizations included shear, bending, and compression.

The results of the intermediate weight screening shown in table 13-5 include temperatures, rib and spar spacings, and weights (lb/ft^2) for the primary structural concepts investigated.

Monocoque Waffle

A parametric aspect ratio study involving 45° x 45° and 0° x 90° waffle panels indicated that a geometrical configuration in which a/b = 2.0, with rib spacing b of 20 in., provides optimum weights. This 20-by-40 in. size was then used for the panel evaluations shown in table 13-6. Since the 45° x 45° grid was more efficient, waffle weights and shapes (including substructure) were determined for the 45° grid to provide input data for obtaining final redundant analysis loads. The details of the monocoque waffle intermediate screening are presented below.

Initial panel aspect ratio and panel dimension investigation – The initial panel aspect ratio and panel dimension investigation encompassed the following main areas:

- Further assessment of the -45° x 45° and 0° x 90° waffle grid was made to provide additional substantiating data for the waffle grid selection (see initial panel screening).

- Aerodynamic pressure effects were considered for designing unflanged -45° x 45° and 0° x 90° waffle plates subjected to combined inplane and out-of-plane loading.

The evaluation matrix for the unflanged -45° x 45° and 0° x 90° waffle grid using inplane loads is shown in table 13-6. As a conservative design approach, only compression loads were considered in the panel sizing. By neglecting the beneficial effects of tension on panel general instability, a small weight penalty was incurred. Panels are located between BL 120 and 220 without heat shields. Assumed temperatures for the comparison were 1400°F and 1600°F for the upper and lower surface panels, respectively. Rene 41' material properties were used. Aspect ratios of 1 and 2 were assumed for panel widths of 20, 40, and 60 in., considering both chordwise and spanwise orientation. A summary of unit weights for this aspect ratio study is shown in table 13-7. The conclusions of the waffle assessment are:

- The 45° x 45° waffle results in lower weight for plate applications (lower surface spanwise orientation).

- The 0° x 90° waffle is lower weight for wide column applications (lower surface spanwise orientation).

- The effective rib cap area (spanwise joint plus rib cap) for both the 45° x 45° and 0° x 90° panels is essentially the same because the distance from the outer pannel surface to the neutral axis is approximately the same.

- The effective spar cap area (chordwise joint plus spar cap) for the 45° x 45° waffle is less than the 0° x 90° waffle since the distance from the outer panel surface to the neutral axis is less for the 45° x 45° waffle.

- Chordwise panel orientation is the most appropriate approach with ribs being placed closer than spars.

The evaluation of normal pressure effects (internal, venting) on the -45° x 45° and 0° x 90° waffle panels is shown in table 13-8. The comparison was based on design loads shown in table 8-2 for the 2g maneuver condition. Panels are between BL 120 - 220 without heat shields. Chordwise panel orientation, aspect ratio of 2.0, and width of 20 in. were considered. Rene' 41 material properties and panel temperature of 1400°F was used. Limit wing pressure data are taken from section 2.

The results of the upper surface panel evaluation are presented in table 13-8. The comparison indicates that upper surface panel weights (for the particular panel size considered) increase approximately 32 percent for both the -45° x 45° and 0° x 90° waffle grids when normal pressures are considered. On the upper surface, unit panel weights of the 0° x 90° waffle grid are slightly less than those for the -45° x 45° waffle grid. Since the upper surface loads are higher in the short panel direction, the weight difference between the waffle grids indicates that the 0° x 90° waffle is also more efficient as a wide column when the effects of pressure are included.

The results of the lower surface panel evaluation shown in table 13-8 indicate that pressure has a significant effect on panel weights. For the -45° x 45° waffle grid, unit panel weights increase 33.5 percent and 49 percent for panel widths of 20 in. and 40 in., respectively. For the 0° x 90° waffle grid, unit panel weights increase 34 percent and 43 percent for panel widths of 20 in. and 40 in., respectively. Thus, the increase in unit panel weight due to pressure is approximately the same for both the -45° x 45° and 0° x 90° waffle grids.

On the lower surface, unit panel weights of the -45° x 45° waffle grid are considerably less than those of the 0° x 90° waffle grid. Since the lower surface loads are higher in the long panel direction, the weight difference between the waffle grids indicates that the -45° x 45° waffle is also more efficient as a plate when the effects of pressure are included.

Since total panel weights for the -45° x 45° waffle grid are less than those for the 0° x 90° waffle grid (see table 13-8), the -45° x 45° waffle grid was selected for the monocoque waffle primary-structure panel concept.

Initial wing geometry (rib and spar spacing). – Initial wing geometry was determined to provide more refined redundant model input data for the monocoque waffle primary-structure concept. The initial rib and spar spacing was determined by the following optimization procedure:

- The panel width was optimized for a chordwise panel orientation and panel aspect ratio of 2.0. These initial assumptions were supported by the comparison of various panel configurations shown in table 13-7.

- The panel aspect ratio was optimized using the panel width determined in the first step.

Panel design for the initial rib and spar spacing was based on constant airloads and thermal strains. Thus, panel thermal loads were proportional to the panel stiffness. This design procedure ensures consistency between redendant model and panel loads. Redundant model airloads depend mainly on equilibrium and, therefore, were assumed to be constant with changes in panel stiffness. Similarly, redundant model thermal strains depend mainly on compatibility conditions and were also assumed to be constant with changes in panel stiffness.

The procedure of section 10 was used for optimization of the -45° x 45° unflanged waffle grid panels subjected to combined inplane and out-of-plane loading. In addition to the initial inplane and pressure loads, an edge eccentricity of ±0.02 inch and an initial deflection due to bowing of 0.001 x b was assumed. Although all three loading conditions were considered, the 2g maneuver condition was the only active design condition.

The panel width optimization matrix is shown in table 13-9. Optimum panel widths were determined for the inboard area between BL 120 - 220 and the outboard area between BL 220 - 350. Lower surface thermal protection for the panel width study consists of heat shields in the outboard area. To select an optimum thermal protection arrangement for the monocoque waffle primary-structure concept, further assessment of the effects of heat shields (with and without insulation) will be considered in the final evaluation. Temperatures are based on preliminary thermal analysis data. A total of 16 panels were optimized for widths of 10, 20, 30 and 40 in. The results of this optimization, including panel weights, dimensions, eccentricities, and maximum deflections, are shown in tables 13-12 and 13-13 for the inboard and outboard areas of the wing, respectively. Notation for the panel dimensions is presented in figure 13-3.

Based on extensional eccentricities from tables 13-10 and 13-11, incremental weights for typical single and double shear joints (figure 13-4) are shown in tables 13-12 and 13-13. Small weight differences between the two joint concepts result. For the determination of the rib and spar requirements, the single shear joint is selected because of design simplicity.

A summary of component wing weights including panels, closeouts, rib/spar webs and caps, and heat shields, is shown in tables 13-14 and 13-15 for the inboard and outboard areas of the wing. Circular-arc corrugated webs of 0.015 in. (minimum gage) analyzed for local instability, general instability, stiffness,

and resistance to flexure-induced crushing are used for both ribs and spars. A minimum gage (0.010-in.) circular-arc corrugated post-supported heat shield is also considered.

Optimization of the rib and spar requirements is shown in figures 13-5 and 13-6. Based on an aspect ratio of 2, the optimum panel width is 20 in. for both the inboard and outboard areas as indicated. Based on the foregoing panel sizes, the corresponding unit wing weights are 8.9 lb/ft^2 for the inboard area and 8.5 lb/ft^2 for the outboard area.

The panel aspect ratio optimization matrix is shown in table 13-16. Optimum panel aspect ratio was determined only for the inboard area. Lower surface heat shields are assumed. Temperatures are based on preliminary thermal analysis data. Eight panels were optimized for a panel width of 20 in. and panel aspect ratios of 1.0, 1.5, 2.0, and 2.5. A summary of component wing weights including panels, closeouts, rib/spar webs and caps and heat shields, is shown in table 13-17. Figure 13-7 indicates that the optimum aspect ratio is approximately 2.5. However, the difference in wing weight for panel aspect ratios between 2.0 and 3.0 is small, i.e., less than one percent.

Monocoque Honeycomb-Core Sandwich

As indicated in the initial panel-weight screening, honeycomb-core sandwich was selected for the final structural analysis. Weights for this panel are not presented in the intermediate screening data of table 13-5. However, an intermediate screening was conducted to determine input for the redundant loads analysis, required for the final structural analysis.

The intermediate screening of the honeycomb-core sandwich concept was accomplished after the final structural sizing of the lightest-weight waffle arrangement and could, therefore, use the final waffle redundant model loads. The honeycomb inboard wing data (table 13-18) includes both smooth and recessed closeouts and indicates that the recessed closeout design results in lower weight. The recessed closeout requires that both face sheets be curved to orient the panel centroidal axis with the substructure fastener, resulting in increased drag and increased local thermal stresses from uneven heating, as well as increased manufacturing complexity.

The most important decision factor, in addition to panel weight, was increased drag. Therefore, total wing aerodynamic performance analysis (drag) was conducted for the two closeout approaches, in terms of fuel increment (as compared to an all-smooth wing). The resulting fuel increments were 9 790 lb for the recessed and 126 lb for the smooth closeout design.

The entire wing weights and the drag penalties are summarized in table 13-18, which shows a vehicle weight advantage of 7416 lb for the smooth closeout design, which was therefore chosen for detail sizing. However, a more gradual recess geometry than that selected would lessen the drag, and since the recessed design has less weight than the smooth design, the recessed design may offer lower wing weight and lower total system cost.

An initial panel aspect ratio (figure 13-7) and panel dimension investigation was conducted (figure 13-8), resulting in minimum-weight geometry of a/b = 2, with a rib spacing b of 40 in. The honeycomb thermal protection was lower surface outboard heat shields and insulation. The geometry for the honeycomb sandwich panels are shown in table 13-19. These panel stiffnesses along with the substructure stiffness were used for input data for obtaining final redundant analysis loads. Table 13-20 indicates weight results for the center ($\mathbb{Q}$ to BL 120), inboard (BL 120 to 212), and outboard (BL 212 to 350) areas of the wing investigation section. A honeycomb sandwich average weight of 6.44 lb/ft^2 was obtained for the total wing investigation section.

Semimonocoque Spanwise

All semimonocoque spanwise-stiffened structures, except the smooth corrugation-stiffened panels, employed heat shields on all exposed surfaces to reduce temperatures and provide aerodynamic smoothness.

The surface panels for each of the spanwise candidates were sized for the inplane and normal loads. The typical results of this analysis are presented in figures 13-9 through 13-15 for panels between BL 120 and 212.

The beaded and tubular panel concepts were based on a constant semiapex angle of 77.5 . This angle was required for fabrication reasons. The elongation, efficiency, and geometry versus semiapex angle are presented in figures 13-16 and 13-17. These calculations were based on a 30.0 in. long panel carrying an inplane load of 2000 lb/in.

The corrugation-stiffened skin panel weight is for the upper surface between BL 120 and 212. The constant geometry parameters used for this section were a 60° interior angle and a flat/slant height ratio of 0.80 as required for fabrication. The trapezoidal corrugation was analyzed for a 60° interior angle and a flat/slant height ratio of 0.85.

During this intermediate structural screening, the corrugation-stiffened skin was eliminated, since it was found to be considerably heavier than the other three candidates. For example, for a 30-in. rib spacing, the upper surface corrugation-stiffened skin panel is 2-1/2 times as heavy as the upper surface trapezoidal corrugation, as shown in table 13-5.

Weight optimization of the tubular concept is presented in figures 13-18 and 13-19 for the representative areas of the wing. The optimum rib spacing is approximately 40 in.; however, definition of the minimum of the curve indicates that the rib spacing can be varied from 38 to 48 in. without appreciably increasing total cross-sectional weights.

Results of weight optimization of the beaded concept are presented in figures 13-20 and 13-21. The optimum rib spacing is approximately 48 in. for the inboard area and 50 in. for the outboard areas. However, as in the case for the tubular panels, rib spacing between 43 and 52 in. can be used without appreciable weight increase. For a 48-in. rib spacing, 0.016-in. gage

thickness panels are required for the upper surface and minimum gage (0.015-in.) for the lower surface. A radius of 1.50 in. is required to provide adequate stiffness and strength to transmit the design loads for the respective panel designs. For a rib spacing of 46 in. minimum-gage panels can be used for both the upper and lower surface panel designs.

Weight optimization of the trapezoidal-corrugation concept is presented in figures 13-22 and 13-23, indicating both wing component and total cross-sectional equivalent thickness. The results indicate rib spacing requirements of approximately 30 in. for both the inboard and outboard areas of the wing. Both upper and lower surface thickness requirements exceed the minimum gage criteria established, with 0.024-in. and 0.020-in. material thickness required, respectively.

The goal of the intermediate screening was the selection of the two lightest-weight semimonocoque spanwise structures for final sizing. These are the tubular and beaded-skin concepts (table 13-5). The trapezoidal corrugation is seen to be about 30 percent heavier than the beaded skin and about 13 percent heavier than the tubular concept. However, a further intermediate screening of the trapezoidal-corrugation concept was conducted using the final semimonocoque spanwise loads presented in section 8. The results were compared with the final beaded and tubular weights (presented later), and the trapezoidal-corrugation concept was still heavier than the other two spanwise concepts. The details of the further intermediate screening of the trapezoidal corrugation are presented below.

The trapezoidal-corrugation primary structure with heat shields on both upper and lower surfaces was assessed on the basis of combined loadings (compression, shear, and bending), material capability (Rene' 41), practicality of design for the given wing cross-section, and detailed thermal analyses. Thermal-protection arrangements with no insulation and with insulation at the lower surface outboard of the one-third wing chord were considered. (Insulation reduces the spanwise thermal gradients and enables a better match between the gradient through the depth of the wing and the fuselage.)

Insulation was placed so as to maintain the 1600°F material limit and to minimize thermal gradients in the spanwise direction and to provide gradient matching between the wing and fuselage, thereby reducing thermal stresses. Figure 8-18 of section 8 shows typical reductions in thermal stresses resulting from proper insulation placement.

Optimum rib and spar spacings were determined by considering surface panels, rib and spar caps and webs, heat shields, closeouts, fasteners, insulation, oxidation penetration, and vertical posts. The surface panels were analyzed for their most critical flight condition, the +2.0-g maneuver.

The 60° circular-arc (sine wave) spar webs were analyzed for total minimum $\bar{t}$ across the three wing areas (A, B, C) for critical shear stability. An optimum spar spacing of 90 in. allowed minimum-gage webs of 0.015-in Rene' 41 in the center (A) and outboard (C) wing areas and 0.018 in. in the inboard (B) section.

From the optimum 90-in. spar spacing, total wing cross-section and various wing element effective thicknesses were determined as a function of rib spacing. The optimization results for the center area (A) for the insulated arrangement are summarized in figure 13-24 and indicate an optimum rib spacing of 30 in.

This same type of rib spacing optimization was accomplished for the remaining areas (B and C) of the insulated arrangement and for the three areas for the uninsulated arrangement, as shown in figures 13-25 to 13-29. In all cases, the rib spacing for minimum wing $\bar{t}$ was low enough for minimum-gage (0.015-in.) rib webs.

As a result of the heat-shield evaluation (described later), the refurbishable corrugated heat shield with multiple supports was used in this analysis. Oxidation weight was based on a depth of oxide penetration commensurate with the exposure time and temperature. The fastener weight represents the head, or nut, section of the fastener.

The summary of optimum rib spacing and unit weights shown in table 13-21 indicates that the insulated arrangement (lower surface outboard) is of least weight as well as being the minimum thermal stress design.

A summary of the trapezoidal-corrugation panel geometrics is presented in tables 13-22 and 13-23.

The component thicknesses and weights for the minimum weight trapezoidal corrugation (insulation outboard) are shown in table 13-24.

Semimonocoque Chordwise

The results for spanwise stiffening eliminated both corrugation-stiffened skin and trapezoidal-corrugation concepts. Of the remaining semimonocoque panel concepts, tubular and beaded, only the tubular buckling analysis had been verified by tests at the time the selection of a panel concept was made for the chordwise weight analysis. Therefore, the tubular concept was selected for intermediate weight analysis. A variation of the tubular concept (convex-beaded) that does not require an aerodynamic fairing on the upper surface and that reduces the exposed bead depth to provide a smoother surface was also considered. This variation permitted a comparison of the least-weight chordwise tubular concept with the least-weight spanwise tubular concept. As a result of the lateral pressure loads and excessive temperatures when unshielded, tubular panels instead of convex-beaded panels were necessary on the lower surface. The rib-spar spacing weight results, including the substructure, are shown in table 13-6. On the basis of these results, the lightest-weight structure consists of tubular lower surface and convex-beaded upper-surface panels, and this construction was selected for final chordwise evaluation. However, a further intermediate screening of chordwise concepts was conducted to evaluate thermal-protection arrangements.

The following tubular and convex-beaded primary-structure and thermal-protection arrangements were assessed on the basis of combined loadings, material capability (Rene' 41), practicality of design for the wing cross-section, and detailed thermal analysis data.

Primary structure and heat-shield arrangement(a)	Insulation Arrangement	Remarks
Upper: tubular Lower: tubular	No	Heat shields required
	Yes(b)	(c)
Upper: convex beaded Lower: tubular	No	Upper surface structural temp increased
	Yes(b)	(c)
Upper: convex beaded Lower: convex beaded	No	Excessive structural temp
Upper: convex beaded Inboard lower: convex beaded Outboard lower: tubular	No	Heat shields reduced structural
	Yes(b)	(c)

(a) Tubular upper surface under fuselage for all arrangements.
Convex beaded: no heat shields.
Tubular: heat shields required.

(b) Insulation on lower surface outboard.

(c) Lower outboard insulation reduced the spanwise thermal gradient.

Since the chordwise-stiffened panels are oriented in the direction of the airflow, the convex-beaded primary structure was used without heat shields. Therefore, thermal gradients for the arrangements investigated varied from small to very large.

The chordwise redundant-model internal loads shown in table 8-17 of section 8 were used for evaluating the various configurations; however, a plane-strain analysis as presented in section 8 was conducted to determine thermal loads for each arrangement.

Optimum rib and spar spacings were determined from data on the surface panels, rib and spar caps and webs, heat shields, closeouts, fasteners, insulation, oxidation penetration, and vertical posts. The surface panels were analyzed for their most critical flight condition.

The 60° circular-arc (sine wave) rib webs were analyzed for the total minimum $\bar{t}$ across the three wing areas (A, B, C) for vertical shear stability. A rib spacing of 60 in. in the center (one-half fuselage) and 75 in. in the inboard (B) and outboard (C) areas allowed minimum-gage webs of 0.015-in. Rene' 41 to be used.

From the optimum rib spacing, total wing cross-section and various wing-element effective thicknesses were determined as a function of spar spacing (figures 13-30 to 13-50). The optimization results for inboard area B (BL 120-212) summarized in figure 13-40 indicate an optimum spar spacing of 24 to 28 in. for the arrangement with a convex upper surface and a tubular lower surface and with lower surface insulation outboard. The minimum-weight spar spacing for wing areas A, B, and C was 24 in. for this concept. Identical spar spacing optimization was accomplished for all chordwise arrangements and for the three areas (A, B, C) of the wing investigation section as shown in figures 13-30 to 13-50. In all cases, the spar spacing for minimum wing $\bar{t}$ was low enough for minimum-gage (0.015 in.) spar webs to be used.

The tubular semiapex angle and the convex-beaded inner semiapex angle were held constant at 77.5°. The bead height-to-width ratio for the unshielded convex-beaded surfaces was held constant at 0.10 to reduce performance (aerodynamic drag) penalties. A summary of the panel geometrics for the various chordwise arrangements is presented in tables 13-25 to 13-31.

As a result of the heat-shield evaluation described later, the refurbishable corrugated heat shield with multiple supports was used in this analysis instead of the corrugated-skin, hat stiffened, clip-supported heat shield design that was used on most of the other intermediate weights. Oxidation weight was based on a depth of oxide penetration commensurate with the exposure time and temperature. The fastener weight represents the head, or nut, section of the fastener.

The summary of optimum spar spacing and unit weights for the chordwise candidates, shown in table 13-32, indicates the importance of insulation placement. The reduced thermal gradients and thermal stresses resulted in weight savings of 10 percent or more for the two minimum-weight arrangements. Also, table 13-32 indicates that the unshielded and uninsulated convex-beaded arrangement is the heaviest. Since the convex-beaded upper surface and tubular

lower surface arrangement (with lower surface insulation outboard) was of the least weight (6.89 lb/ft^2), it was selected for the final structural analysis.

However, at this point in the chordwise investigation, the stiffnesses resulting from the least-weight chordwise structural arrangement were observed to differ from the stiffnesses used for the redundant-model analysis. The primary differences encompassed the shear stiffnesses, the extensional stiffnesses for the upper and lower surface spanwise direction (affecting spar cap geometry), and the extensional stiffnesses for the upper surface chordwise direction (affecting upper surface panel shape). Therefore, a new redundant analysis was conducted with the actual stiffnesses of the least-weight chordwise structural arrangement of table 13-32, and these results were used for the final structural analysis.

FINAL STRUCTURAL WEIGHTS

During final structural sizing of the Rene' 41 primary structure, various thermal-protection arrangements were considered to determine the most compatible arrangement of wing-fuselage temperatures and temperature gradients and to determine the structure with the lowest weight. With respect to the heat shields and insulation, the major objective was to minimize weight and to reduce thermal stress by limiting thermal-stress primary-structural temperatures to a maximum of 1600°F.

Monocoque Waffle Concept

Thermal-protection arrangements for the 45° x 45° waffle primary structure were assessed on the basis of lowest weight, practicality of design for the given wing cross-section, and detailed thermal analysis data. These arrangements were for (1) no heat shields and no insulation, (2) lower surface heat shields outboard of one-third wing chord with and without insulation and, (3) heat shields on entire lower surface with insulation outboard of one-third chord and without insulation.

Final redundant-analysis average internal loads and thermal strains are shown in table 8-4 of section 8 for the thermal-protection arrangement with lower surface heat shields outboard and no insulation. The redundant-model airloads were used for all the thermal-protection arrangements; however, the thermal loads were obtained for other arrangements by plane-strain analyses, which, for the same thermal-protection arrangement, indicated generally good agreement with the redundant-model results of table 8-4, as shown in section 8.

The thermal-analysis data included transient effects on structural temperatures and isotherms generated for the candidate thermal-protection arrangements as presented in section 9. The transient effects were based on a general thermal model, which included effects of heat-shield placement, lower surface insulation, and spar and rib size.

Optimum rib and spar spacing for wing inboard area B (BL 120 to BL 212) was determined for the thermal-protection arrangement with outboard lower surface heat shield and insulation. Forty upper and lower surface panels were optimized for panel-aspect ratios of 0.5, 1.0, 2.0, 3.0, and 4.0 and panel widths of 10, 20, 30, and 40 in. As shown in figure 13-51, the optimum panel width in the inboard area was 20.0 in. and the optimum panel aspect ratio was 1.0 for wing area B. However, final selection of optimum rib and spar spacing was based on a comparison of average unit weights for the entire wing investigation section, in which a panel spanwise width of 20 in. and panel aspect ratios of 1.0 and 2.0 were considered. Average unit weight for aspect ratios of 1.0 was 10.764 lb/ft^2 and for 2.0 was 10.494 lb/ft^2. Consequently, a waffle panel spanwise width of 20 in. and panel aspect ratio of 2.0 (20 in. x 40 in.) was selected for final sizing of the five waffle arrangements.

A summary of average unit weights for the various arrangements of lower surface thermal protection is shown in table 13-33. The arrangement with the lowest weight has heat shields with insulation on the lower surface outboard of the wing one-third chordline. Deleting the outboard insulation results in a 3 percent weight penalty and decreasing the panel aspect ratio from 2 to 1 causes a 2.6 percent weight penalty. Extending the heat shield over the entire lower surface results in a 5.6 percent weight penalty (higher without outboard insulation). Deleting both heat shield and insulation results in an 11 percent weight penalty. The lowest-weight wing was achieved when the thermal-protection arrangement imposed temperatures that resulted in a temperature gradient through the depth of the wing that nearly matched the temperature gradient through the fuselage depth, both at the same station.

A summary of the waffle panel configuration geometrics for the various thermal protection arrangements is presented in tables 13-34 to 13-37 for the center, inboard, and outboard areas of the wing section investigated. Notation for the panel dimensions is presented in figure 13-52. The waffle-concept component weights shown in tables 13-39 to 13-43 include those of panels, single shear cap and closeouts, rib and spar webs, web intersection, Dynaflex-insulated corrugated heat shield, oxidation losses, and fasteners. A spanwise weight distribution was used to obtain an average unit weight for the entire wing cross-section. The waffle panels are seen to represent approximately 55 percent of the total wing weight for the minimum-weight arrangement of table 13-40.

The final structural design offering the lowest weight waffle thermal-protection arrangement are shown in figures 13-53A and B. Center, inboard, and outboard areas (designated A, B, and C) were used for determining total wing weight and cost. A rib spacing of 22.30 in. (in area B) and a spar spacing of 41.05 in. was used so that the one-third wing chord lies along the panel diagonal. This arrangement provides maximum uniformity of panel design.

Out-of-plane loads at the one-third chordline were resisted by full-depth webs along the panel diagonal. A minimum gage (0.015 in.) 60° circular-arc corrugation was used for rib and spar webs. Flush Hi-Lok fasteners were used to attach the upper surface panels to the rib and spar caps. For attachment

of lower surface panels, countersunk screws and nut plates were used. (Removal of the upper surface primary structural panels is accomplished by first removing the lower surface panels.)

At web intersections, combinations of bentup flanges and separate angles were joined by resistance spotwelding. Dynaflex insulation, varying from 0.25 in. in thickness near the leading edge to 0.125 in. inboard, was packaged in Inconel X-750 foil.

Leading edges and heat shields were attached by externally accessible flush screws. Cross-sections of the corrugated heat shield with multiple supports and the segmented leading edge are shown in figure 13-53.

Monocoque Honeycomb-Core Sandwich Concept

The honeycomb-core sandwich primary structure was evaluated with lower surface heat shields and insulation outboard of the one-third wing chord, since this arrangement has the lowest weight for the monocoque waffle concept.

After detailed evaluation, it was determined that Rene' 41 honeycomb-core sandwich could not be adequately brazed by using existing techniques. Therefore, resistance spotwelding was selected for welding the cellular-shaped foil-ribbon core to the face sheets.

The honeycomb-core venting problem was approached in two ways: (1) complete venting to the atmosphere, and (2) sealed panels, evacuated to a low pressure, and filled with helium. Honeycomb-core vented to the atmosphere simplifies heat-shield attachment and fabrication. However, this approach permits oxidation and corrosion (from condensation of water vapor) of core and interior-skin surfaces. Honeycomb-core sealed, evacuated, and filled with helium at 2 psia eliminates oxidation and corrosion of the panel interior, but using existing fabrication techniques the panel pressure seal is extremely difficult to achieve (adequate welding of closeouts). However, since honeycomb sandwich offers a low weight potential and adequate sealing techniques may be developed for future application, the sealed approach was used for this investigation.

Table 8-8 of section 8 shows the final internal loads, resulting from the redundant-model analysis, used for the final structural sizing.

Optimum rib and spar spacing were determined as shown in figure 13-54, considering surface panels, rib and spar caps and webs, heat shields, closeouts, fasteners, insulation, oxidation penetration, and vertical posts. To assure that no weight decrease occurs due to the relieving effect of local thermal gradients, weights were determined with and without thermal gradients. Fifty-four panels were optimized for panel aspect ratios of 1.0, 1.5 and 2.0. Panel widths of 40, 50, and 60 in. were considered. The effective design condition for the center and outboard upper surface panels was cruise and -1/2g maneuver, respectively. All other panels were designed by the +2.0-g maneuver condition.

As indicated in figure 13-54 and table 13-44, a panel aspect ratio of 2.0 and panel width of 40 in. (40 in. x 80 in.) provides minimum weight. This is in agreement with the panel size selected for final redundant-model loads and thermal analysis. A comparison between the shear and extensional thickness used for the honeycomb redundant-model load analysis and the final panel stiffnesses indicated excellent agreement.

A summary of the honeycomb sandwich panel design temperatures and geometry is presented in table 13-45 indicating that the height h varies from 0.71 to 0.96 in. with internal face thicknesses varying from 0.012 to 0.015 in. and external face thicknesses varying from 0.015 to 0.019 in. The maximum face sheet temperatures of table 13-45 were conservatively used to determine material properties for both face sheets and the core. The honeycomb-sandwich component weights shown in table 13-46 include weights of panels, closeouts, caps, webs, web intersection, Dynaflex insulation, corrugated heat shield, oxidation losses, and fasteners. A spanwise weight distribution was used to obtain an average unit weight of 6.47 lb/ft^2 for the entire wing cross-section. The panels represent approximately 59 percent of the wing weight.

A drawing of the final honeycomb-sandwich structural arrangement is shown in figures 13-55 A and B. Center, inboard, and outboard areas (designated A, B, and C) were used for determining total wing weight and cost. Rib spacing of 40 in. and spar spacing of 80 in. were used. A minimum gage (0.015 in.) 60° circular-arc corrugation was used for the rib and spar webs. Flush Hi-Lok fasteners were used to attach the upper surface panels to the rib and spar caps. For attachment of lower surface panels, countersunk screws and nut plates were used. Removal of the upper surface primary structural panels is accomplished by first removing the lower surface panels. At web intersections, combinations of bentup flanges and separate angles were joined by resistance spotwelding.

Dynaflex insulation, varying from 0.25 in. in thickness near the leading edge to 0.125 in. inboard, was packaged in Inconel 750 foil. Heat shields and leading edges were attached by externally accessible flush screws.

Semimonocoque Spanwise Concepts

Two spanwise primary-structure concepts were considered during the final structural sizing. Tubular and beaded-skin primary structures with heat shields on both upper and lower surfaces were assessed on the basis of combined loadings, material capability (Rene' 41), practicality of design for the given wing cross-section, and detailed thermal analyses. Thermal-protection arrangements with no insulation and with insulation at the lower surface outboard of the one-third wing chord were considered. (Insulation reduces the spanwise thermal gradients.)

Tubular. - The internal loads resulting from the spanwise redundant-model analysis are shown in table 8-9 of section 8. These loads were used for evaluating both spanwise structures. Good agreement between assumed and actual stiffenesses were noted. Plane-strain analyses were conducted to determine thermal loads for each thermal-protection arrangement.

Insulation was placed so as to maintain the 1600°F material limit and to minimize thermal gradients in the spanwise direction and to provide a match between gradients through the wing and the fuselage depth, thereby reducing thermal stresses.

Optimum rib and spar spacings were determined by considering surface panels, rib and spar caps and webs, heat shields, closeouts, fasteners, insulation, oxidation penetration, and vertical posts. The surface panels were analyzed for their most critical flight condition, the +2.0-g maneuver.

The 60° circular-arc (sine wave) spar webs were analyzed for total minimum $\bar{t}$ across the three wing areas (A, B, C) for critical shear stability. An optimum spar spacing of 90 in. allowed minimum-gage webs of 0.015-in. Rene' 41 in the center (A) and outboard (C) wing areas and 0.018-in. in the inboard (B) section. The redundant-model shear loads were used for sizing the webs. The determination of the web shear strength was based on the optimization procedure presented in section 11, and subjected to the stated manufacturing constraints in that section. Shear allowables are presented in figures 13-56, 13-57, and 13-58 for temperatures of 1300°F, 1400°F, and 1500°F. The rib and spar cap weights were determined from figures 13-59 and 13-60. Figure 13-60 also includes the basic geometry of the caps.

From the optimum 90-in. spar spacing, total wing cross-section and various wing-element effective thicknesses were determined as a function of rib spacing. The optimization results for center area (A), summarized in figure 13-61, indicate an optimum rib spacing of 50 in. for the tubular concept with insulation. This same type of rib spacing optimization was accomplished for all three areas (A, B, and C) of the wing investigation section and for both thermal protection arrangements as shown in figures 13-61 to 13-66. In all cases, the rib spacing for minimum wing $\bar{t}$ was low enough for minimum-gage (0.015-in.) rib webs.

To provide heat-shield support-clip attachment surfaces, the flats between tubes were set at 0.50 in. The tubular panel semiapex angle was held constant at 77.5°, as in the intermediate sizing.

As a result of the heat-shield evaluation (described later), the refurbishable corrugated heat shield with multiple supports was used in this analysis. Oxidation weight was based on a depth of oxide penetration commensurate with the exposure time and temperature.

The summary of optimum rib spacing and unit weights shown in table 13-47 for the tubular concepts with and without insulation indicates that the insulated arrangement (lower surface outboard) is the lower weight and lower thermal-stress design.

A summary of the panel geometry of the final tubular structure is presented in table 13-48 for the center, inboard, and outboard areas of the wing section investigated. As indicated in table 13-48, the panel geometry is near minimum gage (t = 0.010 in.) for the three wing areas.

The component thicknesses and weights are shown in table 13-49 for primary structural panels, panel closeouts, rib and spar caps, webs, and posts, Dynaflex insulation, corrugated heat shields, oxidation losses, and fasteners. A spanwise weight distribution was used to obtain an average unit weight for the entire wing cross-section. The primary-structure panels are approximately 45 percent of the total wing weight.

The final structural design of the tubular concept is shown in figures 13-67 A & B. The tubular concept has panel dimensions of 90 by 48 in., 90 by 40 in., and 90 by 40 in., respectively, for the three sections from center to outboard.

The vertical rib and spar webs are of 60° circular-arc corrugation full-depth Rene'41 construction melt-through-welded to the rib and spar caps. The caps are of sheetmetal with flanged edges (channels). At the web intersections, the posts are formed from combinations of angles and bentup flanges, joined by resistance spotwelding.

The heat-shield attachment clips are spotwelded to the shield and panel on both surfaces. Since the heat shield is slightly smaller than the structural panel, corrugated cover strips are attached mechanically to the spars. Foil-packaged Dynaflex insulation placement and thickness are indicated in figure 13-67.

Beaded Skin. - Thermal protection arrangements with and without insulation at the lower surface outboard of the one-third chordline were considered to evaluate thermal stresses. The loads of table 8-9 of section 8 were used to evaluate the beaded structure. The tubular structure's optimum 90-in. spar spacing was used to determine total wing cross-section and optimization results for the center area (A), summarized in figure 13-68, indicate an optimum rib spacing of 50 in. for the beaded concept with insulation.

This same type of rib spacing optimization, as shown in figures 13-68 to 13-73, was accomplished for all the three areas (A, B, and C) of the wing investigation section and both thermal-protection arrangements. In all cases, the rib spacing for minimum wing t was low enough for minimum-gage (0.015-in.) rib webs.

To provide heat-shield support-clip attachment surfaces, the flats between beads were set at 0.50 in. The beaded-panel semiapex angle was held constant at 77.5°, as in the intermediate sizing.

The refurbishable corrugated heat shield with multiple supports was used in this analysis. Oxidation weight was based on a depth of oxide penetration commensurate with the exposure time and temperature.

The summary of optimum rib spacing and unit weights shown in table 13-50 for the spanwise candidates indicates that the insulated arrangement (lower surface outboard) is the lower-weight and lower-thermal-stress design.

A summary of the final beaded-panel geometry is presented in table 13-51 for the center, inboard, and outboard areas of the wing section investigated. The panel gages shown in table 13-51 range from a minimum gage of t = 0.015 to t = 0.022; that is, although lower weight than the other concepts, minimum gage is not required.

The component thicknesses and weights are shown in table 13-52 for primary structural panels, panel closeouts, rib and spar caps, webs, and posts, Dynaflex insulation, corrugated heat shields, oxidation losses, and fasteners. A spanwise weight distribution was used to obtain an average unit weight for the entire wing cross-section. The primary-structure panels are approximately 45 percent of the total wing weight.

The final structural design for the beaded concept is shown in figures 13-74 A and B. The panel dimensions are 90 by 50 in., 90 by 50 in., and 90 by 40 in., respectively, for the three sections from center to outboard. Other design aspects of figure 13-74 for the beaded concept are the same as discussed earlier for the tubular concept.

Semimonocoque Chordwise Concept

The weight of the semimonocoque chordwise concept, consisting of tubular panel with heat shields on the lower surface and convex-beaded upper surface without heat shields, was determined with insulation on the lower surface outboard of the one-third chordline. The chordwise redundant-model internal loads shown in table 8-39 of section 8 were used. Detailed transient thermal analyses were conducted to determine local stresses and deflections caused by temperature gradients through the panel structure as presented in section 9.

The 60° circular-arc (sine wave) rib webs were analyzed for the total minimum t across the three wing areas (A, B, C) for vertical shear stability. A rib spacing of 60 in. in the center (one-half fuselage) and 75 in. in the inboard (B) and outboard (C) areas allowed minimum-gage webs of 0.015-in. Rene' 41 to be used.

From the optimum rib spacing, total wing cross-section and various wing-element effective thicknesses were determined as a function of spar spacing as presented in figures 13-75 to 13-77. The optimization results for center area A (℄ to BL 120), summarized in figure 13-75, indicate an optimum spar spacing of 25 in. The minimum-weight spar spacing for wing areas A, B, and C was 24 in. for this concept. In all cases, the spar spacing for minimum wing weight was low enough for minimum-gage (0.015-in.) spar webs to be used.

The tubular semiapex angle and the convex-beaded inner semiapex angle were held constant at 77.5°. The bead height-to-width ratio for the unshielded convex-beaded upper surface panels was held constant at 0.10 to reduce performance (aerodynamic drag) penalties.

As a result of the heat-shield evaluation described later, the refurbishable corrugated heat shield with multiple supports was used in this analysis. Oxidation weight was based on a depth of oxide penetration commensurate with the exposure time and temperature.

A summary of the final panel configuration is presented in table 13-53 for the center, inboard, and outboard areas of the wing-section investigated. As indicated, the tubular-panel configuration for the lower surface and upper surface under the fuselage is near minimum gage (t = 0.010 in.) for the three wing areas. The convex-beaded panel gages are also near minimum gage (t upper = 0.015 in. and t lower = 0.010 in.).

The convex-beaded tubular concept component thicknesses and weights are shown in table 13-54 for primary-structure panels, end closeouts, rib and spar caps, webs, and posts, Dynaflex insulation, corrugated heat shield, oxidation losses, and fasteners. A spanwise weight distribution was used to obtain an average unit weight for the entire wing cross-section. The primary-structure penals are seen to represent approximately 40 percent of the total wing weight.

The final structural design for the chordwise concept shown in figures 13-78 A and B has panel dimensions of 60 by 24 in. and 75 by 24 in. Figure 13-78 also shows panel cross-section for each wing area. The vertical rib and spar webs and caps are identical to those of the spanwise concept.

The lower surface, which is the only surface requiring thermal protection, is shielded from aerodynamic heating by a corrugated heat shield supported on multiple truss-type clips. Dynaflex insulation, packaged in foil, is located on the lower outboard wing surface.

Statically Determinate Concept

The statically determinate structure is a series of spanwise-stiffened beams, decoupled at the chordwise-rib intersections. The slip joints at the beam-rib intersections provide vertical shear continuity only, thereby maintaining the wing contour (shape) but providing neither bending nor axial load paths. Thus, the least-weight semimonocoque spanwise-stiffened panel construction was the logical choice for the detail statically determinate analysis. The least-weight beaded primary structure was evaluated on the basis of combined loadings, weight, practicality of design for the specified wing cross-section, and detailed thermal analyses. Heat shields covered all exposed surfaces and three thermal-protection arrangements were considered: (1) no insulation, (2) insulation on the lower surface at the center and inboard areas, and (3) insulation at the lower surface outboard of the one-third wing chordline.

The second thermal-protection arrangement (insulation on the center and inboard areas) was to investigate structural temperatures even lower than 1600°F to provide minimum-gage panel designs, since the spanwise loads were low. Because of noncontinuous ribs and the allowable wing rotation at the fuselage, wing-to-fuselage temperature and temperature gradient compatibility is not important in this concept.

Internal loads were used, as shown in table 8-40 of section 8, for the no-insulation arrangement. Good agreement between the assumed and the actual final stiffnesses calculated were noted. Because the ribs are discontinuous for this concept, the chordwise airloads and thermal loads are zero, as indicated in table 8-40. Also, the spanwise thermal loads are small, providing a minimum-thermal-stress wing concept.

Detailed transient thermal analyses were conducted for the thermal-protection arrangements to determine local stresses and deflections from temperature gradients through the panel structure, as presented in section 9.

In determining optimum rib and spar spacings, surface panels, caps, web, heat shields, closeouts, fasteners, oxidation penetration, vertical posts, and slip joint assemblies at each rib and spar intersection were considered. Surface panels were analyzed for the most critical condition, the +2.0-g maneuver. A spar spacing of 90 in. was used, with minimum-gage webs of 0.015-in. thickness. However, the spar spacing could be increased since twice as many spars are used to carry the shear as the semimonocoque concept, thus allowing a lower wing weight.

With spar spacing fixed, the rib spacings were varied to determine element sizes and wing weights (figures 13-79 to 13-81). The optimization results for the inboard area (BL 120 - 212) shown in figure 13-80, indicate an optimum rib spacing of 50 in. for the beaded concept with no insulation. This same type of rib-spacing optimization was accomplished for the insulated arrangements and for the three areas (center, inboard, and outboard) of the wing investigation section. All rib spacings resulted in the use of minimum-gage rib webs (0.015 in.).

The beaded-panel semiapex angle was held at 77.5°, the same as for the spanwise concept. To provide heat-shield support-clip attachment surfaces, the flats between beads were set at 0.50 in. The refurbishable heat shield with multiple supports and Dynaflex insulation packaged in foil was used in this analysis.

Structural sizing was not conducted for the third thermal-protection arrangement, with insulation only on the lower surface outboard area, since the outboard panels for the no-insulation arrangement were minimum gage ($t = 0.015$ in.) for the lower surface and near minimum gage (0.016 in.) for the upper surface. Therefore, the use of insulation, with its required packaging, would increase the wing weight above the saving of 0.001 in. on the upper surface.

A summary of unit weights for no-insulation and two thicknesses of insulation inboard, presented in table 13-55, indicates a slight weight advantage for the no-insulation arrangement. Therefore, the fully shielded statically determinate concept with no insulation was selected for detail cost, performance, and reliability evaluation.

A summary for the selected configuration is presented in table 13-56 for the center, inboard, and outboard areas of the wing-investigation section. As indicated, the beaded panel is minimum gage except for the center (A) and inboard (B) upper surface panels. These are not minimum gage because of larger compression airloads.

The statically determinate component thicknesses are shown in table 13-57 for primary structural panels, panel closeouts, rib and spar caps, webs, and posts, corrugated heat shield, exidation losses, and fasteners. A spanwise weight distribution was used to obtain an average unit weight for the entire wing cross-section. As indicated, the average unit weight of this configuration is 5.55 lb/ft^2, and the primary-structure panels represent approximately 35 percent of the total wing weight. The statically determinate fuselage weight incurs a 10 percent penalty over the semimonocoque and monocoque concepts due to additional fuselage skin, local fittings, and concentrated loads. The details of the total fuselage weight penalty are presented in section 22.

The final structural design for the statically determinate beaded concept is shown in figures 13-82 A and B. Panel dimensions are 90 by 60 in. from centerline to BL 120, and 90 by 40 in. from BL 120 outboard. A ball slip joint, providing wing-surface continuity, is located at each spar-rib intersection, with adequate tolerance to permit unrestrained thermal expansion in the chordwise direction.

Rib and spar webs are of 60° circular-arc corrugation (sine-wave) construction, fabricated from Rene 41. The sheetmetal flanged rib and spar caps, which are also fabricated from Rene 41, are melt-through welded to the vertical webs.

Primary-Structure Weight Summary

Table 13-58 presents a summary of the concept weights and associated margins of safety established for each of the six structural concepts. As indicated in the table, the margins of safety were determined for the critical ultimate flight-load condition, panel flutter, vehicle flutter, sonic fatigue, load fatigue, and creep.

Ultimate load analysis. - The margins of safety for the ultimate flight load are zero or near zero for minimum-weight design. However, as shown in table 13-58, the load margin of safety for the beaded concept is as high as 0.30 because of the use of minimum-gage materials.

Panel flutter. - A detailed panel-flutter analysis of the concepts indicates that the panels are stable and substantially exceed the flutter factor-of-safety requirement of 1.3. The panel-flutter margins of safety are shown in table 13-58.

Vehicle flutter analysis. - Vehicle flutter was investigated by applying the results of the redundant analyses to the maximum-weight climb and acceleration region of the trajectory. The investigation showed that an adequate margin on airspeed and dynamic pressure (beyond the required 1.3 factor) is available over the design flight path and that the concepts are not critical in flutter. The margins of safety for vehicle flutter are large, as presented in table 13-58.

Sonic fatigue analysis. - Analyses conducted to determine the effects of random sound pressures on the six concepts indicate that the allowable sound-pressure level (dB/Hz) is greater than the maximum predicted sound-pressure level of the 0.007-q criterion for upper and lower surfaces for both concepts. The application of the 0.002-q criterion on the lower surface during cruise also results in root-mean-square stresses less than fatigue-limit allowable stress. The resulting margins for sonic fatigue are shown in table 13-58. This analysis provides an interim basis for determining the fatigue resistance of the structure on an empirically derived nominal vibratory stress of typical flight hardware. However, for the primary structures of this study, further sonic-fatigue testing is necessary to determine the actual boundary conditions and the detailed design refinements for the primary structure and its attachments.

Fatigue analysis. - Fatigue analysis was conducted to establish allowable design stress levels for primary structures to meet the life requirements specified. The load-fatigue margins of safety are presented in table 13-58 for the tension load surfaces.

Creep analysis. - Creep margins of safety were established for the most critical area for each concept. The effect of compressive thermal strains on creep buckling and tensile thermal strains on total plastic deformation can be neglected, due to stress relaxation. Thus, only airloads were used to determine applied stresses for creep at elevated temperatures. The allowable compressive stresses under creep conditions were determined by using isochronous stress-strain curves. The resulting margins of safety are shown in table 13-58. The critical failure mode for all concepts is creep buckling.

Primary-structure weight comparison. - The wing-section weight investigation resulted in the following ranking of structural concepts: semimonocoque spanwise beaded, semimonocoque spanwise tubular, statically determinate monocoque honeycomb sandwich spanwise beaded, semimonocoque chordwise tubular, and monocoque waffle. However, when the total wing weight is considered (as presented in section 22), the honeycomb sandwich is lower in weight than the statically determinate concept. This is because the honeycomb sandwich has better efficiency in the high-load area of the aft wing.

The double-sheet tubular concept is heavier in weight than the single-sheet beaded concept for the upper surface where bending (due to normal pressure) and inplane compression loads are critical. On the lower surface, where bending due to normal pressure and tension are the design modes, the beaded concept (minimum gage or near minimum gage) is considerably lower in weight than the tubular concept. Therefore, it is concluded that caution should be applied in using only inplane compression weight/strength data for concept selection, since such data shows the tubular panel to be lighter than the beaded panels which is not the case for combined loads.

The spanwise-stiffened concepts are lower in weight than the chordwise, because the thermal stress are highest in the chordwise direction, and the principal airloads act spanwise and added spar cap material is required for chordwise stiffened panel concepts. The high thermal stresses are imposed on the panels of the chordwise concept, whereas only the rib caps of the spanwise concepts are designed for chordwise thermal stresses. When the spanwise tubular concept was compared to the chordwise tubular concept, it was found that a convex-beaded upper surface for chordwise stiffening was lighter than a tubular upper surface. While panel configurations are about equal in weight for the combined conditions, the convex-beaded concept does not involve the weight of heat shields as does the tubular concept. The net result is that the convex-beaded upper surface is lighter.

In comparing the statically determinate and chordwise concepts, the statically determinate design permits a different gradient and a different mean temperature between the wing and fuselage without thermal stress. This concept provides no resistance to thermal bowing in the chordwise direction and no resistance to differential expansion between wing and fuselage. While the statically determinate concept requires additional fuselage and fitting weights, the weight is still less than the chordwise-stiffened concept because of spanwise stiffening and thermal-stress alleviation provided by the statically determinate concept. However, the

statically determinate concept is not lowest in weight because the semimonocoque spanwise concepts also have low thermal stress, require no fittings, and require no added fuselage stiffening.

Results show the waffle to be about 4.0 lb/ft^2 heavier than honeycomb structures. Initial screening (see table 13-1) indicated honeycomb to be heavier than waffle. However, the initial screening was based only on inplane compressive loads for an arbitrarily selected panel size. These factors yielded minimum gage for both waffle and honeycomb panels with total honeycomb weight less favorable because of more edge-member weight. Moreover, waffle is considered to be a more state-of-the-art construction. Therefore waffle was considered for detail analysis. However, later analysis with optimum-size panels (including effects of pressure), show that the honeycomb structure has half the substructure weight of the waffle-panel structure. In addition, when air-pressure loads were included in the analysis, the waffle panels were shown to be less efficient than honeycomb. Consequently, the honeycomb-core sandwich structure is considerably lighter than the waffle monocoque structure. This result indicates that initial screening should include effects of substructure and pressure loads.

Since monocoque panels support biaxial loads, they might be expected to be of minimum weight. However, two factors result in the spanwise semimonocoque structures having less weight than the monocoque structures. The spanwise semimonocoque beaded and tubular concepts are new and were found to be more efficient than the honeycomb-sandwich concept. Another reason that semimonocoque structure is lighter than the monocoque is that chordwise thermal loads are imposed only on the rib caps of the spanwise concept. Monocoque structure, however, provides chordwise stiffening (like the chordwise-stiffened semimonocoque structure) which offers bending resistance to the moment derived from mismatched temperature gradients through the wing and fuselage. A better match of temperatures and gradients might be achieved by using thermal protection on the upper surface, but this would negate the smooth surface offered by monocoque concepts. Also, based on semimonocoque chordwise stiffening results, the reduction in primary-structure weight may be less than the added thermal-protection system weight. The two spanwise semimonocoque concepts each require shields to provide a relatively smooth surface, so the beneficial thermal effects of shields are inherent in the concepts.

TABLE 13-1

INITIAL PANEL WEIGHT SCREENING
OF MONOCOQUE PRIMARY STRUCTURE [a]

Candidate panel configurations	Wing surface & panel temp.	Material	Panel height, in. (a)	$\bar{t}_{Basic}$, in.	Non optimum factor, NOF	$\bar{t}_{Panel}$, in.	$\bar{t}_{Heat\ shield}$, in.	$\bar{t}_{Total}$, in.	$\bar{w}_{Total}$, lb/ft^2
Waffle grid unflanged - 45° x 45°	Upper (1400°F)	René 41	.399	.0308	1.24	.0382	0	.0382	1.64
		Haynes 25	.400	.0311	1.24	.0382	0	.0382	1.83
Waffle grid flanged - 45° x 45°		René 41	.241	.0354	1.30	.0460	0	.0460	1.97
		Haynes 25	.243	.0356	1.30	.0462	0	.0462	2.20
Waffle grid unflanged - 0° x 90°		René 41	.547	.0310	1.38	.0428	0	.0428	1.84
		Haynes 25	.530	.0310	1.38	.0428	0	.0428	2.04
Waffle grid flanged - 0° x 90°		René 41	.312	.0370	1.40	.0518	0	.0518	2.22
		Haynes 25	.321	.0370	1.40	.0518	0	.0518	2.46
Honeycomb sandwich		René 41	.197	.0308	1.80	.0555	0	.0555	2.38
		Haynes 25	.197	.0308	1.80	.0555	0	.0555	2.64
Truss-core sandwich		René 41	.193	.0362	1.50	.0542	0	.0542	2.33
		Haynes 25	.193	.0362	1.50	.0542	0	.0542	2.58
Waffle grid unflanged - 45° x 45°	Lower (1600°F)	René 41	.701	.0514	1.24	.0637	0	.0637	2.73
		Haynes 25	.859	.1040	1.24	.1290	0	.1290	6.13
Waffle grid flanged - 45° x 45°		René 41	.295	.0490	1.30	.0636	0	.0636	2.73
		Haynes 25	(NA)	(NA)	1.30	(NA)	0	(NA)	(NA)
Waffle grid unflanged - 0° x 90°		René 41	.734	.0459	1.38	.0634	0	.0634	2.72
		Haynes 25	1.011	.1018	1.38	.1404	0	.1404	6.68
Waffle grid flanged - 0° x 90°		René 41	.643	.0440	1.40	.0615	0	.0615	2.64
		Haynes 25	.973	.0970	1.40	.1360	0	.1360	6.46
Honeycomb sandwich		René 41	.709	.0363	1.80	.0654	0	.0581	2.80
		Haynes 25	.755	.0953	1.80	.1710	0	.1640	7.80
Truss-core sandwich		René 41	.514	.0606	1.50	.0910	0	.0910	3.80
		Haynes 25	.678	.0978	1.50	.1470	0	.1470	7.00

a Compression panel; aspect ratio, a/b = 2, b = 20 in.

TABLE 13-2

INITIAL SCREENING OF SEMIMONOCOQUE SPANWISE-STIFFENED CONCEPTS[a]

Primary structure Concepts		Surface and panel temperature	Material	Height in.	t_{basic} in.	Non-optimum factor N.O.F.	t_{panel} in.	$t_{heat\ shield}$ in.	t_{total} in.	w_{total} lb/ft^2
Semi-monocoque (spanwise)	Tubular	Upper (1400°F)	René 41	2.00	0.029	1.15	0.0333	0.015	0.0483	2.08
			Haynes 25	2.00	0.029	1.15	0.0333	0.017	0.0503	2.38
	Corrugation stiffened skin		René 41	0.825	0.038	1.20	0.0455	0	0.0455	1.96
			Haynes 25	0.825	0.038	1.20	0.0455	0	0.0455	2.17
	Trapezoidal corrugation		René 41	0.625	0.021	1.20	0.0252	0.015	0.0402	1.72
			Haynes 25	0.625	0.021	1.20	0.0252	0.017	0.0422	2.00
	Beaded		René 41	2.00	0.021	1.17	0.0246	0.015	0.0396	1.70
			Haynes 25	2.00	0.021	1.17	0.0246	0.017	0.0416	1.98
	Tubular	Lower[b]	René 41	2.00	0.029	1.15	0.0333	0.023	0.0563	2.43
			Haynes 25	2.00	0.029	1.15	0.0333	0.025	0.0585	2.78
	Corrugation stiffened skin		René 41	0.825	0.038	1.20	0.0455	0	0.0455	1.96
			Haynes 25	0.825	0.038	1.20	0.0455	0	0.0455	2.17
	Trapezoidal corrugation		René 41	0.625	0.021	1.20	0.0252	0.023	0.0482	2.07
			Haynes 25	0.625	0.021	1.20	0.0252	0.025	0.0502	2.39
	Beaded		René 41	2.00	0.021	1.17	0.0246	0.023	0.0476	2.05
			Haynes 25	2.00	0.021	1.17	0.0246	0.025	0.0496	2.36

[a] a = 43 inches; b = 30.0 inches

[b] Shielded panel temperature 1400°F, unshielded temperature 1600°F

TABLE 13-3

INITIAL SCREENING OF SEMIMONOCOQUE CHORDWISE-STIFFENED CONCEPTS[a]

Primary structure concepts		Surface and panel temperature	Material	Height in.	$\bar{t}$ basic in.	Non-optimum factor N.O.F.	$\bar{t}$ panel in.	$t_{heat\ shield}$ in.	$\bar{t}$ total in	$\bar{w}_{total}$ lb/ft^2
Semi-monocoque (chordwise)	Convex beaded	Upper (1400°F)	René 41	1.60	0.031	1.20	0.0372	0	0.0372	1.60
			Haynes 25	1.60	0.031	1.20	0.0372	0	0.0372	1.77
	Tropezoidal corrugation		René 41	0.625	0.021	1.20	0.0252	0.015	0.0402	1.72
			Haynes 25	0.625	0.021	1.20	0.0252	0.017	0.0422	2.00
	Tubular		René 41	2.00	0.029	1.15	0.0333	0.015	0.0483	2.08
			Haynes 25	2.00	0.029	1.15	0.0333	0.017	0.0503	2.38
			René 41	2.00	0.021	1.17	0.0246	0.015	0.0396	1.70
			Haynes 25	2.00	0.021	1.17	0.0246	0.017	0.0416	1.98
	Convex beaded	Lower	René 41	1.60	0.031	1.20	0.0372	0	0.0372	1.60
			Haynes 25	2.36	0.045	1.20	0.0535	0	0.0535	2.55
	Tropezoidal corrugation		René 41	0.925	0.029	1.20	0.0348	0.023	0.0578	2.48
			Haynes 25	1.650	0.048	1.20	0.0576	0.025	0.0826	3.92
	Tubular		René 41	2.00	0.029	1.15	0.0333	0.023	0.0563	2.43
			Haynes 25	2.00	0.048	1.15	0.0552	0.025	0.0802	3.81
			René 41	2.00	0.021	1.17	0.0246	0.023	0.0476	2.05
			Haynes 25	4.80	0.041	1.17	0.0485	0.025	0.0735	3.50

[a] a = 30.0 inches, b = 43.0 inches

[b] Shielded panel temperature 1400°F, unshielded temperature 1600°F

TABLE 13-4

MANUFACTURING PROCESSES FOR CANDIDATE MONOCOQUE PANEL CONFIGURATIONS

Panel configuration	Manufacturing process
Unflanged waffle grid	Electro-chem-milled waffle grid
Flanged waffle grid	Electro-chem-milled waffle grid Diffusion bonded flanges
Honeycomb sandwich	Brazed face sheets and core Resistance welded core
Truss-core sandwich	Diffusion-bonded face sheets and core

TABLE 13-5

INTERMEDIATE WEIGHT SCREENING RESULTS FOR RENE' 41 PANELS

Primary structure	Location area	Spacing, in.		Design temperature, °F		Weight,[a] lb/ft^2
		Rib	Spar	Lower surface	Upper surface	
Monocoque						
45° by 45° Unflanged waffle	B	20	40	1600	1400	8.90
	C	20	40	1600	1400	8.50
0° by 90° Unflanged waffle	B	20	40	1600	1400	9.24
Semimonocoque spanwise						
Trapezoidal corrugation upper surface panel	B	30	90		1300	1.20[b]
Corrugation stiffened upper surface panel	B	30	90		1400	3.26[b]
Tubular	B	40	90	1400	1300	5.70
	C	44	90	1500	1400	5.11
Beaded-skin	B	48	90	1400	1300	4.93
	C	50	90	1500	1400	4.42
Trapezoidal-corrugation	B	30	90	1400	1300	6.56
	C	31	90	1500	1400	5.64
Semimonocoque chordwise						
Tubular	B	90	46	1400	1300	6.44
Tubular lower convex-beaded upper surfaces	B	90	46	1400	1400	5.92

[a]Panels, heat shields, spars and ribs, and closeouts.

[b]Upper surface panels only.

TABLE 13-6

EVALUATION OF MONOCOQUE WAFFLE GRID PLATE

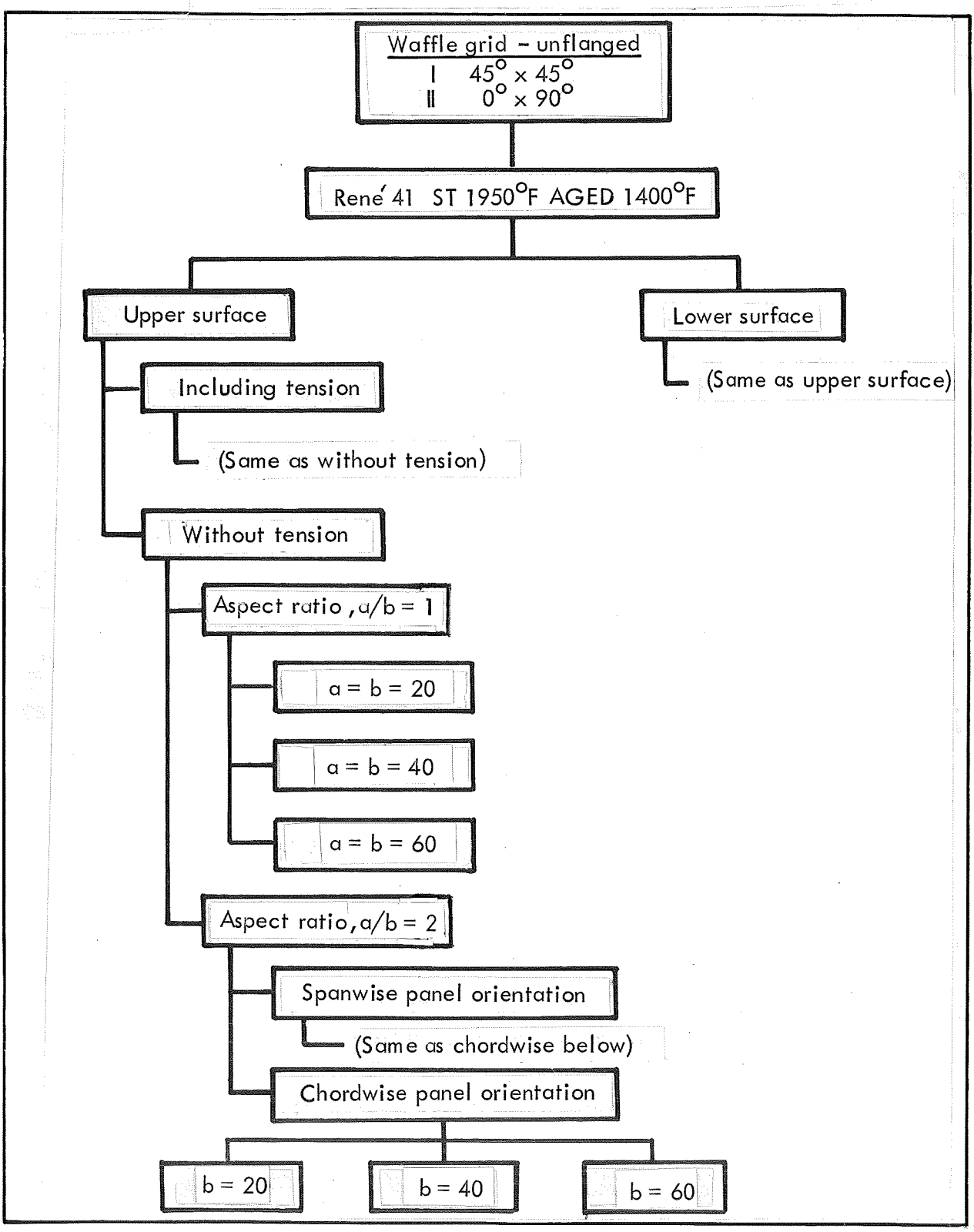

TABLE 13-7

WEIGHT COMPARISON OF MONOCOQUE WAFFLE PANEL DESIGNS (LB/FT^2)

Waffle type	Panel orientation	$45^\circ x 45^\circ$	$0^\circ x 90^\circ$	$45^\circ x 45^\circ$	$0^\circ x 90^\circ$	$45^\circ x 45^\circ$	$0^\circ x 90^\circ$
Geometry	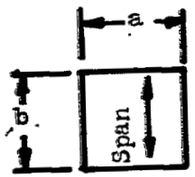	a = 20 in. b = 20 in.		a = 40 in. b = 40 in.		a = 60 in. b = 60 in.	
W_{Upper}, lb/ft^2		1.468	1.597	1.999	2.400	2.545	3.038
W_{Lower}, lb/ft^2		1.968	2.275	2.909	3.254	3.663	4.034
W_{Total}, lb/ft^2		3.436	3.872	4.908	5.654	6.208	7.172
Geometry	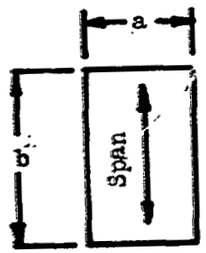	a = 20 in. b = 40 in.		a = 40 in. b = 80 in.		a = 60 in. b = 120 in.	
W_{Upper}, lb/ft^2		1.592	1.625	2.339	2.370	2.970	3.022
W_{Lower}, lb/ft^2		2.687	2.426	3.992	3.396	5.006	4.161
W_{Total}, lb/ft^2		4.279	4.051	6.331	5.766	7.976	7.183
Geometry	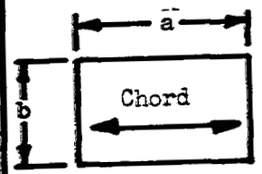	a = 40 in. b = 20 in.		a = 80 in. b = 40 in.		a = 160 in. b = 80 in.	
W_{Upper}, lb/ft^2		1.682	1.594	2.524	2.405	3.196	3.038
W_{Lower}, lb/ft^2		1.940	2.260	2.879	3.246	3.654	4.027
W_{Total}, lb/ft^2		3.622	3.854	5.403	5.651	6.850	7.065

TABLE 13-8

WEIGHT COMPARISON OF UPPER AND LOWER SURFACES OF MONOCOQUE WAFFLE DESIGNS

Panel orientation: chordwise (a = 40 in., b = 20 in., a/b = 2.0)				
Unit panel weight, lb/ft^2	Inplane loads only		Inplane loads plus normal pressure	
	$-45^\circ \times 45^\circ$ waffle	$0^\circ \times 90^\circ$ waffle	$-45^\circ \times 45^\circ$ waffle	$0^\circ \times 90^\circ$ waffle
Upper surface	1.68	1.59	2.23	2.13
Lower surface	1.94	2.26	2.59	3.03
Total	3.62	3.85	4.82	5.16

TABLE 13-9

MONOCOQUE WAFFLE PANEL-WIDTH OPTIMIZATION MATRIX

Panel: -45° x 45° waffle

Chordwise orientation: a/b = 2.0

Condition: +2.0-g maneuver

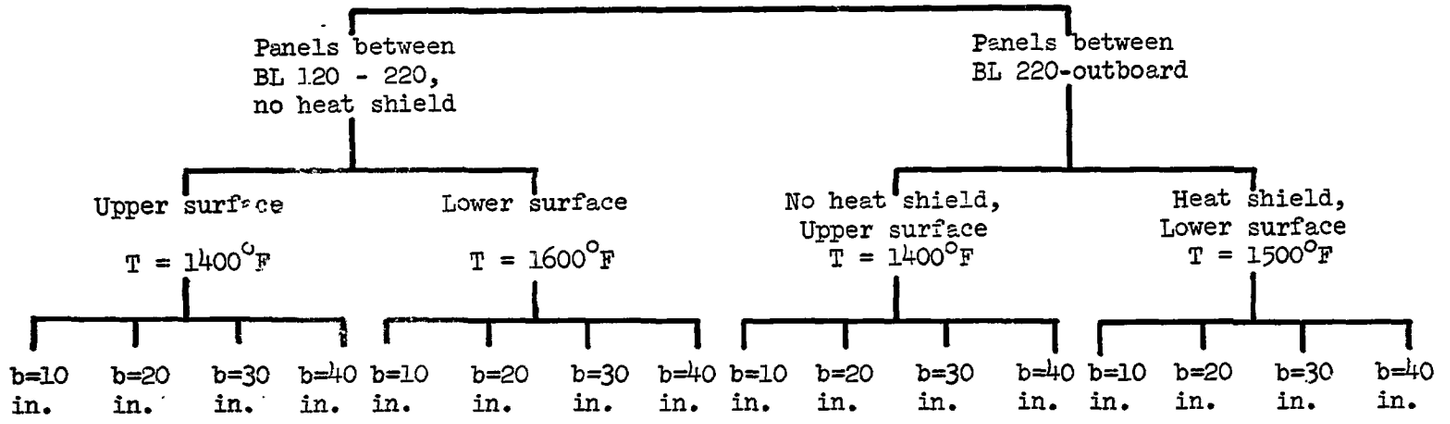

Loads:

In-plane loads and pressure
Edge eccentricity, e = ± 0.02 in.
Initial deflection due to bowing, δ_{max} = 0.001 x b in.

TABLE 13-10

MONOCOQUE WAFFLE DESIGN DATA FOR WING INBOARD AREA

Item	Panels between BL 120 - 220 (No heat shield)							
	Upper surface, temperature = 1400°F				Lower surface, temperature = 1600°F			
b, in.	10	20	30	40	10	20	30	40
W, lb/ft^2	1.6092	2.2717	2.8780	3.473	1.9593	2.6654	3.5467	4.522
$\bar{t}$, in.	0.03750	0.05294	0.067067	0.08093	0.045658	0.06211	0.08265	0.10537
h, in.	0.46386	0.64278	0.82346	1.0176	0.48174	0.61075	0.85226	1.1134
p, in.	1.1735	1.290	1.5267	2.1348	0.83059	0.98772	1.1074	1.3467
t_s, in.	0.020	0.020	0.0207	0.02658	0.0200	0.02656	0.03047	0.03749
t_w, in.	0.02337	0.034575	0.04473	0.059363	0.023408	0.030528	0.035732	0.043176
e_{11}, in.	0.027397	0.059255	0 09114	0.10697	0.037764	0.049423	0.080829	0.10919
e_{33}, in.	0.084623	0.16723	0.2454	0.29206	0.11068	0.14401	0.2268	0.30371
w_o, in.	0.05	0.2	0.4	0.6	0.05	0.2	0.4	0.6

TABLE 13-11

MONOCOQUE WAFFLE DESIGN DATA FOR WING OUTBOARD AREA

Item	Panels between BL 220-outboard							
	No heat shield				Heat shield			
	Upper surface, temperature = 1400°F				Lower surface, temperature = 1500°F			
b, in.	10	20	30	40	10	20	30	40
W, lb/ft^2	1.6259	2.213	2.8348	3.4920	2.3554	2.8892	3.6858	5.1182
$\bar{t}$, in.	0.03789	0.051575	0.066061	0.081375	0.054889	0.067328	0.085892	0.11927
h, in.	0.43594	0.60625	0.78622	0.98251	0.50936	0.60851	0.75804	1.075
p, in.	1.2615	1.3891	1.5423	1.8219	0.95074	1.1414	1.1409	1.8723
t_s, in.	0.0200	0.0200	0.0200	0.021937	0.02138	0.027182	0.028643	0.045184
t_w, in.	0.027428	0.037925	0.047076	0.057268	0.033223	0.040117	0.045690	0.068605
e_{11}, in.	0.026201	0.054414	0.088476	0.12053	0.045538	0.052314	0.078671	0.098853
e_{33}, in.	0.080691	0.15455	0.23713	0.31513	0.12950	0.15011	0.21550	0.27915
w_o, in.	0.05	0.2	0.4	0.6	0.05	0.2	0.4	0.5

TABLE 13-12

MONOCOQUE WAFFLE SINGLE SHEAR JOINT DIMENSIONS

Surface location	X - Direction			Y - Direction			$\Delta\bar{t}$, in.
	t_a, in.	t_b, in.	t_c, in.	t_a, in.	t_b, in.	t_c, in.	
Inboard upper							
b = 10 in.	0.0287	0.0422	0.0374		0.0191		0.02351
b = 20 in.	0.0446		0.0693				0.01835
b = 30 in.	0.0611		0.1015				0.01750
b = 40 in.	0.0734		0.1203				0.01769
Inboard lower							
b = 10 in.	0.0339	0.0750	0.0478	Same as X - Direction	0.0421	Same as X - Direction	0.03168
b = 20 in.	0.0446		0.0627				0.01944
b = 30 in.	0.0633		0.0961				0.01763
b = 40 in.	0.0827		0.1279				0.01745
Outboard upper							
b = 10 in.	0.0281	0.0372	0.0362		0.0228		0.02379
b = 20 in.	0.0422		0.0644				0.01795
b = 30 in.	0.0592		0.0985				0.01718
b = 40 in.	0.0767		0.1315				0.01755
Outboard lower							
b = 10 in.	0.0388	0.0685	0.0562		0.0215		0.03164
b = 20 in.	0.0465		0.0659				0.01878
b = 30 in.	0.0608		0.0930				0.01597
b = 40 in.	0.0833		0.1214				0.01838

TABLE 13-13

MONOCOQUE WAFFLE DOUBLE SHEAR JOINT DIMENSIONS

Surface location	X - Direction			Y - Direction			$\Delta\bar{t}$ in.
	t_a, in.	t_b, in.	t_c, in.	t_a, in.	t_b, in.	t_c, in.	
Inboard upper							
b = 10 in.	0.0392	0.0422	0.0163	0.0334	0.0192	0.0278	0.02237
b = 20 in.	0.0552		0.0482	0.0494		0.0597	0.01786
b = 30 in.	0.0716		0.0804	0.0658		0.0919	0.01728
b = 40 in.	0.0840		0.0992	0.0782		0.1107	0.01774
Inboard lower							
b = 10 in.	0.0526	0.0750	0.0103	0.0444	0.0421	0.0267	0.02845
b = 20 in.	0.0634		0.0252	0.0552		0.0417	0.01804
b = 30 in.	0.0820		0.0587	0.0738		0.0750	0.01681
b = 40 in.	0.1015		0.0904	0.0932		0.1067	0.01700
Outboard upper							
b = 10 in.	0.0374	0.0372	0.0176	0.0338	0.0228	0.0248	0.02274
b = 20 in.	0.0515		0.0458	0.0479		0.0530	0.01752
b = 30 in.	0.0685		0.0799	0.0649		0.0871	0.01696
b = 40 in.	0.0860		0.1129	0.0824		0.1201	0.01750
Outboard lower							
b = 10 in.	0.0559	0.0685	0.0219	0.0442	0.0215	0.0455	0.02961
b = 20 in.	0.0637		0.0317	0.0519		0.0552	0.01795
b = 30 in.	0.0779		0.0587	0.0662		0.0822	0.01542
b = 40 in.	0.1004		0.0872	0.0887		0.1107	0.01833

TABLE 13-14

MONOCOQUE WAFFLE COMPONENT WING WEIGHTS, INBOARD AREA, a/b = 2.0

Panels Between BL 120-220, No Heat Shield

Item		Equivalent panel thickness, $\bar{t}$, in.			
		b = 10 in.	b = 20 in.	b = 30 in.	b = 40 in.
Panels	Upper surface	0.03750	0.05294	0.06707	0.08093
	Lower surface	0.04566	0.06211	0.08265	0.10537
	Total	0.08316	0.11505	0.14972	0.18630
Caps and closeouts, single shear	Upper surface	0.02351	0.01835	0.01750	0.01769
	Lower surface	0.03168	0.01944	0.01763	0.01745
	Total	0.05519	0.03779	0.03513	0.03514
Rib and spar webs [a]		0.109	0.0546	0.0354	0.0272
Total		0.2474	0.2074	0.2213	0.2486

[a] 60° Circular-arc corrugation:

thickness, t = 0.015 in.
average depth, h = 40 in.

TABLE 13-15

MONOCOQUE WAFFLE COMPONENT WING WEIGHTS, OUTBOARD AREA, a/b = 2.0

Panels Between BL 220-350, Heat Shields on Lower Surface Only

Item		Equivalent panel thickness, $\bar{t}$, in.			
		b = 10 in.	b = 20 in.	b = 30 in.	b = 40 in.
Panels	Upper surface	0.03789	0.05158	0.06606	0.08138
	Lower surface	0.05489	0.06733	0.08589	0.11927
	Total	0.09278	0.11891	0.15195	0.20065
Caps and closeouts, single shear	Upper surface	0.02379	0.01795	0.01718	0.01755
	Lower sufrace	0.03164	0.01878	0.01597	0.01838
	Total	0.05543	0.03673	0.03315	0.03593
Rib and spar webs[a]		0.0545	0.0270	0.0182	0.0136
Heat shield[b]		0.0157	0.0157	0.0157	0.0157
Total		0.2184	0.1983	0.2190	0.2659

[a] 60° Circular arc corrugation:

thickness, t = 0.015 in.
average depth, h = 20 in.

[b] Circular arc corrugation:

skin thickness, t_s = 0.010 in.

TABLE 13-16

MONOCOQUE WAFFLE PANEL ASPECT RATIO OPTIMIZATION MATRIX

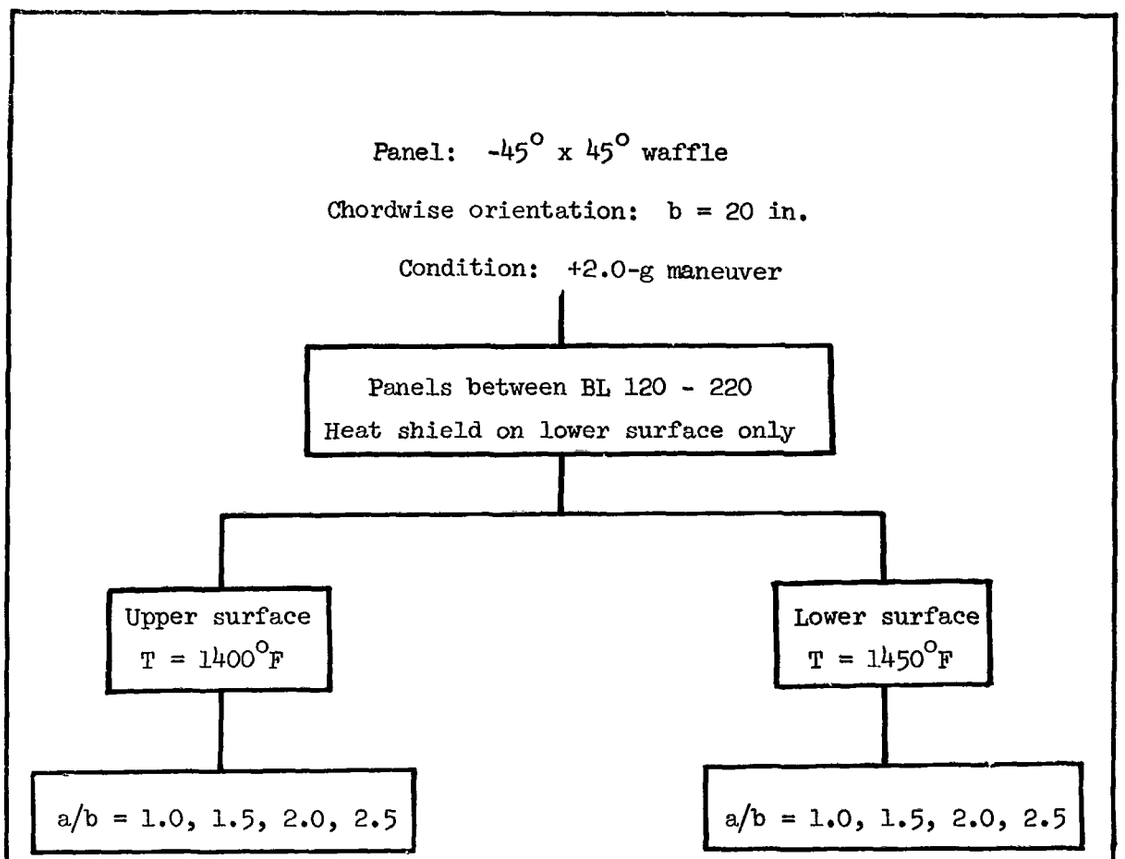

Loads

Pressure and inplane loads
Edge eccentricity, e = + 0.02 in.
Initial deflection due to bowing, δ_{max} = 0.01 x b in.

TABLE 13-17

MONOCOQUE WAFFLE COMPONENT WING WEIGHTS, INBOARD AREA, b = 20 INCHES

Panels Between B.L. 120-220, Heat Shields on Lower Surface Only

Item		Equivalent panel thickness, $\bar{t}$, in.			
		a/b = 1.0	a/b = 1.5	a/b = 2.0	a/b = 2.5
Panels	Upper surface	0.0422	0.0478	0.0522	0.0553
	Lower surface	0.0547	0.0545	0.0530	0.0534
	Total	0.0969	0.1023	0.1052	0.1087
Caps and closeouts, single shear	Upper surface	0.0206	0.0202	0.0207	0.0206
	Lower surface	0.0246	0.0204	0.0175	0.0152
	Total	0.0452	0.0406	0.0382	0.0358
Rib and spar webs [a]		0.0726	0.0605	0.0545	0.0508
Heat shield [b]		0.0157	0.0157	0.0157	0.0157
Total		0.2305	0.2191	0.2137	0.2110

[a] 60° Circular arc corrugation:

thickness, t = 0.015 in.
average depth, h = 40 in.

[b] Circular arc corrugation:

thickness, t = 0.010 in.

TABLE 13-18

HONEYCOMB-CORE SANDWICH PANEL CLOSEOUT COMPARISON

	Recessed 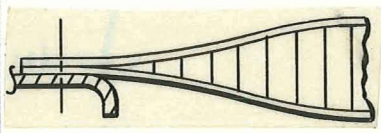		Smooth 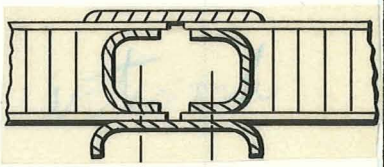	
	lb/ft^2	lb	lb/ft^2	lb
Aero drag panalty		9 790		126
Str. wt.	6.45		6.68	
Wing wt. (9774 ft^2)		63 042		65 290
Wt.		72 832		65 416
Weight saving				7 416

TABLE 13-19

DESIGN DATA FOR MONOCOQUE HONEYCOMB-CORE SANDWICH PANELS[a]

Item	Center		Inboard		Outboard	
	Upper	Lower	Upper	Lower	Upper	Lower
Temp, ^{o}F	1330	1500	1260	1530	1370	1450
W, lb/ft^3	1.78	1.88	1.89	2.24	1.71	1.49
c, lb/ft^3	6.14	5.59	6.13	5.49	5.90	6.02
t, in.	0.0415	0.438	0.0440	0.0522	0.0400	0.0348
h, in.	1.007	0.998	1.258	1.010	0.986	0.672
t_1, in.	0.015	0.0185	0.015	0.0234	0.015	0.015
t_2, in.	0.0148	0.0148	0.0139	0.0185	0.0138	0.0123
t_c, in.	0.002	0.002	0.002	0.002	0.002	0.002
S, in.	0.335	0.369	0.342	0.375	0.349	0.342
Z, in.	0.499	0.446	0.594	0.437	0.437	0.302
Wo, in.	-0.54	1.66	-1.0	1.74	-0.90	-1.0

[a] a = 80 in, b = 40 in, a/b = 2.0

TABLE 13-20

WING UNIT WEIGHTS FOR MONOCOQUE HONEYCOMB-CORE SANDWICH PANELS, INCLUDING SMOOTH CLOSEOUT[a]

Item		Equivalent thickness, $\bar{t}$, in.		
		Center	Inboard	Outboard
Panels[b]	Upper	0.0415	0.0440	0.0400
	Lower	0.0438	0.0522	0.0348
	Total[c]	0.0893	0.1002	0.0788
Smooth cap and closeout	Upper, x	0.00793	0.00807	0.00787
	Upper, y	0.00397	0.00403	0.00393
	Total	0.0119	.0095	0.0118
	Lower, x	0.00787	0.00787	0.00753
	Lower, y	0.00393	0.00393	0.00377
	Total	0.0118	0.0118	0.0113
	Total	0.0237	0.0198	0.0231
Rib and spar webs	Rib web	0.0182	0.0182	0.0091
	Spar web	0.0091	0.0091	0.0046
	Total	0.0273	0.0273	0.0137
Webs intersection	Total	0.000563	0.000563	0.000281
Dynaflex insulation	Insulation	----	----	0.00146
	Packaging	----	----	0.00202
	Total	----	----	0.00348
Corrugated heat shield	Corrugation	----	----	0.01660
	Clip	----	----	0.00485
	Total	----	----	0.02145
Oxidation	Total	0.00047	0.000498	0.005664
Fastener	Total	0.00431	0.00453	0.00403
Total equivalent thickness, in.		0.14564	0.156991	0.150505
Total unit weight, lb/ft^2		6.250	6.737	6.458
Average unit weight, lb/ft^2			6.442	

[a]Insulation and heat shield at outboard lower surface.
[b]a = 80 in., b = 40 in., a/b = 2.
[c]Includes brazing alloy ($\bar{t}_e$ = 0.002 in./panel).

TABLE 13-21

OPTIMUM WING SECTION WEIGHTS AND SPAR/RIB SPACINGS SEMIMONOCOQUE SPANWISE-STIFFENED TRAPEZOIDAL-CORRUGATION PANELS, FURTHER INTERMEDIATE SCREEING

Wing Section Concept[a,b]	Area A		Area B		Area C		Total wing section average unit wt., lb/ft^2
	Unit wt., lb/ft^2	Rib spacing, in.	Unit wt., lb/ft^2	Rib spacing in.	Unit wt., lb/ft^2	Rib spacing, in.	
Trapezoidal corrugation, no insulation	5.682	30	6.616	20	7.794	20	6.760
Trapezoidal corrugation, with insulation	5.555	30	6.551	30	6.451	20	6.170

[a]Heat shields used on all upper and lower surfaces.

[b]All spar spacing = 90 inches.

TABLE 13-22

DETAIL GEOMETRY OF SEMIMONOCOQUE SPANWISE-STIFFENED TRAPEZOIDAL-CORRUGATION PANELS, NO INSULATION

Area	Surface	$\bar{t}$, in.	t, in.	b/d	h, in.	L, in.	Pitch, in.
A (℄-120)	Upper	.0336	.025	.95	0.9	30	3.01
	Lower	.0282	.021	.95	0.7	30	2.34
B (120-212)	Upper	.0269	.020	.95	0.7	20	2.34
	Lower	.0256	.019	.95	0.7	20	2.34
C (212-350)	Upper	.0471	.035	.95	1.10	20	3.68
	Lower	.0309	.023	.95	0.9	20	3.01

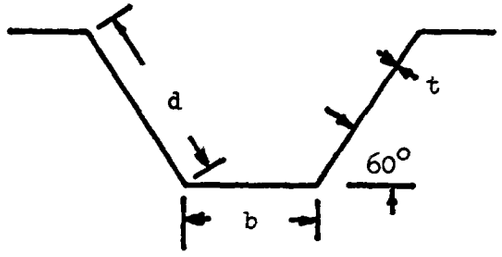

TABLE 13-23

DETAIL GEOMETRY OF SEMIMONOCOQUE SPANWISE-STIFFENED TRAPEZOIDAL-CORRUGATION PANELS, INSULATION LOWER SURFACE BATBOARD

Area	Surface	$\bar{t}$, in.	t, in.	b/d	h, in.	L, in.	Pitch, in.
A (η_L - 120)	Upper	.0336	.025	.95	0.9	30	3.01
	Lower	.0242	.018	.95	0.6	30	2.00
B (120-212)	Upper	.0356	.026	.95	1.0	30	3.12
	Lower	.0336	.025	.95	0.8	30	2.68
C (212-350)	Upper	.0244	.018	.95	0.7	20	2.26
	Lower	.0215	.016	.95	0.7	20	2.34

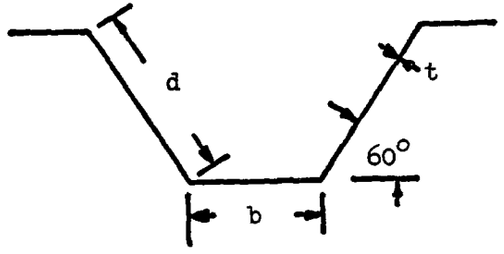

TABLE 13-24

COMPONENTS WEIGHTS FOR SEMIMONOCOQUE SPANWISE-STIFFENED TRAPEZOIDAL-CORRUGATION PANELS

Item	Center t, in.	Inboard t, in.	Outboard t, in.
Panels			
Upper	.0336	.0356	.0244
Lower	.0242	.0236	.0215
Caps			
Spar			
Upper	.0011	.0011	.0011
Lower	.0011	.0011	.0011
Rib			
Upper	.0042	.0031	.0059
Lower	.0045	.0040	.0050
Closeouts	.0074	.0079	.0087
Webs			
Spar	.0084	.0096	.0047
Rib	.0252	.0240	.0230
Posts	.0007	.0007	.0006
Insulation	-	-	.00685
Heat shields	.0131	.0263	.0358
Fasteners	.0036	.0036	.0050
Oxidation	.00234	.00213	.00676
Total (in.)	.1295	.1527	.1503
Unit wt. (lb/ft^2)	5.55	6.55	6.45
Average unit wt. (lb/ft^2)		6.17	

TABLE 13-25

DETAIL GEOMETRY OF SEMI-MONOCOQUE CHORDWISE-STIFFENED, TUBULAR PANELS, NO INSULATION

Area	Surface	$\bar{t}$, in.	t, in.	R, in.	b, in.	L, in.	Pitch, in.	Critical Condition
A	Upper	.02575	.010	.75	.50	30	1.964	Cruise
$\mathcal{C}_L$-120	Lower	.03359	.013	.80	.50	30	2.062	2g
B	Upper	.03319	.013	.65	.50	30	1.769	-0.5g
120-212	Lower	.03889	.015	.85	.50	30	2.160	2g
C	Upper	.02553	.010	.65	.50	30	1.769	2g
212-350	Lower	.08299	.031	1.85	.50	30	4.112	2g

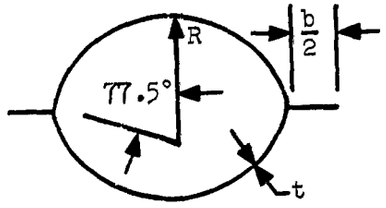

TABLE 13-26

DETAIL GEOMETRY OF SEMIMONOCOQUE CHORDWISE-STIFFENED TUBULAR PANELS, WITH INSULATION

Area	Surface	$\bar{t}$, in.	t, in.	R, in.	b, in.	L, in.	Pitch, in.	Critical Condition
A	Upper	.03144	.012	1.05	.50	30	2.550	Cruise
C_L -120	Lower	.03953	.015	1.20	.50	30	2.843	Cruise
B	Upper	.03064	.012	.65	.50	30	1.769	2g
120-212	Lower	.04172	.016	.95	.50	30	2.355	2g
C	Upper	.02510	.010	.50	.50	30	1.476	-0.5g
212-350	Lower	.03064	.012	.65	.50	30	1.769	2g

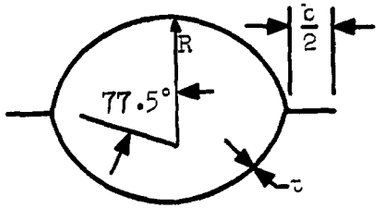

TABLE 13-27

DETAIL GEOMETRY OF SEMIMONOCOQUE CHORDWISE-STIFFENED CONVEX-BEADED UPPER/TUBULAR LOWER PANELS, NO INSULATION[a]

TUBULAR

Area	Surface	$\bar{t}$, in.	t, in.	R, in.	b, in.	Pitch, in.	Critical Condition
A η_L-120	Upper	.02540	.010	.60	.50	1.672	Cruise
	Lower	.02564	.010	.70	.50	1.867	Cruise
B 120-212	Lower	.03064	.012	.65	.50	1.769	2g
C 212-350	Lower	.07194	.027	1.60	.50	3.624	2g

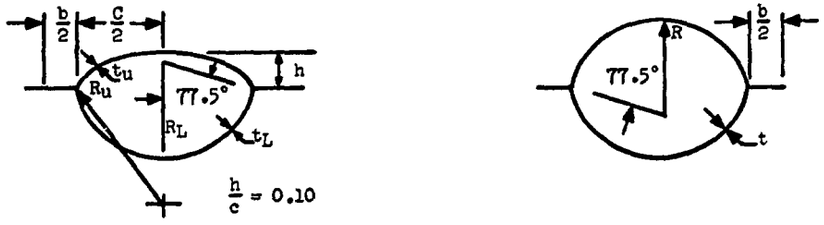

CONVEX BEADED

Area	Surface	$\bar{t}$, (in.)	t_{up}, (in.)	t_{low}, (in.)	R_{up}, (in.)	R_{low}, (in.)	b, (in.)	Pitch, in.	Critical Condition
B 120-212	Upper	.03037	.016	.011	1.726	.68	.50	1.828	2g
C 212-350	Upper	.03378	.019	.011	2.538	1.00	.50	2.453	−0.5g

[a] Panel lengths are 20 in.

TABLE 13-28

DETAIL GEOMETRY OF SEMIMONOCOQUE CHORDWISE-STIFFENED, CONVEX-BEADED UPPER/TUBULAR LOWER PANELS, WITH INSULATION[2]

TUBULAR

Area	Surface	$\bar{t}$, in.	t, in.	R, in.	b, in.	Pitch, in.	Critical Condition
A $\mathcal{C}_L$ -120	Upper	.02575	.010	.75	.50	1.964	Cruise
	Lower	.02607	.010	.95	.50	2.355	Cruise
B 120-212	Lower	.03347	.013	.75	.50	1.964	2g
C 212-350	Lower	.02779	.011	.55	.50	1.574	2g

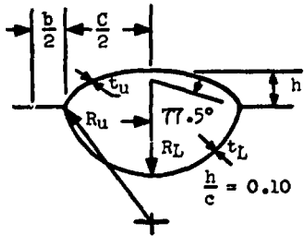

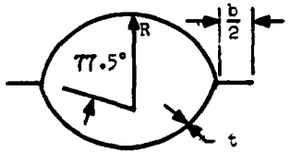

CONVEX BEADED

Area	Surface	$\bar{t}$, in.	t_{up}, in.	t_{low}, (in.)	R_{up}, (in.)	R_{low}, (in.)	b, (in.)	Pitch, in.	Critical Condition
B 120-212	Upper	.03036	.016	.011	1.675	.66	.50	1.789	2g
C 212-350	Upper	.03036	.016	.011	2.285	.90	.50	2.257	~0.5g

(1) Panel lengths are 20 in.

TABLE 13-29

DETAIL GEOMETRY OF SEMIMONOCOQUE CHORDWISE-STIFFENED CONVEX-BEADED BOTH SURFACES, NO INSULATION[a]

Area	Surface	$\bar{t}$, in.	t_{up}, in.	t_{low}, in.	R_{up}, in.	R_{low}, in.	b, in.	Pitch, in.
A $\mathbb{Q}_L$ - 120	Upper[b]	.0251	.010	-	0.50	-	0.50	1.476
A $\mathbb{Q}_L$ - 120	Lower	.0439	.025	.014	2.716	1.070	0.50	2.589
B 120-212	Upper	.0314	.017	.011	1.675	0.50	0.50	1.789
B 120-212	Lower	.0724	.042	.022	4.823	1.90	0.50	4.210
C 212-350	Upper	.0328	.018	.011	2.513	0.99	0.50	2.433
C 212-350	Lower	.1055	.066	.028	5.70	2.25	0.50	4.890

[a]Panel lengths are 20 in.
[b]Tubular panels upper surface from $\mathbb{Q}_L$ - BL 120

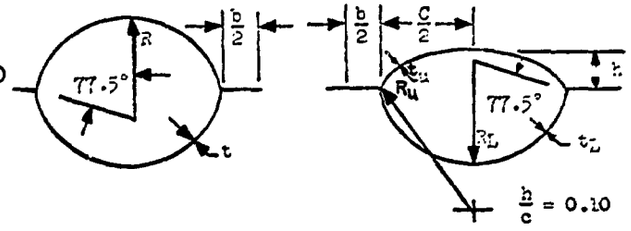

TABLE 13-30

DETAIL GEOMETRY OF SEMIMONOCOQUE CHORDWISE-STIFFENED CONVEX-BEADED/TUBULAR LOWER OUTBOARD[a]

TUBULAR

Area	Surface	$\bar{t}$, in.	t, in.	R, in.	b, in.	Pitch, in.	Critical Condition
A ℄-120	Upper	.02540	.010	.60	.50	1.672	Cruise
B 120-212	Lower	.03376	.015	.80	.50	2.062	2g
C 212-350	Lower	.04134	.016	.80	.50	2.062	2g

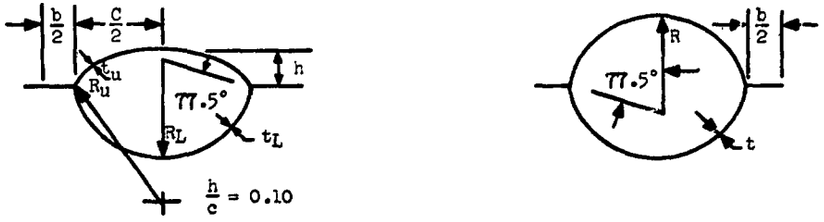

CONVEX BEADED

Area	Surface	$\bar{t}$, in.	t_{UP}, in.	t_{LOW}, in.	R_{UP}, in.	R_{LOW}, in.	b, in.	Pitch, in.	Critical Condition
A ℄-120	Lower	.07613	.046	.022	3.376	1.33	.50	3.097	2g
B 120-212	Upper	.03368	.018	.012	1.675	.66	.50	1.789	2g
C 212-350	Upper	.03042	.017	.010	2.513	.99	.50	2.433	−0.5g

[a] Panel lengths are 20 in.

TABLE 13-31

DETAIL GEOMETRY OF SEMIMONOCOQUE CHORDWISE-STIFFENED CONVEX-BEADED/TUBULAR LOWER OUTBOARD, WITH INSULATION

TUBULAR

Area	Surface	$\bar{t}$, in.	t, in.	R, in.	b, in.	Pitch, in.	Critical Condition
A ℄-120	Upper	.02553	.010	.65	.50	1.769	Cruise
B 120-212	Lower	.03876	.015	.80	.50	2.062	2g
C 212-350	Lower	.03048	.012	.60	.50	1.672	2g

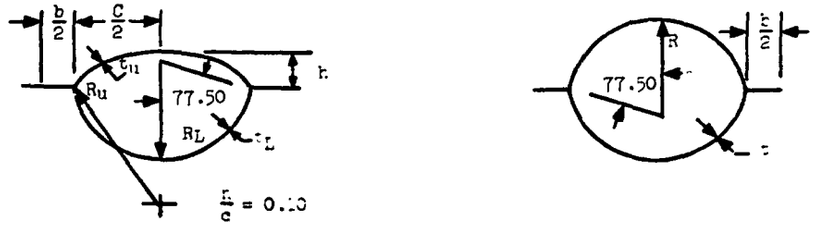

CONVEX BEADED

Area	Surface	$\bar{t}$, in.	t_{UP}, in.	t_{LOW}, in.	R_{UP}, in.	R_{LOW}, in.	b, in.	Pitch, in.	Critical Condition
A ℄-120	Lower	.10579	.067	.028	3.96	1.56	.50	3.546	2g
B 120-212	Upper	.03036	.016	.011	1.675	.66	.50	1.789	2g
C 212-350	Upper	.02934	.016	.010	2.310	.91	.50	2.277	−0.5g

[a] Panel lengths are 20 in.

TABLE 13-32

INTERMEDIATE SCREENING WEIGHTS FOR CHORDWISE-STIFFENED CANDIDATE CONCEPTS[a]

Concept	Spar spacing, in.	Weights, lb/ft^2				Normalized weights (to least-weight)
		Inboard area (A)	Center area (B)	Outboard area (C)	Average for wing section	
Tubular	30	6.512	7.259	8.681	7.563	1.10
Tubular with insulation [b]	30	7.242	7.289	6.426	6.933	1.01
Convex beaded upper, tubular lower[c]	20	7.052	6.978	8.466	7.590	1.10
Convex beaded upper, tubular lower with insulation[b,c]	24	7.278	7.111	6.417	6.894	1.00 Least weight
Convex beaded	20	7.410	7.702	8.862	8.059	1.17
Convex beaded upper and lower inboard, tubular lower outboard	20	8.882	7.498	6.880	7.729	1.12
Convex beaded upper and lower inboard, tubular lower outboard with insulation[c]	20	10.291	7.355	6.288	7.618	1.11

[a]Rib spacing: 60 inches for area A
75 inches for area B, C

[b]Upper wing surface under fuselage: tubular construction.

[c]"With insulation" indicates lower surface outboard only.

TABLE 13-33
WEIGHTS OF MONOCOQUE WAFFLE PANEL AND
VARIOUS THERMAL-PROTECTION ARRANGEMENTS

Aspect ratio	Thermal-protection arrangement		Weight, lb/ft^2			
	Heat shields	Insulation	Center area A	Inboard area B	Outboard area C	Weighted average
2	Lower surface outboard area	Yes	10.717	12.033	9.437	10.494[a]
2	Lower surface outboard area	No	10.355	11.896	10.637	10.811
1	Lower surface outboard area	Yes	10.668	11.645	10.367	10.764
2	Entire lower surface	No	11.785	11.427	11.698	11.670
2	Entire lower surface	Outboard area	11.343	11.506	10.609	11.084
2	None	No	10.298	11.664	12.907	11.652

[a]Lowest weight.

TABLE 13-34

DESIGN TEMPERATURES AND GEOMETRY FOR MONOCOQUE WAFFLE PANELS, PARTIAL HEAT SHIELD AT OUTBOARD AREA LOWER SURFACE

	Center		Inboard		Outboard	
	Upper	Lower	Upper	Lower	Upper	Lower
Item \ Temp., °F	1330	1500	1260	1530	1385	1550
W, lb/ft^2	3.159	2.425	3.519	3.313	3.084	2.859
$\bar{t}$, in.	0.07360	0.05651	0.08200	0.07721	0.07186	0.06662
h, in.	0.7186	0.5797	0.7488	0.6744	0.6622	0.5944
p, in.	1.036	0.9196	1.0143	1.023	1.087	1.051
t_s, in.	0.02043	0.02296	0.0200	0.02724	0.0200	0.02641
t_w, in.	0.04025	0.02814	0.04410	0.04030	0.04483	0.03789
e_{11}, in.	0.08653	0.04955	0.09842	0.06674	0.07957	0.05227
e_{33}, in.	0.2275	0.1423	0.2520	0.1851	0.2093	0.1492
w_o, in.	0.3021	0.2265	0.3307	0.2571	0.3276	0.2569

TABLE 13-35

DESIGN TEMPERATURES AND GEOMETRY FOR MONOCOQUE WAFFLE PANELS, PARTIAL HEAT SHIELD AT OUTBOARD AREA LOWER SURFACE, WITH INSULATION

	Center		Inboard		Outboard	
	Upper	Lower	Upper	Lower	Upper	Lower
Item \ Temp., °F	1330	1500	1260	1530	1370	1450
W, lb/ft^2	3.039	2.821	3.392	3.529	2.935	1.942
$\bar{t}$, in.	0.07082	0.06575	0.07904	0.08224	0.06840	0.04525
h, in.	0.7078	0.6213	0.7259	0.7143	0.6436	0.4642
p, in.	1.076	0.7991	1.031	1.022	1.105	0.8305
t_s, in.	0.0210	0.0200	0.02015	0.02683	0.02001	0.0200
t_w, in.	0.03975	0.03097	0.04395	0.04205	0.04375	0.02395
e_{11}, in.	0.08106	0.06969	0.09274	0.07582	0.07457	0.03582
e_{33}, in.	0.2162	0.1870	0.2395	0.2065	0.1982	0.1052
w_o, in.	0.2877	0.2994	0.3319	0.2544	0.3222	0.1339

TABLE 13-36

DESIGN TEMPERATURES AND GEOMETRY FOR MONOCOQUE WAFFLE PANELS, HEAT SHIELD ON ENTIRE LOWER SURFACE

	Center		Inboard		Outboard	
	Upper	Lower	Upper	Lower	Upper	Lower
Item \ Temp., °F	1075	1265	1200	1390	1385	1550
W, lb/ft^2	3.792	2.352	3.350	2.628	2.728	3.905
$\bar{t}$, in.	0.08836	0.05482	0.07806	0.06125	0.06357	0.09100
h, in.	0.7909	0.6235	0.7155	0.5742	0.6222	0.8176
p, in.	1.008	1.194	1.081	0.9755	1.185	1.122
t_3, in.	0.02012	0.02708	0.02129	0.02585	0.0200	0.02538
t_w, in.	0.04565	0.02810	0.04514	0.03200	0.04368	0.04746
e_{11}, in.	0.1084	0.04150	0.08730	0.04702	0.06801	0.09820
e_{33}, in.	0.2740	0.1255	0.2286	0.1364	0.1838	0.2584
w_o, in.	0.3503	-0.2328	0.3425	-0.3088	0.3537	0.208

TABLE 13-37

DESIGN TEMPERATURES AND GEOMETRY FOR MONOCOQUE WAFFLE PANELS, HEAT SHIELD ON ENTIRE LOWER SURFACE, WITH INSULATION AT OUTBOARD AREA

	Center		Inboard		Outboard	
	Upper	Lower	Upper	Lower	Upper	Lower
Item \ Temp., °F	1075	1265	1200	1390	1365	1425
W, lb/ft^2	3.689	2.120	3.253	2.792	2.780	3.009
$\bar{t}$, in.	0.08597	0.04941	0.07581	0.06507	0.06478	0.07011
h, in.	0.7668	0.5985	0.7082	0.5927	0.6248	0.6269
p, in.	1.021	1.197	1.122	0.9779	1.184	1.054
t_s, in.	0.02016	0.02597	0.02204	0.02619	0.0200	0.02597
t_w, in.	0.04605	0.02475	0.04487	0.03415	0.04467	0.03945
e_{11}, in.	0.1033	0.03619	0.08243	0.05125	0.06938	0.05917
e_{33}, in.	0.2625	0.1113	0.2188	0.1468	0.1866	0.1660
w_o, in.	0.3743	-0.2668	0.3186	-0.2563	0.3775	0.2851

TABLE 13-38

DESIGN TEMPERATURES AND GEOMETRY FOR MONOCOQUE WAFFLE PANELS, NO HEAT SHIELD AND NO INSULATION

	Center		Inboard		Outboard	
	Upper	Lower	Upper	Lower	Upper	Upper
Item \ Temp., °F	1325	1504	1261	1534	1420	1655
W, lb/ft^2	3.267	2.295	3.611	3.133	2.964	5.228
$\bar{t}$, in.	0.07614	0.05347	0.08144	0.07301	0.06908	0.1218
h, in.	0.7303	0.5707	0.7604	0.6512	0.6624	1.1177
p, in.	1.062	1.189	1.065	0.9582	1.155	2.426
t_s, in.	0.02124	0.02817	0.02123	0.02563	0.02104	0.06039
t_w, in.	0.04196	0.02807	0.04633	0.03701	0.04410	0.07153
e_{11}, in.	0.08763	0.03444	0.09782	0.06472	0.07433	0.07418
e_{33}, in.	0.2306	0.1060	0.2521	0.1793	0.1994	0.2244
w_o, in.	0.3106	-0.2991	0.3455	0.2423	0.2823	0.1013

TABLE 13-39

COMPARISON WEIGHTS FOR MONOCOQUE WAFFLE CONCEPT, PARTIAL HEAT SHIELD AT OUTBOARD AREA LOWER SURFACE

Item		Equivalent thickness, in.		
		Center	Inboard	Outboard
Panels	Upper	0.07360	0.08200	0.07186
	Lower	0.05651	0.07721	0.06662
	Total	0.13011	0.15921	0.13848
Cap and closeout, single shear	Upper, rib direction	0.01886	0.02052	0.01797
	Upper, spar direction	0.00943	0.01026	0.00898
	Total	0.02829	0.03078	0.02695
	Lower, rib direction	0.01319	0.01657	0.01440
	Lower, spar direction	0.00659	0.00829	0.00720
	Total	0.01978	0.02486	0.02160
	Total	0.04807	0.05564	0.04855
Rib and spar webs	Rib web	0.0363	0.0363	0.0182
	Spar web	0.0182	0.0182	0.0091
	Total	0.0545	0.0545	0.0273
Web intersection	Total	0.00225	0.00225	0.001125
Dynaflex insulation	Insulation	--	--	--
	Packaging	--	--	--
	Total	--	--	--
Corrugated heat shield	Corrugation	--	--	0.01660
	Clip	--	--	0.00485
	Total	--	--	0.02145
Oxidation	Total	0.00097	0.000216	0.005552
Fastener	Total	0.00541	0.00541	0.00541
Total equivalent thickness, in.		0.24131	0.27723	0.24789
Total unit weight, lb/ft^2		10.355	11.896	10.637
Average unit weight, lb/ft^2		10.811		

TABLE 13-40

BREAKDOWN OF WING WEIGHTS FOR MONOCOQUE WAFFLE PANELS WITH LOWER SURFACE OUTBOARD HEAT SHIELD AND INSULATION[a]

Item		Equivalent thickness $\bar{t}$, in.		
		Center, A	Inboard, B	Outboard, C
Panels	Upper	0.0708	0.0790	0.0684
	Lower	0.0658	0.0822	0.0452
Caps (minimum gage)	Spar, upper	0.00173	0.00173	0.00173
	Spar, lower	0.00173	0.00173	0.00173
	Rib, upper	0.00345	0.00345	0.00345
	Rib, lower	0.00345	0.00345	0.00345
Closeouts	Upper	0.0222	0.0245	0.0207
	Lower	0.0180	0.0217	0.0108
Webs	Rib web	0.0363	0.0363	0.0182
	Spar web	0.0182	0.0182	0.0091
Web intersections	Total	0.00225	0.00225	0.00112
Insulation	Total	–	–	0.00348
Heat shields	Corrugation	–	–	0.0166
	Clip	–	–	0.00485
Oxidation	Total	0.00047	0.00050	0.00566
Fasteners	Total	0.00541	0.00541	0.00541
Total equivalent thickness, in.		0.2498	0.2804	0.2199
Total unit weight, lb/ft^2		10.72	12.03	9.44
Average unit weight, lb/ft^2		10.49		

[a] a = 40 in., b = 20 in., a/b = 2.

TABLE 13-41

COMPONENT WEIGHTS FOR MONOCOQUE WAFFLE CONCEPT, HEAT SHIELD ON ENTIRE LOWER SURFACE

Item		Equivalent thickness, in.		
		Center(A)	Inboard (B)	(Outboard (C)
Panels	Upper	0.08836	0.07806	0.06357
	Lower	0.05482	0.06125	0.09100
	Total	0.14318	0.13931	0.15457
Cap and closeout, single shear	Upper, rib direction	0.02201	0.01927	0.01653
	Upper, spar direction	0.01101	0.00964	0.00826
	Total	0.03302	0.02891	0.02479
	Lower, rib direction	0.01325	0.01330	0.02161
	Lower, spar direction	0.00662	0.00665	0.01080
	Total	0.01987	0.01995	0.03241
	Total	0.05289	0.04886	0.05720
Rib and spar webs	Rib web	0.0363	0.0363	0.0182
	Spar web	0.0182	0.0182	0.0091
	Total	0.0545	0.0545	0.0273
Web intersection	Total	0.00225	0.00225	0.001125
Dynaflex insulation	Insulation	--	--	--
	Packaging	--	--	--
	Total	--	--	--
Corrugated heat shield	Corrugation	0.0105	0.0105	0.0166
	Clip	0.00448	0.00448	0.00485
	Total	0.01498	0.01498	0.02145
Oxidation	Total	0.00143	0.00098	0.005552
Fastener	Total	0.00541	0.00541	0.00541
Total equivalent thickness, in.		0.27464	0.26629	0.27261
Total unit weight, lb/ft^2		11.785	11.427	11.698
Average unit weights, lb/ft^2		11.670		

TABLE 13-42

COMPONENT WEIGHTS FOR MONOCOQUE WAFFLE CONCEPTS, HEAT SHIELD ON ENTIRE LOWER SURFACE, WITH INSULATION AT OUTBOARD AREA[a]

Item		Equivalent thickness, in.		
		Center (A)	Inboard (B)	Outboard (C)
Panels	Upper	0.08597	0.07581	0.06478
	Lower	0.04941	0.06507	0.07011
	Total	0.13538	0.14088	0.13489
Cap and closeout, single shear	Upper, rib direction	0.02131	0.01878	0.01674
	Upper, spar direction	0.01065	0.00939	0.00837
	Total	0.03196	0.02817	0.02511
	Lower, rib direction	0.01229	0.01398	0.01541
	Lower, spar direction	0.00614	0.00699	0.00770
	Total	0.01843	0.02097	0.02311
	Total	0.05039	0.04914	0.04822
Rib and spar webs	Rib web	0.0363	0.0363	0.0182
	Spar web	0.0182	0.0182	0.0091
	Total	0.0545	0.0545	0.0273
Web intersection	Total	0.00225	0.00225	0.001125
Dynaflex insulation	Insulation	--	--	0.00146
	Packaging	--	--	0.00202
	Total	--	--	0.00348
Corrugated heat shield	Corrugation	0.0105	0.0105	0.0166
	Clip	0.00448	0.00448	0.00485
	Total	0.01498	0.01498	0.02145
Oxidation	Total	0.00143	0.00098	0.0053$\frac{1}{2}$6
Fastener	Total	0.00541	0.00541	0.00541
Total equivalent thickness, in.		0.26434	0.26814	0.24723
Total unit weight, lb/ft^2		11.343	11.506	10.609
Total unit weight, lb/ft^2		11.084		

[a] a = 40 in., b = 20 in.

TABLE 13-43

COMPONENT WEIGHTS FOR MONOCOQUE WAFFLE CONCEPT, NO HEAT SHIELDS AND NO INSULATION[a]

Item		Equivalent thickness, in.		
		Center	Inboard	Outboard
Panels	Upper	0.07614	0.08144	0.06908
	Lower	0.05347	0.07301	0.1218
	Total	0.12961	0.15445	0.19088
Cap and closeout, single shear	Upper, rib direction	0.01923	0.02080	0.01753
	Upper, spar direction	0.00962	0.01040	0.00877
	Total	0.02885	0.03120	0.02360
	Lower, rib direction	0.01225	0.01586	0.03188
	Lower, spar direction	0.00613	0.00793	0.01594
	Total	0.01838	0.02379	0.04782
	Total	0.04723	0.05499	0.07412
Rib and spar webs	Rib web	0.0363	0.0363	0.0182
	Spar web	0.0182	0.0182	0.0091
	Total	0.0545	0.0545	0.0273
Web intersection	Total	0.00225	0.00225	0.001125
Dynaflex insulation	Insulation	--	--	--
	Packaging	--	--	--
	Total	--	--	--
Corrugated heat shield	Corrugation	--	--	--
	Clip	--	--	--
	Total	--	--	--
Oxidation	Total	0.000976	0.000224	0.001932
Fastener	Total	0.00541	0.00541	0.00541
Total equivalent thickness, in.		0.23998	0.27182	0.30077
Total unit weight, lb/ft^2		10.298	11.664	12.907
Average unit weight, lb/ft^2		11.652		

[a](a = 40 in., b = 20 in.)

TABLE 13-44

AVERAGE WING UNIT WEIGHTS FOR VARIOUS PANEL WIDTHS AND ASPECT RATIOS, MONOCOQUE HONEYCOMB-CORE SANDWICH PANELS

Aspect ratio, a/b \ Panel width, b, in.	Average wing unit weight, lb/ft^2			
	30	40	50	60
1.0	-	6.959	6.782	6.822
1.5	-	6.608	6.576	6.805
2.0	6.712	6.473	6.508	-

TABLE 13-45

FINAL TEMPERATURES AND GEOMETRY FOR MONOCOQUE HONEYCOMB-CORE SANDWICH PANELS WITH OUTBOARD LOWER SURFACE HEAT SHIELD AND INSULATION [a,b]

		Center		Inboard		Outboard	
		Upper	Lower	Upper	Lower	Upper	Lower
Max. face sheet temp., °F	-0.5-g	1003	1263	1313	1335	1595	1412
	+2.0-g	1026	1534	1245	1572	1408	1515
	Cruise	1277	1327	1130	1340	1123	1315
$W^{(c)}$, lb/ft^2		1.820	1.800	1.760	1.970	1.990	1.520
ρ_c, lb/ft^3		7.600	7.120	6.690	7.070	5.740	6.160
$\bar{t}$, in.		0.042	0.042	0.041	0.046	0.046	0.035
h, in.		0.935	0.898	0.950	0.937	0.963	0.714
t_1, in.		0.015	0.015	0.015	0.018	0.018	0.015
t_2, in.		0.014	0.015	0.014	0.015	0.018	0.012
t_c, in.		0.002	0.002	0.002	0.002	0.002	0.002
S, in.		0.271	0.291	0.308	0.294	0.358	0.334
$\bar{Z}$, in.		0.450	0.449	0.461	0.420	0.492	0.319
$W_o^{(d)}$, in.		-0.910	1.610	-0.820	0.230	1.160	-0.950

[a] a 80 in., b 40 in., a/b 2.0.

[b] Effective design condition underlined.

[c] Nominal, does not include core flanges and corrugations.

[d] Midpanel deflection.

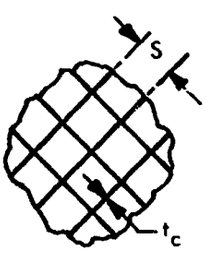

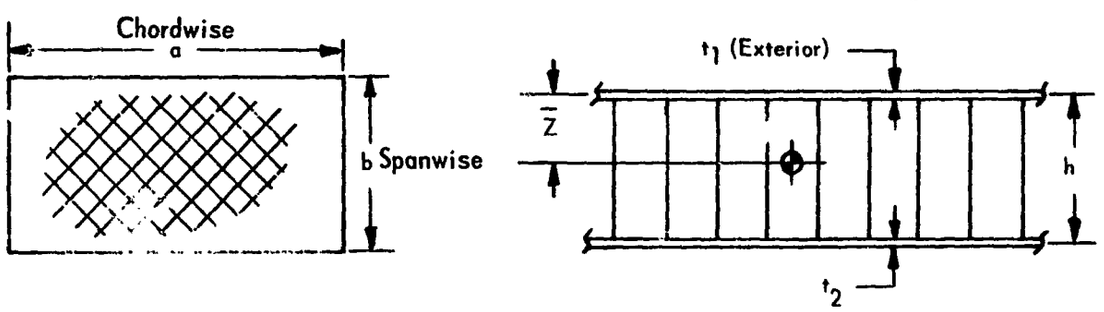

$\bar{t}$ = panel equivalent thickness

w = panel equivalent unit weight

ρ_c = density

TABLE 13-46

BREAKDOWN OF WING WEIGHTS FOR MONOCOQUE HONEYCOMB-CORE SANDWICH PANELS WITH LOWER SURFACE OUTBOARD HEAT SHIELD AND INSULATION

Item		Equivalent thickness, $\bar{t}$, in.		
		Center, A	Inboard, B	Outboard, C
Panels	Upper[a]	0.0449	0.0434	0.0480
	Lower[a]	0.0443	0.0482	0.0372
Caps (minimum gage)	Spar, upper	0.00097	0.00097	0.00097
	Spar, lower	0.00097	0.00097	0.00097
	Rib, upper	0.00195	0.00195	0.00195
	Rib, lower	0.00195	0.00195	0.00195
Closeouts	Upper	0.00878	0.00888	0.00888
	Lower	0.00868	0.00878	0.00848
Webs	Rib web	0.0182	0.0182	0.0091
	Spar web	0.0091	0.0091	0.0046
Web intersections	Total	0.00056	0.00056	0.00028
Insulation	Total	–	–	0.00348
Heat shields	Corrugation	–	–	0.01660
	Clip	–	–	0.00485
Oxidation	Total	0.00110	0.00077	0.00599
Fasteners	Total	0.00417	0.00421	0.00404
Total equivalent thickness, in.		0.1456	0.1479	0.1573
Total unit weight, lb/ft^2		6.25	6.35	6.75
Average unit weight, lb/ft^2		6.47		

[a]Includes weight due to core corrugation and flanges.

TABLE 13-47

OPTIMUM WING SECTION FINAL WEIGHTS AND SPAR/RIB SPACINGS FOR SEMONOMOCOQUE SPANWISE-STIFFENED TUBULAR CONCEPTS[a,b]

Wing Section	Area A		Area B		Area C		Total Wing Section Average unit wt., lb/ft^2
Concept	Unit wt., lb/ft^2	Rib spacing, in.	Unit wt., lb/ft^2	Rib spacing, in.	Unit wt., lb/ft^2	Rib spacing, in.	
Tubular, no Insulation	4.73	50	5.55	40	7.11	20	5.89
Tubular, insulation	4.82	48	5.61	40	5.70	40	5.38

[a]Heat shields used on all upper and lower surfaces of all concepts.

[b]Spar spacing = 90 inches.

TABLE 13-48

FINAL GEOMETRY FOR SEMIMONOCOQUE
SPANWISE-STIFFENED TUBULAR PANELS

Wing Area	Surface	$\bar{t}$, in.	t, in.	R, in.	L, in.	Pitch, in.
A (C_L - 120)	Upper	0.0292	0.011	1.500	50	3.429
	Lower	0.0258	0.010	0.800	50	2.062
B (120-212)	Upper	0.0287	0.011	0.950	40	2.355
	Lower	0.0284	0.011	0.800	40	2.062
C (212-350)	Upper	0.0258	0.010	0.750	40	1.964
	Lower	0.0254	0.010	0.600	40	1.672

$\bar{t}$ - panel equivalent thickness.
L - panel length (rib spacing).
b - 0.5 in. flat.
Pitch - center-to-center of stiffener.
Critical flight condition all wing areas +2.0 g.

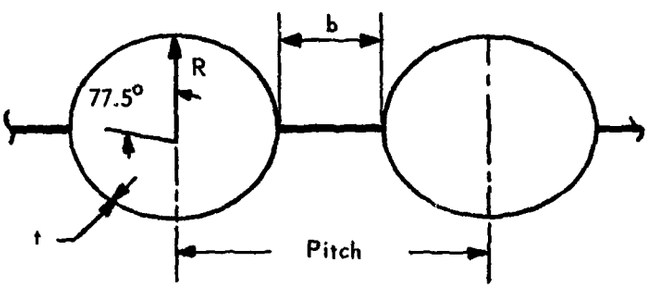

TABLE 13-49

BREAKDOWN OF WING WEIGHTS FOR SEMIMONOCOQUE SPANWISE STIFFENED TUBULAR PANELS WITH FULL HEAT SHIELDS AND LOWER SURFACE OUTBOARD INSULATION[a]

Item		Equivalent thickness, $\bar{t}$, in.		
		Center, A	Inboard, B	Outboard, C
Panels	Upper Lower	0.0292 0.0258	0.0287 0.0284	0.0258 0.0254
Caps	Spar, upper Spar, lower	0.0011 0.0011	0.0011 0.0011	0.0011 0.0011
	Rib, upper Rib, lower	0.0027 0.0032	0.0028 0.0034	0.0032 0.0028
Closeouts	Upper Lower	0.0032 0.0020	0.0029 0.0025	0.0024 0.0021
Webs	Rib web Spar web	0.0151 0.0084	0.0180 0.0096	0.0120 0.0047
Web intersections	Total	0.00042	0.00050	0.00029
Insulation	Total	–	–	0.00685
Heat shields	Total	0.0131	0.0263	0.0358
Oxidation	Total	0.00453	0.00246	0.00633
Fasteners	Total	0.00254	0.00294	0.00294
Total equivalent thickness, in.		0.1124	0.1307	0.1328
Total unit weight, lb/ft^2		4.82	5.61	5.70
Average unit weight, lb/ft^2		5.38		

[a]Area A: a = 90, b = 50, a/b = 1.8.

Area B and C: 2 = 90, b = 40, a/b = 2.25.

TABLE 13-50

OPTIMUM WING SECTION FINAL WEIGHTS AND SPAR/RIB SPACINGS FOR SEMIMONOCOQUE SPANWISE-STIFFENED BEADED PANELS[a,b]

Wing Section	Area A		Area B		Area C		Total wing section average unit wt., lb/ft^2
Concept	Unit wt., lb/ft^2	Rib spacing in.	Unit wt., lb/ft^2	Rib spacing, in.	Unit wt., lb/ft^2	Rib spacing, in	
Beaded, no insulation	4.27	50	5.19	40	6.99	20	5.59
Beaded, insulation	4.46	50	5.38	50	5.37	40	5.06

[a] Heat shields used on all upper and lower surfaces.

[b] Spar spacing = 90 inches.

TABLE 13-51

FINAL GEOMETRY FOR SEMIMONOCOQUE SPANWISE-STIFFENED BEADED PANELS

Wing Area	Surface	$\bar{t}$, in.	t, in.	R, in.	L, in.	Pitch, in.
A C_L - BL 120	Upper	0.0263	0.020	1.150	50	5.491
	Lower	0.0196	0.015	1.050	50	5.100
B BL 120-212	Upper	0.0262	0.020	1.100	40	5.296
	Lower	0.0224	0.017	1.250	40	5.881
C BL 212-350	Upper	0.0221	0.017	0.900	40	4.515
	Lower	0.0197	0.015	1.150	40	5.491

$\bar{t}$ = panel equivalent thickness.
L = panel length (rib spacing).
b = 0.5 in. flat.
Pitch = center-to-center of stiffener.
Critical flight condition all wing areas = +2.0 g.

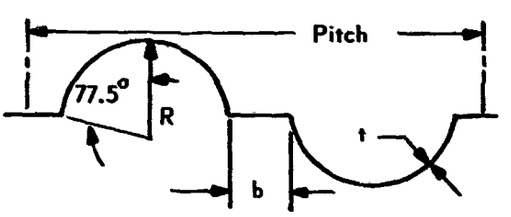

TABLE 13-52

DETAIL BREAKDOWN OF WING WEIGHTS FOR SEMIMONOCOQUE SPANWISE-STIFFENED BEADED PANELS WITH FULL HEAT SHIELDS AND LOWER SURFACE OUTBOARD INSULATION[a]

Item	Equivalent thickness, $\bar{t}$, in.		
	Center, A	Inboard, B	Outboard, C
Panels			
Upper	0.0263	0.0262	0.0221
Lower	0.0196	0.0224	0.0197
Caps			
Spar, Upper	0.0011	0.0011	0.0011
Spar, Lower	0.0011	0.0011	0.0011
Rib, Upper	0.0027	0.0028	0.0032
Rib, Lower	0.0032	0.0034	0.0028
Closeouts			
Upper	0.0037	0.0038	0.0030
Lower	0.0040	0.0053	0.0036
Webs			
Spar	0.0084	0.0096	0.0047
Rib	0.0151	0.0180	0.0120
Posts	0.00042	0.00050	0.00029
Insulation	–	–	0.00685
Heat shield	0.0131	0.0263	0.0358
Oxidation	0.00254	0.00173	0.00602
Fasteners	0.00254	0.00294	0.00294
Total, in.	0.1039	0.1253	0.1252
Unit wt., lb/ft^2	4.46	5.38	5.37
Average unit wt., lb/ft^2		5.06	

[a]Area A: a = 90 in., b = 50 in.

Area B and C: a = 90 in., b = 40 in.

TABLE 13-53

FINAL GEOMETRY FOR SEMIMONOCOQUE CHORDWISE-STIFFENED TUBULAR AND CONVEX BEADED PANELS

Panel Concept	Area	Surface	$\bar{t}$, in.	t, in.	R, in.	Pitch, in.	Critical Condition
Tubular	A C_L-120	Upper	0.0286	0.011	0.900	2.257	Cruise
	A C_L-120	Lower	0.0261	0.010	0.950	2.355	Cruise
	B BL 120-212	Lower	0.0337	0.013	0.850	2.160	+2.0-g
	C BL 212-350	Lower	0.0254	0.010	0.600	1.672	+2.0-g

Convex Beaded	Area	Surface	$\bar{t}$, in.	t_u in.	t_ℓ in.	R_u in.	R_ℓ in.	Pitch, in.	Critical Condition
	B BL 120-212	Upper	0.0292	0.016	0.010	2.031	0.800	2.062	+2.0-g
	C BL 212-350	Upper	0.0382	0.022	0.012	2.538	1.000	2.453	-0.5-g

Panel length = 24 in. (spar spacing)
b = 0.5 in. flat
$\bar{t}$ = panel equivalent thickness

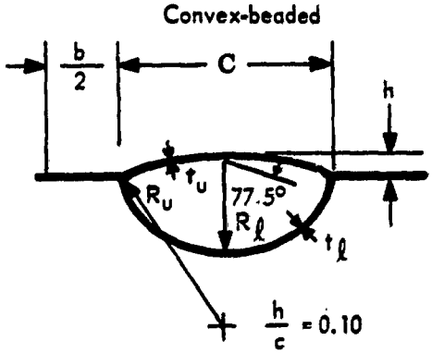

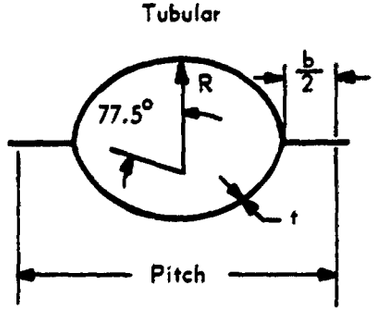

TABLE 13-54

DETAIL BREAKDOWN OF WING WEIGHTS FOR SEMIMONOCOQUE CHORDWISE-STIFFENED TUBULAR/CONVEX-BEADED PANELS WITH FULL LOWER SURFACE HEAT SHIELD AND OUTBOARD LOWER SURFACE INSULATION [a]

Item	Equivalent thickness, $\bar{t}$, in.		
	Center, A	Inboard, B	Outboard, C
Panels			
Upper	0.0286	0.0292	0.0381
Lower	0.0261	0.0337	0.0254
Caps			
Spar, Upper	0.0070	0.0069	0.0051
Spar, Lower	0.0070	0.0083	0.0041
Rib, Upper	0.00167	0.00163	0.00145
Rib, Lower	0.00167	0.00163	0.00145
Closeouts			
Upper	0.00865	0.00420	0.00491
Lower	0.00805	0.00613	0.00348
Webs			
Spar	0.0329	0.0300	0.0176
Rib	0.0150	0.0155	0.0056
Posts	0.00131	0.0010	0.00058
Insulation	–	–	0.00685
Heat shields	0.0143	0.0143	0.0230
Oxidation	0.00525	0.00173	0.00588
Fasteners	0.0044	0.0041	0.0041
Total, in.	0.1619	0.1584	0.1476
Unit wt, lb/ft^2	6.95	6.80	6.33
Average unit wt, lb/ft^2		6.67	

[a]Area A: a = 24 in., b = 60 in.

Area B and C: a = 24 in., b = 75 in.

TABLE 13-55

WEIGHTS OF STATICALLY DETERMINATE PANEL AND VARIOUS THERMAL-PROTECTION ARRANGEMENTS

Panel concept[a]	Thermal-protection system[b]	Item, in. $\frac{\bar{t}}{L}$ (c)	Center Area A	Inboard Area B	Outboard Area C	Average	Weight, lb/ft^2 Average
Beaded skin	Heat shields, no insulation	$\frac{\bar{t}}{L}$	0.1214 / 60	0.1399 / 50	0.1292 / 40	0.1293	5.550
Beaded skin	Heat shields, 1/8 in. insulation lower surface from $\mathcal{C}_L$ to BL 212 (Areas A and B)	$\frac{\bar{t}}{L}$	0.1223 / 60	0.1390 / 50	0.1292 / 40	0.1294	5.554
Beaded skin	Heat shields, 1/4 in. insulation lower surface from $\mathcal{C}_L$ to BL 212 (Areas A and B)	$\frac{\bar{t}}{L}$	0.1209 / 60	0.1416 / 50	0.1292 / 40	0.1296	5.562

[a] Lowest-weight semimonocoque spanwise-stiffened concept.

[b] Heat shields on all exposed wing areas.

[c] L = rib spacing.

TABLE 13-56

FINAL GEOMETRY FOR LOWEST WEIGHT STATICALLY DETERMINATE PANELS

Wing area	Surface	$\bar{t}$, in.	t, in.	R, in.	L, in.	Pitch, in.
A C_L - 120	Upper	0.0314	0.024	1.000	60	4.905
	Lower	0.0211	0.016	1.200	60	5.686
B BL 120-212	Upper	0.0291	0.022	1.300	50	6.077
	Lower	0.0253	0.019	1.600	50	7.248
C BL 212-350	Upper	0.0206	0.016	0.750	40	3.929
	Lower	0.0199	0.015	1.350	40	6.272

$\bar{t}$ = panel equivalent thickness.
L = panel length (rib spacing).
b = 0.5 in. flat.
Critical flight condition on all wing areas = +2.0-g

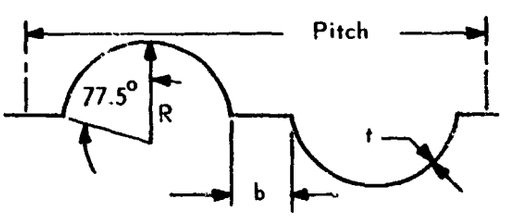

TABLE 13-57

BREAKDOWN OF WING WEIGHTS FOR STATICALLY DETERMINATE PANELS WITH FULL HEAT SHIELDS AND NO INSULATION[a]

Item		Equivalent thickness, $\bar{t}$, in.		
		Center, A	Inboard, B	Outboard, C
Panels	Upper	0.0314	0.0291	0.0206
	Lower	0.0211	0.0253	0.0199
Caps	Spar, upper	0.0022	0.0022	0.0022
	Spar, lower	0.0022	0.0022	0.0022
	Rib, upper	0.00135	0.0020	0.0025
	Rib, lower	0.00165	0.0020	0.0025
Closeouts	Upper	0.00338	0.00408	0.0026
	Lower	0.00387	0.00482	0.0041
Webs	Rib webs	0.0126	0.0144	0.0120
	Spar webs	0.0157	0.0147	0.0084
Web intersections	Total	0.00039	0.00044	0.00032
Insulation	Total		–	–
Heat shields		0.0131	0.0263	0.0359
Oxidation	Total	0.00231	0.00162	0.00714
Fasteners	Total	0.00226	0.00254	0.00294
Vertical shear fittings		0.0076	0.00819	0.00594
Total, in.		0.1214	0.1399	0.1292
Unit wt, lb/ft^2		5.21	6.00	5.54
Average unit wt, lb/ft^2			5.55	

[a]Area A: a = 90 in., b = 60 in.
Area B: a = 90 in., b = 50 in.
Area C: a = 90 in., b = 40 in.

TABLE 13-58

STRUCTURAL MARGINS OF SAFETY

Concept	Surface / Section	Ultimate load		Panel flutter[a]		Wing flutter	Sonic fatigue[b]		Load fatigue[b]		Creep[c]	
		Upper	Lower	Upper	Lower		Upper	Lower	Upper	Lower	Upper	Lower
Monocoque	A	0.00	0.00	d	83.0	1.3+	11.2	9.66	5.82	4.52	2.70	4.68
Waffle	B	0.00	0.00	135.0	135.0		13.2	13.1	2.31	6.77		
	C	0.00	0.00	92.0	6.77		10.1	1.16	1.50	2.89		
	A	0.00	0.00	d	42.6	1.3+	5.54	5.90	3.01	1.89	2.28	2.59
Honeycomb	B	0.00	0.00	46.2	51.1		5.62	6.04	0.70	1.46		
	C	0.00	0.00	58.4	5.31		7.04	0.96	0.36	1.32		
Semimonocoque spanwise	A	0.03	0.43	d	3.00	1.3+	2.16	1.22	4.75	0.13	5.00	1.82
Beaded	B	0.04	0.30	7.90	8.69		2.76	2.51	11.33	0.54		
	C	0.04	0.30	5.71	8.79		1.80	0.18	3.05	1.06		
	A	0.00	0.10	d	2.69	1.3+	3.09	1.47	11.89	0.15	3.68	1.56
Tubular	B	0.03	0.09	7.11	5.53		2.75	2.38	8.41	0.34		
	C	0.00	0.13	5.79	3.88		1.92	0.00	1.55	0.37		
Semimonocoque chordwise	A	0.02	0.01	d	12.4	1.3+	5.16	4.84	6.78	2.78	1.14	0.68
Tubular	B	0.00	0.16	51.5	12.8		2.53	5.86	0.17	2.92		
	C	0.04	0.00	53.8	18.7		3.98	0.65	0.29	2.05		
Statically determinate	A	0.10	0.01	d	2.61	1.3+	1.88	1.17	2.58	0.003	6.35	1.42
Beaded	B	0.03	0.08	5.72	7.30		2.68	2.66	4.32	0.54		
	C	0.13	0.01	4.64	11.90		1.33	0.31	1.53	1.52		

[a] (λ/λ_{CR}) value for panel flutter.

[b] MS = (F/f)-1. For sonic fatigue, F = rms stress, f = normalized stress; for fatigue, F = fatigue allowable. f = applied limit stress.

[c] Critical area ℄ to BL 120. Critical failure mode for all areas – creep buckling at t = 6680 hr, except for the chordwise concept which is critical for creep buckling at t = 30 hr.

[d] Surface not exposed to airflow.

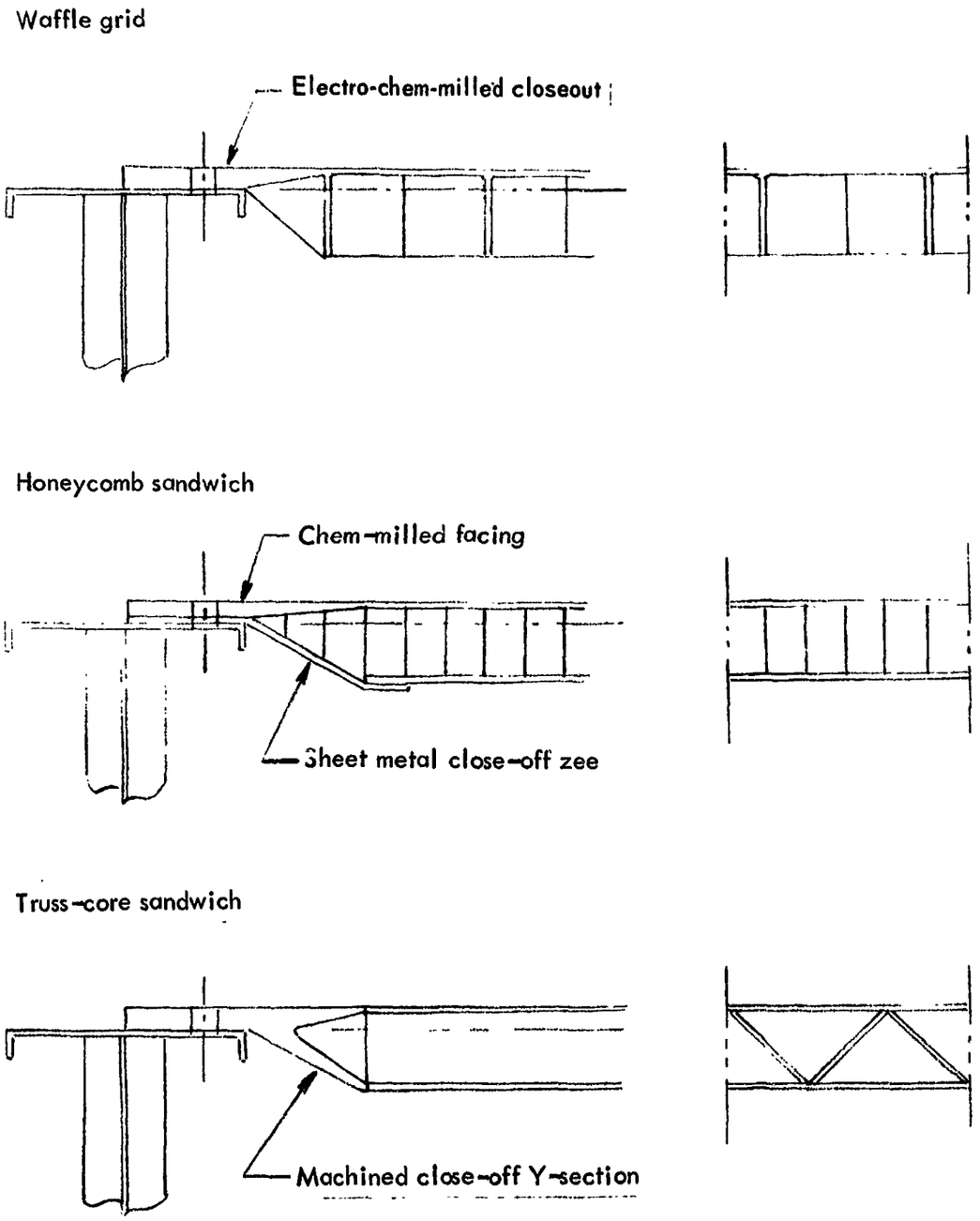

Figure 13-1. Typical edge closeouts for candidate monocoque panel configurations

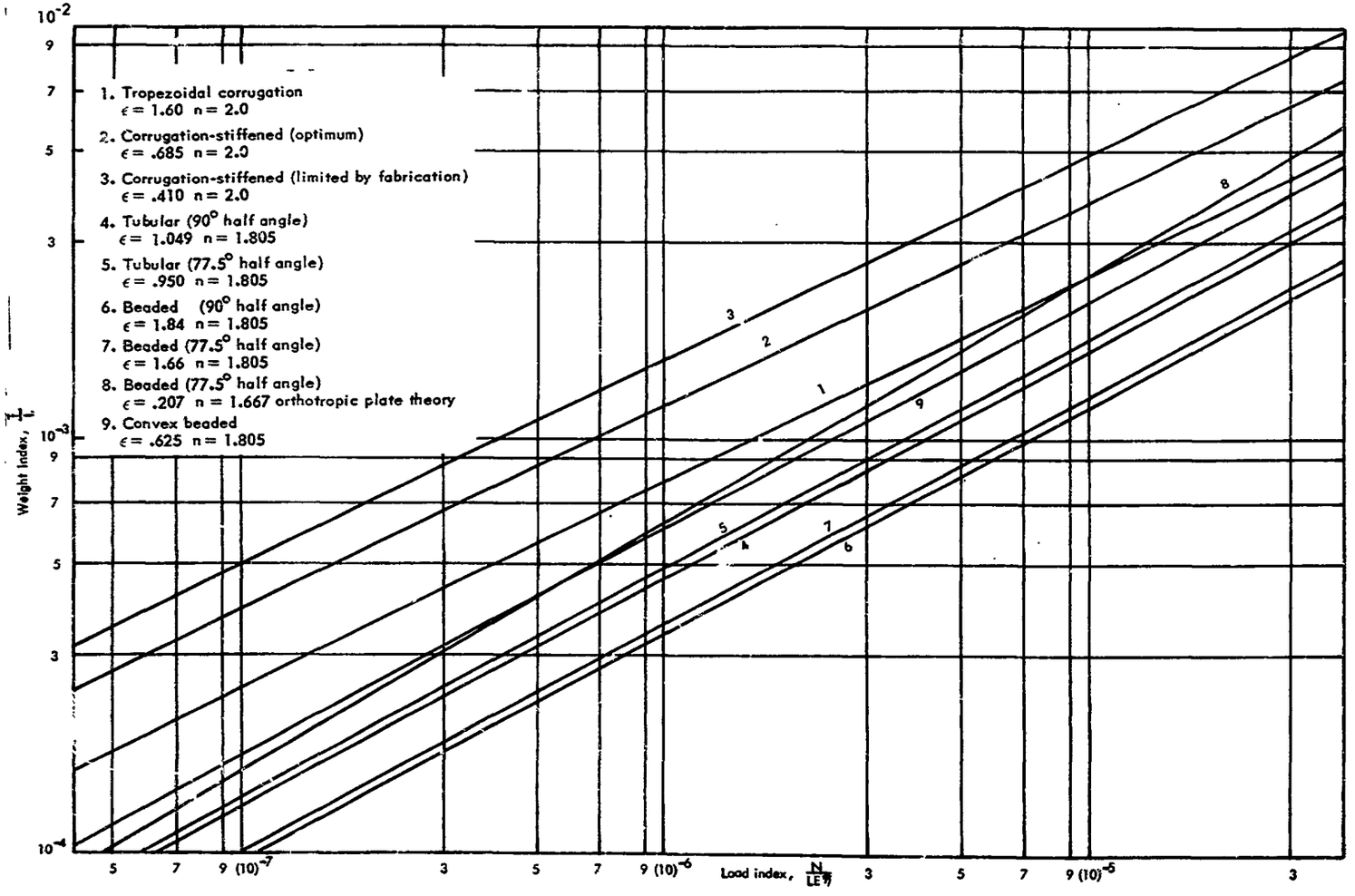

Figure 13-2. Semimonocoque stiffened panels, wide column curves

Panel dimensions: (All dimensions in inches)

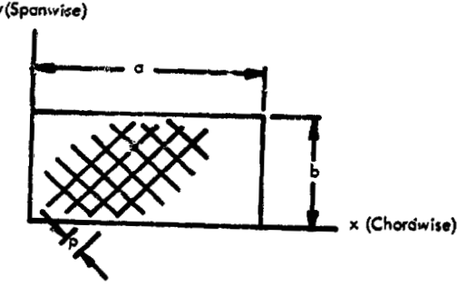

Waffle dimensions:

- h - overall waffle height
- p - pitch of stiffeners
- t_s - skin thickness
- t_w - stiffener thickness
- $\bar{t}$ - panel equivalent thickness

Miscellaneous:

- e_{11} - extensional eccentricity
- e_{33} - shear eccentricity
- w_o - maximum panel deflection

Figure 13-3. Notation for monocoque waffle panel design data

Single shear joint

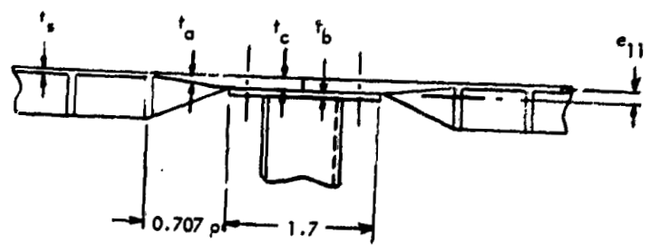

$$t_a = \frac{1}{2}(t_s + t_c)$$

$$t_c = \frac{1}{2}t_s + e_{11}$$

Double shear joint

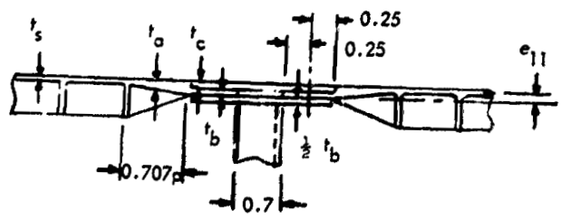

$$t_a = \frac{1}{2}\left(t_s + (t_b + t_c)\right)$$

Figure 13-4. Monocoque waffle cap and closeout detail

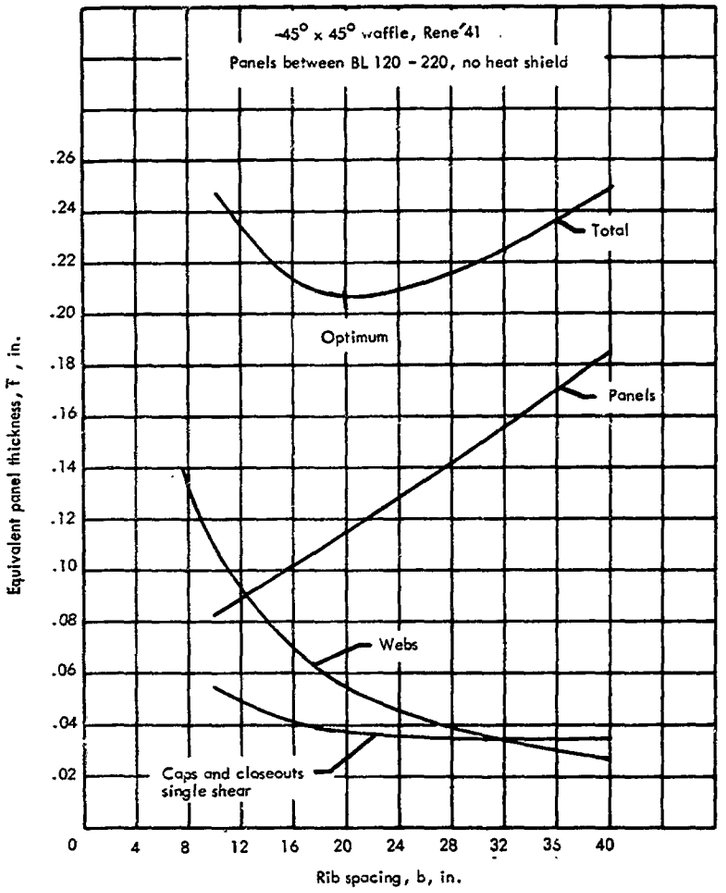

Figure 13-5. Monocoque waffle panel-width optimization for inboard wing area, a/b = 2.0

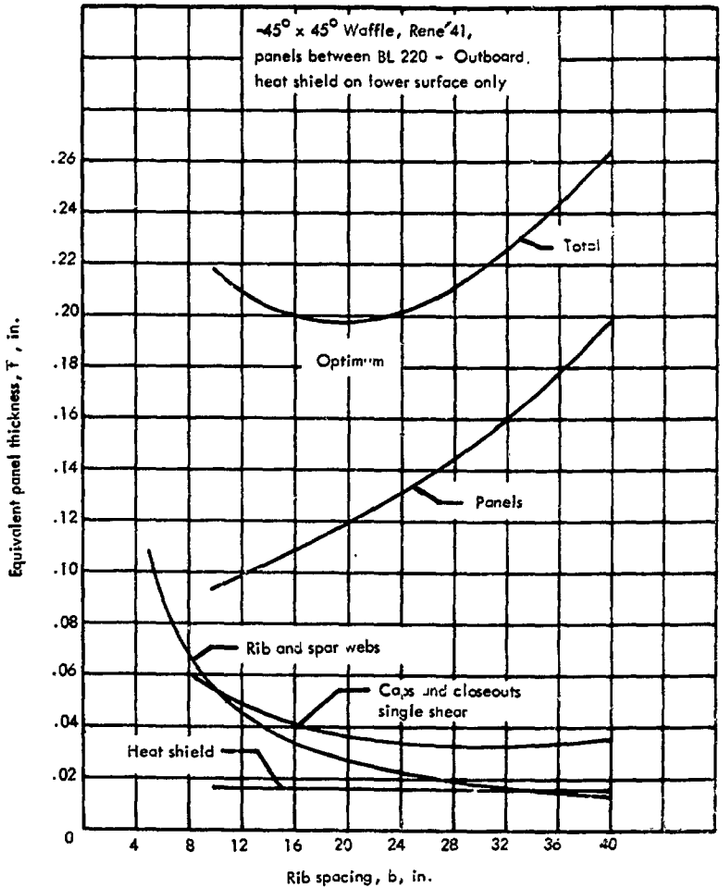

Figure 13-6. Monocoque waffle panel-width optimization for outboard wing area, a/b = 2.0

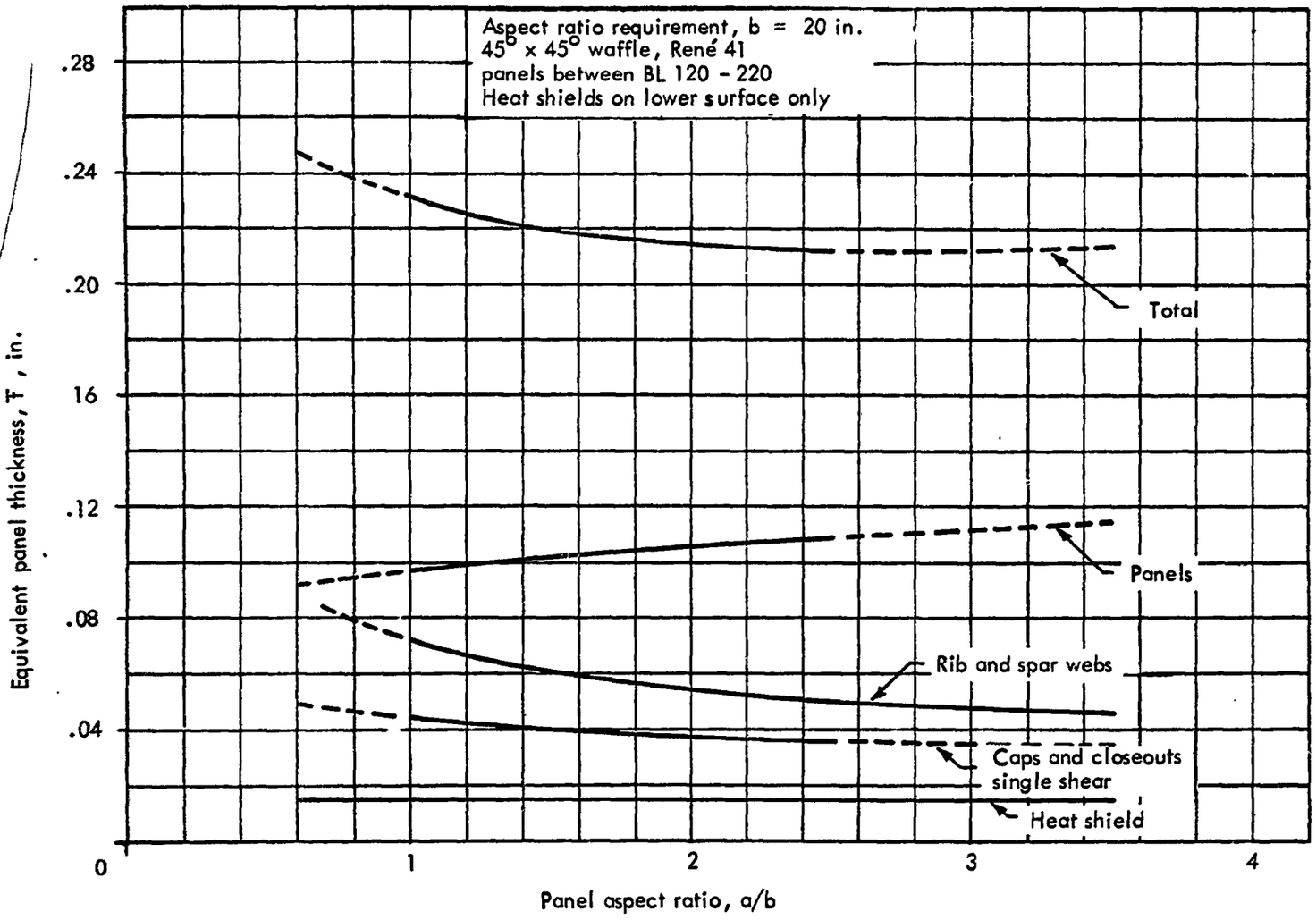

Figure 13-7. Panel aspect ratio optimization for inboard wing area of monocoque waffle concept, b = 20 in.

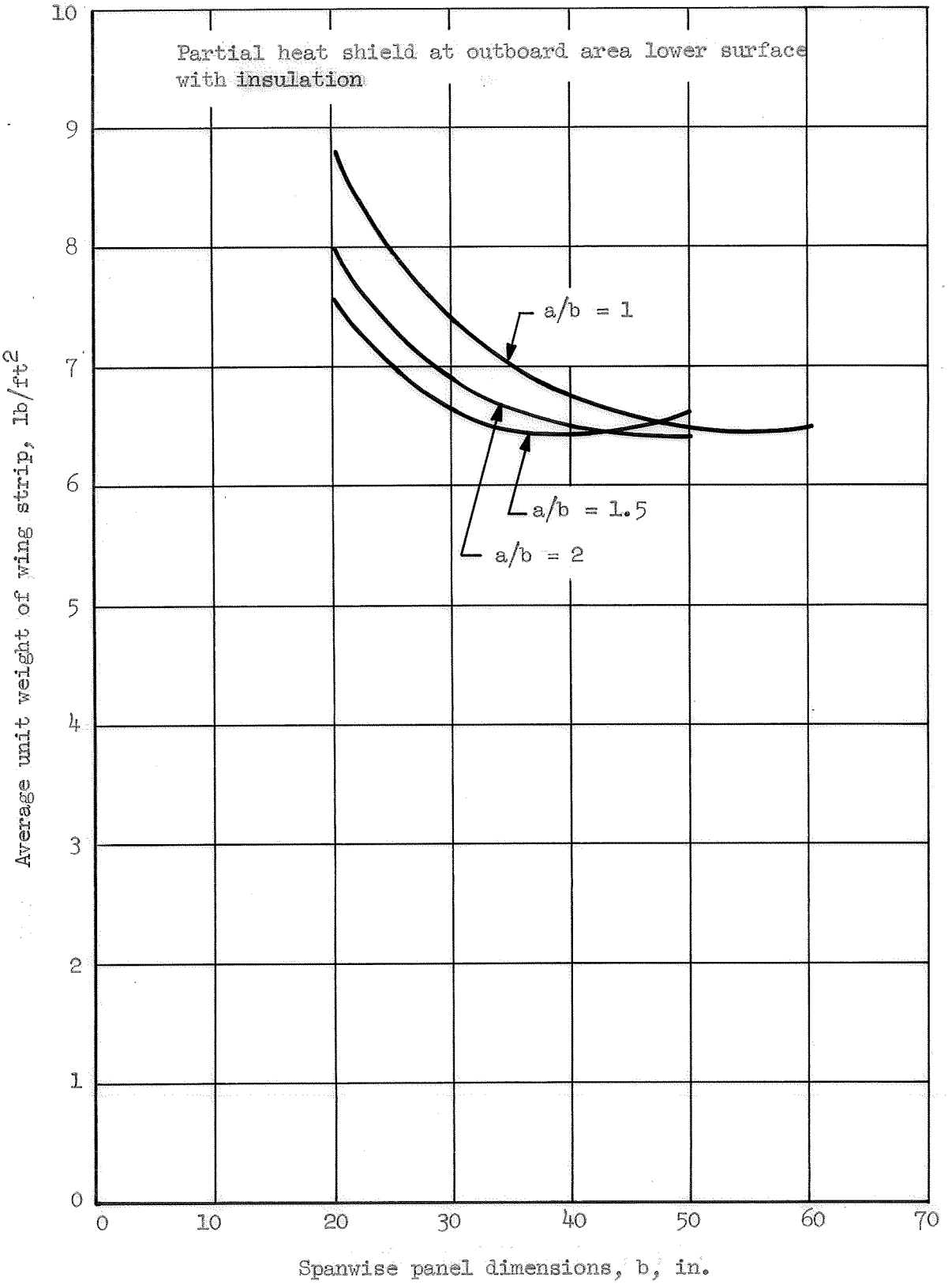

Figure 13-8 Monocoque honeycomb sandwich panel sizes

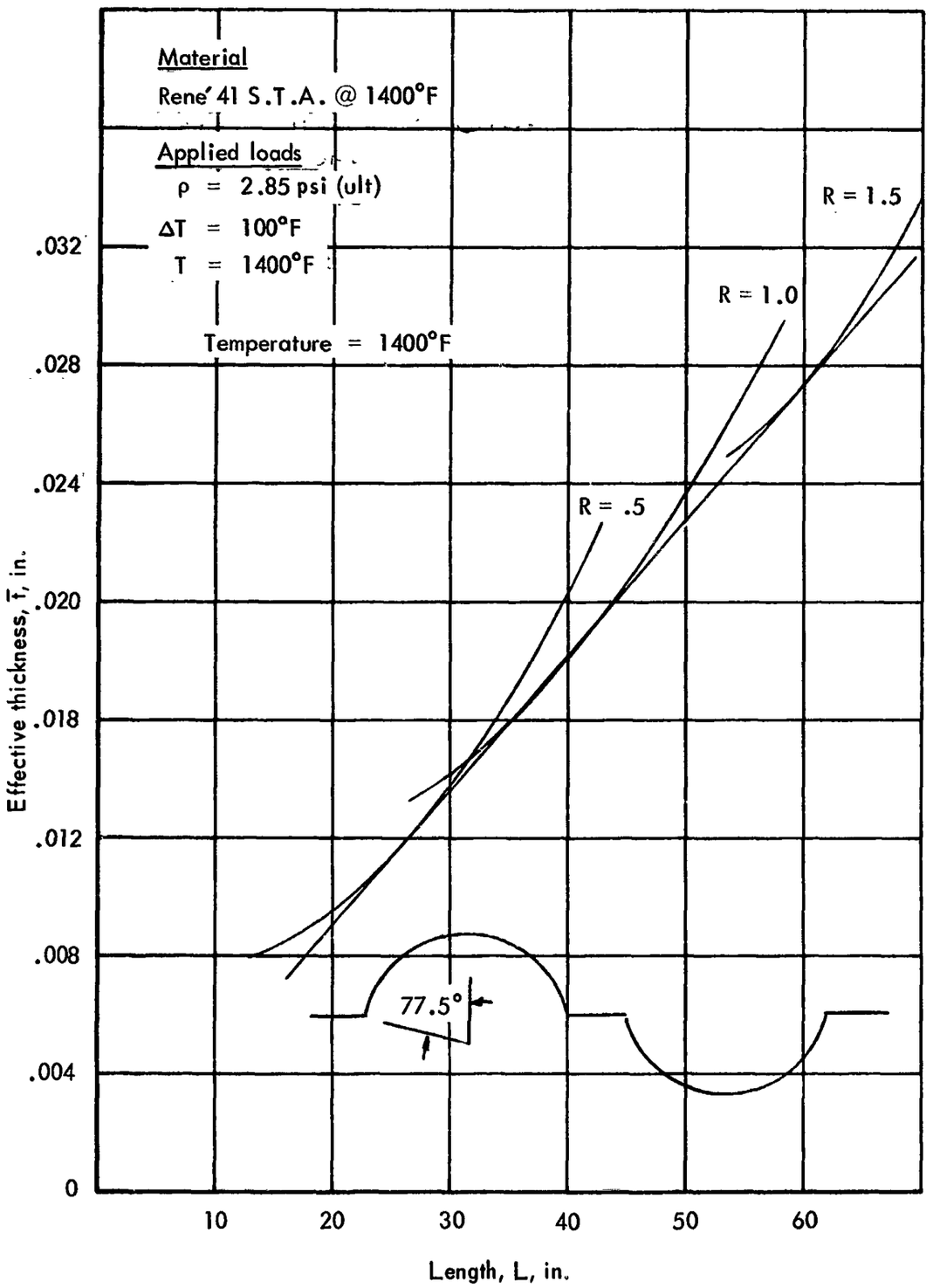

Figure 13-9. Effective thickness versus length of semimonocoque spanwise-stiffened beaded panels, lower surface, BL 120 - BL 220

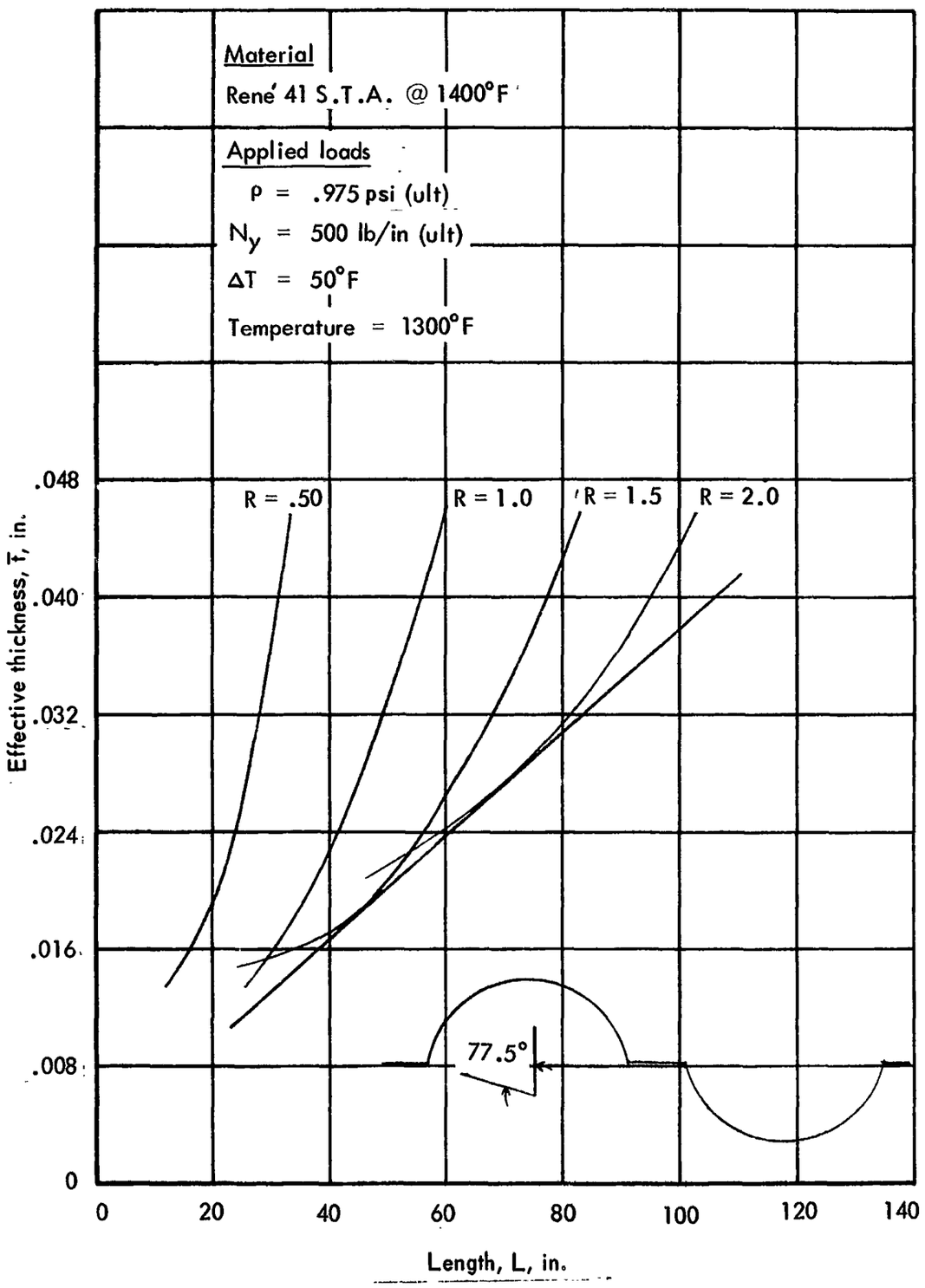

Figure 13-10. Effective thickness versus length of semimonocoque spanwise-stiffened beaded panels, upper surface, centerline to BL 220

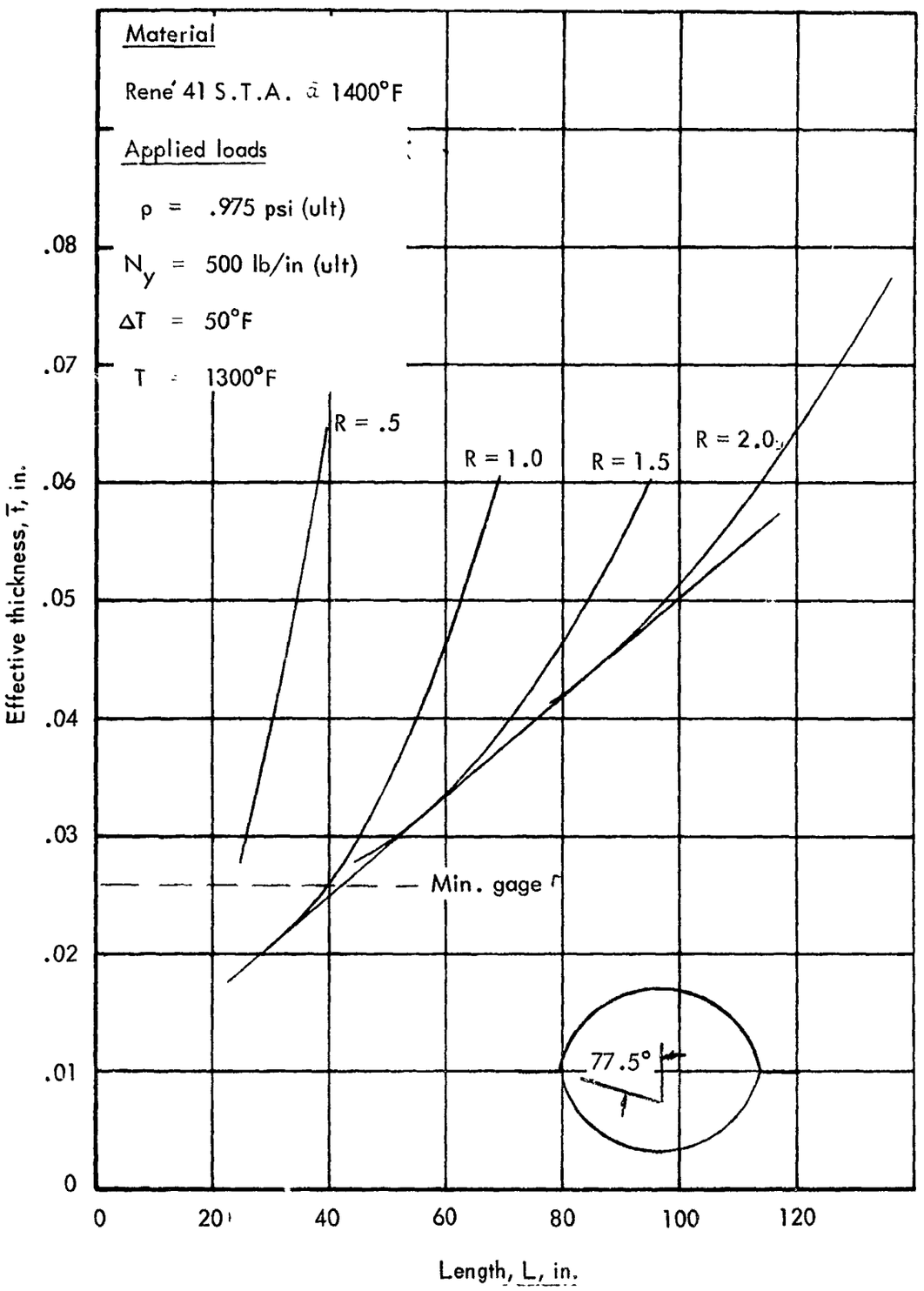

Figure 13-11. Effective thickness versus length of semimonocoque spanwise-stiffened tubular panels, upper surface, centerline to BL 220

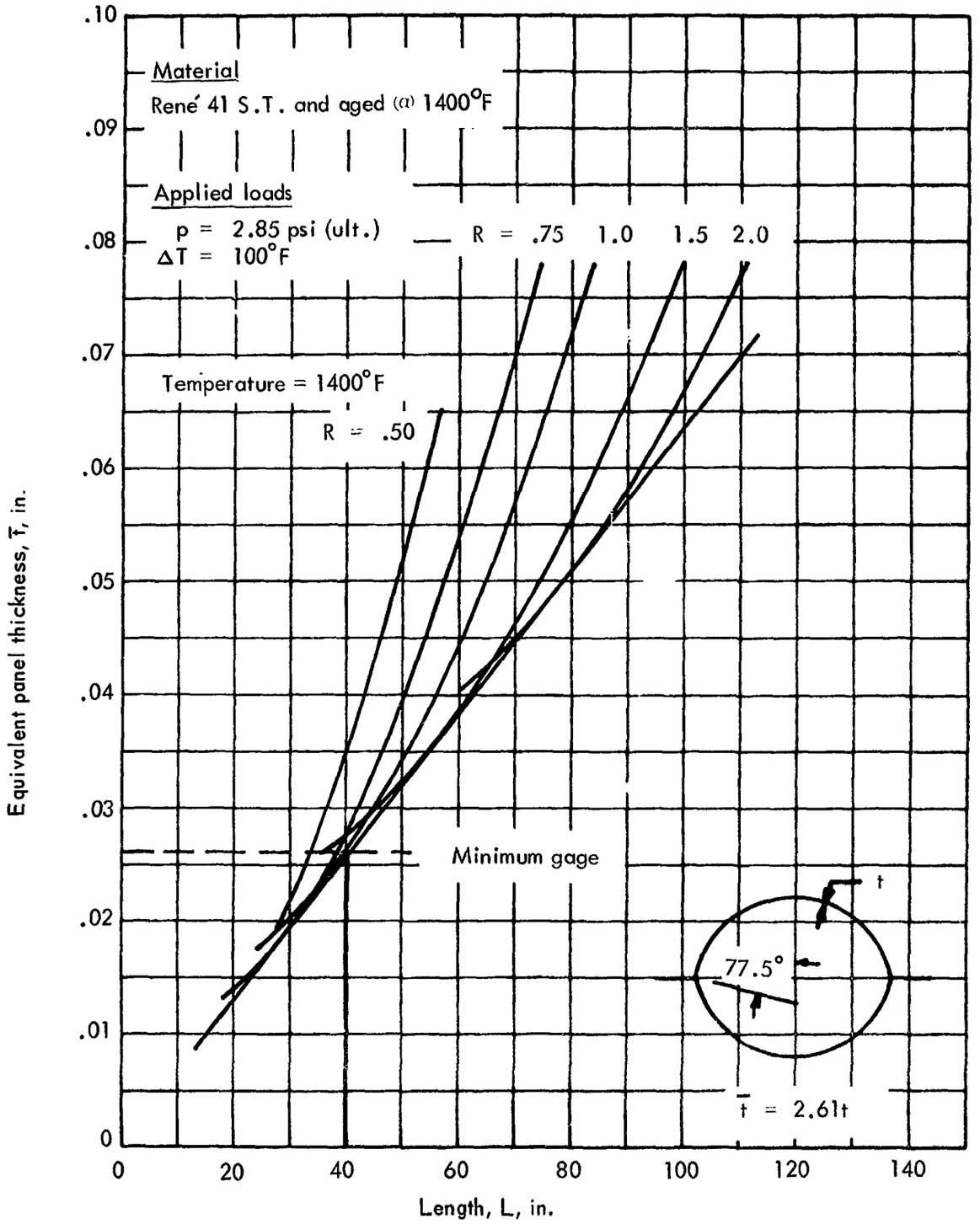

Figure 13-12. Effective thickness versus length of semimonocoque spanwise-stiffened tubular panels, lower surface, [illegible]

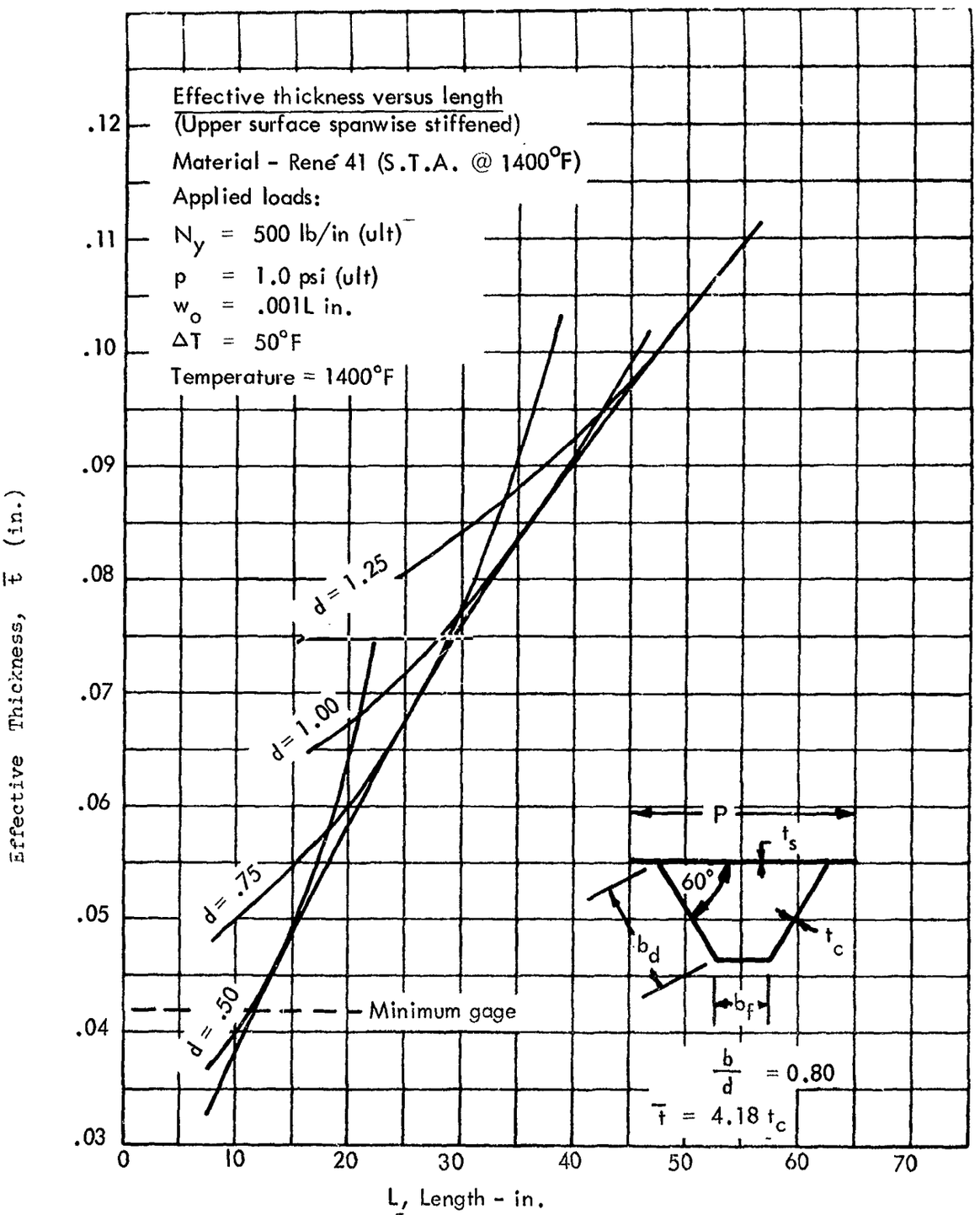

Figure 13-13. Effective thickness versus length of semimonocoque spanwise-corrugation stiffened panels, upper surface, BL 120 to BL 212

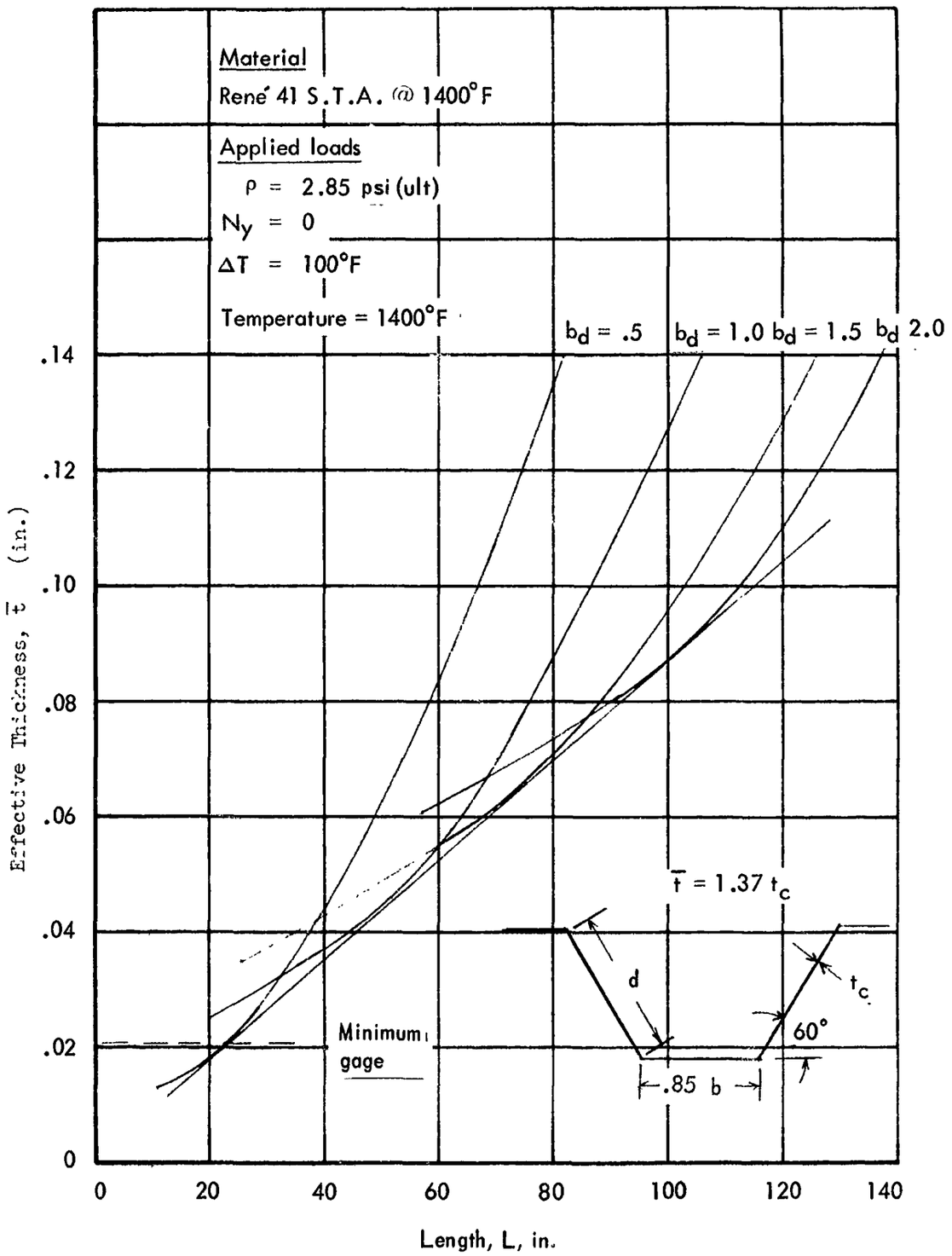

Figure 13-14. Effective thickness versus length of semimonocoque spanwise-trapezoidal corrugated panels, lower surface, BL 120 to BL 220

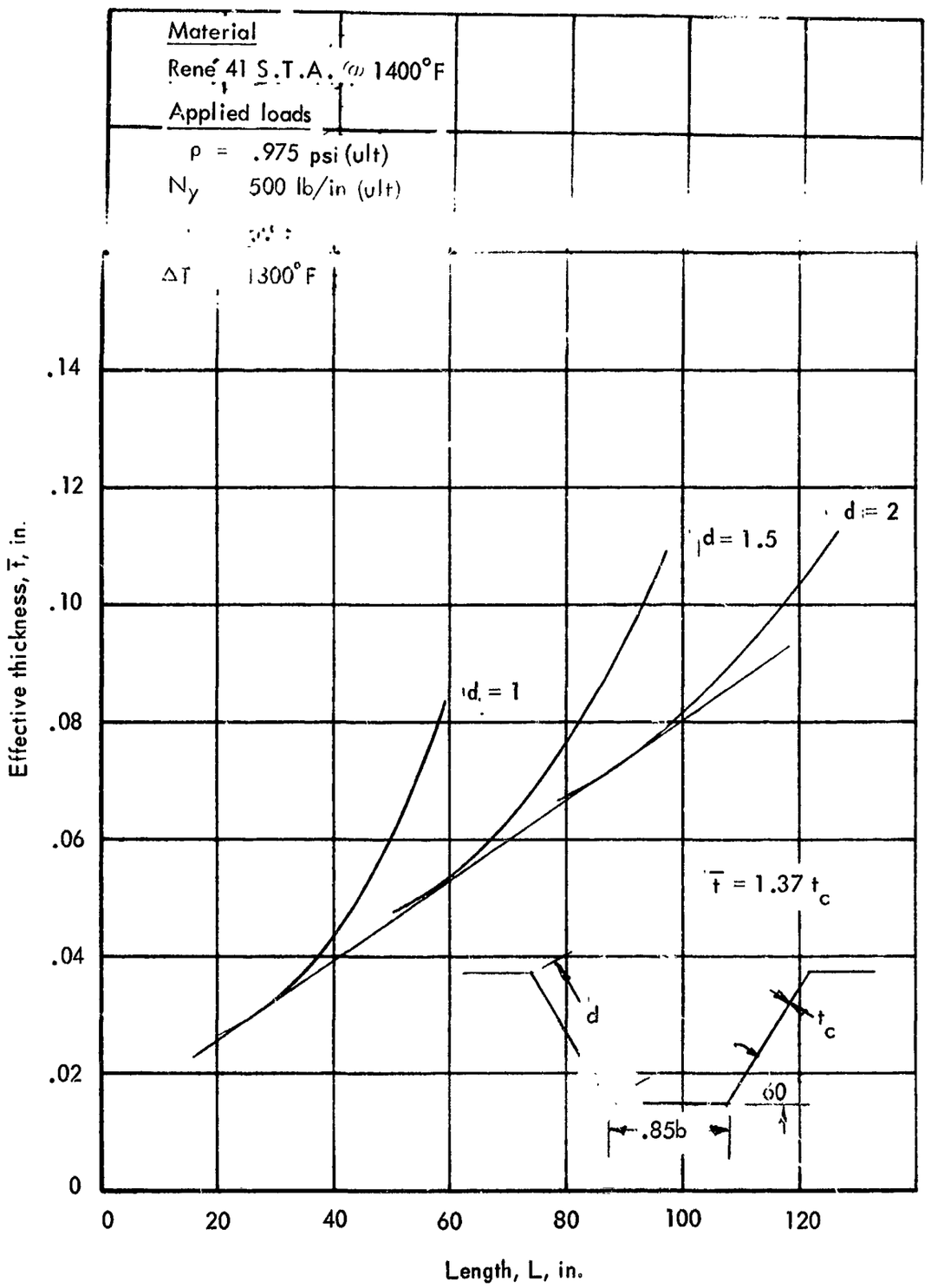

Figure 13-15. Effective thickness versus length of semimonocoque spanwise-trapezoidal corrugated panels, upper surface, centerline to BL 220

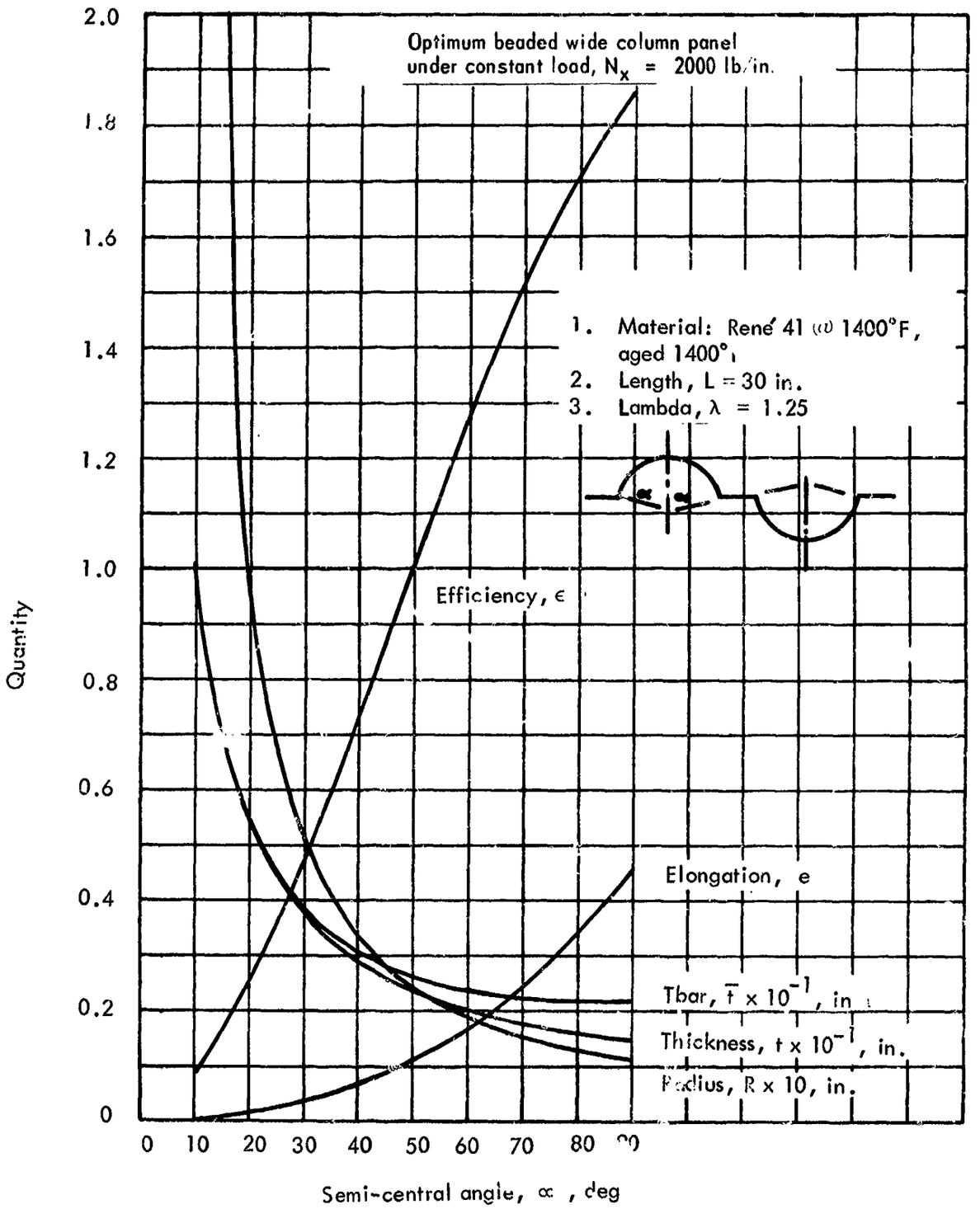

Figure 13-16. Optimum semimonocoque spanwise-stiffened beaded concept

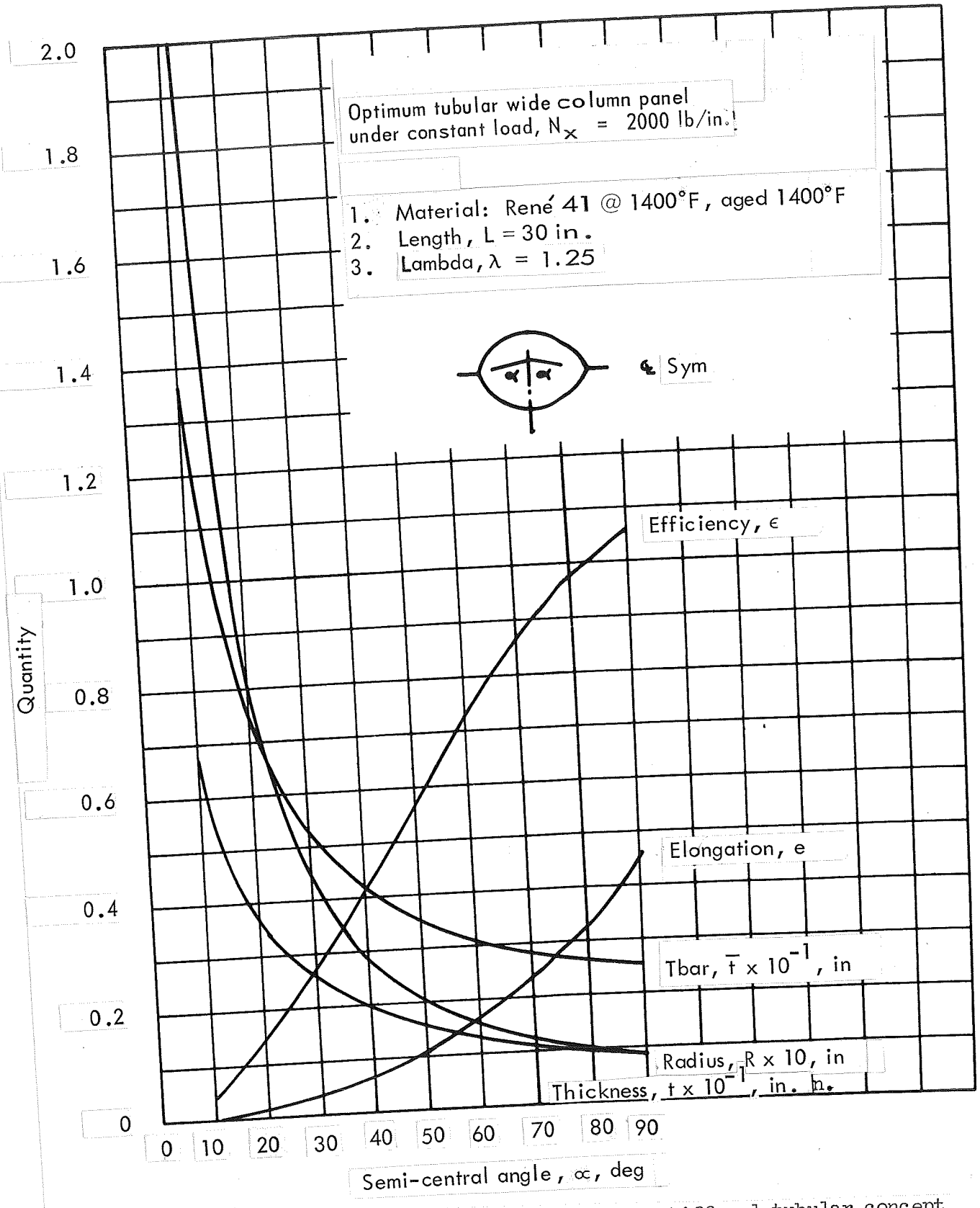

Figure 13-17. Optimum semimonocoque spanwise-stiffened tubular concept

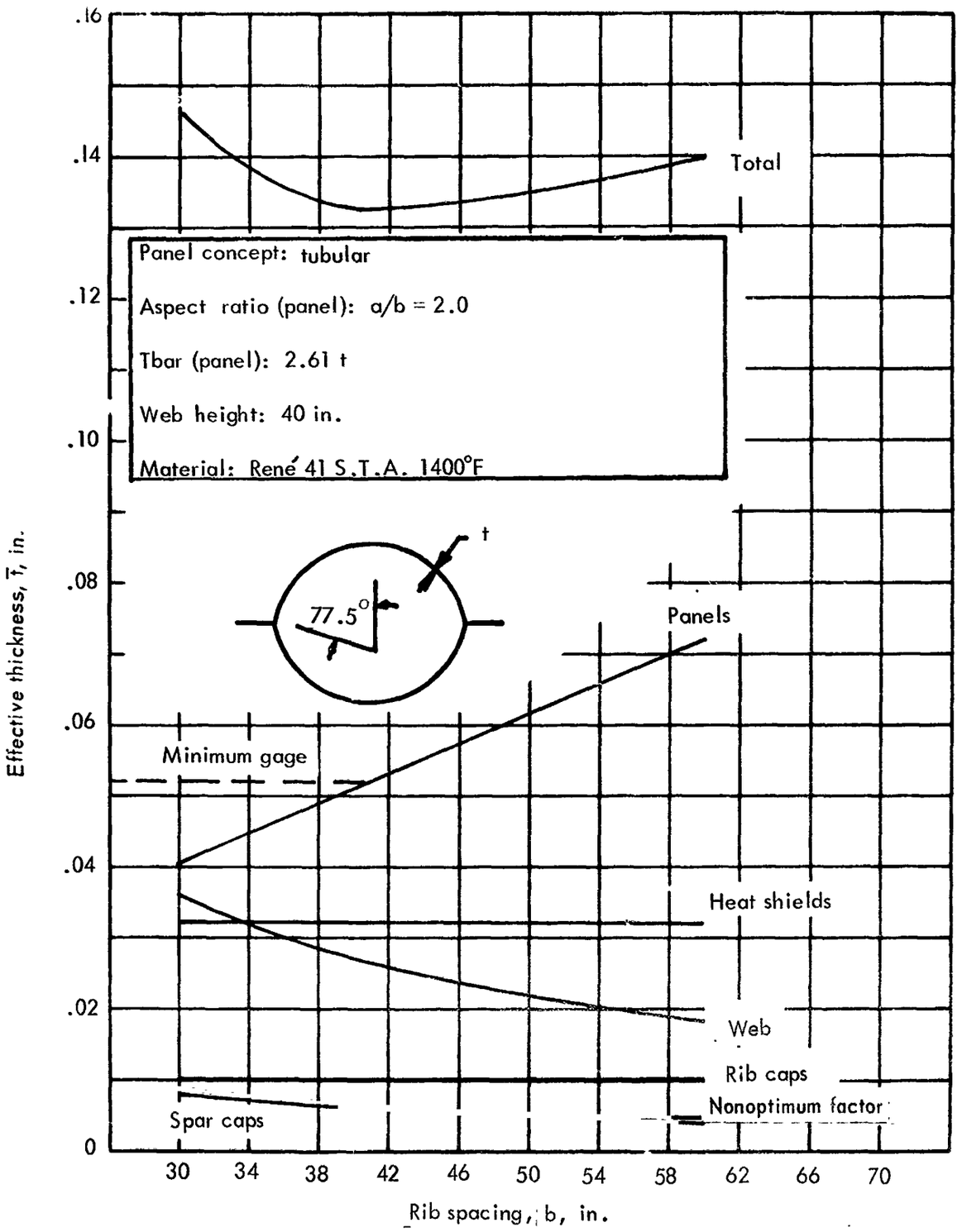

Figure 13-18. Weight optimization of semimonocoque spanwise-stiffened tubular panels, BL 120 to BL 212

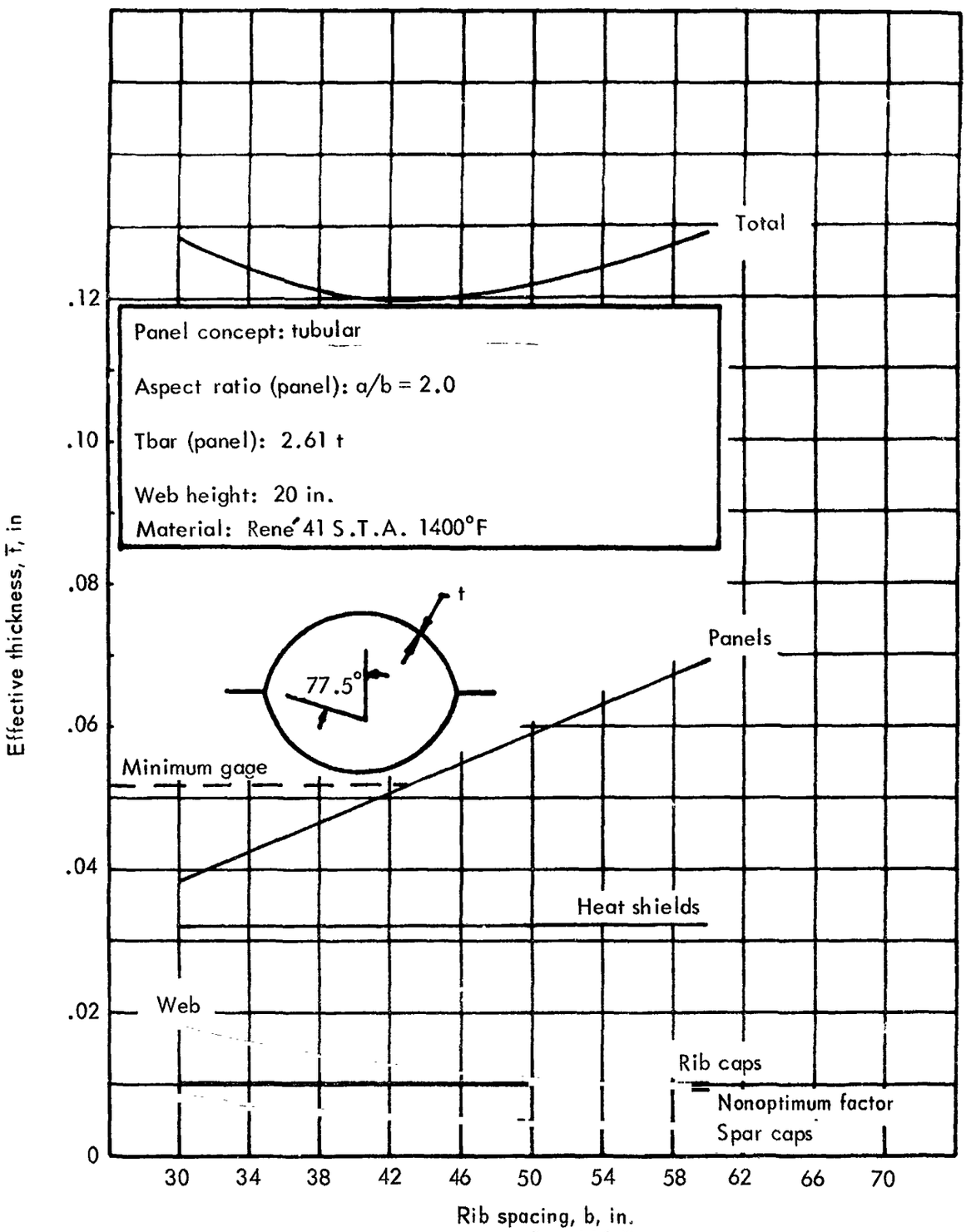

Figure 13-19. Weight optimization of semimonoque spanwise-stiffened tubular panels, BL 212 to BL 350

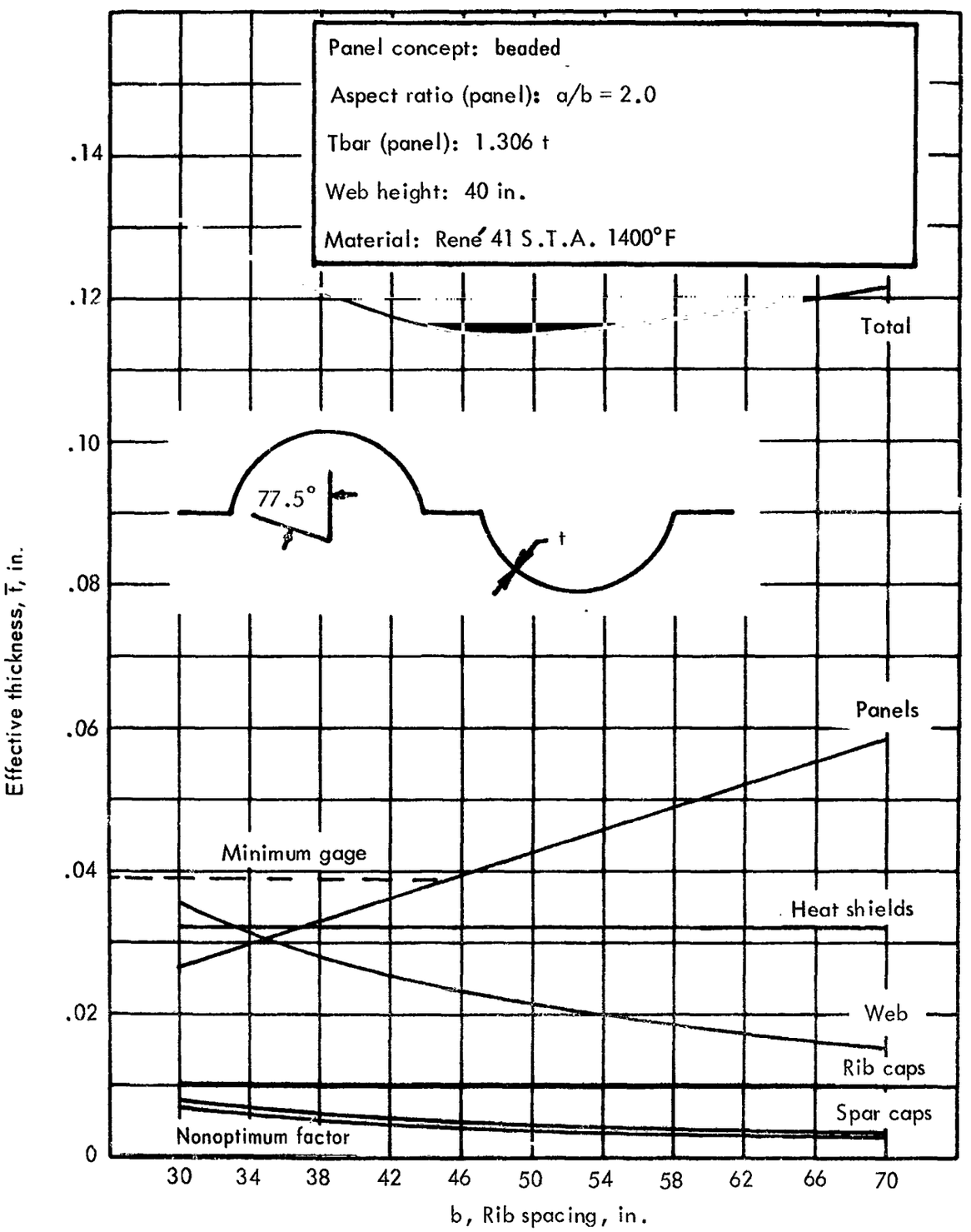

Figure 13-20. Weight optimization of semimonocoque spanwise-stiffened beaded panels, BL 120 to BL 212

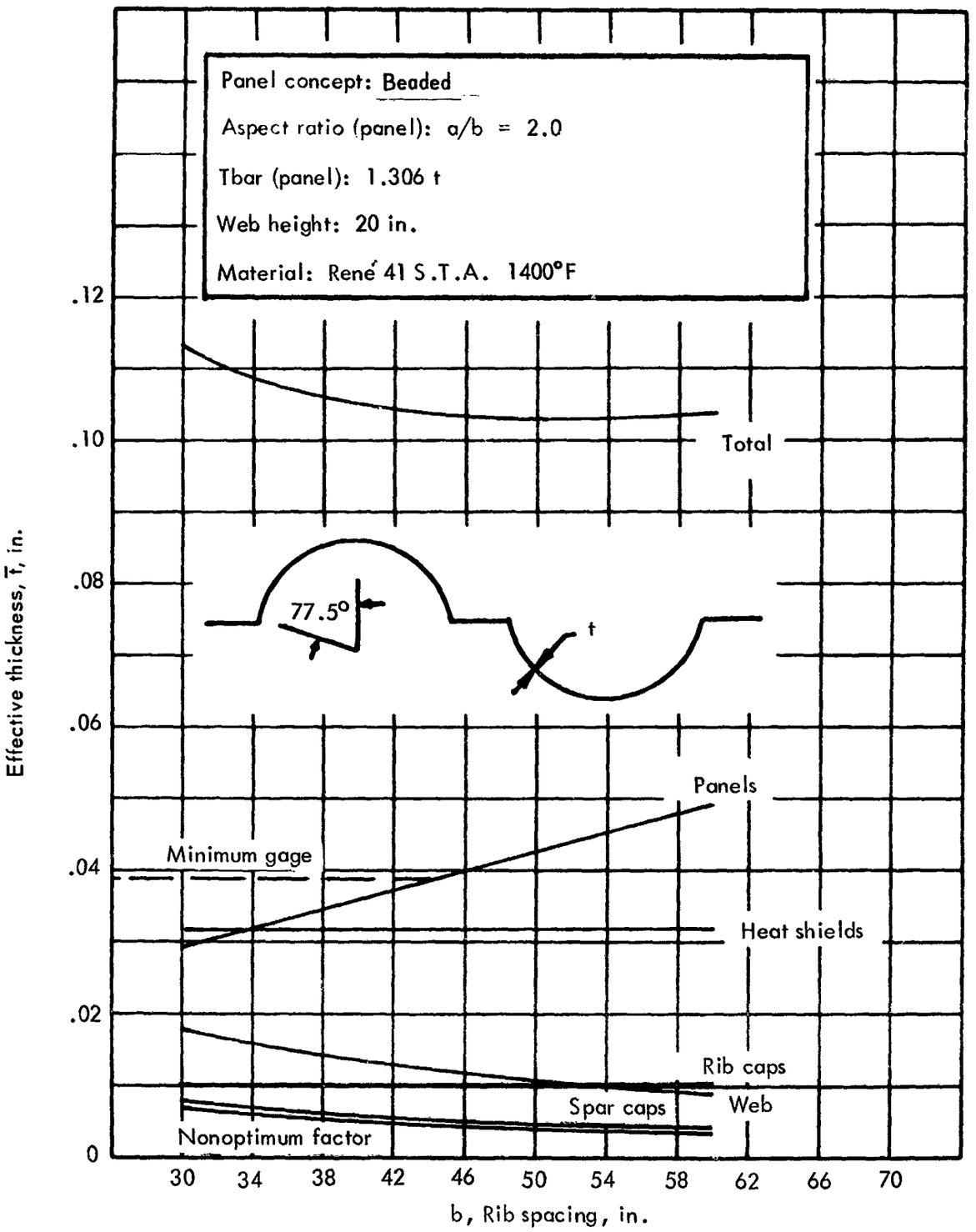

Figure 13-21. Weight optimization of semimonocoque spanwise-stiffened beaded panels, BL 212 to BL 350

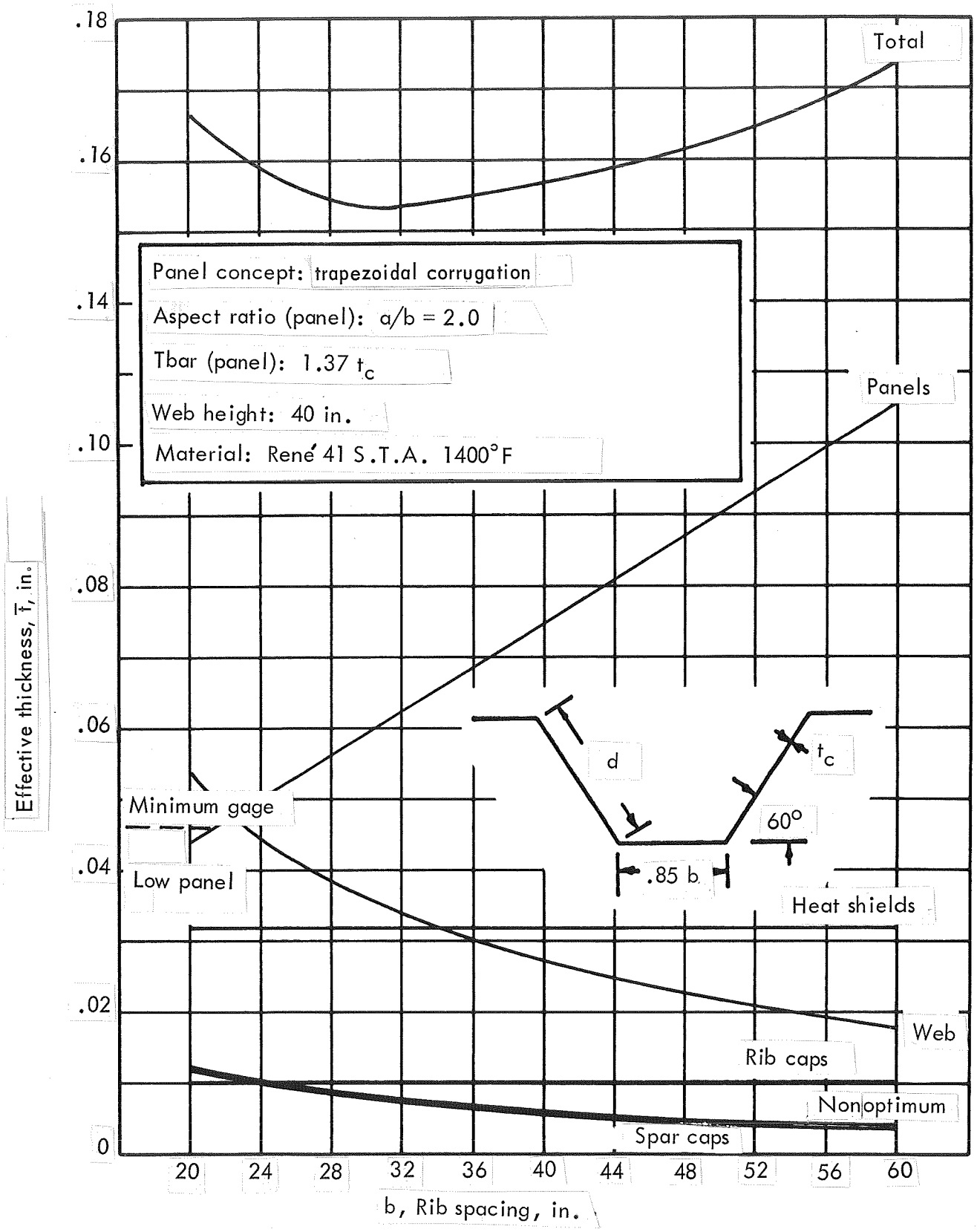

Figure 13-22. Weight optimization of semimonocoque spanwise-trapezoidal-corrugated panels, BL 120 to BL 212

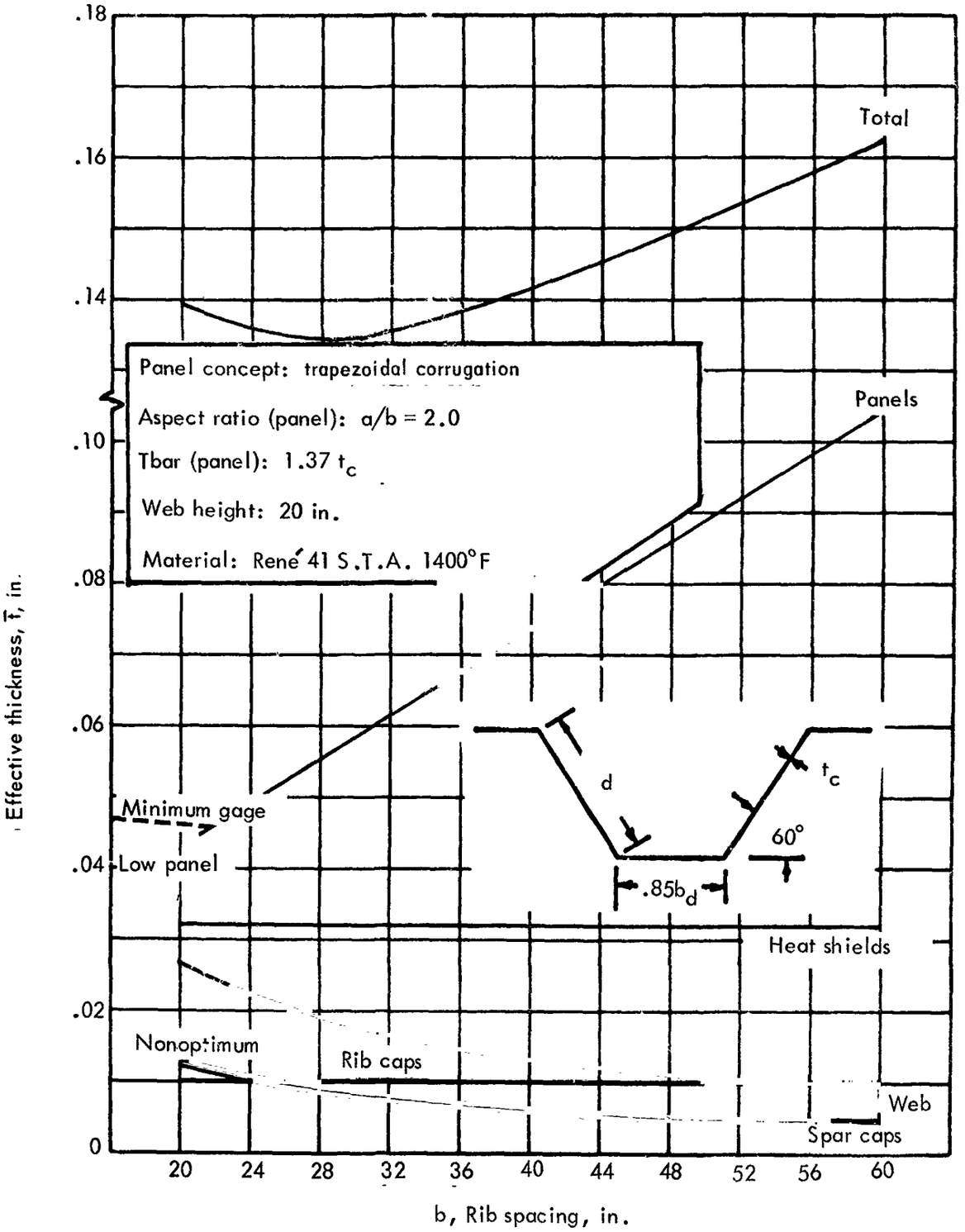

Figure 13-23. Weight optimization of semimonocoque spanwise trapezoidal-corrugated panels, BL 212 to BL 350

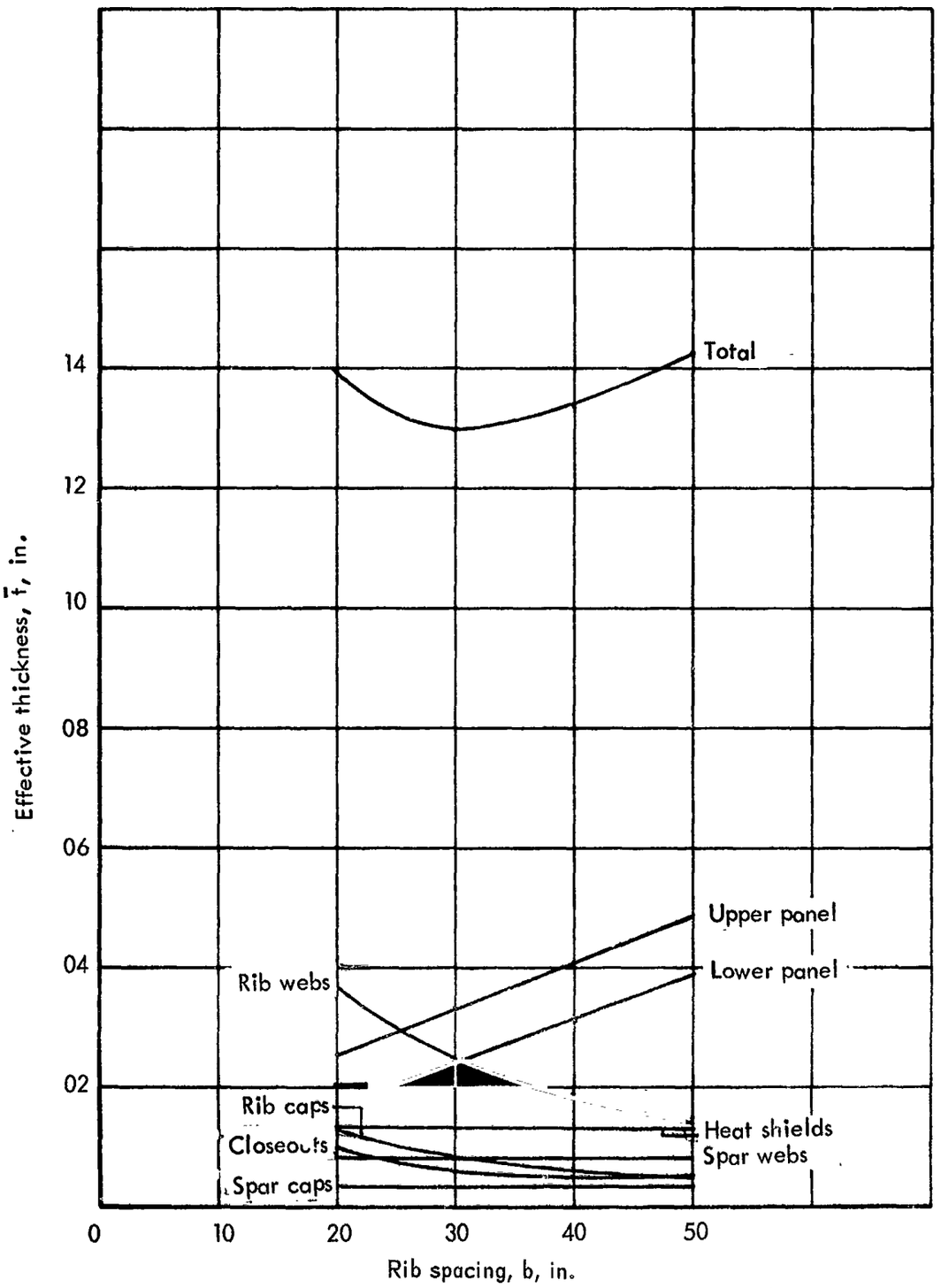

Figure 13-24. Weight optimization of wing area A ($\mathcal{L}$ to BL 120) of semimonocoque spanwise trapezoidal-corrugated panels, insulation outboard lower surface

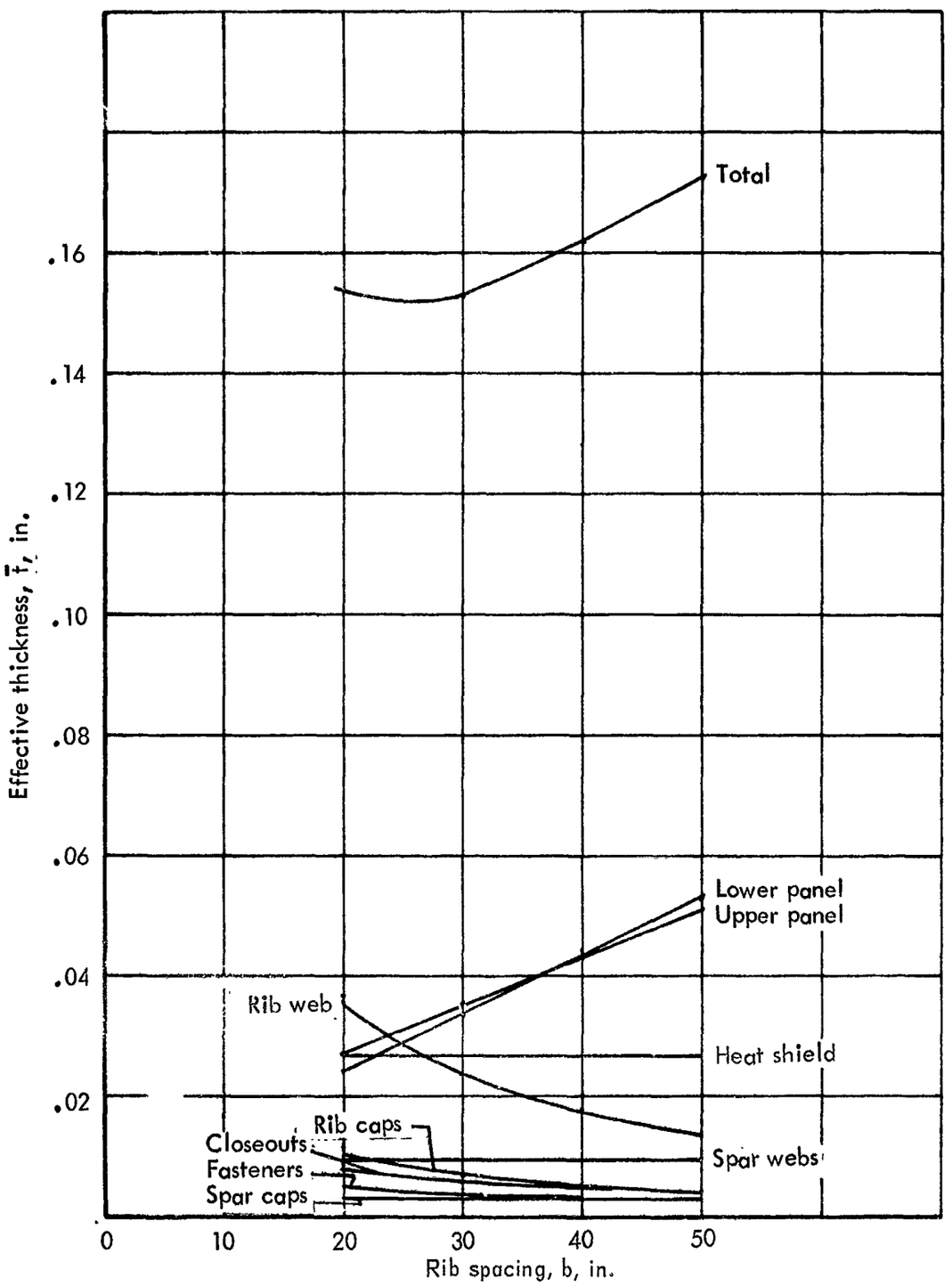

Figure 13-25. Weight optimization of wing area B (BL 120 to BL 212) of semi-monocoque spanwise trapezoidal-corrugated panels, insulation outboard lower surface

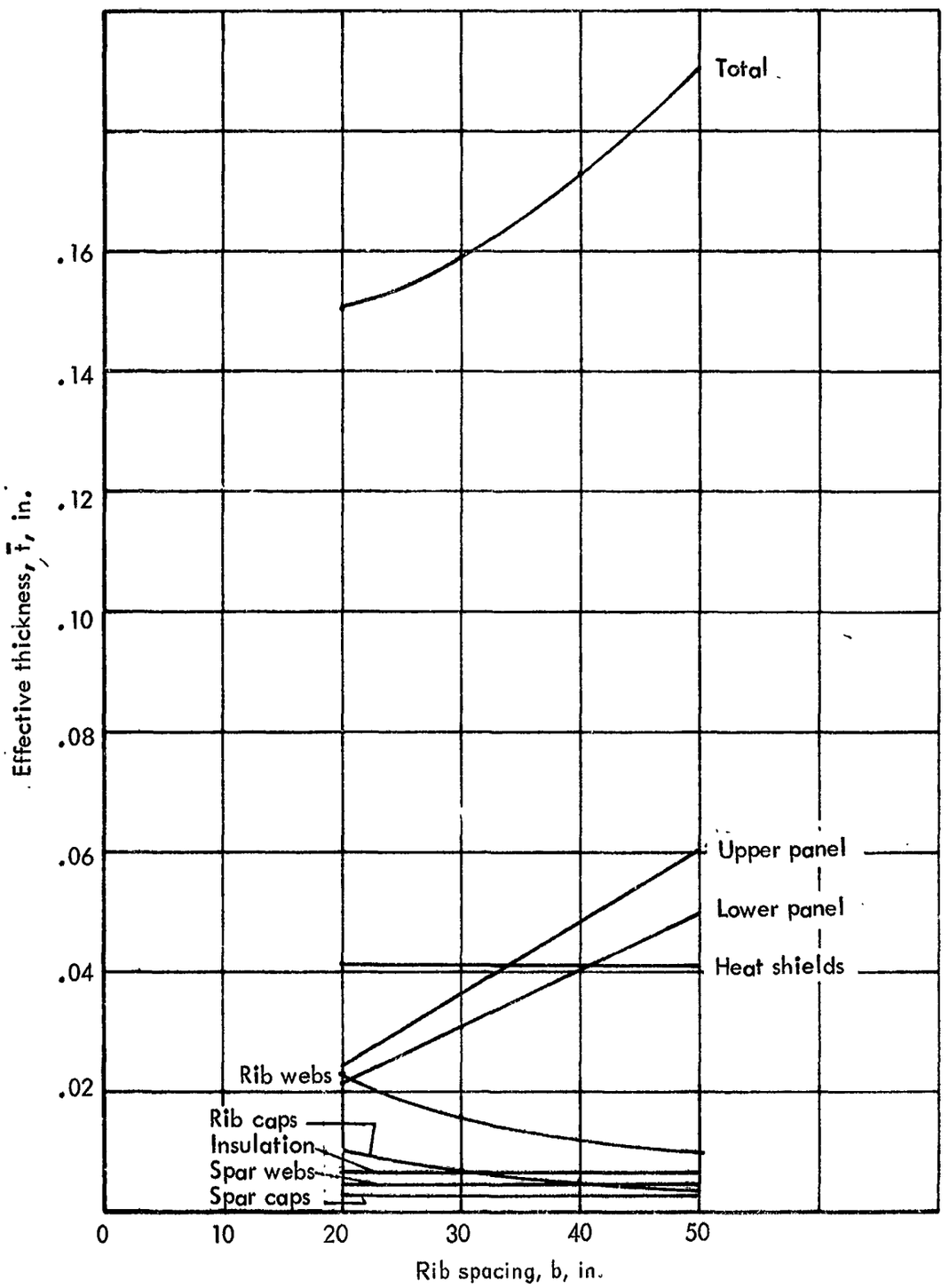

Figure 13-26. Weight optimization of wing area C (BL 212 to BL 350) of semi-monocoque spanwise trapezoidal-corrugated panels, insulation outboard lower surface

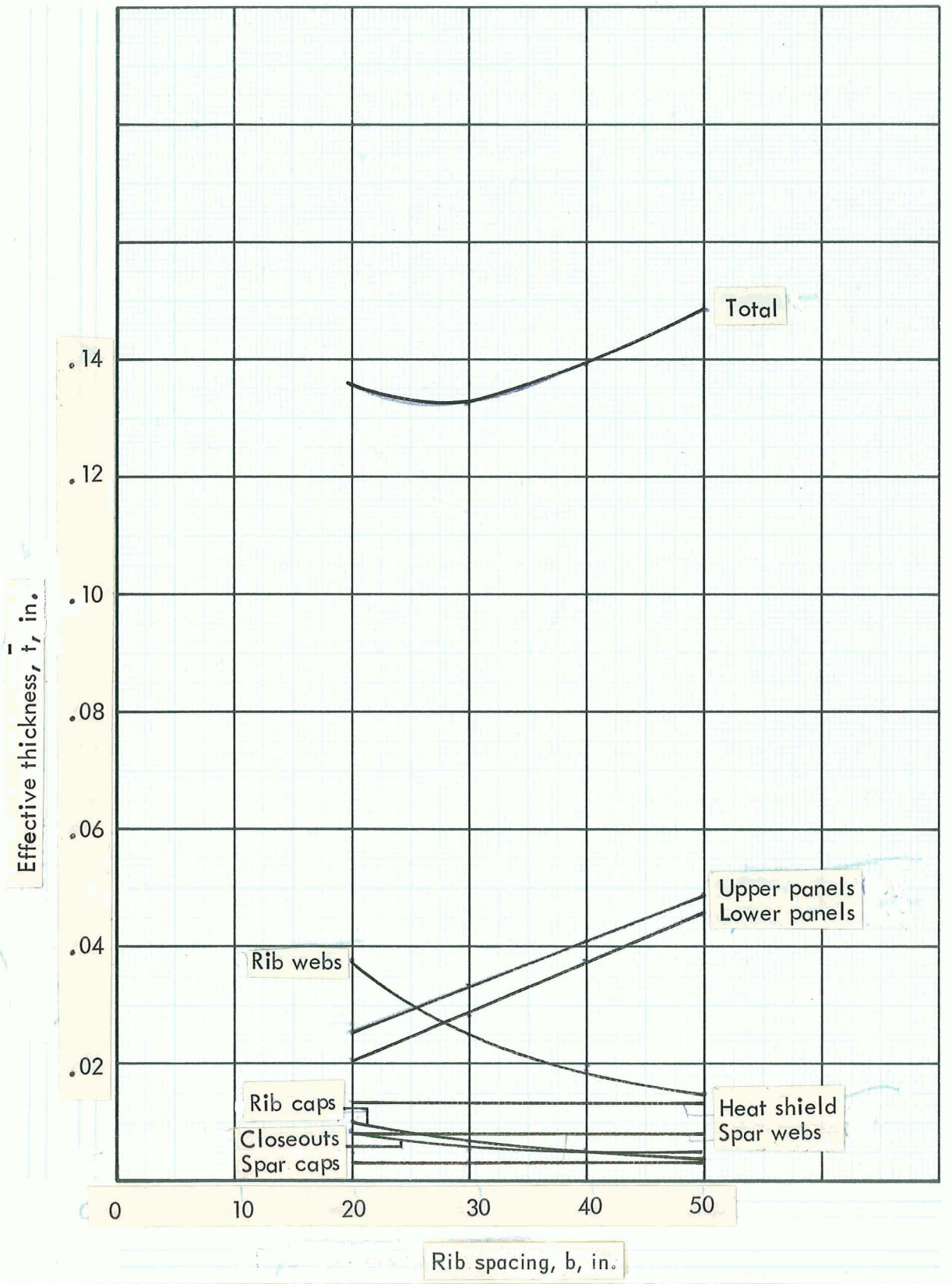

Figure 13-27. Weight optimization of wing area A ($\mathcal{L}$ to BL 120) of semimonocoque spanwise trapezoidal-corrugated panels, no insulation

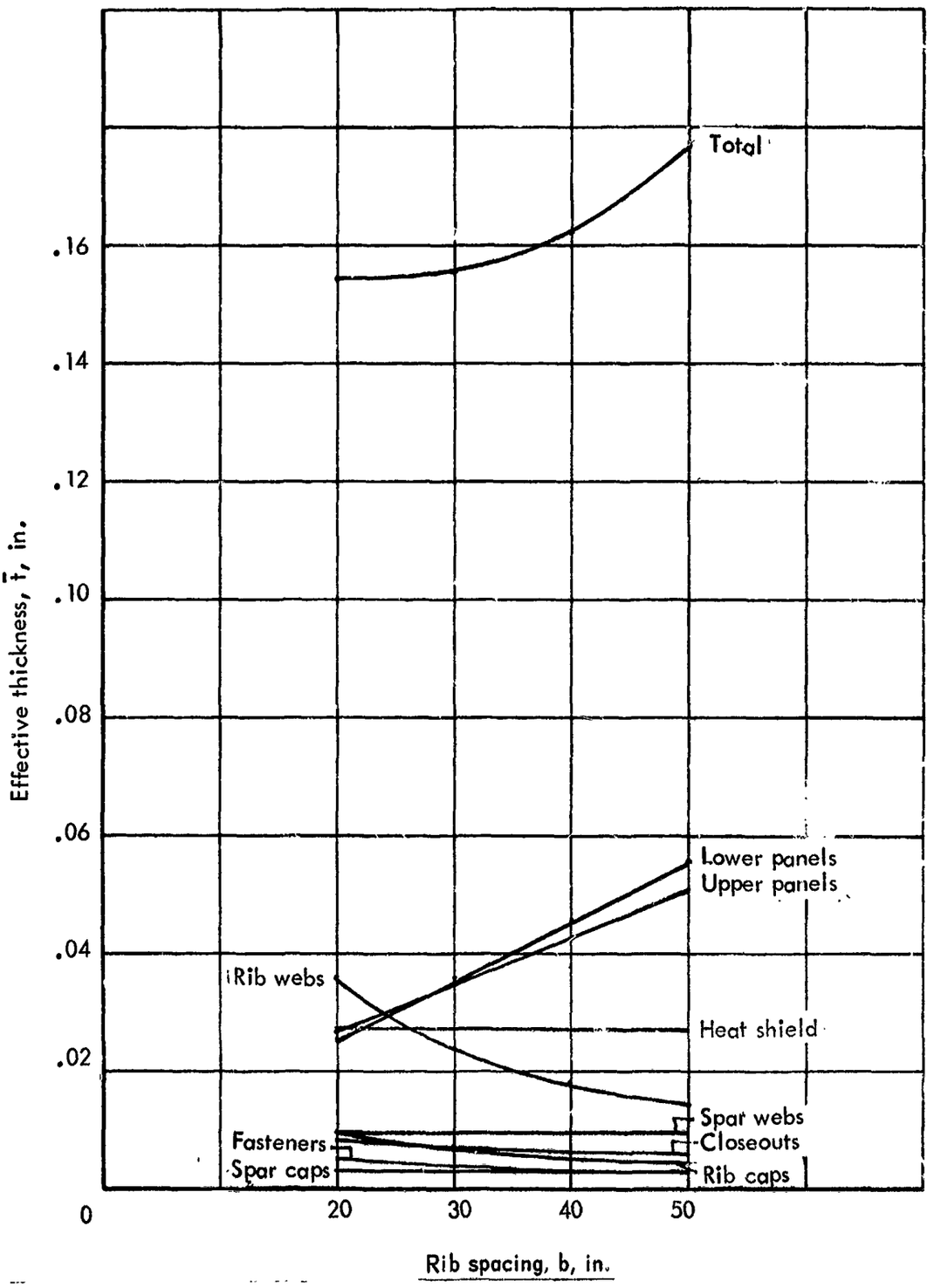

Figure 13-28. Weight optimization of wing Area B (BL 120 to BL 212) of semi-monocoque spanwise trapezoidal-corrugated panels, no insulation

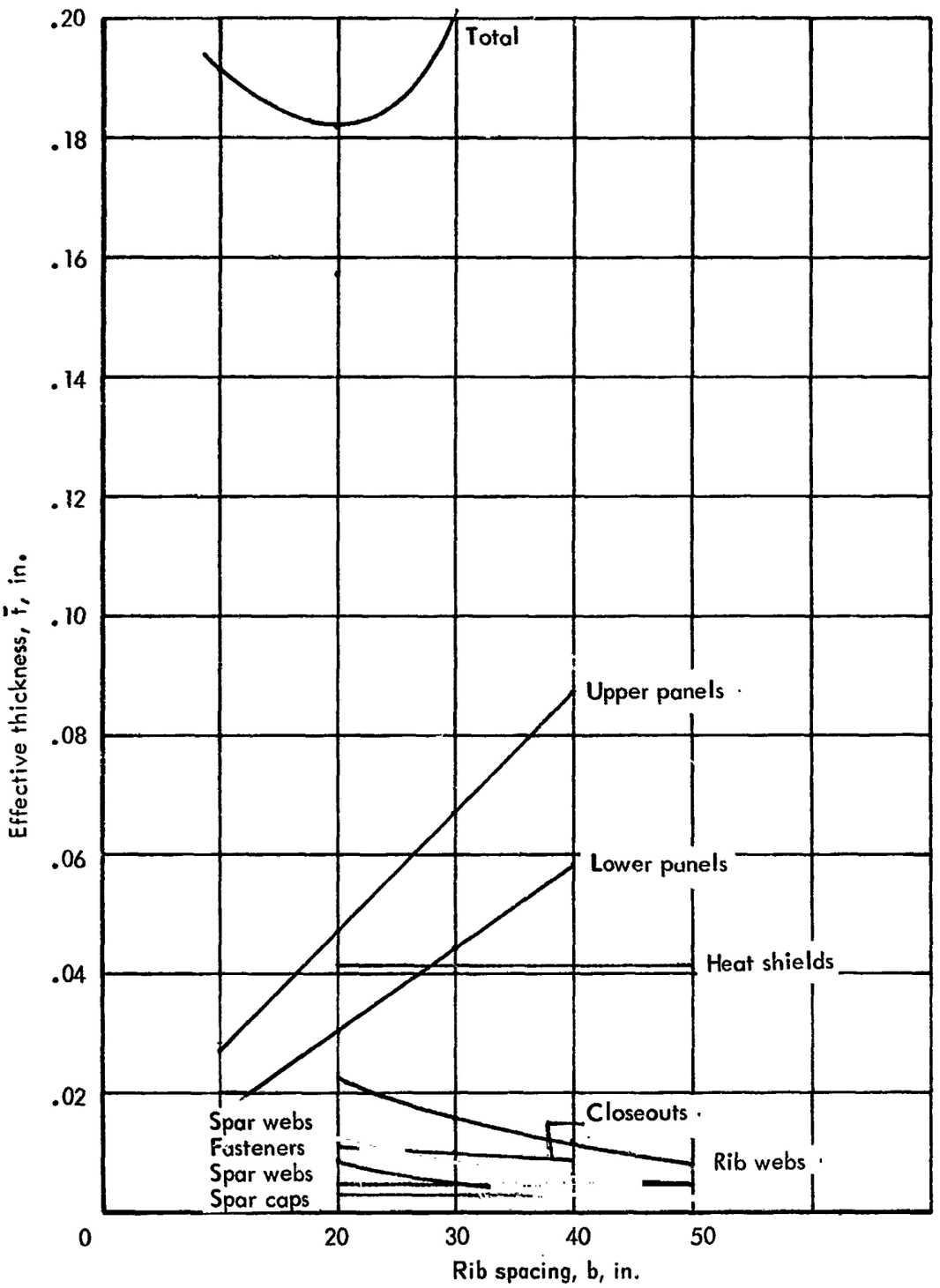

Figure 13-29. Weight optimization of wing C (BL 212 to BL 350) of semimonocoque spanwise trapezoidal-corrugated panels, no insulation

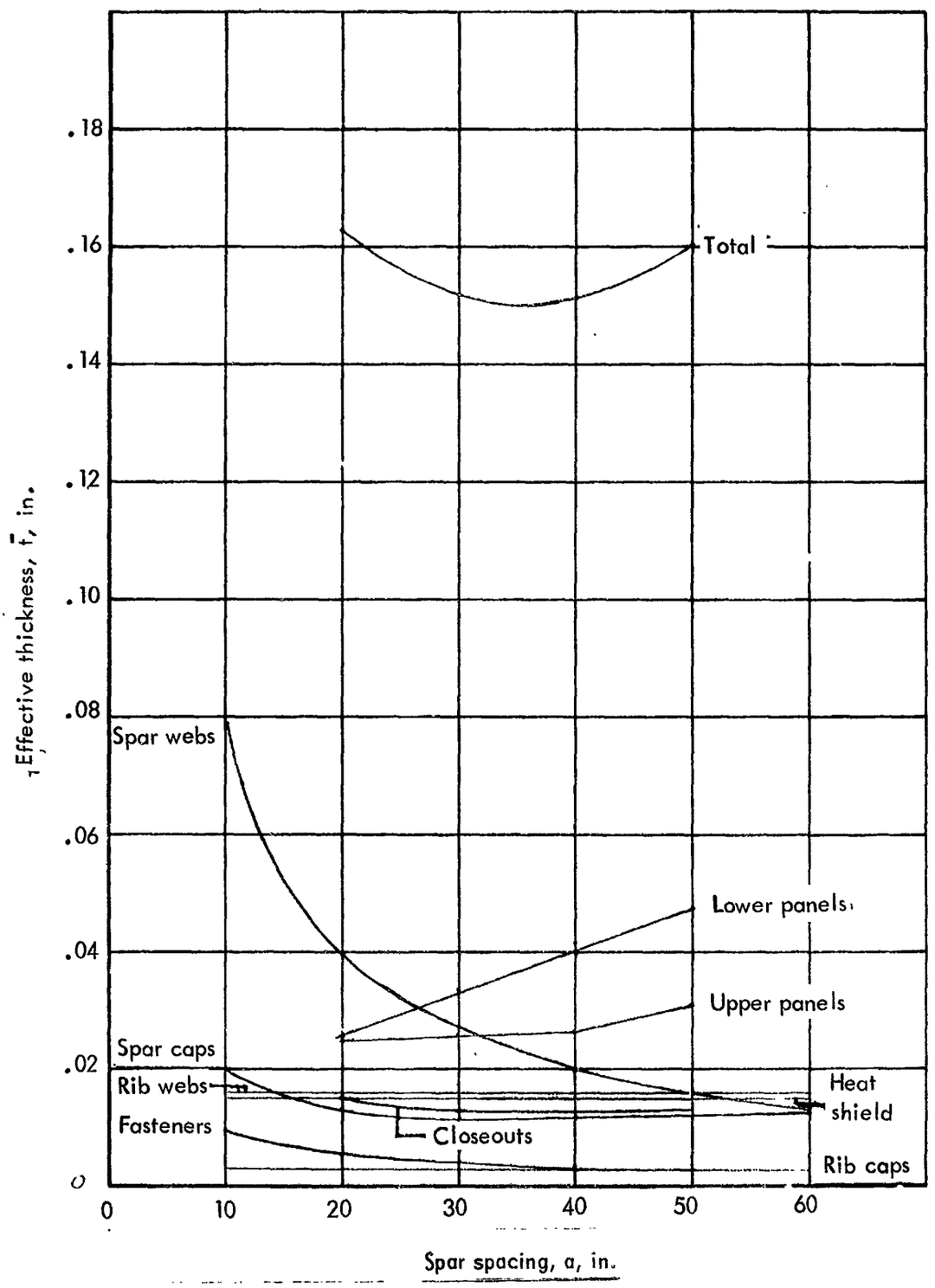

Figure 13-30. Weight optimization of wing area A ($\mathbb{Q}$ to BL 120) of semimonocoque chordwise-stiffened tubular panels, no insulation

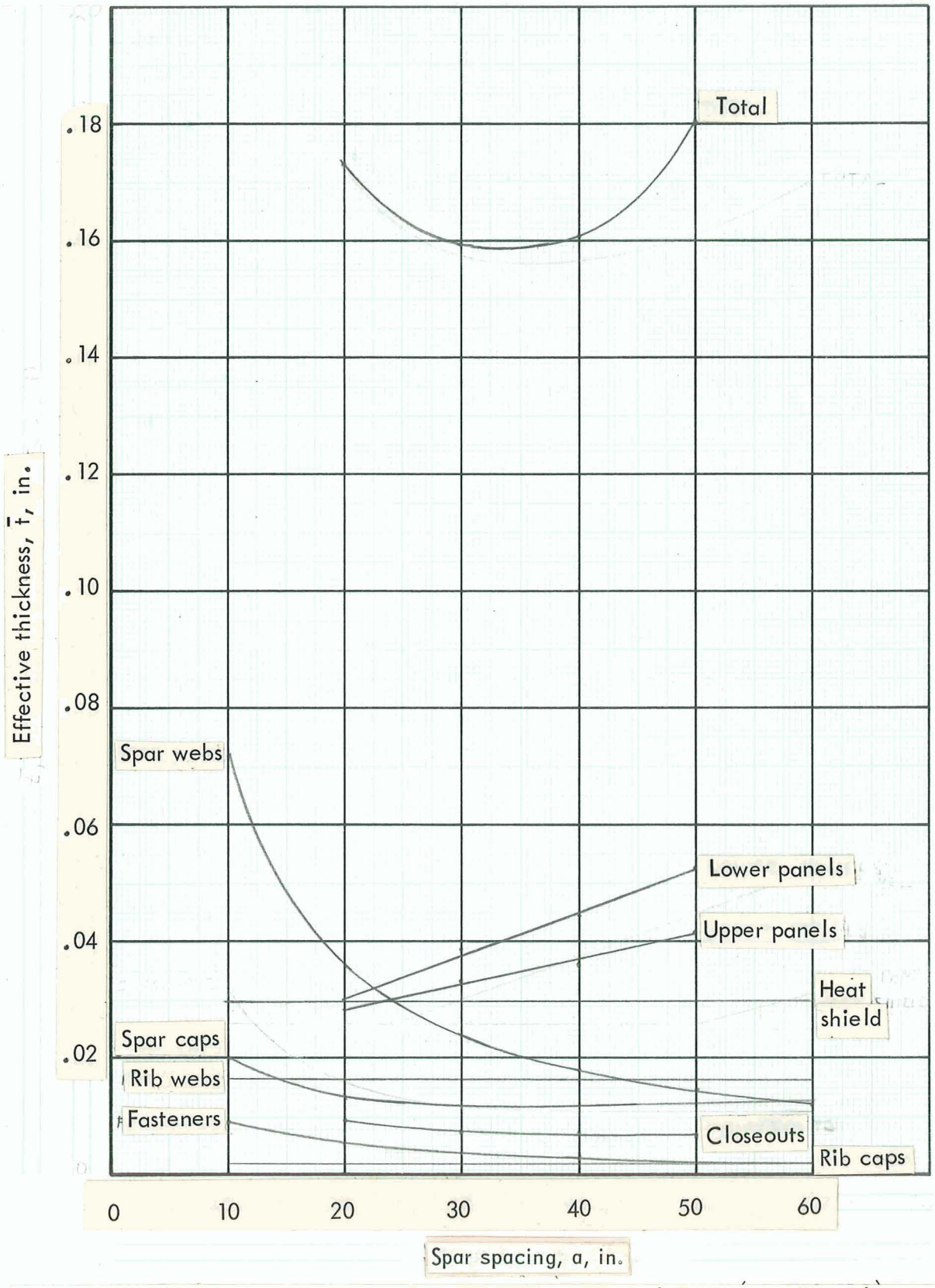

Figure 13-31. Weight optimization of wing area B (BL 120 to BL 212) of semi-monocoque chordwise-stiffened tubular panels, no insulation

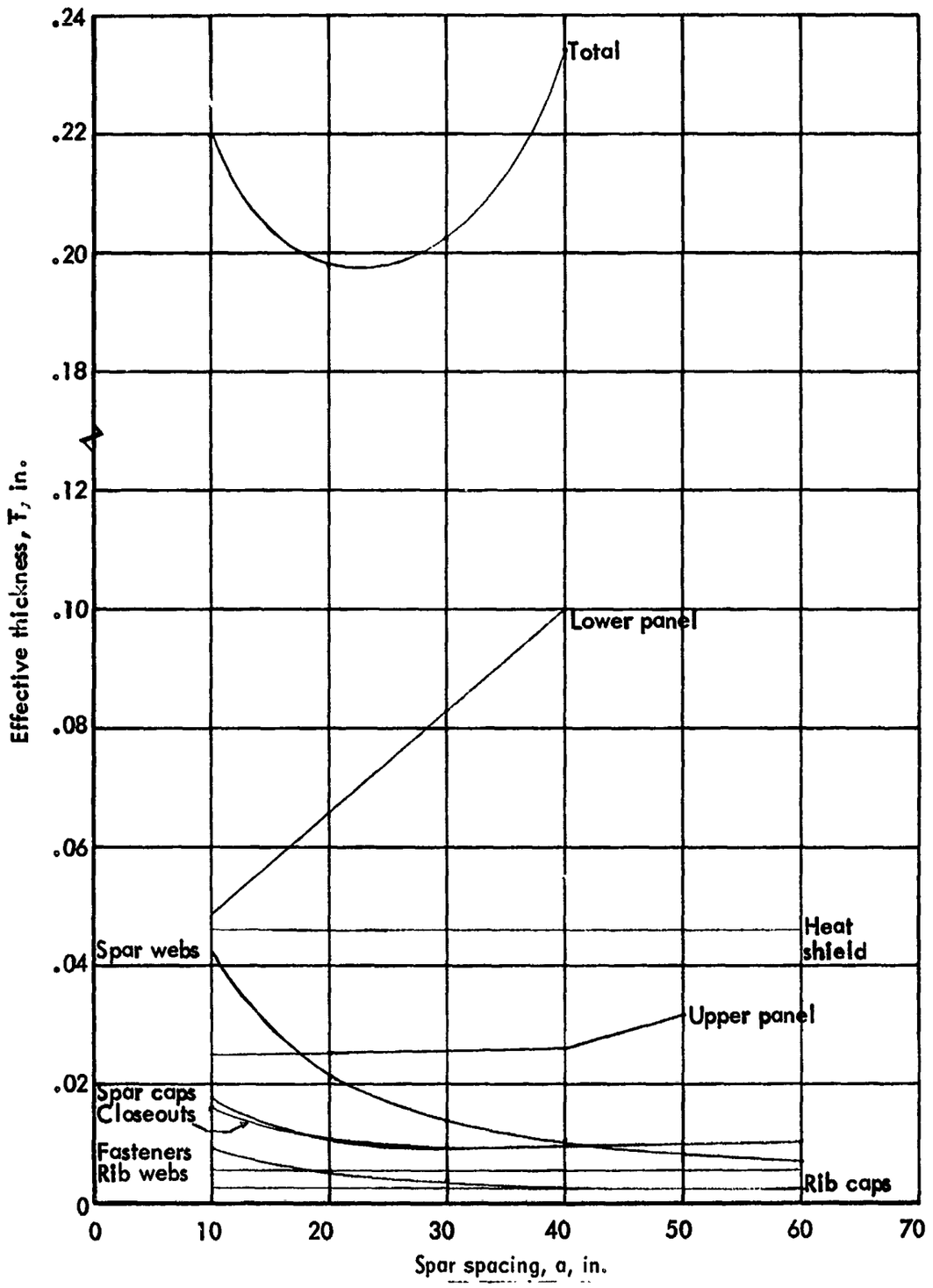

Figure 13-32. Weight optimization of wing area C (BL 212 to BL 350) of semi-monocoque chordwise-stiffened tubular panels, no insulation

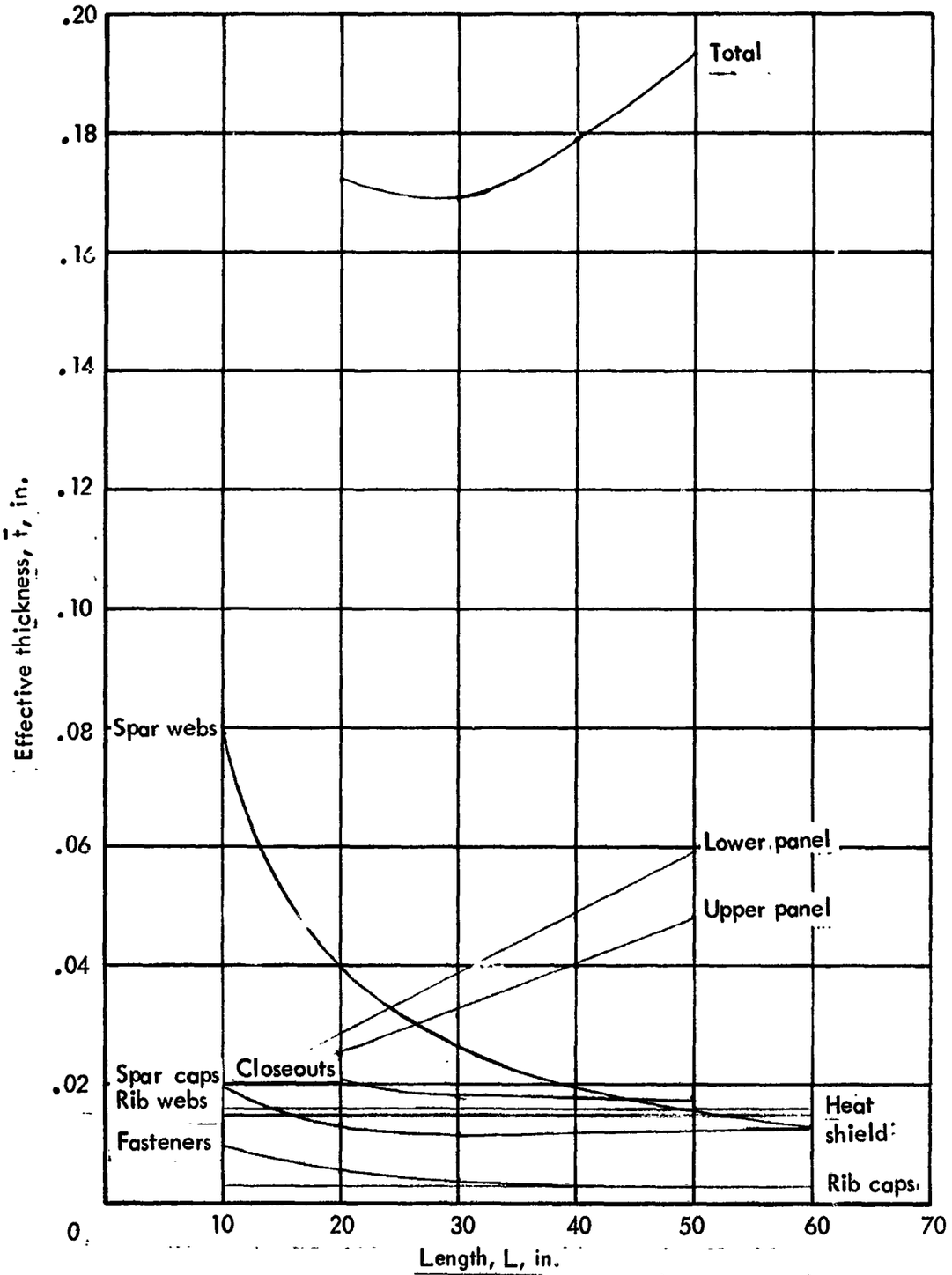

Figure 13-33. Weight optimization of wing area A (℄ to BL 120) of semimonocoque chordwise-stiffened tubular panels, with insulation

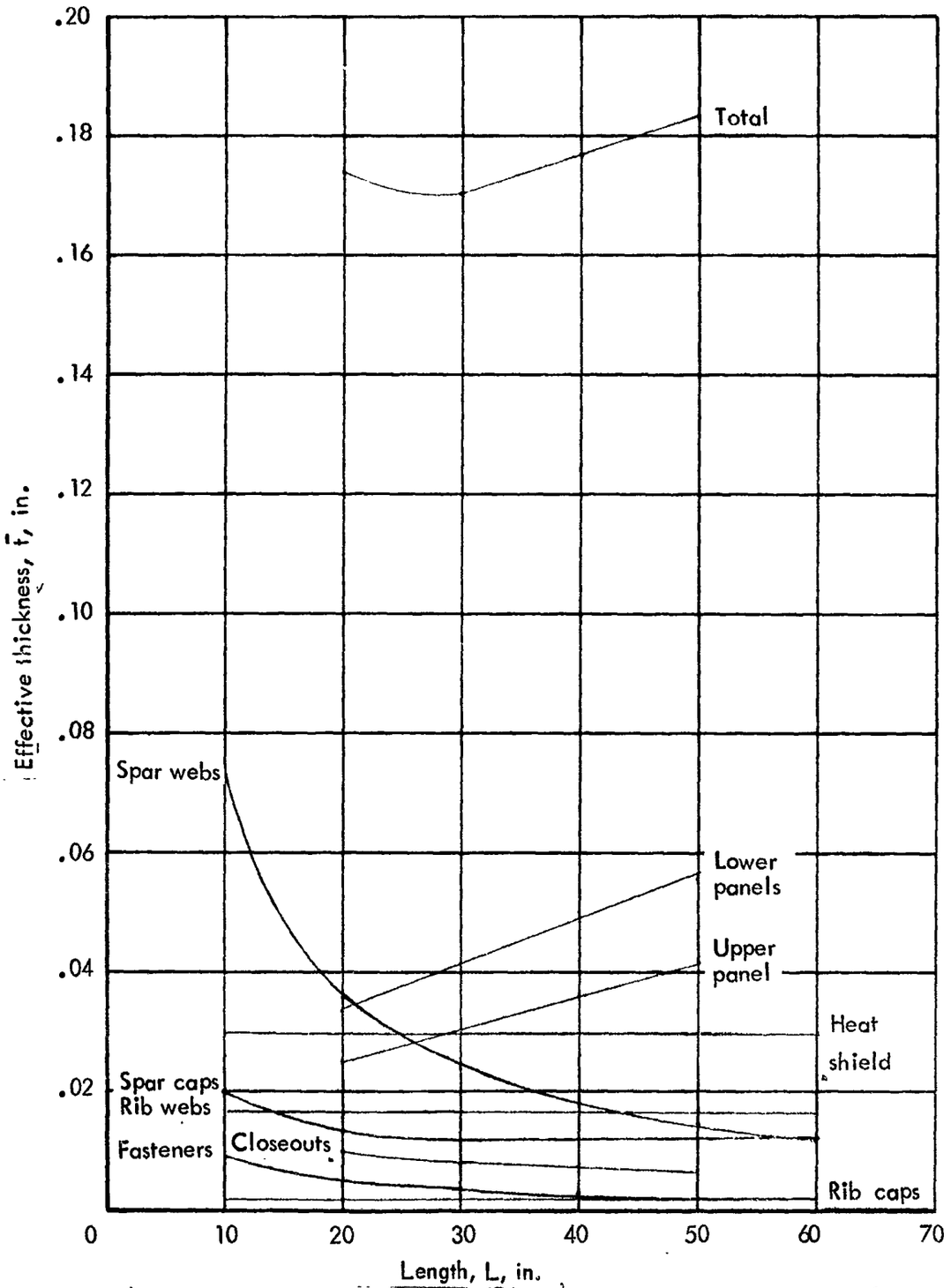

Figure 13-34. Weight optimization of wing area B (BL 120 to BL 212) of semi-monocoque chordwise-stiffened tubular panels, with insulation

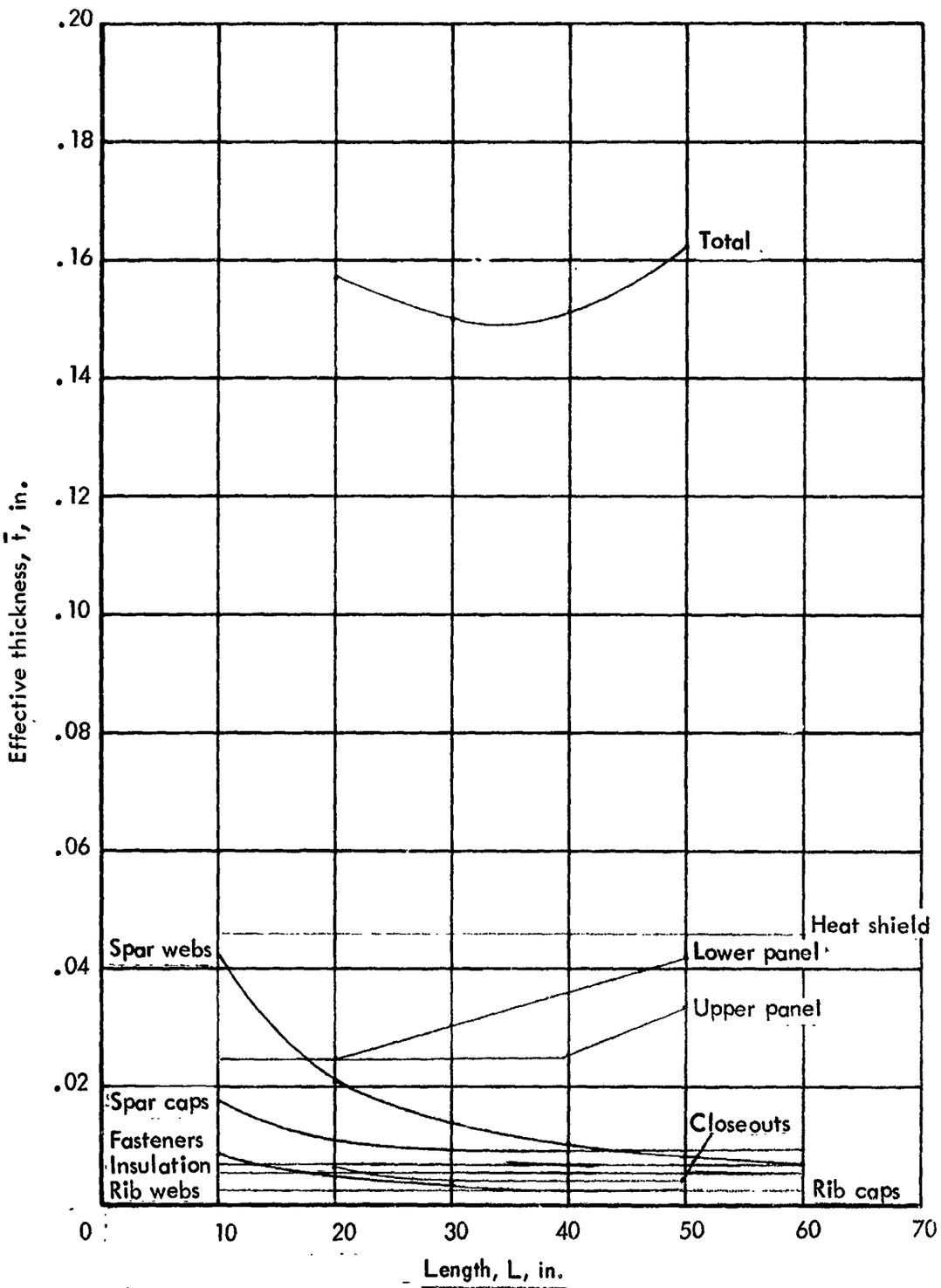

Figure 13-35. Weight optimization of wing area C (BL 212 to BL 350) of semi-monocoque chordwise-stiffened tubular panels, with insulation

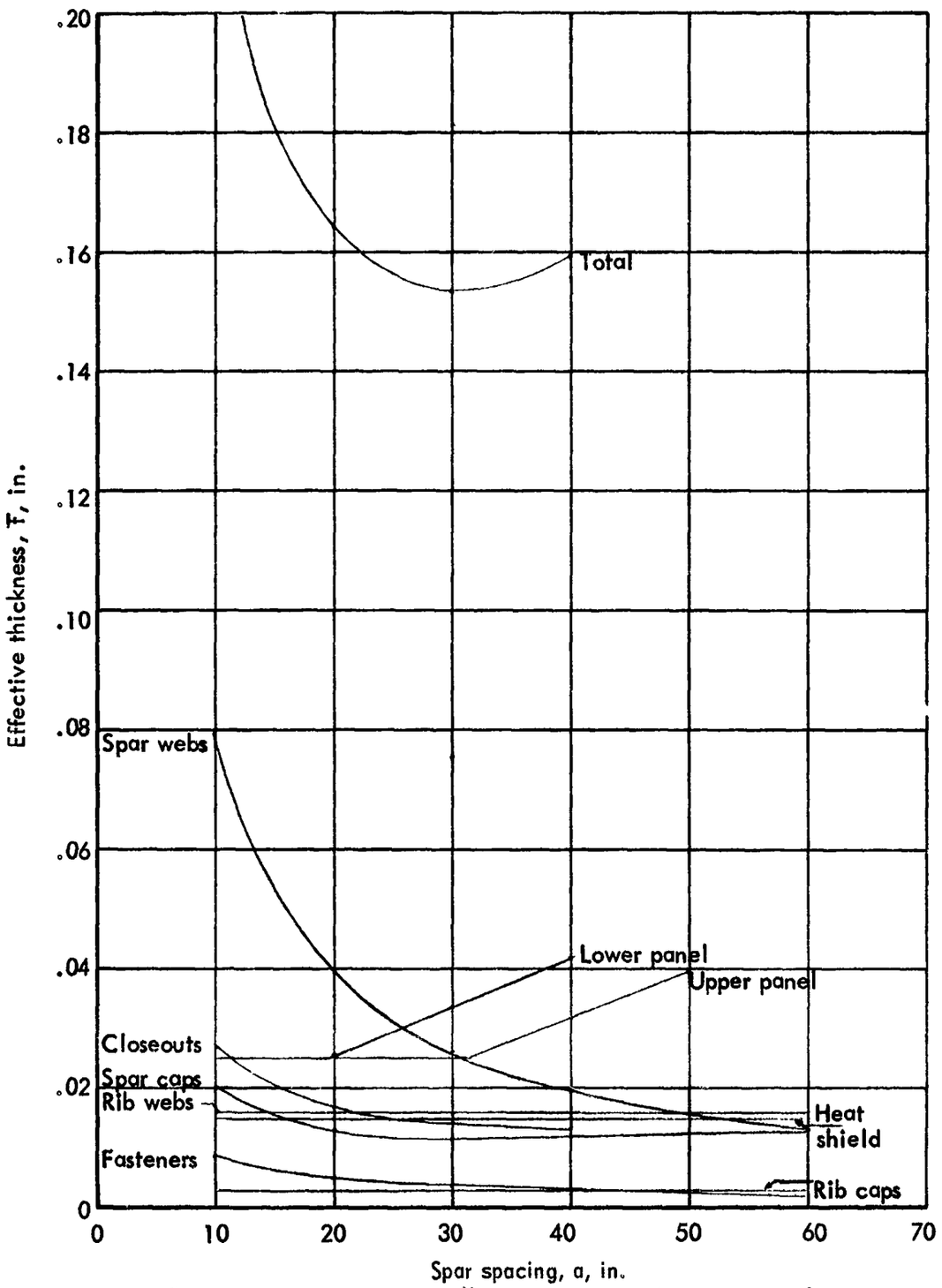

Figure 13-36. Weight optimization of wing area A (℄ to BL 120) of semimonocoque chordwise-stiffened convex-beaded upper/tubular lower panels, no insulation

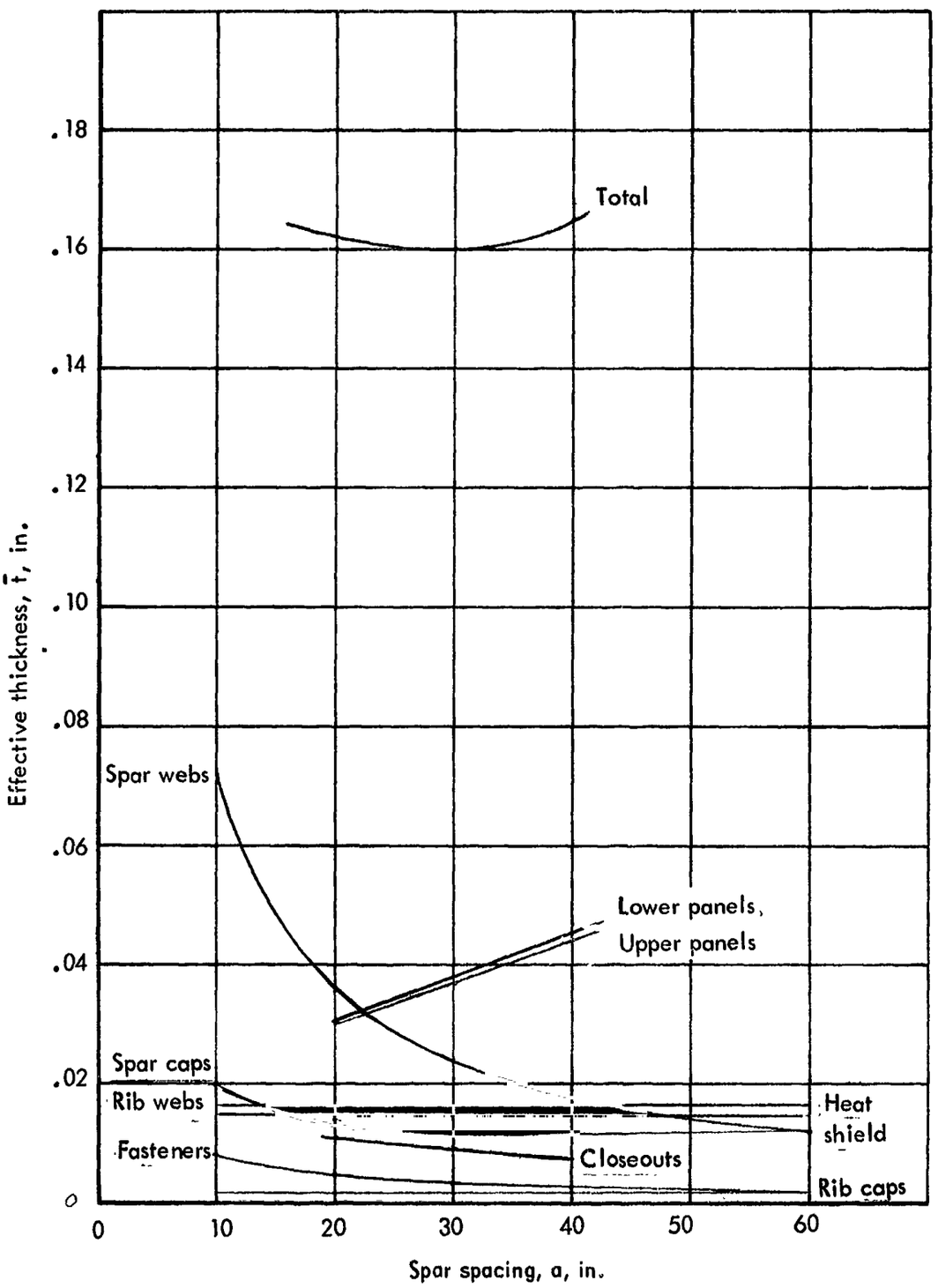

Figure 13-37. Weight optimization of wing area B (BL 120 to BL 212) of semi-monocoque chordwise-stiffened convex-beaded upper/tubular lower panels, no insulation

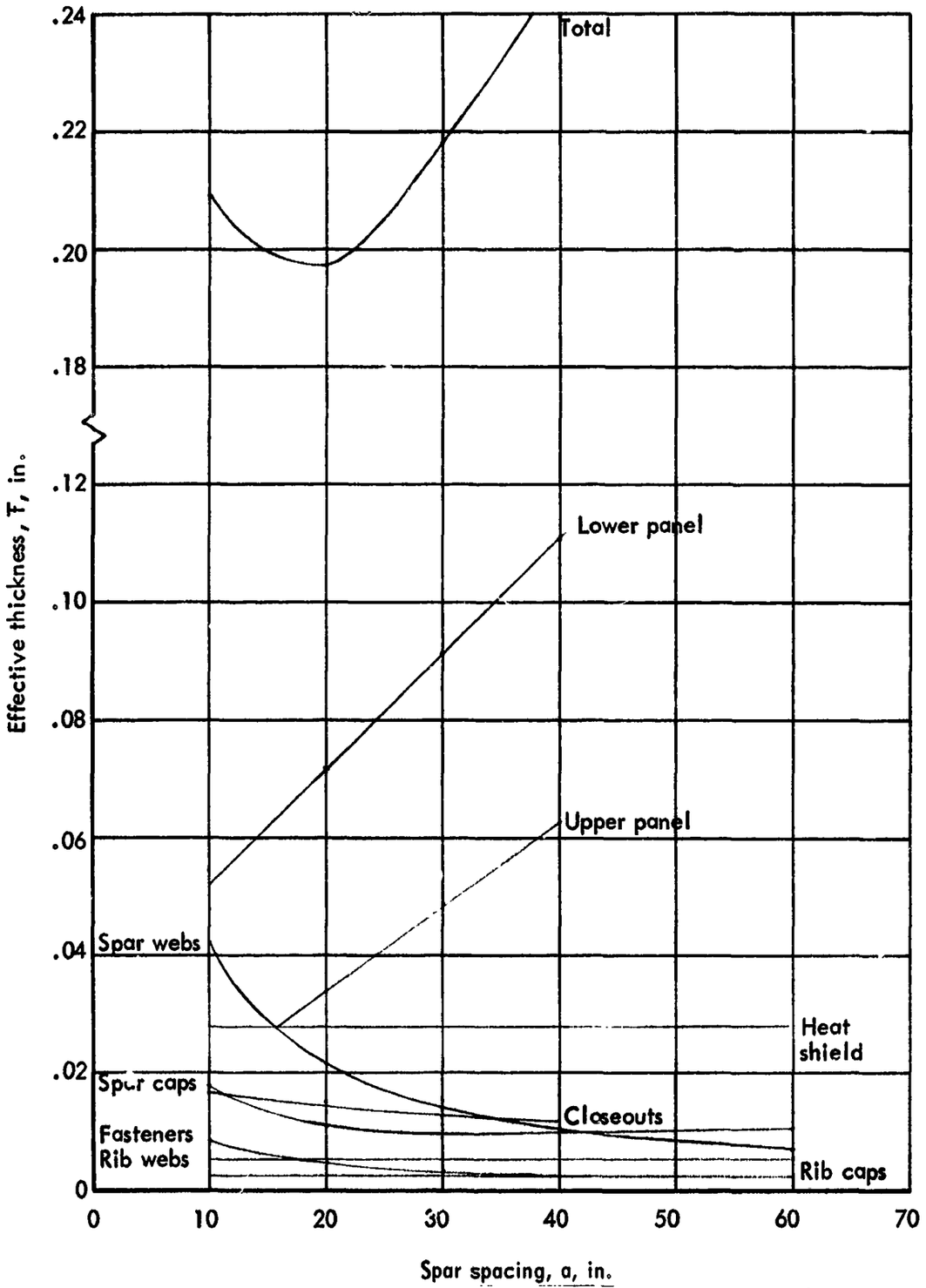

Figure 13-38. Weight optimization of wing area C (BL 212 to BL 350) of semi-monocoque chordwise-stiffened convex-beaded upper/tubular lower panels, no insulation

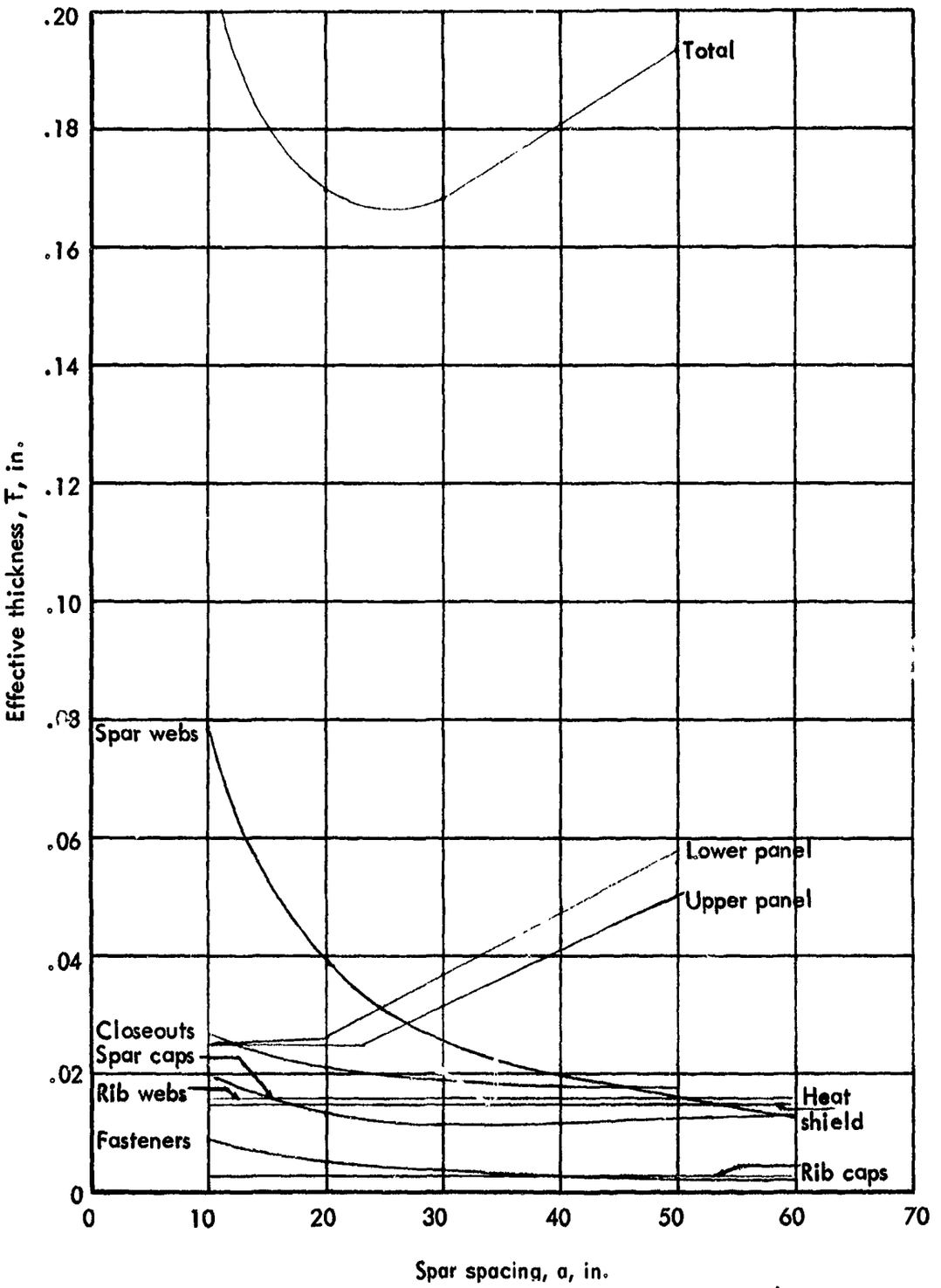

Figure 13-39. Weight optimization of wing area A (℄ to BL 120) of semimonocoque chordwise-stiffened convex-beaded upper/tubular lower panels, with insulatio

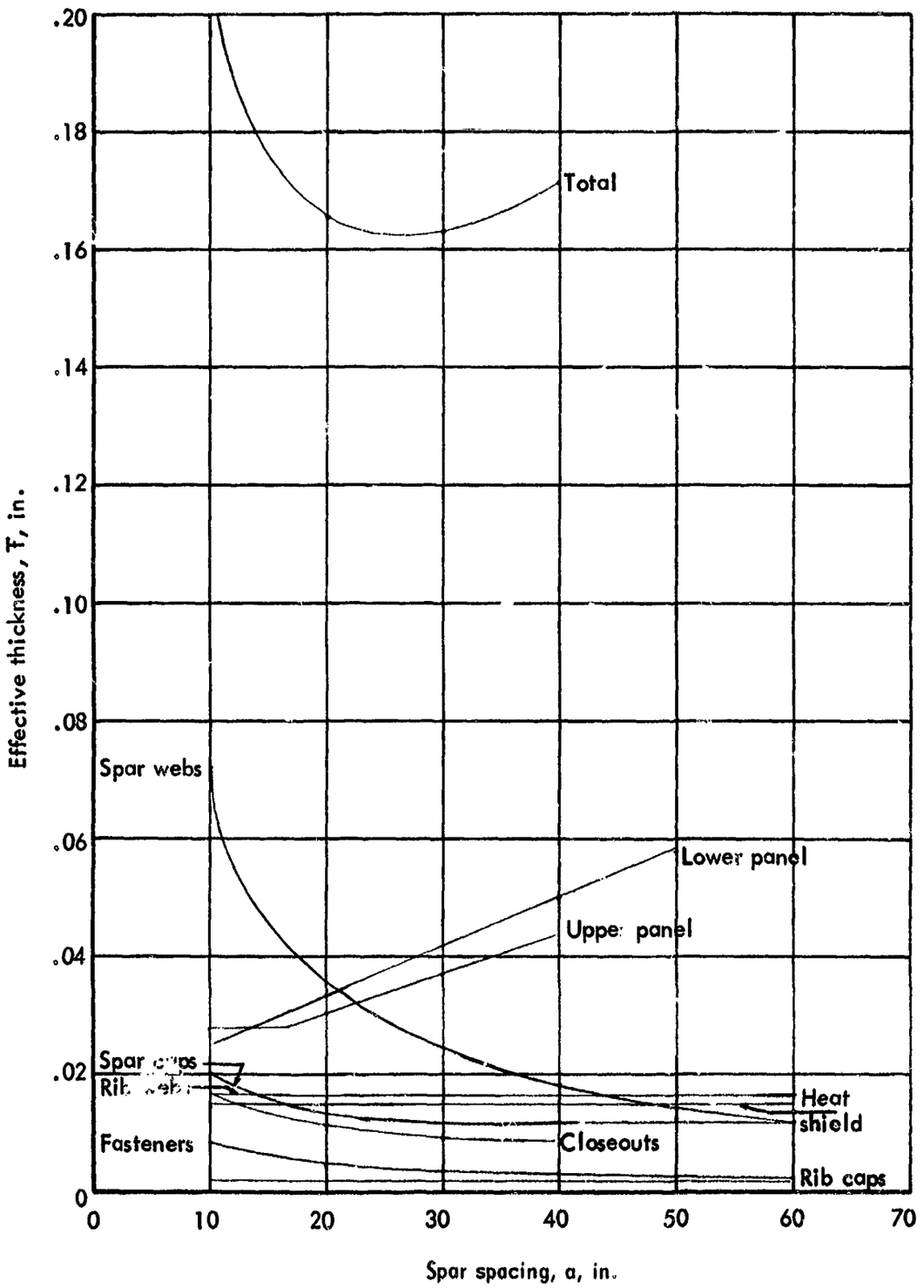

Figure 13-40. Weight optimization of wing area B (BL 120 to BL 212) of semi-monocoque chordwise-stiffened convex-beaded upper/tubular lower, with insulation

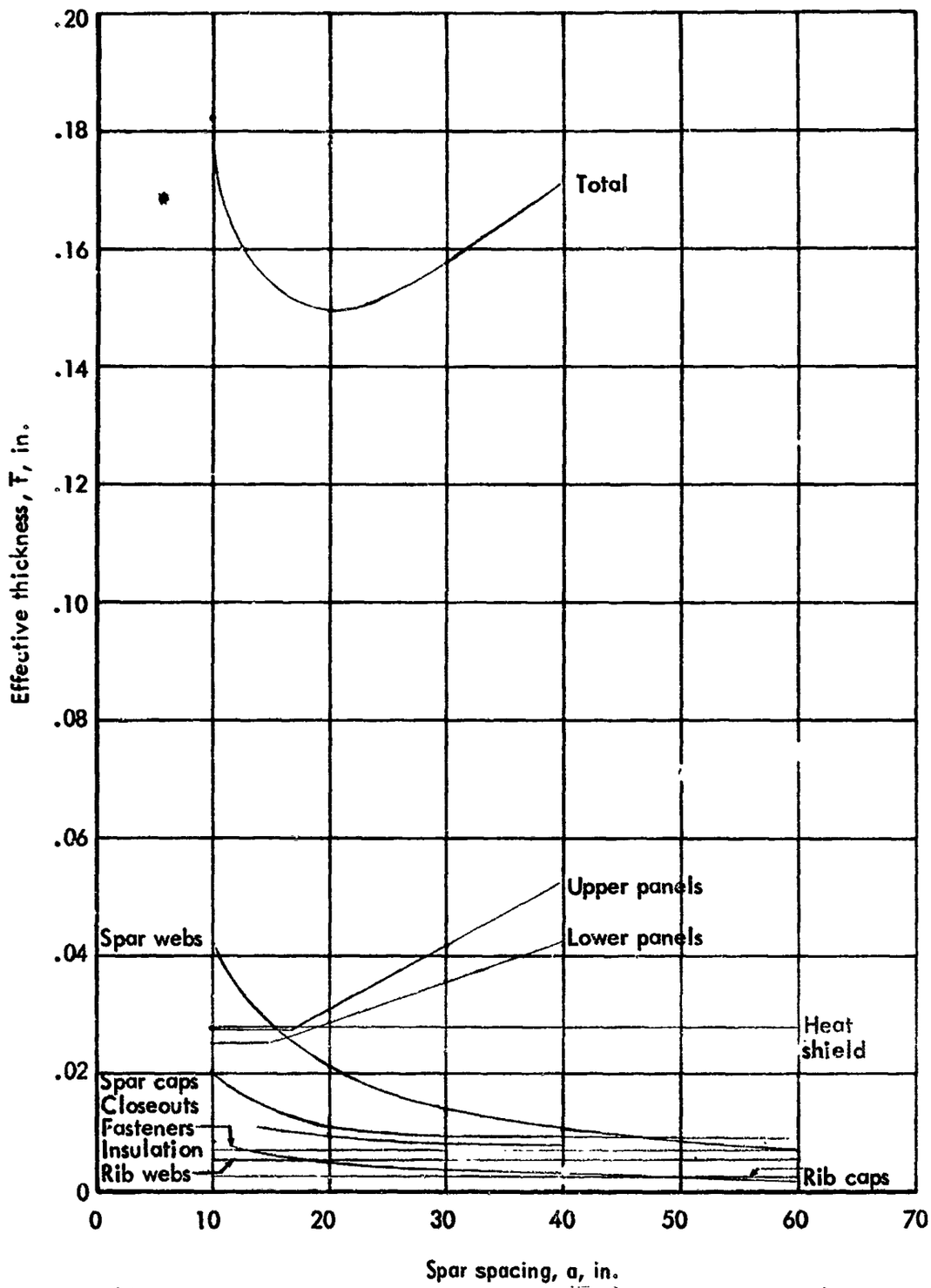

Figure 13-41. Weight optimization of wing area C (BL 212 to BL 350) of semi-monocoque chordwise-stiffened convex-beaded upper/tubular lower panels, with insulation

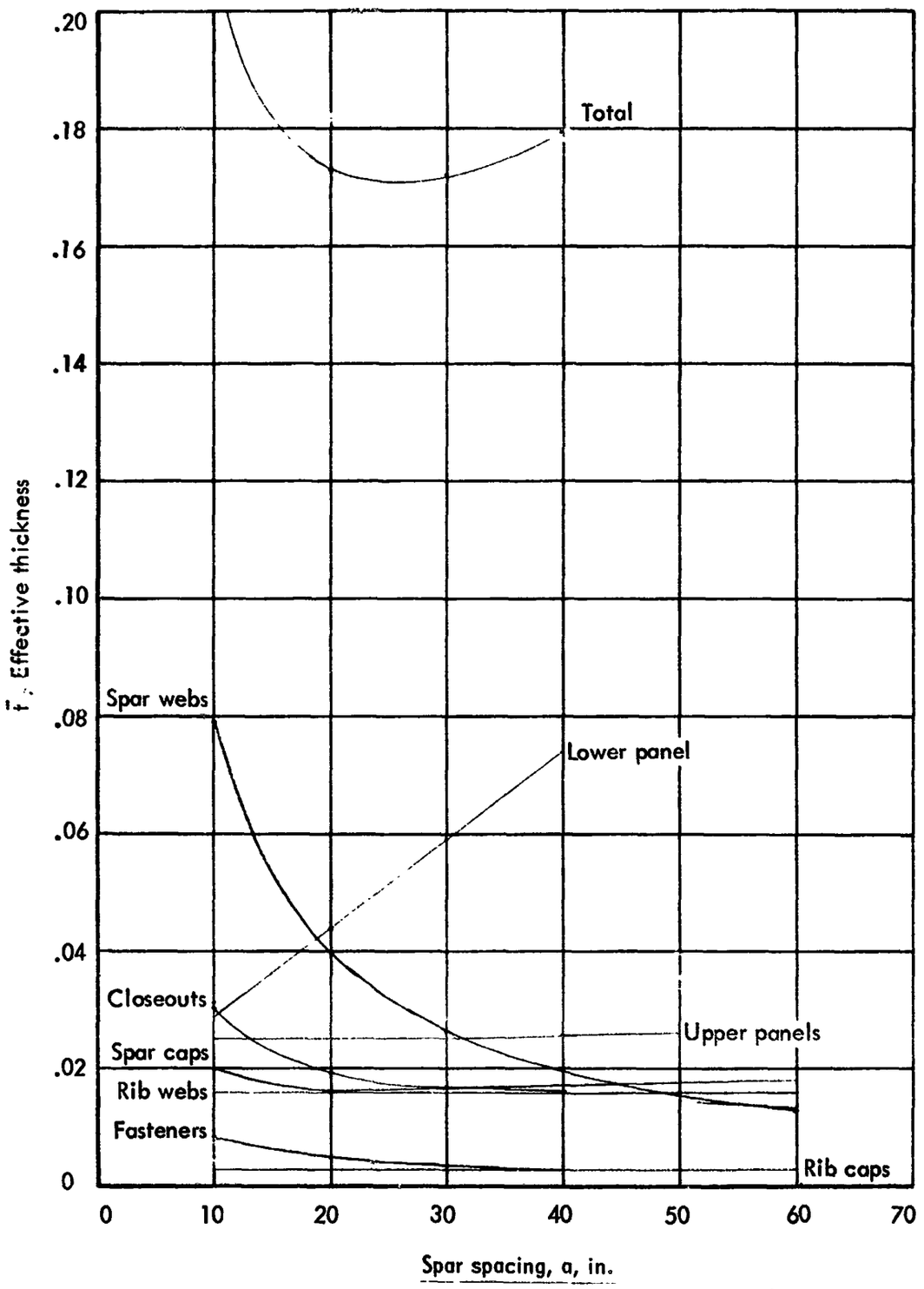

Figure 13-42. Weight optimization of wing area A ($\mathbb{Q}$ to BL 120) of semimonocoque chordwise-stiffened convex-beaded panels, no insulation

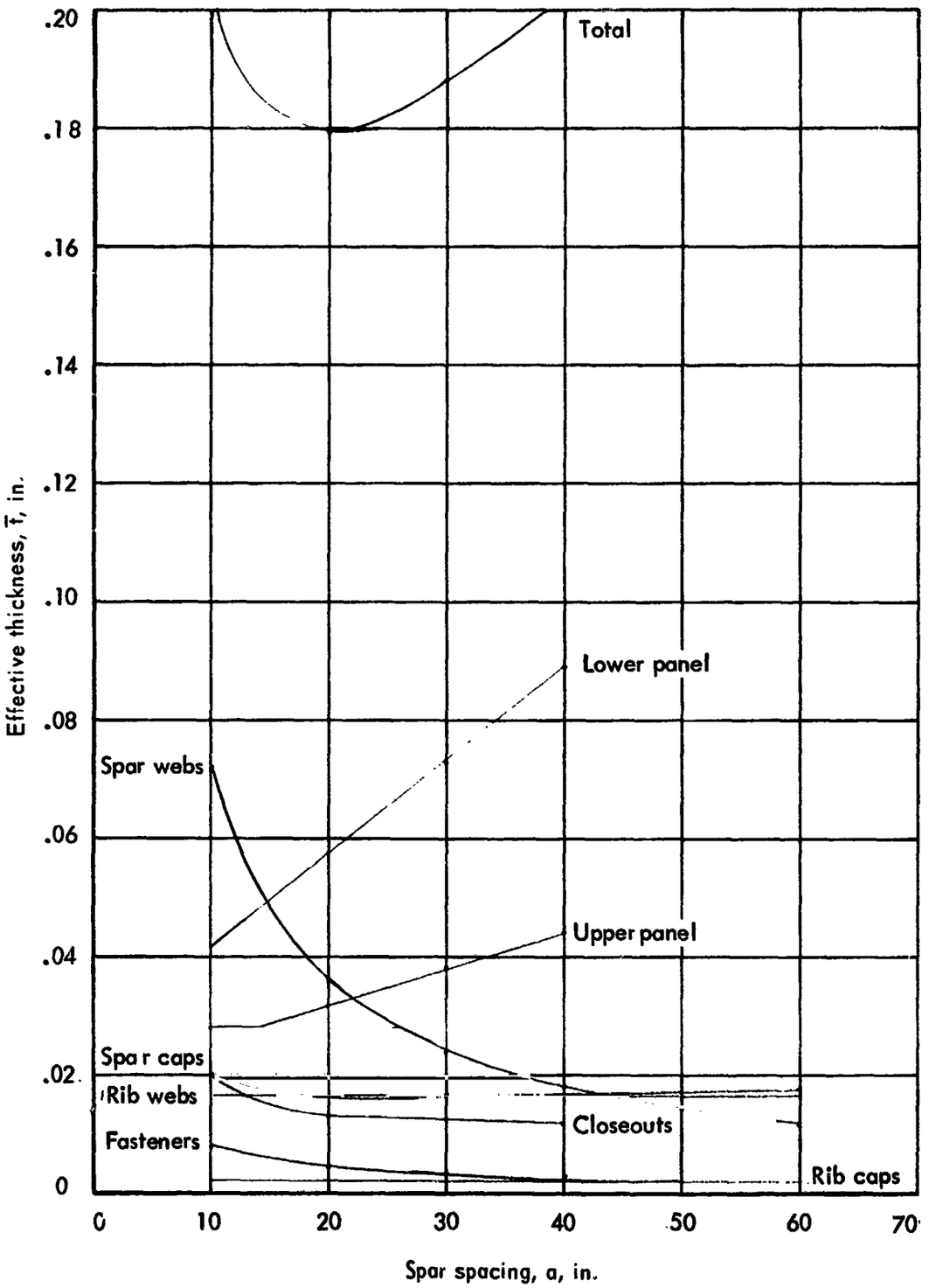

Figure 13-43. Weight optimization of wing area B (BL 120 to BL 212) of semi-monocoque chordwise-stiffened convex-beaded panels, no insulation

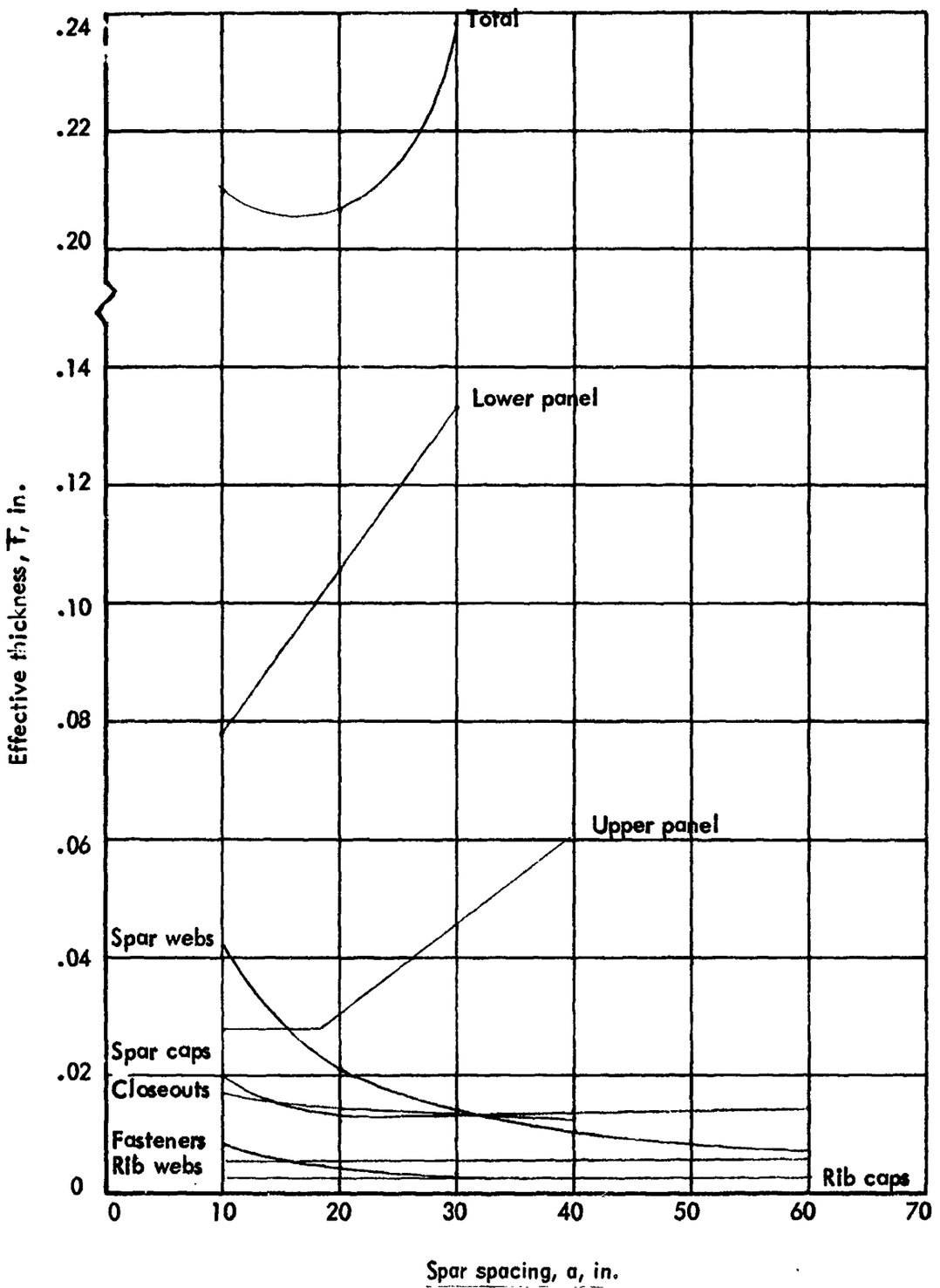

Figure 13-44. Weight optimization of wing area C (BL 212 to BL 350) of semi-monocoque chordwise-stiffened convex-beaded panels, no insulation

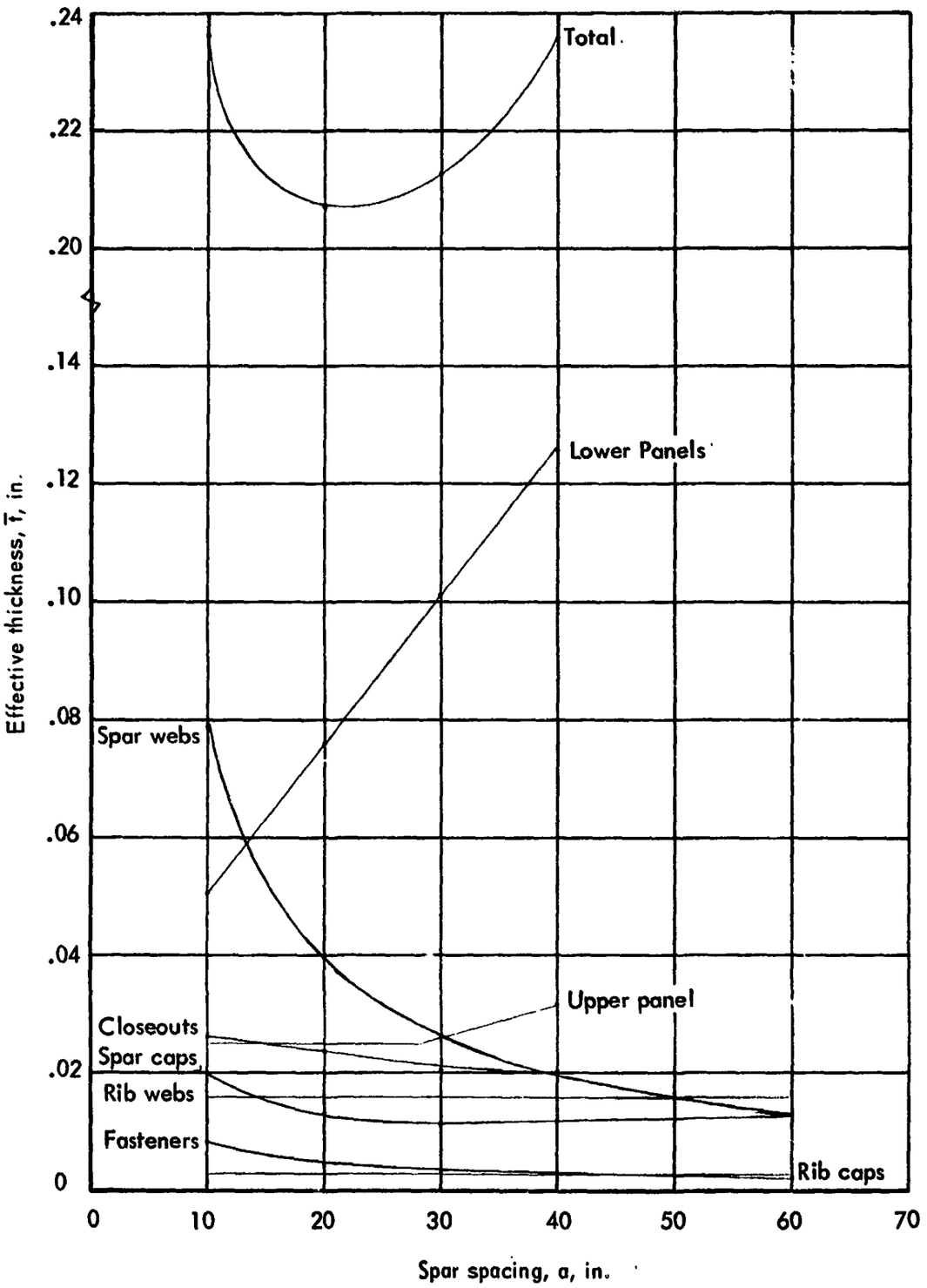

Figure 13-45. Weight optimization of wing area A (℄ to BL 120) of semimonocoque chordwise-stiffened convex-beaded/tubular lower outboard no insulation

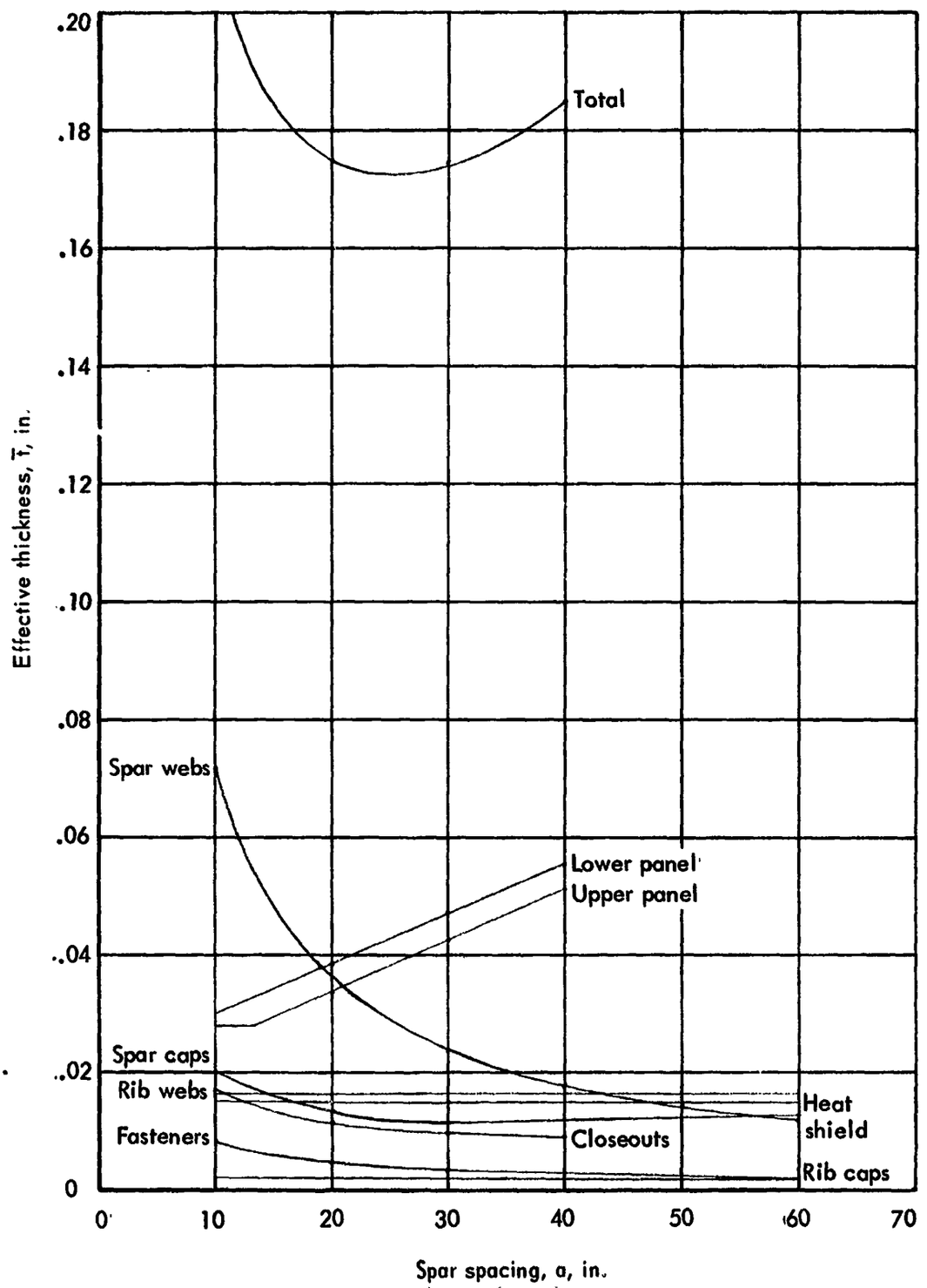

Figure 13-46. Weight optimization of wing area B (BL 120 to BL 212) of semi-monocoque chordwise-stiffened convex-beaded/tubular lower outboard, no insulation

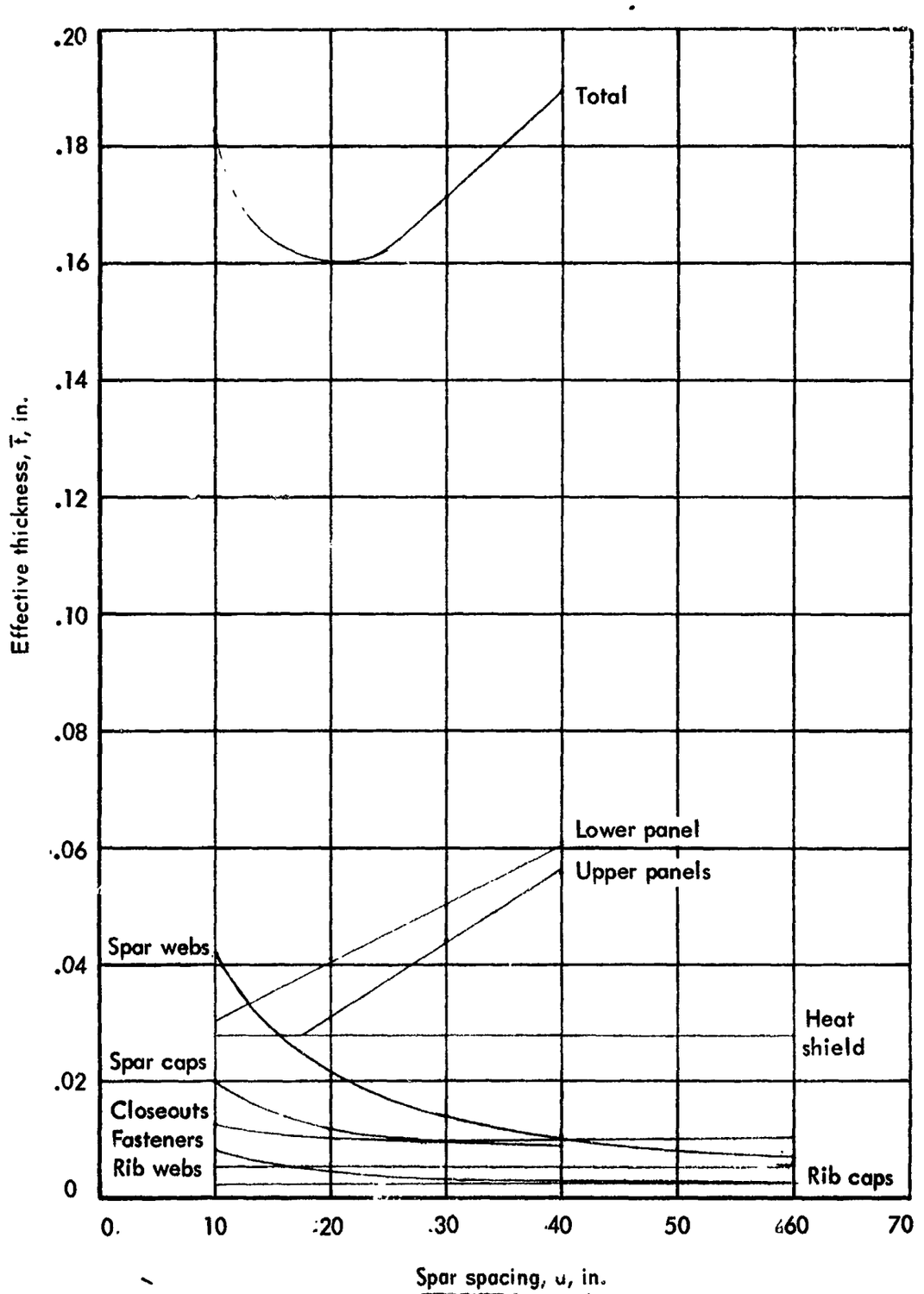

Figure 13-47. Weight optimization of wing area C (BL 212 to BL 350) of semi-monocoque chordwise-stiffened convex-beaded/tubular lower outboard, no insulation

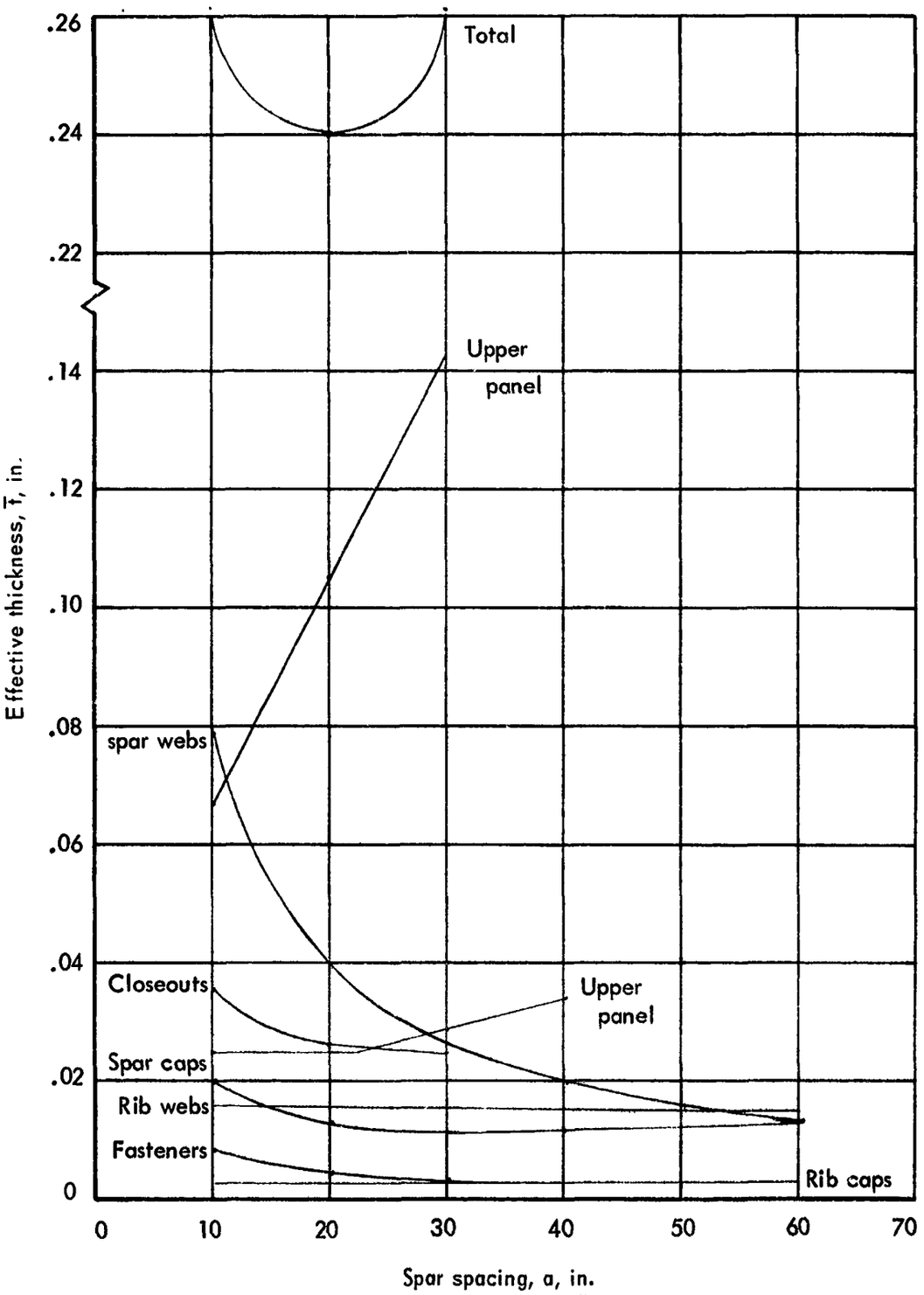

Figure 13-48. Weight optimization of wing area A ($\mathcal{L}$ to BL 120) of semimonocoque chordwise-stiffened convex-beaded/tubular lower outboard, with insulation

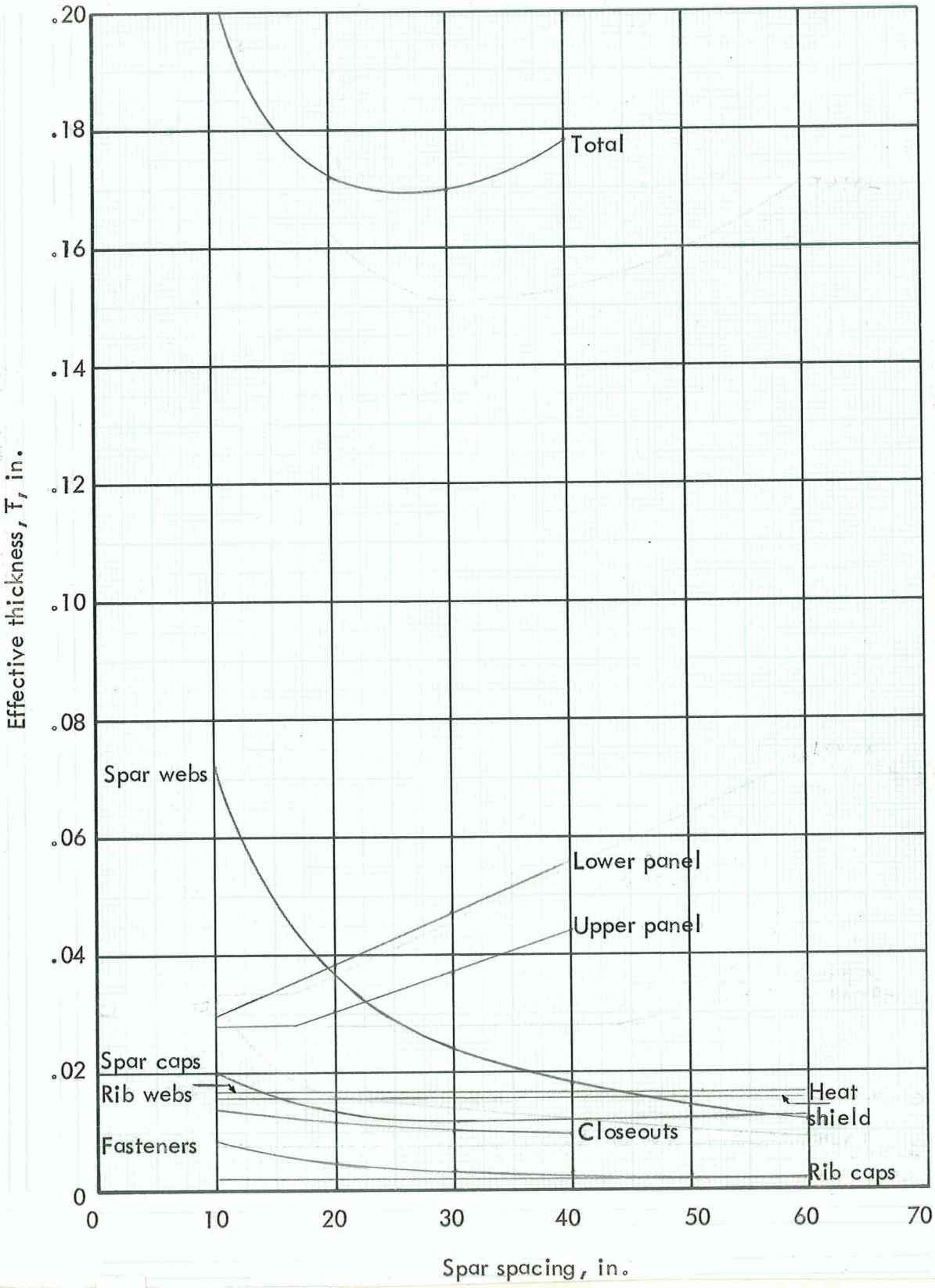

Figure 13-49. Optimization of wing area B (BL 120 to BL 212) of semimonocoque chordwise-stiffened convex-beaded/tubular lower outboard, with insulation

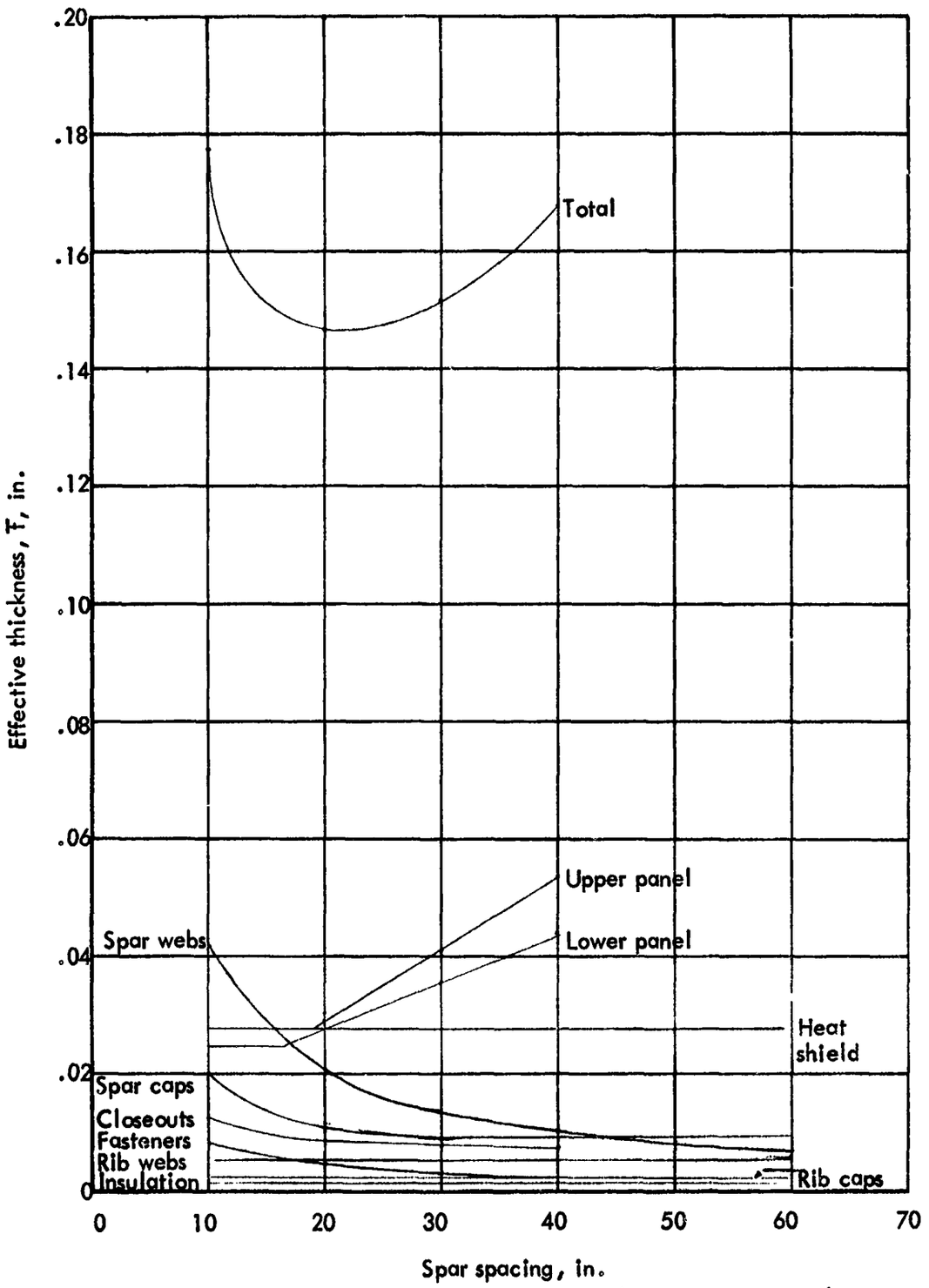

Figure 13-50. Weight optimization of wing area C (BL 212 to BL 350) of semi-monocoque chordwise-stiffened convex-beaded/tubular lower outboard, with insulation

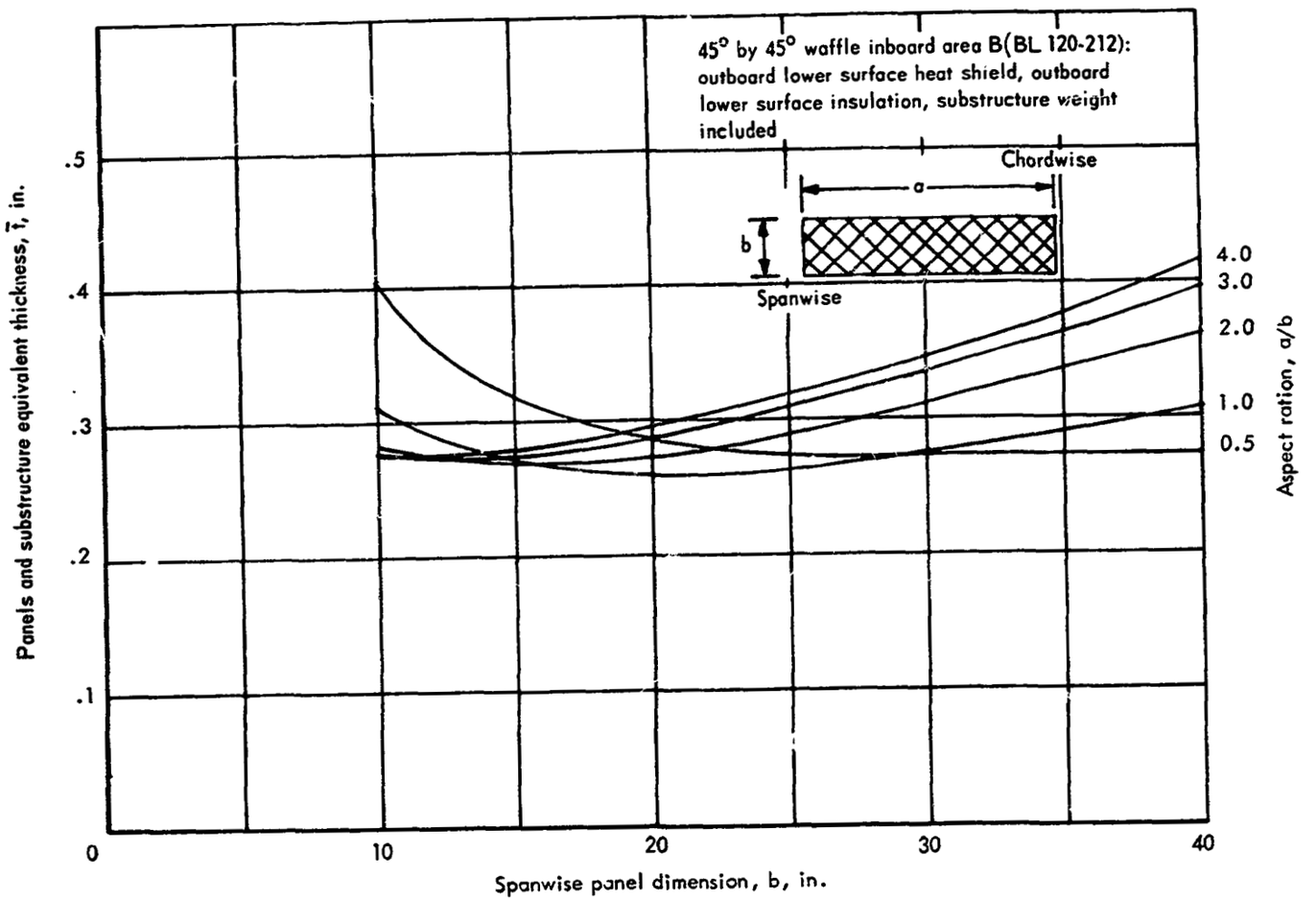

Figure 13-51. Aspect ratio weight summary, waffle construction

Panel dimensions: (All dimensions in inches)

($panwise)

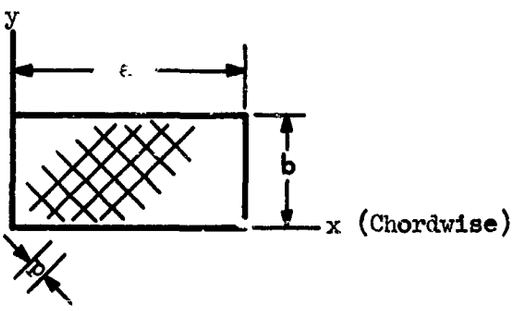

Waffle dimensions:

- h – overall waffle height
- p – pitch of stiffeners
- t_s – skin thickness
- t_w – stiffener thickness
- $\bar{t}$ – panel equivalent thickness

Miscellaneous:

- e_{11} – extensional eccentricity
- e_{33} – shear eccentricity
- w_o – maximum panel deflection

Figure 13-52 Notation for monocoque waffle panel design data

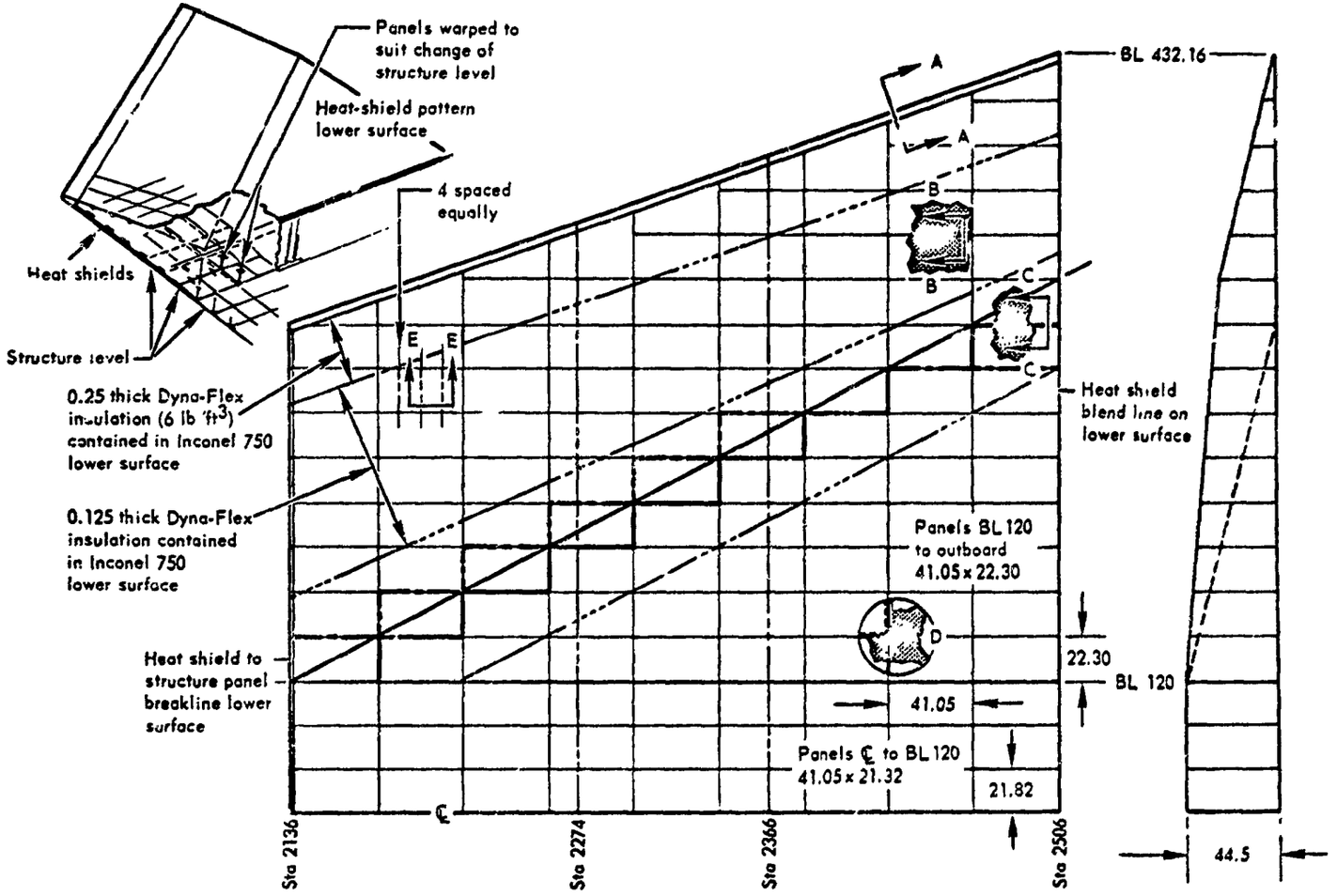

Figure 13-53. Final design of monocoque waffle primary structure concept

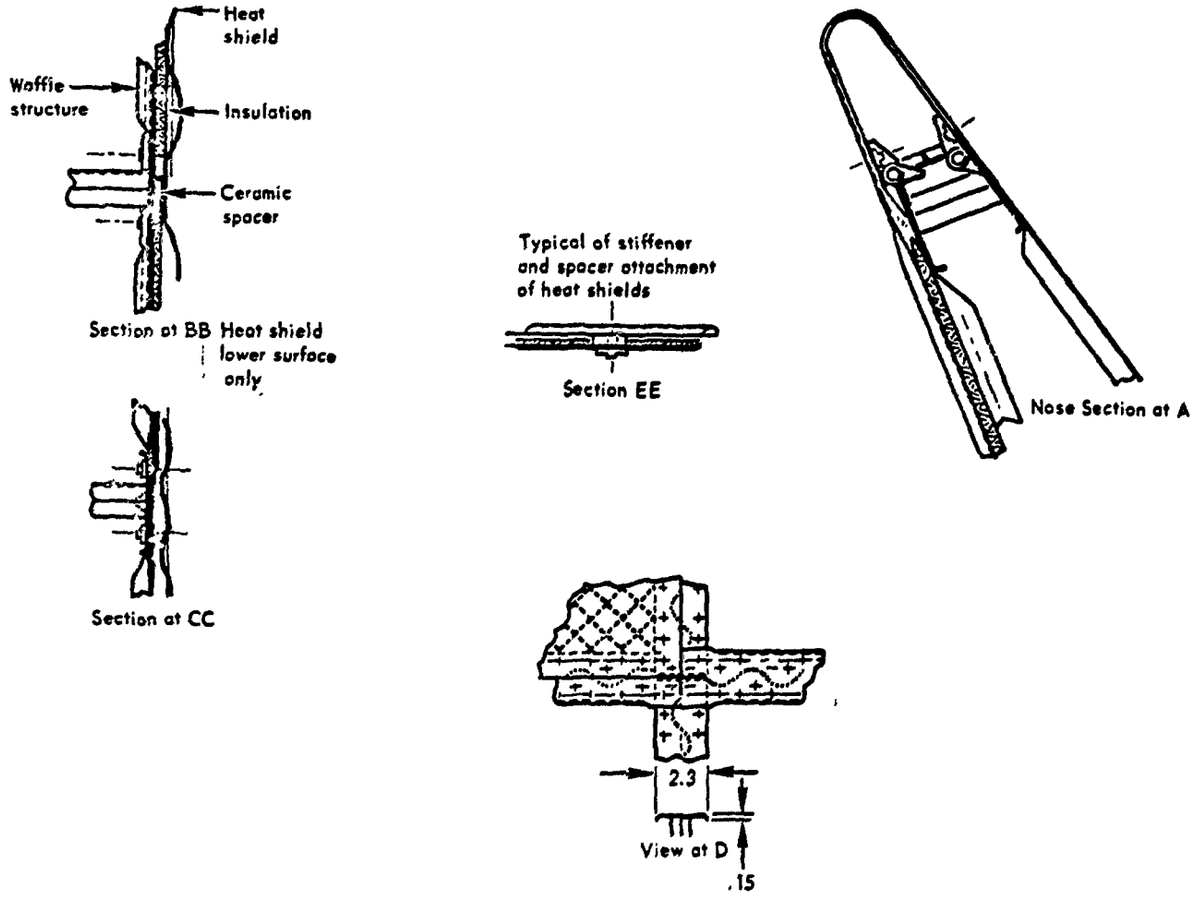

Figure 13-53. Final design of monocoque waffle primary-structure concept (Cont.)

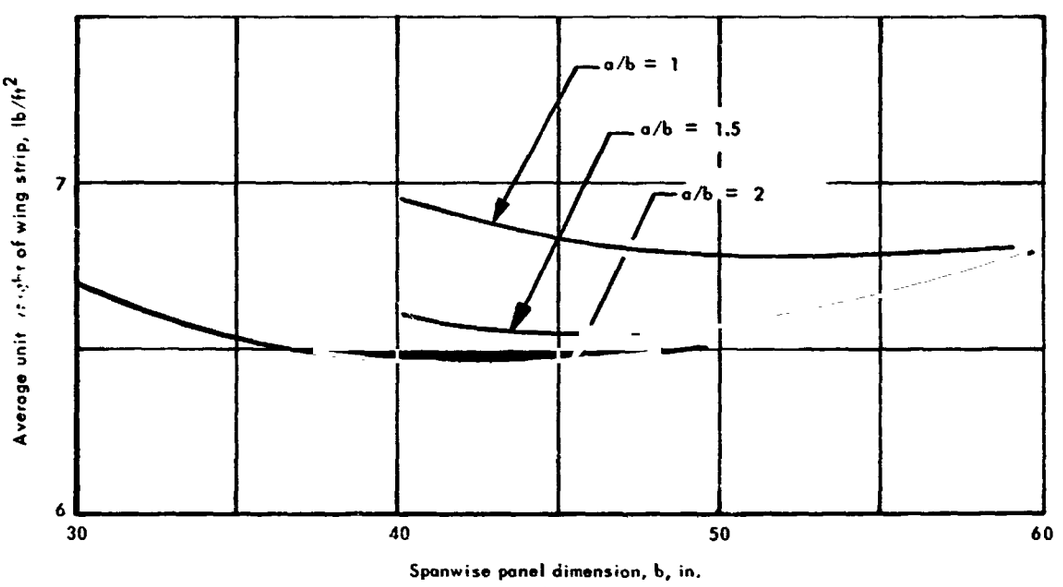

Figure 13-54 Honeycomb-core sandwich panel size requirements

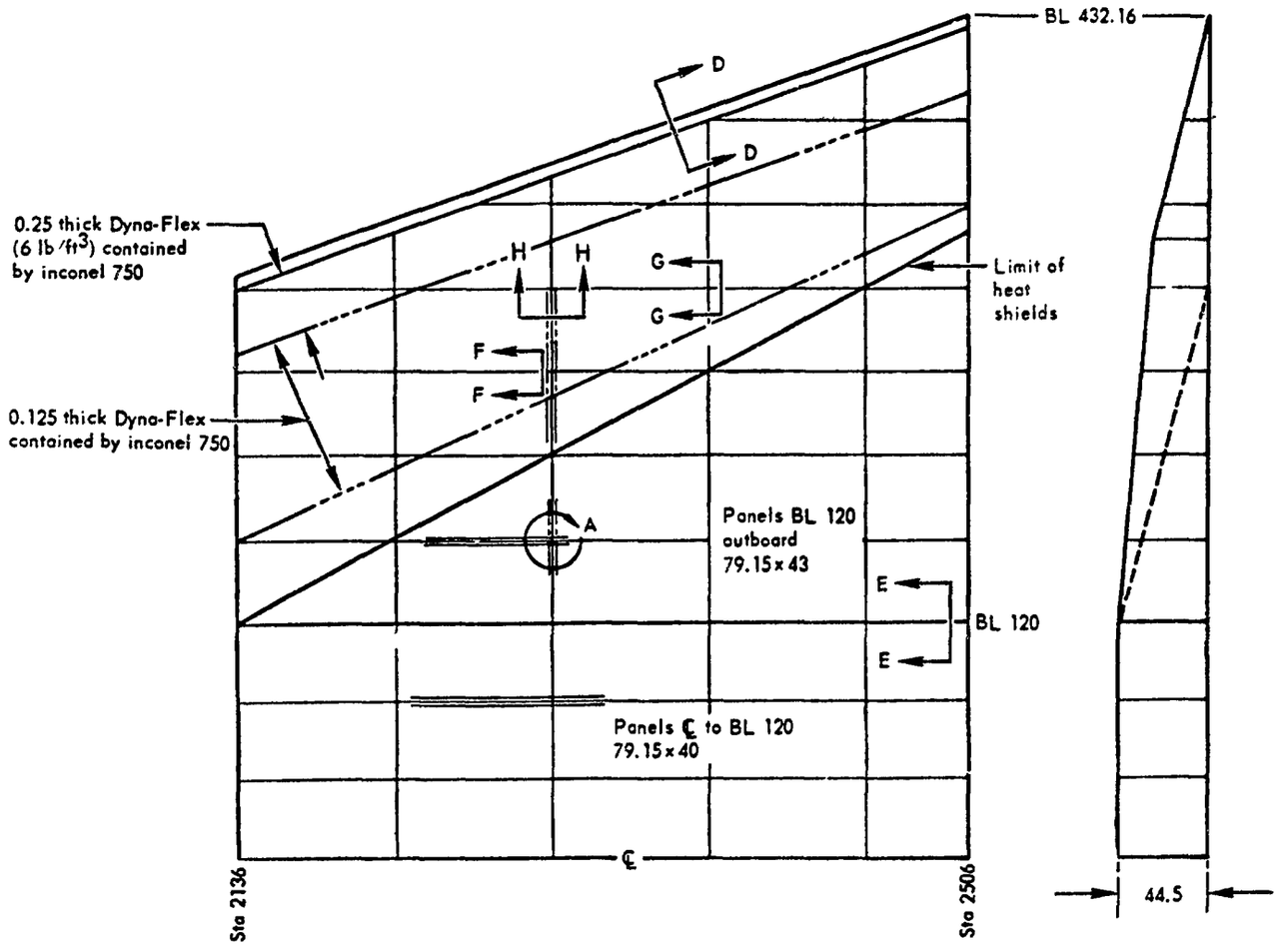

Figure 13-55 Final design of monocoque honeycomb-core sandwich primary-structure concept

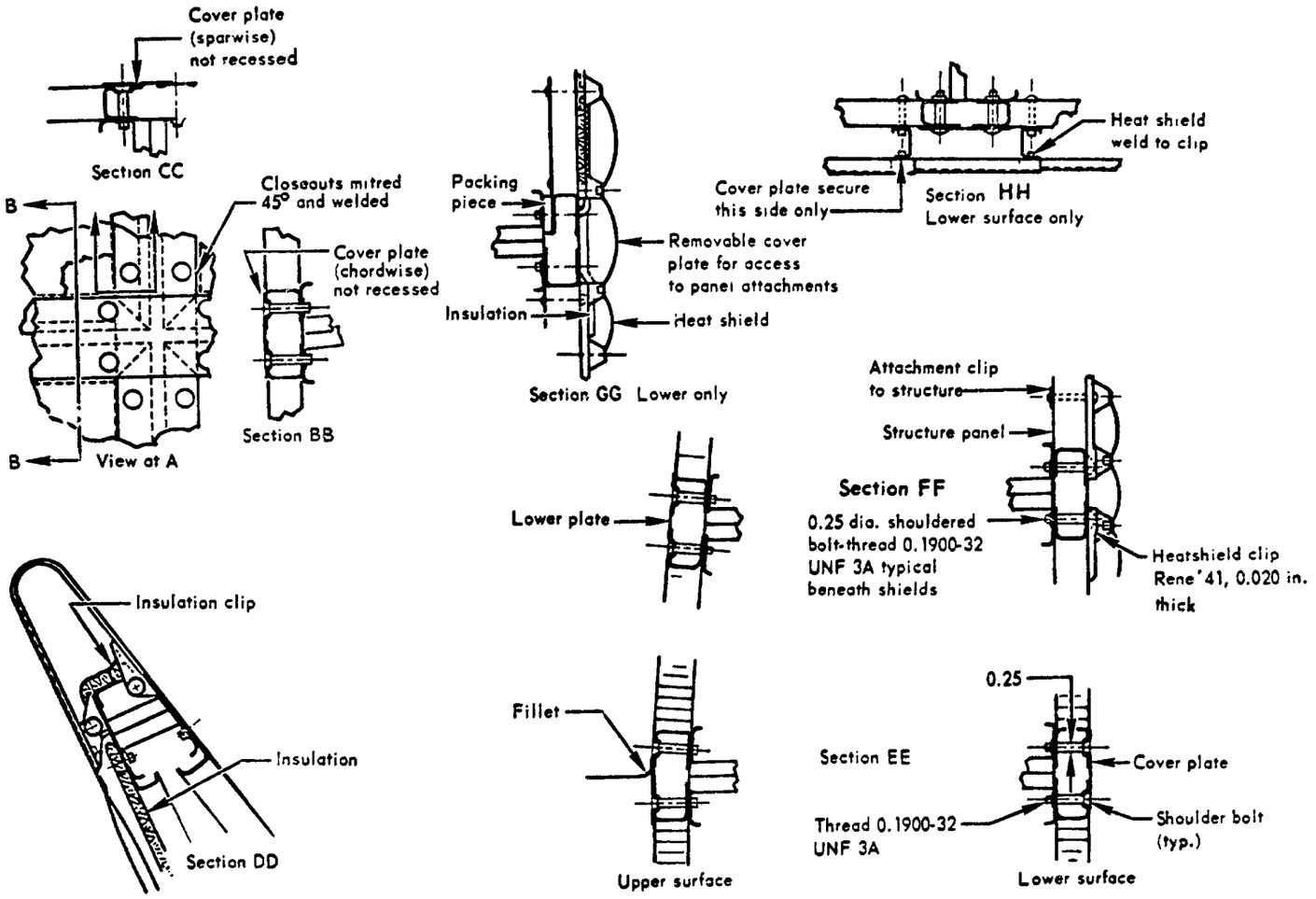

Figure 13-55. Final design of monocoque honeycomb-core sandwich primary-structure concept (Cont.)

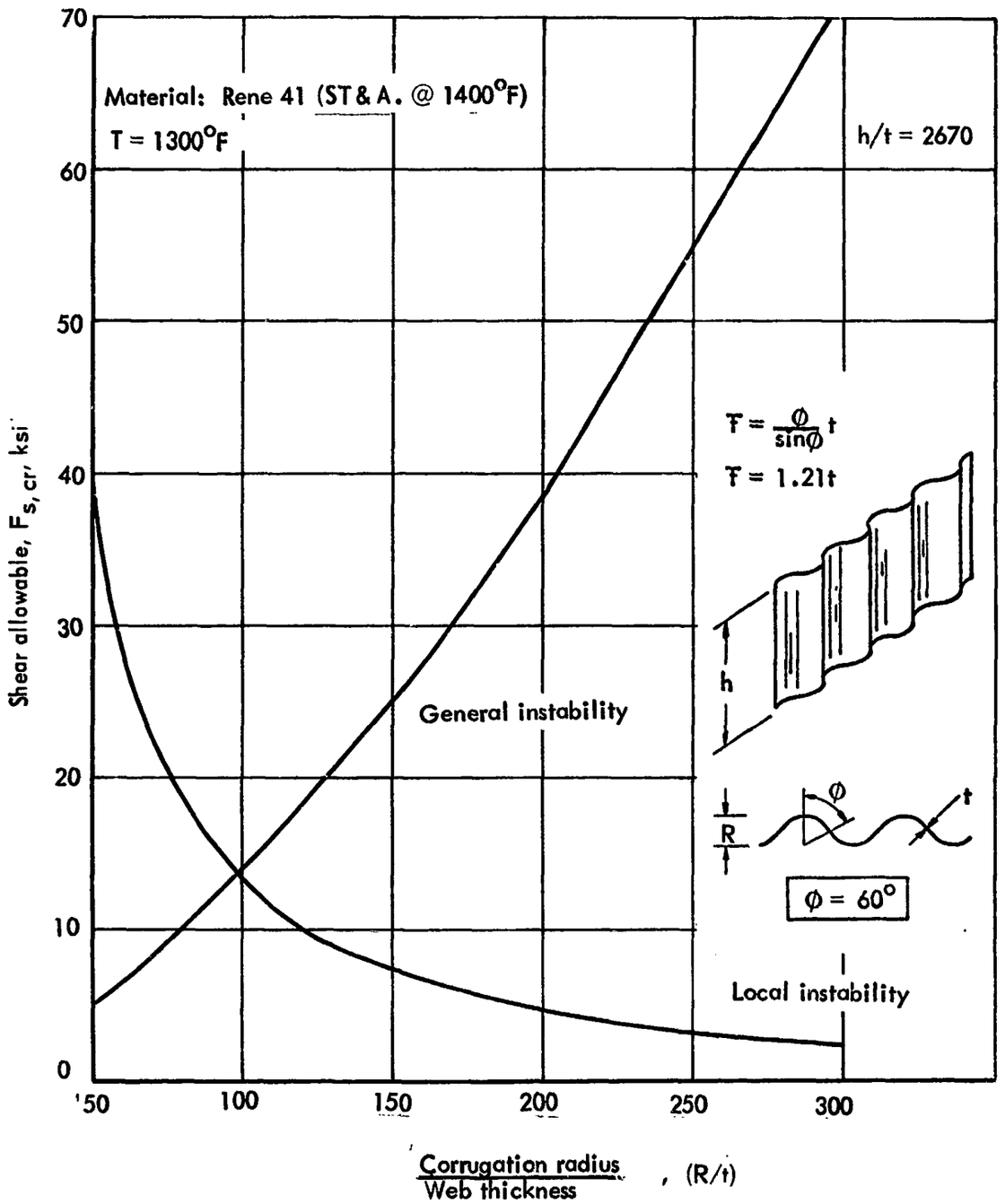

Figure 13-56. Shear allowable versus R/t of vertical circular-arc webs at 1300°

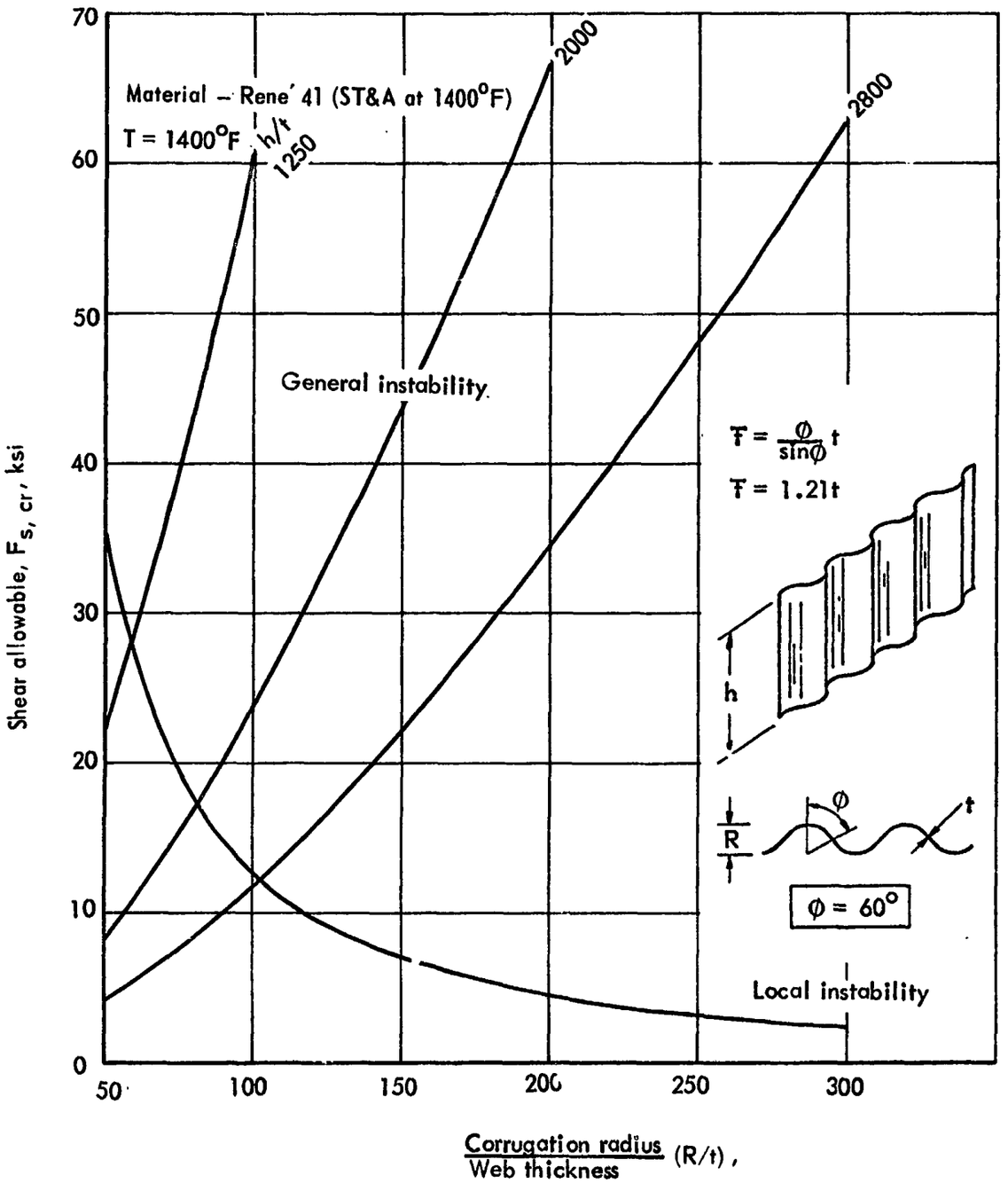

Figure 13-57. Shear allowable versus R/t of vertical circular-arc webs at 1400°F

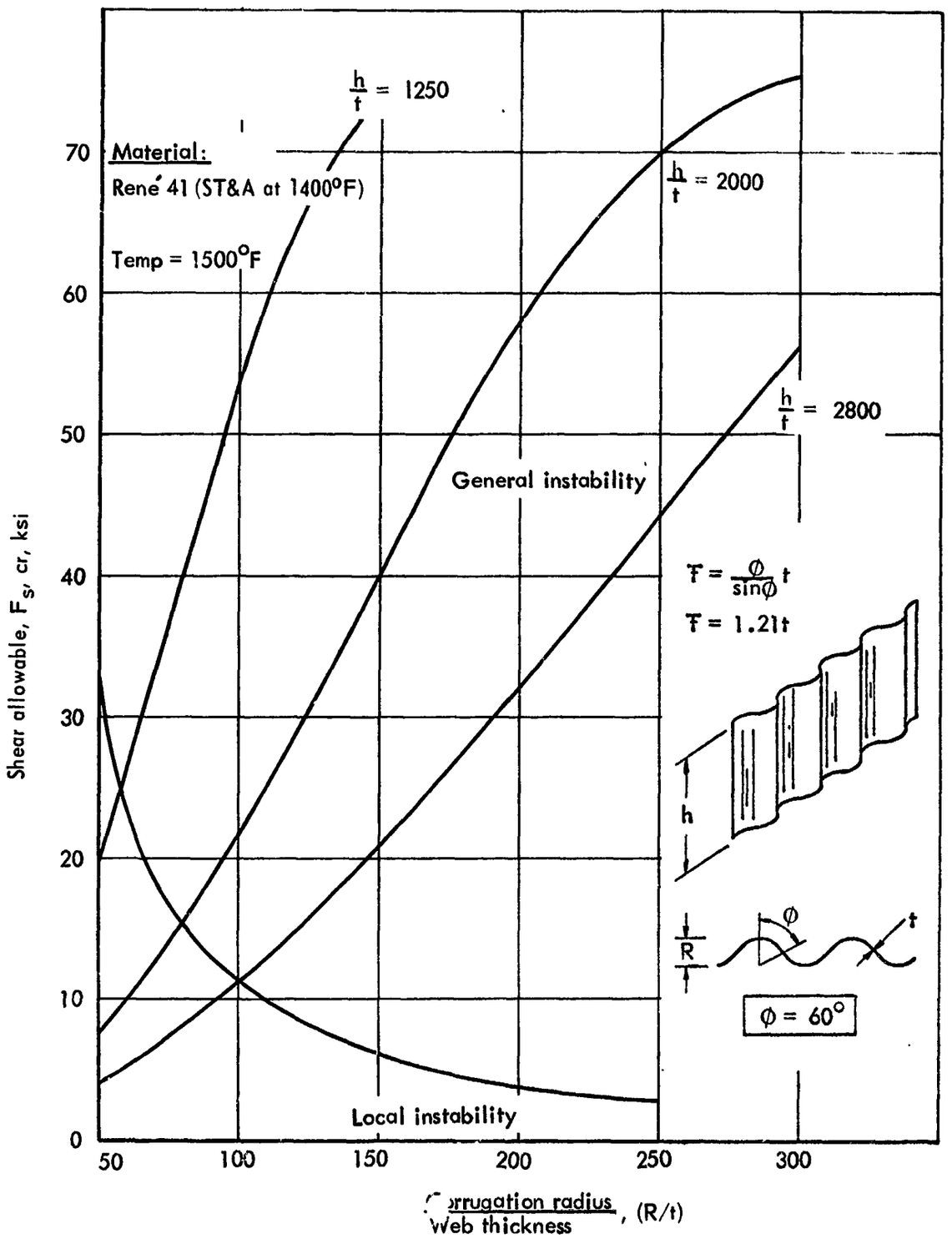

Figure 13-58. Shear allowable versus R/t of vertical circular-arc webs at 1500°F

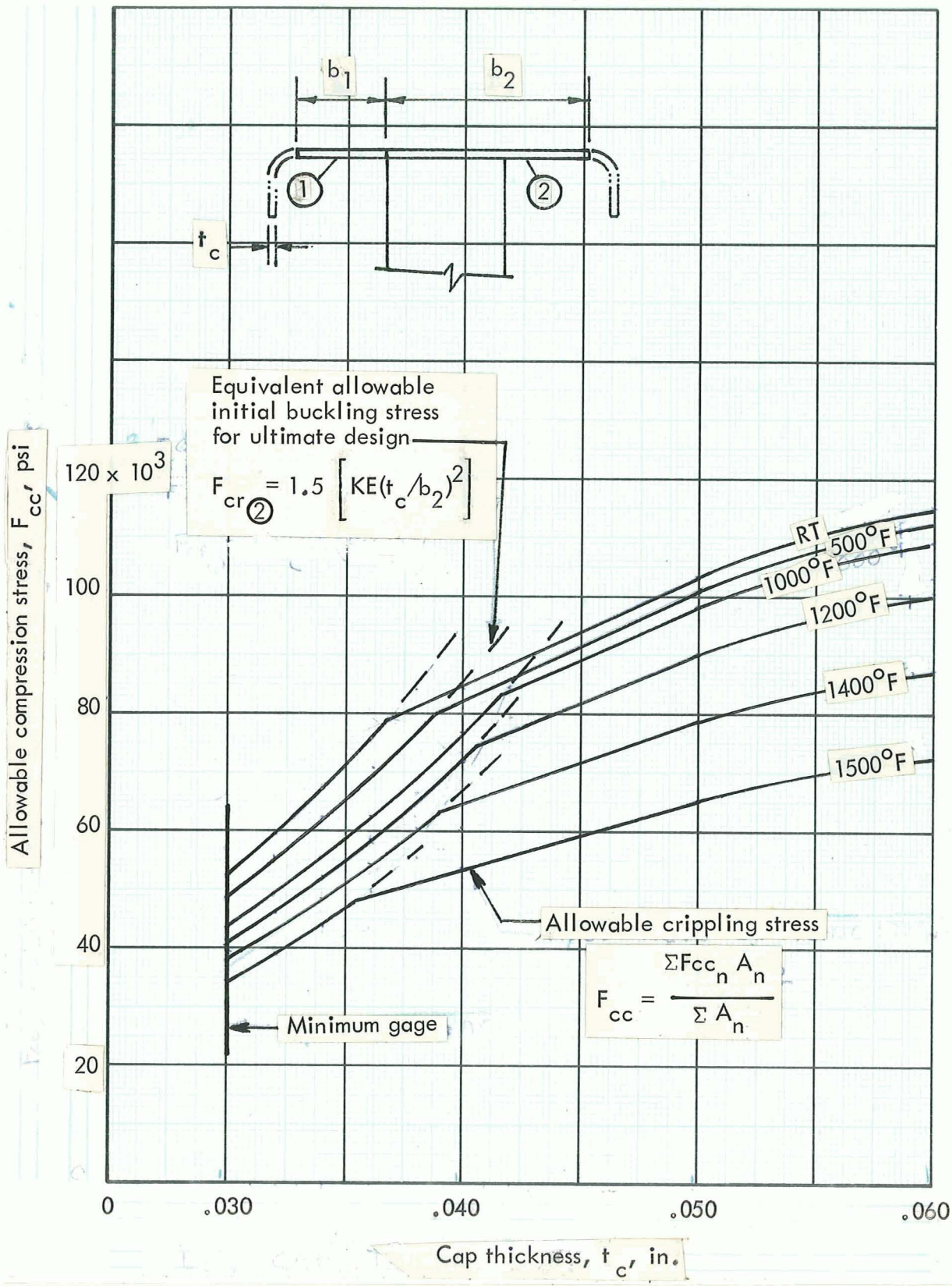

Figure 13-59. Allowable compression stress versus thickness of rib and spar caps

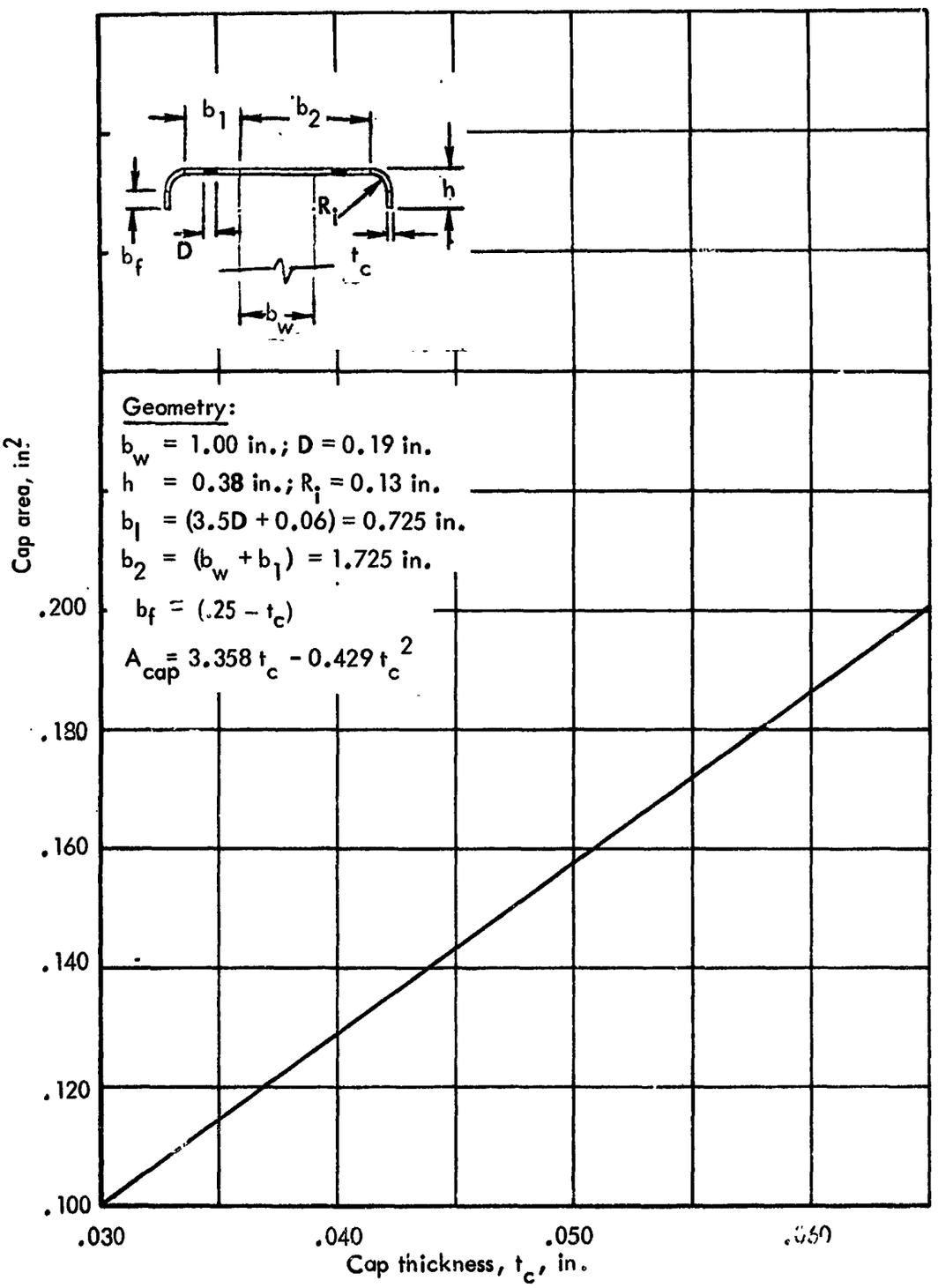

Figure 13-60. Cap area vs thickness of rib and spar caps

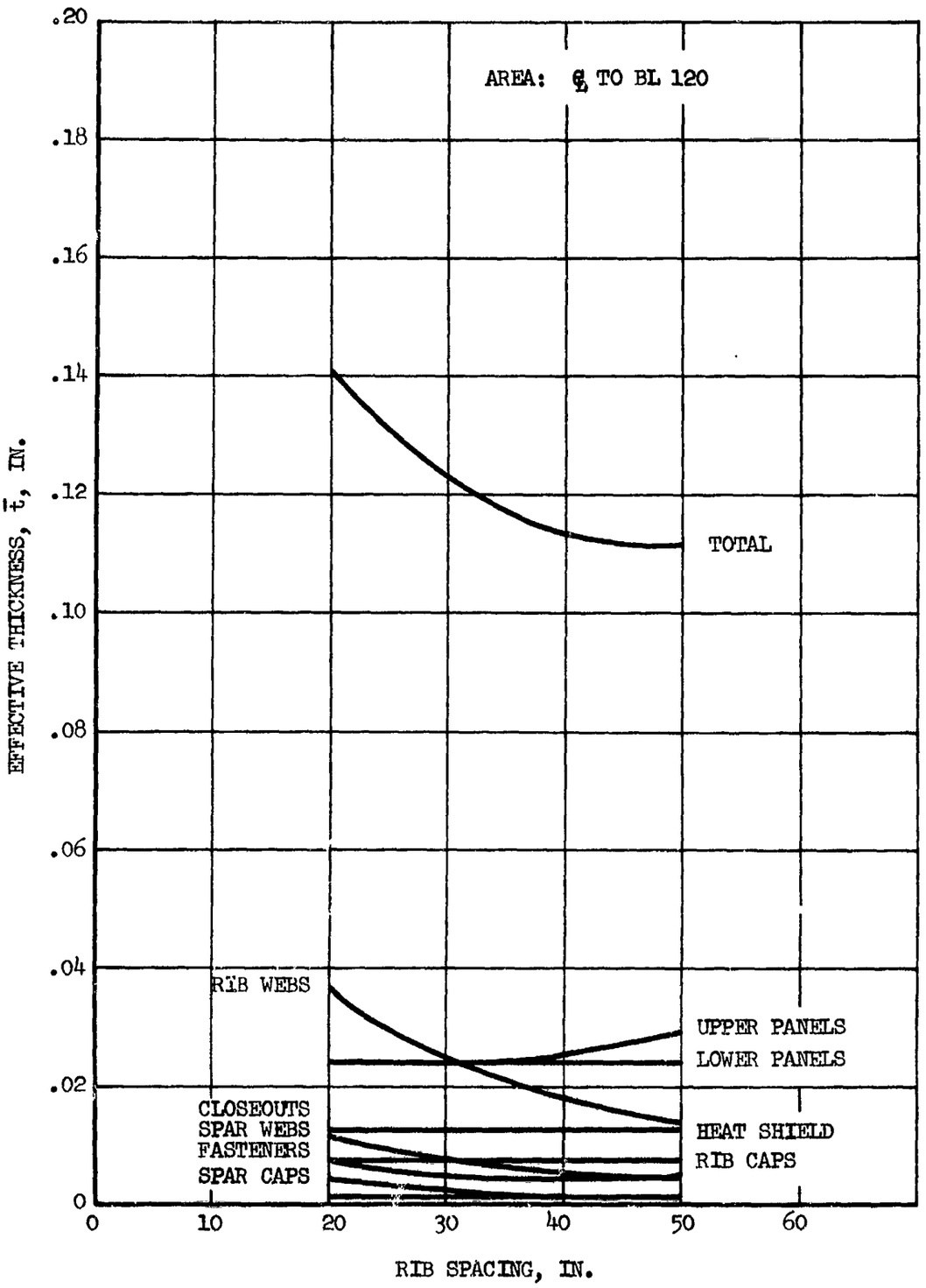

Figure 13-61 Optimum rib spacing for center area of semimonocoque spanwise-stiffened tubular panels with heat shields and partial insulation outboard

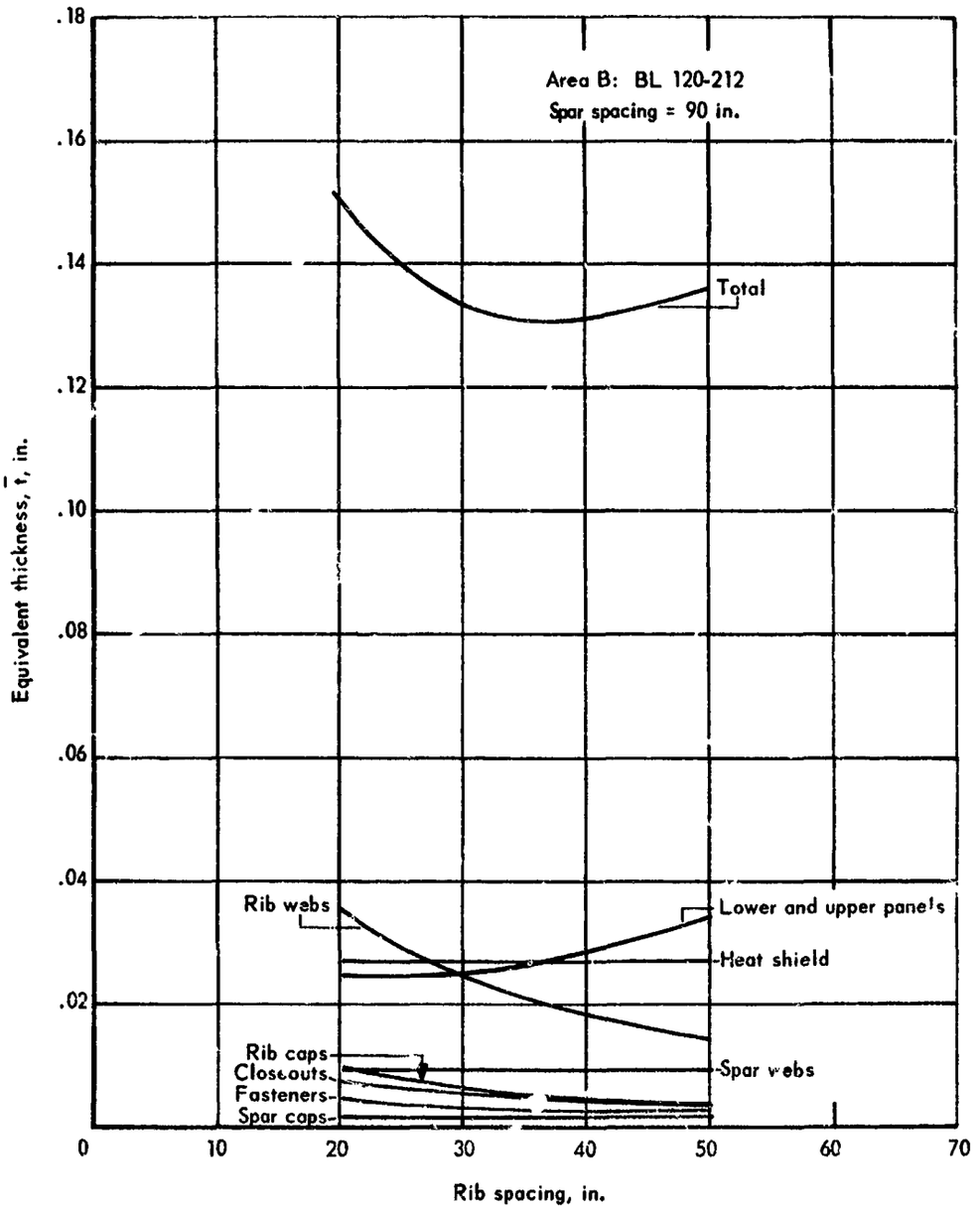

Figure 13-62 **Optimum rib spacing for spanwise-stiffened tubular panels with partial insulation outboard**

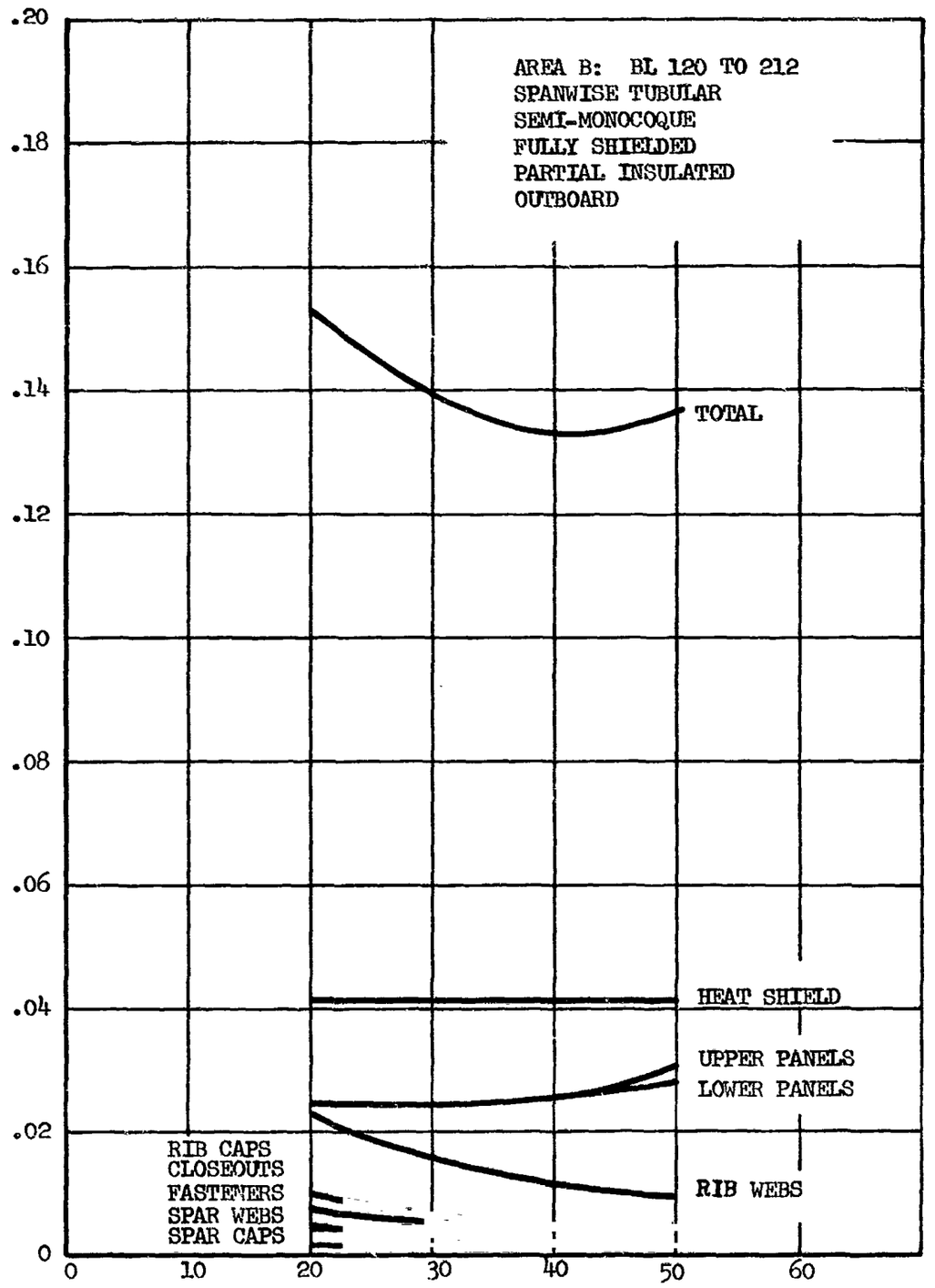

Figure 13-63 Optimum rib spacing for outboard area of semimonocoque spanwise-stiffened tubular panels with heat shields and partial insulation outboard

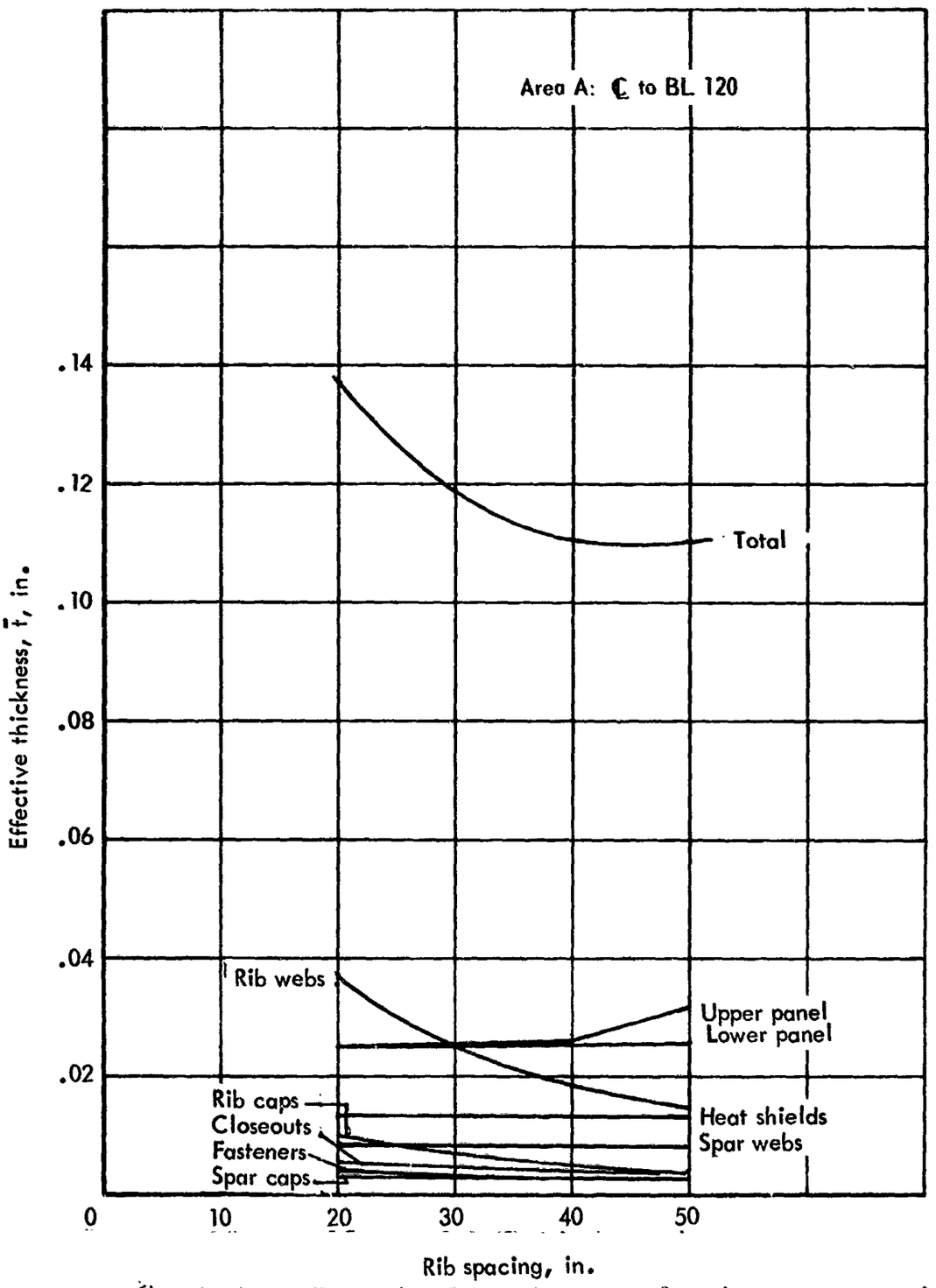

Figure 13-64. Optimum rib spacing for center area of semimonocoque spanwise-stiffened tubular panels with no insulation

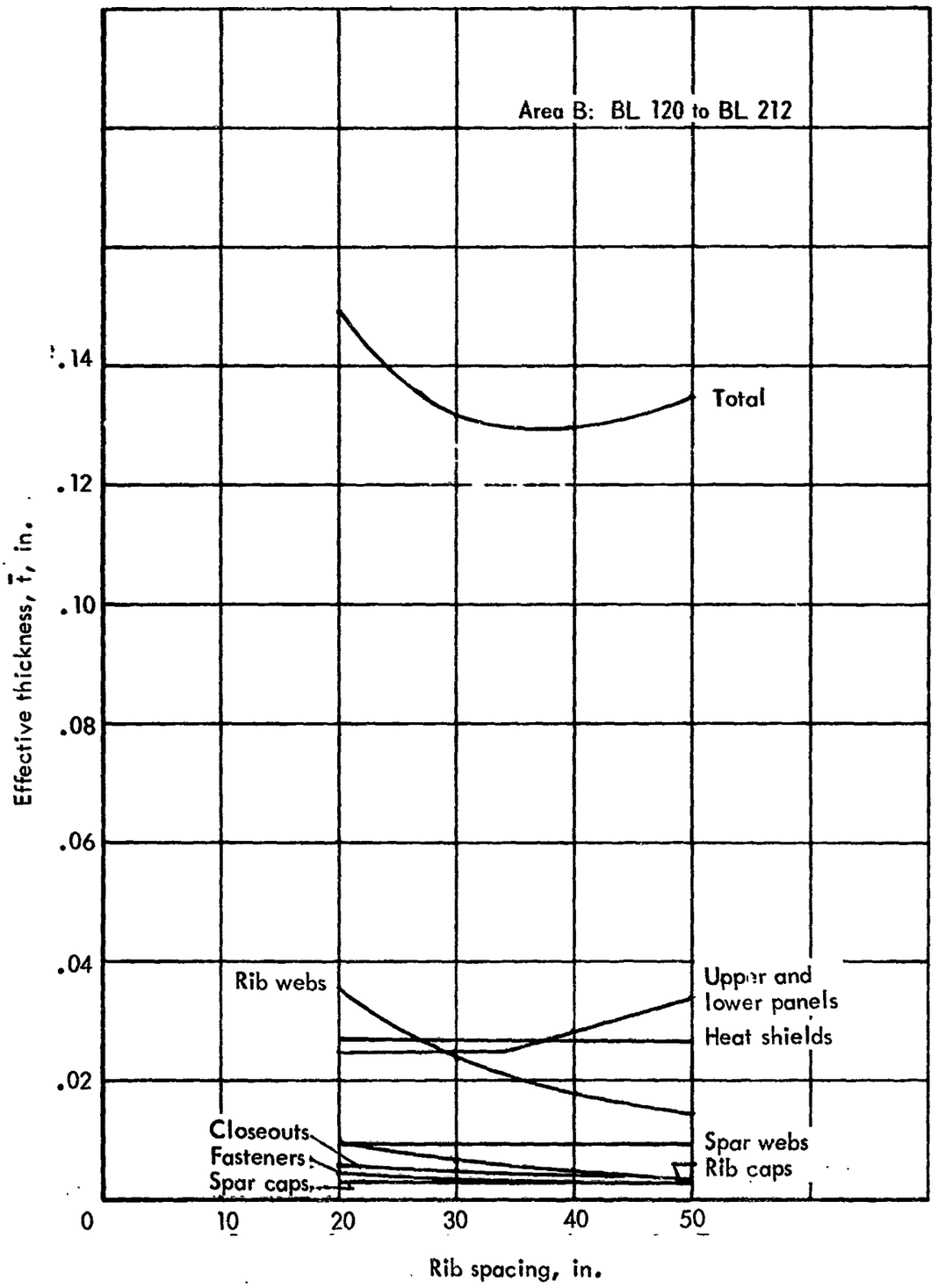

Figure 13-65. Optimum rib spacing for inboard area of semimonocoque spanwise-stiffened tubular panels with no insulation

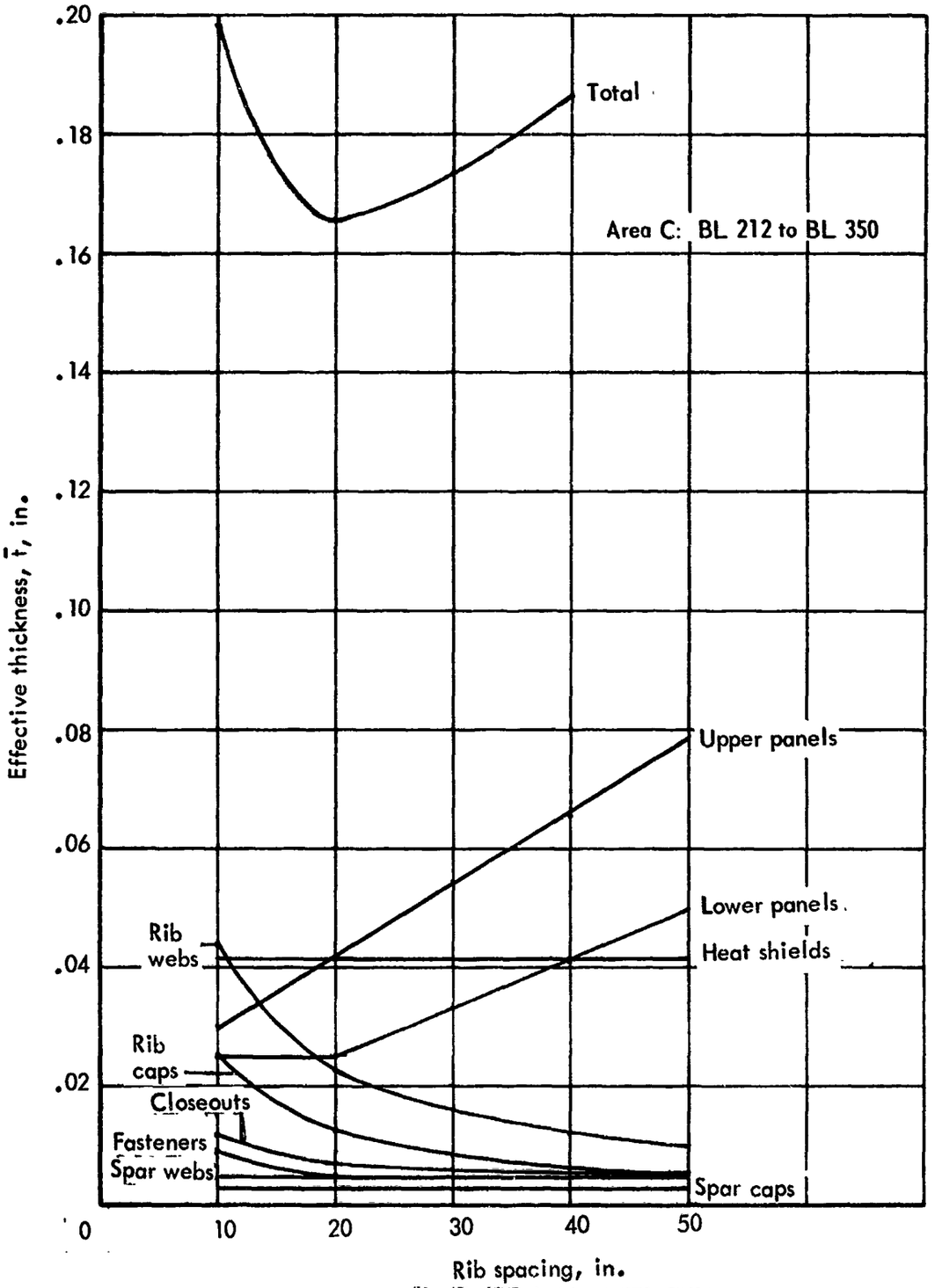

Figure 13-66. Optimum rib spacing for outboard area of semimonocoque spanwise-stiffened tubular panels with no insulation

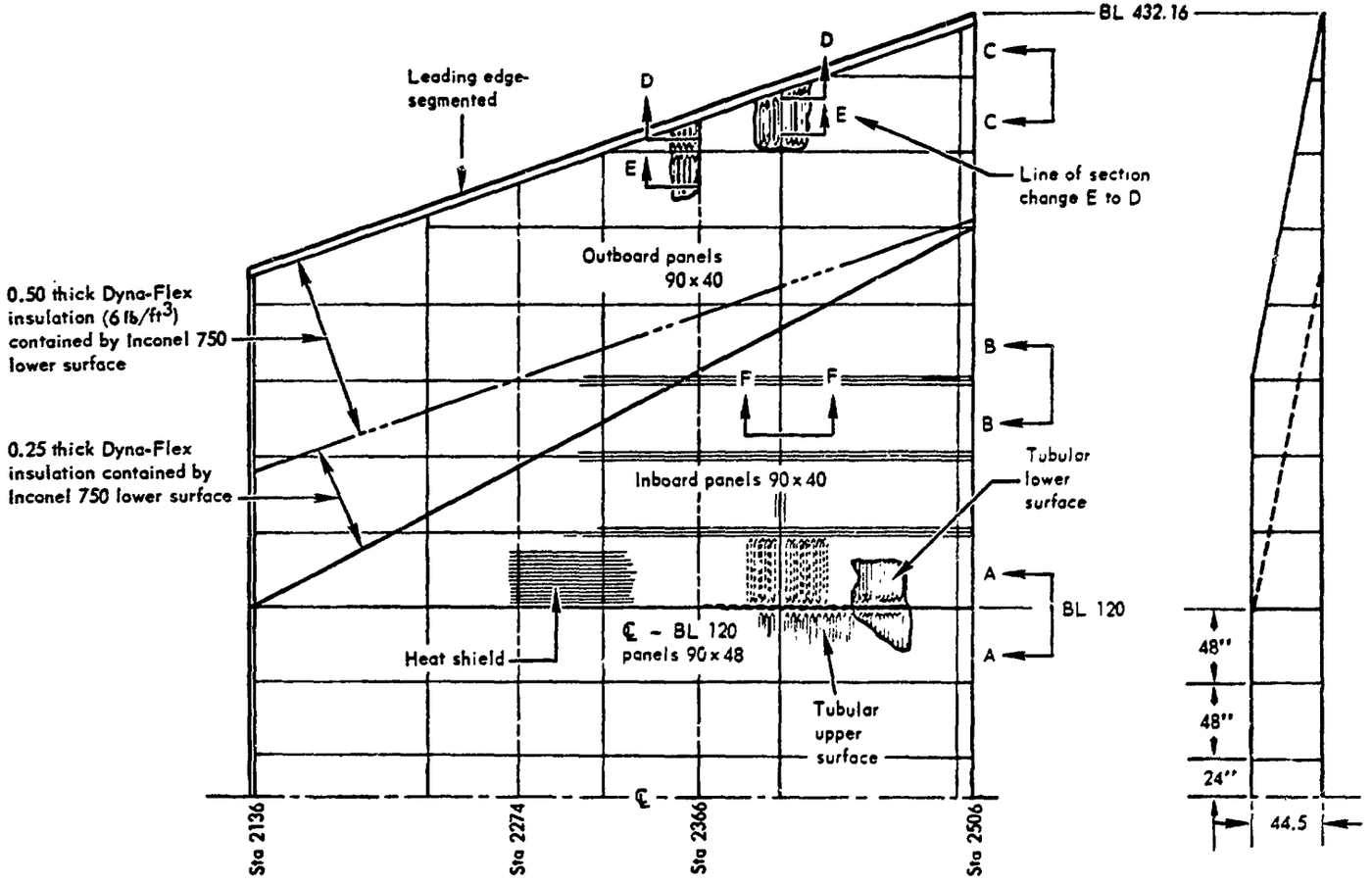

Figure 13-67. Final design of semimonocoque spanwise-stiffened tubular primary-structure concept

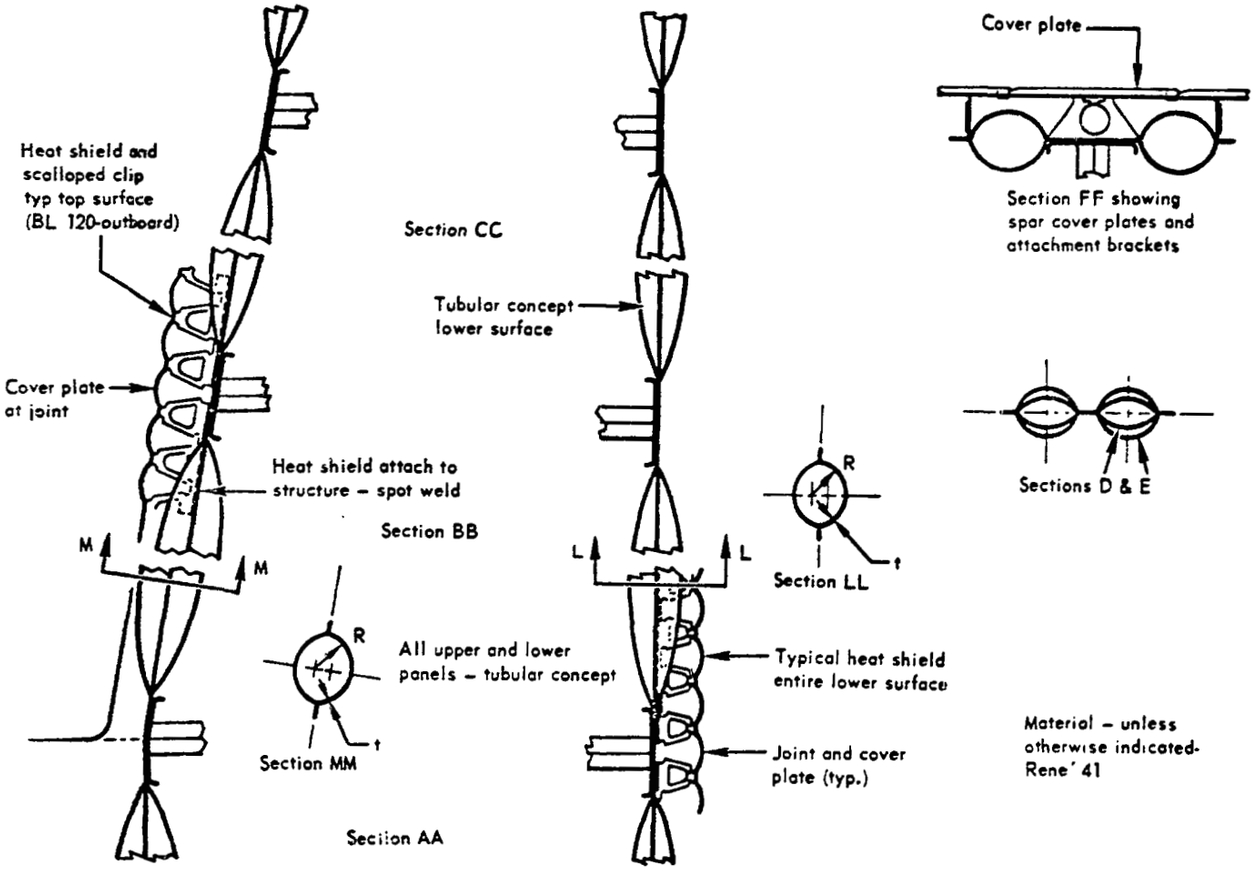

Figure 13-67. Final design of semimonocoque spanwise-stiffened tubular primary-structure concept (Cont.)

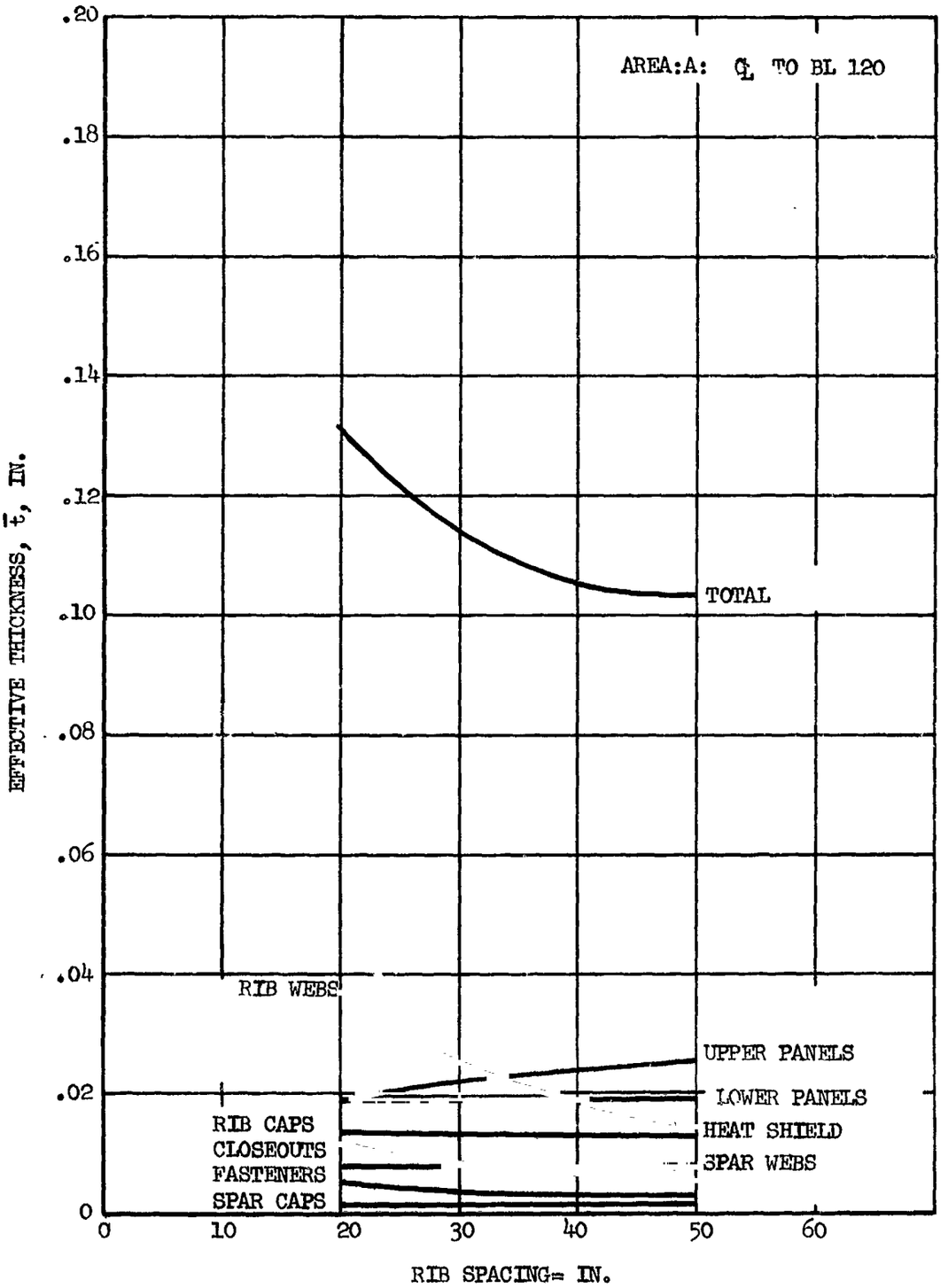

Figure 13-68 Optimum rib spacing for center area of semimonocoque spanwise-stiffened beaded panels with heat shields and partial insulation outboard

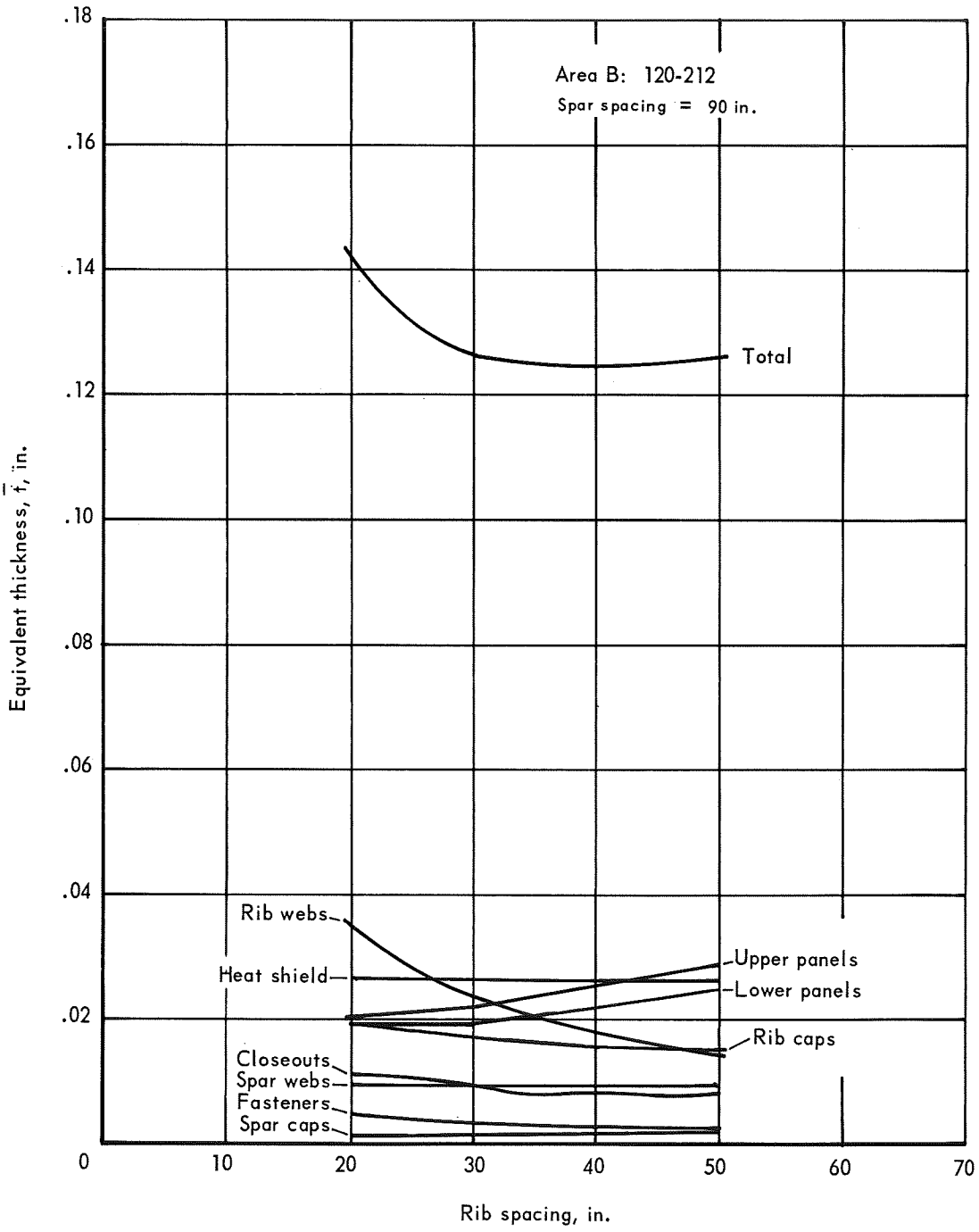

Figure 13-69 Optimum rib spacing for semimonocoque beaded skin concept

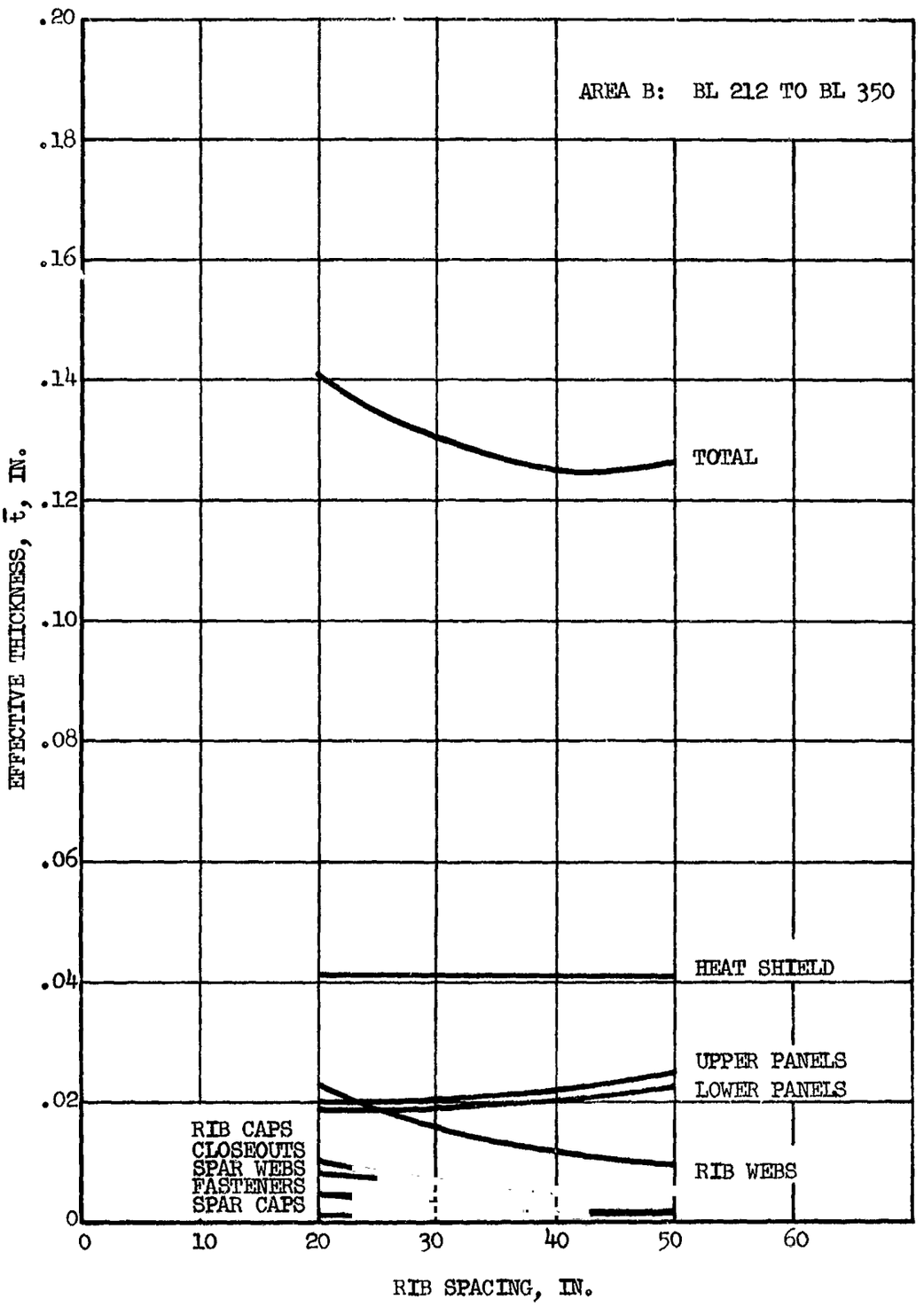

Figure 13-70 Optimum rib spacing for outboard area of semimonocoque spanwise-stiffened beaded panels with heat shields and partial insulation outboard

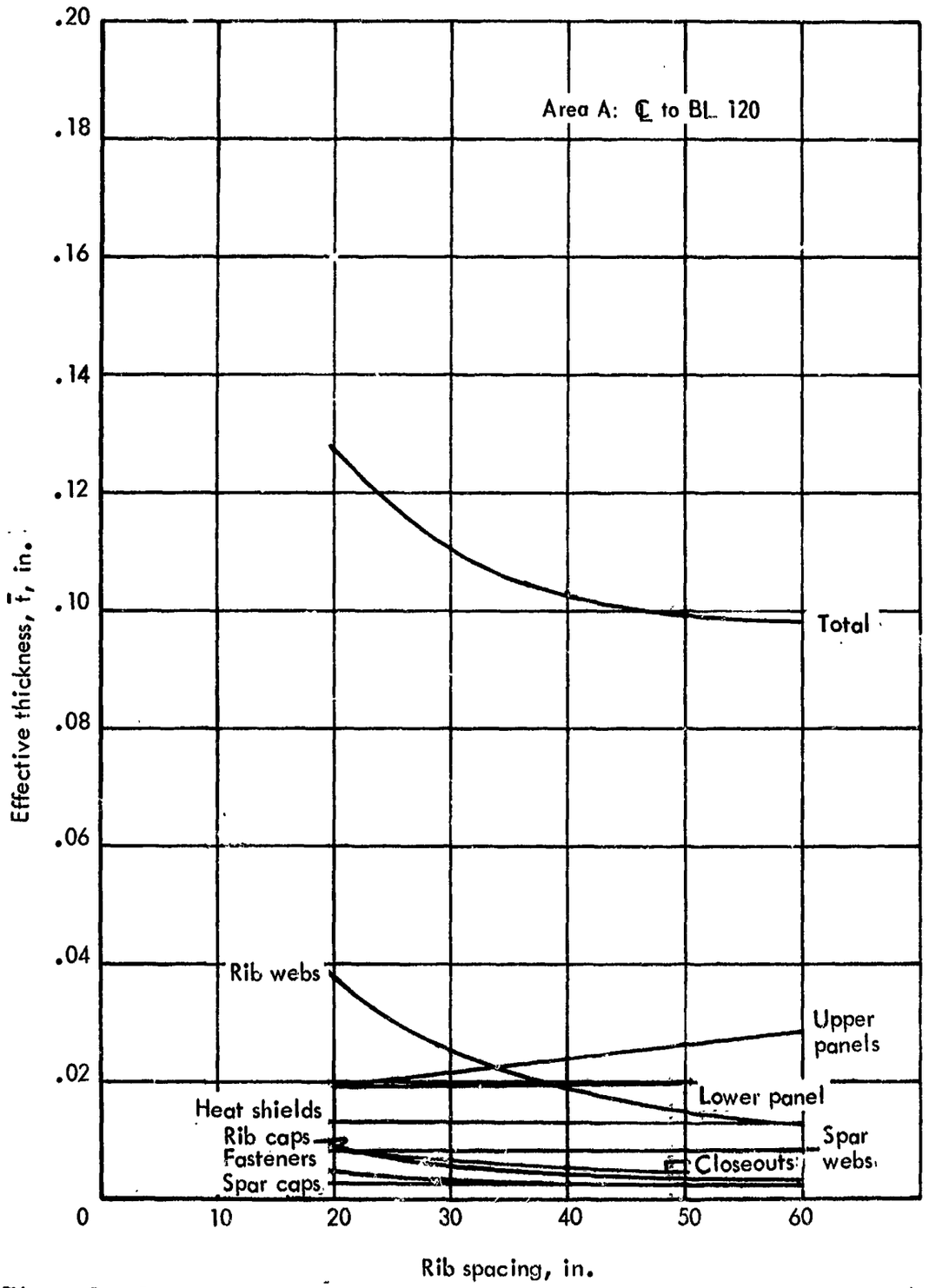

Figure 13-71. Optimum rib spacing for center area of semimonocoque spanwise-stiffened beaded panels with no insulation

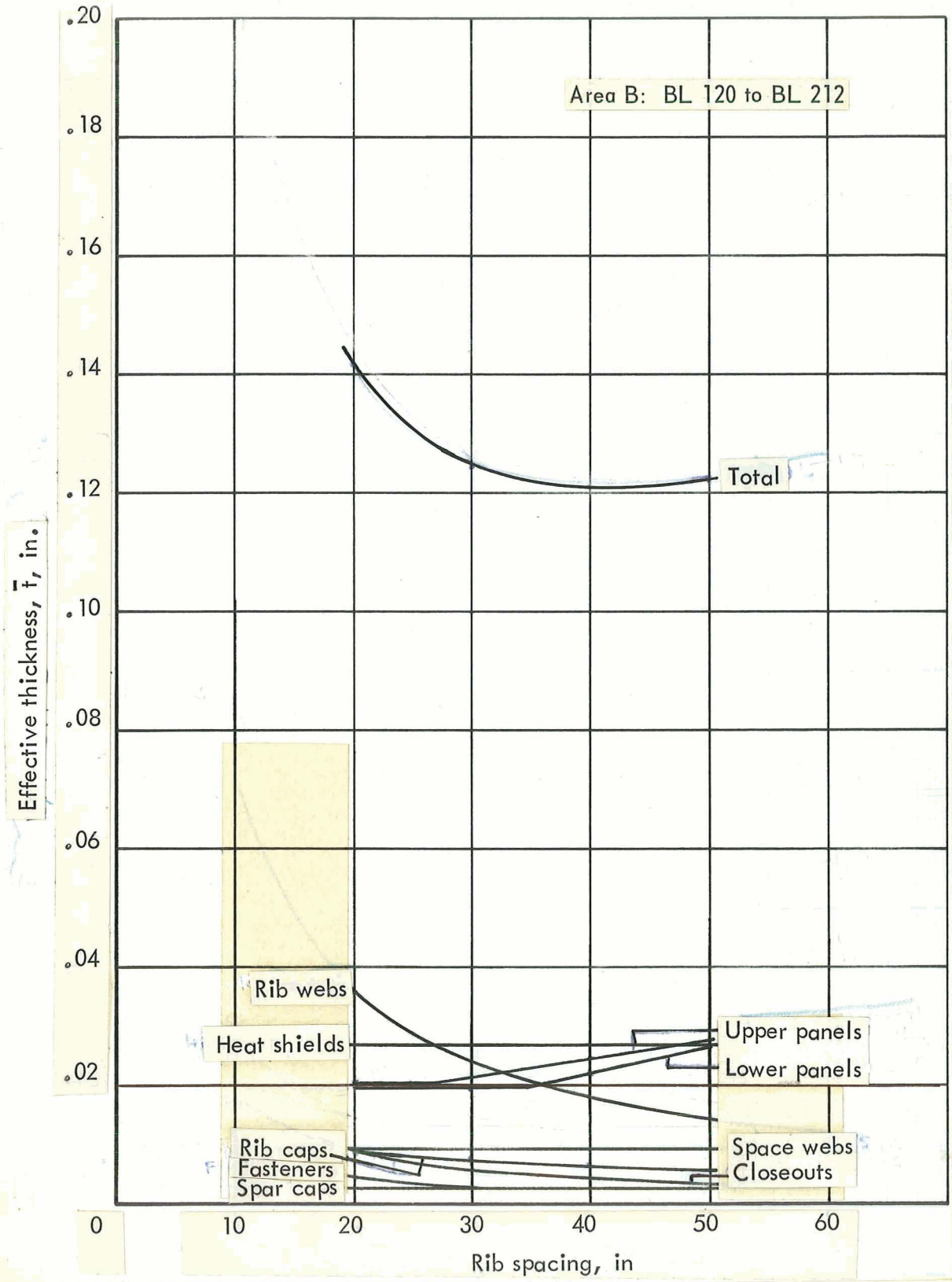

Figure 13-72. Optimum rib spacing for inboard area of semimonocoque spanwise-stiffened beaded panels with no insulation

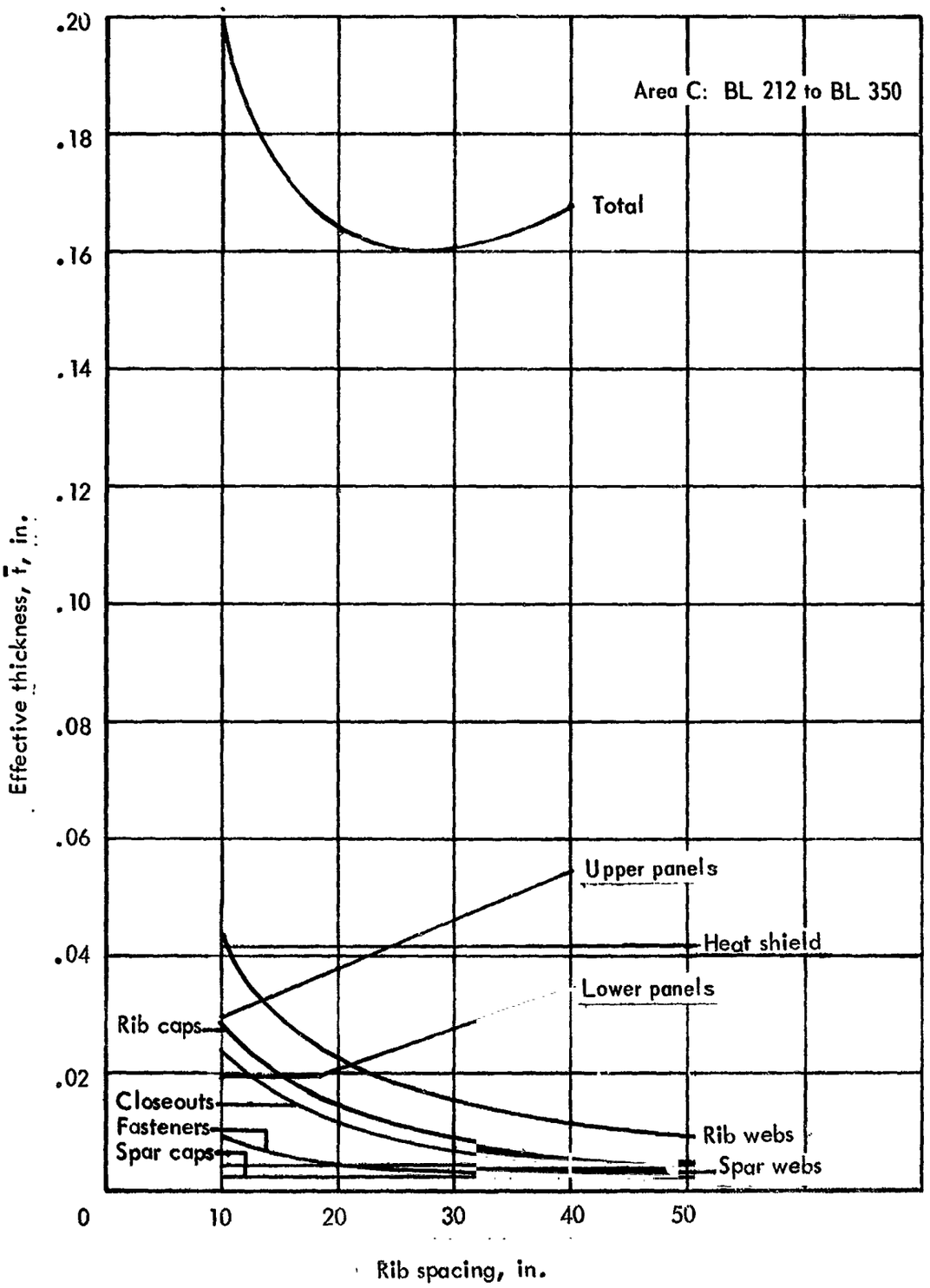

Figure 13-73. Optimum rib spacing for outboard area of semimonocoque spanwise-stiffened beaded panels with no insulation

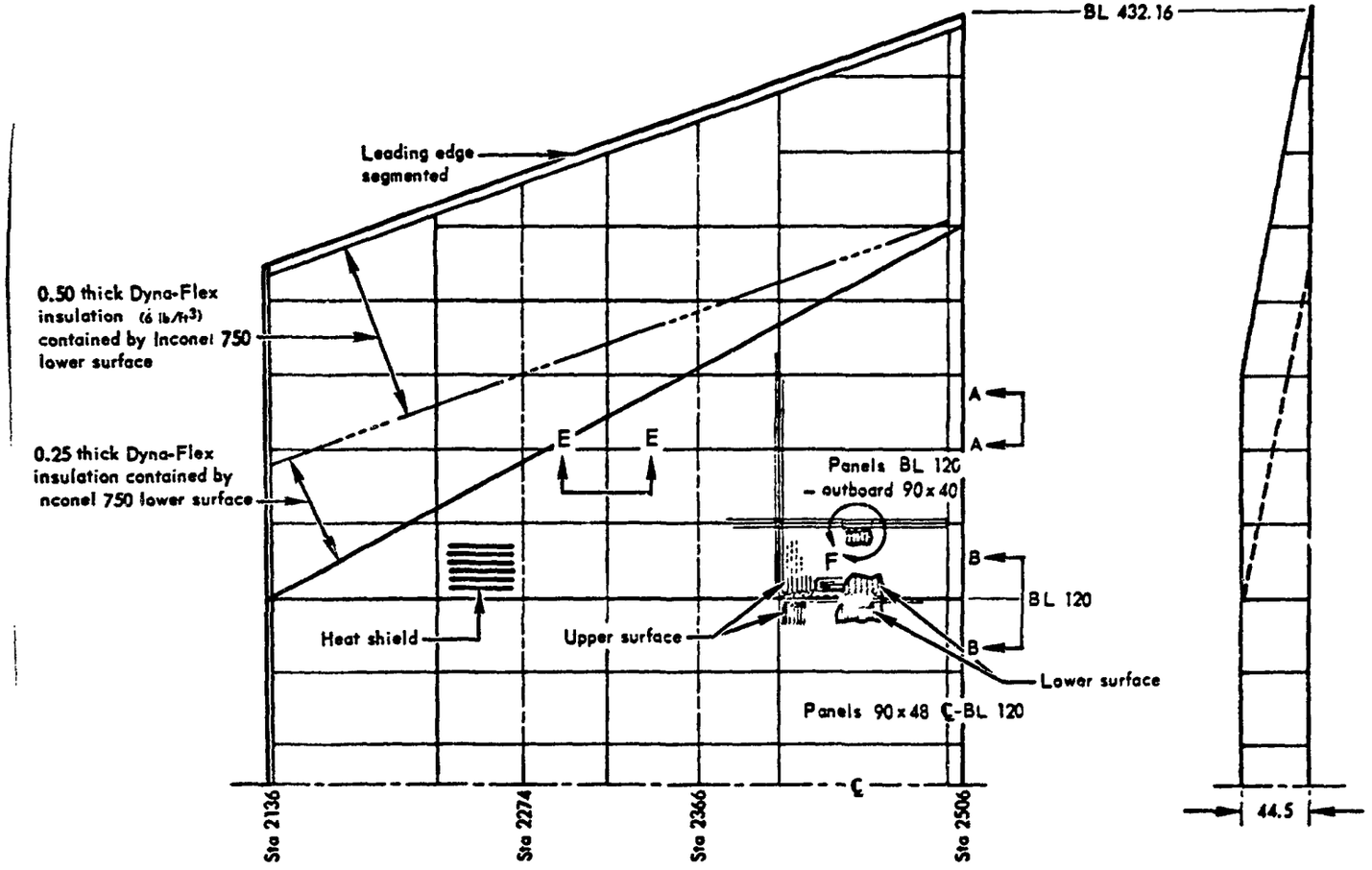

Figure 13-74. Final design of semimonocoque spanwise-stiffened beaded primary-structure concept

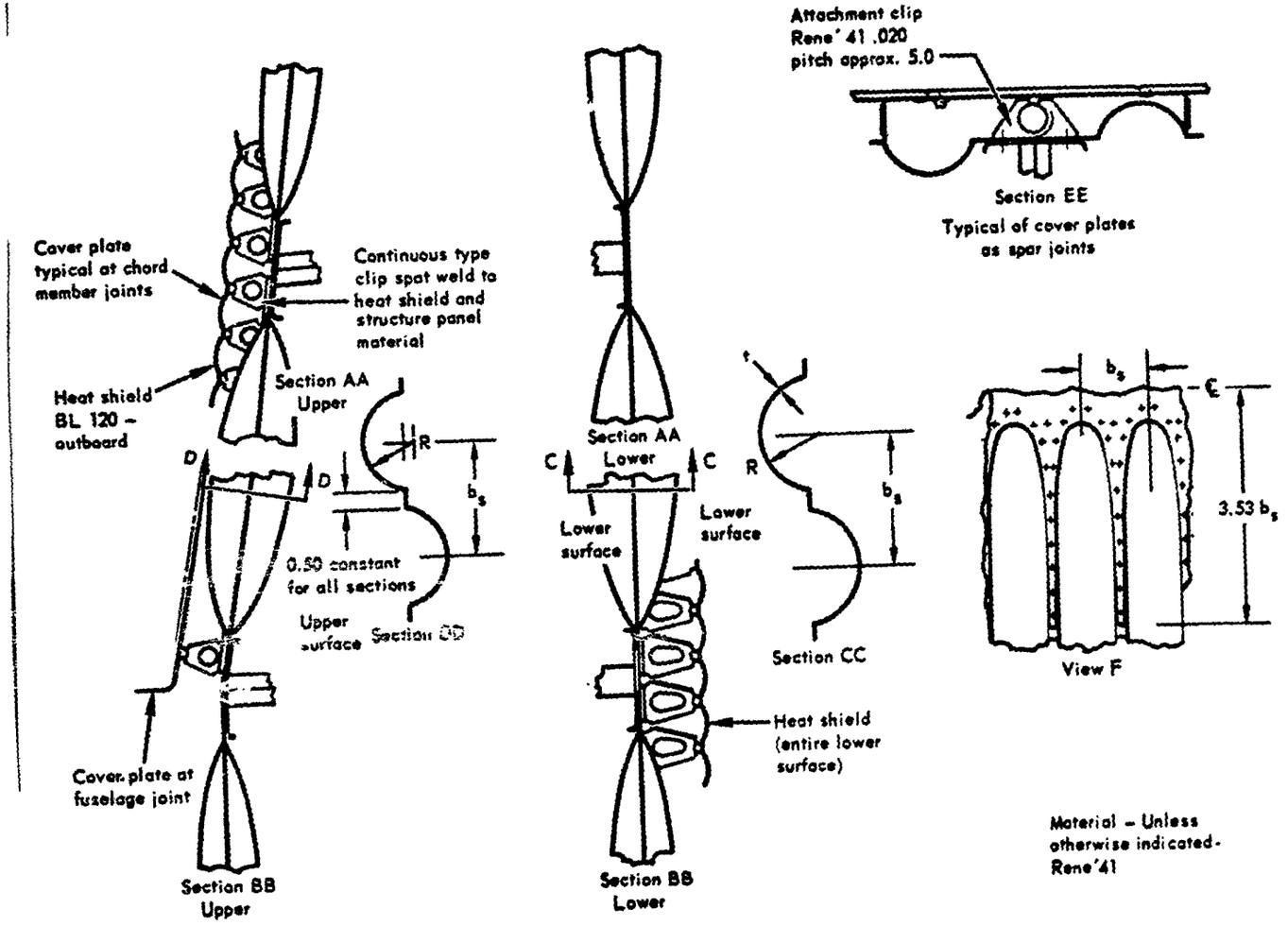

Figure 13-74. Final design of semimonocoque spanwise-stiffened beaded primary-structure concept (Cont.)

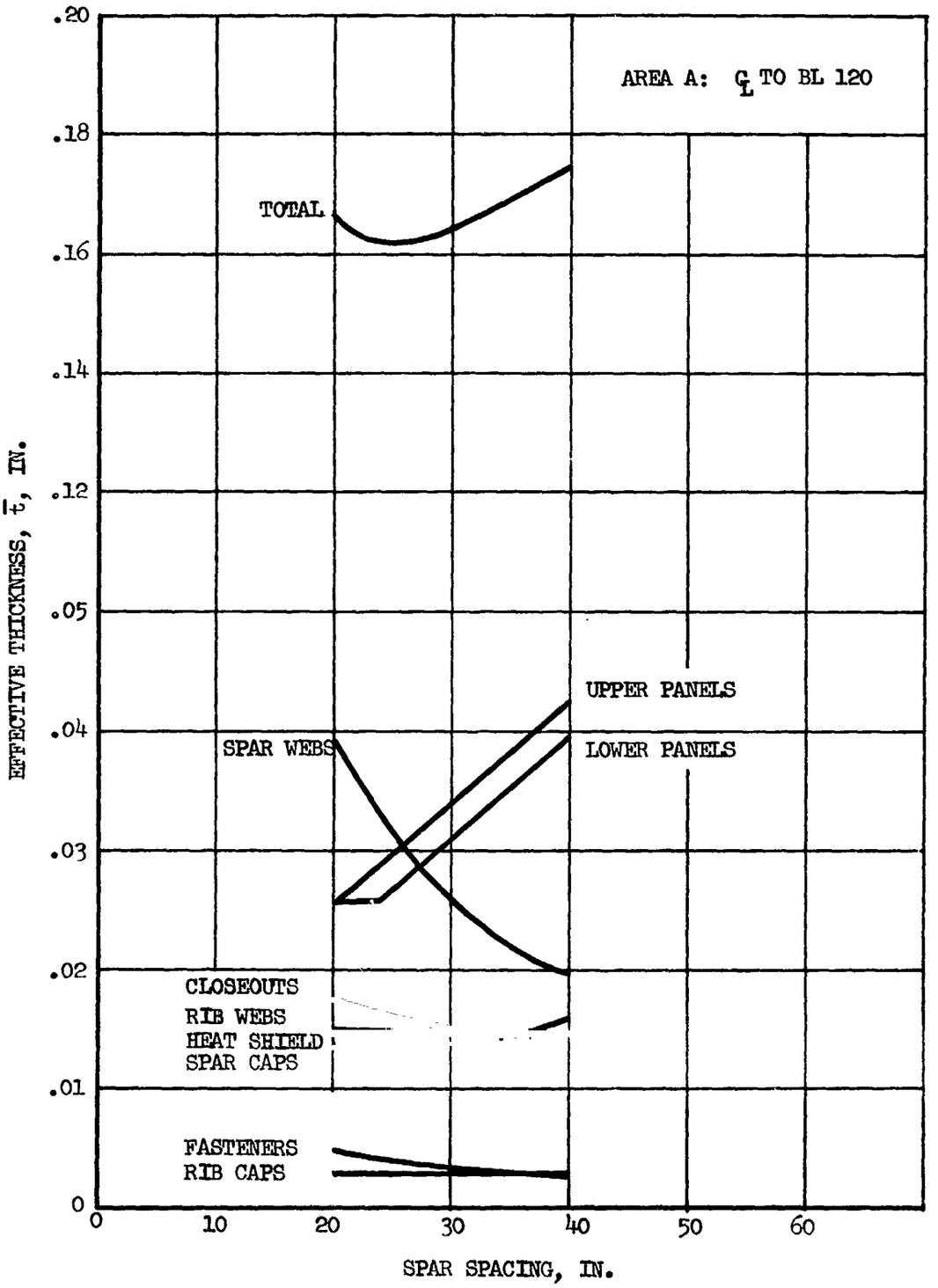

Figure 13-75 Optimum spar spacing for center area of semimonocoque chordwise-stiffened tubular lower surface and convex-beaded upper surface with lower heat shields and partial insulation outboard

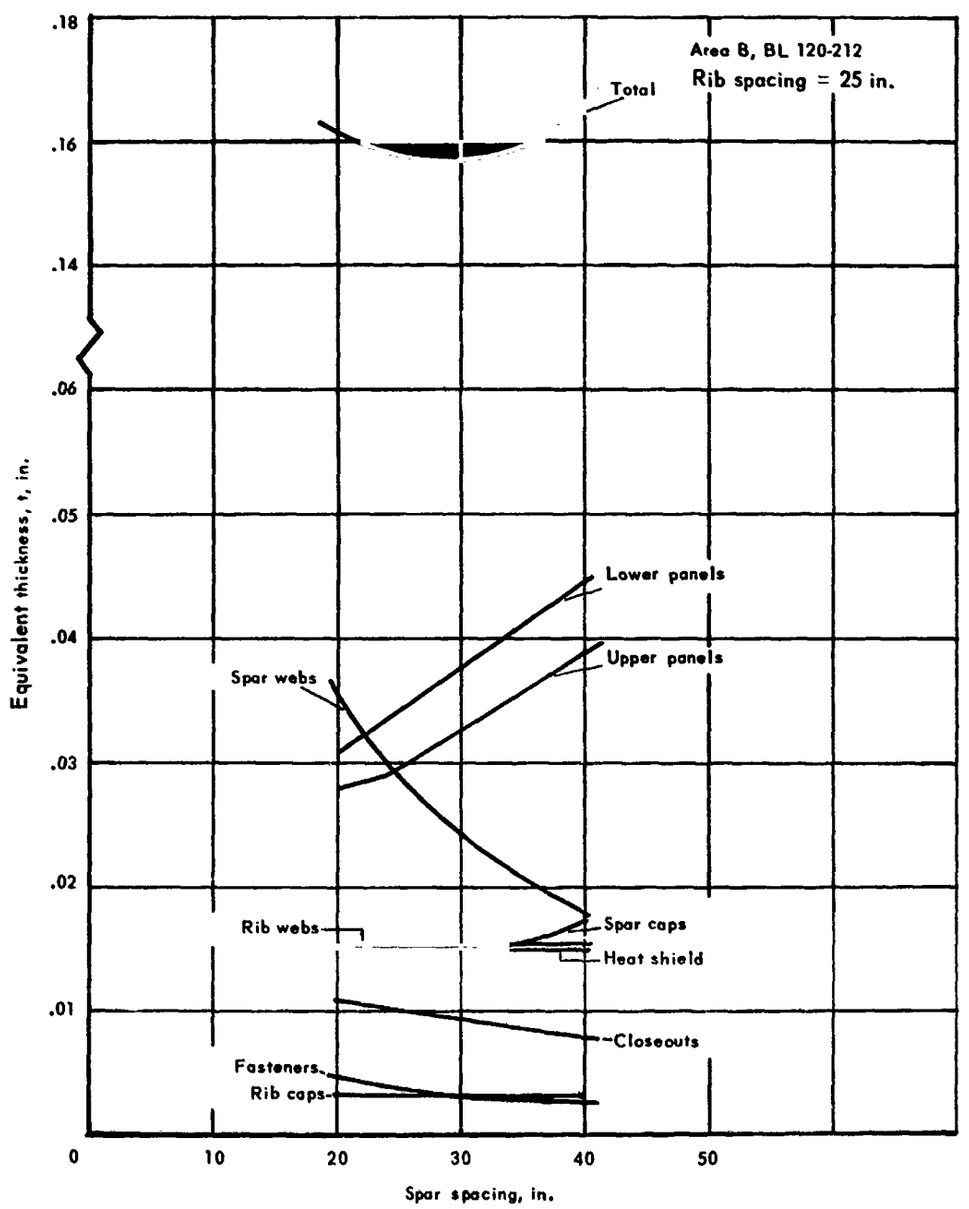

Figure 13-76 Optimum spar spacing for semimoncoque chordwise stiffened concept

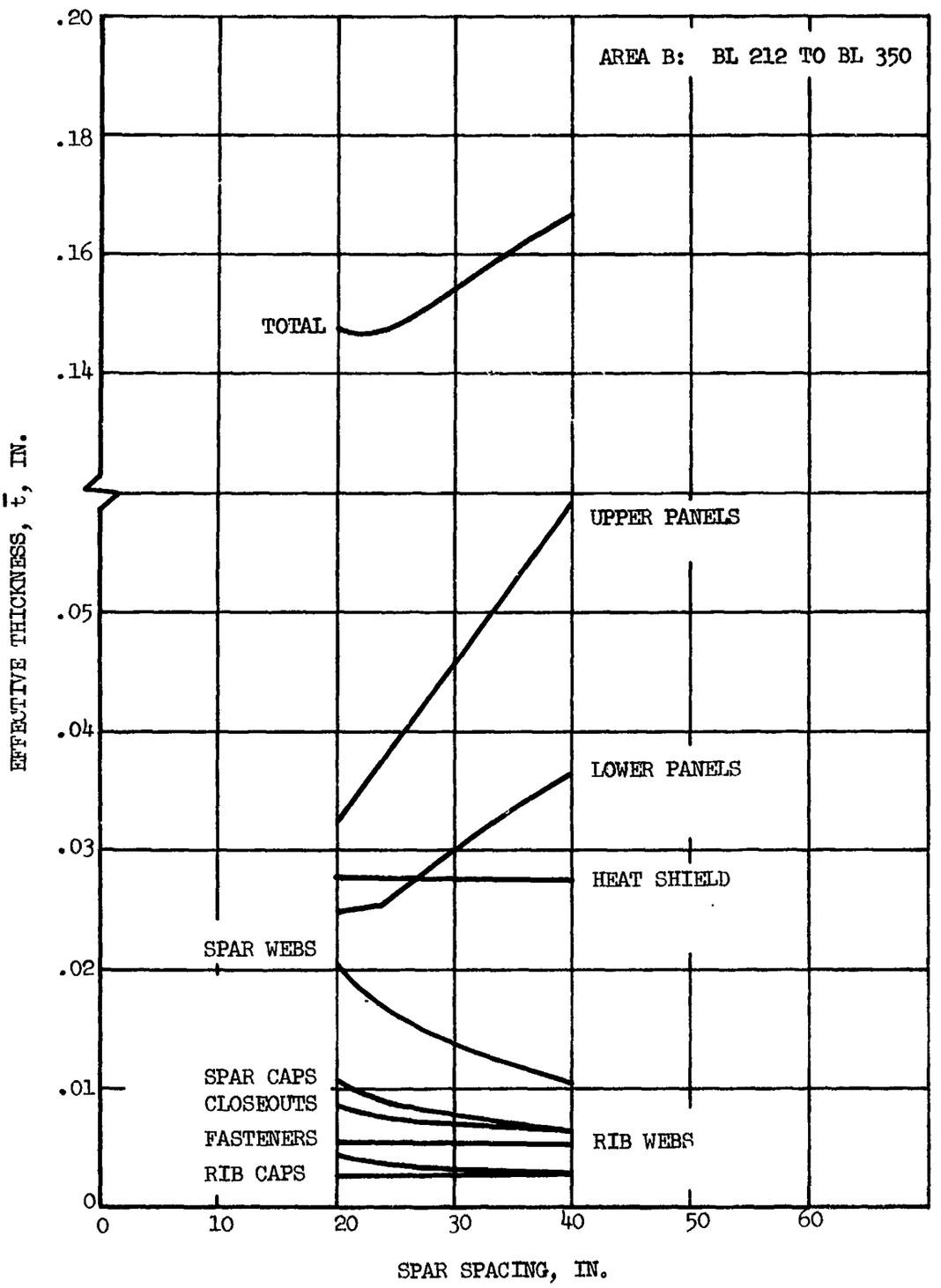

Figure 13-77 Optimum spar spacing for outboard area of semimonocoque chordwise-stiffened tubular panels with lower surface heat shield and partial insulation outboard

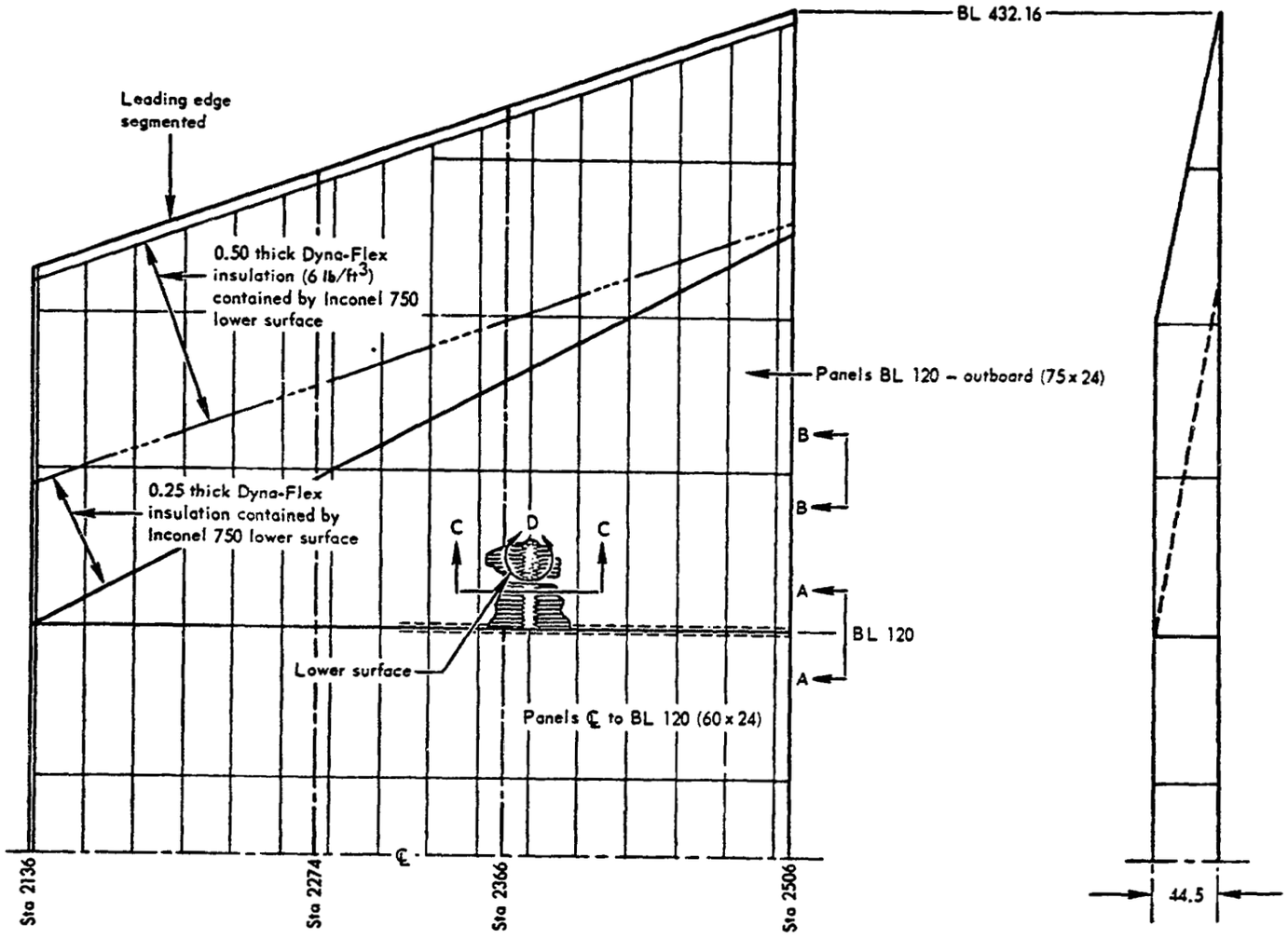

Figure 13-78. Final design of semimonocoque chordwise-stiffened primary-structure concept

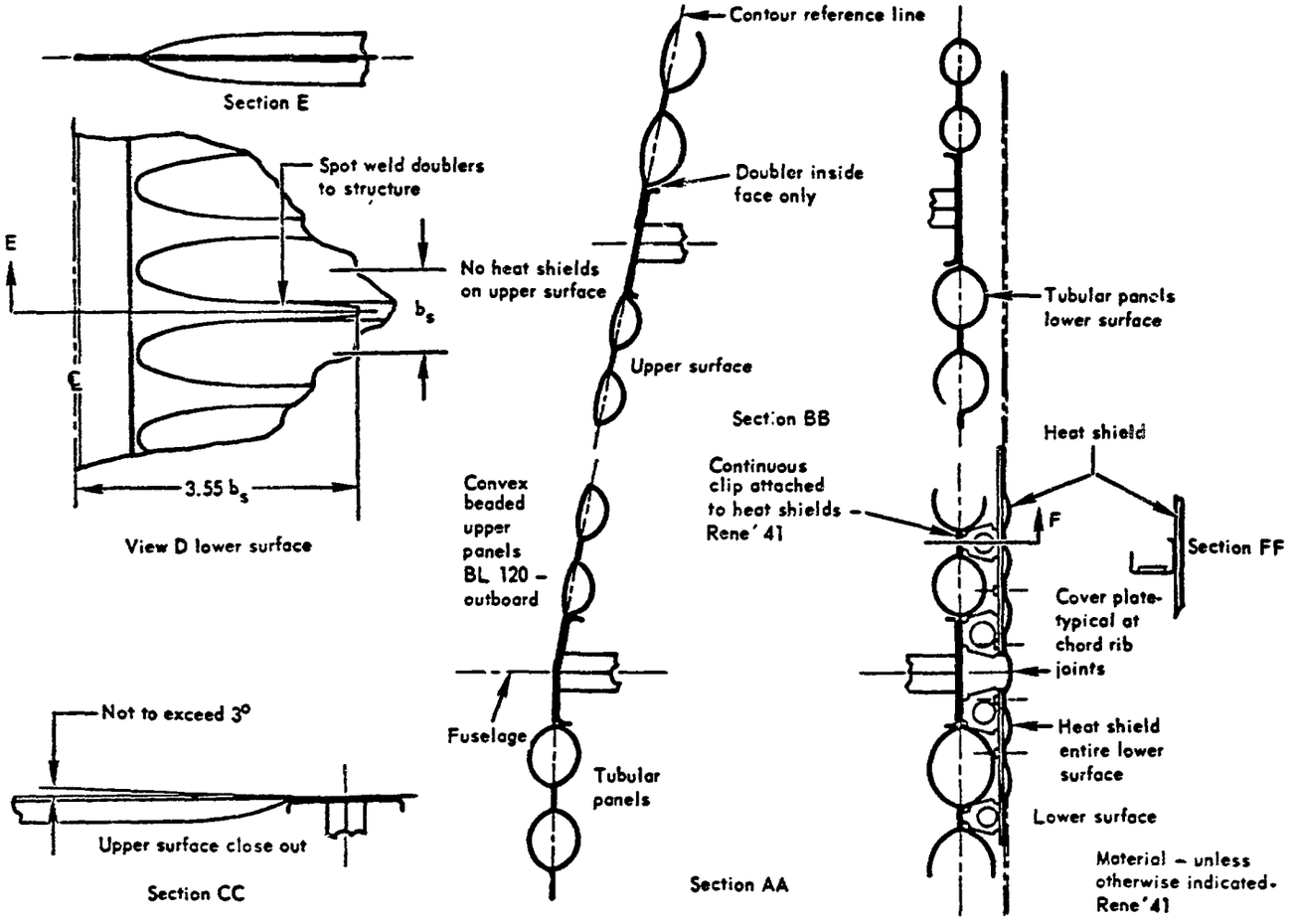

Figure 13-78. Final design of semimonocoque chordwise-stiffened primary-structure concept (Cont.)

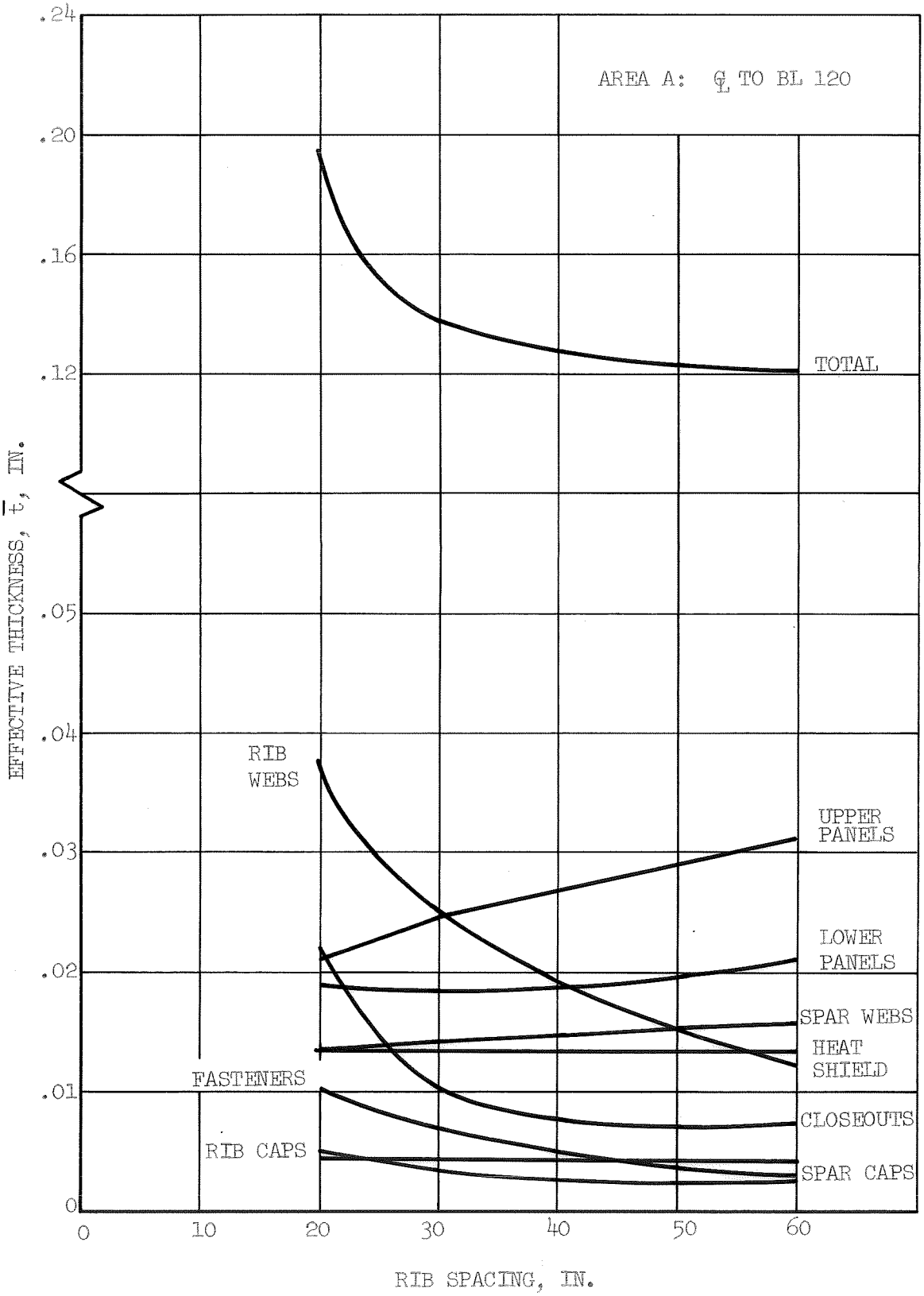

Figure 13-79 Optimum rib spacing for center area of statically determinate beaded panels with heat shields and no insulation

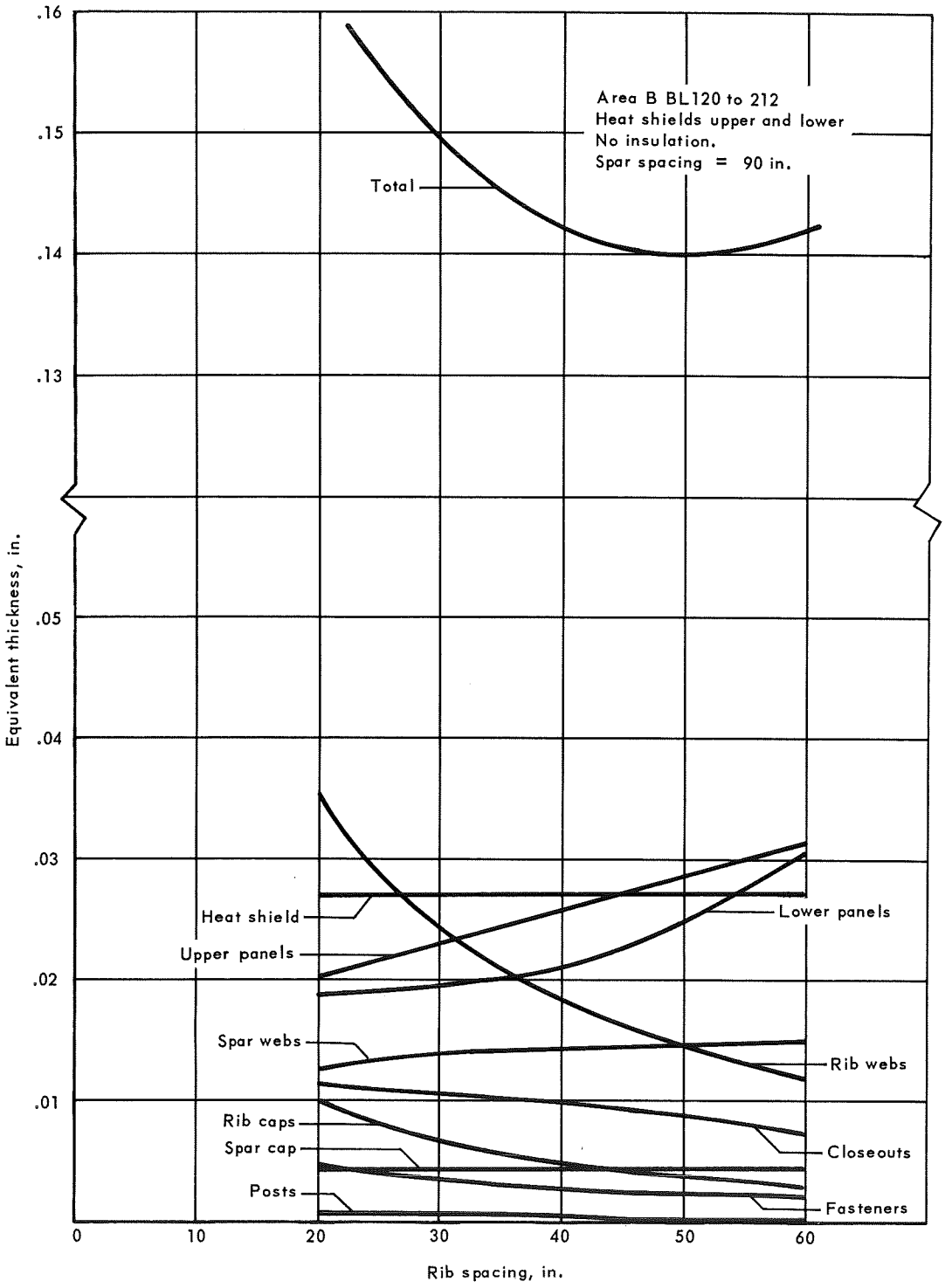

Figure 13-80 Optimum rib spacing for statically determinate beaded concept

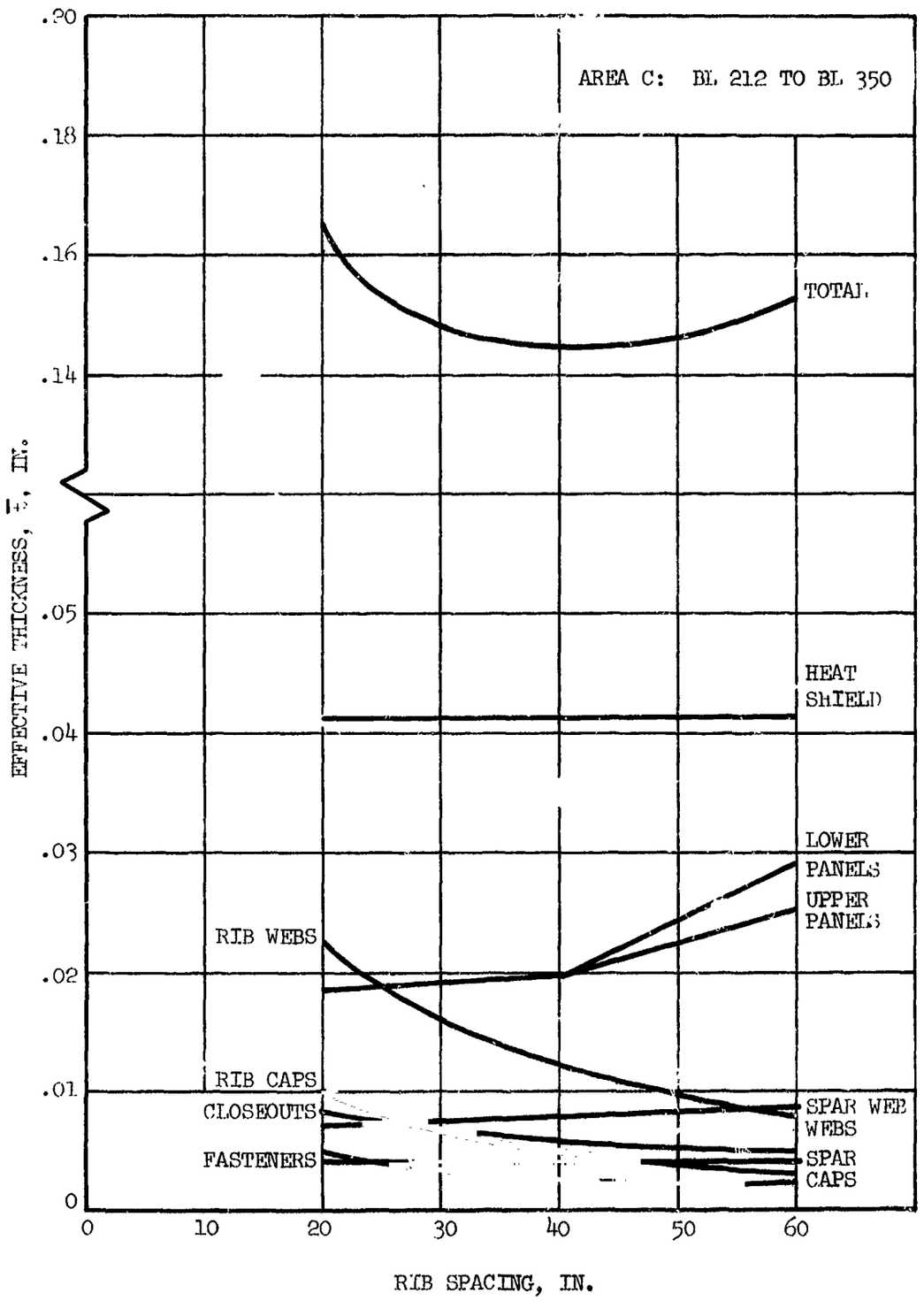

Figure 13-81 Statically determinate concept optimum rib spacing

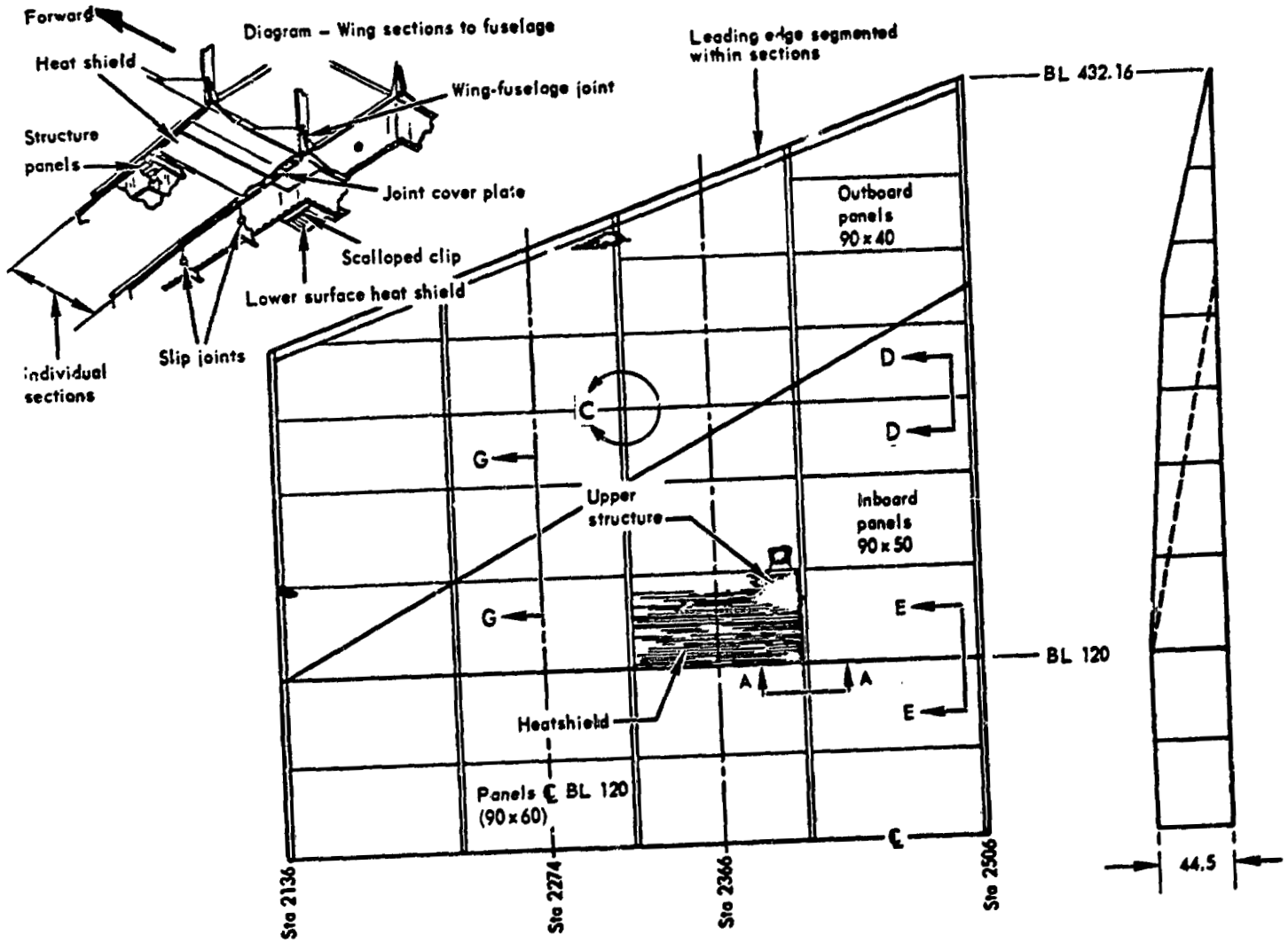

Figure 13-82. Final design of statically determinate beaded primary-structure concept

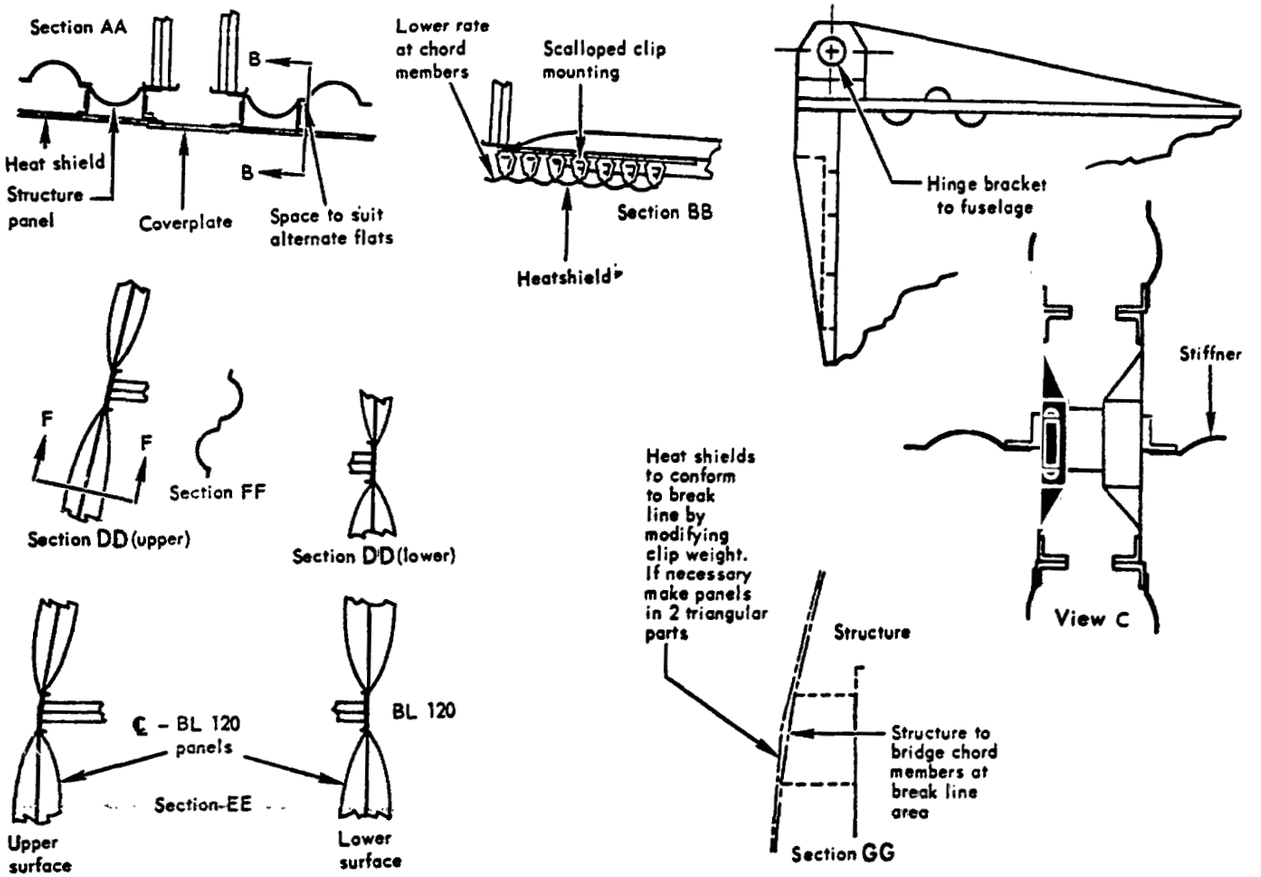

Figure 13-82. Final design of statically determinate beaded primary-structure concept (Cont.)

Section 14

PANEL FLUTTER ANALYSIS

by

G. W. Davis, L. E. Fogg, and C. C. Richie

CONTENTS

TABLES

SYMBOLS

$\bar{A}_x, \bar{A}_y$	Panel geometry parameters
a,b	Panel dimension in x and y coordinates
BL	Butt line
C	Stiffness parameter, $D_{12}/(D_1 D_2)^{1/2}$
D_1, D_2, D_{12}	Stiffness coefficients of governing differential equations
E	Modulus of elasticity
I	Moment of inertia
K	Deflectional spring constant per unit length
$\bar{K}$	Deflectional spring constant, $Kb^3/\pi^3 D_2$
ℓ	Length
M	Mach number
p	Pitch of panel stiffeners and heat shield clips
q	Dynamic pressure of airstream
T	Temperature
β	$(M^2 - 1)^{1/2}$
λ	Dynamic pressure parameter
λ_{cr}	Value of dynamic pressure parameter at flutter

Section 14

PANEL FLUTTER ANALYSIS

The results of the analytical flutter investigation indicate all wing surfaces exposed to the aerodynamic environment remain stable throughout the entire flight trajectory.

CRITERIA

The surface panels were analyzed by use of the method presented by Bohon and Anderson (ref. 14-1), which includes the influence of spring-supported edges.

A factor of safety of 1.3 on the dynamic pressure and a test correlation factor of 2.0 is used. This results in the theoretical critical dynamic pressure to cause flutter being greater than 2.6 times the actual dynamic pressure at the critical point of the flight trajectory.

The critical point of the flight trajectory was evaluated from the maximum value of the $q/\beta E$ parameter, where

q = dynamic pressure, psi

$\beta = \left[(\text{Mach No.})^2 - 1\right]^{1/2}$

E = Young's modulus of the structure at the temperature corresponding to the point of the flight trajectory being evaluated

This parameter was evaluated at 7, 20.6, and 40 minutes into the flight, and the critical point of the flight trajectory was determined to occur at 7 minutes into the flight. Consequently, the stiffness of the unshielded primary structural panels was based on a temperature of 500°F, and for the shielded areas the heat shield, support clip, and panel temperatures were 500°F, 350°F, and 200°F, respectively.

Where refurbishable heat shields are used, the spring constants include the flexibility of the heat shield edge closeout, the support clip, and the primary structural panel. The primary structural panel is regarded as shielded from the aerodynamic environment when the refurbishable heat shield is employed. However, where modular or permanently attached heat shields are used, both the heat shield and the primary structural panel are required to be flutter free. Unshielded primary structural panels are analyzed and required to be flutter free with edge spring supports based on the flexibility of the panel edge closeout and the structure to which it is attached.

PRIMARY STRUCTURAL PANELS

Monocoque Waffle

The waffle concept has heat shields on the lower outboard surface only. In all other areas the structural panel is subjected to the aerodynamic environment. The panels have an aspect ratio of 2 and dimensions of 20 inches by 40 inches, with the long dimension parallel to the airstream. The edge of the panel is attached to the spar and rib flanges. The effective spring constant of the unshielded panels is based on the flexibility of the spar/rib flange, the panel edge thickness, and the panel edge closeout. A schematic drawing for this closeout area is shown in table 14-1. The spar/rib flange was assumed to be cantilevered from a point halfway between the centerline and the edge of the corrugated web, with an inflection point occurring at the panel-to-flange attachment point. The stiffness of the tapered panel edge closeout was assumed to vary according to the square of the tapered length. On the basis of these assumptions and by use of the strain energy of bending for this system, the equation for the spring constant was determined. The spring constant equation, spring constants, and related stiffnesses for the panel edge closeout are summarized in table 14-1. It was assumed that the leading and trailing edges were simply supported and the streamwise edges were elastically supported with the aforementioned spring constant.

The heat shield on the lower surface of the outboard segment of the wing is corrugated in the streamwise direction and is supported on hat-shaped clips spaced at 10 inches in the streamwise direction. The effective spring constant is based on the combined flexibility of the support clips and the waffle primary structural panels. The equations for the spring constants, stiffnesses, and geometry for the clips and the primary structural panels are shown in tables 14-2 and 14-3, respectively. The critical dynamic pressure parameter as defined in the criteria section occurs at 7.0 minutes into the flight. At this time the temperature of the heat shield, the clip, and the panel are 500°F, 350°F, and 200°F, respectively.

All areas of the wing are stable and exceed the flutter factor of safety requirements as defined in the criteria section. Table 14-4 summarizes the principal flutter parameters and results. The minimum factor of safety of 6.77 occurs on the lower surface heat shield between BL 304 and 350.

Monocoque Honeycomb

The honeycomb concept has the identical thermal protection arrangement as the waffle concept – heat shields on the lower surface outboard area of the wing. The panels have an aspect ratio of 2 and dimensions of 40 inches by 80 inches, with the long direction parallel to the airstream. The panel has a channel closeout stiffening the two face sheets, with an upper-surface splice plate for load transfer between adjacent panels. The lower face sheet is attached to the spar and rib flanges.

The effective spring constants for the unshielded panels are based on the combined flexibility of the spar/rib flange, panel edge thicknesses, and the panel closeout. The closeout geometry and the assumptions made for the solution of the spring constant are shown in table 14-5. The spring constants for these unshielded areas are summarized in table 14-6.

The heat shields on the lower surface of the outboard segment are corrugated in the streamwise direction and attached to the primary structural panels by clips spaced approximately 11.4 inches. The heat shield spring constants, which are composed of the heat shield clip and primary structure panels, are shown in tables 14-2 and 14-3.

All areas of the wing are stable, with the minimum factor of safety of 5.31 occurring on the shielded lower surface between BL 212 and 304. The principal flutter parameters and results are shown in table 14-6.

Semimonocoque Spanwise

The tubular and beaded concepts have refurbishable heat shields on both upper and lower surfaces. These heat shields are the corrugated concept with multiple supports. The shield is stiffened in the streamwise direction and attached to the primary structural panels by clips spaced approximately 13.1 inches in the spanwise direction. The panel width is equal to the rib spacing, which is 50 inches, 40 inches, and 40 inches from center to outboard areas, respectively, for both concepts.

Since these concepts are completely shielded, the spring constants are based on the combined flexibility of the heat shield support clips and the primary structure panels. These equations and spring constants are shown in tables 14-2 and 14-3. The heat shields for all wing areas for both the tubular and beaded concepts are stable and meet the required factor of safety. The principal flutter parameters and results are shown in tables 14-7 and 14-8. The minimum factor of safety for both concepts occurs on the lower surface heat shield located between the centerline and BL 120, $\lambda_{cr}/\lambda = 2.69$ for the tubular and $\lambda_{cr}/\lambda = 3.0$ for the beaded concept.

Semimonocoque Chordwise

The chordwise concept has tubular primary structure panels on the lower surface and convex beaded panels on the upper surface. The lower surface requires heat shield for thermal protection and aerodynamic smoothness. The shields, which are stiffened in the spanwise direction, are attached to the primary structure by clips spaced 13.1 inches in the streamwise direction. The panel dimensions for both upper and lower surface primary structure panels are 75 inches by 25 inches spanwise and chordwise, respectively.

The spring constants on the lower surface heat shields are based on the combined flexibility of the heat shield clip and tubular panel. The clip spring constants are summarized in table 14-2. The spring constant equation and stiffnesses for the lower surface panels are shown in table 14-3.

The unshielded upper surface spring constants are based on the combined flexibility of the spar flange thickness and panel closeout geometry. The spar flange was assumed to be cantilevered from a point halfway between the centerline and the edge of the corrugated web. The stiffness of the panel edge closeout was assumed to vary according to the square of the tapered length. The closeout spring constants for the upper exposed panels are shown in table 14-9. The related dimensions and stiffnesses as well as the spring constant equation are contained in this table.

Both upper and lower surfaces are stable and have factors of safety against flutter, λ_{cr}/λ , that exceed the required factor of safety of 2.6. The minimum factor of safety of 12.4 occurs on the lower surface between the centerline and BL 120. The principal flutter parameters and results of the analysis are summarized in table 14-10.

Statically Determinate

This concept has refurbishable heat shields on both upper and lower surfaces with corrugations in the streamwise direction. The heat shields are attached to the primary structural panels by clips spaced 13.1 inches in the streamwise direction. The primary structural panels used on this concept are the spanwise stiffened beaded configuration.

The panel widths are equal to the rib spacing and are 60, 50, and 40 inches from center to outboard area respectively. Since all surfaces are shielded, the effective spring constant was calculated from the combined flexibility of the heat shield support clips and the primary structural panels. These spring constant calculations are shown in tables 14-2 and 14-3

The heat shields are stable and have factors of safety against flutter that exceed the required factor of safety of 2.6. The minimum factor of safety occurs on the lower surface heat shield between the centerline and BL 120. The principal flutter parameters and results are summarized in table 14-11.

HEAT SHIELD CANDIDATE ANALYSIS

A detailed panel flutter analysis of each of the candidate heat shield concepts was conducted by use of the method and criteria discussed in the criteria section. Both refurbishable and permanently attached heat shields were analyzed. The heat shield designs investigated are described in Section 20. The effective spring constant is based on the combined flexibility of the support clips and the primary structural panel.

A typical tubular panel was assummed with a radius of 1.0 inch, a thickness of 0.010 inch and a pitch of 2.4526 inches. For the analysis of the panel with permanently attached heat shields, the effective spring constant was based on the combined flexibility of the rib flange, the panel edge thickness (including doubler), and the tapered end closeout of the tube. The critical dynamic pressure parameter occurs at 7.0 minutes into the flight.

The refurbishable heat shields are stable and have factors of safety against flutter, λ_{cr}/λ , that exceed the required value of 2.6. However, the primary structural panel of the permanently attached (modular) concepts has an allowable flutter parameter that is less than the applied dynamic pressure; consequently, it would flutter. The principal flutter parameters and results are summarized in table 14-12.

REFERENCE

14-1 Bohon, Herman; and Anderson, Melvin S.: The Role of Boundary Conditions on Flutter of Orothotropic Panels. AIAA Journal, Vol. 4, No. 7, R41-1248, July 1966.

TABLE 14-1

WAFFLE CLOSEOUT SPRING CONSTANTS

Wing location	T, °F	E, psi	P pitch, in.	t_c, in.	D_{11}, lb-in.	D_B, lb-in.	D_E, lb-in.	K, lb/in./in.
℄ – 120 (Lower)	500	29.7×10^6	0.799	.0797	28 900	1 253	27 647	7 640
120 – 212 (Lower)	500	29.7	1.022	.0892	47 100	1 756	45 368	8 920
212 – 350* (Lower)	–	–	–	–	–	–	–	–
120 – 212 (Upper)	500	29.7	1.031	.1028	47 400	2 690	44 772	10 240
212 – 350 (Upper)	500	29.7	1.105	.0845	32 350	1 490	30 869	6 840

$$\frac{1}{K} = \frac{877.08}{E} + \frac{0.38\,P^2}{D_E}\,\mathrm{LOG}_e\left(\frac{D_{11}}{D_B}\right) + 0.707\,\frac{P^3}{D_E} + \frac{0.0183}{D_B} + \left[\frac{.2042P - .707P^3\,(D_B/D_E)}{(D_E D_B)^{1/2}}\right] \tan^{-1}\left(\frac{D_E}{D_B}\right)^{1/2}$$

*Surface has heat shield

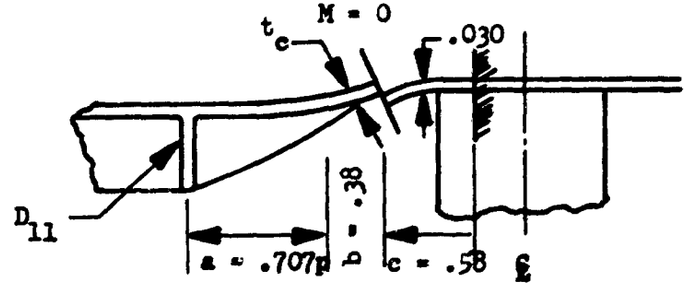

TABLE 14-2

HEAT SHIELD CLIP SPRING CONSTANTS

Concept	Wing location	Clip temp °F	Material	ℓ_1 in.	I_1 in.^{4} x 10^{-6}	ℓ_2 in.	I_2 in.^{4} x 10^{-6}	h in.	ℓ_3 in.	I_3 in.^{4} x 10^{-6}	ℓ_4 in.	I_4 in.^{4} x 10^{-6}	Pitch in.	E_s psi	K_{Clip} lb/in./in.
Semimonocoque, spanwise (tubular and beaded) and statically determinate	120-212 (Upper)	350	René 41	0.167	0.314	0.100	0.314	0.700	0.750	10.8	0.300	1.22	1.22	30.34	1034
	212-350 (Upper)	350	René 41	0.167	0.570	0.100	0.570	0.600	0.650	12.5	0.300	2.24	1.52	30.34	1444
	ℓ_2 - 120 (Lower)	350	René 41	0.167	0.314	0.100	0.314	0.600	0.650	10.8	0.300	1.22	1.22	30.34	1056
	120-212 (Lower)	350	René 41	0.167	0.314	0.100	0.314	0.600	0.650	10.8	0.300	1.22	1.22	30.34	1056
	212-304 (Lower)	350	René 41	0.167	0.696	0.100	0.696	0.600	0.650	14.1	0.300	2.75	1.88	30.34	1407
	304-350 (Lower)	350	TD NiCr	0.167	1.645	0.100	1.645	0.600	0.650	18.5	0.300	6.41	3.18	20.0	1119
Semimonocoque, chordwise	ℓ_2 - 120 (Lower)	350	René 41	0.167	2.16	0.150	2.16	0.700	0.750	14.9	0.300	1.08	2.843	30.34	831
	120-212 (Lower)	350	René 41	0.167	2.16	0.150	2.16	0.700	0.750	14.9	0.300	1.08	2.355	30.34	1003
	212-304 (Lower)	350	René 41	0.167	5.13	0.150	5.13	0.700	0.750	18.0	0.300	1.56	1.769	30.34	2016
	304-350 (Lower)	350	TD NiCr	0.167	9.36	0.150	9.36	0.700	0.750	24.2	0.300	4.68	1.769	20.0	2894
Monocoque, honeycomb	212-304 (Lower)	350	René 41	0.167	0.696	0.100	0.696	0.600	0.650	14.1	0.300	2.75	1.88	30.34	1407
	304-350 (Lower)	350	TD NiCr	0.167	1.645	0.100	1.645	0.600	0.650	18.5	0.300	6.41	3.18	20.0	1119

$$K_{Clip} = \frac{E}{K_{Pitch}} \Big/ \ell_1^2 \left[\frac{\ell_1}{3I_1} + \frac{\ell_2}{I_2} + \frac{2h^2}{I_3 \ell_3} + \frac{\ell_4}{I_4} \right]$$

TABLE 14-3

PANEL SPRING CONSTANT FOR SHIELDED AREAS

Concept	Wing location	Surface	Material	Panel temp, °F	E, psi x 10^6	$\bar{I}$, $in.^4/in.$	b_{HS}, in.	D, lb-in. x 10^3	b_{Panel}, in.	K_{Panel}, lb/in./in.
Semimonocoque, spanwise, tubular	120-212	Upper	René 41	200	30.97	.00677	13.1	209.7	40	82.4
	212-350	Upper	René 41	200	30.97	.00360	13.1	111.5	40	43.8
	℄ -120	Lower	René 41	200	30.97	.00420	13.1	130.1	50	20.9
	120-212	Lower	René 41	200	30.97	.00462	13.1	143.1	40	56.2
	212-350	Lower	René 41	200	30.97	.00218	13.1	67.5	40	26.5
Semimonocoque, spanwise, beaded	120-212	Upper	René 41	200	30.97	.00850	13.1	263.2	40	103.6
	212-350	Upper	René 41	200	30.97	.00464	13.1	143.7	40	56.5
	℄ -120	Lower	René 41	200	30.97	.00576	13.1	178.4	50	28.7
	120-212	Lower	René 41	200	30.97	.00954	13.1	295.4	40	116.2
	212-350	Lower	René 41	200	30.97	.00702	13.1	217.4	40	85.5
Semimonocoque, chordwise	℄ -120	Lower	René 41	200	30.97	.00616	13.1	190.8	24	578.5
	120-212	Lower	René 41	200	30.97	.00625	13.1	193.6	24	587.0
	212-350	Lower	René 41	200	30.97	.00218	13.1	67.5	24	204.7
Monocoque, waffle	212-350	Lower	René 41	200	30.97	.00033	13.1	10,238	20	51.2
Monocoque, honeycomb	212-350	Lower	René 41	200	30.97	.00375	13.1	116,200	40	39.8
Statically determinate	120-212	Upper	René 41	200	30.97	.0134	13.1	414.9	50	67.1
	212-350	Upper	René 41	200	30.97	.0029	13.1	89.9	40	35.4
	℄ -120	Lower	René 41	200	30.97	.0082	13.1	253.9	60	19.8
	120-212	Lower	René 41	200	30.97	.0182	13.1	563.6	50	90.6
	212-350	Lower	René 41	200	30.97	.0099	13.1	306.6	40	121.2

$$K_{Panel} = \left(\frac{384}{5}\right) \frac{D_{Panel} (b)_{hs}}{(b)^4_{Panel}}$$

TABLE 14-4

MONOCOQUE WAFFLE PANEL FLUTTER PARAMETERS

Location		Center	Inboard		Outboard
Surface		Lower	Upper	Lower	Upper
$D_1 = D_2$, lb-in.	(a)	28 900	47 400	47 100	32 350
D_{12}, lb-in.	(b)	76 300	124 500	124 700	85 400
K, lb/in./in.		7 640	10 240	8 920	6 840
$\bar{K}$	(c)	96.9	68.8	72.4	70.1
C	(d)	2.642	2.625	2.649	2.636
$-\bar{A}_x$	(e)	21.1	21.0	21.2	21.1
$(\lambda'_{cr})^{1/3}$	(f)	3.4	3.4	3.4	3.4
$(q/\beta)_{cr}$, psi		305	495	498	340
$(q/\beta)_{cr}/(q/\beta)$	(g)	83	135	135	92

(a) Flexural stiffness

(b) Twisting stiffness, $D_{12} = D_3 = D_1 + 2D_{33}$

(c) $\bar{K} = K b^3/\pi^3 D_2$, where $b = 20$ inches

(d) $C = D_{12}/(D_1 D_2)^{1/2}$

(e) $-\bar{A}_x = 2 (a/b)^2 D_{12}/D_1$, where $a = 40$ inches

(f) $(\lambda'_{cr})^{1/3} = (2qb^3/\beta D_1)^{1/3} (D_1/D_{12})^{1/2}$; from figure 4, reference 14-1; ($C = 7.07$ and $\bar{K} = 50$)

(g) $q/\beta = 3.68$ psi at 7.0 minutes

TABLE 14-4 (Concluded)

			Lower Surface[k]	
			BL 212-304	BL 304-350
$(D_1)_{Panel}$,	lb-in.	(a)	10 680	10 680
K_{Panel},	lb/in./in.	(b)	51.2	51.2
$(D_2)_{HS}$,	lb-in.	(c)	2 376	1 560
$(D_{12})_{HS}$,	lb-in.	(d)	6.100	4.005
λ		(e)	3.098	4.724
$-\bar{A}_y$		(f)	0.000142	0.000143
K_{Clip},	lb/in./in.	(g)	28,180	18,576
$\bar{K}$,	lb/in./in.	(h)	51.1	51.07
$\bar{\bar{K}}$		(i)	0.693	1.056
λ_{cr}		(j)	25	32
λ_{cr}/λ			8.07	6.77

(a) $(D_1)_{Panel} = E\,(\bar{I}_1)_{Panel}$; $E = 30.97 \times 10^6$ psi

(b) $K_{Panel} = (384/5)\,(D_1)_{Panel}\,(b)_{HS}/(b)^4_{Panel}$

(c) $(D_2)_{HS} = E\,(\bar{I}_2)_{HS}$; $E = 29.7 \times 10^6$ psi

(d) $(D_{12})_{HS} = \left(\frac{S}{b_S}\right)\frac{Et^3}{12\,(1+\nu)} = \left(\frac{1.047R + b_f}{b_S}\right)\frac{Et^3}{15.6}$

(e) $\lambda = 2\,(q/\beta)\,(b^3/D_2)_{HS} = 7.37\,(b^3/D_2)_{HS}$

(f) $-\bar{A}_y = 2\,(b/a)^2_{HS}\,(D_{12}/D_2)_{HS}$

(g) $E_{Clip} = 30.34 \times 10^6$ psi (René 41 clips @ T = 350°F); $E_{Clip} = 20 \times 10^6$ psi (TD NiCr clips @ T = 350°F)

(h) $\frac{1}{\bar{K}} = \frac{1}{K_{Panel}} + \frac{1}{K_{Clip}}$

(i) $\bar{\bar{K}} = \frac{K}{\pi^3}\,(b^3/D_2)_{HS}$

(j) λ_{cr} from Figure 2, reference 14-1.

(k) Heat shield panels and clips; René 41 between BL 212-304; TD NiCr between BL 304-350.

TABLE 14-5

MONOCOQUE HONEYCOMB SPRING CONSTANT EQUATIONS
(UNSHIELDED)

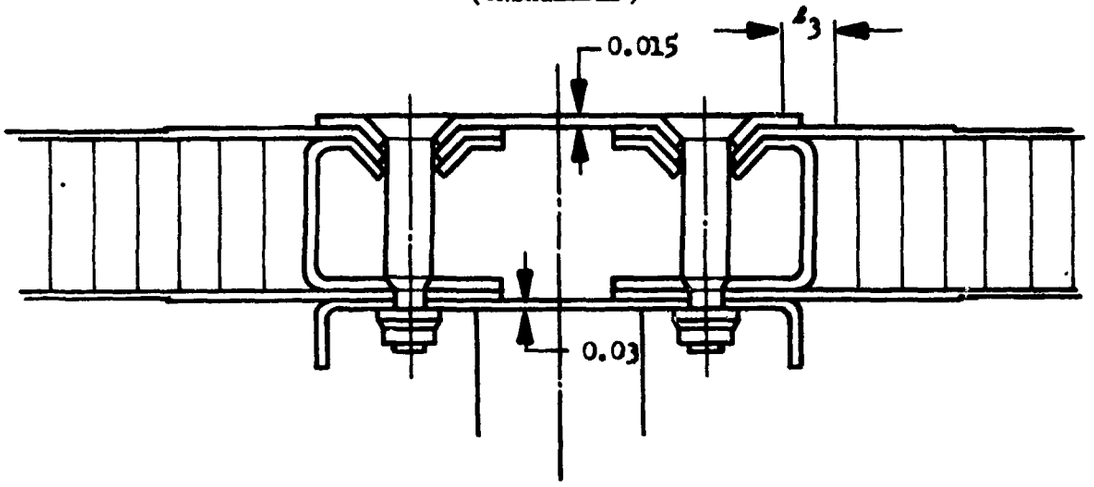

Assumptions

(1) Cap and closeout have same slope, θ, due to clamping by shoulder bolt.

(2) Head of shoulder bolt permits inward movement but resists outward movement.

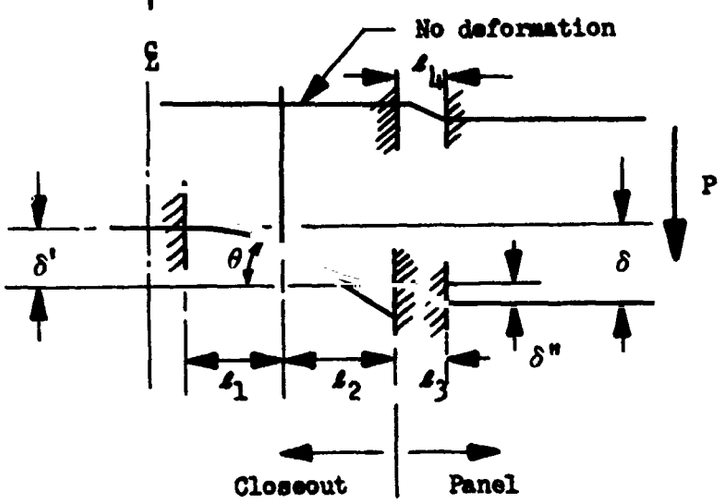

Closeout deflection equation: $\delta_{Total} = \delta = \delta' + \delta''$

$$\delta' = \frac{P\ell^3}{3E}\left(\frac{I_1 + I_2}{I_1 I_2}\right) - \frac{P\ell^3}{4E}\frac{(I_2 - I_1)^2}{I_1 I_2 (I_1 + I_2)} \quad ; \quad \ell = \ell_1 = \ell_2$$

Panel deflection equation:

$$\delta'' = \frac{P\ell^3}{12 (EI_3 + EI_4)} \quad ; \quad \ell = \ell_3 = \ell_4$$

Spring constant:

$$\frac{1}{K} = \frac{1}{K'} + \frac{1}{K''} \qquad \text{where} \qquad K' = P/\delta' \quad K'' = P/\delta''$$

TABLE 14-6

HONEYCOMB SANDWICH PANEL FLUTTER EVALUATION

Location		Center	Inboard		Outboard
Surface		Lower	Upper	Lower	Upper
$D_1 = D_2 = D_{12}$, in.-lb	(a)	193 530	209 770	231 900	265 000
K, lb/in./in.	(b)	1210.34	1210.34	1210.34	1210.34
$\bar{K}$	(c)	12.909	11.909	10.773	9.427
C	(d)	1.0	1.0	1.0	1.0
$-\bar{A}_x$	(e)	8.0	8.0	8.0	8.0
$(\lambda'_{cr})^{1/3}$	(f)	4.7	4.7	4.7	4.7
$(q/\beta)_{cr}$		156.98	170.15	188.10	214.95
$(q/\beta)_{cr}/(q/\beta)$	(g)	42.62	46.20	51.07	58.36

(a) Flexural and twisting stiffness

(b) Deflectional spring constant per unit width

(c) $\bar{K} = Kb^3/\pi^3 D_2$, where b = 40 in.

(d) $C = D_{12}/(D_1 D_2)^{1/2}$

(e) $-\bar{A}_x = 2 (a/b)^2 D_{12}/D_1$, where a = 80 in.

(f) $(\lambda'_{cr})^{1/3} = (2qb^3/\beta D_1)^{1/3} (D_1/D_{12})^{1/2}$, from figure 5, reference 14-1, ($\bar{K}$ = 10)

(g) q/β = 3.683 psi at t = 7.0 minutes

TABLE 14-6 (Concluded)

Location			Outboard(k)	
Surface			212-304	304-350
$(D_1)_{Panel}$,	lb-in.	(a)	116 197	116 197
K_{Panel},	lb-in./in.	(b)	39.809	39.809
$(D_2)_{HS}$,	lb-in.	(c)	2328	3900
$(D_{12})_{HS}$,	lb-in.	(d)	5.9768	8.838
λ		(e)	4.7125	2.813
$-\bar{A}_y$		(f)	0.000418	.000369
K_{Clip},	lb/in./in.	(g)	1407.0	1119.0
$\bar{K}$,	lb/in./in.	(h)	38.714	38.462
$\bar{K}$		(i)	0.7898	0.4737
λ_{cr}		(j)	25	20
λ_{cr}/λ			5.305	7.10

(a) $(D_1)_{Panel} = E(\bar{I}_1)_{Panel}$, $E = 31.0 \times 10^6$ psi

(b) $K_{Panel} = (384/5)(D_1)_{Panel}(b)_{HS}/(b)^4_{Panel}$

(c) $(D_2)_{HS} = E(\bar{I}_2)_{HS}$, $E = 29.1 \times 10^6$ psi

(d) $(D_{12})_{HS} = \left(\frac{S}{b_S}\right)\frac{Et^3}{12(1+\nu)} = \left(\frac{1.047R + b_f}{b_S}\right)\frac{Et^3}{15.6}$

(e) $\lambda = 2(q/\beta)(b^3/D_2)_{HS} = 7.366\,(b^3/D_2)_{HS}$

(f) $-\bar{A}_y = 2(b/a)^2_{HS}(D_{12}/D_2)_{HS}$

(g) $E_{Clip} = 30.34 \times 10^6$ psi

(h) $\frac{1}{\bar{K}} = \frac{1}{K_{Panel}} + \frac{1}{K_{Clip}}$

(i) $\bar{K} = \frac{K}{\pi^3}\left(\frac{b^3}{D_2}\right)_{HS}$

(j) λ_{cr} from figure 2, reference 14-1

(k) Heat shield material René 41, 212-304; TD NiCr, 304-350

TABLE 14-7

PANEL FLUTTER REQUIREMENTS – SEMIMONOCOQUE, TUBULAR

Surface			Upper		Lower			
Location stations, BL			120-212	212-350	85 - 120	120-212	212-304	304-350[j]
$(t)_{HS}$		in.	0.10	0.012	0.010	0.010	0.014	0.019
$(b_s)_{HS}$		in.	1.22	1.52	1.22	1.22	1.88	2.50
$(R)_{HS}$		in.	0.91	1.15	0.91	0.91	1.40	1.90
$(b_f)_{HS}$		in.	0.31	0.39	0.31	0.31	0.48	0.64
$(\bar{I})_{HS}$		$in.^4/in.$	22×10^{-6}	43×10^{-6}	22×10^{-6}	22×10^{-6}	72×10^{-6}	180×10^{-6}
$(D_2)_{HS}$	(a)	lb-in.	653.4	1277.1	653.4	653.4	2138.4	3510.0
$(D_{12})_{HS}$	(b)	lb-in.	1.971	3.450	1.971	1.971	5.407	9.017
D_{12}/D_2			0.00292	0.00270	0.00292	0.00292	0.00253	0.00257
b		in.	13.1	13.1	13.1	13.1	13.1	13.1
λ	(c)		25.32	12.96	25.32	25.32	7.738	4.714
a		in.	40	40	50	40	40	40
$-\bar{A}_y$	(d)		0.000626	0.000580	0.000401	0.000626	0.000542	0.000551
$(K)_{Clip}$	(e)	lb/in./in.	1034.0	1444.0	1056.0	1056.0	1407.0	1119.0
$(K)_{Panel}$	(f)	lb/in./in.	82.4	43.8	20.9	56.2	26.5	26.5
K	(g)	lb/in./in.	76.318	42.511	20.494	53.360	26.010	25.887
$\bar{K}$	(h)		8.47	2.41	2.27	5.92	0.882	0.535
λ_{cr}	(i)		180	75	68	140	30	20
λ_{cr}/λ			7.11	5.79	2.69	5.53	3.88	4.24

(a) $D_2 = (\bar{I}\,E)_{HS}$, $T_{HS} = 500^{\circ}F$, $(E)_{HS} = 29.7 \times 10^6$ psi

(b) $D_{12} = \left(\frac{S}{b_S}\right)\frac{Et^3}{12(1+\nu)} = \left(\frac{1.047\,R + b_f}{b_S}\right)\frac{Et^3}{15.6}$

(c) $\lambda = 2(q/\beta)\,b^3/D_2 = 7.36\,b^3/D_2$; time = 7.0 minutes, q = 1500 psf, M = 3.0

(d) $-\bar{A}_y = 2\left(\frac{b}{a}\right)^2\left(\frac{D_{12}}{D_2}\right)$

(e) $T_{Clip} = 350^{\circ}F$; $E_{Clip} = 30.34 \times 10^6$ psi

(f) $T_{Panel} = 200^{\circ}F$; $E_{Panel} = 30.97 \times 10^6$ psi; $E_{Panel} = \frac{384}{5}(D_1)_{Panel}\,(b)^4_{HS}/(b)^4_{Panel}$

(g) $\frac{1}{K} = \frac{1}{(K)_{Clip}} + \frac{1}{(K)_{Panel}}$

(h) $\bar{K} = \frac{K\,b^3}{\pi^3 D_2}$

(i) λ_{cr} from reference 14-1, figure 2

(j) Heat shield material René 41; except lower surface BL 304-350, TD NiCr

TABLE 14-8

PANEL FLUTTER REQUIREMENTS – SEMIMONOCOQUE, SPANWISE, BEADED

Surface			Upper		Lower			
Location stations, BL			120-212	212-350	0 - 120	120-212	212-304	304-350[j]
$(t)_{HS}$		in.	0.010	0.012	0.010	0.010	0.014	0.019
$(b_s)_{HS}$		in.	1.22	1.52	1.22	1.22	1.88	2.50
$(R)_{HS}$		in.	0.91	1.15	0.91	0.91	1.40	1.90
$(b_f)_{HS}$		in.	0.31	0.39	0.31	0.31	0.48	0.64
$(\bar{I})_{HS}$		$in.^4/in.$	22×10^{-6}	43×10^{-6}	22×10^{-6}	22×10^{-6}	72×10^{-6}	180×10^{-6}
$(D_2)_{HS}$	(a)	lb-in.	653.4	1277.1	653.4	653.4	2138.4	3510.0
$(D_{12})_{HS}$	(b)	lb-in.	1.971	3.450	1.971	1.971	5.407	9.017
D_{12}/D_2			0.00292	0.00270	0.00292	0.00292	0.00253	0.00257
b		in.	13.1	13.1	13.1	13.1	13.1	13.1
λ	(c)		25.32	12.96	25.32	25.32	7.738	4.714
a		in.	40.0	40.0	50.0	40.0	40.0	40.0
$-\bar{A}_y$	(d)		0.000626	0.000580	0.000401	0.000626	0.000542	0.000551
$(K)_{Clip}$	(e)	lb/in./in.	1034.0	1444.0	1056.0	1056.0	1407.0	1119.0
$(K)_{Panel}$	(f)	lb/in./in.	103.4	56.47	28.72	116.1	85.44	85.44
K	(g)	lb/in./in.	94.00	54.35	27.96	104.6	80.55	79.38
$\bar{K}$	(h)		10.4	3.08	3.10	11.61	2.73	1.64
λ_{cr}	(i)		200	74	76	220	68	46
λ_{cr}/λ			7.90	5.71	3.00	8.69	8.79	9.76

(a) $D_2 = (\bar{I}\,E)_{HS}$; $T_{HS} = 500^{\circ}F$, $(E)_{HS} = 29.7 \times 10^6$ psi

(b) $D_{12} = \left(\frac{S}{b_S}\right) \frac{Et^3}{12\,(1+\nu)} \left(\frac{1.047\,R + b_f}{b_S}\right) \frac{Et^3}{15.6}$

(c) $\lambda = 2\,(q/\beta)\,b^3/D_2 = 7.36\,b^3/D_2$; time = 7.0 minutes, q = 1500 psf, M = 3.0

(d) $-\bar{A}_y = 2\left(\frac{b}{a}\right)\left(\frac{D_{12}}{D_2}\right)$

(e) $T_{Clip} = 350^{\circ}F$; $E_{Clip} = 30.34 \times 10^6$ psi

(f) $T_{Panel} = 200^{\circ}F$; $E_{Panel} = 30.97 \times 10^6$ psi

(g) $\frac{1}{K} = \frac{1}{(K)_{Clip}} + \frac{1}{(K)_{Panel}}$

(h) $\bar{K} = \frac{K\,b^3}{\pi^3 D_2}$

(i) λ_{cr} from reference 14-1, figure 2

(j) Heat shield material René 41; except BL 304-350, TD NiCr

TABLE 4-9

SEMIMONOCOQUE, CHORDWISE CLOSEOUT SPRING CONSTANT

Wing Location	a, in.	b, in.	c, in.	t_b, in.	t_c, in.	I_{ao}, $in.^4/in.$	I_b, $in.^4/in$	I_c, $in.^4/in.$	I_e, $in.^4/in.$	E, PSI	K, lb/in./in.
120-212 Upper	3.124	0.605	0.612	0.060	0.053	.00196	.000018	.000012	.001942	29.7×10^6	426.1
212-350 Upper	3.906	0.605	0.612	0.054	0.038	.00400	.000013	.000004	.003987	29.7×10^6	352.1

$$\frac{1}{K} = \frac{c^3}{3EI_c} + \frac{b^3}{3EI_b} + \frac{2a^3}{EI_e} + 2\left[\frac{ab^2 - a^3\,(I_b/I_e)}{E\,(I_e\,I_b)^{\frac{1}{2}}}\right] \tan^{-1}\left(\frac{I_e}{I_b}\right)^{\frac{1}{2}} + \frac{a^2 b}{EI_e}\left[\mathrm{LOG}_e\left(\frac{I_e+I_b}{I_b}\right)\right]$$

I_{ao} = Panel Inertia

$I_a = (I_{ao}-I_b)\left(\frac{X}{a}\right)^2 + I_b$

$I_b = \frac{t_b^3}{12}$

$I_c = \frac{t_c^3}{12}$

$I_e = I_{ao} - I_b$

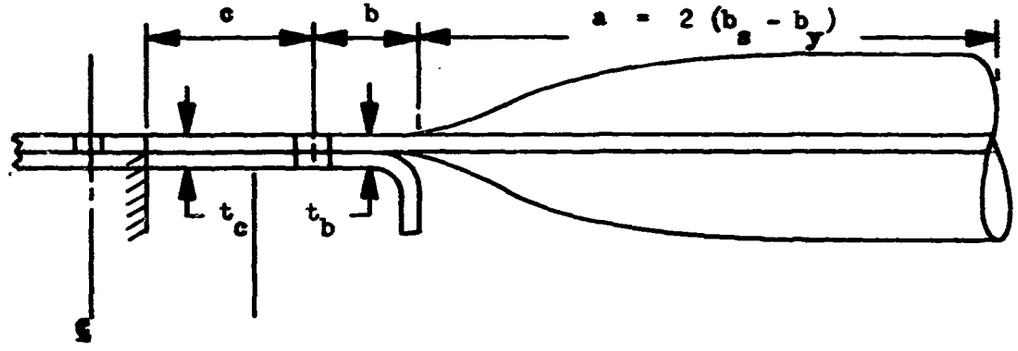

I_c = Cap Thickness, In.

I_b = Cap + Panel Thickness, in

t_c = Cap thickness, in.

t_b = Cap plus panel thickness, in.

TABLE 14-10

PANEL FLUTTER REQUIREMENTS – SEMIMONOCOQUE, CHORDWISE

Surface			Upper		Lower			
Location stations, BL			120-212	212-350	0 - 120	120-212	212-304	304-350(j)
$(t)_{HS}$		in.	–	–	0.012	0.012	0.015	0.019
$(b_s)_{HS}$		in.	–	–	1.22	1.22	1.92	2.60
$(R)_{HS}$		in.	–	–	0.91	0.91	1.42	1.92
$(b_f)_{HS}$		in.	–	–	0.31	0.31	0.49	0.67
$\bar{I}$		$in.^4/in.$	1960×10^{-6}	4000×10^{-6}	23×10^{-6}	23×10^{-6}	80×10^{-6}	200×10^{-6}
D_2	(a)	lb-in.	58 000	119 000	683.1	683.1	2376.0	3900.0
D_{12}	(b)	lb-in.	27 900	57 200	3.405	3.405	6.615	8.838
D_{12}/D_2			0.481	0.481	0.00498	0.00498	0.00278	0.00227
b		in.	24.0	24.0	13.1	13.1	13.1	13.1
λ	(c)		1.754	0.855	24.22	24.22	6.964	4.243
a		in.	75	75	60	75	75	75
$-\bar{\lambda}_y$	(d)		.0985	.0985	.000475	.000304	.000170	.000138
$(E)_{Clip}$	(e)	lb/in./in.	–	–	831.0	1003.0	2016.0	2894.0
$(E)_{Panel}$	(f)	lb/in./in.	426.1	352.1	578.5	587.0	204.7	204.7
E	(g)	lb/in./in.	426.1	352.1	341.1	370.3	185.8	191.2
$\bar{E}$	(h)		3.3	1.3	36.2	39.3	5.67	3.55
λ_{cr}	(i)		90	46	300	310	130	90
λ_{cr}/λ			51.5	53.8	12.4	12.8	18.7	21.2

(a) $D_2 = (\bar{I}\,E)_{HS}$; $T_{HS} = 500°F$, $(E)_{HS} = 29.7 \times 10^6$ psi

(b) $D_{12} = \left(\frac{s}{b_s}\right)\frac{Et^3}{12(1+\nu)} = \left(\frac{1.047\,R + b_f}{b_s}\right)\frac{Et^3}{15.6}$ (for heat shields); $D_{12} = D_3 = GJ/2$ (upper surface primary structure)

(c) $\lambda = 2\,(q/\beta)\,b^3/D_2 = 7.36\,b^3/D_2$; time = 7.0 minutes, q = 1500 psf, M = 3.0

(d) $-\bar{\lambda}_y = 2\left(\frac{b}{a}\right)^2\left(\frac{D_{12}}{D_2}\right)$

(e) $T_{Clip} = 350°F$; $E_{Clip} = 30.34 \times 10^6$ psi

(f) $T_{Panel} = 200°F$; $E_{Panel} = 30.97 \times 10^6$ psi (lower surface); $T_{Panel} = 500°F$; $E = 29.7 \times 10^6$ psi (upper surface)

(g) $\frac{1}{E} = \frac{1}{(E)_{Clip}} + \frac{1}{(E)_{Panel}}$

(h) $\bar{E} = \frac{E\,b^3}{\pi^3 D_2}$

(i) λ_{cr} from reference 14-1, figure 2

(j) Heat shield material Rene' 41; except BL 304-350, TD NiCr

TABLE 14-11

PANEL FLUTTER REQUIREMENTS – STATICALLY DETERMINATE

Surface			Upper		Lower			
Location stations, BL			120-212	212-350	ℓ - 120	120-212	212-304	304-350 (j)
$(t)_{HS}$		in.	0.010	0.012	0.010	0.010	0.014	0.019
$(b_s)_{HS}$		in.	1.22	1.52	1.22	1.22	1.88	2.50
$(R)_{HS}$		in.	0.91	1.15	0.91	0.91	1.40	1.90
$(b_f)_{HS}$		in.	0.31	0.39	0.31	0.31	0.48	0.64
$(\bar{I})_{HS}$		$in.^4/in.$	22×10^{-6}	43×10^{-6}	22×10^{-6}	22×10^{-6}	72×10^{-6}	180×10^{-6}
$(D_2)_{HS}$	(a)	lb-in.	653.4	1277.1	653.4	653.4	2138.4	3510.0
$(D_{12})_{HS}$	(b)	lb-in.	1.971	3.450	1.971	1.971	5.407	9.017
D_{12}/D_2			0.00292	0.00270	0.00292	0.00292	0.00253	0.00257
b		in.	13.1	13.1	13.1	13.1	13.1	13.1
λ	(c)		25.32	12.96	25.32	25.32	7.738	4.714
a		in.	50	40	60	50	40	40
$-\bar{A}_y$	(d)		0.00040	0.00058	0.00026	0.00040	0.00054	0.00055
$(K)_{Clip}$	(e)	lb/in./in.	1034.3	1111	1056.0	1056.0	1107.0	1119.0
$(K)_{Panel}$	(f)	lb/in./in.	67.1	35.4	19.8	90.1	121.2	121.2
K	(g)	lb/in./in.	63.0	34.5	19.4	83.4	111.6	109.0
$\bar{K}$	(h)		6.98	1.96	2.13	9.25	3.78	2.25
λ_{cr}	(i)		145	60	66	185	92	68
λ_{cr}/λ			5.72	4.64	2.61	7.30	11.9	14.4

(a) $D_2 = (\bar{I}\,E)_{HS}$, $T_{HS} = 500^{\circ}F$, $(E)_{HS} = 29.7 \times 10^6$ psi

(b) $D_{12} = \left(\frac{S}{b_S}\right)\frac{Et^3}{12(1+\nu)} = \left(\frac{1.047\,R + b_f}{b_S}\right)\frac{Et^3}{15.6}$

(c) $= 2\,(q/\beta)\,b^3/D_2 = 7.36\,b^3/D_2$; time = 7.0 minutes, q = 1500 psf, M = 3.0

(d) $-\bar{A}_y = 2\left(\frac{b}{a}\right)^2\left(\frac{D_{12}}{D_2}\right)$

(e) $T_{Clip} = 350^{\circ}F$; $E_{Clip} = 30.34 \times 10^6$ psi

(f) $T_{Panel} = 200^{\circ}F$; $E_{Panel} = 30.97 \times 10^6$ psi

(g) $\frac{1}{K} = \frac{1}{(K)_{Clip}} + \frac{1}{(K)_{Panel}}$

(h) $\bar{K} = \frac{K\,b^3}{\pi^3 D_2}$

(i) λ_{cr} from reference 14-1, figure 2

(j) Heat shield material René' 41; except BL 304-350, TD NiCr

TABLE 14-12

SUMMARY OF HEAT SHIELD PANEL FLUTTER ANALYSIS

			Refurbishable heat shields				Permanently attached heat shields (modules)			
			Corrugated skin			Flat skin, dimple stiffened, clip supported	Primary structural panel			
			Hat stiffened, clip supported	Continuous simple support	Continuous multiple supports					
$(t)_{HS}$		in.	0.010	0.010	0.010	0.015	t_{panel}		in.	0.010
$(b_s)_{HS}$		in.	1.24	1.24	1.24		b_s		in.	2.453
$(R)_{HS}$		in.	0.91	0.91	0.91		R		in.	1.00
$(b_f)_{HS}$		in.	0.32	0.32	0.32		b_f		in.	0.5
$(I)_{HS}$		$in.^4/in.$	22.2×10^{-6}	22.2×10^{-6}	22.2×10^{-6}	26×10^{6}	E		$in.^4/in.$	0.006894
D_2	(a)	lb-in.	659.34	659.34	659.34	773	D_1	(j)	lb-in.	19.8
D_{12}	(b)	lb-in.	1.954	1.954	1.954	290	D_2	(e)	lb-in.	204,800
D_{12}/D_2			0.002964	0.002964	0.002964	0.375	D_{12}	(b)	lb-in.	76,600
b		in.	15.3	15.3	13.1	15.3	b		in.	46
λ	(c)		39.98	39.98	25.09	34.1	λ	(k)		0.075
a		in.	15.3	46	46	15.3	a		in.	92
$-\bar{A}_y$	(d)		0.00592?6	0.0006557	0.0004807	0.75	$-\bar{A}_x$	(l)		31,000
$(K)_{CLIP}$	(e)	lb/in./in.	314.9	60.3	66.5	332.5				
$(K)_{PANEL}$	(f)	lb/in./in.	56.0	56.0	56.0	56.0	K_{EDGE}	(m)	lb/in./in.	101
K	(g)	lb/in./in.	47.5	29.0	27.9	47.9	$\bar{K}$	(h)		1.55
$\bar{K}$	(h)		8.33	5.09	3.07	7.17	C	(n)		38.1
λ_{cr}	(i)		180	120	85	180	λ_{cr}	(o)		0.033
λ_{cr}/λ			4.5	3.0	3.4	5.3	λ_{cr}/λ			0.44
			Stable	Stable	Stable	Stable				Flutters

(a) $D_2 = (\bar{I}\ E)$, T = 500°F, E = 29.7×10^6 psi

(b) $D_{12} = \left(\frac{s}{b_s}\right) \frac{E\ t^3}{12(1+\nu)} = \left(\frac{1.047\ R + b_f}{b_s}\right) \frac{E\ t^3}{15.6}$ (for heat shield)

$D_{12} = D_3 = G\ J/2$ (for primary structural panel)

(c) $\lambda = 2\ (q/s)\ b^3/D_2 = 7.36\ b^3/D_2$; time = 7.0 minutes, q = 1500 psf, M = 3.0

(d) $-\bar{A}_y = 2 \left(\frac{b}{a}\right)^2 \left(\frac{D_{12}}{D_2}\right)$

(e) T_{clip} = 350°F; $E_{clip} = 30.34 \times 10^6$ psi

(f) T_{panel} = 200°F; $E_{panel} = 30.97 \times 10^6$ psi

(g) $\frac{1}{K} = \frac{1}{(K)_{clip}} + \frac{1}{(K)_{panel}}$

(h) $\bar{K} = \frac{K\ b^3}{\pi^3 D_2}$

(i) λ_{cr} from Reference 14-1 Figure 2

(j) $D_1 = \frac{(2t)^2}{12} E$; t = 500°F, E = 29.7×10^6 psi

(k) $\lambda = 2\ (q/s)\ b^3 (D_1/D_{12})^{3/2}/D_1$

(l) $-\bar{A}_x = 2\ (a/b)^2\ (D_{12}/D_1) > 1000$, indicates highly orthotropic.

(m) K_{EDGE} includes flexibility of rib cap and runout of tube closeout.

(n) $C = D_{12}/(D_1 D_2)^{1/2}$

(o) λ_{cr} from Reference 14-1

Section 15

VEHICLE FLUTTER

by

R. F. O'Connell

CONTENTS

ILLUSTRATIONS

SYMBOLS

C_L	Lift coefficient
g	Gravitational acceleration
Hz	Hertz
M	Mach number
q	Dynamic pressure
V_{keas}	Equivalent airspeed
α	Angle of attack

Section 15

VEHICLE FLUTTER

Flutter analysis of the hypersonic cruise vehicle was conducted to assure that the structural concepts were not flutter critical. This investigation was limited to symmetrical modes in keeping with the redundant analyses. Previous studies of flutter response of long, slender vehicles have indicated that asymmetric flutter is not likely to be critical for the overall vehicle (configurations having tip fins may require local stiffening to avoid asymmetric flutter).

The critical flutter condition is expected to occur during the heavy weight climb/acceleration phase of the trajectory as maximum $C_{L_\alpha} q$ is attained. The variation of the parameter $C_{L_\alpha} q$ with Mach number during climb is shown in figure 15-1. Symmetric flutter response at Mach 2.75, 520 000 pounds vehicle gross weight, was analyzed using piston-theory aerodynamics for the wing and slender-body aerodynamics for the forebody. The level of aerodynamic forces was modified to give a $C_{L_\alpha} q$ of 0.0215 lb/deg-sq ft based on the wing reference area.

Using the computer program of reference 15-1, vehicle flutter analyses were performed for the monocoque, semimonocoque spanwise, semimonocoque chordwise, and statically determinate structural concepts. The resultant damping coefficients and frequencies versus equivalent airspeed for the first three modes are shown in figures 15-2 through 15-5. (Higher order modes were included in the analyses but were determined to be of little significance.) In general, the vehicle modes exhibit the low frequencies typical of long slender configurations.

The first mode is comprised primarily of fuselage bending, while the second mode principally indicates wing bending about the longitudinal axis. Response frequencies of both flutter evaluations are similar. The third mode shape, consisting of combined second fuselage bending and outer wing bending, exhibits a slightly lower frequency than the third mode resulting from the preliminary flutter analysis. This mode displays negative damping throughout the velocity range investigated. No positive damping was indicated throughout the speed range investigated. The speed range considered extends well b vond the required 1.3 factor on dynamic pressure. Therefore, it is conclu that high margin on airspeed and dynamic pressure is available over t.. design flight path and that the structural concepts are not critical in flutter. It was not required to conduct a vehicle flutter analysis for the monocoque honeycomb sandwich concept. This concept was investigated after the final analysis of all the other concepts was complete. Since the wing stiffness of the honeycomb sandwich concept was similar to the other concepts, which provided high margins on airspeed and dynamic pressure, it was concluded that this concept was not critical in flutter.

REFERENCES

15-1 Lockheed Flutter and Matrix Algebra System (FAMAS).

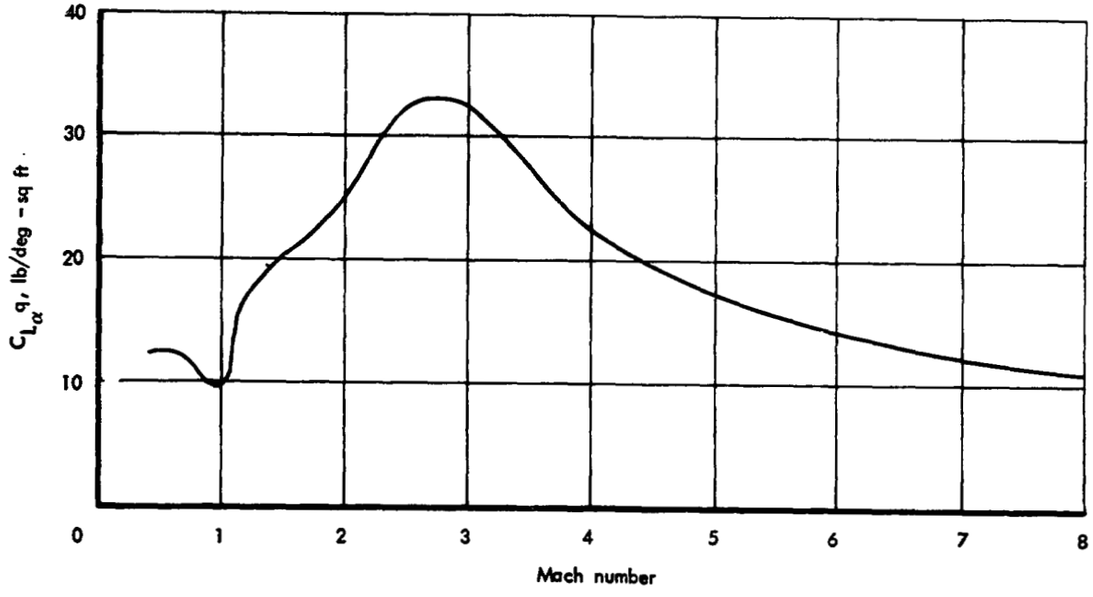

Figure 15-1. $C_{L_\alpha} q$ vs Mach number for vehicle trajectory

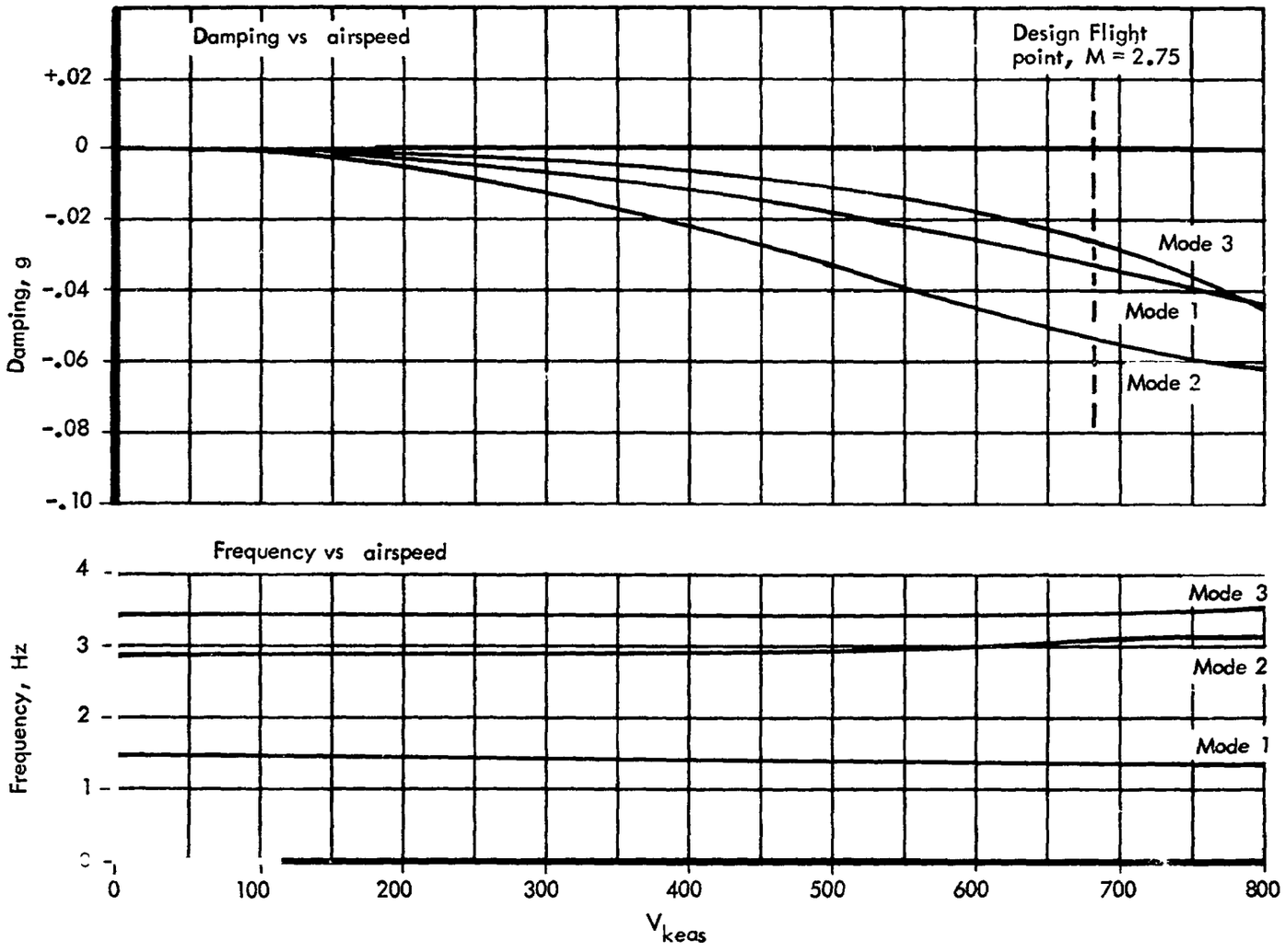

Figure 15-2. Damping coefficient and frequency vs equivalent airspeed monocoque waffle concept

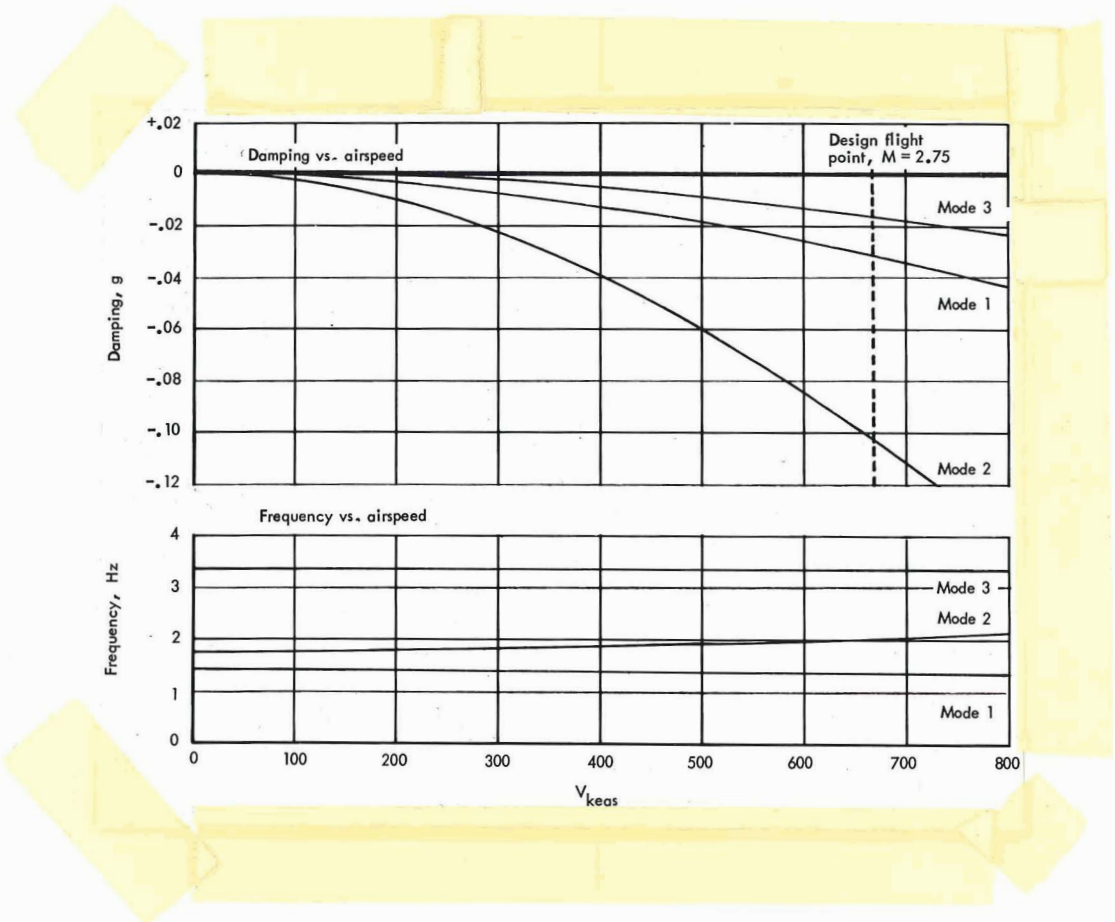

Figure 15-3. Damping coefficient and frequency vs equivalent airspeed semi-monocoque spanwise concept

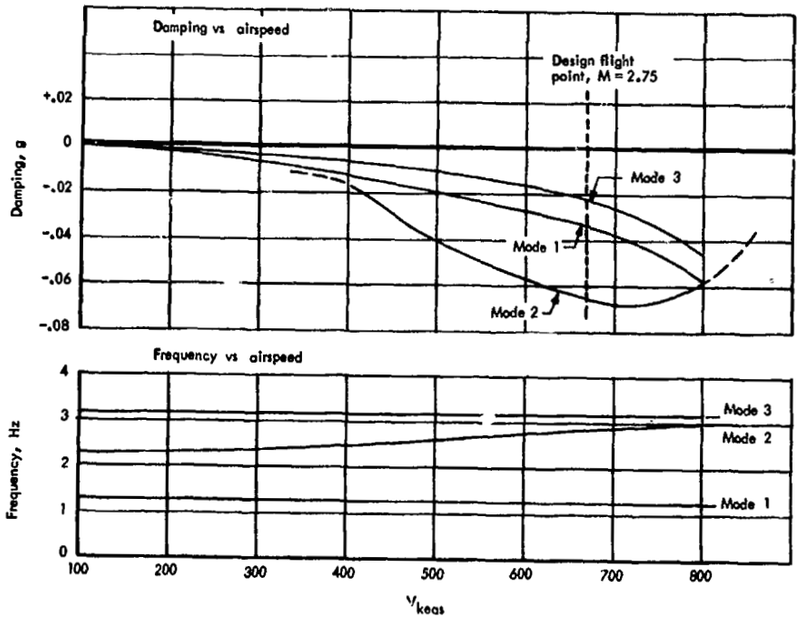

Figure 15-4. Damping coefficient and frequency vs equivalent airspeed semi-monocoque chordwise concept

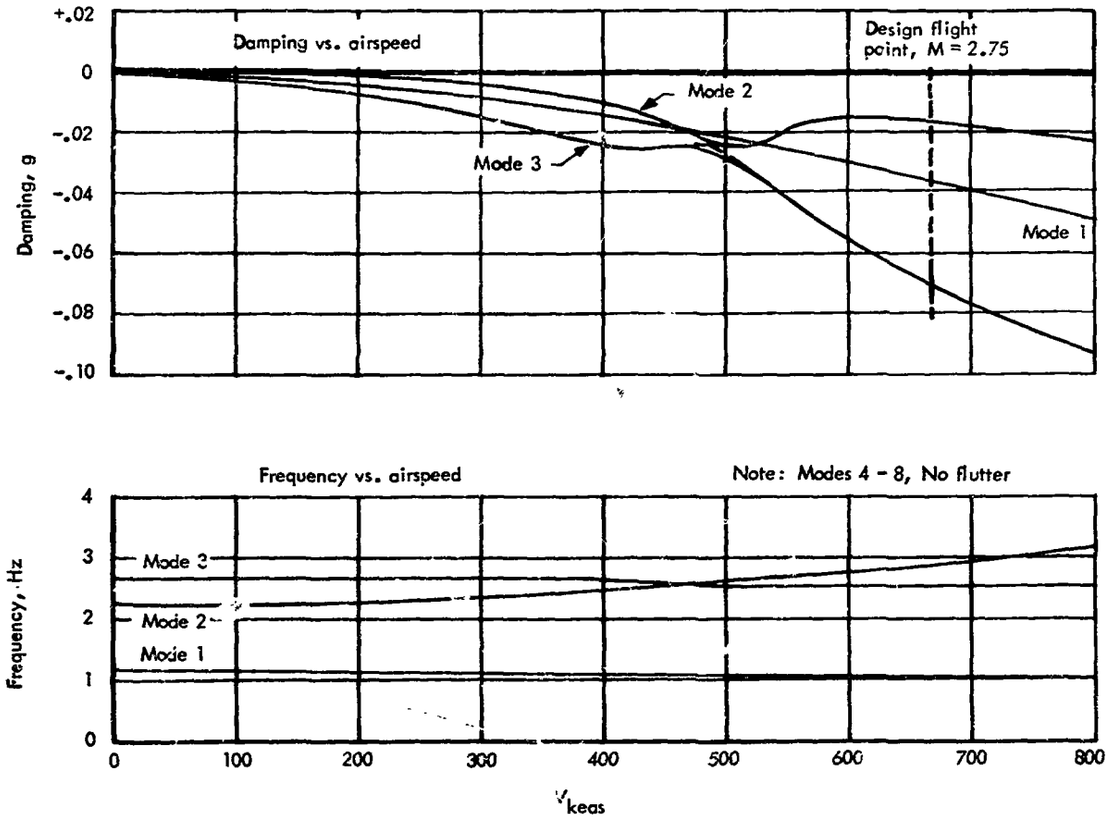

Figure 15-5. Damping coefficient and frequency vs equivalent airspeed statically determinate concept

Section 16

SONIC FATIGUE ANALYSIS

by

B. C. Wollner, I. F. Sakata, H. H. Armstrong,
C. C. Richie, G. W. Davis

CONTENTS

TABLES

ILLUSTRATIONS

SYMBOLS

A	Panel cross section area; effective moment arm
a, b	x and y distances between simply supported edges of plates
B	Panel width
BL	Butt line
C	End fixity coefficient; empirical constant used for calculating rms flange stress
D	Directivity correction used in calculating the overall sound pressure level
D_1, D_2, D_3	Stiffness coefficients of governing differential equation
dB	Decibels
E	Modulus of elasticity
FS	Factor of safety
f_o	Resonant frequency
g	Gravitational acceleration
Hz	Hertz
h	Height
I	Moment of inertia
K	187.61, emperical constant used in equation 16-6
K_t	E_{temp}/E_{RT}, material correction factor
L	Panel length
M	Bending moment; Mach number
N	Number of loading cycles
p	Pressure
psd	Power spectral density

q	Dynamic pressure
R	Reynolds number; reduction factor used in equation 16-5; radius
rms	Root mean square
t	Thickness
t_f	Flange thickness
$\bar{t}$	Equivalent panel thickness
w	Deflection
X	Distance from leading edge; distance from sound source
x, y, z	Rectangular Cartesian coordinates
Z	Distance from "neutral" axis to extreme fiber
Δ	Boundary layer thickness
δ	Damping ratio
ϕ_0	Root mean square pressure density
ρ	Material density
σ_f	Root mean square flange stress
σ_0	Normalized stress
σ_{rms}	Allowable root mean square stress
σ_s	Unit pressure stress
$\bar{\sigma}$	Root mean square stress

Section 16
SONIC FATIGUE ANALYSIS

Adequate resistance of the wing structure to the acoustic loading for the life cycle span (10 000 hours) was determined by theoretical methods of analysis supplemented by empirical data.

BOUNDARY LAYER AND NOISE CRITERIA

Boundary layer and engine noise levels are considered to establish acoustic (sonic) fatigue effects. For the wing study area, the boundary layer noise is the primary condition contributing to sonic fatigue for the wing structural concepts.

Estimated overall sound pressure levels (OASPL) for boundary layer noise were determined, based on the criterion (ref. 16-1) that overall root mean square pressure is 0.7 percent of free stream dynamic pressure for laminar and turbulent flow conditions. For transition from laminar to turbulent flow, the criterion is based on an overall root mean square pressure that is 2.2 percent of the freestream dynamic pressure. The resultant values, as shown in figure 16-1, are found to be 10 db higher than those for 0.7 percent q. The 0.022 q criterion is based on recent flight test data from the X-15 program, which indicated the possibility that a higher relation between noise level and dynamic pressure than found in reference 16-1 may exist.

Boundary layer thickness (Δ) is computed using an extension of the method suggested in reference 16-2.

$$\frac{\Delta}{X} = \frac{0.113M^{0.8}}{R^{0.2}} \qquad (16\text{-}1)$$

where

X = the distance from the leading edge

M = the Mach number at the edge of the boundary layer

R = the local Reynolds number

Maximum octave sound pressures occur in the 2400 - 4800 Hz octave band for body panels and in the 4800 - 9600 Hz octave band for wing panels. Since fundamental panel frequencies were anticipated to fall within the 37.5 - 150 Hz octave band, sound pressure levels within this range were determined as shown in figure 16-1.

Sound pressure levels from engine noise were determined using the thrust and flow relationships for the Pratt and Whitney STF-219 turbojet engine. An overall power level (PWL) of 186 dB re 10^{-13} watts is produced. The overall sound pressure level (OASPL) is determined as:

$$OASPL = PWL + D - 10 \log_{10} 2\pi X^2 \qquad (16\text{-}2)$$

where

D = a directivity correction, -15 dB at 150°F from the jet axis

X = the distance from the exhaust nozzle, 52 feet to the aft edge of the wing study area

The most severe sonic environment on the wing study area due to engine noise is thus defined by an OASPL of 129 dB. The sound pressure level in the octave band corresponding to fundamental panel frequency (37.5-150 Hz) is 122 dB at takeoff. This decreases rapidly as speed is increased, with the influence at stations forward of the exhaust disappearing as sonic speed is attained. The variations of OASPL with time due to boundary layer noise indicate values in excess of those due to engine noise (fig. 16-1). Therefore, the latter are not considered critical for design, and the acoustic environment due to boundary layer is used to dictate design requirements.

A comparison of acoustic fatigue effects due to boundary layer noise for the 0.007 q and the 0.022 q criteria are contained in table 16-1. For ease of computation, the vehicle life is conservatively considered to be composed of three loading levels: one based on maximum pressure during the basic mission, one at maximum dynamic pressure (2200 psf) during the positive maneuver, and one at a nominal dynamic pressure (2000 psf) during the specific maneuver excursion. Except for the lower outboard area, the wing is conservatively analyzed for the maneuver (2200 psf) at an OASPL for 10^{10} loading cycles. Using the maneuver sonic criteria is conservative since the maneuver perturbation requires only 16 hours of the 10 000-hour life. The 0.022 q criteria is valid only during cruise, as discussed below. Root mean square (rms) pressure and power spectral density (psd) in both the second and third octave bands are included. Pressure increases by a factor of 3 are produced under the more severe criterion and power spectral density levels are increased by a factor of 10.

LAMINAR-TURBULENT TRANSITION CRITERIA

Transition from laminar to turbulent flow at the wing leading edge is assumed to occur at a freestream Reynolds number of 130 000 based on leading edge diameter. Flow over both the wing upper and lower surface is assumed turbulent whenever the leading edge is turbulent. For laminar leading edge flow, transition on the wing lower surface is assumed to begin when the ratio of momentum thickness Reynolds number to local Mach number equals 150. Transition on windward upper surfaces occurs under the same conditions as for the lower surface. Flow over leeward upper surfaces is assumed turbulent for all flight conditions.

Flow field analysis for the design trajectory indicated that leading edge flow is turbulent throughout climb and through the trajectory perturbations. Immediately after the 2.0-g maneuver, the leading edge Reynolds number drops below 130 000 and decreases until the end of cruise. Flight angle of attack remains above 8°, however, so all wing upper surfaces are leeward and flow there remains turbulent. Since turbulent flow is a stable condition and laminar flow is unstable, it is impossible to predict exactly when flow at the leading edge will shift from turbulent to laminar, if at all. If leading edge flow does become laminar as soon as possible, a laminar-to-turbulent transition line will occur on the lower surface within three feet of the leading edge, measured along the wing chord line during the cruise portion of flight. The area of applicability of this criteria is shown in figure 16-2, indicating only a small region of the panel affected. The analyzed area is localized near the end closeout of the panels adjacent to the leading edge structure.

METHOD OF ANALYSIS

Fatigue effects of random sound pressure on the wing structure are determined by analytical and empirical approaches of references 16-3, -4 and -5.

The following basic assumptions are postulated for the structural response, resulting stress levels, and fatigue damage:

1. Stresses that contributed to the sonic fatigue damage are significant only in the primary structural resonant modes.

2. Lightly damped structure will respond significantly in only one mode when exposed to random excitation.

3. The fatigue failure resulting from random sound pressure excitation can be interpreted as a quasi-sinusoidal response whose frequency is that of the significant mode and whose amplitude has a random variation. The peak probability distribution is Rayleighian (ref. 16-5).

4. The randomness of the pressure input can be defined statistically as the probability rate of occurrence of instantaneous pressure. The instantaneous distribution is Gaussian (ref. 16-5).

5. For single mode response, the sound pressure correlation is unity; i.e., the pressure everywhere on the surface under the random pressure load is in phase.

6. Fatigue damage is accumulated at a linear rate (ref. 16-5).

Structural Response

The response of the structure, when excited by random sound pressure, may in many instances be complex and is due largely to the structural configuration itself where the skin panels and support structure are dynamically coupled. For these analyses, it is assumed that the structure under study will respond as a single degree-of-freedom system. Structural response to random sound pressure levels can therefore be expressed by Miles' theory (ref. 16-6). This assumption may not be realistic in many instances, but, for more complex structural configurations it serves quite well in estimating the lowest resonant frequencies. This approach has great practical value in that the vibratory motion of a complex structure generally exhibits its maximum displacement and stress amplitude at its lowest resonant frequency. Miles' theory is dependent on structural damping ratios, response frequency, and normalized stress response, which are discussed briefly in the following paragraphs.

Structural Damping

The amplitude of the displacement and dynamic stress in the structure, when excited at any resonant mode, is dependent on the damping ratio. Most of the fatigue damage can be expected to accumulate when the response is in the least damped mode. Damping ratio (δ) in the range of 0.010 to 0.020 is usually considered for these analyses; here, the conservative value of 0.010 is used.

Response Frequency

Determination of the structural response frequency is another important consideration in sonic fatigue analyses. It is assumed that the maximum sonic fatigue damage will be accumulated in the lower frequency modes of the structural configuration, and, therefore, it is important to determine a close approximation of these resonant frequencies. For analytical purposes, the response frequency is determined and then the sound pressure level is chosen to be the octave band level corresponding to this frequency. Due to the complexity of the structure and the interaction between members, it is very difficult in many instances to predict the exact resonant frequencies; historical test data and/or response tests are required to better define structural response. For analytical purposes, response frequencies for the various structural members are determined from beam and plate theory (ref. 16-7).

Normalized Stress

As noted previously, structural response to random pressure fluctuations is expressed by Miles' theory with the rms stress as:

$$\overline{\sigma}^2 = \frac{\pi}{4\delta} f_0 \phi_0 \sigma_0^2 \qquad (16\text{-}3)$$

where:

$\overline{\sigma}$ = rms stress

δ = the damping ratio

f_0 = resonant frequency of the system

ϕ_0 = root mean square pressure density (psi^2/Hz)

σ_0 = normalized stress

The normalized stress response to a unit pressure closely approximates the static stress response to a unit pressure; therefore, basic plate and beam theories are used in determining this parameter for structural sizing. In addition, the normalized stress (σ_0) is equal to 90 percent σ_s, resulting from a unit pressure loading. Bending stresses in plates and supports and axial stresses in members are determined from basic theories. Through Miles' equation, rms stresses due to the various random conditions are determined for fatigue life predictions.

Flange Stress

Adequate support structure sizing is essential, since the prying action of the attach flange on its fasteners causes stresses in the flange. This is sometimes critical if the thickness of the flange is less than the skin thickness or if the moment arm, A, as shown below, is out of proportion relative to panel width, as may be the case with a large bend radius or overhang of the cap flange due to corrugated webs (ref. 16-5).

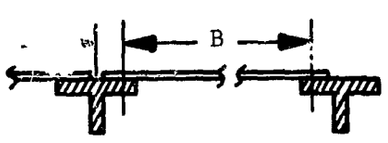

Test Data

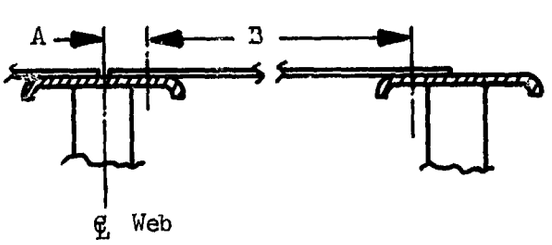

Corrugated Web

The rms flange stress resulting from a unit load is determined from the following empirical equation:

$$\sigma_f = \frac{CBA\sqrt{f_0\,\phi_0}}{t_f^2} \qquad (16\text{-}4)$$

where:

σ_f = rms flange stress

B = panel width

A = effective moment arm

t_f = flange thickness

$\sqrt{f_0\,\phi_0}$ = rms sound pressure, psi

C = empirical constant = 21.3 for double flange
= 42.6 for single flange

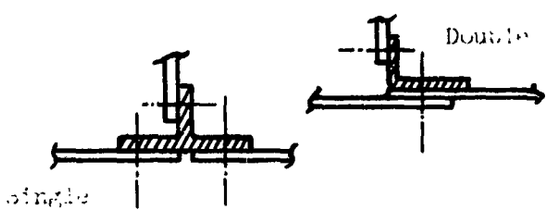

Fatigue Curves and Allowables

The René 41 random fatigue curves presented in figure 16-3 are used for the sonic fatigue analyses. These data are results of narrow-band random amplitude bending fatigue tests conducted on sharply notched René 41 specimens. Theoretical life predictions were made for the random loading tests by using the Palmgren-Miner cumulative damage rule and two different peak stress distributions, the distribution determined from the tests and the classical Rayleigh distribution. The data indicate that, for short lives, a progressive loss of fatigue strength occurred with increase in temperature. For long lives, fatigue strength decreased from room temperature to 700°F, but did not decrease further at 1400°F. The René 41 heat shield panel stresses were compared to the 10 000 psi fatigue allowable (endurance limit stress).

The lower outboard surface heat shield TD NiCr allowables were based on the analysis discussed in section 17 (fatigue). Figure 16-4 shows a total strain versus cycles to failure for TD NiCr from 1600° to 2400°F for three factors of safety. The methods of reference 16-8 were employed to derive the curves and a factor of safety (F.S.) of 1.5 is recommended (ref. 16-8) to assure that all test results fall above the curve. Table 16-2 shows the allowable stresses for factors of safety (on stress) of 1.0, 1.5, and 2.0. The 9530 psi allowable at F.S. = 1.5 is conservatively used in the analysis for TD-NiCr shields and heat shield clips.

Scatter Factor and Design Life

A scatter factor of 2.0 is used to bracket the normal spread in fatigue life. This factor accounts for scatter fatigue data, for tolerances in manufacturing and materials, for unknowns in analysis techniques, and for scatter in environment.

The analysis presented is based on a Rene' 41 allowable rms stress of 10 000 psi at 700° to 1400°F (fig. 16-3) which corresponds to an extrapolated endurance limit greater than 10^{10} cycles. Should a conversion from cycles to time be desirable, the following equation is appropriate.

$$\text{time (hr)} = \frac{RN}{3600\ f_0} \qquad (16\text{-}5)$$

where:

R = reduction factor = 0.50 (for scatter factor = 2.0)

N = cycles

f_0 = fundamental panel frequency, Hz

Design Nomographs and Service Life Curves

Results of sonic fatigue development tests and full scale tests of several types of aircraft structures are compiled and are used to produce acoustic fatigue design charts for aluminum and titanium alloy (ref. 16-3 and 16-4). These data are combined with applicable theory to derive the relationship that yields the capability of a panel to withstand sonic fatigue due to random acoustic excitation. This empirical relationship relates the allowable spectrum level (dB/Hz) to the geometric and material parameters by the following equation:

$$\text{Allowable dB/Hz} = K + 20 \log (\sigma_{rms}) + 10 \log \delta - 5 \log (E/\rho) - 5 \log (g) + 20 \log \left(\frac{A^{1/4} I^{3/4}}{ZL} \right) \qquad (16\text{-}6)$$

where

		Rene' 41	TD NiCr
K	= empirical constant = 187.61		
σ_{rms}	= allowable rms stress (psi)	10,000	9530
δ	= structural damping ratio (C/C_0)	0.01	0.01
E	= modulus of elasticity (psi)	31.6×10^6	21×10^6
ρ	= material density (lb/cu in.)	0.298	0.306
g	= acceleration of gravity (in./sec^2)		
A	= panel cross sectional area (in.^{2}/in.)		
I	= panel moment of inertia (in.^{4}/in.)		
Z	= distance to extreme fiber (in.)		
L	= panel length (in.)		

For both the René 41 and TD NiCr constants shown above, equation 16-6 becomes

$$\text{Allowable dB/Hz} = 195 - 5 \log K_t + 20 \log \left(\frac{A^{1/4} I^{3/4}}{ZL} \right) \qquad (16\text{-}7)$$

where

$$K_t = E_{temp} / E_{RT}$$

Validation of Analyses

Since a sonic fatigue prevention program involves many variables difficult to model analytically, laboratory development tests are necessary to complement analyses. These development tests are required to support the detail design, evaluate new design concepts and materials, and substantiate analytical fatigue life predictions; all of these are aimed at developing minimum weight and minimum cost structures.

FATIGUE ANALYSIS RESULTS

Margins of safety are shown for primary structural panels, rib and spar caps, heat shield panels, and heat shield clips.

Monocoque Primary Structure

The monocoque primary structure results are shown for waffle and honeycomb sandwich panels. The flexural rigidities, D_1, D_2, D_3, and other constants are discussed in reference 16-9.

Waffle - The natural frequency (f_o) of the waffle panels is solved using orthotropic plate theory (ref. 16-10). The basic differential equation is

$$D_1\frac{\partial^4 w}{\partial x^4} + 2D_3\frac{\partial^4 w}{\partial x^2 \partial y^2} + D_2\frac{\partial^4 w}{\partial y^4} = q \qquad (16\text{-}8)$$

where $q = -\frac{\rho\bar{t}}{g}\ddot{w}$ (load term)

and the deflection, $w = \sum_{m=1}^{\infty}\sum_{n=1}^{\infty}\phi_{mn}\sin\frac{m\pi x}{a}\sin\frac{n\pi y}{b}$

the solution is $\frac{\rho\bar{t}}{g}\ddot{\phi}_{mn} + \lambda\phi_{mn} = 0$

where $\lambda_{mn} = D_1\left(\frac{m\pi}{a}\right)^4 + 2D_3\left(\frac{m\pi}{a}\right)^2\left(\frac{n\pi}{b}\right)^2 + D_2\left(\frac{n\pi}{b}\right)^4$

leading to

$$f_o = \frac{1}{2\pi}\left[\frac{g\lambda_{mn}}{\rho\bar{t}}\right]^{\frac{1}{2}} \text{ Hz} \qquad (16\text{-}9)$$

for the lowest frequency, and $a = 20$, $b = 40$ in.:

$$f_o = \frac{\pi}{2a^2}\left[\frac{g}{\rho\bar{t}}(17D_1 + 8D_3)\right]^{\frac{1}{2}} \text{ Hz} \qquad (16\text{-}10)$$

The rms stress (eq. 16-3) is solved using $\delta = 0.01$ and the normalized stress (σ_0) equal to 90 percent of the maximum unit pressure stress (σ_s) in the skin or the stiffener.

The results are summarized in table 16-3, where margins of safety based on the 10 000 psi allowable are also shown. All margins are high, with the lowest (1.16) based on the 2.2 percent q.

Honeycomb sandwich panels - The natural frequency (lowest mode) of honeycomb sandwich panels are given by reference 16-11:

$$f_0 = \frac{\pi}{2}\left(\frac{gD}{\rho t}\right)^{\frac{1}{2}}\left(\frac{1}{a^2}+\frac{1}{b^2}\right) \qquad (16\text{-}11)$$

for $a = 40$, $b = 80$, René 41

$$f_0 = 0.04417\left(\frac{D}{t}\right)^{\frac{1}{2}} \text{ Hz} \qquad (16\text{-}12)$$

RMS stress: The normalized stress (σ_0) is equal to 90 percent of the unit pressure stress:

$$\sigma_0 = \frac{(0.9)M}{ht_{min}} = \frac{146.45}{ht_{min}} \qquad (16\text{-}13)$$

where

$M_{max} = 0.1017(40)^2 = 162.72$ in.-lb (ref. 16-12)

t_{min} = thinnest face thickness

RMS stress, ref eq. (16-3),

$$\bar{\sigma} = \left(\frac{\pi}{4\delta}\right)^{\frac{1}{2}}\left(f_0\,\phi_0\right)^{\frac{1}{2}}\sigma_0$$

for $\delta = 0.01$, $\bar{\sigma} = 8.86\,\sigma_0(f_0\phi_0)^{1/2}$

The results are summarized in table 16-4, where margins of safety are shown for rms stress based on the 10 000 psi allowable. Margins of safety above 5.0 are seen to exist except on the lower outboard panels, where use of the 2.2 percent q criteria results in M.S. = 0.96, which is still large.

Semimonocoque and Statically Determinate Primary Structure

The sonic fatigue results for the spanwise and chordwise stiffened primary structural panels are shown in table 16-5. The margins of safety are based on rms stress predictions and the 10 000 psi endurance limit allowable. The lowest margins for each construction occur on the lower surface outboard where the high transition line sound pressure level (0.022 q) is considered applicable. The minimum margin of 0.0 for the "sheet-metal" constructions occurs on the tubular panels where minimum gages and low moments of inertia (light static loads) make the designs more susceptible to fatigue damage.

The first mode bending frequency, f_0, from reference 16-7 is:

$$f_0 = C\left[\frac{K_t\ EIg}{wL^4}\right]^{\frac{1}{2}} \text{ Hz} \qquad (16\text{-}4)$$

where

C = 1.57 for pinned ends

K_t = a temperature correction = E_{temp}/E_{RT}

$w = \bar{t}\rho$

L = panel width, in.

Rib and Spar Caps

The margins of safety for the rib and spar caps are shown for each structural concept.

Monocoque waffle - The maximum rectangular panel reactions on the rib and spar caps due to lateral pressure sonic loading are approximately equal on the long and short side (ref. 16-12):

$$(R)_{max} = \frac{pa}{2}$$

where a is the short side of the panel. Equation (16-4) can then be used for both spar and rib caps, provided the short side panel dimension is used for B in equation (16-4). The results are shown in table 16-6. The outboard 8 inches of the spar and the leading edge beam require 0.033-inch thicknesses to meet the 0.022 q criteria.

Monocoque honeycomb sandwich - The waffle methods are pertinent, using the 40-inch short side dimension for the honeycomb panels. The results are also shown in table 16-6, but here the last 8 inches of the spar and the leading edge, beam thickness requirement is 0.043-inch to satisfy the 0.022 sonic requirement.

Semimonocoque spanwise - For spanwise stiffening, the sonic fatigue pressure loadings are reacted by the rib caps. The rib cap designs are identical for the beaded and tubular and the resulting margins of safety are shown in tables 16-7 and 16-8. The leading edge beam cap thickness is greater for the beaded because the higher panel natural frequencies cause a higher rms stress.

Semimonocoque chordwise - Chordwise sonic fatigue pressure loadings are reacted by the wing spars. The spar cap margins are shown in table 16-9. Use of the 0.022 q criteria results in large flange stress in the last 6 to 8 inches outboard adjacent to the leading edge. A local 0.010-inch doubler is sufficient to provide positive margins of safety.

Statically determinate - The critical rib cap margins of safety for the spanwise stiffened, statically determinate concept are shown in table 16-10. The leading edge beam cap requires a thickness of 0.049 to meet the 0.022 q criterion.

Heat Shield Sonic Fatigue

Analyses were conducted to determine the effects of random sound pressures on the multisupport corrugation heat shield and to define the requirements imposed by the established criteria. The analytical approach presented in the semimonocoque primary structure evaluation was used to determine estimated allowable sound pressure levels (dB/Hz) and panel/clip stresses due to the random sound pressures. The heat shield panel natural frequencies were based on a 7-span beam analysis and stresses determined.

The heat shield is René 41 except for the BL 304 to 350 lower surface which is fabricated of TD NiCr.

The maximum moment (M), due to a 7-span beam is equal to $0.10\ p^2$ for calculating σ_o, the normalized stress due to a unit of loading (1.0 psi).

The resulting margins of safety are shown in table 16-11 where the following values were used for rms stress allowable ($\bar{\sigma}$).

René 41	10 000 psi
TD NiCr	9 530 psi

Positive margins are noted throughout.

Heat Shield Clips

The heat shield clips are analyzed using the equation (16.4). The resulting margins of safety are shown in table 16-12 for the allowables noted above.

REFERENCES

16-1 Dyer, I.; Franken, P.A.; and Ungar, E. E.: Noise Environments of Flight Vehicles, Noise Control, January-February 1960.

16-2 Eldred, K.; Roberts, W.; and White, R.: Structural Vibrations in Space Vehicles, WADD TR 61-62.

16-3 Lockheed-California Company: Structural Life-Assurance Manual (SLM No. 5, Sonic Fatigue Prevention).

16-4 McGowan, P.R.; et al: Structural Design for Acoustic Fatigue, ASD TDR 63-820, October 1963.

16-5 Lockheed Georgia Company: LG 1VS58-1-3 C5A Final Sonic Fatigue Analysis, February 1968.

16-6 Miles, J.W.: On Structural Damage Under Random Loading, Journal of the Aeronautical Sciences, Volume 30, No. 11, November 1954.

16-7 Fredberg, C.R.; and Kemter, E.N.: Elements of Mechanical Vibration, John Wiley and Sons, Inc., New York, 1949.

16-8 Manson, S.S.: Thermal Stress and Low-Cycle Fatigue, McGraw Hill Co. 1966

16-9 Hubka, R.E.: Structural Optimization of Six Different Types of Rectangular Plates Subjected to Combined and Biaxial-Compressive Loading, Lockheed-California Company, LR 21662, 1968.

16-10 Timoshenko, S.; and Gere, J.: Theory of Elastic Stability, McGraw Hill Co., Second Edition, 1961.

16-11 Timoshenko, S.: Vibration Problems in Engineering, Van Nostrand Co., Third Edition, 1955.

16-12 Timoshenko, S; and Woinowsky-Kreiger, S.: Theory of Plates and Shells, Second Edition, McGraw Hill Co., 1959.

16-13 Philips, E. P.: Fatigue of René 41 Under Constant and Random Amplitude Loading at Room and Elevated Temperatures, NASA TN D3075, Langley Research Center, November 1968.

TABLE 16-1

ACOUSTIC FATIGUE CRITERIA
10 000 HOUR LIFE
$37.5 < f_o < 150$ Hz

Loading Level	Time	Overall Sound Pressure Level, OASPL			
		P = 0.007q		P = 0.022[a]	
p (psf)	seconds	RMS pressure, psi	PSD $(psi)^2/Hz$	RMS pressure, psi	PSD $(psi)^2/Hz$
1500[b]	35.98×10^6	0.0080	1.707×10^{-6}	0.0251	1.680×10^{-5}
2000[c]	10.92×10^3	0.0095	2.43×10^{-6}		
2200[d]	11.40×10^3	0.0100	2.67×10^{-6}		

[a]Valid only during cruise.
[b]Based on maximum pressure during the basic mission.
[c]Based on nominal pressure during maneuver excursion.
[d]Based on maximum dynamic pressure during positive maneuver.

Table 16-2

SONIC FATIGUE ALLOWABLES FOR TD NiCr - LOWER OUTBOARD HEAT SHIELD

Factor of Safety	$\Delta\epsilon^{(a)}$	$\Delta\epsilon/2$	Temp ^oF (Cruise)	10^6 E psi	f Allow psi $(E)\left(\frac{\Delta\epsilon}{2}\right)$
1.0	0.00225	0.001125	1500	12.7	14300
1.5	0.0015	0.00075	1500	12.7	9530
2.0	0.00112	0.00056	1500	12.7	7110

[a]Total reversible strain for one cycle for 10^7 cycles (fig. 16-4)

TABLE 16-3

MONOCOQUE BAFFLE SONIC FATIGUE ANALYSIS, PRIMARY STRUCTURAL PANEL

Wing Surface	BL Location	Criteria %q	Predicted Sound Pressure Level: OBL dB	Φ_o 10^{-6} (psi)^3 Hz table 16-1	Spectrum Level dB/Hz	$\bar{t}$ in.^{2}/in.	Geometry: D_1 10^5 in.-lb	D_3 10^5 in.-lb	Temp ^oF Cruise	$(E)_{Temp}$ 10^6 psi	f_o Hz eq (16-10)	σ_s Skin psi	σ_s Stiffener psi	σ_o (-q) $(\sigma_s)_{max}$ psi	$\bar{\sigma}$ rms Stress psi & 86 $\sigma_o\sqrt{f_o \Phi_o}$	M.S. Margin of Safety $\frac{10000}{\bar{\sigma}} - 1$
Waffle																
Upper	$\mathcal{Q}_L$-120	0.7	128	2.67	115	0.0708	0.8292	0.8687	1250	24.2	148.7	2550	5140	4620	816	11.25
Lower	$\mathcal{Q}_L$-120					0.0658	0.2294	0.6060	1320	23.6	128.8	2080	6350	5710	933	9.6
Upper	120-212					0.0790	0.4011	1.053	1120	25.1	155.2	2500	4330	3900	704	13.2
Lower	120-212					0.0822	0.3746	0.9924	1310	23.6	147.4	2030	4500	4050	712	13.0
Upper	212-350	0.7	128	2.67	115	0.0684	0.2816	0.7423	1000	25.8	140	1940	5320	5240	900	10.1
Lower	212-350	2.2	132	16.8	123	0.0453	0.0959	0.2322	1150	24.0	95.6	1410	14510	13060	4637	1.1

TABLE 16-4

MONOCOQUE HONEYCOMB SANDWICH SONIC FATIGUE ANALYSIS, PRIMARY STRUCTURAL PANELS

Wing Surface	BL Location	Criteria %q	Predicted Sound Pressure Level: OBL dB	Φ_o 10^{-6} (psi)^3 Hz table 16-1	Spectrum Level dB/Hz	Geometry: t_1 in.	t_2 in.	h in.	D 10^6 lb-in.	Temp ^oF Cruise	E_{Temp} 10^6 psi	f_o Hz eq (16-12)	$\bar{t}$ in.	σ_o psi	$\bar{\sigma}$ psi rms Stress	M.S. $\frac{10\,000}{\bar{\sigma}} - 1$
Honeycomb																
Upper	$\mathcal{Q}_L$-120	0.7	128	2.67	115	0.0150	0.0139	0.935	0.1655	1280	23.9	87.4	0.0423	11300	1530	5.54
Lower	$\mathcal{Q}_L$-120					0.0150	0.0150	0.900	0.1556	1330	23.4	85.0	0.0420	10900	1450	5.90
Upper	120-212					0.0150	0.0141	0.950	0.1773	1130	24.6	91.7	0.0411	10900	1510	5.62
Lower	120-212					0.0184	0.0150	0.939	0.1865	1340	23.4	89.1	0.0458	10400	1420	6.04
Upper	212-350	0.7	128	2.67	115	0.0175	0.0182	0.964	0.2240	1120	24.6	97.5	0.0460	8700	1244	7.04
Lower	212-350	2.2	132	16.8	123	0.0150	0.0122	0.714	0.0885	1320	23.6	89.8	0.0354	16800	5100	0.96

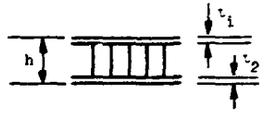

panel sizes: a = 60 in.
b = 40 in.

PRECEDING PAGE BLANK NOT FILMED.

TABLE 16-5

PRIMARY STRUCTURE SONIC FATIGUE ANALYSIS, SEMIMONOCOQUE AND STATICALLY DETERMINATE PANELS

Wing Surface	BL Location	Criteria q	Predicted Sound Pressure Level ϕ_o $10^{-6}\ \frac{(psi)^2}{Hz}$	OBI, dB	Spectrum Level dB/Hz	Geometry A $in.^2/in.$	I $in.^4/in.$	Z in.	L in.	Temp °F Cruise	k_t E/F_{RT}	f_o Hz (a)	Allowable Sound Pressure Level dB/Hz (b)	σ_o psi (c)	$\bar{\sigma}$ psi rms Stress (d)	Margin of Safety M.S. (e)	Panel Concept
Upper	℄-120	0.007	2.67	128	115	0.0263	0.00937	0.901	50	1320	0.746	65.6	124.2	27000	3170	2.16	
Lower	℄-120	0.007	2.67	128	115	0.0196	0.00576	0.823	50	1330	0.745	59.6	121.3	24200	4500	1.22	
Upper	120-212	0.007	2.67	128	115	0.0262	0.00850	0.962	40	1130	0.805	101.0	125.7	16300	2660	2.76	Chordwise
Lower	120-212	0.007	2.67	128	115	0.0224	0.00954	0.879	40	1260	0.766	113.0	125.3	18500	2550	2.51	Spanwise
Upper	212-350	0.007	2.67	128	115	0.0221	0.00424	0.705	40	1130	0.805	81.6	123.3	27300	3570	1.94	Beaded
Lower	212-350	0.022	16.8	132	123	0.0197	0.00702	0.901	40	1250	0.770	104.1	123.6	22900	5490	0.19	
Upper	℄-120	0.007	2.67	128	115	0.0293	0.01830	1.175	50	1320	0.746	86.7	127	13100	2450	3.09	
Lower	℄-120	0.007	2.67	128	115	0.0258	0.00420	0.626	50	1330	0.745	44.2	122	41200	4050	1.47	Semimonocoque
Upper	120-212	0.007	2.67	128	115	0.0287	0.00677	0.745	40	1130	0.805	86.5	126	16200	2670	2.75	Spanwise
Lower	120-212	0.007	2.67	128	115	0.0284	0.00462	0.626	40	1260	0.766	70.1	125	21400	2960	2.38	Chordwise
Upper	212-350	0.007	2.67	128	115	0.0255	0.00363	0.539	40	1130	0.805	66.8	124	23200	3440	1.94	
Lower	212-350	0.022	16.8	132	123	0.0254	0.00213	0.470	40	1250	0.770	51.1	123	33500	12000	0.00	
Upper	℄-120	0.007	2.67	128	115	0.0286	0.0260	0.705		1345	0.74	216.7	130.0	7614	1623	5.16	
Lower	℄-120	0.007	2.67	128	115	0.0261	0.0062	0.744	24	1343	0.74	230.5	129.6	7750	1711	4.84	
Upper	120-212	0.007	2.67	128	115	0.0292	0.0020	0.526	24	994	0.84	132.1	125.2	17042	2336	2.53	Semimonocoque
Lower	120-212	0.007	2.67	128	115	0.0337	0.0062	0.666	24	1196	0.78	208.9	131.0	6750	1457	5.86	Chordwise
Upper	212-350	0.007	2.67	128	115	0.0382	0.0040	0.669	24	945	0.85	163.7	128.3	10940	2008	3.98	
Lower	212-350	0.022	16.9	132	123	0.0254	0.0022	0.470	24	1113	0.81	146.2	126.6	13540	6075	0.65	
Upper	℄-120	0.007	2.67	128	115	0.0314	0.00827	0.734	60	1300	0.74	39.0	123.4	38300	3470	1.88	
Lower	℄-120	0.007	2.67	128	115	0.0211	0.00322	0.940	60	1330	0.73	47.1	121.0	46900	4600	1.17	Semimonocoque
Upper	120-212	0.007	2.67	128	115	0.0291	0.01345	1.019	50	1100	0.81	77.8	125.6	21900	2720	2	Statically
Lower	120-212	0.007	2.67	128	115	0.0253	0.01815	1.25	50	1250	0.77	84.5	125.6	19430	2734	2.00	Determinate
Upper	212-350	0.007	2.67	128	115	0.0206	0.0029	0.588	40	1160	0.793	66.4	121.6	36500	4300	1.33	Beaded Skin
Lower	212-350	0.022	16.8	132	123	0.0199	0.00945	1.058	40	1300	0.74	120.8	124.6	19140	7640	0.31	

[a] First mode bending frequency (ref 16-7), $f_o = C\left[k_t\, EIg/wL^4\right]^{1/2}$.

[b] Allow dB/Hz = $195 - \log k_t + 20 \log \left(\frac{A^{\frac{1}{4}} I^{\frac{3}{4}}}{2L}\right)$.

[c] Normalized stress, σ_o = 90% of unit pressure stress = $\frac{0.90\, L^2 Z}{8I}$.

(d) Mean square stress, $\bar{\sigma} = \sigma_o \left(\frac{\pi f_o \phi_o}{4\, o\, \delta}\right)^{1/2}$, where $\delta = 0.01$.

(e) M.S. = $(10\,000/\bar{\sigma}) - 1.0$.

PRECEDING PAGE BLANK NOT FILMED

TABLE 16-6

RIB AND SPAR CAP SONIC FATIGUE, MONOCOQUE CONCEPTS

	Surface	Location BL	Critical cap R = Rib S = Spar	Criteria %q	ϕ_o 10^{-6} $(psi)^2/Hz$	f_o Hz	$\sqrt{f_o \phi_o}$ B panel width short side in.	t_{cap}	σ_f RMS (eq 16-4) stress lb/in.^{2}	M.S. $\frac{1000}{\sigma_f} - 1$
WAFFLE	Upper	℄-120	R & S	.7	2.67	148.7	20	0.030	5900	0.69
	Lower	℄-120	R & S	.7	2.67	128.8	20	0.030	5500	.82
	Upper	120-212	R & S	.7	2.67	155.2	20	0.030	6020	.66
	Lower	120-212	R & S	.7	2.67	147.4	20	0.030	5870	.70
	Upper	212-350	R & S	.7	2.67	140.0	20	0.030	5720	.75
	Lower	212-342	R & S	.7	2.67	95.6	20	0.030	4730	1.11
	Lower	342-350	SPAR	2.2	16.8	95.6	20	0.033	9800	.02
	L.E.Beam			2.2	16.8	95.6	20	0.033	9800	.02
HONEYCOMB	Upper	℄-120	R & S	.7	2.67	87.4	40	0.030	9040	.106
	Lower	℄-120	R & S	.7	2.67	85.0	40	0.030	8910	.122
	Upper	120-212	R & S	.7	2.67	91.7	40	0.030	9260	.080
	Lower	120-212	R & S	.7	2.67	89.1	40	0.030	9130	.095
	Upper	212-350	R & S	.7	2.67	97.5	40	0.030	9550	.047
	Lower	212-342	R & S	.7	2.67	69.8	40	0.030	8080	.237
	Lower	342-350	SPAR	2.2	16.8	69.8	40	0.043	9860	.014
	L.E.Beam			2.2	16.8	69.8	40	0.043	9860	.014

TABLE 16-7

RIB CAP SONIC FATIGUE, BEADED CONCEPT

Surface	Location BL	Criteria %q	ϕ_0 $(psi)^2/Hz$ 10^{-6}	f_0 Hz (panel)	$\sqrt{f_0 \phi_0}$ 10^{-3}	B Panel Width	t Cap in.	$\sigma_f^{(a)}$ stress eq (16-4) psi	M.S. Margin of Safety $\frac{10000}{\sigma_f} - 1$
Upper	℄ -120	0.7	2.67	65.6	13.234	50	.043	4760	1.10
Lower	℄ -120			59.6	12.61	50	.050	3360	1.98
U	120-212			101	16.42	40	.035	7140	0.40
L	120-212			113	17.37	40	.043	5000	1.00
U	212-350			81.6	14.76	40	.039	5170	0.93
L	212-350	.7	2.67	104.1	16.67	40	.034	7680	0.30
L	LE Beam	2.2	16.8	104.1	41.82	40	.048	9670	0.03

[a]Doubler added to outboard 6 to 8 inches of spar.

TABLE 16-8

RIB AND SPAR CAP SONIC FATIGUE, TUBULAR PRIMARY STRUCTURE

Surface	Location BL	Concept (Critical Cap)	Criteria %q	ϕ_0 $(psi)^2 Hz$ 10^{-6} Units	f_0 Hz Panel	$\sqrt{f_0 \phi_0}$ psi	B Panel Width	t Cap in.	σ_f Stress $lb/in.^2$	M.S. $\frac{10\,000}{\sigma_f} - 1$
U	8 to 120	Rib caps	.7	2.67	86.7	.01521	50	.043	5475	.83
L	8 to 120	Rib caps	.7	2.67	44.2	.01086	50	.050	2900	2.45
U	120 to 212	Rib caps	.7	2.67	86.5	.0152	40	.035	6600	.52
L	120 to 212	Rib caps	.7	2.67	70.1	.01368	40	.043	3940	1.54
U	212 to 350	Rib caps	.7	2.67	66.8	.01335	40	.039	4700	1.13
L	212 to 350	Rib caps	.7	2.67	51.1	.01168	40	.034	5380	.859
L	L. E. Beam	L. E. Beam	2.2	16.8	51.1	.0293	40	.040	9750	.026

A = 0.625 in.

C = 21.3

σ_f Allow = 10 000 psi.

Rene' 41, at 1400F 10^{10} cycles

TABLE 16-9

RIB AND SPAR CAP SONIC FATIGUE CONCEPT, CHORDWISE CRITICAL, SPAR CAPS

Surface	Location BL	Sonic Criteria %q	ϕ_0 $(psi)^2/Hz$ 10^{-6} $\frac{psi^2}{Hz}$	f_0 Hz (panel)	$\sqrt{f_0 \phi_0}$ 10^{-3} psi	B Panel Width in.	t Cap in.	σ_f rms stress eq. (16-4) psi	M.S. Margin of Safety $\frac{10000}{\sigma_f} - 1$
Upper	$\mathcal{L}$ -120	0.7	2.67	216.7	24.1	24	.054	2636	2.79
Lower	$\mathcal{L}$ -120			230.8	24.8		.054	2720	2.68
Upper	120-212			132.1	18.8		.053	2140	3.67
Lower	120-212			208.9	23.6		.064	1840	4.43
Upper	212-350			163.7	20.9		.038	4630	1.16
Lower	212-342	0.7	2.67	146.2	19.8		.030	7010	.43
	342-350	2.2	16.8	146.2	49.6	24	.040	9900	.01

[a] Doubler added to outboard 6 to 8 in. of spar.

TABLE 16-10

RIB AND SPAR CAP SONIC FATIGUE CONCEPT, STATICALLY DETERMINATE CRITICAL CAPS, RIB CAPS

Surface	Location BL	Sonic Criteria %q	ϕ_0 10^{-6} psi^2 Hz	$\sqrt{f_0}$ $\sqrt{cps}$	B Width in.	t Cap in.	σ_f rms stress eq.(16-4) psi	M.S. Margin of Safety $\frac{10000}{\sigma_f} - 1$
Upper	$\mathcal{L}$ -120	0.7	2.67	6.243	60	.030	9060	0.104
Lower	$\mathcal{L}$ -120			6.86	60	.030	9950	0.012
Upper	120-212			8.82	50	.031	9980	0.002
Lower	120-212			9.72	50	.033	9710	0.031
Upper	212-350			8.146	40	.030	7900	0.266
Lower	212-350	0.7	2.67	10.992	40	.031	9950	0.005
Lower	LE Beam	2.2	16.8	10.992	40	.049	9990	0.001

TABLE 16-11
HEAT SHIELD SONIC FATIGUE

Surface and BL	Material	Criteria ξ_q	Predicted Sound Pressure Level			Geometry				Temp (Cruise) ^{o}F	K_t E_T/E_{RT}	f_o eq.(16-14) Hz	Allow SPL eq (16-7) dB/Hz	σ_o (1) psi	$\bar{\sigma}$ RMS eq.(16-8) psi	M.S. Margin of Safety
			OBL dB	Spectrum Level dB/Hz	$10^{-6}\ \frac{(psi)^2}{Hz}$	$\bar{t}$ $in.^2/in.$	I $in.^4/in.$	Z in.	L in.							
Upper θ_L -120	None															
Lower θ_L -120	Rene 41	0.7	128	115	2.67	.0103	2.2	.361	13.1	1330	.75	74.1	117.3	42 820	52-0	0.87
Upper 120-212						.0103	2.2	.361		955	.54	78.4	117.5	42 820	5490	0.32
Lower 120-212						.0103	2.2	.361		1350	.74	75.6	117.3	42 820	5320	0.33
Upper 212-350						.0125	4.3	.376		1240	.52	98.3	120.4	27 300	3280	1.55
Lower 212-204	Rene 41	0.7	128	115	2.67	.0143	7.2	.394		1460	.69	129.1	122.6	20 160	3350	2.28
Lower 304-350	TD NiCr	2.2	132	123	16.8	.0191	18.0	.126	13.1	1230	.623	111	127	10 810	4140	1.30

[a] $\sigma_o = \frac{(.09)\,L^2 z}{I}$

TABLE 16-12

HEAT SHIELD CLIPS SONIC FATIGUE

Matl	Criteria %q	Surface	Location	f_0 Hz (Heat shield)	ϕ_0 $(psi)^2/Hz$	t_f reqd in. Eq.(16-4)	t (Actual)	M.S. $\left(\frac{t}{t_{req'd}}\right)^2-1$
René 41	0.7	U	120-212	78.4	2.67×10^{-6}	0.014	0.023	1.70
		U	212-350	98.3		0.015	0.026	2.00
		L	0-120	74.1		0.014	0.23	1.70
		L	120-212	73.6		0.014	0.023	1.70
René 41	0.7	L	212-304	109.1	2.67×10^{-6}	0.0154	0.030	2.79
TD NiCr	2.2	L	305-350	111	16.8×10^{-6}	0.025	0.037	1.19

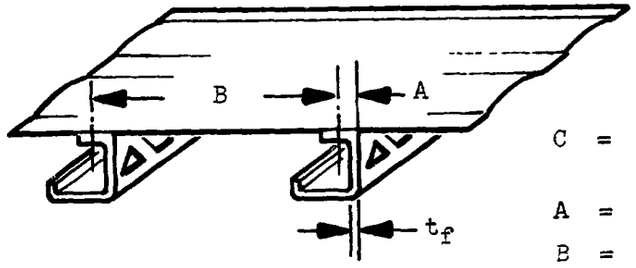

C = 42.6 empirical factor for single flange

A = 0.25

B = 13.1

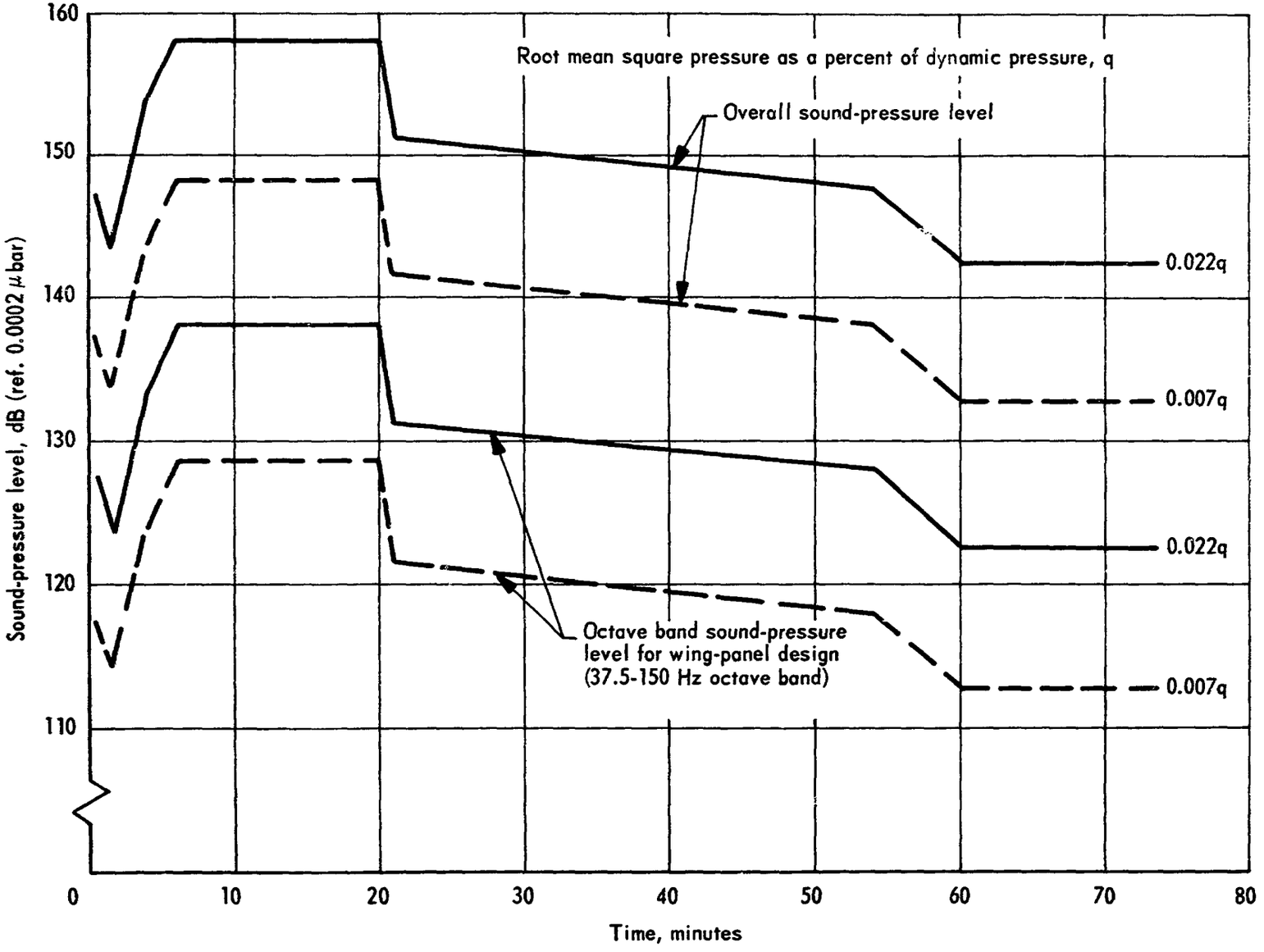

Figure 16-1. Variation of boundary layer noise during design trajectory

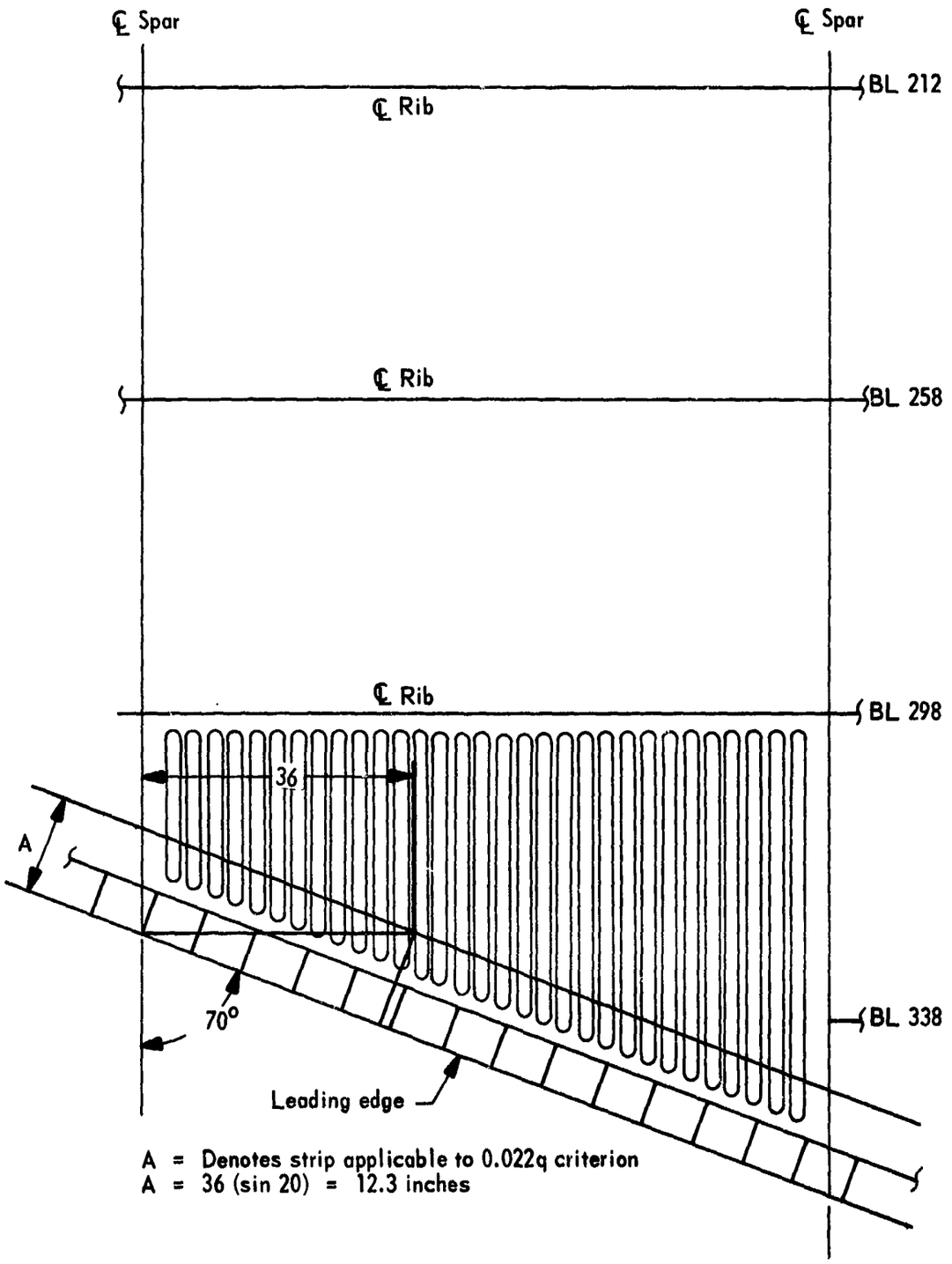

Figure 16-2. Wing area applicable to the 0.022 q criteria

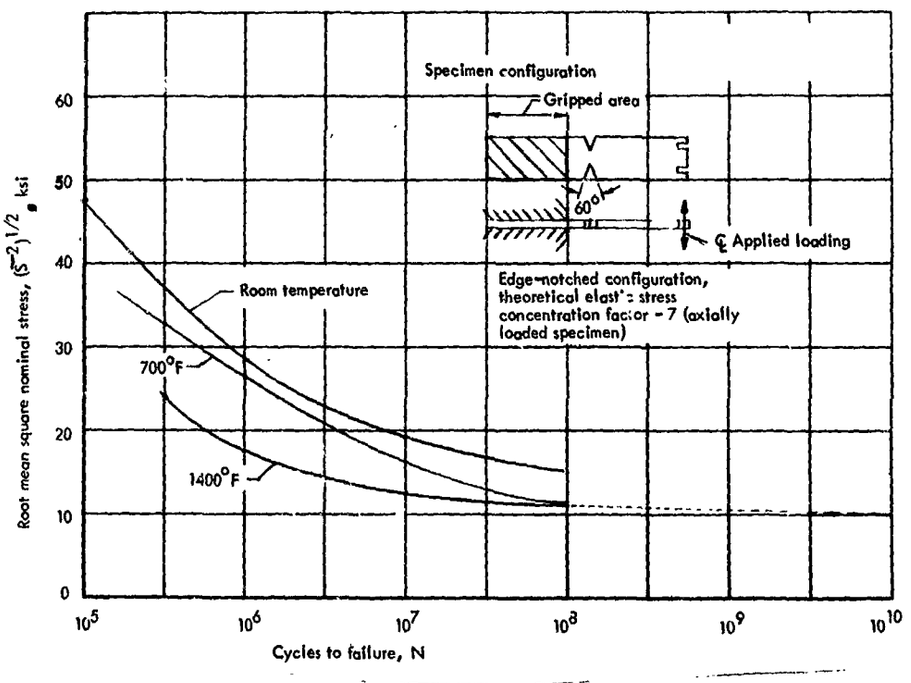

Figure 16-3. Random-loading fatigue curves - René 41

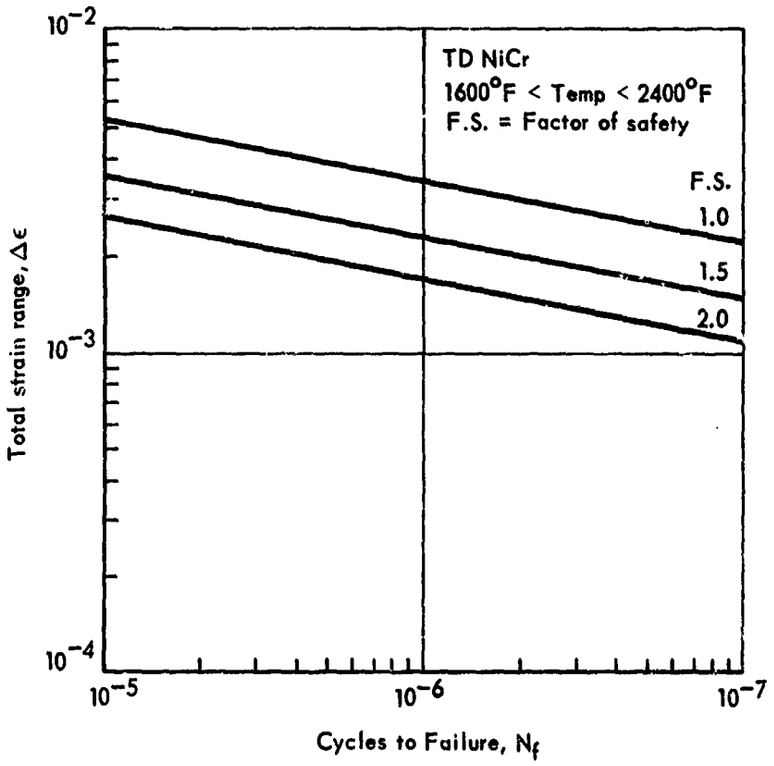

Figure 16-4. TD NiCr Fatigue Allowables

Section 17

FATIGUE ANALYSIS

by: I. F. Sakata, C. C. Richie, H. H. Armstrong, B. C. Wollner

CONTENTS

TABLES

ILLUSTRATIONS

SYMBOLS

BL	Butt line
C	Distance from neutral axis to extreme fiber
c.g.	Center of gravity
D	Calculated life utilization ratio
E	Modulus of elasticity
$F_{f,o}$	Fatigue allowable stress for operational load condition
$F_{f,n}$	Fatigue allowable stress
$F_{f,u}$	Fatigue allowable stress for ultimate load condition
F_{tu}	Tensile ultimate strength
F_{ty}	Tensile yield strength
f_a	Alternating stress
f_m	Mean stress
g	Gravitational acceleration
H	Altitude
I	Moment of inertia, $in.^4$
K	Fatigue quality index
K_t	Stress concentration factor
k	Number of stress levels
L	Length
L_c	Calculated life
L_l	Life span in hours represented in the spectra
M	Fuselage body bending moment; Mach number

MS	Margin of safety
N	Number of cycles
N_i	Number of loading cycles to failure for the i^{th} stress level from the relevant constant-life diagram
N_x, N_y, N_{xy}	Extensional forces and shear force in xy coordinate system per unit length
n	Cumulative number of occurrences
n_i	Number of loading cycles at the i^{th} stress level
n_z	Load factor in. z direction
p	Pressure
q	Dynamic pressure
R	Reduction coefficient used to assure a specified probability of obtaining a test life equal to or greater than the calculated life
RT	Room temperature
T	Temperature
t	Time; thickness
$\bar{t}$	Equivalent thickness
Z	I/C section modulus
α	Angle of attach
Δ_p	Differential pressure
ϵ	Strain
Σ	Summations
Σ_n	Cumulative number of occurrences

Section 17

FATIGUE ANALYSIS

Analyses were conducted to establish allowable design stress levels for fatigue evaluation of primary structure and heat shield concepts to meet the specified life requirements of 10 000 hours. The factors considered for selection of the design stress levels included operational utilization, corresponding loading spectra and environmental conditions, temperature, and structural fatigue quality (ref. 17-1).

The loading spectra, including the ground-air-ground cycle effect, were combined to obtain a total spectra for cumulative damage evaluation. Constant life diagrams for Rene' 41 at room temperature, and at various elevated temperatures using a $K_t = 4.0$ (stress concentration factor) were used. Although the design goal is to achieve the lowest practical fatigue quality index, a minimum value of 4.0 was selected based on previous experience. Early service failures are characterized by K values greater than 4; whereas, parts which have demonstrated adequate service life invariably give K values less than 4. Experimental evaluation of designs with reasonable simulation of the loading spectra is essential to demonstrate acceptable fatigue quality, in addition to care given to details during design and fabrication of structural elements.

A fatigue scatter factor of 1.5 was used for the nominal vehicle design.

FATIGUE SPECTRA

A fatigue spectrum was established for determination of cyclic loadings on the vehicle with the specified maneuver perturbation occurring every tenth flight for the 10 000-hour vehicle life.

The altitude-Mach number schedule (fig. 17-1) was divided into seven segments (table 17-1) consisting of three during ascent, two during cruise, and two during descent, so that typical load levels could be defined within each segment. A spectrum of load occurrence was developed for each segment. The vehicle altitude within each segment was related to load factor, thus defining the frequency of exceedance of a given load level within each segment (fig. 17-2). These individual spectra were summed to obtain a cumulative frequency of exposure to cyclic loading.

A frequency of exceedance of c.g. load factor was established for each segment of the design trajectory as shown in figure 17-2. These spectra were based on previous studies for a supersonic transport (ref. 17-2) with an initial ascent along a similar profile. Since the SST airplane operates in a lower Mach-altitude environment, extension of the load factor experience to the hypersonic cruise vehicle is conservative.

The spectra for inflight cyclic loading (fig. 17-2) was used to construct a cumulative flight loading spectra (fig. 17-3). The spectra were obtained for the three flight regimes (ascent, cruise (including maneuver), and descent) so that pertinent temperature effects could be properly taken into account. Cumulative frequencies in excess of the defined load factor excursions were based on Maneuver Load Spectrum C of MIL-A-8866(ASG). Application of this portion of the flight loading spectra for determination of the fatigue strength is complicated by the requirement that the limit load is considered to occur 10 percent of the time, which precludes a single-occurrence load level.

A ground-handling cycle (taxi considerations) is included in figure 17-3, to permit definition of forces on the vehicle throughout the contemplated ground-air-ground cycle. Since design loads on the vehicle are defined by flight loading conditions at cruise altitudes, it was necessary to adjust vehicle loads associated with ground-handling/landing criteria to satisfy the limit load envelope.

Landing criteria were selected as 2-g acceleration at the nose gear for a single occurrence per life and $\pm$ 0.33-g for a single occurrence per flight.

The criteria set forth in the foregoing paragraph were considered as limit.

The cruise diagram of figure 17-3 includes the -0.5-g and the +2.0-g maneuvers with 1.0-g cruise represented by the apex (i.e., M = -30 x 10^6 in.-lb; n = 100 000). The +2.0-g maneuver condition is represented by the point described by the intersection of the cruise line with the extreme left vertical line (i.e., M = -60 x 10^6 in.-lb; n = 811). The -0.5-g maneuver condition is represented by the cruise-line intersection with 811 cumulative number of occurrences which corresponds to -18 x 10^6 in.-lb of bending moment.

WING FATIGUE SPECTRA DEVELOPMENT

The spectra for fatigue evaluation of the wing was assumed to be similar to that described for fuselage bending (figure 17-3). Initially, the assumption was made that the wing stresses were proportional to the bending moments presented in figure 17-3 (i.e., 30 x 10^6 in.-lb = 30 000 psi for cruise). Based on this proportionality, maximum, minimum, and mean stresses were established for ascent, cruise (including maneuver), descent, and taxi. The corresponding applied cycles were compared with the allowable cycles using the appropriate constant life diagrams and, through the theory of linear cumulative damage, the service life was determined. The initial results yielded a calculated life greater than 10 000 hours (with a scatter factor of 1.5); therefore, the stresses were increased until the specified life was obtained. The cumulative spectra used to determine the allowable fatigue design stress are presented in figure 17-4, indicating representative values of mean stress (f_m) and alternating stress (f_a) that result in 10 000 hours of life.

Applied stress relationships (air plus thermal stresses) greater than those specified, result in less life and correspondingly smaller stresses will result in increased life.

ALLOWABLE DESIGN FATIGUE STRESS DETERMINATION

Discrete loading spectra were derived based on the established cumulative loading spectra and used for cumulative damage evaluation (fig.17-4; table 17-2). Constant life diagrams for René 41 at room temperature, 700°F, 1100°F, and 1400°F (figs. 17-5 through 17-8) and appropriate S-N curves (fig. 17-9) for a $K_t = 4.0$ were used.

The Palmgren-Miner theory of linear cumulative fatigue damage was used to determine the required service life. The basic equation is expressed as follows:

$$D = \frac{n_1}{N_1} + \frac{n_2}{N_2} + \cdots + \frac{n_i}{N_i} + \cdots + \frac{n_k}{N_k} = \sum_{i=1}^{k} \frac{n_i}{N_i}$$

where D = calculated life utilization ratio

n_i = number of loading cycles applied at the i^{th} stress level

N_i = number of loading cycles to failure for the i^{th} stress level from the relevant constant-life diagram. The relevant constant-life diagram is the one which applies to the material and fatigue quality index of the section under consideration

$\frac{n_i}{N_i}$ = cycle ratio

k = number of stress levels considered

The method of analysis using the above equation as a basis is as follows:

1. Select a fatigue quality index K for the section under consideration ($K_t = 4.0$).

2. Obtain loading spectra and temperatures associated with applicable phase of spectra.

3. Obtain constant-life diagrams for $K_t = K$ for René 41 at applicable temperatures (figs. 17-5 through 17-8).

4. Convert applied limit loads to stresses (since constant-life diagrams are presented as percent of room temperature strength, loads are converted to stresses as a percentage of the room-temperature ultimate tensile strength).

5. Calculate the cycle ratio of each loading case and add the cycle ratios to obtain the life utilization ratio "D" (table 17-3).

6. Calculate the life in hours for the section under consideration by

$$L_c = \frac{R\, L_1}{D}$$

where L_c = calculated life

L_1 = the life span in hours represented in the spectra used in the analysis

R = a reduction coefficient used to assure a specified probability of obtaining a test life equal to or greater than the calculated life

Using a reduction coefficient of 0.667 (which corresponds to a scatter factor for nominal design equal to 1.5), a calculated life of 10 000 hours was determined (table 17-3). This life-time corresponds to the total life requirement of the vehicle and indicates that for the assumed alternating stress levels and the number of applied cycles and temperatures, the operating 1g stress level (f_m) during cruise is 46 000 psi. The basic material allowables, as well as allowable tensile stresses for fatigue for both cruise and maneuver conditions are presented in table 17-4. The operational stresses (F_{fo}) reflect allowables applicable for service life calculations. The ultimate value for F_{fn} is an equivalent value for comparative purposes, with the minimum value (underlined) governing the design. Reduction of design stresses to the minimum values provides a structural system which meets the specified life requirement of 10 000 hours.

Monocoque Waffle

The 45° x 45° waffle panel limit air and thermal loads are summarized in table 17-5 for both the cruise and 2g maneuver conditions. Unit inplane loads (N_x and N_y) were input into the computer program (Section 10) to determine unit internal stresses (table 17-6). Also, unit pressure (ΔP) lateral loads were input and the resulting stresses are shown in table 17-6. The tensile inplane loads and the limit pressure loads for the 2g and cruise conditions are summarized in table 17-7 where they are multiplied by the unit cases and summed to arrive at the predicted fatigue levels for the wing study area. These stresses are compared to the appropriate fatigue allowables to arrive at margins of safety. The minimum margins are tabulated; the lowest being 1.50 on the upper skin outboard for the cruise condition.

Monocoque Honeycomb Sandwich

The limit air and thermal loads for the 2-g maneuver and cruise condition are shown in table 17-8. Table 17-9 summarizes the fatigue analysis, including margins of safety. The stress resultants for unit cases of pressure and inplane loads for the 40 x 80 in. panels are given. These are multiplied by the tensile

inplane loads and predicted pressures, also shown. The stresses are summed and compared with the appropriate fatigue allowables to obtain margins of safety. The minimum margin (0.36) is seen to occur on the upper outboard surface for the cruise condition.

Semimonocoque and Statically Determinate

The fatigue analysis results and margins of safety for the four "sheet" metal" wing constructions are shown in tables 17-10 (cruise) and 17-11 (2-g maneuver). The air load inplane loads, N, are the critical "x" or "y" direction loads, as are the thermal strains. The three stress components are:

inplane stress: $f_1 = N/t$

thermal stress: $f_2 = \epsilon$

bending stress: $f_3 = \frac{MZ}{I}$ where $M = \frac{pL^2}{8}$

The sum of these stresses are compared with the appropriate fatigue allowables (table 17-4) to determine the margins of safety. The minimum margin (0.003) occurs on the statically determinate center lower surface ($\mathfrak{E}$ to BL 120), for the 2-g condition. The 60-in. rib spacing causing large bending stresses due to lateral pressures was the major stress contributor in this analysis.

Spar and Rib Cap Fatigue

The caps for spars and ribs are subject to fatigue analysis where they must support primary thermal loads and air loads without panel support. That is, for the spanwise-stiffened concepts the rib caps are considered, and for chordwise stiffening the spar caps are considered. The lowest margins of safety occur during cruise and are shown in tables 17-12 and 17-13. The combined air and thermal stresses are not applicable when the net stress is compression. Large margins, in excess of 1.0, exist for all concepts.

REFERENCES

17-1 Structural Life Assurance Manual. Lockheed-California Company, 1968.

17-2 Airframe Design. Lockheed-California Company, Volume 11-C, LR19839.

TABLE 17-1

TIME SEGMENTS FOR SPECTRA DEFINITION

	Segment	Time, t, min	Altitude H, ft	Mach No., M	Dyn Press, q psf	Angle of attack, α degrees
ASCENT		0				
	1		38 000	1.6	600	4.3
		6.0				
	2		62 000	3.85	1500	2.8
		13.0				
	3		84 000	6.50	1500	4.35
		19.9				
CRUISE	4		111 000	8.00	630	9.31
		36.0				
	5		115 000	8.00	530	9.6
		52.2				
DESCENT	6		112 500	7.15	475	9.7
		62.0				
	7		84 000	3.45	390	5.75
		72.4				

TABLE 17-2

DISCRETE LOADING SPECTRA DERIVED FROM CUMULATIVE LOADING SPECTRA FOR S_m = CONSTANT

Given cumulative loading spectrum			Derived discrete loading spectrum	
Condition	Alternating stress level, f_a, psi	Cumulative No. of cycles, Σn	Alternating stress level, f_a, psi	No. of cycles applied at f_a, n
Taxi, Room temp		100 000		
	5 000	4 000	2 500	96 000
	10 000	180	7 500	3 820
	15 000	8	12 500	172
	18 500	1	16 750	7
Ascent, 700°F	0	10 000		
	5 000	350	2 500	9 650
	10 000	13	7 500	337
	14 000	1	12 000	12
Cruise, 1400°F	0	100 000		
	5 000	33 000	2 500	67 000
	10 000	11 500	7 500	21 500
	15 000	4 000	12 500	7 500
	20 000	1 300	17 500	2 700
	22 500	1 000	21 250	300
	22 500	1	22 500	999
Descent, 1100°F	0	1 400		
	5 000	150	2 500	1 250
	10 000	17	7 500	133
	15 000	2	12 500	15
	16 700	1	15 850	1

TABLE 17-3

LIFE UTILIZATION RATIO FOR K_t = 4.0

Reference		f_m,	f_a,	Applied cycles,	Allowable cycles,	Cycle ratio,	$\sum \frac{n}{N}$
No.	Condition	% F_{tu} at RT	% F_{tu} at RT	n	N		
1	Taxi,	35.7	1.47	9.6×10^4	10^7	.010	
2	Room	(60 700 psi)	4.41	3.82×10^3	5×10^5	.008	
3	Temp		7.35	1.72×10^2	5×10^4	-	
4			9.85	7	3.6×10^4	-	.018
1	Ascent,	20.7	1.47	9.65×10^3	10^7	.001	
2	700°F	(35 200 psi)	4.41	3.37×10^2	5×10^5	.001	
3			7.06	12	10^5	-	.002
1	Cruise,	27.1	1.47	6.7×10^4		.007	
2	1400°F	(46 000 psi)	4.41	2.15×10^4	1.3×10^5	.165	
3			7.35	7.5×10^3	4.4×10^4	.170	
4			10.3	2.7×10^3	1.8×10^4	.150	
5			12.5	3.0×10^2	9.3×10^3	.032	.524
6	Maneuver	27.1	13.2	9.99×10^2	8.2×10^3	.121	.121
1	Descent,	14.25	1.47	1.25×10^3	10^7	-	
2	1100°F	(24 200 psi)	4.41	1.33×10^2	2.3×10^5	.001	
3			7.35	1.5x10	7×10^4	-	
4			9.3	1	4.5×10^4	-	.001
							.666

René 41; F_{tu} = 170 000 lb/in.^{2}, room temp

$$L_c = \frac{R\,L_1}{D} = \frac{(.667)(10\,000)}{(.666)} = 10\,000 \text{ hours}$$

where

L_c = calculated life (hours)

R = reduction coefficient = 0.667 (scatter factor = 1.5)

L_1 = life span represented in spectra (hours)

D = life utilization ratio

TABLE 17-4

ALLOWABLE TENSILE STRESSES, RENE'41

(Design life of 10 000 hours)

Reference	Temp °F	Ultimate		Limit		Operational
		F_{tu},[a] psi	F_{fu}, psi	F_{ty},[b] psi	2/3 F_{tu}, psi	F_{fo},[c] psi
Basic Material	RT	170 000		130 000	113 333	46 000
Cruise	1400	129 000	90 000	108 000	86 000	46 000
Maneuver	1400	129 000	133 400	108 000	86 000	68 500

[a] F_{tu} $_{1400^{\circ}F}$ = (0.76)(170 000) = 129 000 psi (min.)

[b] F_{ty} $_{1400^{\circ}F}$ = (0.83)(130 000) = 108 000 psi (min.)

fatigue design allowable stress:

[c] F_{fn}, = Operational stress.

For cruise, F_{fo} = $\left|(27.1)(170\ 000) \div (100)\right|$ = 46 000 psi

For maneuver, F_{fo} = $\left|(27.1 + 13.2)(170\ 000)\right|$ (100)

= 68 000 psi

Equivalent allowable ultimate stress:

F_{fu} = 1.3 x 1.5 F_{fo}

TABLE 17-5

MONOCOQUE WAFFLE FATIGUE LIMIT LOADS, CRUISE AND +2.0-g CONDITIONS

	Cruise Condition[a]					
Location / Direction	Center		Inboard		Outboard	
	Upper	Lower	Upper	Lower	Upper	Lower
N_x, Air	- 39	-120	- 36	-109	- 17	- 69
N_x, Thermal	-436	-415	440	-289	546	-226
$\sum N_x$	-475	-535	404	-398	529	-295
N_y, Air	-198	189	-187	174	- 82	85
N_y, Thermal	- 62	- 45	-105	- 23	- 83	69
$\sum N_y$	-260	144	-292	151	-165	154
N_{xy}, Air	- 10	1	- 90	73	- 77	68
N_{xy}, Thermal	- 38	- 26	82	- 9	106	- 9
$\sum N_{xy}$	- 48	- 25	- 8	64	29	59

	+2.0-g Maneuver Condition[a]					
Location / Direction	Center		Inboard		Outboard	
	Upper	Lower	Upper	Lower	Upper	Lower
N_x, Air	- 78	-261	- 74	-235	- 13	-116
N_x, Thermal	360	-289	616	-493	395	-437
$\sum N_x$	282	-550	542	-728	382	-553
N_y, Air	-439	412	-414	394	-203	197
N_y, Thermal	- 50	45	- 88	40	-152	98
$\sum N_y$	-489	457	-502	434	-355	-295
N_{xy}, Air	- 29	10	-212	143	-179	163
N_{xy}, Thermal	0	7	118	- 18	- 52	- 12
$\sum N_{xy}$	- 29	17	- 94	125	-231	151

[a]Limit loads

TABLE 17-6

MONOCOQUE WAFFLE UNIT STRESSES

Wing Area	Surface	Unit Stiffener Stress, psi						Unit Skin Stress, psi									Temp. °F
		$f_{w,e}$ Based on unit Nx = 100 lb/in.	$f_{w,n}$ Based on unit Nx = 100 lb/in.	$f_{w,e}$ Based on unit Ny = 100 lb/in.	$f_{w,n}$ Based on unit Ny = 100 lb/in.	$f_{w,e}$ Based on unit p = 1.00 psi	$f_{w,n}$ Based on unit p = 1.00 psi	$f_{x,s}$ Based on unit Nx = -100 lb/in.	$f_{y,s}$ Based on unit Nx = -100 lb/in.	$f_{xy,s}$ Based on unit Nx = -100 lb/in.	$f_{x,s}$ Based on unit Ny = -100 lb/in.	$f_{y,s}$ Based on unit Ny = -100 lb/in.	$f_{xy,s}$ Based on unit Ny = -100 lb/in.	$f_{x,s}$ Based on unit p = 1.00 psi	$f_{y,s}$ Based on unit p = 1.00 psi	$f_{xy,s}$ Based on unit p = 1.00 psi	
Center	Upper	-123.78	-123.78	-595.33	-595.33	-5 137	- 5 137	-3106.6	210.88	0	198.99	-3216.6	0	2551	2551	0	1345
	Lower	-129.33	-129.33	-621.93	-621.93	-6 348	- 6 348	-3222.9	189.59	0	164.91	-3368.0	0	3075	3075	0	1340
Inboard	Upper	-106.81	-106.81	-556.77	-556.77	-4 333	- 4 333	-3130.4	282.54	0	281.51	-3215.1	0	2497	2497	0	1003
	Lower	-109.65	-109.65	-517.53	-517.53	-4 499	- 4 499	-2649.2	189.04	0	199.61	-2681.1	0	2029	2029	0	1306
Outboard	Upper	-126.69	-126.69	-612.03	-612.03	-5 821	- 5 821	-3203.8	211.15	0	192.30	-1334.5	0	2938	2938	0	845
	Lower	-175.07	-175.07	-736.78	-736.78	-14 510	-14 510	-3364.5	145.22	0	71.808	-3645.0	0	4407	4407	0	878

TABLE 17-7

MONOCOQUE WAFFLE FATIGUE ANALYSIS

Wing Area	Surface	Load Condition	Nx (lb/in.)	Ny (lb/in.)	p (psi)	Stiffener Stress, psi			Skin Stress, psi			Fatigue Allowable F_f, psi	MS(a)
						f_a' psi	f_b' psi	$f_a'+f_b'$ psi	f_a' psi	f_b' psi	$f_a'+f_b$ psi		
Center	Upper	Cruise	-	-	±0.50	0	± 2 569	+ 2 569	0	±1276	+ 1 276	46 000	16.91
	Lower	Cruise	-	+144	-0.73	895	4 634	5 529	4 850	-2245	+ 2 605	46 000	7.32
Inboard	Upper	Cruise	404	-	±0.50	428	± 2 167	2 595	12 645	+1249	+13 894	46 000	2.31
	Lower	Cruise	-	151	-0.97	780	4 364	5 144	4 048	-1968	+ 2 080	46 000	7.94
Outboard	Upper	Cruise	529	-	±0.5	672	± 2 911	3 583	16 949	±1469	+18 418	46 000	1.50
	Lower	Cruise	-	154	-0.735	1135	10 665	11 800	5 613	-3239	+ 2 374	46 000	2.89
Center	Upper	+2.0g	282	-	±0.5	347	± 2 569	2 916	8 762	±1276	10 038	68 500	5.82
	Lower	+2.0g	-	457	-0.97	2843	6 158	9 001	15 392	-2983	12 409	68 500	4.52
Inboard	Upper	+2.0g	542	-	±0.5	580	+ 2 167	2 747	16 965	±1249	18 214	68 500	2.76
	Lower	+2.0g	-	434	-1.46	2248	6 569	8 817	11 636	-2962	8 674	68 500	6.77
Outboard	Upper	+2.0g	382	-	±0.5	485	± 2 911	3 396	12 239	±1469	13 708	68 500	4.00
	Lower	+2.0g	-	295	-0.98	2174	14 220	16 394	10 753	-4319	6 434	68 500	3.17

(a) $MS = \frac{F_f}{f} - 1$

TABLE 17-8

MONOCOQUE HONEYCOMB SANDWICH FATIGUE LIMIT LOADS, CRUISE AND +2.0g CONDITIONS

	Cruise Condition[a,b]					
Location / Direction	Center		Inboard		Outboard	
	Upper	Lower	Upper	Lower	Upper	Lower
N_x, Air	- 96	- 73	- 78	- 95	- 22	- 21
N_x, Thermal	-903	-506	+688	-305	+1058	+429
$\sum N_x$	-999	-579	+610	-400	+1036	+408
N_y, Air	-157	+146	-136	+132	- 57	+ 56
N_y, Thermal	-158	-177	- 99	-125	+ 31	+109
$\sum N_y$	-315	- 31	-235	+ 7	- 26	+165
N_{xy}, Air	+ 4	- 12	- 67	+ 43	+ 44	+ 37
N_{xy}, Thermal	+ 50	+ 49	+ 36	- 71	+ 266	+220
$\sum N_{xy}$	+ 54	+ 37	- 31	+ 28	+ 310	+257

	+2.0g Condition[a,b]					
Location / Direction	Center		Inboard		Outboard	
	Upper	Lower	Upper	Lower	Upper	Lower
N_x, Air	-205	-152	-170	-198	- 52	- 33
N_x, Thermal	+518	-593	+692	-738	+348	-181
$\sum N_x$	+313	-745	+522	-936	+296	-214
N_y, Air	-334	+301	-302	+287	-124	+124
N_y, Thermal	- 65	+ 57	- 74	+ 77	-120	+134
$\sum N_y$	-399	358	-376	+364	-244	+258
N_{xy}, Air	+ 13	+ 2	-155	- 99	- 98	- 76
N_{xy}, Thermal	- 12	- 35	+ 84	+139	- 98	+132
$\sum N_{xy}$	+ 1	- 33	- 71	+ 40	-196	+ 56

[a] Limit loads

[b] Positive value tension, negative value compression

TABLE 17-9

MONOCOQUE HONEYCOMB SANDWICH FATIGUE ANALYSIS

Wing area	Surface	Unit stresses, psi			Load conditions	Actual loads			Actual stresses, psi			Fatigue allowable F_f psi	(a) MS
		f_x Based on N_x = -1000 lb/in.	f_y Based on N_y = -1000 lb/in.	f_x Based on p = 1.00 psi		N_x lb/in.	N_y lb/in.	p psi	f_a psi	f_b psi	f_a+f_b psi		
Center	Upper	34 556	34 556	12 492	CRUISE	-	-	±0.50	-	6 426	6 426	46 000	6.16
	Lower	33 357	33 357	12 091	CRUISE	-	-	-0.73	-	8 826	8 826	46 000	4.21
Inboard	Upper	34 315	34 315	12 115	CRUISE	610	-	±0.50	20 932	6 058	26 990	46 000	0.70
	Lower	29 948	29 948	11 591	CRUISE	-	7	-0.97	210	11 243	11 453	46 000	3.02
Outboard	Upper	28 032	28 032	9 670	CRUISE	1036	-	±0.50	29 041	4 835	33 876	46 000	0.36
	Lower	36 803	36 803	18 726	CRUISE	-	165	-0.74	6 072	13 764	19 836	46 000	1.32
Center	Upper	34 556	34 556	12 492	+2.0-g	313	-	±0.50	10 816	6 246	17 062	68 500	3.01
	Lower	33 357	33 357	12 091	+2.0-g	-	358	-0.97	11 942	11 728	23 670	68 500	1.89
Inboard	Upper	34 315	34 315	12 115	+2.0-g	522	-	±0.50	17 912	6 058	23 970	68 500	1.86
	Lower	29 948	29 948	11 591	+2.0-g	-	364	-1.46	10 901	16 923	27 824	68 500	1.46
Outboard	Upper	28 032	28 032	9 670	+2.0-g	296	-	±0.50	8 297	4 835	13 132	68 500	4.22
	Lower	36 803	36 803	18 726	+2.0-g	-	258	-0.98	9 495	18 351	27 846	68 500	1.46

(a) $MS = \frac{F_f}{f} - 1$

TABLE 17-10

SEMIMONOCOQUE AND STATICALLY DETERMINATE PRIMARY STRUCTURE
FATIGUE ANALYSIS, CRUISE CONDITION

Concept	Wing Surface	BL location	Environment (limit)				Geometry				Modulus of elasticity	M	Air load stress	Thermal stress	Bending stress	Σ^f	Margin of safety
			Airload N lb/in.	Thermal strain ϵ 10^{-6} in./in.	Pressure p lb/in.^{2}	Temp T ^oF	Range length ℓ in.	Area E in.^{2}/in.	Neutral axis Z in.	Moment of inertia I in.^{4}/in.	E 10^6 lb/in.^{2} $K_E(31.6)$	$\frac{\text{in. lb}}{\text{in.}}$	f_1 lb/in.^{2}	f_2 lb/in.^{2}	f_3 lb/in.^{2}	f_t $f_1+f_2+f_3$ lb/in.^{2}	MS $\frac{46000}{f_t} - 1$
Tubular	Upper	℄ -120	-138	- 74	0.50	1320	50	0.0293	1.175	0.0153	23.3	156.3	-4710	- 1 760	10 040	3 570	11.89
	Lower	℄ -120	158	- 4.6	-0.73	1330	50	0.0258	0.626	0.0042	23.8	228	6100	- 110	34 000	40 000	0.15
	Upper	120-212	-119	- 73.5	0.50	1130	40	0.0281	0.745	0.00677	25.4	100	-4240	- 1 870	11 000	4 890	8.41
	Lower	120-212	136	27.6	-0.97	1260	40	0.0284	0.626	0.00462	24.2	194	4800	670	26 300	31 770	0.45
	Upper	212-350	- 47	- 67	0.50	1130	40	0.0254	0.470	0.00218	25.4	100	-1850	- 1 700	21 560	18 011	1.55
	Lower	212-350	37	33	-0.73	1250	40	0.0254	0.470	0.0022	24.2	147	1450	800	31 300	33 550	0.37
Beaded	Upper	℄ -120	-138	- 74	0.50	1320	50	0.0263	0.901	0.00937	23.8	156	-5250	- 1 760	15 000	8 000	4.75
	Lower	℄ -120	158	- 4.6	-0.73	1330	50	0.0196	0.823	0.00576	23.8	228	8060	- 110	32 600	40 550	0.13
	Upper	120-212	-119	- 73.5	0.50	1130	40	0.0262	0.862	0.00850	25.4	100	-4540	- 1 870	10 140	3 730	11.33
	Lower	120-212	136	27.6	-0.97	1260	40	0.0224	0.979	0.00954	24.2	194	6070	670	19 900	26 700	0.72
	Upper	212-350	- 47	- 67	0.50	1130	40	0.0221	0.705	0.00464	25.4	100	-2130	- 1 700	15 200	11 370	3.05
	Lower	212-350	37	33	-0.73	1250	40	0.0197	0.901	0.00702	24.2	147	1880	800	18 900	21 600	1.13
Chordwise	Upper	℄ -120	- 73	-1530	0.5	1345	24	0.0286	0.705	0.0060	23.4	36	-2550	-17 350	4 230	N.A.	N.A.
	Lower	℄ -120	-130	-1210	-0.73	1343	24	0.0261	0.744	0.0062	23.4	53	-4950	-28 310	6 360	N.A.	N.A.
	Upper	120-212	- 80	1230	0.50	994	24	0.0292	0.526	0.0020	26.3	36.0	-2730	32 500	9 500	29 300	0.17
	Lower	120-212	-161	- 297	-0.97	1196	24	0.0337	0.666	0.0062	24.7	70	-4750	- 7 340	7 520	N.A.	N.A.
	Upper	212-350	- 69	1180	0.50	945	24	0.0382	0.669	0.0040	26.6	36.0	-1800	31 500	6 020	35 720	0.29
	Lower	212-350	- 26	192	-0.735	1113	24	0.0254	0.470	0.0022	25.6	52.6	-1020	4 900	11 200	15 080	2.05
Statically determinate	Upper	℄ -120	-150	- 15.8	0.50	1300	60	1.0314	0.784	0.00827	23.4	225	-4780	- 3 700	21 330	12 850	2.58
	Lower	℄ -120	+150	19	-0.73	1330	60	0.0211	0.94	0.00822	23.8	328	7110	450	37 510	45 070	0.02
	Upper	120-212	-126	45.5	0.50	1100	50	0.0291	1.019	0.01345	25.6	156	-4330	1 160	11 820	8 650	4.32
	Lower	120-212	126	- 28.3	-0.97	1250	50	0.0253	1.254	0.01815	24.2	303	4980	- 680	20 930	25 230	0.823
	Upper	212-350	- 47.3	12.3	0.50	1160	40	0.0206	0.588	0.00291	25.0	100	-2300	310	20 210	18 220	1.53
	Lower	212-350	45.7	- 13.9	-0.735	1300	40	0.0199	1.058	0.00995	23.4	147	2300	325	15 630	18 255	1.52

LIMIT LOADS, STRAINS, AND STRESSES SHOWN

N.A.: NOT APPLICABLE, COMPRESSIVE STRESSES $M = p\frac{\ell^2}{8}$ $f_1 = N/t$ $f_2 = E\epsilon$ $f_3 = \frac{MZ}{I}$ F_F = 46 000 lb/in.^{2} fatigue allowable

TABLE 17-11

SEMIMONOCOQUE AND STATICALLY DETERMINATE PRIMARY STRUCTURE FATIGUE ANALYSIS, 2g MANEUVER LIMIT LOADS

Concept	Wing Surface	BL location	Environment: Air load N lb/in.	Environment: Thermal strain ϵ 10^{-6} in./in.	Environment: Lateral Pressure p lb/in.^{2}	Environment: Temp T ^{o}F	Geometry: Panel length l in.	Geometry: Area $\bar{t}$ in.^{2}/in.	Geometry: Moment of inertia I in.^{4}/in.	Neutral axis Z in.	Modulus of elasticity E 10^6 lb/in.^{2}	Bending moment M in. lb/in.	Air load stress f_1 lb/in.^{2}	Thermal stress f_2 lb/in.^{2}	Bending stress f_3 lb/in.^{2}	ΣStress f_t $f_1+f_2+f_3$	Margin of safety MS $\frac{68,500}{f_t} - 1$
Tubular	Upper	℄ -120	-289	- 26.5	0.5	1220	50	0.0293	0.0183	1.175	24.6	156.3	- 9 360	- 650	10 030	- 480	(a)
	Lower	℄ -120	320	54	-0.97	1350	50	0.0258	0.0042	0.626	23.4	303	12 400	1 260	45 180	58 840	0.16
	Upper	120-212	-255	- 36.6	0.5	1300	40	0.0281	0.00677	0.745	23.9	100	- 9 070	- 870	11 000	1 060	63.6
	Lower	120-212	296	56.4	-1.46	1420	40	0.0284	0.00462	0.626	22.5	292	10 420	1 270	39 560	51 250	0.34
	Upper	212-350	-101	- 77	0.5	1330	40	0.0254	0.00218	0.470	22.4	100	- 3 980	- 1 720	21 560	15 860	3.32
	Lower	212-350	110	118	-0.98	1350	40	0.0254	0.0022	0.470	23.3	196	4 330	2 750	41 870	48 950	0.40
Beaded	Upper	℄ -120	-289	- 26.5	0.5	1220	50	0.0263	0.00937	0.901	24.6	156.3	-11 000	- 650	15 000	3 350	19.4
	Lower	℄ -120	320	54	-0.97	1350	50	0.0196	0.00576	0.813	23.4	303	16 330	1 260	43 310	60 900	0.13
	Upper	120-212	-255	- 36.6	0.5	1300	40	0.0262	0.00850	0.862	23.9	100	- 9 730	- 870	10 140	- 460	(a)
	Lower	120-212	296	56.4	-1.46	1420	40	0.0224	0.00954	0.979	22.5	292	13 210	1 270	29.970	44 450	0.54
	Upper	212-350	-101	- 77	0.5	1330	40	0.0227	0.00464	0.705	22.4	100	- 4 570	- 1 720	15 200	8 910	6.69
	Lower	212-350	110	118	-0.98	1350	40	0.0197	0.00708	0.901	23.3	196	5 580	2 750	24 940	33 270	1.06
Chordwise	Upper	℄ -120	-154	406	0.5	1232	24	0.0286	0.0060	0.705	24.5	36	- 5 380	9 950	4 230	8 800	6.78
	Lower	℄ -130	-281	-357	-9.97	1358	24	0.0261	0.0062	0.744	23.3	70	-10 770	- 8 320	8 380	-10 710	(a)
	Upper	120-212	-181	697	0.5	1277	24	0.0292	0.0020	0.526	24.1	36	- 6 200	16 800	9 500	20 100	2.41
	Lower	120-212	-349	-341	-1.46	1392	24	0.0337	0.0062	0.666	22.8	105	-10 360	- 7 770	11 290	- 6 840	(a)
	Upper	212-350	- 75	-132	0.5	1373	24	0.0382	0.0040	0.669	23.2	36	- 1 960	- 3 060	6 020	1 000	67.5
	Lower	212-350	71	-193	-0.98	1382	24	0.0254	0.0022	0.470	23.0	.6	- 2 800	- 4 440	15 070	7 830	7.75
Statically determinate	Upper	℄ -120	-316	-134	0.5	1220	60	0.0314	0.00827	0.784	24.6	225	-10 030	- 3 300	21 330	8 000	7.56
	Lower	℄ -120	314	150	-0.97	1350	60	0.0211	0.00822	0.94	23.4	436.5	14 900	3 510	49 910	68 320	0.003
	Upper	120-212	-274	- 74	0.5	1300	50	0.0291	0.01345	1.019	23.9	156.3	- 9 420	- 1 770	11 820	630	107.7
	Lower	120-212	286	73.5	-1.46	1420	50	0.0253	0.01815	1.254	22.5	456.2	11 300	1 650	31 520	44 470	0.54
	Upper	212-350	-103	- 44	0.5	1430	40	0.0206	0.00291	0.588	22.4	100	- 5 000	- 990	20 210	14 220	3.82
	Lower	212-350	109	37.6	-0.98	1550	40	0.0199	0.00995	1.058	19.2	196	5 030	720	20 840	26 590	1.58

$M = p\frac{l^2}{8}$ $f_1 = N/\bar{t}$ $f_2 = E\epsilon$ $f_3 = \frac{MZ}{I}$ F_F = 68,500 lb/in.^{2} (maneuver fatigue allowable)

(a) Not applicable; compression stress

TABLE 17-12

RIB CAP FATIGUE, SEMIMONOCOQUE SPANWISE TUBULAR AND SEMIMONOCOQUE SPANWISE BEADED
CRUISE LIMIT LOADS AND TEMPERATURES

Surface	BL location in.	N_x Air load lb/in.	ϵ_x Thermal strain 10^{-6} in/in.	Rib spacing in.	P Air load lb N_x (SPAC)	A_{CAP} $in.^2$ (a)	f_A Air stress $lb/in.^2$ P/A	f_T Thermal $lb/in.^2$ (E_T) (ϵ_X) (b)	f_{total} $lb/in.^2$	MS $\frac{F_F}{F_{total}} - 1$ $\frac{46\,000}{F_F} - 1$
Upper	℄ -120	-66.2	-1484	50	-3310	0.227	-14 580	-35 319	-49 900	(c)
Lower	℄ -120	-91.8	-1569	50	-4590	0.249	-18 430	-37 342	-55 770	(c)
Upper	120-212	-65.6	- 215	40	-2620	0.205	-12 780	-54 601	-18 240	(c)
Lower	120-212	-92.8	- 827	40	-3710	0.227	-16 344	-20 013	-36 357	(c)
Upper	212-350	-33.3	932	40	-1330	0.217	- 6 129	23 673	17 540	1.62
Lower	212-350	-52.3	542	40	-2090	0.203	-10 300	13 120	2 820	15.31

[a] Includes effective skin.

[b] Temp. and E_T.

[c] Not applicable for compression.

TABLE 17-13

SPAR CAP FATIGUE, SEMIMONOCOQUE CHORDWISE CRUISE LIMIT LOADS AND TEMPERATURES

Surface	Station location in.	N_y Air load lb/in.	ϵ_y Thermal strain 10^{-6} in./in.	SPAR spacing in.	P Air load lb N_y (SPAC)	A_{CAP} $in.^2$ (a)	f_A Air stress $lb/in.^2$ P/A	f_T Thermal $lb/in.^2$ $(E_T)(\epsilon_y)$ (b)	f_{total} $lb/in.^2$	M.S. $\frac{F_F}{F_{total}} - 1$
Upper	C -120	-227	-345	24	-5450	.260	-20 961	-8060	-29 010	(c)
Lower	C -120	208	-301	24	4990	.260	19 200	-7040	12 160	2.78
Upper	120-212	-215	-200	24	-5160	.258	-20 000	-5260	-25 260	(c)
Lower	120-212	195	-180	24	4680	.289	16 190	-4450	11 740	2.92
Upper	[illegible]	- 93	- 35.4	24	-2230	.215	-10 380	- 940	-11 320	(c)
Lower	212-350	95	95.4	24	2280	.191	11 940	2440	14 380	2.20

[a] Includes effective skin

[b] Temp. and E_T

[c] Not applicable for compression.

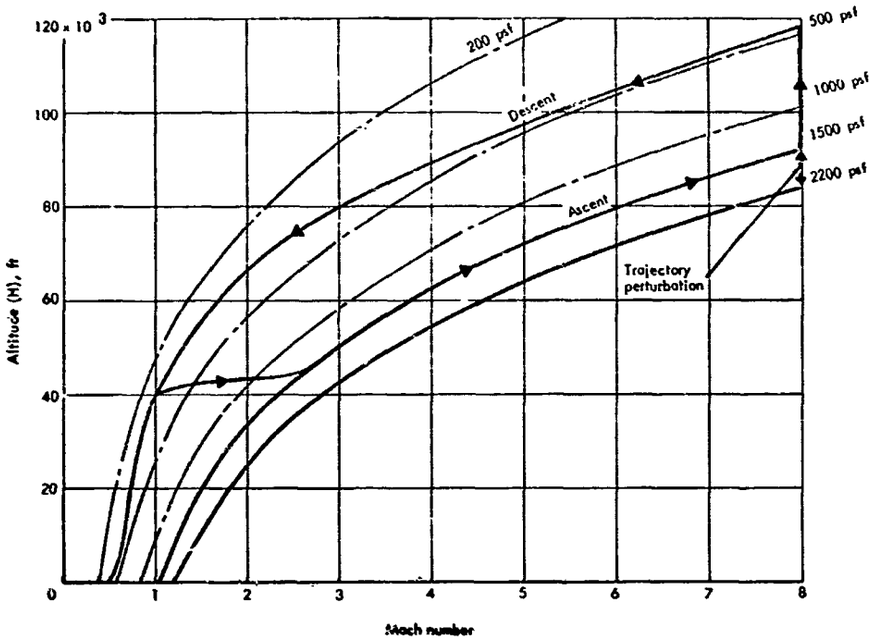

Figure 17-1. Hypersonic cruise airplane design trajectory

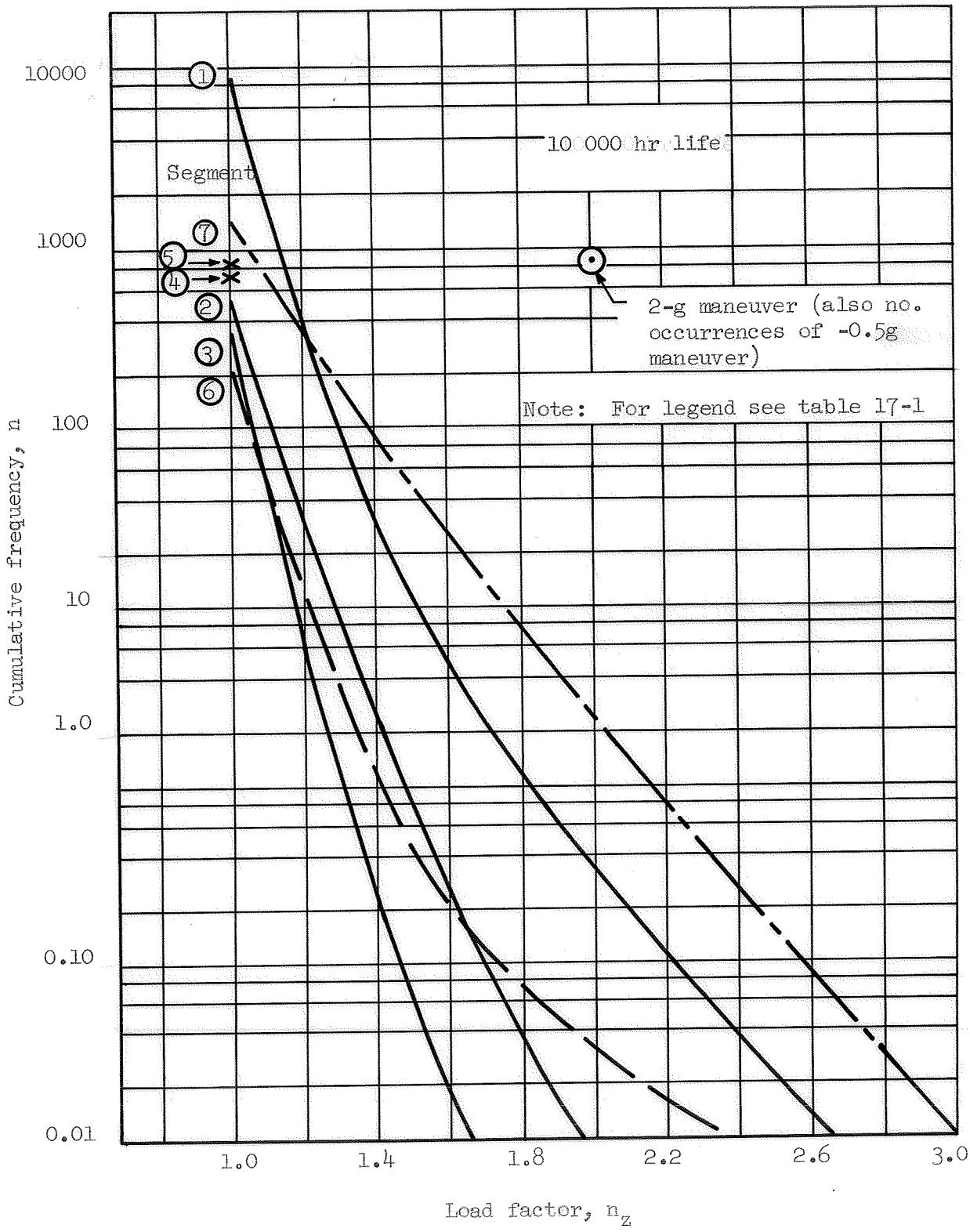

Figure 17-2. Frequency of exceedance of c.g. load factor

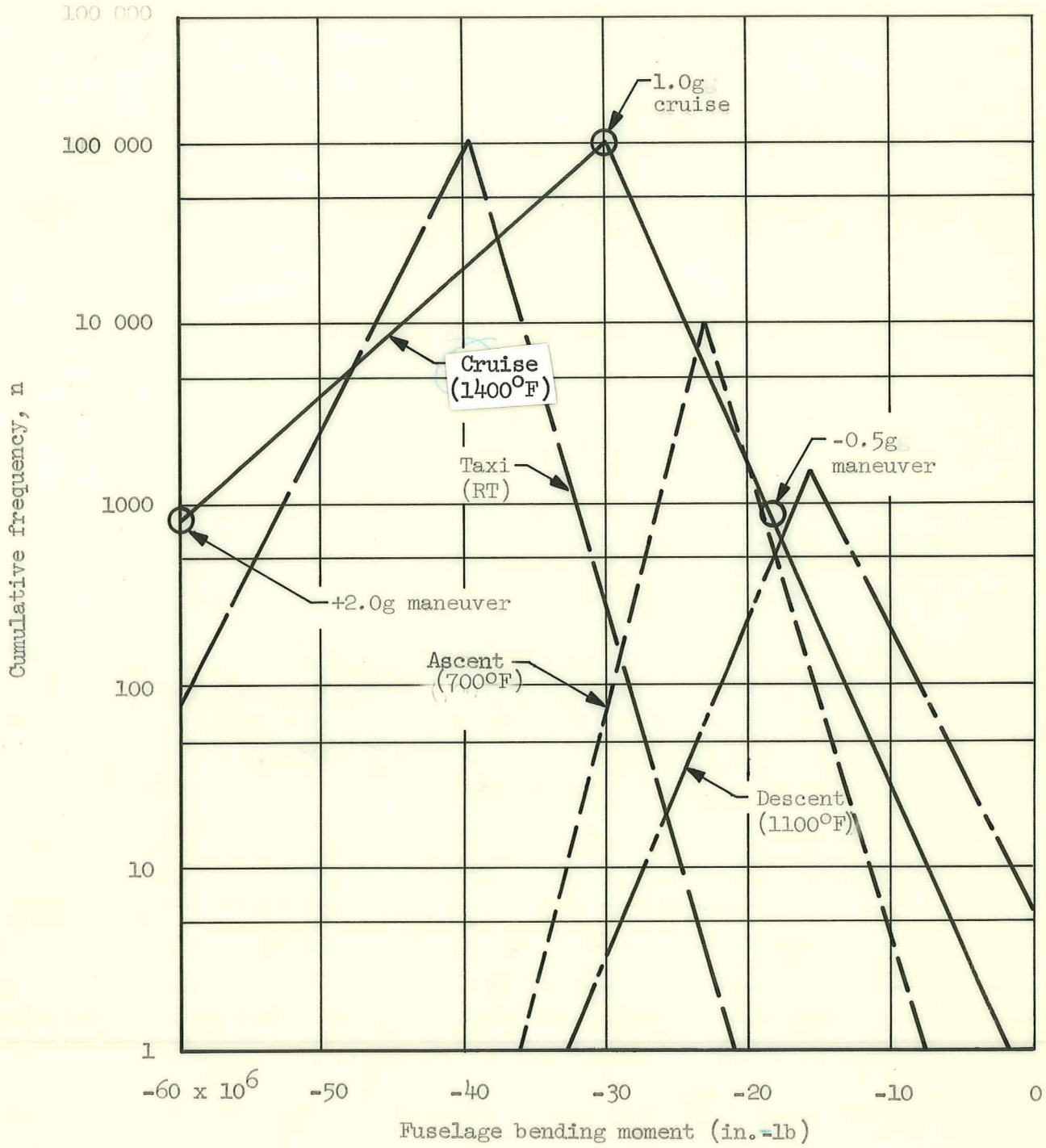

Figure 17-3. Frequency of exceedance of longitudinal bending moment at station 2364 - 10 000-hour life

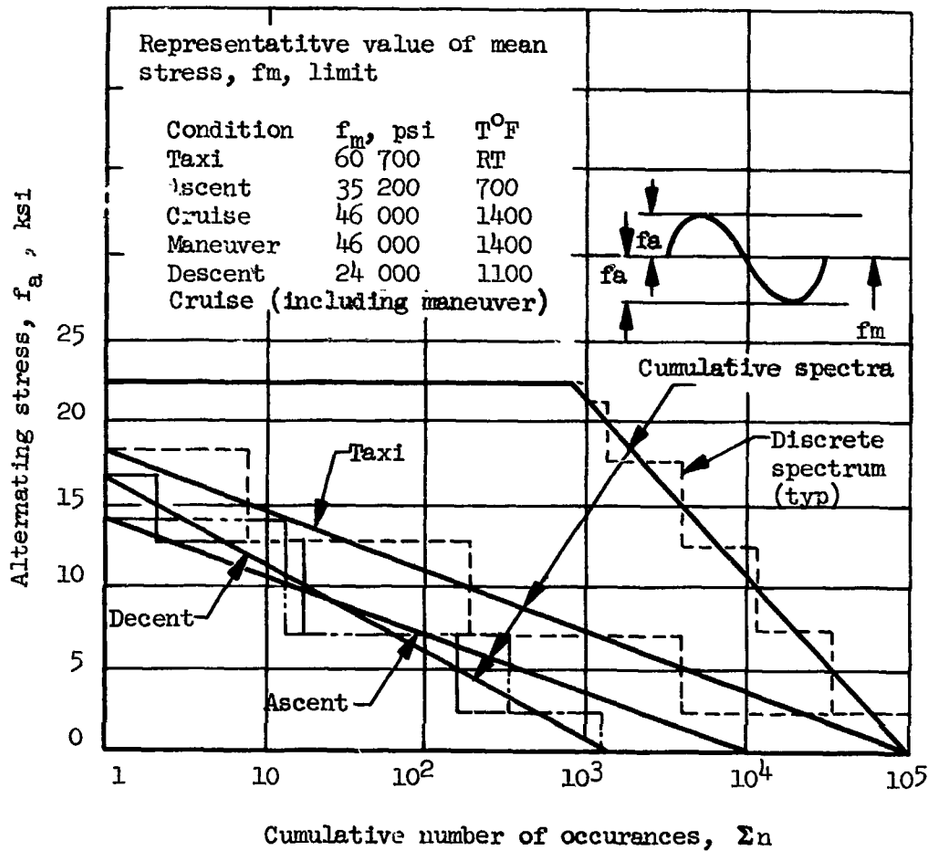

Figure 17-4. Fatigue spectra for wing structure life determination

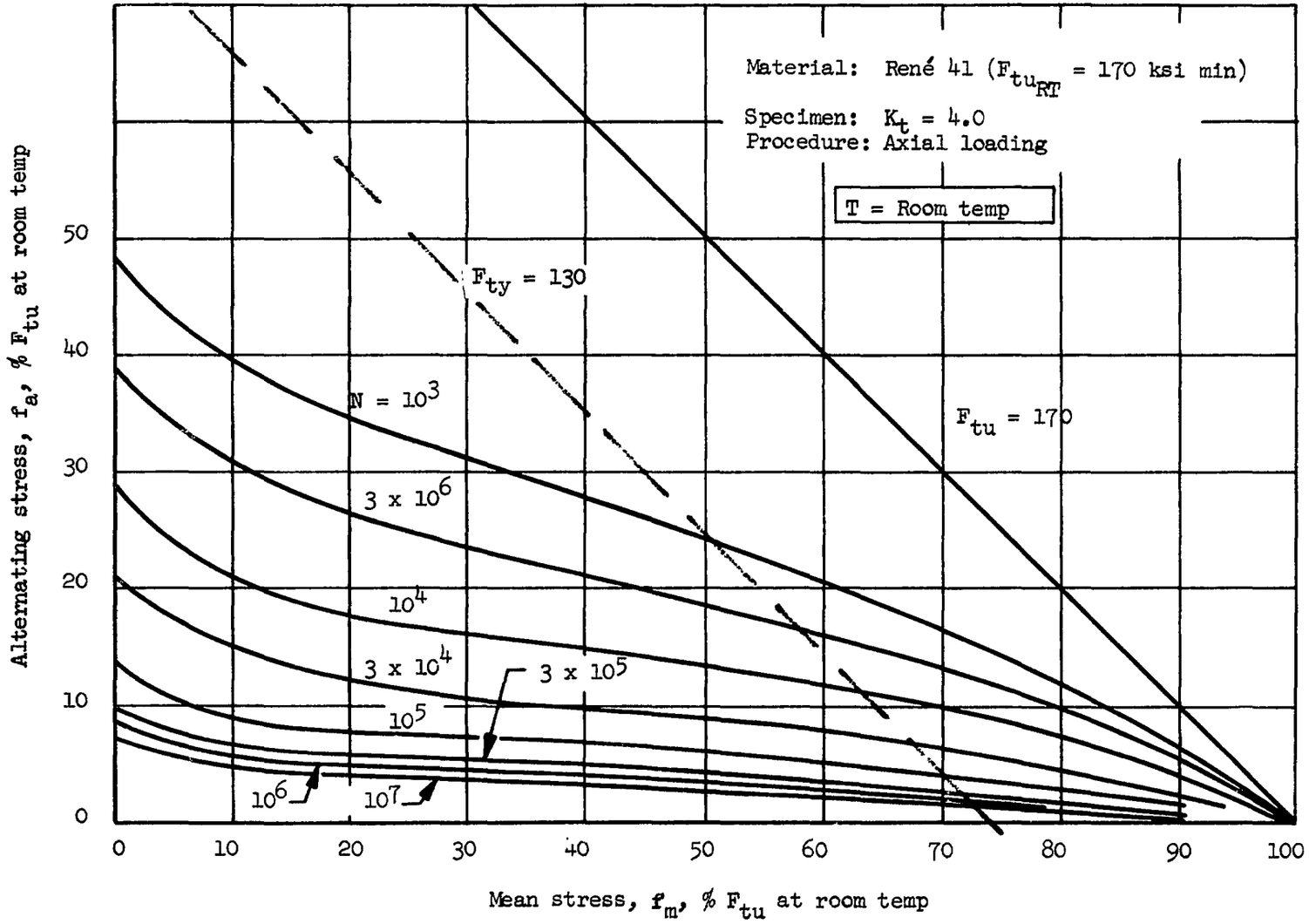

Figure 17-5. Constant life diagram – René 41 (K_t = 4.0) – room temp

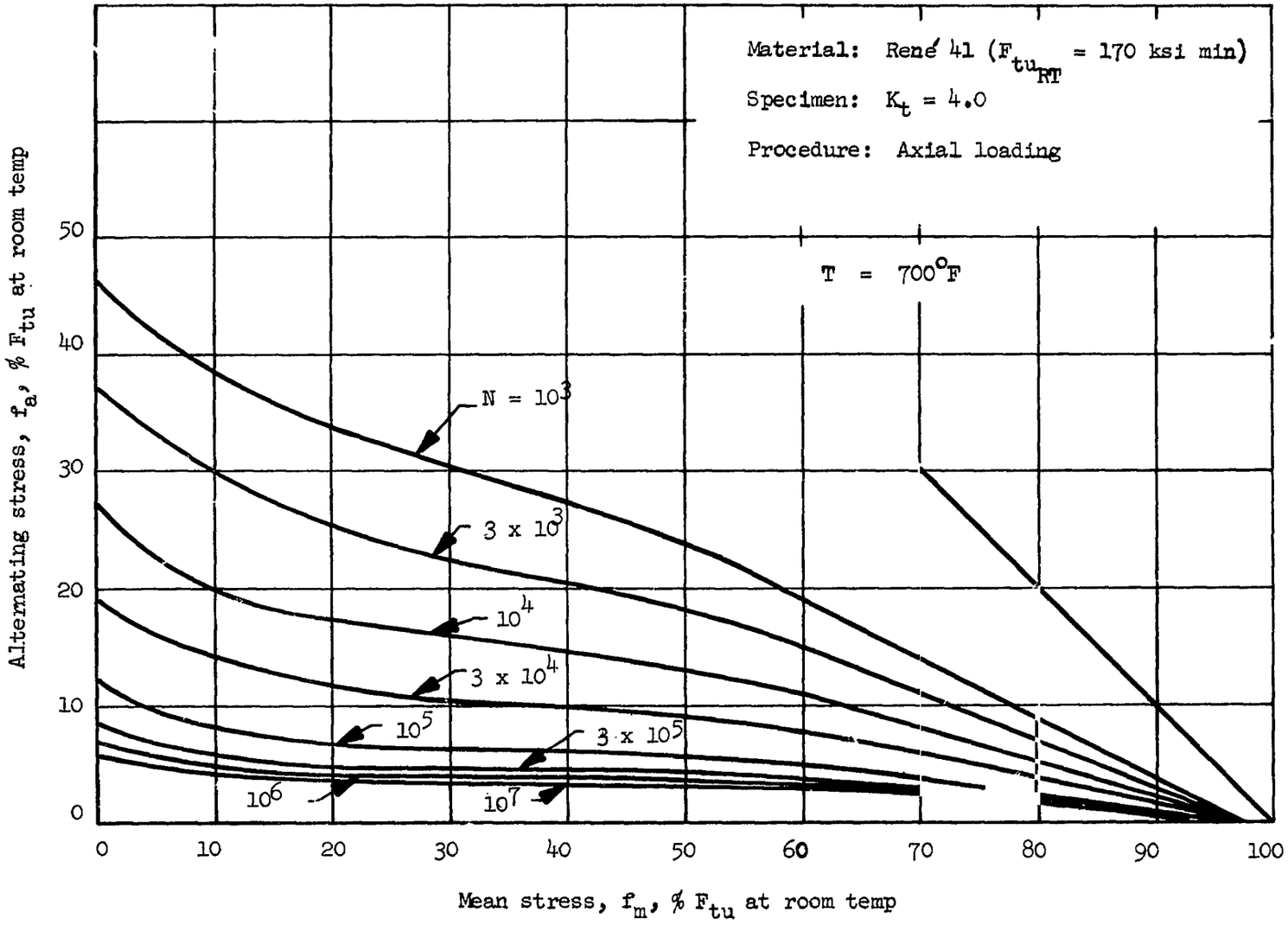

Figure 17-6. Constant life diagram – René 41 (K_t = 4.0) ~ 700°F

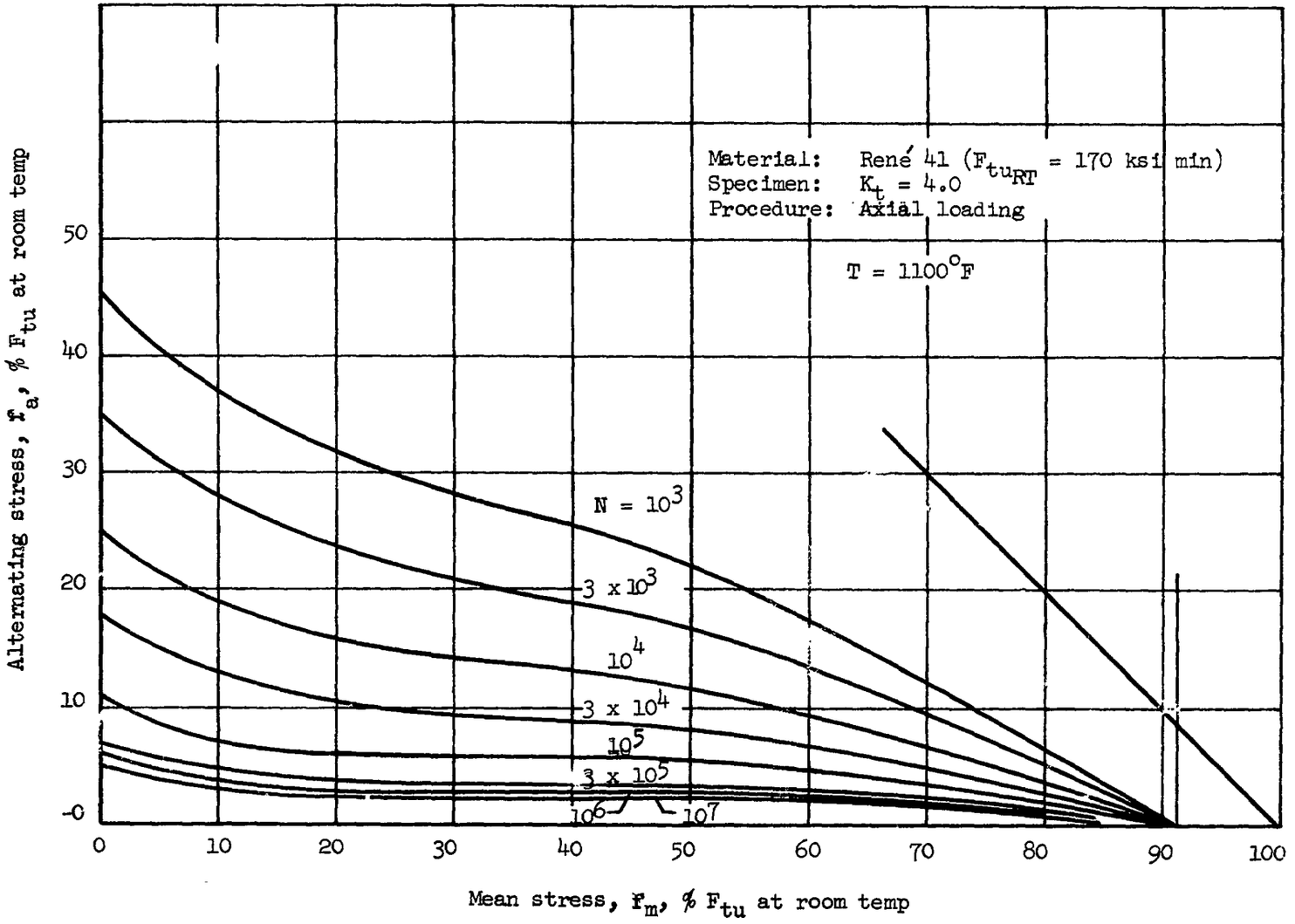

Figure 17-7. Constant life diagram – René 41 (K_t = 4.0) – 1100°F

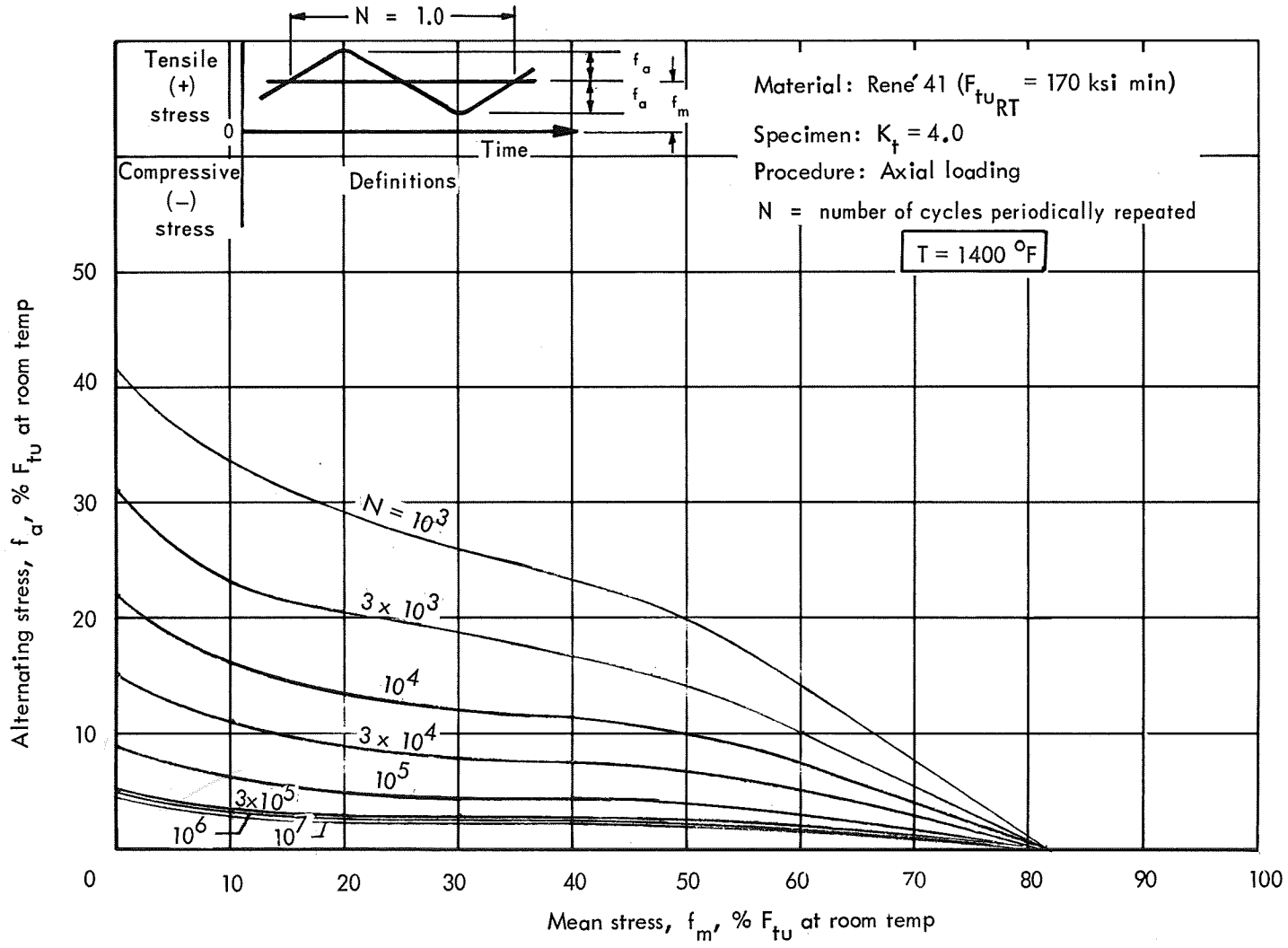

Figure 17-8. Constant life diagram, René 41 (K_t = 4.0) - 1400°F

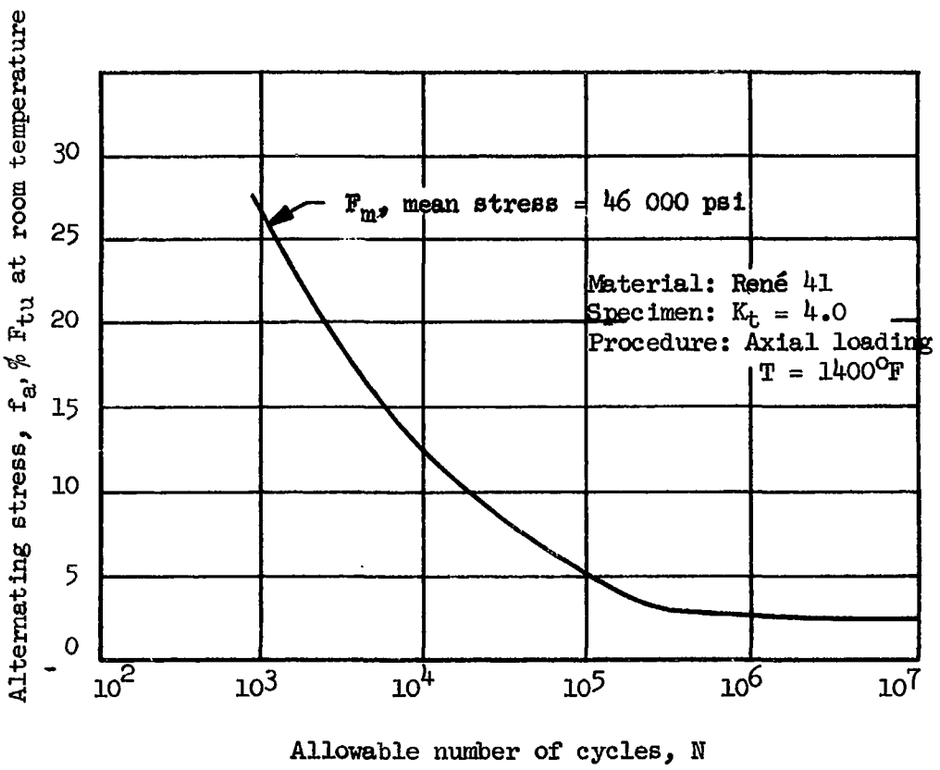

FIGURE 17-9 S/N Curve for Rene' 41 at 1400 F(K_t = 4.0)

Section 18

CREEP

by

C. C. Richie

CONTENTS

TABLES

ILLUSTRATIONS

SYMBOLS

BL	Butt line
b	Width of panel flat
E	Modulus of elasticity
E_{el}	Elastic modulus of elasticity
F_{cy}	Compressive yield strength
f_c	Compressive stress
f_{cc}	Compressive crippling stress
$f_{c,cr}$	Compressive buckling stress
$f_{l,th}$	Thermal stress for lower surface of center area
$f_{u,th}$	Thermal stress for upper surface of center area
f_x, f_y, f_{xy}	Extensional stresses and shear stress in xy coordinate system
g	Gravitational acceleration
MS	Margin of safety
N_x, N_y, N_{xy}	Extensional forces and shear force in xy coordinate system per unit length of section
n, n_o	Material constants used in creep equations, also n is shape parameter determined from stress-strain curve of the material
p	Pressure
R	Radius
T	Temperature
t	Time; material thickness
t_c	Cap thickness
ϵ	Strain

ϵ_x, ϵ_y, γ	Extensional strains and shear strain in xy coordinate system
$\epsilon_{equiv.}$	Equivalent uniaxial strain based on octahedral shear stress theory
σ	Stress
σ_o, σ_c	Material constants
η_S	$\frac{E_s}{E}$, Secant plasticity factor
η_T	$\frac{E_t}{E}$, Tangent plasticity factor

Section 18

CREEP

CREEP DESIGN CRITERIA

Creep design criteria considered creep buckling and permanent deformation of 0.5 percent for a vehicle life of 10 000 hours. To evaluate creep effects, the following assumptions were made:

1. The allowable compressive stresses under creep conditions can be approximated by using the isochronous stress-strain curves as if they were actual stress-strain curves (ref. 18-1).

2. Stress relaxation of thermal strains can be approximated using the theory of total creep deformation presented in reference 18-2.

3. The creep material properties are based on the average temperature during cruise and the total time at cruise (6680 hours, including a scatter factor of 1.5) for a vehicle life of 10 000 hours.

The criteria used for evaluating stress relaxation is based on the theory of total creep deformation presented in reference 18-2. In this theory, the assumptions are as follows:

(1) Elastic deformations are considered small compared with plastic or creep deformations.

(2) Plastic (slip) deformation with strain hardening, measured by the plastic strain ϵ in the presence of stress σ, can be expressed in the form:

$$\epsilon = \left(\frac{\sigma}{\sigma_o}\right)^{n_o}$$

where σ_o and n_o are material constants

(3) The viscous flow under constant uniaxial stress, σ, during the secondary stage of creep can be represented in the form of a power law:

$$\frac{d\epsilon}{dt} \qquad \left(\frac{\sigma}{\sigma_c}\right)^{n}$$

where σ_c and n are material constants.

Based on assumptions (1) through (3), the total creep rate can be expressed in the form:

$$\frac{d\epsilon}{dt} = \frac{d}{dt}\left(\frac{\sigma}{\sigma_o}\right)^{n_o} + \left(\frac{\sigma}{\sigma_c}\right)^{n} \tag{18-1}$$

Integration gives

$$\epsilon = \left(\frac{\sigma}{\sigma_o}\right)^{n_o} + \int_o^t \left(\frac{\sigma}{\sigma_c}\right)^{n} dt \tag{18-2}$$

assuming

$$\epsilon = \epsilon^{(o)} = \left(\frac{\sigma}{\sigma_o}\right)^{n_o} \quad \text{for} \quad t = 0$$

and $\sigma > 0$. For σ = constant, equation (18-2) can be expressed in the form:

$$\epsilon = \epsilon^{(o)} + vt$$

where $v = \left(\frac{\sigma}{\sigma_c}\right)^{n}$ is the corresponding creep rate in secondary creep.

Stress relaxation due to creep of Rene' 41 was evaluated by considering a constant thermal strain and gradually diminishing thermal stresses. Based on creep data presented in reference 18-3 for Rene' 41 at a temperature of 1300°F, the material constants for the creep power law are:

$n = n_o = 1.0$

$\sigma_o = 41.44 \times 10^6$ psi

$\sigma_c = 9.615 \times 10^9$ psi

Thus, from equation (18-1)

$$0 = \frac{d}{dt}\left(\frac{\sigma}{\sigma_o}\right) + \left(\frac{\sigma}{\sigma_c}\right)$$

$$0 = \frac{\sigma_c}{\sigma_o}\frac{d\sigma}{\sigma} + dt$$

$$0 = \frac{\sigma_c}{\sigma_o}\ln\left(\frac{\sigma_2}{\sigma_1}\right) + (t_2 - t_1)$$

$$t_2 - t_1 = \frac{\sigma_c}{\sigma_o}\ln\left(\frac{\sigma_1}{\sigma_2}\right) \tag{18-3}$$

Stress relaxation for the chordwise semimonocoque concept is shown in figure 18-1. Based on equation (18-3), these results show that the upper surface panel thermal stress decays exponentially from $\sigma_1 = -36\ 000$ psi to $\sigma_2 = -100$ psi in 1360 hours and the lower surface panel thermal stress decreases from $\sigma_1 = -29\ 000$ psi to $\sigma_2 = -100$ psi in 1320 hours. From this example, the following conclusions are evident:

1. Thermal stress relaxation of René 41 at temperatures near 1300°F is very significant.

2. Creep effects produce redistribution of thermal stress.

3. Residual stress buildup due to creep significantly reduces thermal stresses.

An exact determination of the redistribution of thermal stresses in transient creep due to cyclic variation of stresses and temperature in a complex redundant structure is beyond the scope of this study. Hence, the foregoing simplified criteria was used for evaluation of creep effects.

CREEP EVALUATION RESULTS

Creep evaluation of primary structural concepts encompassed monocoque panels and semimonocoque panels and rib/spar caps. Creep design criteria included creep buckling and permanent deformation of 0.5 percent. Compressive in-plane loads only were used to determine creep buckling margins of safety. Factors of safety were for limit loads and a scatter factor of 1.5 was applied to creep design life. The wing location selected for creep evaluation was the center area under the fuselage (BL 0-120). This area was selected because of maximum compressive loads and temperatures during cruise. Equations used for stress analysis of the monocoque and semimonocoque concepts are presented in sections 10 and 11, respectively. Isochronous stress strain curves for the average temperature under the fuselage during cruise, T = 1300°F, were used to determine creep buckling strengths and plastic creep deformation.

Since creep was assumed to occur predominantly during cruise, the cruise in-plane loads, thermal strains, and pressure loads were selected for the creep evaluation.

Only steady-state aerodynamic pressures were considered for the creep evaluation. Wing vent pressures are transient pressure loads occurring during a small fraction of the vehicle life and, therefore, are not considered.

Because of thermal stress relaxation, two elapsed times were considered for the creep buckling criteria. All structural concepts were evaluated for the time at cruise, including the scatter factor of 1.5, t = 6680 hours, based on a vehicle life of 10 000 hours, corresponding to the minimum difference

between the isochronous yield strength and the time-dependent thermal stress (see fig. 18-1). Typical stress-strain states for 30 hours and the design creep life are shown in figure 18-2. Since thermal stress relaxation produces permanent creep deformation, figure 18-1 shows that maximum permanent deformation and minimum thermal stress occur at $t = 6680$ hours.

Results of the creep evaluation indicate that the monocoque and semimonocoque primary structural concepts are adequate with respect to creep buckling analysis of monocoque and semimonocoque panels for the creep design life, $t = 6680$ hours. The lower surface panel for the statically determinate concept has the minimum panel margin of safety of 1.42. Results of the permanent creep deformation analysis of the primary structural panel concepts for the creep design life are shown in table 18-2. The minimum panel margin of safety of 2.16 occurs for the upper surface panel of the semimonocoque chordwise concept. Comparison of tables 18-1 and 18-2 shows that creep buckling is the governing panel criteria for all but the upper surface panel of the semimonocoque chordwise concept at $t = 6680$ hours. Creep buckling and plastic strain analysis results for the semimonocoque beam cap concepts are shown in tables 18-3 and 18-4, respectively. Minimum margin of safety of 0.37 occurs for the upper surface spar caps for the semimonocoque chordwise concept. The statically determinate concept has no chordwise stiffness and, therefore, no evaluation was required. Results of the creep buckling analysis of the semimonocoque chordwise concept for a time of 30 hours, corresponding to the minimum difference between isochronous yield strength and time-dependent yield stress, are shown in table 18-5. Comparison of tables 18-1 and 18-5 shows that the minimum creep buckling margin of safety for the chordwise semimonocoque concept occurs for a time of 30 hours.

Typical creep materials data and creep buckling allowables required for the creep evaluation are shown in figures 18-3 through 18-9. Isochronous stress strain curves for Rene' 41 at the 1300°F design temperature are shown in figure 18-3. Isochronous plasticity reduction factors for the creep design life and a time of 30 hours are shown in figures 18-4 and 18-5, respectively. Local creep buckling strength of a circular-arc for times of 6680 hours and 30 hours is shown in figures 18-6 and 18-7, respectively. Figure 18-8 presents initial creep buckling of semimonocoque rib caps for the design temperature of 1300°F and time of 6680 hours. A comparison of semimonocoque cap crippling and initial buckling stresses is shown in figure 18-9. Initial creep buckling of the caps is seen to be the governing allowable compressive stress.

REFERENCES

18-1 Gatewood, B. E.: Thermal Stresses. McGraw-Hill Book Co., 1957, page 134.

18-2 Falke, K. G. Odqvist: Mathematical Theory of Creep and Creep Rupture. Oxford, 1966.

18-3 Aarnes, M. N.; Tuttle, M. M.: Presentation of Creep Data for Design Purposes. ASD TR-61-216, June 1961.

18-4 Manson, S. S.: Thermal Stress and Low Cycle Fatigue. 1966.

TABLE 18-1

ANALYSIS OF CREEP BUCKLING.[a,b]; t = 6680 HOURS

Concept	Monocoque				Semimonocoque							
	-45° x 45° Waffle[c]		Honeycomb sandwich		Spanwise, tubular		Spanwise, beaded		Chordwise		Statically determinate	
Surface BL 0-120	Upper	Lower	Upper	Lower	Upper	Lower	Upper	Lower	Upper	Lower	Upper	Lower
T, °F	1345	1340	1277	1327	1320	1330	1320	1330	1345	1343	1320	1330
N_x (d)	-39	-120	-96	-73	—	—	—	—	-73	-130	—	—
N_y (d)	-198	189	-157	146	-138	156	-138	156	—	—	-150	150
N_{xy} (d)	10	1	4	-12	4	2	4	2	12	2	0	0
p[e]	0	-0.23	0	-0.23	0	-0.23	0	-0.23	0	-0.23	0	-0.23
f_x[f]	-818	-4574	-3317	-5216	—	—	—	—	-2550	-8290	—	—
f_y[f]	-6287	-479	-5425	-2781	-4720	-10 750	-5250	-10 300	—	—	-4780	-11 800
f_{xy}	185	20	138	-400	164	75	180	150	560	105	0	0
Fcr	26 300	28 700	28 700	28 700	21 500	27 500	31 500	29 000	27 250	25 250	35 000	28 500
MS	2.70	4.68	2.28	2.59	3.68	1.56	5.0	1.82	9.7	2.05	6.35	1.42

[a] Material: Rene' 41, sta 1400°F, T = 1300°F, t = 6680 hr.

[b] Stresses based on limit in-plane and pressure loads for cruise condition.

[c] Waffle skin.

[d] Airloads only.

[e] Not including vent pressure.

[f] Compression only.

TABLE 18-2

ANALYSIS OF PERMANENT CREEP DEFORMATION [a,b]

Concept	Monocoque				Semimonocoque							
Surface BL 0-120	$-45^{\circ} \times 45^{\circ}$ Waffle[c]		Honeycomb sandwich		Spanwise, tubular		Spanwise, beaded		Chordwise		Statically determinate	
Strain x 10^{-6}	Upper	Lower	Upper	Lower	Upper	Lower	Upper	Lower	Upper	Lower	Upper	Lower
ϵ_x, Thermal	-890	-769	-1259	-657	–	–	–	–	-1530	-1210	–	–
ϵ_y, Thermal	146	153	167	34	-74	-5	-74	-5	–	–	-16	19
γ, Thermal	106	-71	192	185	15	108	15	108	228	109	0	0
ϵ_x, Total	[illegible]	-769	-1259	-657	–	–	–	–	-1530	-1210	–	–
ϵ_y, Total	146	153	167	34	-74	245	-74	350	–	–	-16	369
γ, Total	106	-71	192	185	15	108	15	108	228	109	0	0
ϵ_{eq}[e]	988	864	1391	747	78	308	78	397	1580	1225	16	369
MS[f]	4.06	4.78	2.59	5.69	Large	Large	Large	Large	2.16	3.08	Large	Large

[a] Material: René 41, sta 1400°F, T = 1300°F, t = 6680 hr.

[b] Based on limit airload and thermal strain for cruise condition.

[c] Waffle skin.

[d] $\epsilon_{total} = \epsilon_{airload} + \epsilon_{thermal}$: total plastic creep strain.

[e] $\epsilon_{eq} = (\epsilon_x^2 + \epsilon_y^2 - \epsilon_x \epsilon_y + 3\gamma^2)^{1/2}$; equivalent unixial strain based on octahedral shear stress theory.

[f] $MS = \epsilon_{max}/\epsilon_{eq} - 1$, where $\epsilon_{max} = 0.5\%$.

TABLE 18-3

BEAM CAP CREEP BUCKLING; τ = 6680 HOURS

Concept	Wing Location	Item	f_c, psi	$f_{c,cr}$ psi	MS
Semimonocoque, spanwise	$\mathcal{L}$ - 120 (upper)	Rib caps	-14 700	24 000	+0.63
	$\mathcal{L}$ - 120 (lower)	Rib caps	-18 500	28 000	+0.51
Semimonocoque, chordwise	$\mathcal{L}$ - 120 (upper)	Spar caps	-21 200	29 000	+0.37
	$\mathcal{L}$ - 120 (lower)	Spar caps	-19 100	29 000	+0.52
Statically determinate	$\mathcal{L}$ - 120 (upper)	Rib caps	No chordwise cap stiffness - not critical in creep buckling		
	$\mathcal{L}$ - 120 (lower)	Rib caps			

TABLE 18-4

CAP PLASTIC STRAIN ANALYSIS

Concept	Wing location	ϵ_{th}, in./in. x 10^{-6}	f_{air}, psi	ϵ_{air}[b], in./in. (plastic) x 10^{-6}	ϵ_{total}, in./in. x 10^{-6}	ϵ_{total}, %	MS[c]
Semimonocoque, spanwise[a] (rib caps)	C_L - 120 (upper)	-1490	-14 700	-200	-1690	-0.169	1.97
	C_L - 120 (lower)	-1570	-18 500	-400	-1970	-0.197	1.53
Semimonocoque, chordwise (spar caps)	C_L - 120 (upper)	-345	-21 200	-550	-895	-0.0895	4.60
	C_L -120 (lower)	-302	-19 100	-450	-752	-0.075	5.65
Statically determinate (rib caps)	"NO CHORDWISE STIFFNESS"						

[a] Semimonocoque, spanwise tubular & beaded have identical caps and loads.

[b] Plastic strain.

[c] $MS = \epsilon_{max}/\epsilon_{total} - 1$, where $\epsilon_{max} = 0.5\%$.

TABLE 18-5

ANALYSIS OF CREEP BUCKLING,[a,b] t = 30 HOURS

(Concept: semimonocoque, chordwise)

Surface (BL 0-120)	Upper	Lower
T_1 °F	1345	1343
N_x, Airload	-915	-130
N_x, Thermal	-73	-663
N_x, Total	-988	-793
p, psi[c]	0	-0.23
f_x, psi[c]	-34 550	-41 105
$f_{c,cr}$	74 000	69 000
MS	1.14	0.68

[a] Material: Rene 41, sta 1400°F, T = 1300 °F, t = 30 hr

[b] Stresses based on limit in-plane and pressure loads for cruise condition.

[c] Not including vent pressure.

[d] Compression only.

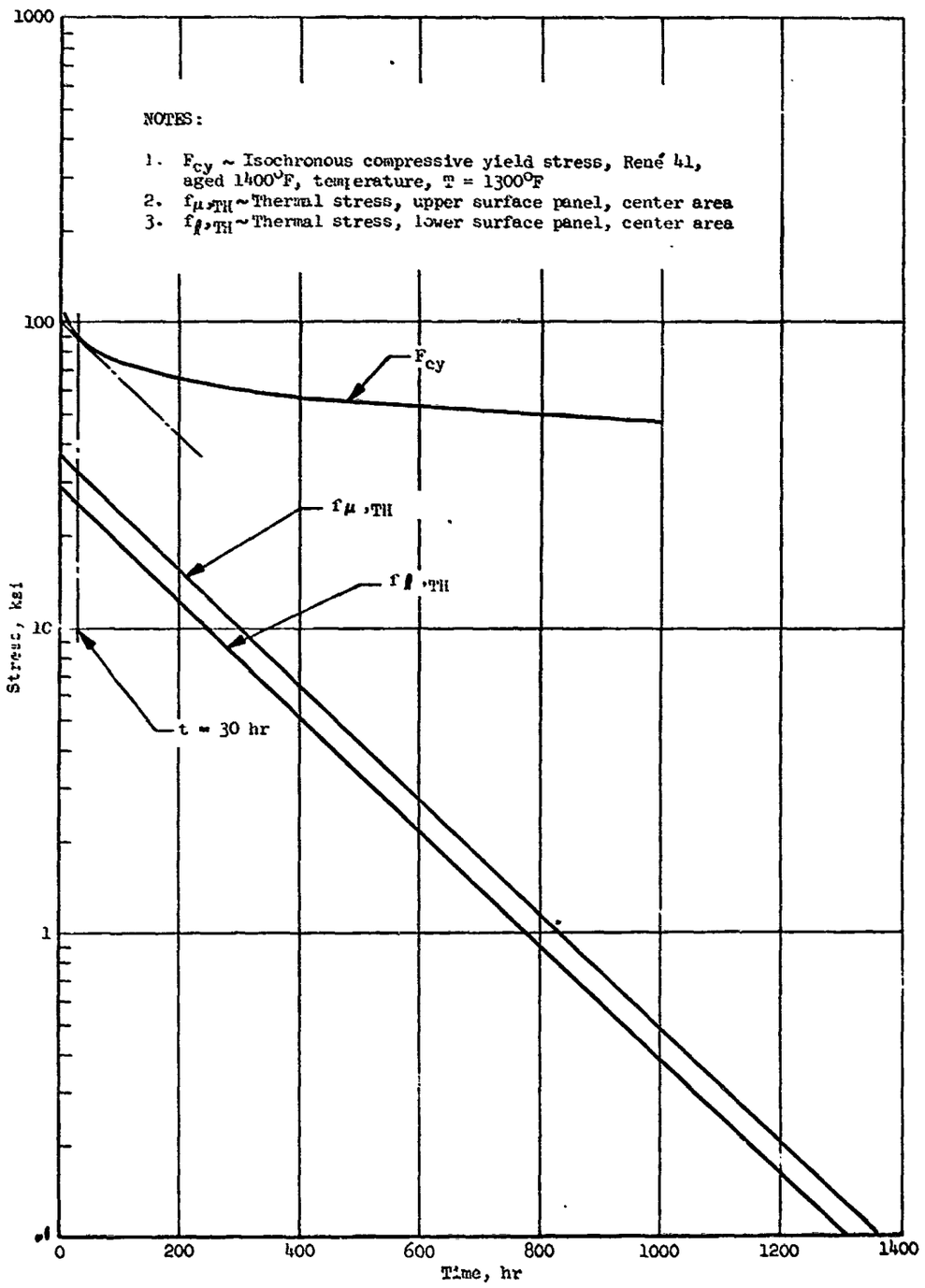

Figure 18-1 Semimonocoque chordwise thermal stress relaxation

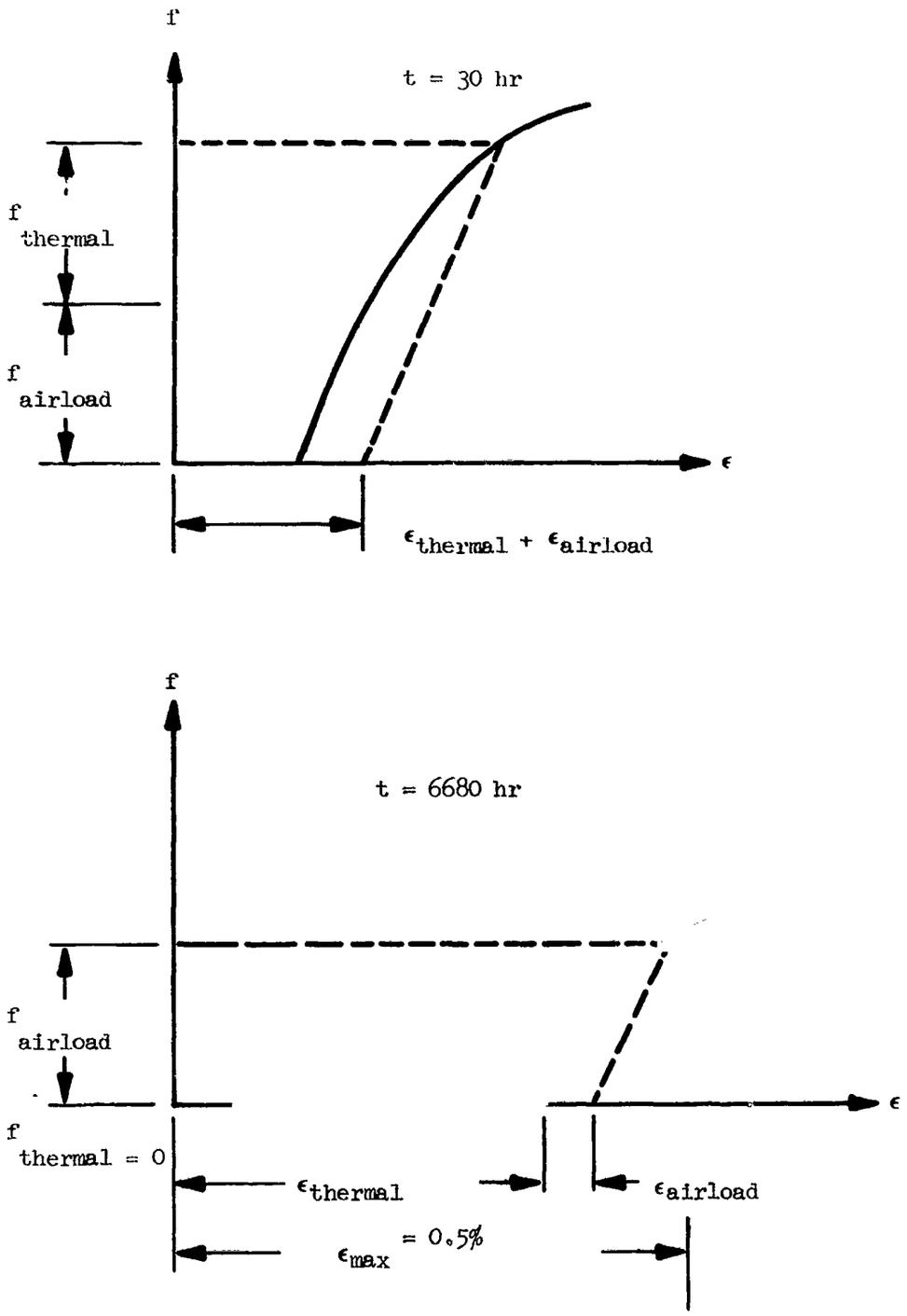

Figure 18-2 Typical stress-strain states for t = 30 hr and t = 6680 hr

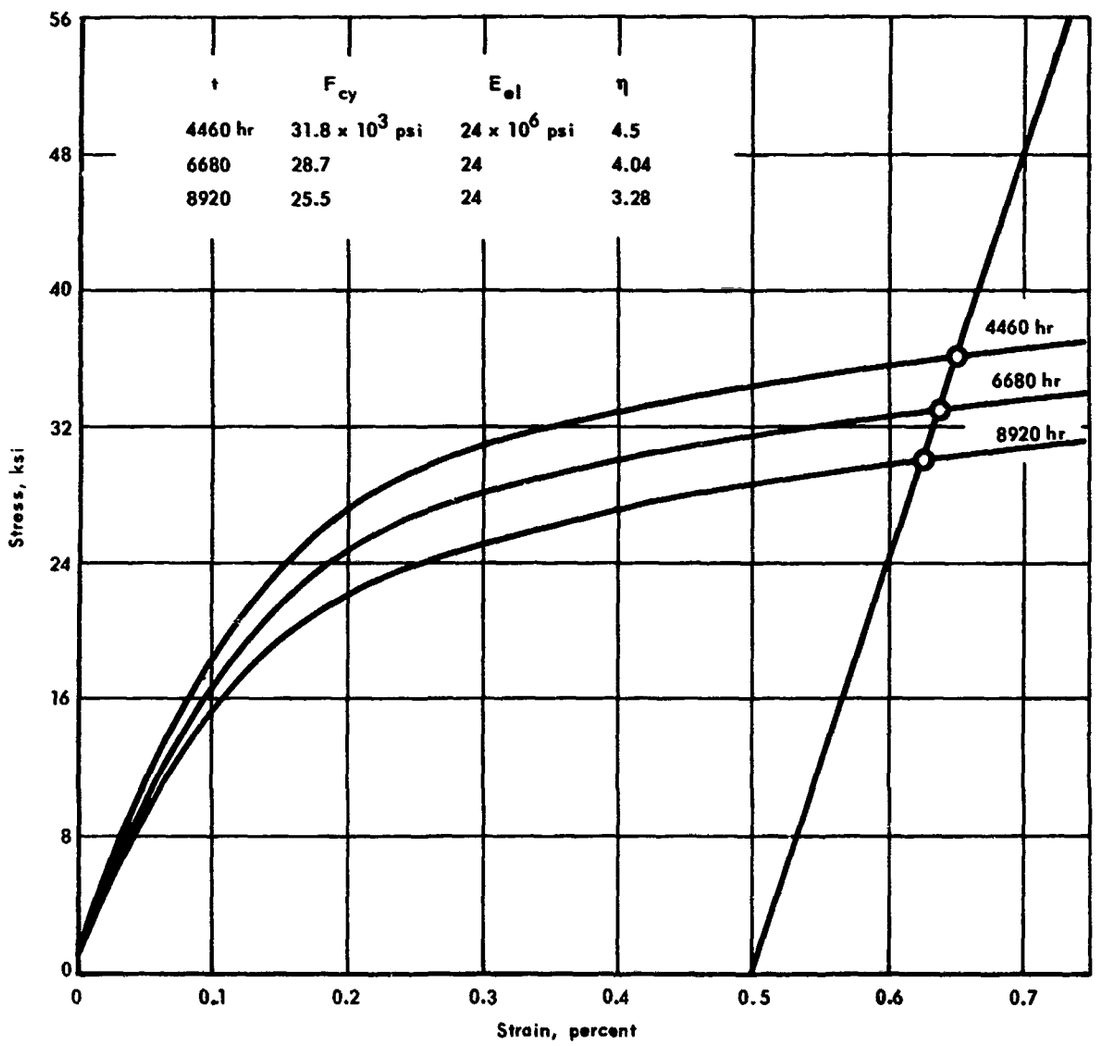

Figure 18-3 Typical isochronous stress-strain diagram for 1400°F aged Rene' 41 sheet (0.020-0.080), T = 1300°F

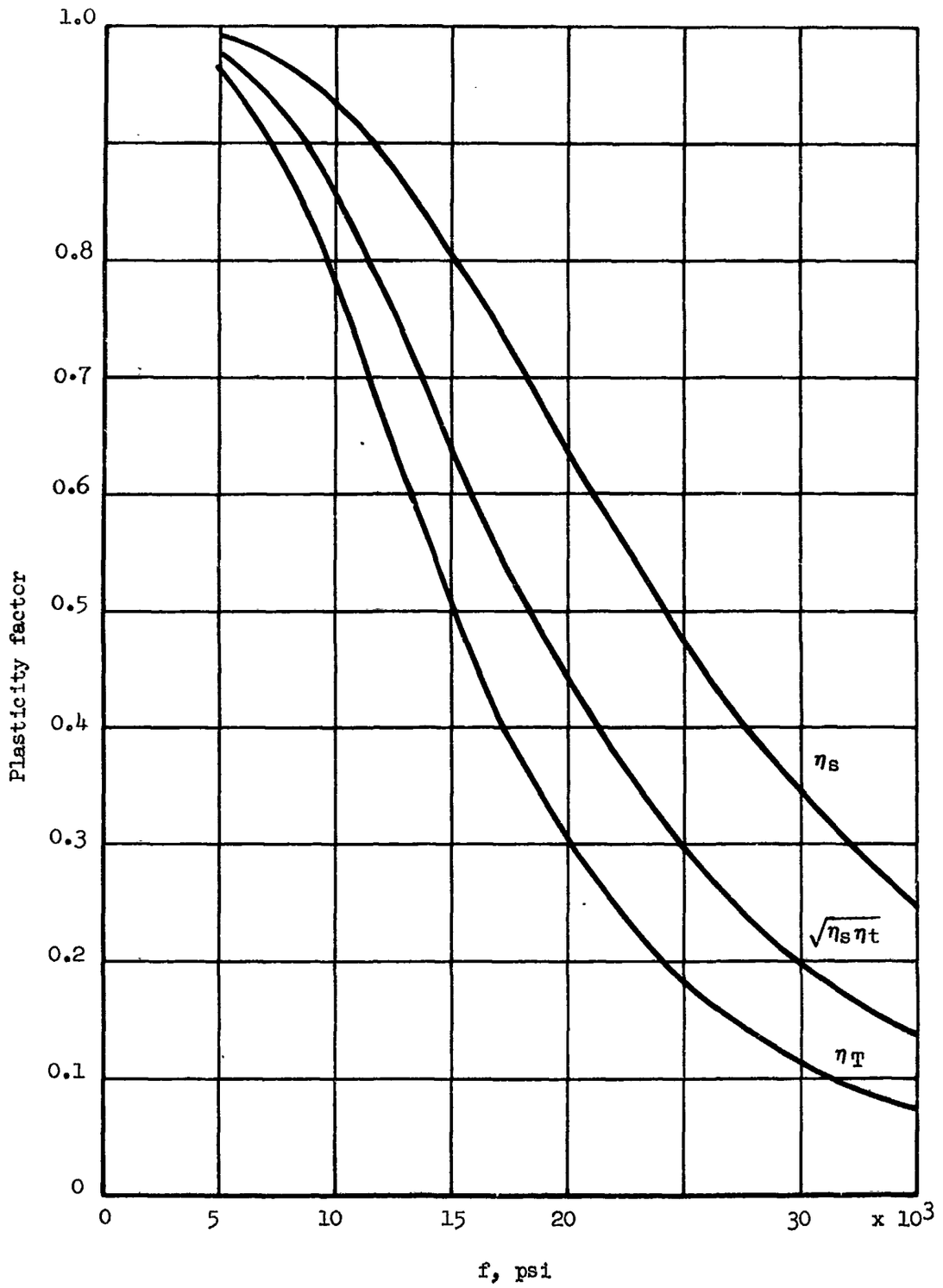

Figure 18-4 Isochronous plasticity reduction factors for Rene'41, sta 1400°F, T = 1300°F, t = 6680 hr

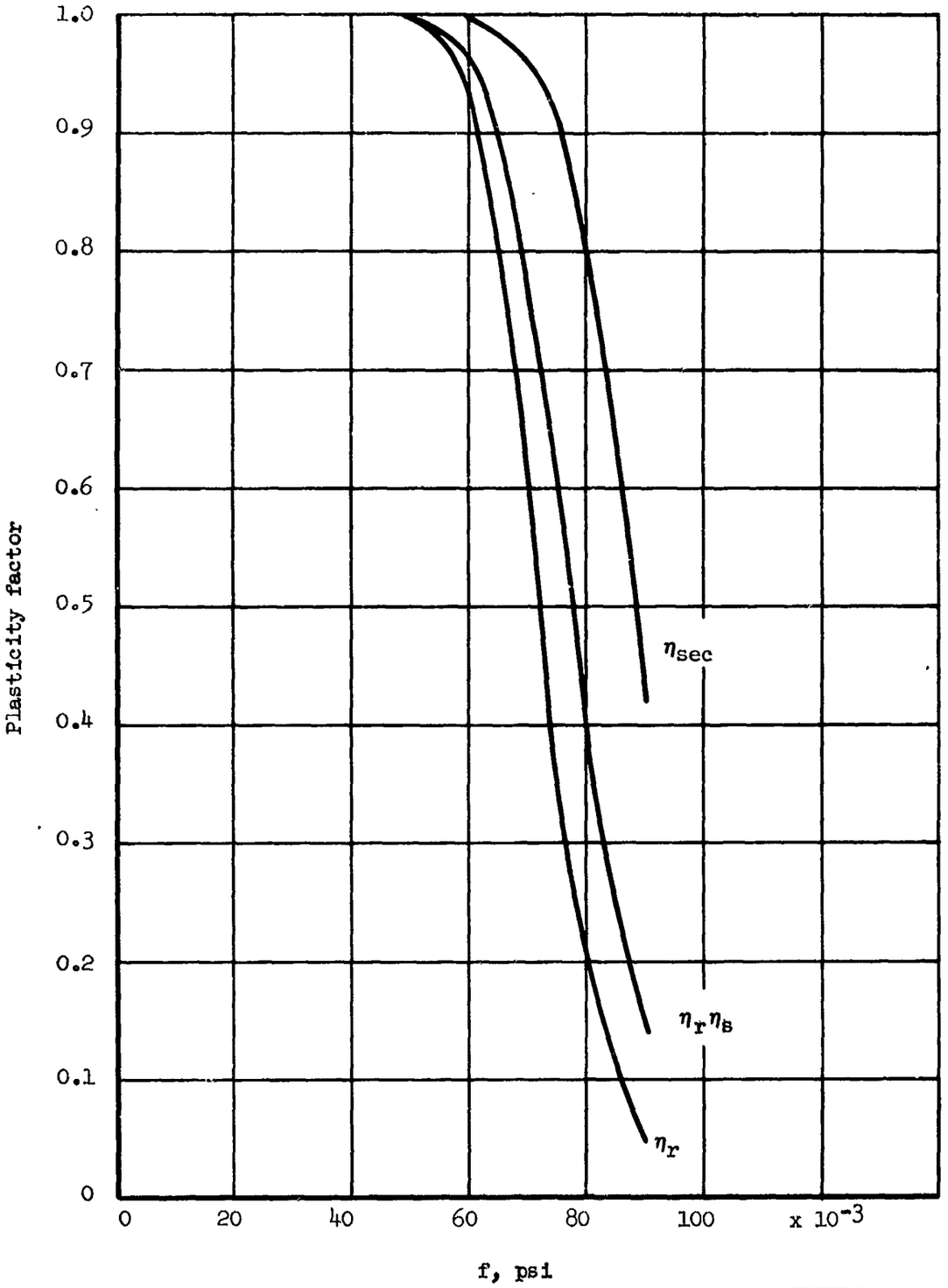

Figure 18-5 Isochronous plasticity reduction factors for Rene' 41, sta 1400°F, T = 1300°F, t = 30 hr

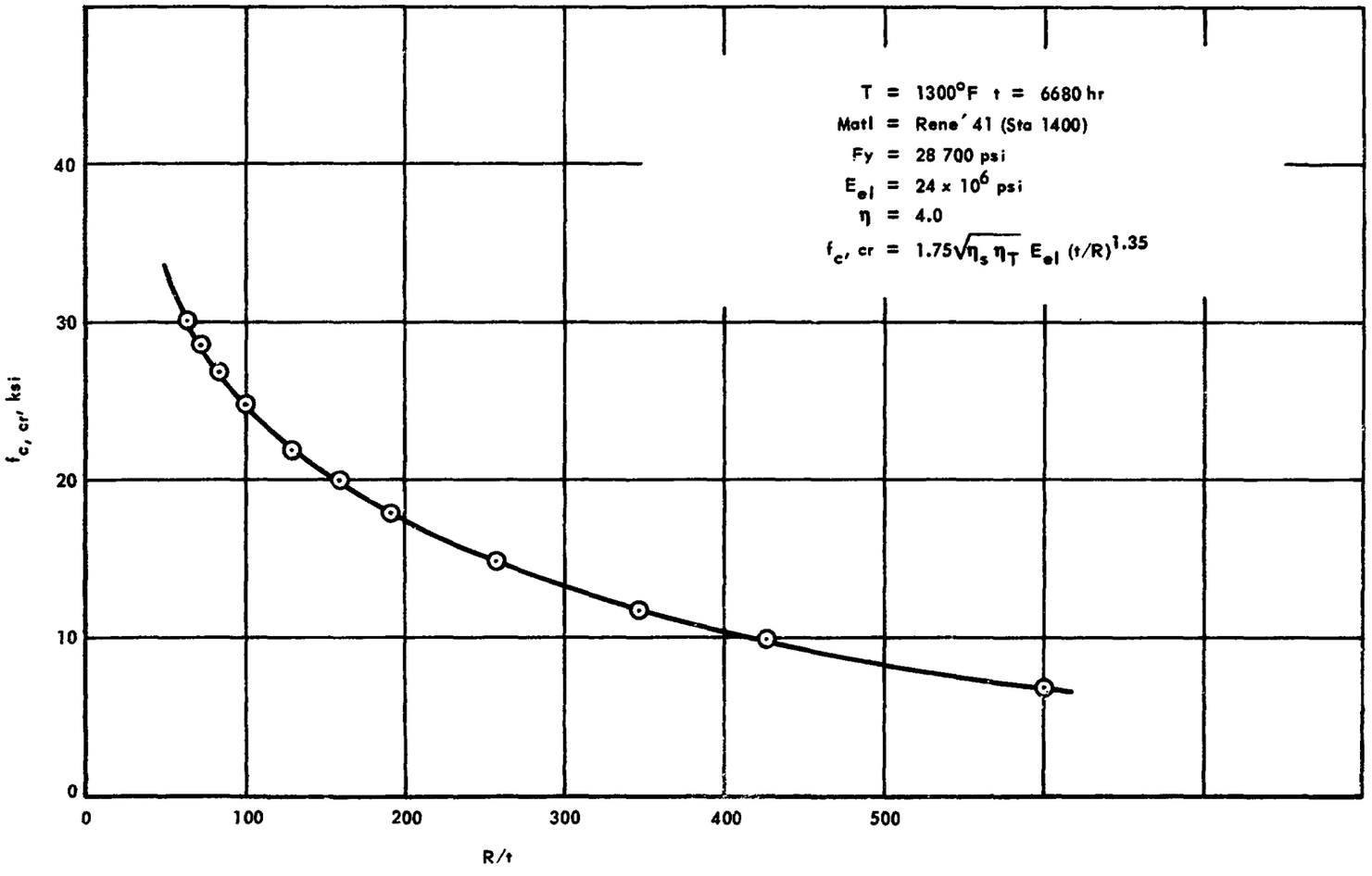

Figure 18-6 Local arc buckling, t = 6680 hr

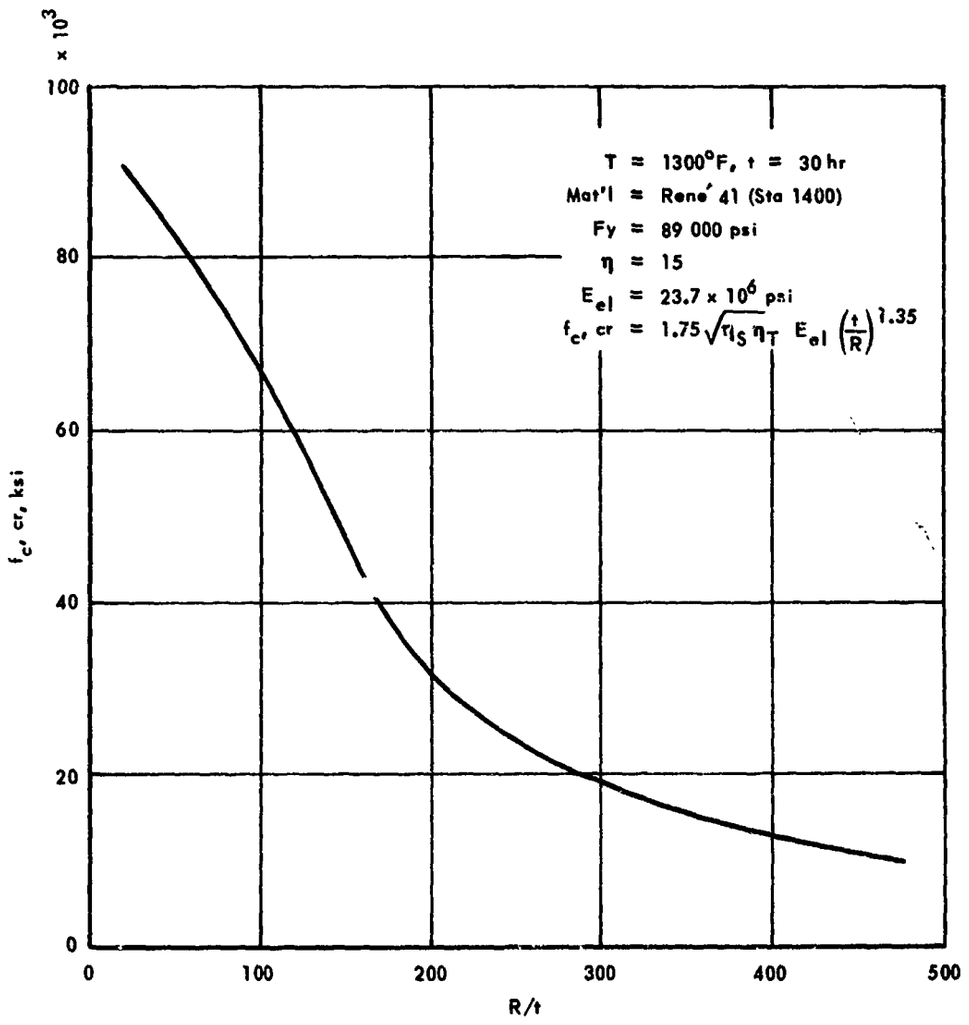

Figure 18-7 Local arc buckling, t = 30 hr

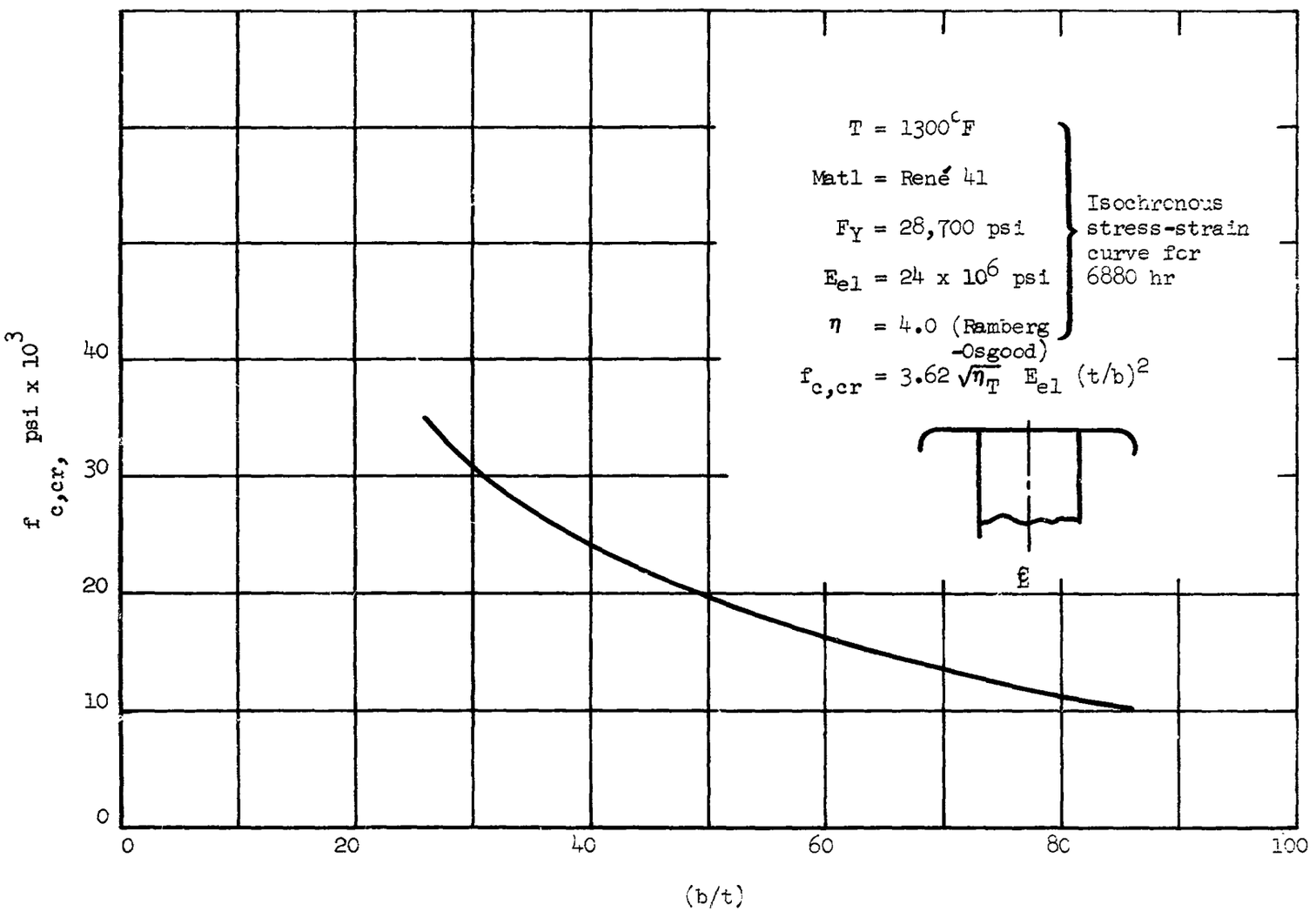

Figure 18-8 Initial buckling of rib cap

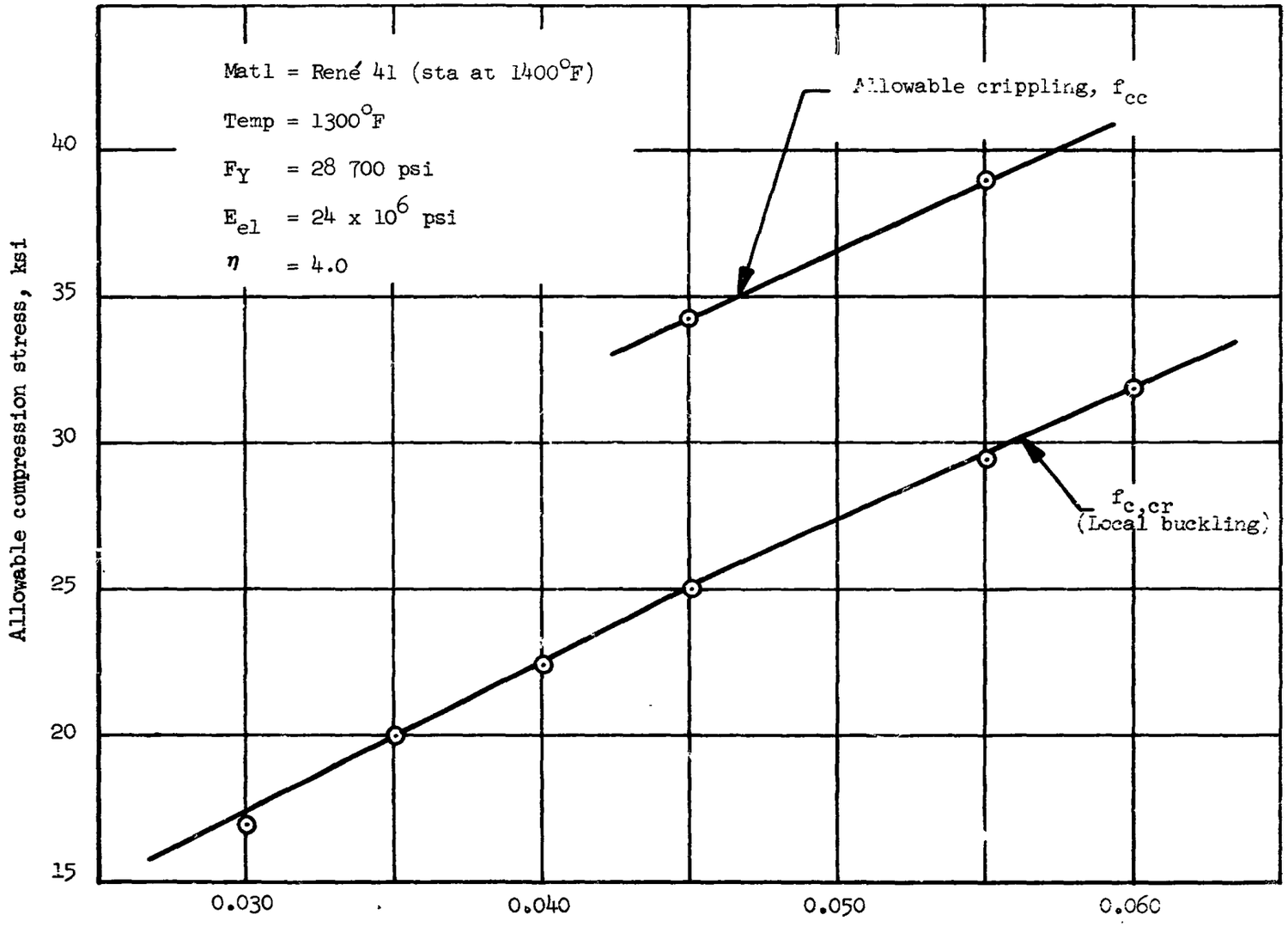

Figure 18-9 Cap creep ouckling analysis

Section 19

OPTIMIZATION PROCEDURE FOR HEAT SHIELDS

by

C. C. Richie

CONTENTS

TABLES

ILLUSTRATIONS

SYMBOLS

b	Width of flat for corrugated heat shields; width of flat plate for buckling analysis
E	Modulus of elasticity
e	Deflection; elongation
$F_{0.7}$	Stress corresponding to modulus of $0.7\ E_{el}$
f	Stress
h	Height
I	Moment of Inertia
k	Compressive bucking coefficient
L	Length
M	Bending moment
N	Extensional forces per unit of length
n	Shape parameter
p	Pitch
R	Radius
r	Radius of curvature
t	Thickness
$\bar{t}$	Equivalent panel thickness
x,y,z,	Rectangular cartesian coordinates
w	Panel deflection
Z	Distance from neutral axis to extreme fiber.

α	Semi-apex angle for corrugation stiffened heat shields; ratio of M_O/M_I
β	Parameter as defined by equation 19-25
ξ	Parameter as defined by equation 19-14
η	Plasticity factor
λ	Ratio as defined by equation 19-17
ν	Poissons ratio

Subscripts

b	Denotes bending
cr	denotes critical or minimum value
el	Elastic
I	Denotes quantity at inner fiber
O	Denotes quantity at outer fiber
sec	Denotes Secant values
tan	Denotes tangent value
th	Abbreviation for thermal
x,y,z	Denotes direction in rectangular cartesian coordinates.

SECTION 19

OPTIMIZATION PROCEDURE FOR HEAT SHIELDS

Equations of the computer programs which were used to determine minimum weight configurations in the evaluation of refurbishable and permanently attached heat shields are presented in this section. The refurbishable heat shield concepts are:

Corrugated skin, hat-section stiffened, clip supported

Corrugated skin, simply supported

Corrugated skin, multiple supports

Flat skin, dimple-stiffened, clip supported.

The permanently attached concepts which are of the corrugated skin configuration are:

Modular, simply supported

Modular, cantilevered

The heat shield panels are assumed to be separated by flexible joints which alleviate inplane loading.

The function of the heat shields is to protect the primary structure in a high-temperature environment due to aerodynamic heating and to provide a smoother aerodynamic surface than afforded by some of the structural panel concepts. Even though they are vented, the heat shields are subjected to pressure loading due to fluctuation of the pressure.

The analysis, which is formulated for the closed-form method of optimization, is discussed in four categories: (1) panel loading, (2) stress analysis, (3) local buckling analysis, and (4) closed-form equations.

PANEL LOADING

The aerodynamic pressure is assumed to act positively and negatively on the heat shields.

Corrugated Heat Shield

Bending moments of the corrugated skin heat shield, produced by the pressure loading, are dependent on the type of supports and on the spacing of the supports. The heat shield reaction, moment, and deflection indices due to pressure loading are pre ented in table 19-1. These results can be obtained by using any one of the many methods available for calculating the loads and deflections of continuous beams; i.e., area-moment, moment distribution, etc. In addition, the corrugated heat shield with multiple supports is subjected to bending moments produced by nonuniform thermal deflection of the supports and bowing of the stiffened panels of the primary structure under loading. The heat shield bending moment due to nonuniform thermal deflection of the supports is shown in table 19-2. These data, which are presented as a moment index, are for heat shields with 3, 4, and 5 supports.

The bending moment on the corrugated heat shield with multiple support due to bowing of the stiffened panels of the primary structure under loading is as follows:

A conservative approximation of the primary-structure panel deflection due to thermal bowing is

$$e = \frac{e_{th}}{(1 - N/N_{cr})} \tag{19-1}$$

where the deflection due to thermal bowing e_{th} is defined in section 12 by equation 12-4, and as indicated in the above equation a beam column magnification factor is used.

Assuming the heat shield is subjected to the same deflection as the primary structure due to the continuous supports between shield and primary structure, the radius of the curvature r for the heat shield is

$$r = \frac{L^2}{8e} \tag{19-2}$$

where the length L is measured in the heat-shield stiffened direction, chordwise. The heat shield bending moment can then be written as

$$M = \frac{EI}{r} \tag{19-3}$$

Flat Skin, Dimple-Stiffened Heat Shield

The flat skin, dimple-stiffened heat shield (figure 19-1) has four symmetrically located discrete supports (posts). Approximations of the moments and deflections of the heat shield are determined with the finite difference solution of reference 19-1. Moment and deflection indices due to pressure loading are presented in the reference for various coordinates of the plate (figure 19-2). The deflection indices were used for evaluations of the heat shield performance penalty.

STRESS ANALYSIS

The stresses of the corrugated skin heat shield (figure 19-3) are

$$f_{y,O} = \frac{M_y z_O}{\bar{I}_y} \tag{19-4}$$

$$f_{y,I} = \frac{M_y z_I}{\bar{I}_y}$$

where the subscripts O and I denote quantities at the outer and inner extremities of the corrugation, neglecting the thickness t. The moment is considered positive when it produces a compressive stress in the outer surface of the heat shield.

The stresses for the hat-section stiffeners and support clips used for the corrugated heat shield were determined as follows: The hat-section stresses are evaluated by equation 19-4 at the maximum-moment location, midway between support clips. The hat-section stiffener cross section is shown in figure 19-4. The stress for the support clips is

$$f = \frac{N}{t} \tag{19-5}$$

and the maximum stress level occurs on the upright member of the clip. The support clip geometry is shown in figure 19-4.

The stresses for the truss-type continuous clips used on both the simply supported and multiple supported corrugated heat shield concepts are evaluated by equations 19-4 and 19-5. This clip design is shown in figure 19-4.

Stresses of the flat skin, dimple stiffened heat shield are

$$f_{x,\ell} = \frac{M_x z_\ell}{\bar{I}}$$

$$(\ell = 0, I) \qquad (19\text{-}5)$$

$$f_{y,\ell} = \frac{M_y z_\ell}{\bar{I}}$$

The moments are positive when they produce compressive stresses in the outer skin. The stresses for the support clips used on the flat-skin, dimple-stiffened heat shield are evaluated by equation 19-5.

LOAD BUCKLING ANALYSIS

Corrugated Skin Heat Shield

The buckling stress of the circular-arc segment is approximated by equation (12-14) of section 12, which is

$$f_{b,cr} = k_o \bar{\eta}_{c,0} E_{el} \left(\frac{t}{R}\right)^n \qquad (19\text{-}6)$$

in which

$$k_o = 1.75, \quad n = 1.35$$

and

$$\bar{\eta}_{c,0} = \left(\eta_{sec} \eta_{tan}\right)^{1/2} \qquad (19\text{-}7)$$

Treating the plate element as a long, simply supported plate, the expression of the buckling stress is

$$f_{b,cr} = k_I \frac{\bar{\eta}_{c,I} E_{el}}{1 - \nu_{el}^2} \left(\frac{t}{b}\right)^2 \qquad (19\text{-}8)$$

where $\bar{\eta}_c = \eta_{ST}$, which is given by equation (10-12a) of section 10.

Flat Skin, Dimple Stiffened Heat Shield

Spacing of the dimples, which are in the inner skin of the flat skin dimple-stiffened heat shield, is the same in the x and y directions. The outer and inner skins are then treated as square plates with post supports at the four corners, and the heat shield is analyzed for local instability with the buckling equation

$$f_{b,cr,\ell} = \frac{k_\ell \pi^2 \bar{\eta}_\ell E_{el}}{12(1 - \nu_{el}^2)} \left(\frac{t_\ell}{p}\right)^2 \qquad (\ell = 0,I) \qquad (19\text{-}9)$$

in which

$$\bar{\eta} = \left(\eta_{tan}\right)^{1/2}$$

and with the interaction equation

$$\left(f_x/f_{b,cr}\right)_\ell + \left(f_y/f_{b,cr}\right)_\ell = 1 \qquad (\ell = 0,I) \qquad (19\text{-}10)$$

The plasticity coefficient η_{tan} is based on the stresses f_x and f_y, the equivalent stress of which is determined with octahedral shear stress theory. NASA stated that buckling coefficients obtained from some of their test data ranged from 1.0 to 1.5. Hence, $k_0 = k_I = 1$ was used for the present investigation.

CLOSED FORM EQUATIONS

Corrugated Skin Heat Shield

In the formulation of the closed-form equations of optimization for the corrugated skin heat shield, the maximum moment (absolute value) is applied positively and negatively and the local buckling stresses of the arc and the flat are equal and are based on the extreme fiber stresses. The analysis is simplified by assuming that the stress gradient through the cross section is linear. In addition, the geometry is constrained so that the maximum stresses at the top and bottom of the corrugation are equal; i.e., the centroid of the cross section is at the mid-height of the corrugation. Hence, when b, R, and t are eliminated from equations (19-6) and (19-8), an expression for the optimum stress is obtained as

$$\left(\frac{f_{y,Opt}}{F_{0.7}}\right)^{\frac{1}{n}} = (2\lambda \sin\alpha)^{\frac{2}{2-n}} \left[\frac{(k_o\bar{\eta}_o)^{\frac{2}{n}}}{\bar{k}_I\bar{\eta}_I}\right]^{\frac{1}{2-n}} \left(\frac{E_{el}}{F_{0.7}}\right)^{\frac{1}{n}} \qquad (19\text{-}11)$$

in which

$$\lambda = \frac{b}{R} = \left(2\,\frac{\frac{\sin\alpha}{\alpha} - \cos\alpha}{1 - \cos\alpha} - 1\right)\frac{\alpha}{\sin\alpha} \qquad (19\text{-}12)$$

and

$$\bar{k}_I = \frac{k_I\pi^2}{12(1 - \nu_{el}^2)}$$

The geometry of the corrugated heat shield can now be defined as

$$\frac{b}{M^{1/2}} = \left(\frac{1}{2\lambda \sin\alpha}\right)^{\frac{n-1}{2-n}} \left(\frac{\bar{k}_I \bar{\eta}_{c,I}}{k_0 \bar{\eta}_{c,0}}\right)^{\frac{1}{2(2-n)}} \left(\frac{\xi_1}{f_{y,Opt}}\right)^{1/2}$$

$$\frac{p}{M^{1/2}} = \left(\frac{1}{2\lambda \sin\alpha}\right)^{\frac{n-1}{2-n}} \left(\frac{1+\lambda}{\lambda}\right) \left(\frac{\bar{k}_I \bar{\eta}_{c,I}}{k_0 \bar{\eta}_{c,0}}\right)^{\frac{1}{2(2-n)}} \left(\frac{\xi_1}{f_{y,Opt}}\right)^{1/2} \qquad (19\text{-}13)$$

$$\frac{R}{M^{1/2}} = \left(\frac{1}{2\lambda \sin\alpha}\right)^{\frac{1}{2-n}} \left(\frac{\bar{k}_I \bar{\eta}_{c,I}}{k_0 \bar{\eta}_{c,0}}\right)^{\frac{1}{2(2-n)}} \left(\frac{\xi_1}{f_{y,Opt}}\right)^{1/2}$$

$$\frac{t}{M^{1/2}} = (2\lambda \sin\alpha)^{\frac{1}{2-n}} \left(\frac{k_0 \bar{\eta}_{c,0}}{\bar{k}_I \bar{\eta}_{c,I}}\right)^{\frac{1}{2(2-n)}} \left(\frac{\xi_1}{f_{y,Opt}}\right)^{1/2}$$

where

$$\xi_1 = \frac{\left[(1-\cos\alpha)\phi_2 - \phi_3\right]\phi_1}{\phi_2\phi_4 - 2\alpha\phi_3^2} \qquad (19\text{-}14)$$

in which

$$\phi_1 = 2(1+\lambda)\sin\alpha$$

$$\phi_2 = 1 + \lambda\frac{\sin\alpha}{\alpha}$$

$$\phi_3 = \frac{\sin\alpha}{\alpha} - \cos\alpha \qquad (19\text{-}15$$

$$\phi_4 = \alpha - 3\sin\alpha\cos\alpha + \cdots\cos^2\alpha$$

The equation of the average thickness is

$$\frac{\bar{t}}{M^{1/2}} = \frac{1}{1+\lambda}\left(\frac{\alpha}{\sin\alpha} + \lambda\right)(2\lambda\sin\alpha)^{\frac{1}{2-n}}\left(\frac{k_O\,\bar{\eta}_{c,O}}{\bar{k}_I\,\bar{\eta}_{c,I}}\right)^{\frac{1}{2(2-n)}}\left(\frac{\xi_1}{f_{y,Opt}}\right)^{1/2} \qquad (19\text{-}16)$$

Aerodynamic requirements require that a constraint be imposed on the height/pitch ratio of the corrugation, $(h/p) = 0.10$. Hence, for a specified value of (h/p), the angle of equations (19-11) through (19-16) can be obtained from the expression

$$1 - \cos\alpha - 2(\sin\alpha + \lambda\sin\alpha)\left(\frac{h}{p}\right) = 0$$

and equation (19-12). For a given moment and material, the dimensions of the minimum weight design of the corrugated heat shield are now defined within the constrained geometry.

When the last of equations (19-13)yielded a stress which was less than the minimum gage, the spacing of the supports was increased until the full strength potential of the optimum configuration of minimum gage was utilized.

The allowable stress for the hat-section stiffener is based on the cross section element that has the minimum crippling stress. The thickness of this element was varied until crippling failure occurred at the same stress level as the applied bending stress. The crippling stress was determined from Stress Memo 80 of reference 19-2. The allowable stress for the support clips is based on the column buckling stress of the upright member (see figure 19-4) This stress is evaluated in section 12 by equation 12-8. The same procedure as described for the hat section stiffener is utilized to attain minimum thickness clips.

The weight of the truss-type support clips, which are used on the simply supported and multiple supported heat shield concepts, was determined by varying the shield-to-support attachment flange thickness until the allowable stress, the bending modulus of rupture, is equal to the applied bending stress, equation 19-4. The upright member was analyzed for bending and compression stresses, equations 19-4 and 19-5. In all cases, the designing element for the clip was the attachment flange. The thickness determined from the flange analysis provided sufficient clip stiffness for heat shield flutter analysis. The clip height h is determined so that sufficient clearance is provided between the deflected shield and the primary structure.

Flat Skin, Dimple Stiffened Heat Shield

In designing the flat skin, dimple-stiffened heat shield, a constraint was imposed on the elongation due to dimpling of the inner skin. Assuming that the dimple is a cone ($r = 0$), the elongation is defined as

$$e = \frac{\pi R^2/\sin\alpha - \pi R^2}{\pi p^2/4}$$

or

$$c = 4\left(\frac{h}{p}\right)^2 \frac{\tan\alpha}{\cos\alpha}\,(1 - \sin\alpha) \qquad (19\text{-}17)$$

To obtain expressions of the thickness and stress ratios of the two faces, let

$$M_0 = \max\,(M_x, M_y)_{cr,o} \qquad (19\text{-}18a)$$

$$M_I = \max\,(|M_x|, |M_y|) \qquad (19\text{-}18b)$$

$$\alpha = M_0/M_I \qquad (19\text{-}18c)$$

where the quantities of equation (19-18a) are buckling moments of the outer face and those of equation (19-18b), buckling moments of the inner face.

Using equations (19-9), (19-10), and (19-18), the thickness ratio can be expressed as

$$\lambda = t_0/t_I = \left(\gamma\,\frac{\bar{k}_I\bar{\eta}_I}{\bar{k}_0\bar{\eta}_0}\right)^{1/3} \qquad (19\text{-}19)$$

in which

$$\bar{k}_\ell = \frac{k_\ell \pi^2}{12(1 - \nu_{el}^2)} \qquad (\ell = 0, I) \qquad (19\text{-}20)$$

From equations (19-8) and (19-18),

$$\lambda = \gamma\,\frac{f_I}{f_0} \qquad (19\text{-}21)$$

First eliminating γ and then λ from equations (19-19) and (19-21) yields

$$\lambda = \frac{t_O}{t_I} = \left(\frac{\bar{k}_I}{\bar{k}_O}\frac{\bar{\eta}_I}{\bar{\eta}_O}\frac{f_O}{f_I}\right)^{1/2} \tag{19-22}$$

and

$$\frac{f_I}{f_O} = \left(\frac{1}{\gamma}\right)^{2/3}\left(\frac{\bar{k}_I\bar{\eta}_I}{\bar{k}_O\bar{\eta}_O}\right)^{1/3} \tag{19-23}$$

Note that the stresses f_O and f_I are direct results of the moments M_O and M_I.

The expression for the average thickness is ($r = 0$)

$$\bar{t} = t_I\left[1 + \lambda + \pi\frac{\tan\alpha}{\cos\alpha}\left(\frac{h}{p}\right)^2(1 - \sin\alpha)\right] \tag{19-24}$$

Solving equation (19-17) for (h/p), substituting the resulting equation and equation (19-22) into equation (19-24) and then using equations 19-5, 19-9, 19-10, and 19-22 gives

$$\frac{\bar{t}}{M_I^{1/2}} = \left[\frac{h}{e}\frac{(1 - \sin\alpha)(1 + \beta)^2\tan\alpha}{(\bar{k}_I\bar{\eta}_I E_{el} f_I)\cos\alpha}\right]^{1/4}\left[1 + \frac{\pi e}{\eta_I} + \left(\frac{\bar{k}_I}{\bar{k}_O}\frac{\bar{\eta}_I}{\bar{\eta}_O}\frac{f_O}{f_I}\right)^{1/2}\right] \tag{19-25}$$

where

$$\beta = \min\left(\frac{M_x}{M_y}, \frac{M_y}{M_x}\right)$$

As already stated, the loading of the heat shields is applied positively and negatively. Hence, $M_O/M_I = \gamma = 1$. The average thickness of the optimum configuration is then determined by minimizing equation (19-25) with respect to f_I. Note that equation (19-25) can be expressed in terms of M_O with the use of equation (19-18c).

With the stress f_I known, dimensions of the minimum weight configuration are determined with the following equations:

$$\frac{h}{M_I^{1/2}} = \frac{(1+\beta)^{1/2}}{(f_I)^{3/4}} \left[\frac{e}{4} \frac{\cos\alpha}{(1-\sin\alpha)\tan\alpha} \bar{k}_I \bar{\eta}_I E_{el}\right]^{1/4}$$

$$\frac{p}{M_I^{1/2}} = \frac{(1+\beta)^{1/2}}{(f_I)^{3/4}} \left[\frac{4}{e} \frac{(1-\sin\alpha)\tan\alpha}{\cos\alpha} \bar{k}_I \bar{\eta}_I E_{el}\right]^{1/4} \qquad (19\text{-}26)$$

$$\frac{t_I}{M_I^{1/2}} = (1+\beta)^{1/2} \left[\frac{4}{e} \frac{(1-\sin\alpha)\tan\alpha}{\cos\alpha} \frac{1}{\bar{k}_I \bar{\eta}_I E_{el}} \frac{1}{f_I}\right]^{1/4}$$

The weight of the clip supports for this heat shield is determined by the same procedure as described for the hat-section skin-stiffened corrugated heat shield concept.

REFERENCES

19-1 Plank, P. P.; and MacMiller, C. J.: Analytical Investigation of Candidate Thermal-Structural Concepts Applicable to Wing, Fuselage and Inlet Structure of a Manned Hypersonic Vehicle, AFFDL-TR-66-15(Confidential) 1966.

19-2 Lockheed-California Company, Engineering Stress Memo Manual 80.

TABLE 19-1

REACTION, MOMENT, AND DEFLECTION COEFFICIENTS DUE TO PRESSURE FOR THE CORRUGATED HEAT SHIELD

Type of support	X/L (in.)	Number of supports	$\frac{R}{qL}$	$\frac{M}{qL^2}$	$\frac{wD}{qL^4}$
Simply supported	0.000	2	0.500	0.125	0.0130
	0.100	2	0.500	0.075	0.0050
	0.207	2	0.500	0.021	0.0006
Multiple supports	–	3	1.250(1)	0.125(1)	0.0054
	–	5	1.143	0.107	0.0065
	–	7	1.135	0.106	0.0065

Notes:

1. Maximum reaction R and moment M for the multiple supported shield occurs over the second support.
2. Maximum deflection w for multiple supported shield occurs during the first span.
3. Definitions:

   R = reaction, lb/in.
   L = length, in.
   q = pressure, $lb/in.^2$
   M = bending moment, in.-lb/in.
   D = bending stiffness of corrugated heat shield, $lb\text{-}in.^2$
   w = deflection, in.

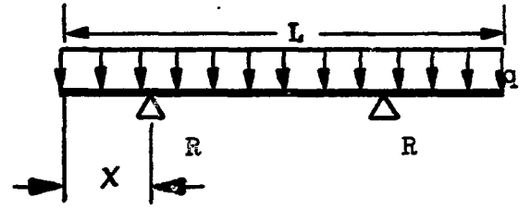

Simply supported

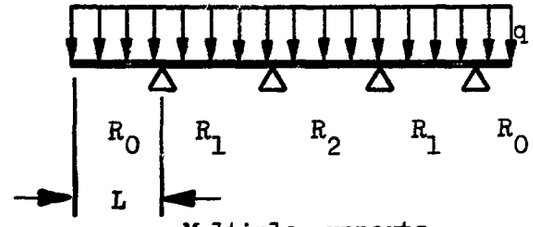

Multiple supports

TABLE 19-2

MOMENT COEFFICIENT DUE TO NONUNIFORM THERMAL DEFLECTION OF THE SUPPORTS FOR THE CORRUGATED HEAT SHIELD

	Location	Number of supports			Units
		3	4	5	
Moment coefficients at supports	R_1	-3.00	-1.20	-1.72	$\frac{ML}{w_{th.}D}$
	R_2	-	-	+0.86	

Notes:

1. Definitions:

   M = bending moment, in.-lb/in.
   L = length, in.
   $w_{th.}$ = thermal expansion of end clips, $\alpha \Delta th.$
   D = bending stiffness of corrugated heat shield

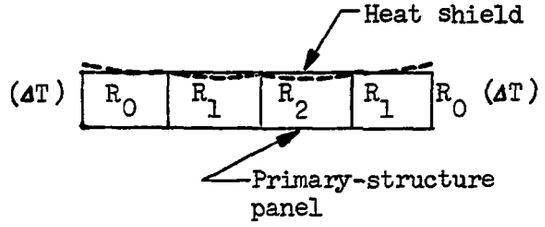

2. Assumptions:

   The end clips are subjected to a temperature change ΔT of $50^{\circ}F$; none of the other clips are subjected to thermal expansion.

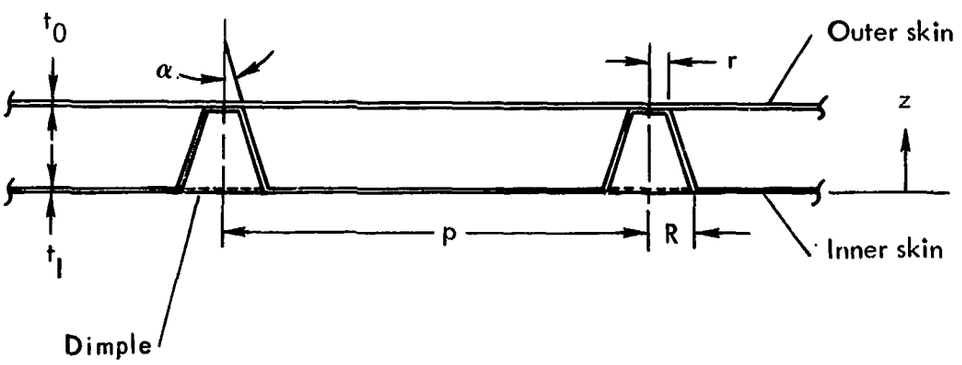

Figure 19-1 Cross section of flat skin, dimple-stiffened heat shield

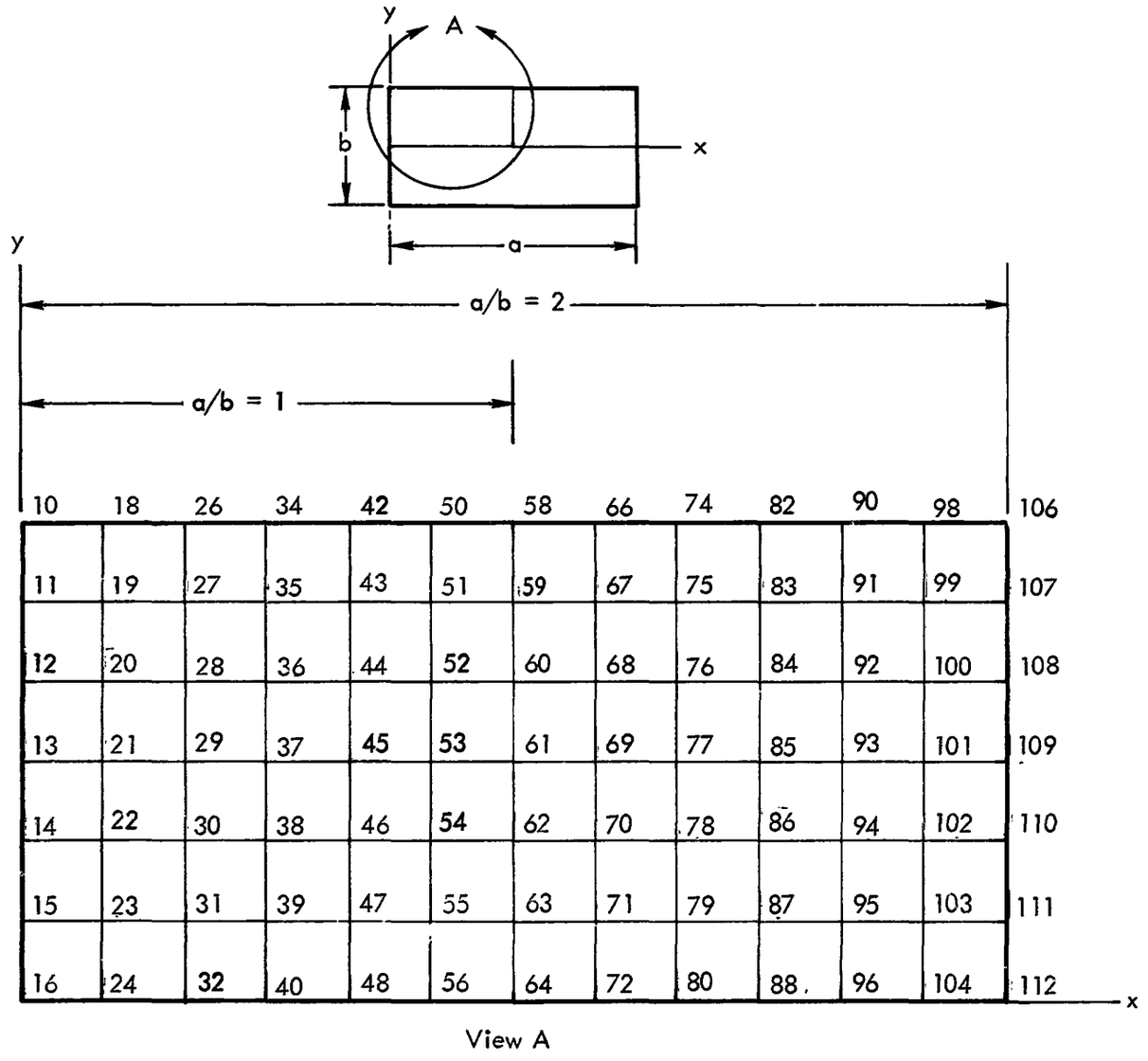

View A

Figure 19-2 Grid of finite difference solution of reference 19-1 for post-supported sandwich plate. Fictitious grid points along boundaries are omitted

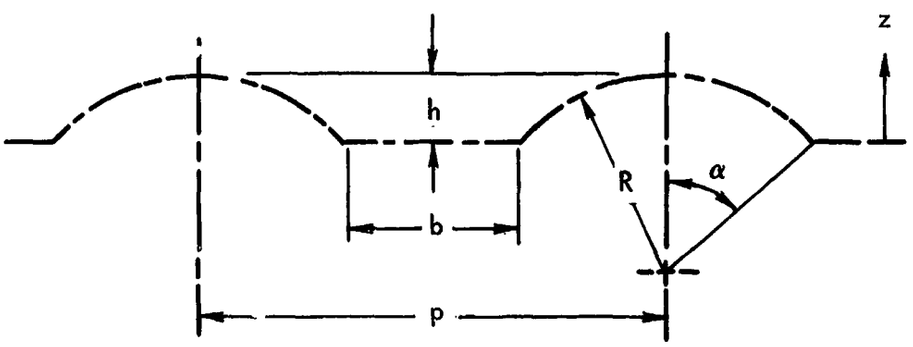

Figure 19-3 Cross section of corrugated skin heat shield

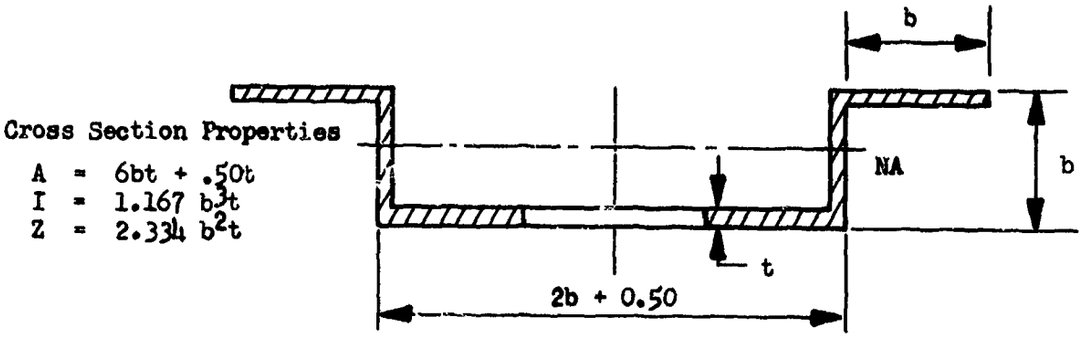

Hot-section stiffener cross-section for the post-supported corrugated heat shield

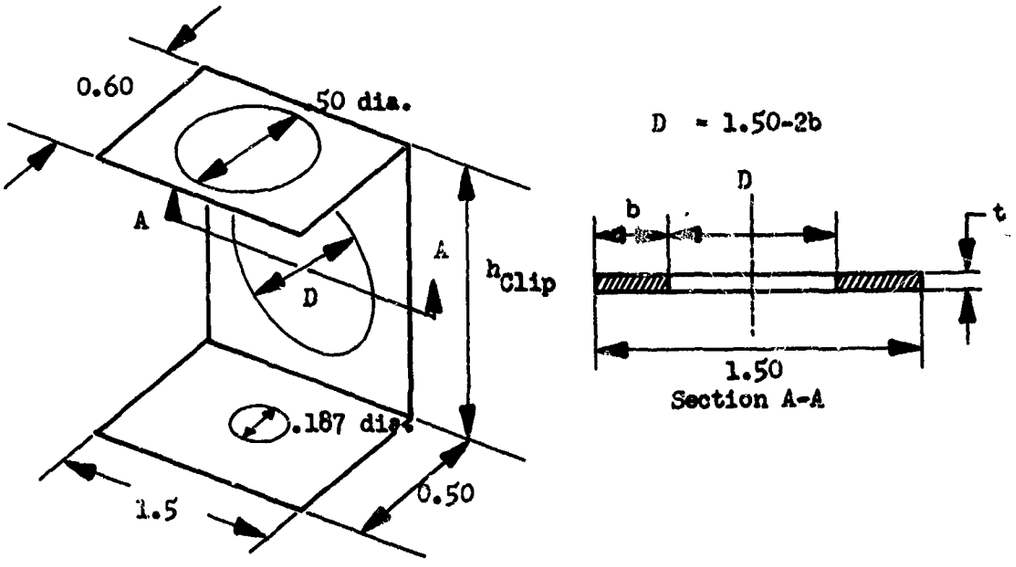

Support clip geometry for the post-supported corrugated and flat-skin dimple-stiffened heat shield concepts

Figure 19-4 Heat shield support clip geometry

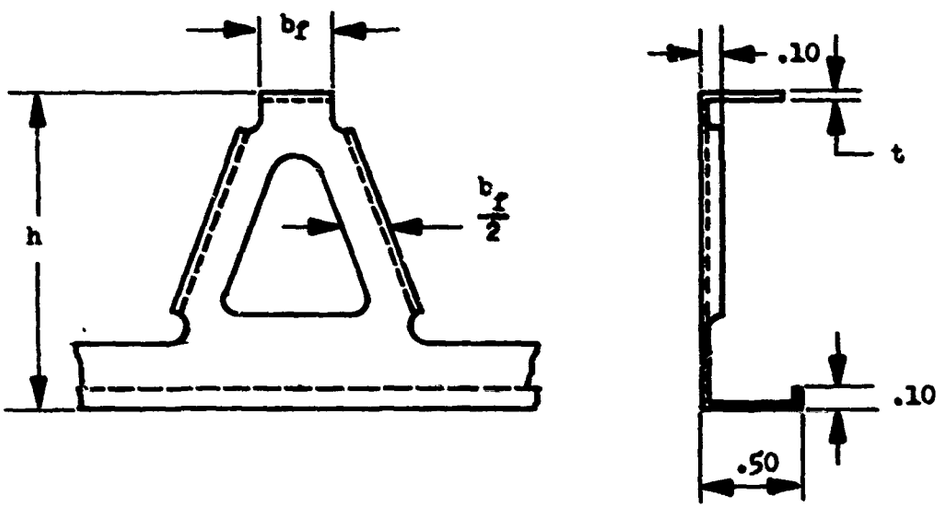

Support clip geometry for the simply supported and multiple supported corrugated heat shield

Figure 19-4 Heat shield support clip geometry (Concluded)

Section 20

HEAT SHIELD WEIGHT ANALYSIS

by

W. A. Claus, C. C. Richie, F. T. Bevan

CONTENTS

TABLES

ILLUSTRATIONS

SYMBOLS

a,b	x and y distances between simply supported edge of panels
a/b	Aspect ratio of the panel
BL	Butt line
b_f	Flat width of heat shield corrugation
b_s	Pitch
D	Diameter
FS	Fuselage station
g	Gravitational acceleration
h	Height
L	Length of span
p	Pressure; pitch
q	Dynamic pressure
R	Radius
T	Temperature
t	Thickness
t_c	Thickness of corrugated heat shield
$\bar{t}$	Equivalent panel thickness
δ	Deflection
$\Sigma\bar{t}$	Summation of equivalent panel thickness

Subscripts

chan	Indicates quantity pertains to cap
clip	Indicates quantity pertains to clip
corr	Indicates quantity pertains to corrugated heat shield
hat	Indicates quantity pertains to hat
hs	Denotes quantity associated with heat shields
max	Denotes maximum value
oxid	Denotes quantity pertains to oxidation
panel	Denotes quantity pertains to panel
truss	Denotes quantity pertains to truss-type clips

Section 20

HEAT-SHIELD WEIGHT ANALYSIS

The heat-shield weight analysis consisted of an initial weight investigation (including cost, performance, and reliability) of several concepts and a final structural sizing of the most promising heat-shield concept.

INITIAL WEIGHT EVALUATION

The initial heat-shield weight analysis for both refurbishable and permanently attached shields was made in terms of temperature requirements, materials, aspect ratio, and width, and was based on a multiple of the overall primary load-carrying dimensions of a typical semimonocoque spanwise tubular panel.

The refurbishable heat-shield concepts considered were as follows:

(1) Corrugated skin, hat section stiffened with clip supports

(2) Corrugated skin with simple supports

(3) Corrugated skin with multiple supports

(4) Flat double skin, dimple stiffened with clip supports

The permanently attached heat-shield evaluations included the following concepts:

(1) Modular, simply supported

(2) Modular, cantilevered

Figure 20-1 shows heat-shield temperature versus distance from the leading edge along FS 2360 (wing investigation section). The data are for a typical semimonocoque spanwise concept with insulation on the lower surface outboard of the one-third chordline. The upper surface temperatures of figure 20-1 are for the -0.5-g condition. As indicated in the figure, the lower surface temperature varies from 1945° to 1555°F with a reduction to 1900°F after 5 inches. The upper surface heat-shield temperatures range from 1785°F to 1280°F. In view of the temperature range, Haynes 25, René 41, and TD NiCr were evaluated as candidate materials.

Equivalent thicknesses $\bar{t}$ or weights were determined for the corrugated concept, using a maximum bending moment of 17 in.-lb/in. These weights for various temperatures are shown in figure 20-2 with the corresponding corrugation geometry shown in table 20-1. The results indicate that Rene 41 is the most suitable material for heat-shield application below 1800°F. Rene 41 was selected for heat-shield applications below 1800°F and TD NiCr was selected for temperatures above 1800°F. TD NiCr is used on the first 71 inches of the lower surface. The welding of TD NiCr is difficult; therefore, riveted construction was considered.

Using Rene 41, the evaluation of both refurbishable and permanently attached heat shields was conducted by providing an arrangement of heat shields to protect a typical spanwise tubular panel (46 inches by 92 inches). The design temperature was 1600°F for transient pressures of ± 1.0 psi (ultimate). However, in addition to the pressure loading, the corrugated multiple-support concept included bending due to nonuniform thermal deflection of the multiple supports and bowing of the panel due to thermal gradients, pressure, and inplane loading.

Minimum gage for the corrugated and modular heat shields is 0.010 inch. For the flat skin dimple stiffened heat shield, the minimum gage of the outer skin is 0.015 inch and of the innerformed skin 0.010 inch.

The basic data obtained for each candidate heat shield included a plot of $\bar{t}$ versus panel size, maximum deflection versus panel size, and drawings showing structural arrangement and typical dimensions.

Refurbishable Heat Shield Concept

Corrugated hat section stiffened, clip supported heat shield. – The heat shield shown in figures 20-3 and 20-4 is formed by a corrugated sheet supported by a hat section stiffener at about one-tenth of the corrugation length from each end of the shield. Corrugation amplitude is one-tenth the corrugation pitch. A flat between corrugation arcs enables the hat sections to be attached. The attachment is made by resistance spotwelding. The support clip is also attached to the hat section by resistance spotwelding.

Mounting of the shields is performed from outside the shield through an access hole at each of the four attachments per shield. A flanged nut is resistance spotwelded to the primary structural panel, a super mica washer is used, the shield is installed, and a socket head screw fastens the standoff support clip to the nutplate. Each access hole is located at the center of a corrugation at about one-quarter span of the shield, and each hole is closed after assembly with a pronged cap.

The effect of several support locations on the maximum heat shield bending moment is presented in section 19. The optimum support location for equal magnitude of bending moment at the supports and mid span is 20.7 percent of the span. However, to stiffen the corrugation near the "overhang"

edges and prevent flattening of the ends, the support location selected was 10.0 percent of the span. This support location increases the maximum bending moment by a factor of 3.5.

The support clips are rotated so as to place the plane of the web normal to a line joining opposed attach points. This orientation of the support clips allows for bidirectional thermal expansion and gives shear stiffness to the supports in any direction.

A summary of design data for the corrugation, hat section, and support clip is shown in figure 20-3. The lowest weight shield has a minimum gage corrugation thickness of 0.010 inch, aspect ratio of 1.0, and width of 15.3 inches. Minimum gage for the hat section stiffener is 0.020 inch. Figures 20-5 and 20-6 show panel size versus effective thickness and panel size versus deflection, respectively. The deflection consists of corrugation and hat section deflection and does not include thermal deflections. For an aspect ratio of 1.0 and width of 15.3 inches, the maximum deflection is 0.380 inch. Figure 20-7 shows a parametric study of effective thickness versus temperature for a panel aspect ratio of 1.0 and width of 23.0 inches.

Corrugated heat shield with simple supports. - The short corrugated heat shield shown in figure 20-8 consists of a corrugated sheet supported by simple supports at about one-tenth of the corrugation length from each end of each shield. Shields overlap at the trailing edge forming shingles. Corrugation amplitude is one-tenth the corrugation pitch. A flat is provided between corrugation arcs to enable attachment of the truss-type support clip. The attachment is made by at least two spotwelds at each flat. The support clip is also attached to the primary-structure panel by resistance spot-welding. The support clip is stamped from flat sheet and rubber formed. Support clips at one end of a shield are stiffened by gussets in the shield lengthwise direction to transmit drag shear to the primary structure.

Mounting of the heat shields is performed before the primary structural panel is installed. If necessary, removal of the shields is accomplished by: (1) removing cover plates between adjacent primary-structure panels, (2) removing primary-structure panel, and (3) drilling out spotwelds attaching the support clips and primary structure panel. To replace the heat shield, rivets are installed in place of the drilled-out spotwelds.

Spanwise thermal expansion due to thermal gradients between the heat shield and primary-structure panel is allowed by bending of the circular-arc portion of the corrugated skin. Chordwise thermal expansion is permitted by deflection of the support clips at one end of the shield. Gusset clips are provided at the other end of the shield to resist inplane shear in the short dimension of the panel.

A summary of design data for the corrugation and support clip is shown in figure 20-8. The support clips are sized one the basis of eccentrically applied compressive loads due to pressure. The lowest weight shield has a minimum gage corrugation thickness of 0.010 inch and length of 15.3 inches.

Figure 20-9 shows heat shield length versus effective thickness and heat shield length versus maximum deflection. For a length of 15.3 inches, the maximum deflection is 0.360 inch.

Corrugated heat shield with multiple supports. – The heat shield shown in figures 20-10 and 20-11 consists of a corrugated skin supported by multiple rows of truss-type supports. The corrugated skin is of the same size as the primary-structure panel. Spans between the supports are a multiple of the primary-structure panel size. Other details of design and installation are similar to those for the simply supported heat shield concept discussed in the preceeding section.

In addition to pressure, loads for the multisupported heat shield include bending due to nonuniform thermal deflection of the supports and bowing of panel substructure due to thermal gradients, pressure, and inplane loading.

Provisions for differential inplane thermal expansion between the heat shield and primary-structure panel are similar to those for the simply supported heat shield concept discussed in the preceeding section, except that one row of clips at the panel centerline is perpendicular to the others to resist inplane shear in the long dimension of the panel.

A summary of design data for the corrugation and support clip is shown in figure 20-10. Sizing of the support clips is based on eccentrically applied compressive loads due to pressure. The lowest weight shield has a minimum gage corrugation thickness of 0.010 inch, a span of 13.1 inches, and 8 rows of support clips. Figures 20-12 and 20-13 show support span versus effective thickness and support span versus maximum deflection, respectively. For a span of 13.1 inches, the maximum deflection is 0.242 inch.

Flat skin, dimple stiffened, clip supported heat shield. – The heat shield shown in figures 20-14 and 20-15 consists of a flat skin stiffened isotropically by a formed sheet. The formations in the sheet are truncated cones and each cone is resistance spotwelded to the flat sheet. Support clips are located in the flats of the primary structural panel and are near as possible to the location for minimum heat shield deflection (section 19).

Mounting of the shields is performed from the outside by means of flush socket head screws at each of the four attach points. The socket head screws then fasten to flanged nuts which are resistance spotwelded to the support clips. The support clips are resistance spotwelded to the primary structural panel.

The support clips are rotated so as to place the plane of the web normal to a line joining opposed attach points. This orientation of the support clips allows for bidirectional thermal expansion and gives shear stiffness to the supports in any direction.

A summary of design data for the heat shield is shown in figure 20-14. The lowest weight shield has a minimum gage flat skin thickness of 0.015 inch, a minimum gage dimpled skin thickness of 0.010 inch, aspect ratio of 1.0, and width of 15.3 inches. Figures 20-16 and 20-17 show panel size versus effective thickness and panel size versus maximum deflection, respectively. For an aspect ratio of 1.0 and width of 15.3 inches, the maximum deflection is 0.173 inch.

Permanently Attached Heat Shield Concept

Modular, simply supported, interlocking joint heat shield. - The heat shield shown in figures 20-18 and 20-19 consists of corrugated sheets that are simply supported at the ends and shingled with rearward facing steps. On the forward end of the corrugated sheet, a joggle is formed and finger slots are cut. In the flats of the aft end of the corrugated sheet, standoff supports are provided. Various types of standoff supports were considered, including:

(1) Truncated conical dimples drawn in the corrugated sheet

(2) Flanged cups spotwelded to the shield

(3) Spacers projection welded to the shield.

Truncated conical dimples were selected for the standoff supports.

The shield is mounted by sliding the joggled end under the adjacent upstream shield and resistance spotwelding the dimpled end to the primary-structure panel.

At joints between shields, the joggle minimizes aerodynamic drag. Finger slots on the joggled end permit chordwise differential thermal expansion between the heat shield and primary-structure panel. Spanwise differential thermal expansion is allowed by bending of the circular-arc portion of the corrugated sheet.

A summary of design data for the corrugation is shown in figure 20-20. The lowest weight heat shield has a minimum gage corrugation thickness of 0.010 inch and maximum allowable length of four times the pitch (i.e., 10.44 inches) of the primary-structure panel. The maximum allowable length is due to high bending in the wing panel tube wall from reactions at the heat shield simple supports. Figure 20-21 shows heat shield length versus effective thickness, including the effect of overlapping joints. Figure 20-22 shows heat shield length versus maximum deflection. For a length of 10.44 inches, the maximum deflection is 0.195 inch, not including thermal or support deflection.

Modular, cantilevered heat shield. - The heat shield shown in figures 20-23 and 20-19 consists of corrugated sheets that are cantilevered at the forward end and shingled with rearward facing steps. The forward end of the corrugated sheet is curved to fit the circular-arc portion of the primary-structure panel. The curved end of the heat shield is attached directly to the circular-arc portion of the primary-structure panel by at least two resistance spotwelds located in the flats of the corrugated sheet.

Spanwise differential thermal expansion due to thermal gradients between the heat shield and primary-structure panel is allowed by deformation of the circular-arc portion of the corrugated sheet. Since the shingled heat shield is only attached at the forward end, chordwise thermal expansion is permitted by the rearward facing overlapping joints.

A summary of design data for the corrugation is shown in figure 20-23. The lowest weight heat shield has a minimum gage corrugation thickness of 0.010 inch and maximum allowable length of one pitch (i.e., 2.61 inches) of the primary-structure panel. The maximum allowable length is due to high bending in the wing panel tube wall from the cantilever moment and shear. Figure 20-24 shows heat shield length versus effective thickness, including the effect of overlapping joints. Figure 20-25 shows heat shield length versus maximum deflection. For a length of 2.61 inch, the maximum deflection is 0.0073 inch, not including thermal or support deflection.

Heat Shield Thermal Analysis

Heat shield isotherms at the three specified flight conditions (-0.5-g, +2.0-g, and cruise) have been shown in section 9 with the isotherm presentations for the different primary-structure concepts. Mean temperatures for the heat shields were derived assuming a single flat sheet with an equivalent mass thickness $\overline{t}$ of 0.011 inch. The effect of corrugations was neglected but is assumed small because boundary layer flow is nearly parallel to the corrugations. The start of the corrugations at the leading edge experiences higher local heating due to the ramp effect of the corrugation closeout. An estimate of 25-percent increase in the local heat transfer coefficient due to a 3-degree maximum chordwise slope yields a local temperature increase of 90°F at peak heating conditions on the upper and lower surfaces.

Various heat shield attachment methods were examined to determine local effects on heat shield and panel temperatures. Table 20-2 shows temperatures derived for a direct attachment method in which the heat shield is spotwelded or riveted directly to the circular-arc stiffened panel. The analysis was performed at one wing location (FS 2366, BL 270) for upper and lower surfaces without insulation. Panel and heat shield temperatures were found to be unaffected except at the attachment point, where direct aerodynamic heating occurs through the heat shield. A local "hot spot" of approximately 85°F above normal panel temperature is shown for the upper panel at the -0.5-g condition and for the lower panel at the +2.0-g condition. For all conditions, the attachment point temperature is between the panel and heat shield temperatures. Application of these results to the modular heat shield concepts is direct; i.e., temperatures at the attachment points are between heat shield and panel temperatures.

Two methods of attaching the heat shield to the panel with standoff clips were also investigated. The first method holds the heat shield in place with clips which connect a flat portion of the panel to a continuous hat section on the inside surface of the heat shield. The lower wing surface with no insulation was analyzed at one location (FS 2366, BL 270). Figure 20-26 shows temperatures

at the attachment point for three flight conditions for this first attachment method. Temperature differences are 155°F across the hat and 115°F across the clip at the +2.0-g condition. Differences are under 100°F for the other flight conditions. Temperature for the section of heat shield enclosed by the hat is seen to vary by less than 10°F from the temperature for the heat shield away from the hat. Where the hat section is attached to the shield, the higher thermal capacity and conduction to the interior at these points cause temperature lag during the transients and reduced temperature at cruise, compared to the normal heat shield temperature. The higher inner structure temperatures shown for the -0.5-g condition are caused by rapidly reduced heating rates, hence lower temperatures, on the heat shield when the lower surface is at negative angle of attack. Structural panel temperatures are unaffected by the presence of the hat and clip, except during the +2.0-g condition, when reduced exposure to the heat shield at peak temperature reduces local panel peak temperatures by about 50°F.

The second clip attachment method examined assumes that the clip directly connects the heat shield to the flat portion of the panel, as with the multiple support concept. The analysis was performed for upper and lower surfaces at an inboard location (BL 166) and at an insulated outboard location (BL 300), and for the lower surface under the fuselage (BL 60). Table 20-3 shows temperature differences across the support clip derived for the three flight conditions for this method of attachment. The 535°F differential shown for the outboard lower surface at +2.0-g is due primarily to the insulation which isolates the primary structure and forces the shield to high temperatures during the peak heating condition. Thermal resistance through the clip from shield to panel was calculated to be about four times the normal thermal resistance through the insulation and radiation air space at this location. Thus the effect of the clip on local shield and panel temperatures is minor. This is evidenced by comparing the derived differentials across the clip, shown in table 20-2, with the temperature differences from heat shield to panel, based on the detailed panel model, shown in table 20-4. Agreement is good, considering that the additional thermal capacity and conduction path of the clip are not included in the detailed panel analysis. The effect of the clip on the heat shield at these locations is shown in table 20-5, which lists the temperature difference from the crest of a corrugation on the heat shield to an adjacent clip attachment point. Except for the surfaces experiencing peak heating during transients, the temperature difference is not more than 50°F. The higher differentials at transient conditions are caused by the thermal lag at the attachment point, due to a higher mass per exposed area compared to the corrugation skin.

An analysis was also conducted to determine temperatures of the flat skin, dimple stiffened heat shield concept for comparison with corrugated heat shield temperatures. Table 20-6 shows temperatures for the upper and lower heat shields at four locations on the wing for three flight conditions. The outboard locations are shown with and without insulation on the lower surface. Temperatures are presented for the external skin [T(1) for upper surface and T(6) for lower surface], for the top of the dimple at the attachment point with the external skin [T(2) for upper surface and T(5) for lower surface], and for the internal skin [T(3) for upper surface and T(4) for lower surface]. Temperature differences from the top of the dimple to the inner skin, T(2) to T(3) and T(5) to

T(4), are less than 10°F except during the transient conditions, when the differences for surfaces undergoing peak heating (upper surface at -0.5-g, lower surface at 2.0-g) are on the order of 50°F. Peak temperature differentials from external to internal skin, T(1) to T(3) and T(6) to T(4), for locations without lower surface insulation occur at the -0.5-g condition on the upper surface (100° to 150°F); at the +2.0-g condition on the lower surface (110° to 160°F); and at the cruise condition on the upper surface (130°F). With insulation, the peak temperature differential occurs on the upper surface (220°F) at the -0.5-g condition. The peak differentials for all other conditions, upper or lower surface, with or without insulation, are not more than 70°F.

Temperatures for the corrugated heat shield derived from the isotherm analysis for structural panels are presented in table 20-7 for direct comparison with the dimple stiffened heat shield temperatures in table 20-6.

Temperatures for the external skin of the dimple stiffened heat shield are generally 0° to 70°F cooler than corrugated heat shield temperatures, except for the lower surface at -0.5-g and cruise conditions. For these conditions, the corrugated heat shield is up to 40°F cooler. A comparison of the effects of both heat shield concepts on semimonocoque structural panels showed that peak panel temperatures are about the same (within 100°F) with either heat shield concept, except for the outboard locations with insulation. At these locations, peak panel temperatures are 150° to 200°F lower with the dimple stiffened heat shield than with the corrugated heat shield.

Summary of Initial Weight Evaluation

A summary of heat shield data is presented in table 20-8. On the basis of weight and deflection, the data show that the corrugated heat shield with multiple supports is the leading candidate for the refurbishable shield; for the permanently attached shield, the simply supported modular shield is lower in weight. Also, the multiple-supported shield is of large single-piece construction and affords appreciable cost advantages.

For the refurbishable shield, the flat-skinned concept reduces the flow disturbances and local heating due to cross flow from that of the corrugated concepts, but it entails a weight penalty.

Panel flutter analyses of the heat shields were also conducted (as presented in section 14). When refurbishable heat shields were considered, the spring constants included the flexibility of the heat-shield edge closeout, the support clip, and the primary-structure panel. The primary-structure panel is regarded as shielded from the aerodynamic environment when the refurbishable heat shield is employed. However, when modular, or permanently attached heat shields were considered, both the shield and the primary-structure panel were required to be flutter free.

The refurbishable shields are stable; they have panel flutter factors of safety exceeding the required 1.3. On the other hand, the permanently attached shields are flutter critical, because the primary-structure panel has an allowable flutter parameter that is less than the applied dynamic pressure. This is because the chordwise stiffness of the spanwise-oriented tubular concept is low. In decreasing the rib and spar spacing to overcome this condition, the total wing substructure weight is increased significantly beyond that of the refurbishable shield (additional $\bar{t}$ = 0.204 inch or 8.7 lb/ft^2).

Results of analyses to determine effects of random sound pressures indicate that the upper surface and lower surface inboard heat shields and support clips satisfy the 0.007-q and 0.022-q criteria as required.

Considering the weight results shown in table 20-8, and cost, performance, and reliability data presented in later sections, the corrugated heat shield with multiple supports was selected for application to the several primary-structure concepts.

FINAL HEAT SHIELD STRUCTURAL SIZING

The corrugated heat shield concept was applied to the various primary structure concepts in obtaining total concept weight. Typical heat shield design and weight data for the spanwise semimonocoque concept are shown in tables 20-9 and 20-10, respectively. For the chordwise semimonocoque concept, typical heat shield design and weight data are shown in tables 20-11 and 20-12, respectively. For the monocoque concept, typical heat shield weight data are shown in table 20-13. For each primary-structure concept, the effect of oxidation is included in the total heat shield weight. TD NiCr is used on the lower surface outboard area between BL 304 and BL 350, and Rene 41 is used on the remaining upper and lower surface areas. Since a support spacing of 13.1 inches was determined least weight at a location where minimum gage René 41 shields were required for least weight, and since this spacing was used for all concepts requiring shields, not all heat shields are minimum gage nor least weight. For shields thicker than minimum gage, a weight reduction is achievable by reducing the support spacing; actually all analyses conducted indicate that support spacing should be reduced until the shield is minimum gage to result in least weight. However, the reduction in spacing would have to be in multiples of the pitch of the primary-structure panel configuration (tubular and beaded) and hence maximum spacing for minimum gage shield (least weight) might not be attainable. Also closer supports mean more fasteners, welding, and labor, so fabrication cost must be considered; but total system cost is not as sensitive to fabrication cost as to weight, so in the final analysis the maximum support spacing (compatible with the primary-structure configuration) in which a minimum gage shield can be utilized is probably the optimum weight design.

TABLE 20-1

HEAT SHIELD MATERIAL COMPARISON SUMMARY[a]

Temp., °F	Haynes 25				René 41				TD NiCr			
	t_c in.	b_f in.	b_s in.	t_{corr}[b] in.	t_c in.	b_f in.	b_s in.	t_{corr}[b] in.	t_c in.	b_f in.	b_s in.	t_{corr}[b] in.
1400	.013	.51	2.01	0.014	0.010	0.21	0.83	0.010				
1500	.014	.49	1.89	0.014	0.010	0.26	1.02	0.010	0.0145	0.50	1.97	0.015
1600	.015	.64	2.53	0.016	0.010	0.31	1.20	0.010				
1700	.016	.70	2.73	0.017	0.012	0.39	1.52	0.012				
1800	.017	.73	2.86	0.018	0.017	0.67	2.65	0.018	0.017	0.060	2.30	0.018
1900					0.020	0.82	3.20	0.021	0.019	0.65	2.50	0.020
2000									0.020	0.70	2.75	0.021
2200									0.024	0.87	3.40	0.025
2400									0.027	1.07	4.20	0.028

[a]Constants: Panel length = 92.0 in.; Support span = 13.1 in.; Number of supports = 8.

[b]t = Equivalent thickness of corrugation only; support clips not included.

TABLE 20-2

TEMPERATURES FOR DIRECT ATTACHMENT OF CORRUGATED HEAT SHIELD TO SEMIMONOCOQUE TUBULAR PANELS

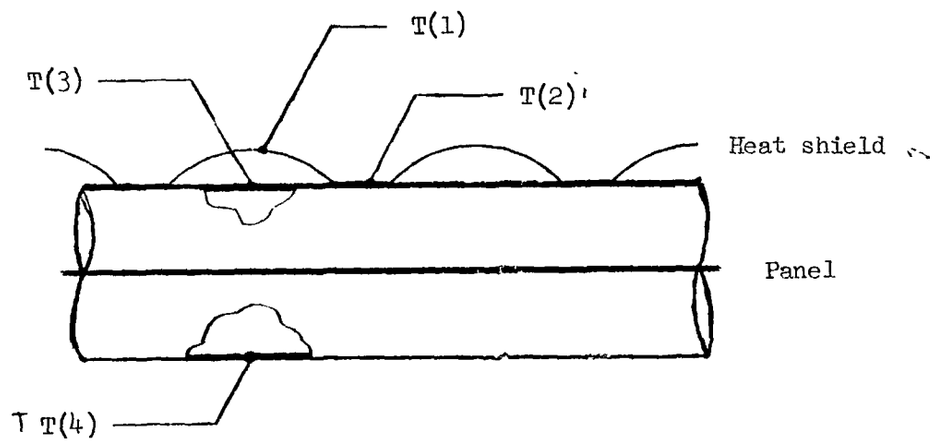

Location	Condition		Temperature,[a] °F -0.5g	2.0g	Cruise
Upper surface	Heat shield[b]	T(1)	1650	1350	965
	Attach point	T(2)	1585	1375	1010
	Panel exterior	T(3)	1500	1400	1080
	Panel interior	T(4)	1420	1435	1190
Lower surface	Panel interior	T(4)	1415	1485	1280
	Panel exterior	T(3)	1415	1600	1360
	Attach point	T(2)	1395	1600	1400
	Heat shield[b]	T(1)	1370	1715	1420

[a]Temperatures at FS 2366, BL 270.

[b]No insulation.

TABLE 20-3

TEMPERATURE DIFFERENTIAL ACROSS MULTIPLE CLIP SUPPORT FOR CORRUGATED HEAT SHIELD

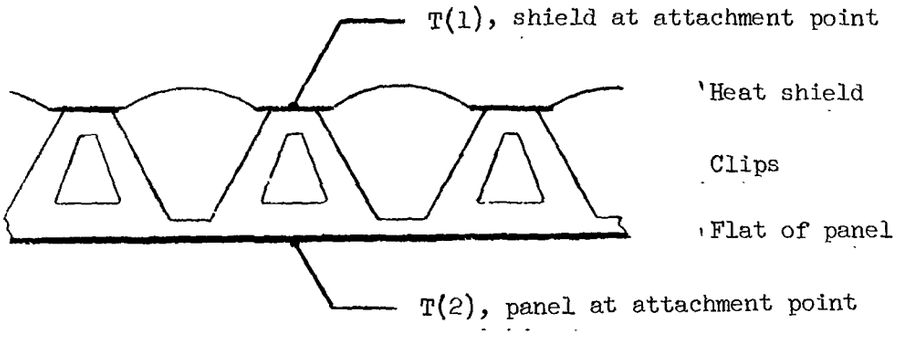

		Temperature differential, T(1) - T(2), °F		
Condition	Location	BL 60[a]	BL 166[a]	BL 300[a,b]
-.5g	Upper surface	-	0	+275
	Lower surface	+115	+ 85	+175
2.0g	Upper surface	-	- 90	+110
	Lower surface	+295	+280	+535
Cruise	Upper surface	-	-250	-130
	Lower surface	-5	+130	+295

[a] Temperatures at FS 2366, semimonocoque primary structure, upper and lower heat shield, no insulation.

[b] With insulation at lower surface.

TABLE 20-4

TEMPERATURE DIFFERENTIAL FROM HEAT SHIELD TO SEMIMONOCOQUE PANELS

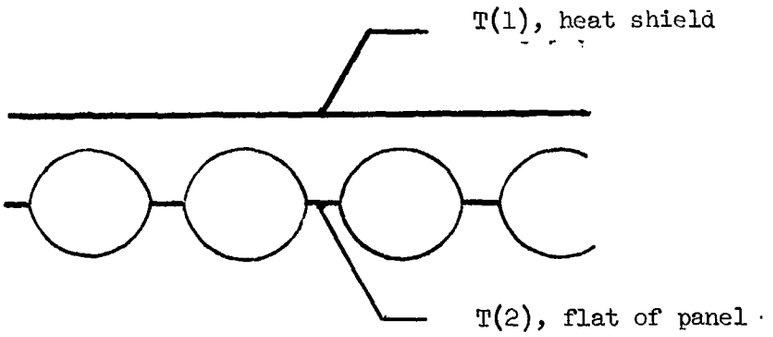

		Temperature differential, T(1) − T(2), °F		
Condition	Location	BL 60[a]	BL 166[a]	BL 300[a,b]
-0.5g	Upper surface	-	+125	+260
	Lower surface	+135	- 20	+ 80
2.0g	Upper surface	-	- 75	- 20
	Lower surface	+275	+225	+440
Cruise	Upper surface	-	-165	- 90
	Lower surface	0	+ 90	+370

[a] Temperatures at FS 2366, semimonocoque primary structure, upper and lower heat shield, no insulation

[b] With insulation at lower surface

TABLE 20-5

TEMPERATURE DIFFERENTIAL FROM CREST OF CORRUGATION ON HEAT SHIELD TO ADJACENT CLIP ATTACHMENT POINT

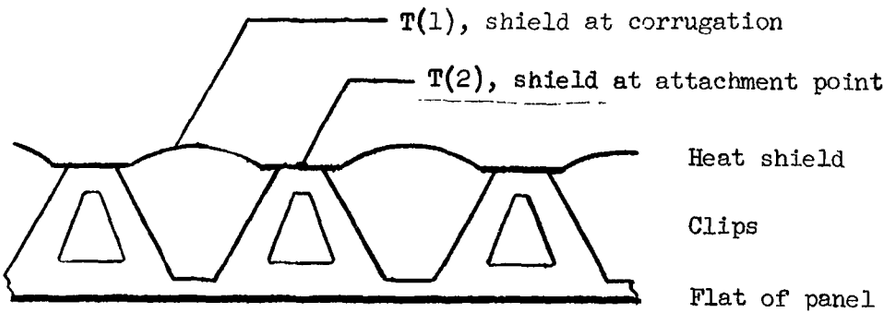

		Temperature differential, T(1) - T(2), °F		
Condition	Location	BL 60[a]	BL 166[a]	BL 300[a,b]
-0.5g	Upper surface	-	+115	+145
	Lower surface	-40	- 50	+ 40
2.0g	Upper surface	-	- 50	- 40
	Lower surface	+80	+ 75	+ 55
Cruise	Upper surface	-	- 50	- 25
	Lower surface	0	+ 10	+ 50

[a] Temperatures at FS 2366, semimonocoque primary structure, upper and lower heat shield, no insulation.

[b] With insulation at lower surface.

TABLE 20-6

TEMPERATURES FOR FLAT SKIN DIMPLE STIFFENED HEAT SHIELD CONCEPT

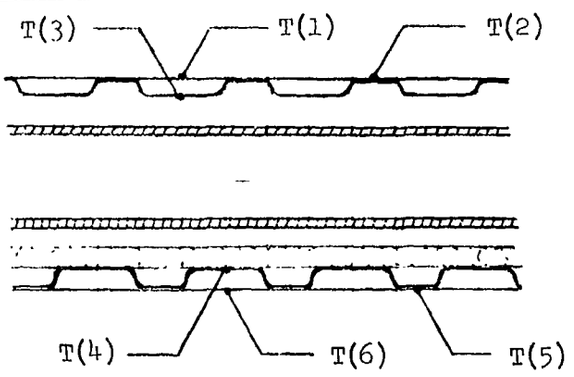

Condition	Location	Temperatures,[a] °F					
		BL 60	BL 166	BL 258	BL 258	BL 350	BL 350
	Insulation	None	None	None	.25 in.	None	.50 in.
-0.5g	External skin, T(1)	-	1305	1585	1550	1675	1640
	Attach point, T(2)	-	1220	1470	1370	1565	1475
	Internal skin, T(3)	-	1200	1435	1325	1530	1425
	Internal skin, T(4)	1190	1300	1400	1465	1480	1540
	Attach point, T(5)	1195	1300	1400	1460	1480	1535
	External skin, T(6)	1235	1300	1375	1405	1450	1475
2.0g	External skin, T(1)	-	1155	1355	1305	1420	1375
	Attach point, T(2)	-	1190	1380	1275	1460	1365
	Internal skin, T(3)	-	1195	1385	1270	1465	1355
	Internal skin, T(4)	1340	1445	1550	1640	1645	1725
	Attach point, T(5)	1385	1485	1590	1660	1690	1750
	External skin, T(6)	1545	1605	1685	1710	1775	1795
Cruise	External skin, T(1)	-	885	950	835	1005	875
	Attach point, T(2)	-	1000	1065	860	1125	890
	Internal skin, T(3)	-	1010	1075	860	1140	890
	Internal skin, T(4)	1340	1285	1350	1445	1415	1525
	Attach point, T(5)	1345	1295	1365	1450	1435	1530
	External skin, T(6)	1340	1340	1410	1445	1480	1520

[a]Temperatures at FS 2366, semimonocoque primary structure.

TABLE 20-7

TEMPERATURES FOR CORRUGATED HEAT SHIELD DERIVED FROM SEMIMONOCOQUE PRIMARY STRUCTURE ISOTHERM ANALYSIS

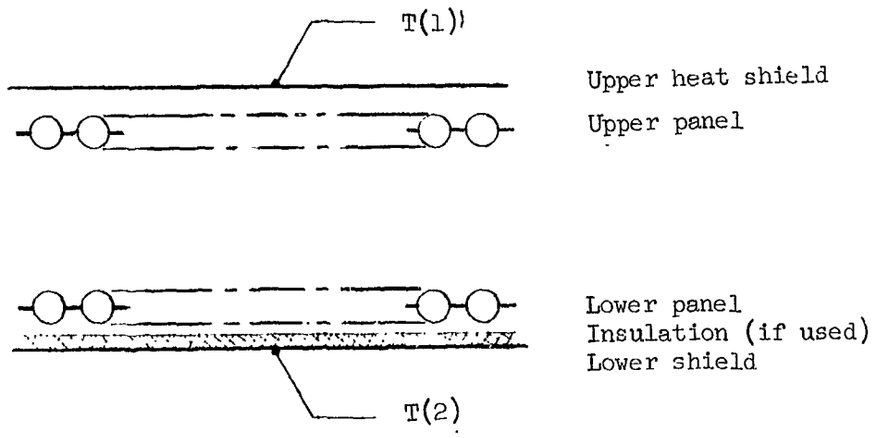

Condition	Location	Temperature,[a] °F					
		BL 60	BL 166	BL 258	BL 258	BL 350	BL 350
	Insulation	none	none	none	.25 in.	none	.50 in.
-0.5g	Upper shield, T(1)	-	1370	1620	1590	1700	1675
	Lower shield, T(2)	1245	1280	1360	1365	1430	1435
2.0g	Upper shield, T(1)	-	1180	1335	1320	1425	1380
	Lower shield, T(2)	1555	1600	1685	1745	1775	1845
Cruise	Upper shield, T(1)	-	945	990	910	1050	935
	Lower shield, T(2)	1340	1325	1385	1415	1455	1500

[a] Temperatures at FS 2366.

TABLE 20-8

SUMMARY OF HEAT SHIELD DATA

Heat shield concept		Panel aspect ratio	Support spacing, in.	Maximum deflection, in. (b)	$\Sigma\bar{t}$ in.	Weight,
Refurbishable	Corrugated skin hat-section stiff. with clip supports	1	15.3	0.380	0.0165	0.707
	Corrugated skin with simple supports	--	15.3	0.360	0.0147	0.630
	Corrugated skin with multiple supports	–	13.1	0.242	0.0131	0.562
	Flat-skin dimple-stiffened with clip supports		15.3	0.173	0.0298	1.28
Permanently attached	Modular, simply supported	–	10.4 (c)	0.195 (d)	0.0118	0.507
	Modular, cantilevered	–	2.61 (c)	0.0073 (d)	0.0123	0.528

[a] Design temperature = 1600°F; oxidation effects not included.

[b] Thermal deflections not included.

[c] Maximum length allowed due to high bending in wing-panel tube wall from heat-shield loads.

[d] Local deflections of supports not included.

TABLE 20-9

TYPICAL HEAT SHIELD AND CLIP DESIGN DATA, SPANWISE SEMIMONOCOQUE CONCEPT

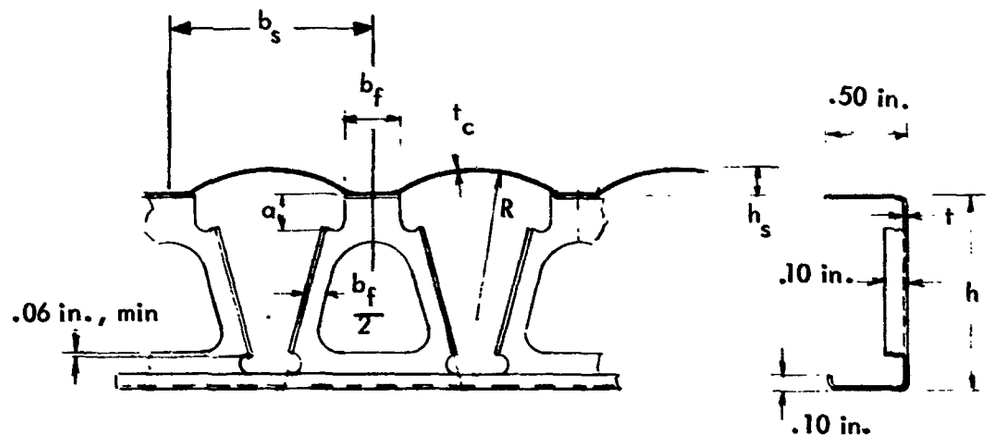

Surface	BL	a, in.	b_f, in.	h, in.	b_s, in.	R, in.	t	t_c	h_s
Upper	120-212	.10	.31	1.362	1.22	.91	.023	.012	.122
Upper	212-350	.15	.39	1.172	1.52	1.15	.026	.014	.152
Lower	0-120	.10	.31	1.172	1.22	.91	.023	.012	.122
Lower	120-212	.10	.31	1.172	1.22	.91	.023	.012	.122
Lower	212-304	.10	.48	1.172	1.88	1.40	.023	.014	.188
Lower[a]	304-350	.10	.64	1.172	2.5	1.88	.037	.019	.250

[a]TD-NiCr heat shield and clips.

TABLE 20-10

HEAT SHIELD AND SUPPORT WEIGHT SUMMARY, TYPICAL HEAT SHIELDS ON SEMIMONOCOQUE SPANWISE CONCEPTS

Surface	BL	Heat-shield design temperature, °F	$\bar{t}_{hs}$, in.	$\bar{t}_{oxid}$, in.	$\bar{t}_{clip}$, in.	$\Sigma \bar{t}$, in.	Unit weight, lb/ft^2
Upper	120 to 212	1600	0.0103	0.00005	0.00294	0.0133	0.570
Upper	212 to 350	1700	0.0125	0.00066	0.00300	0.0162	0.693
Lower	$\mathcal{L}$ to 120	1600	0.0103	0.00055	0.00280	0.0136	0.586
Lower	120 to 212	1600	0.0103	0.00093	0.00280	0.0140	0.602
Lower	212 to 350	1750[a] 1900[b]	0.0142 0.0196	0.00505 0.00207	0.00346 0.00855[c]	0.0252[d]	1.082

[a]BL 212 to BL 304.

[b]BL 304 to BL 350, TD NiCr heat shield and clips.

[c]Includes fasteners.

[d]Weighted average.

TABLE 20-11

TYPICAL HEAT SHIELD AND CLIP DESIGN DATA, CHORDWISE SEMIMONOCOQUE CONCEPT

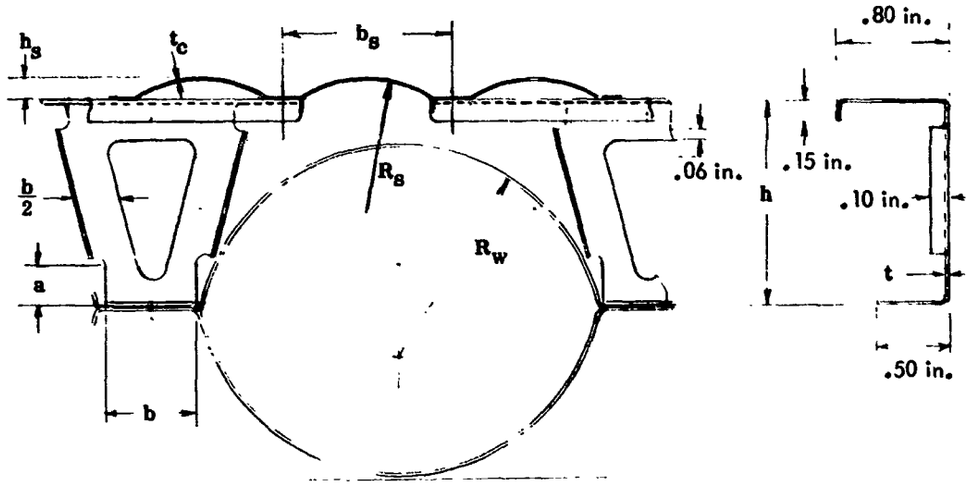

Geometry:

Surface	BL	a, in.	b, in.	h, in.	t, in.	R_s, in.	b_s, in.	b_f in.	t_c in.
Upper	120-212	.15	.40	1.183	.029	.91	1.22	.31	.011
Upper	212-350	.15	.40	1.183	.032	1.19	1.58	.40	.014
Lower	0-120	.30	.66	1.439	.027	.91	1.22	.31	.012
Lower	120-212	.30	.66	1.439	.027	.91	1.22	.31	.012
Lower	212-304	.30	.66	1.439	.036	1.42	1.92	.49	.015
Lower[a]	304-350	.30	.66	1.439	.044	1.92	2.60	.67	.019

[a]TD-NiCr heat shield and clips.

TABLE 20-12

HEAT SHIELD AND SUPPORT WEIGHT SUMMARY, TYPICAL HEAT SHIELDS ON SEMIMONOCOQUE CHORDWISE CONCEPT

Surface	BL	Heat shield design temperature, ^{o}F	$\bar{t}_{hs}$, in.	$\bar{t}_{oxid}$, in.	$\bar{t}_{clip}$, in.	$\Sigma\bar{t}$, in.	Unit weight, lb/ft^2
Upper	120 - 212	1600	.0103	.00005	.00413	.01448	.621
Upper	212 - 350	1700	.0130	.00066	.00435	.01821	.781
Lower	0 - 120	1600	.0103	.00055	.00404	.01489	.639
Lower	120 - 212	1600	.0103	.00093	.00404	.01527	.655
Lower	212 - 350	1750[a]	.0149	.00505	.00539	.0280	1.201
		1900[b]	.0210	.00505	.00658		

[a] BL 212 - 304.

[b] BL 304 - 350, TD-NiCr heat shield and clips.

[c] Including fasteners.

[d] Weighted average.

TABLE 20-13

HEAT SHIELD AND SUPPORT WEIGHT SUMMARY, TYPICAL HEAT SHIELDS ON MONOCOQUE CONCEPTS

Surface	BL	Heat shield design temperature, ^{o}F	$\bar{t}_{hs}$, in.	$\bar{t}_{oxid}$, in.	$\bar{t}_{clip}$, in.	$\Sigma \bar{t}$, in.	Unit weight, lb/ft^2
Lower	C - 120	1600	0.0150	0.00055	0.00448	0.01553	0.666
Lower	120 - 212	1600	0.0150	0.00093	0.00448	0.01591	0.684
Lower	212 - 350	1750[a] 1900[b]	0.0149 0.0203	0.00505 0.00207	0.00408 0.01048[c]	0.0269	1.157

[a] Design temperature = 1750°F, BL 212 - 304.

[b] BL 304 - 350, TD-NiCr heat shield and clips,

[c] Including fasteners.

[d] Weighted average.

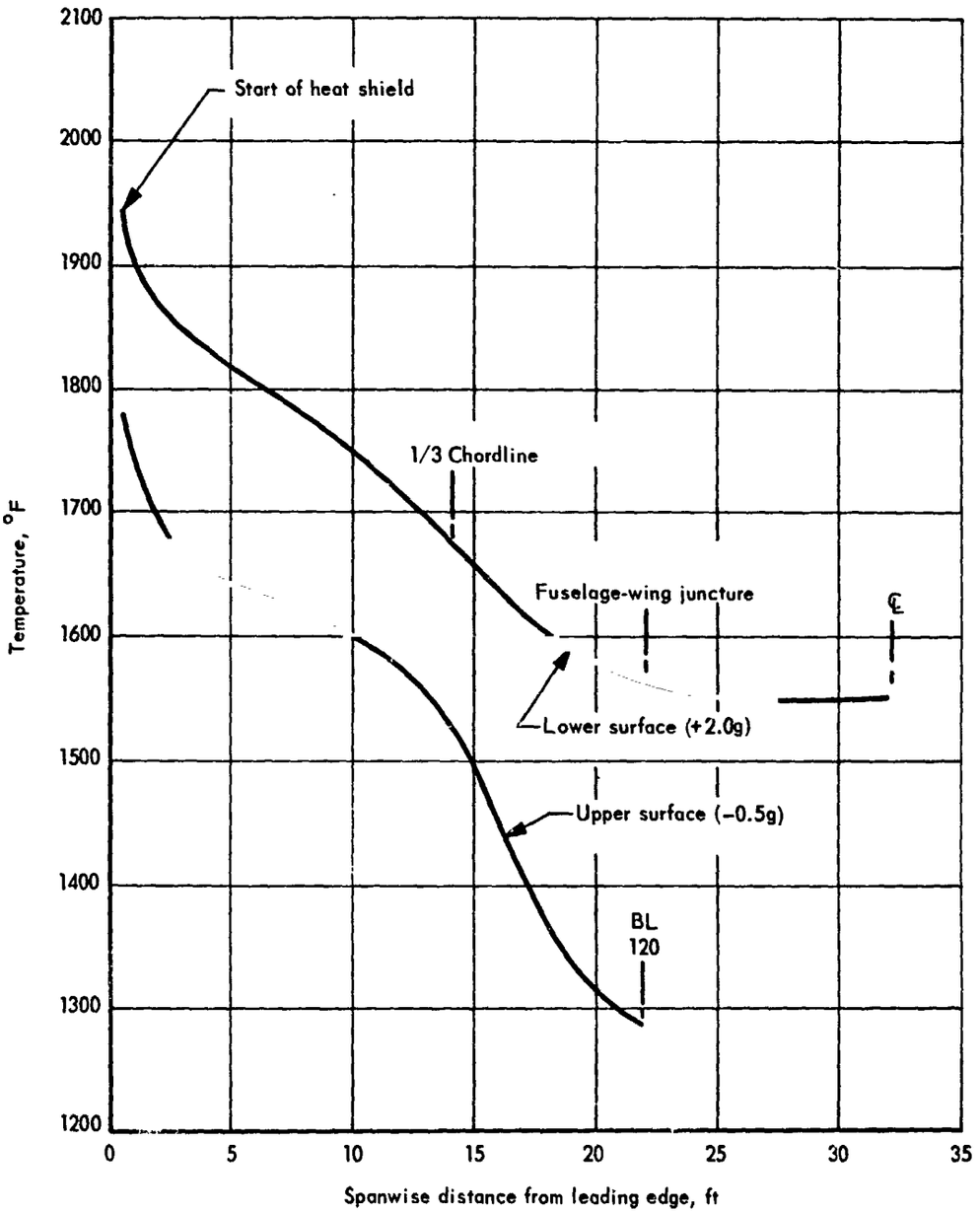

Figure 20-1. Heat-shield temperature vs spanwise distance from leading edge along station 2360

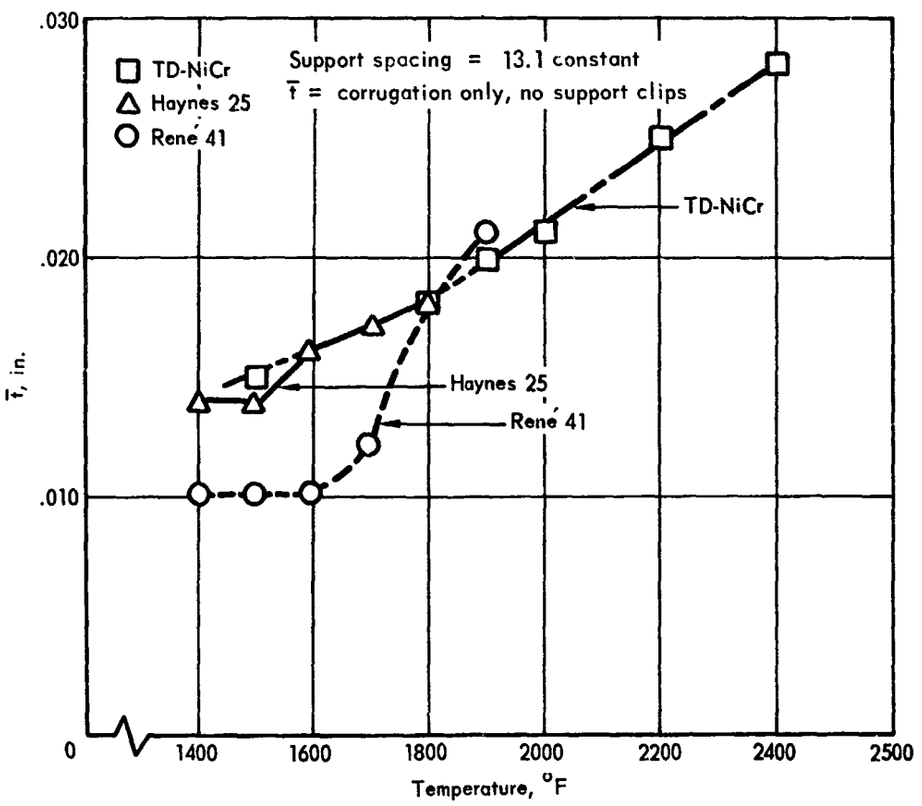

Figure 20-2. Heat shield material comparison

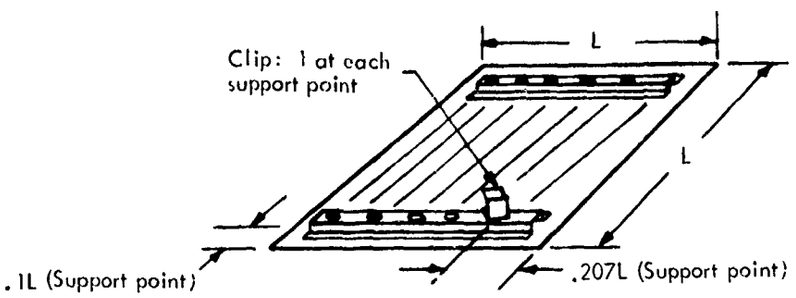

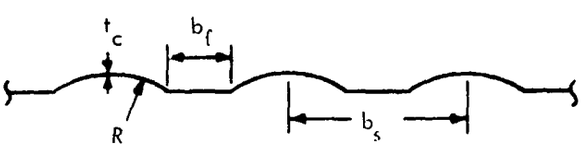

Corrugation section

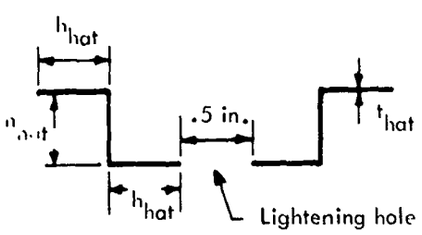

Hat section

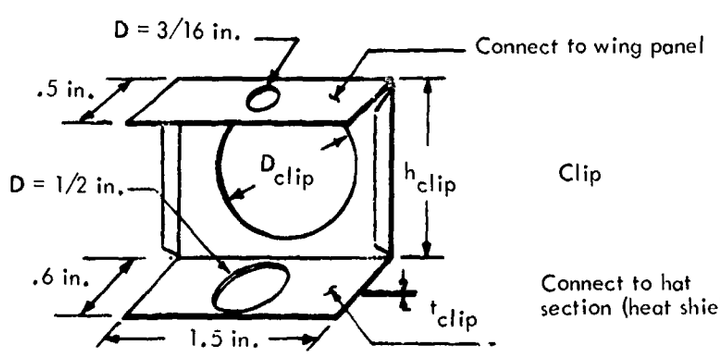

Clip

Connect to hat section (heat shield)

	Panel data				Heat section data		Clip data			Weight data			Deflection
Panel length, in.	b_f, in.	b_s, in.	t_c in.	R, in.	t_{hat}, in.	h_{hat}, in.	D_{clip}, in.	h_{clip}, in.	t_{clip}, in.	$\bar{t}_{shield}$ [a], in.	$\bar{t}_{clip}$, in.	$\Sigma\bar{t}$, in.	δ_m, in.
15.3	.32	1.24	.010	.910	.020	.250	1.30	1.31	.039	.0151	.0014	.0165	.380
23.0	.47	1.84	.016	1.360	.020	.320	1.30	1.49	.044	.0198	.0008	.0206	.557

[a] $\bar{t}_{shield} = \bar{t}_{panel} + \bar{t}_{hat}$

Figure 20-3. Corrugated heat shield concept, hat section stiffened and clip suppo. ted (refurbishable)

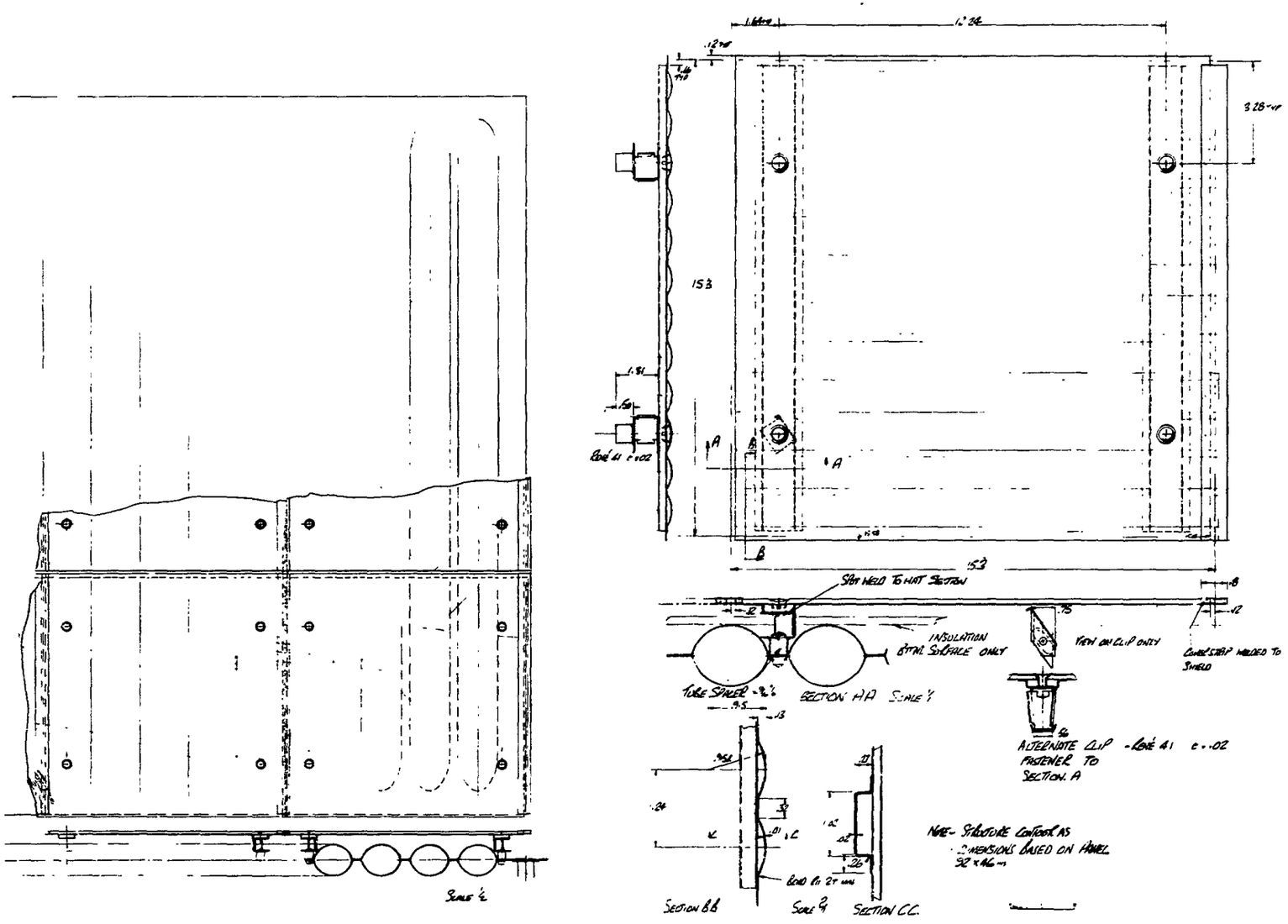

Figure 20-4. Corrugated heat shield concept, hat section stiffened and clip supported (refurbishable)

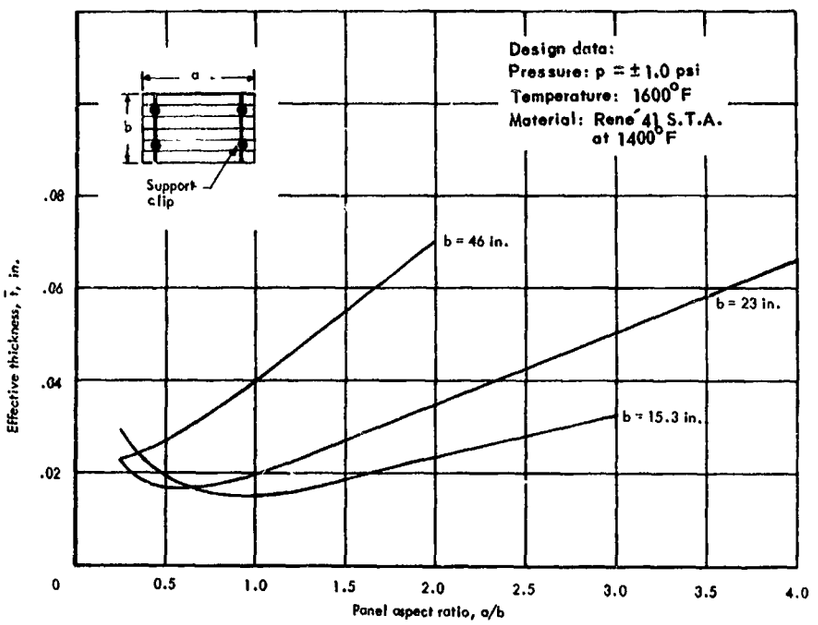

Figure 20-5. Panel size vs $\bar{t}$ for corrugated heat shields with hat sections and clip support

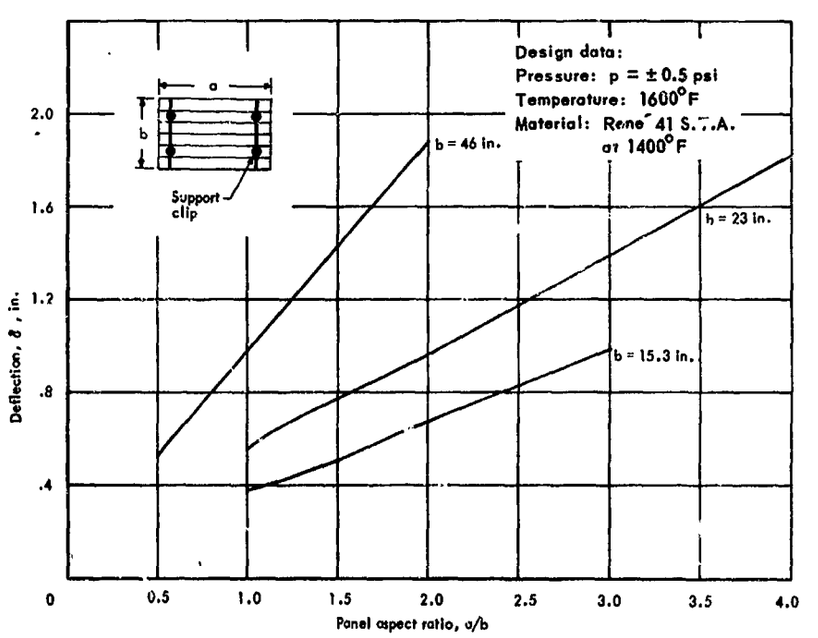

Figure 20-6. Panel size vs total deflection for corrugated heat shields with hat section and clip supports

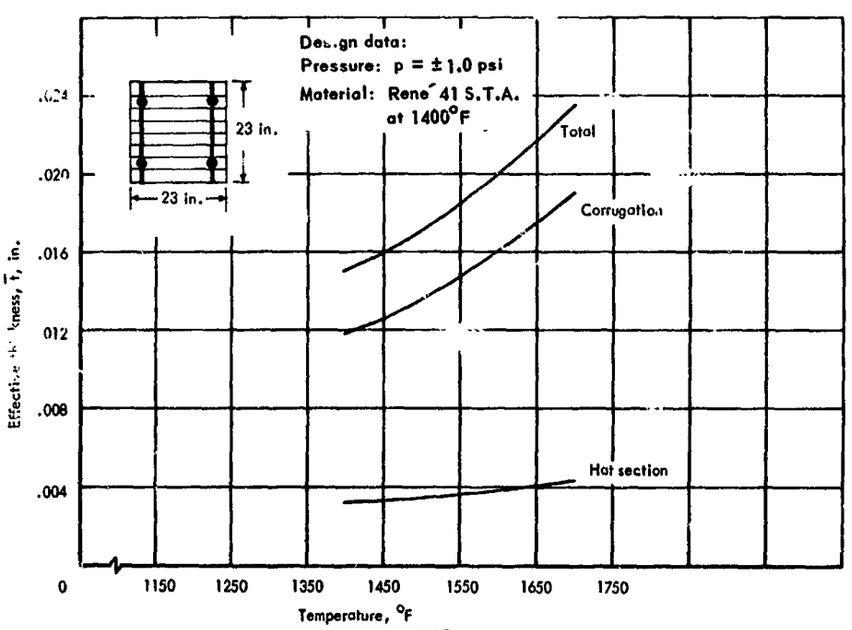

Figure 20-7. Temperature vs $\bar{t}$ for corrugated heat shields with hat sections and clip supports

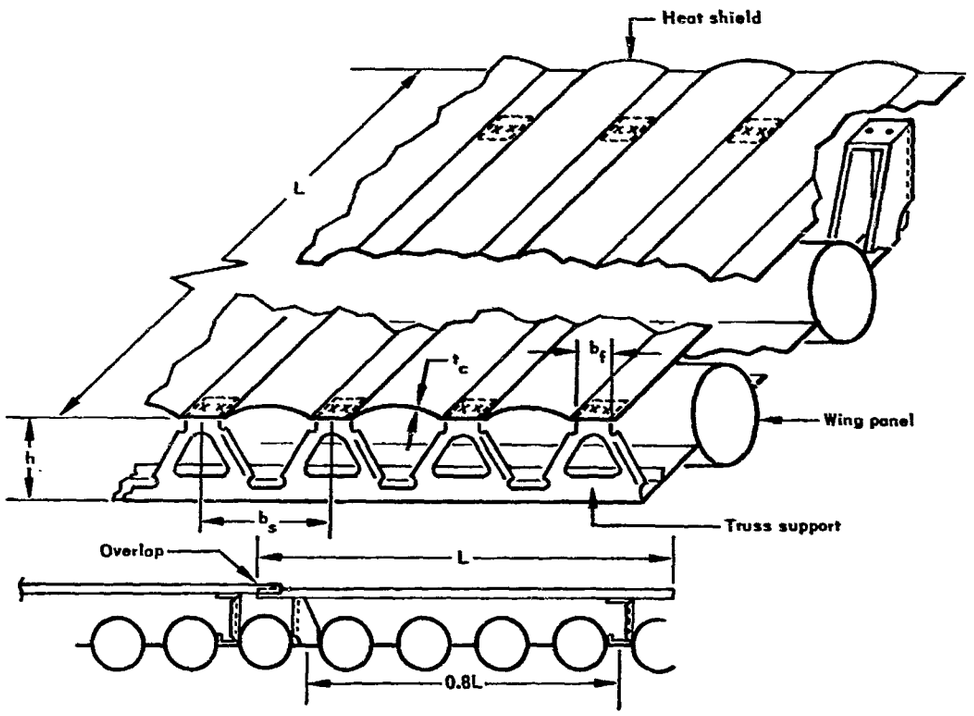

Geometry:

Panel length in.	b_f, in.	b_s, in.	t_c, in.	R, in.	h, in.	t, in.	$\bar{t}_{chan}$, in.	$\bar{t}_{shield}$, in.	$\bar{t}$, in.	δ_{max}, in.
15.3	.32	1.25	.010	0.910	1.172	.023	0.0042	.0105	0.0147	.360
23	.47	1.85	.016	1.360	1.362	.023	0.00294	.016	0.0189	.483

Figure 20-8. Corrugated heat shield concept with simply supported ends (refurbishable)

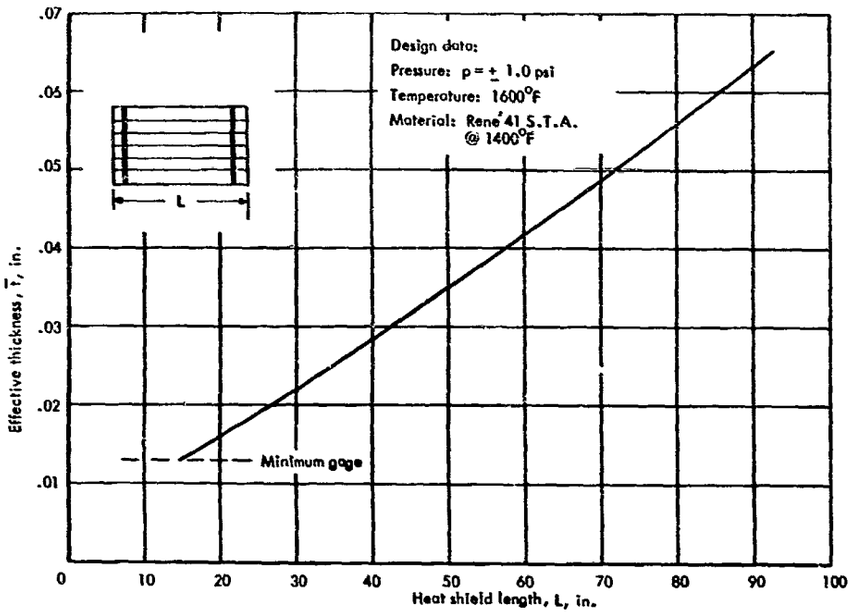

Panel length vs $\bar{t}$

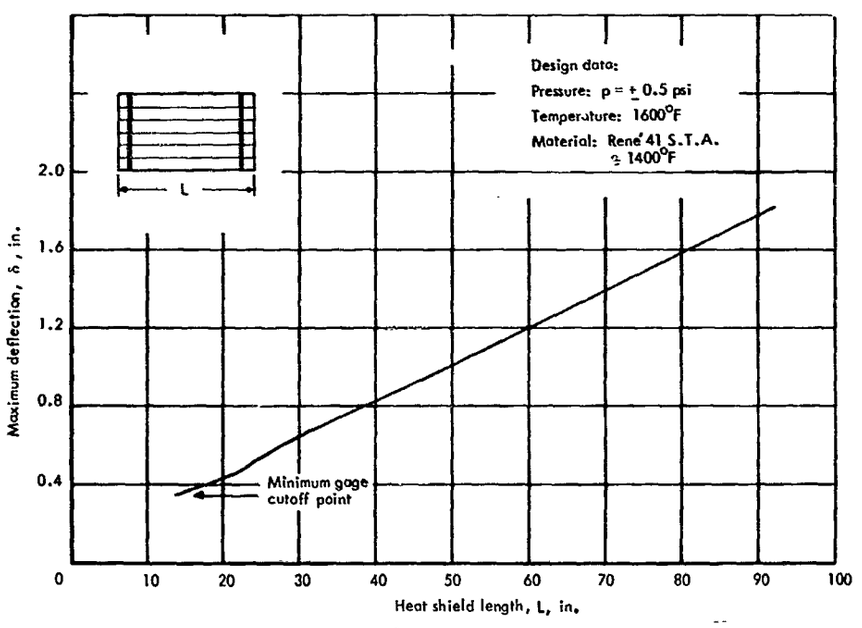

Panel length vs deflection

Figure 20-9. Effective thickness and deflection for corrugated heat shield with simple supports

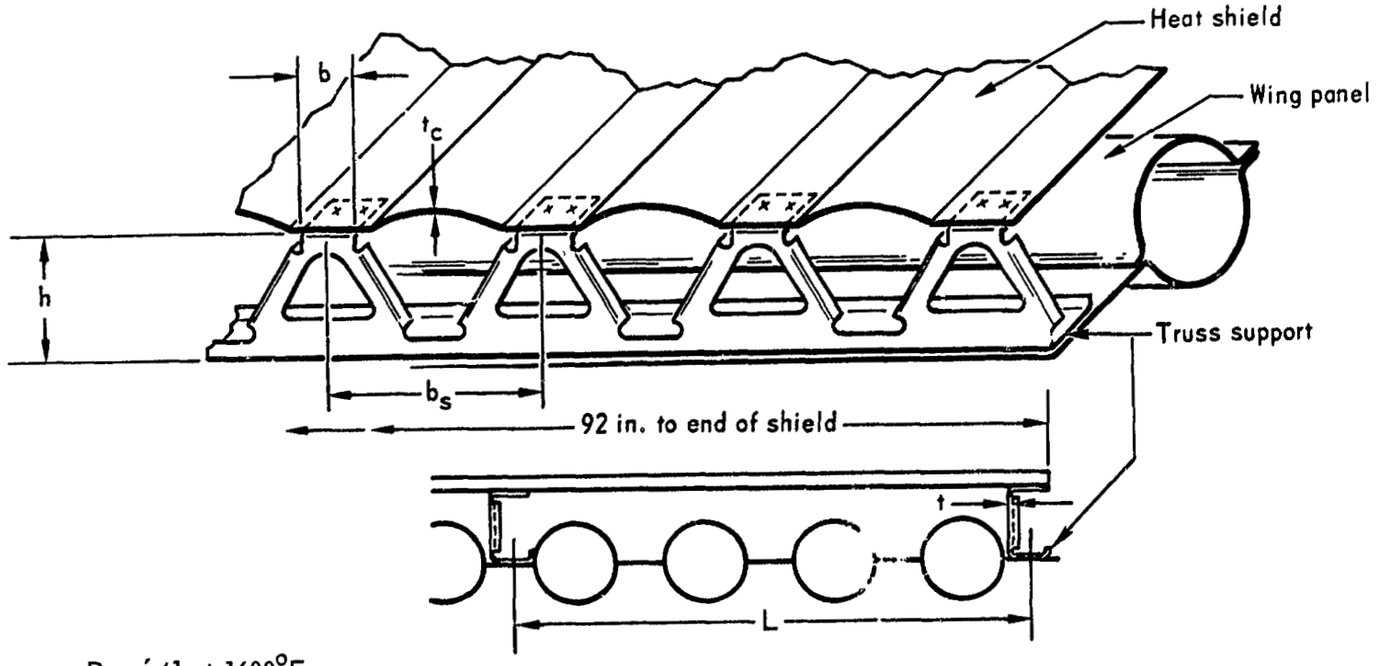

Geometry: Rene' 41 at 1600°F

Panel length	Support span, in.	Supports required	t_c, in.	b_f, in.	b_s, in.	t, in.	h, in.	$\bar{t}_{truss}$ in.	$\bar{t}_{corr}$, in.	$\Sigma\bar{t}$, in.	δ, in.
92	13.1 (a)	8	.010	.31	1.20	.023	1.172	.0028	.0103	.0131	.242
92	15.3	7	.0122	.37	1.48	.023	1.190	.00245	.0124	.01485	.260
92	23.0	5	.0185	.57	2.20	.023	1.277	.00175	.0190	.02075	.347

[a] Minimum-weight design

Figure 20-10. Corrugated heat shield concept with multiple (refurbishable)

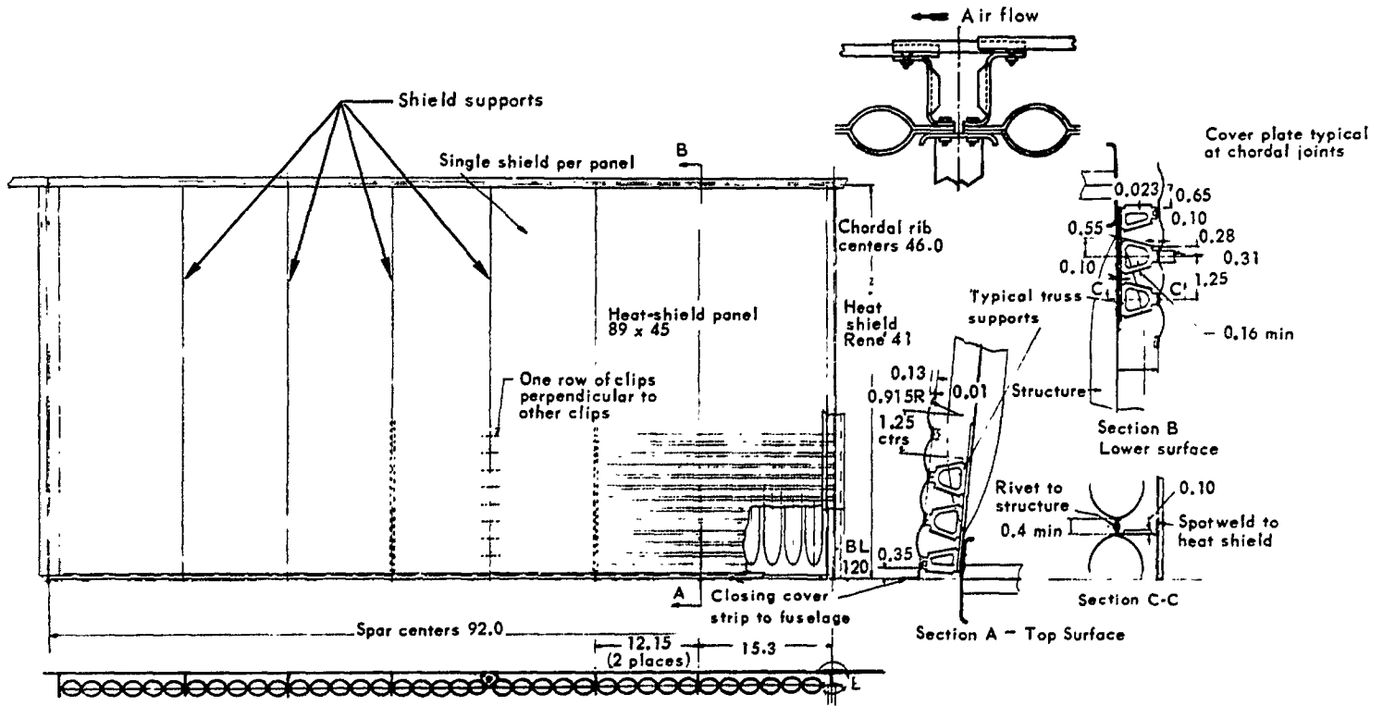

Figure 20-11. Heat shield with multiple supports (refurbishable)

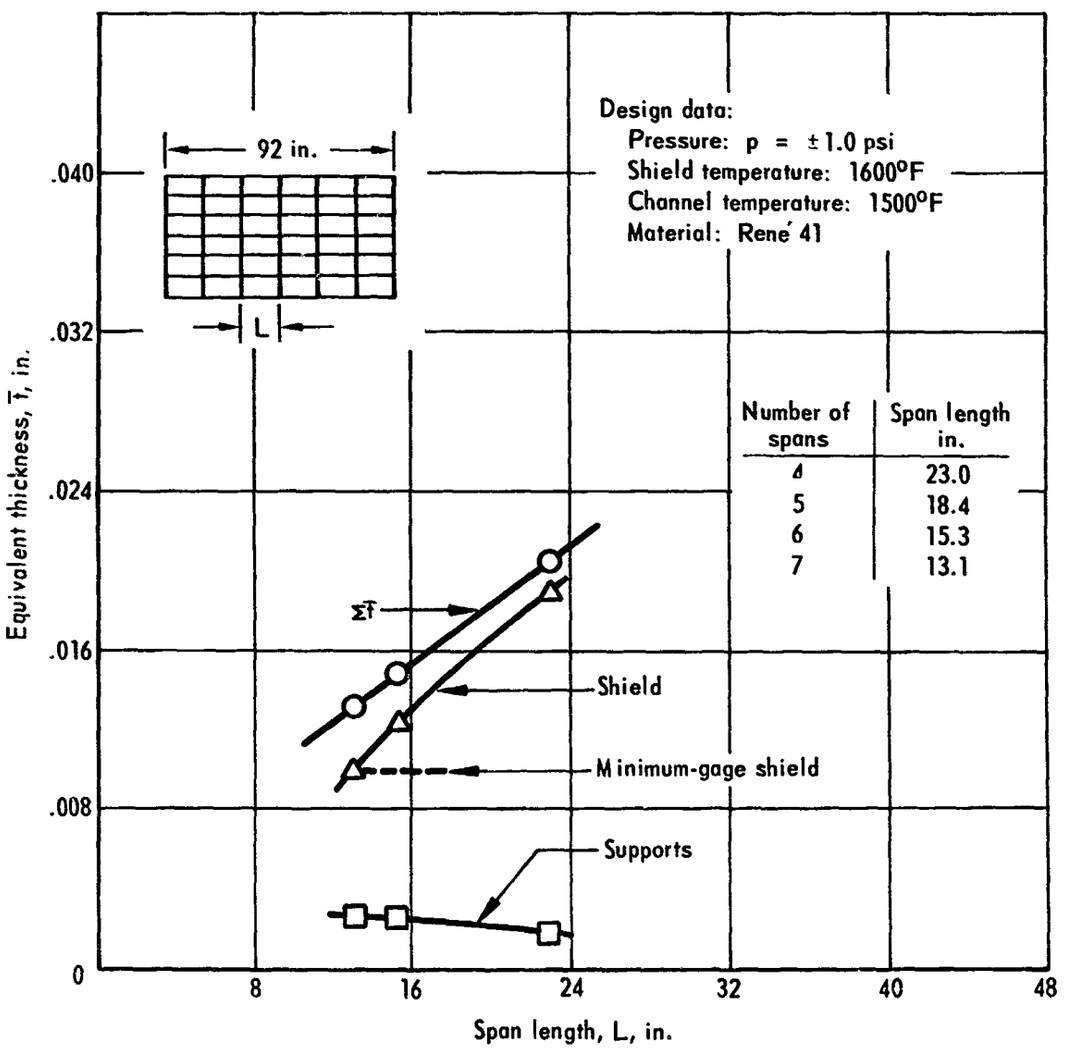

Figure 20-12. Span length vs $\bar{t}$ for multisupported corrugated heat shield

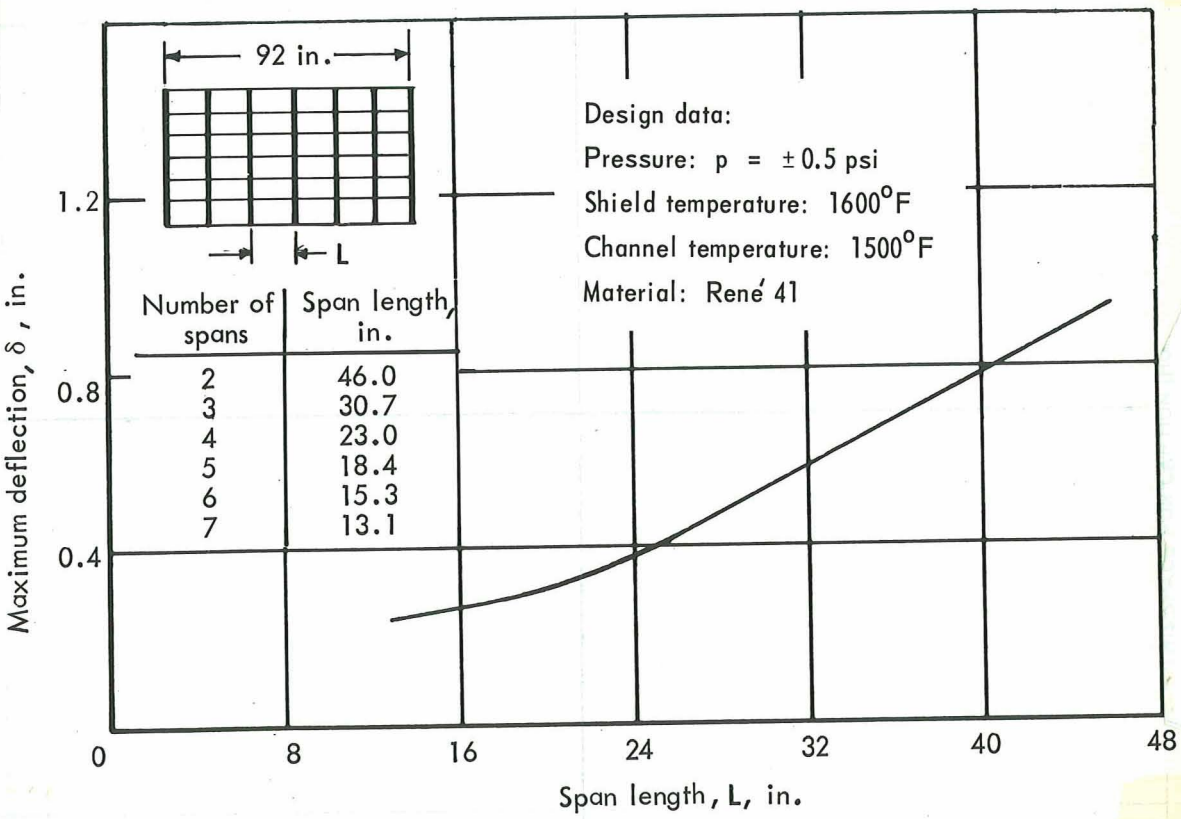

Figure 20-13. Span length vs deflection for multisupported corrugated heat shield

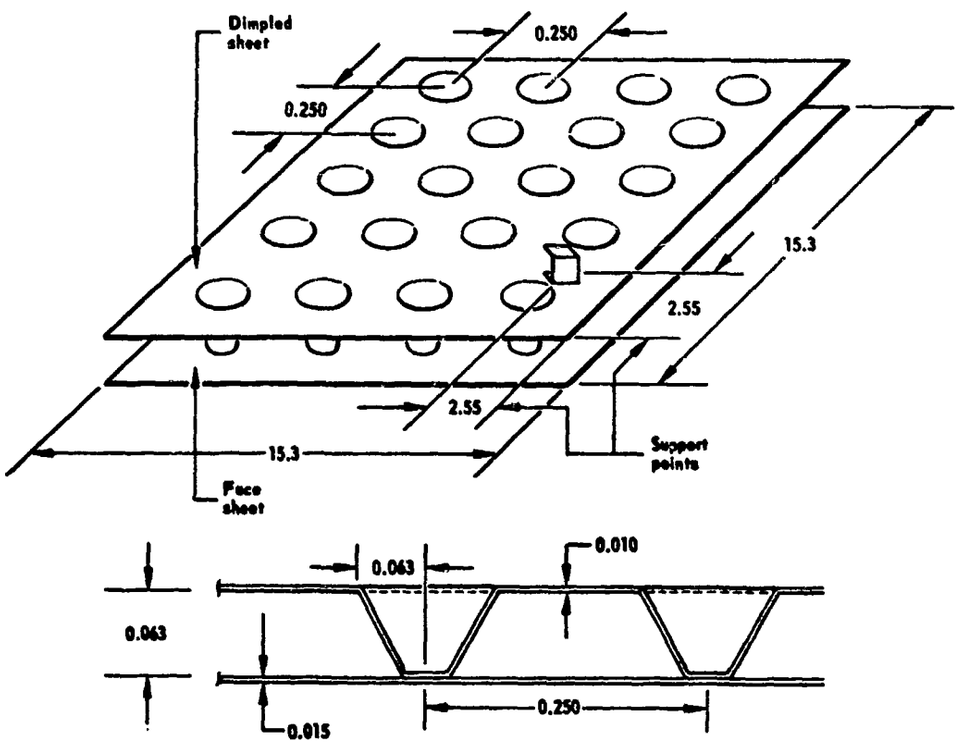

Geometry:

L, in.	p, in.	R, in.	h, in.	t_c, in.	t_s, in.	δ, in.	$\bar{t}_{panel}$, in.	$\bar{t}_{shield}$, in.
15.3	.250	.063	.063	.010	.015	.173	.0284	.0298
23.0	.310	.077	.077	.017	.017	.480	.035	.0353

- Material: Rene' 41
- Design temperature: 1600°F
- $\bar{t}_{shield} = \bar{t}_{panel} + \bar{t}_{clip}$ (from corrugated concept)

Figure 20-14. Flat skin dimple stiffened heat shield concept with clip supports (refurbishable)

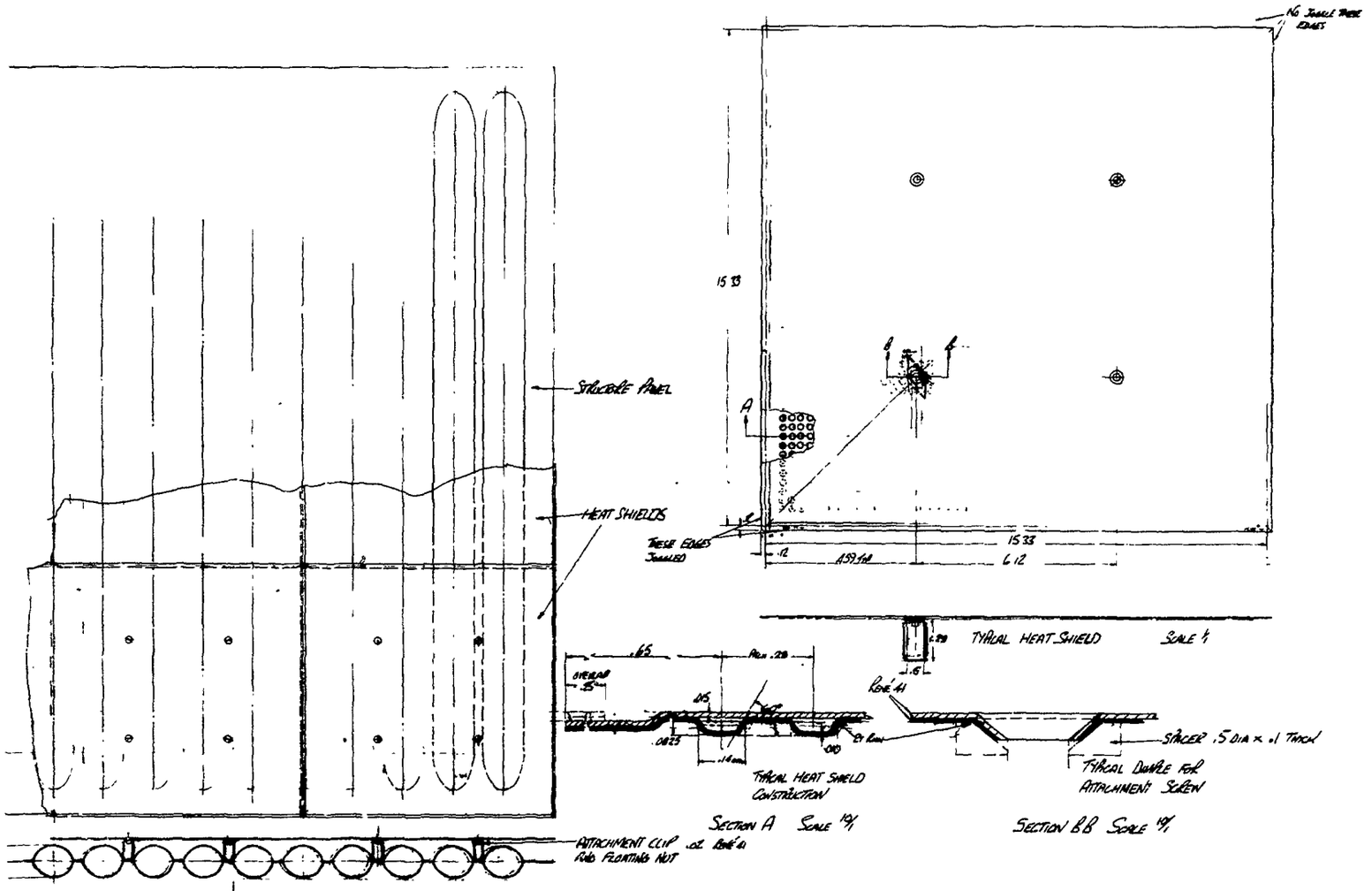

Figure 20-15. Heat shields, flat skin, dimple stiffened with clip supports (refurbishable)

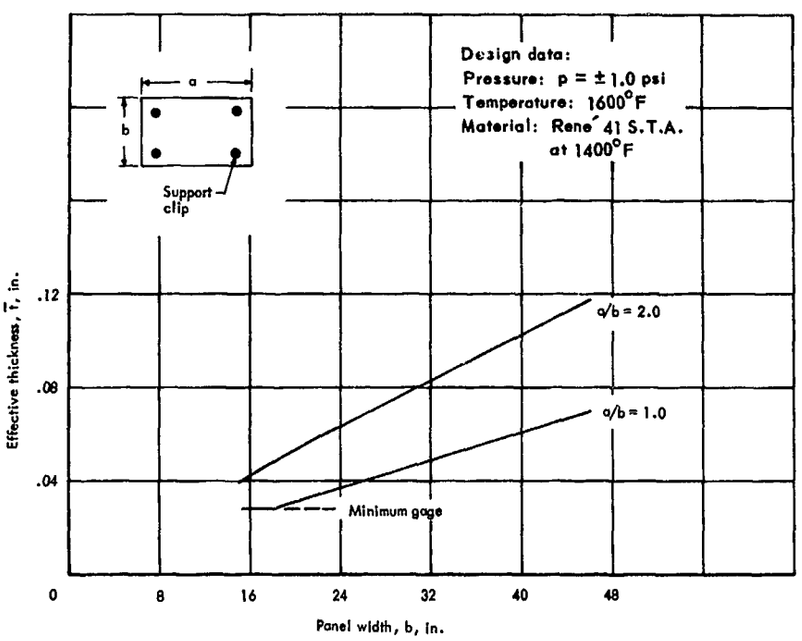

Figure 20-16. Panel size vs $\bar{t}$ for dimpled concept heat shields

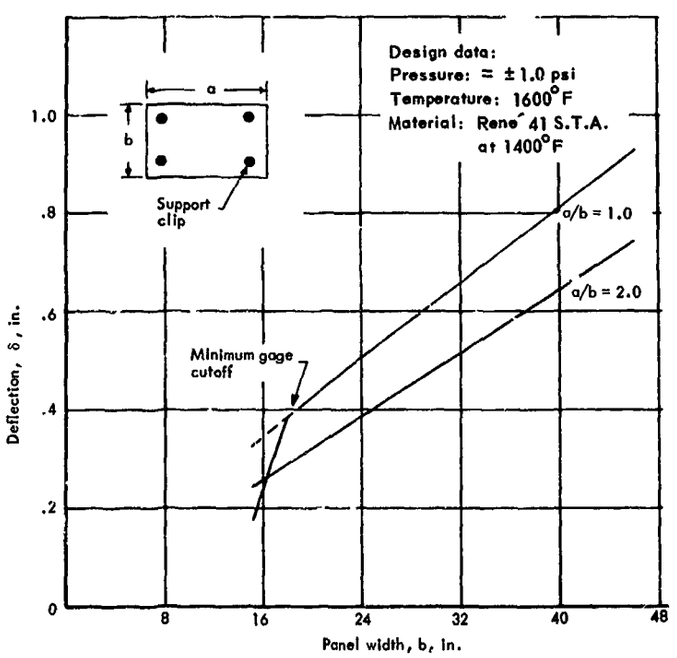

Figure 20-17. Deflection vs panel size for dimpled concept heat shields

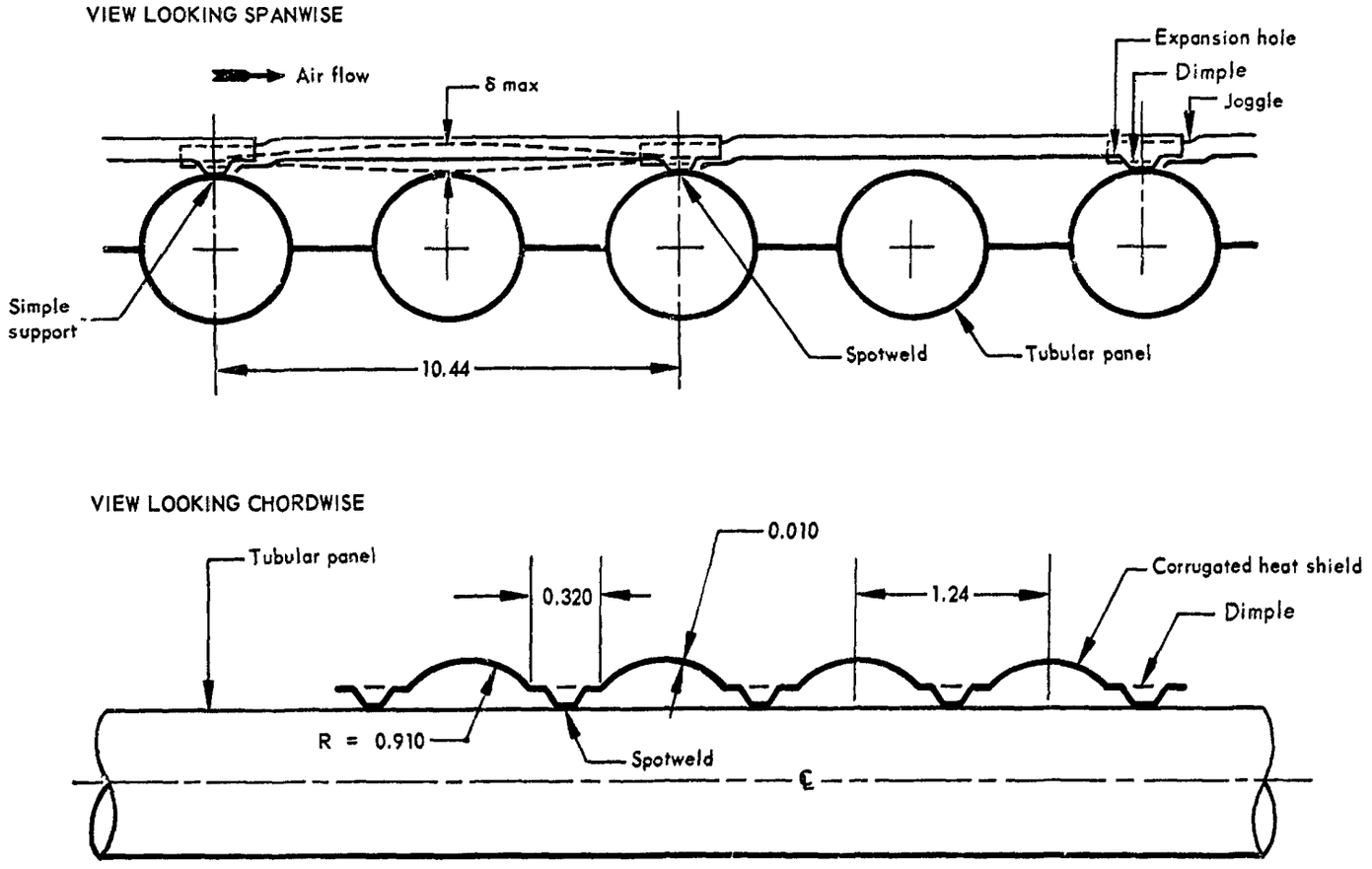

Figure 20-18. Simply supported modular heat shield concept with interlocking joint (permanently attached)

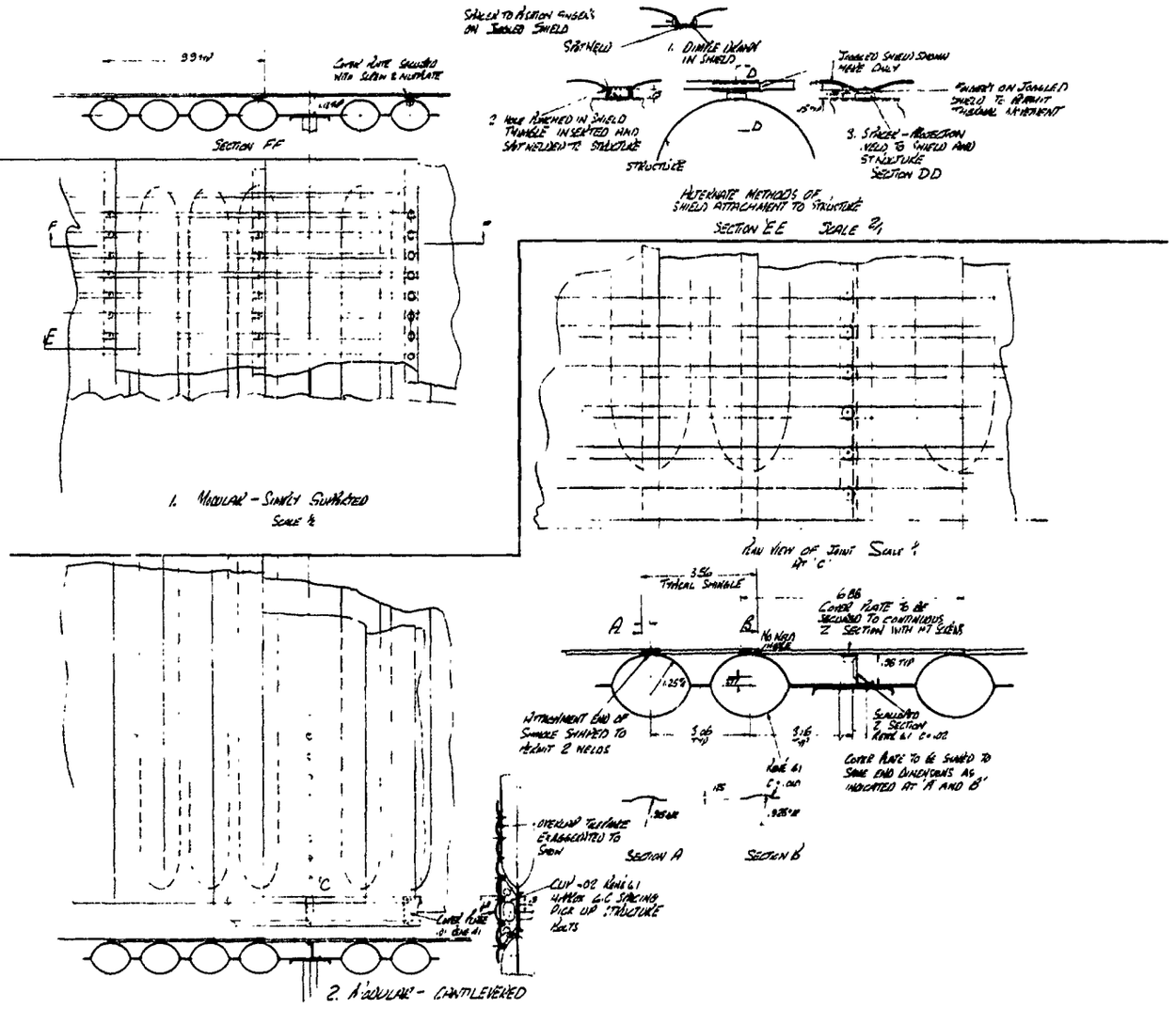

Figure 20-19. Heat shield, modular, simply supported and cantilevered (permanently attached)

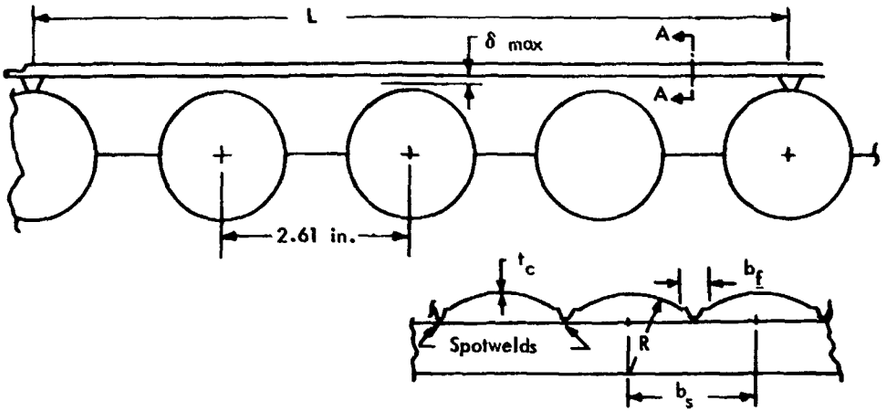

Section A-A

Geometry:

L_{opt}, in.	t_c, in.	R, in.	b_f, in.	b_s, in.	$\bar{t}$, in.	δ_{max}, in.
10.44	.010	.910	.320	1.24	.0118	.195

Figure 20-20. Simply supported modular heat shield concept (permanently attached)

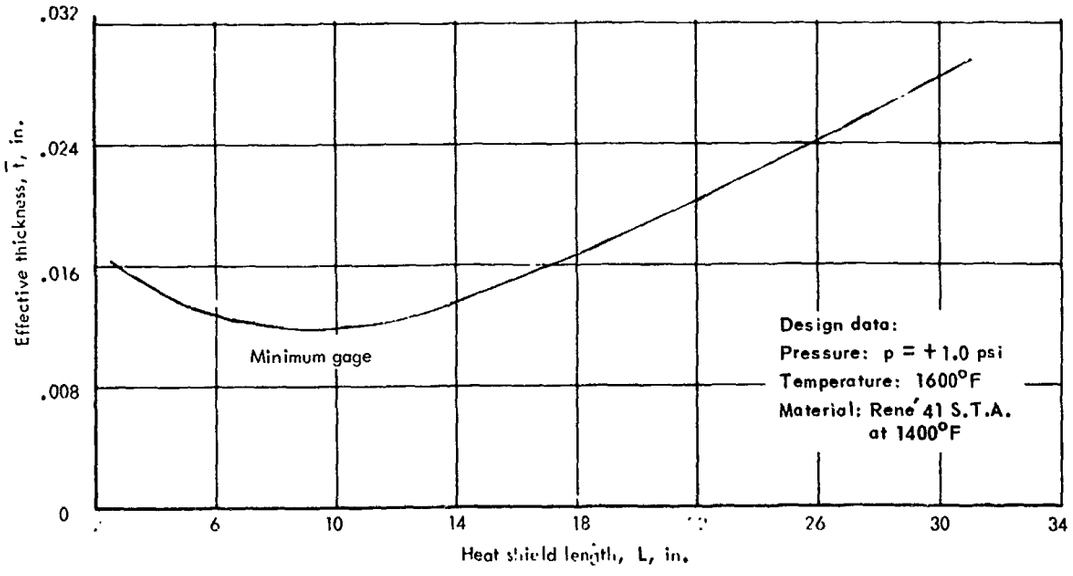

Figure 20-21. Length vs $\bar{t}$ for modular heat shield concept with simple supports

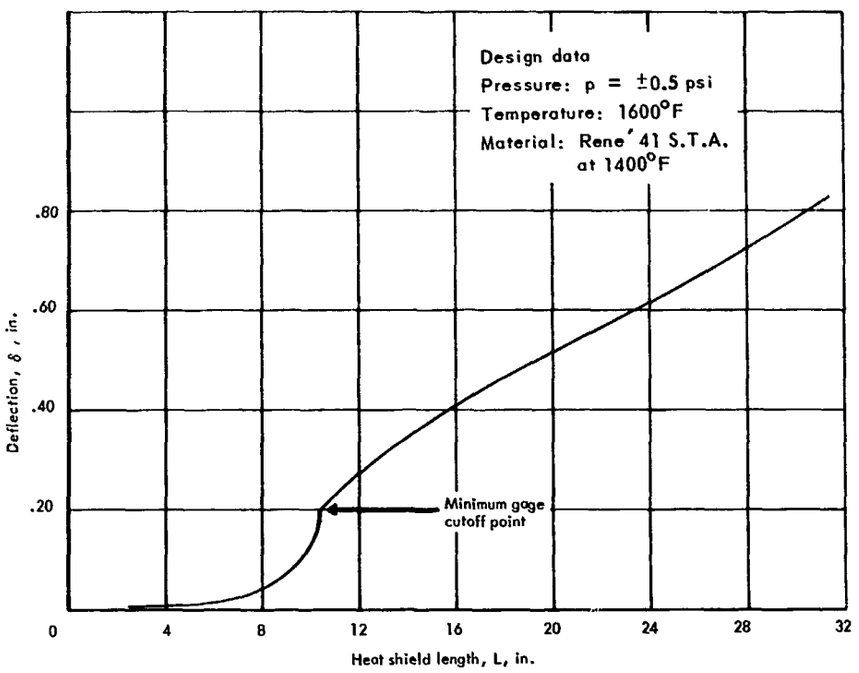

Figure 20-22. Length vs δ for modular heat shield concept with simple supports

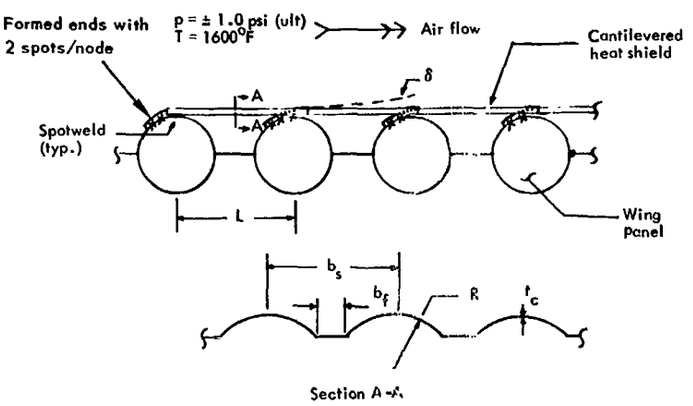

L_{opt}, in. a	t_c, in.	R, in.	b_f, in.	b_s, in.	$\bar{t}$, in.	δ in. b
2.61	.010	.910	.320	1.24	.0123	.0073

a. Maximum allowable length due to high bending in wing panel tube wall from cantilever moment.

b. Does not include thermal deflection or support deflection.

Figure 20-23. Cantilevered modular heat shield (permanently attached)

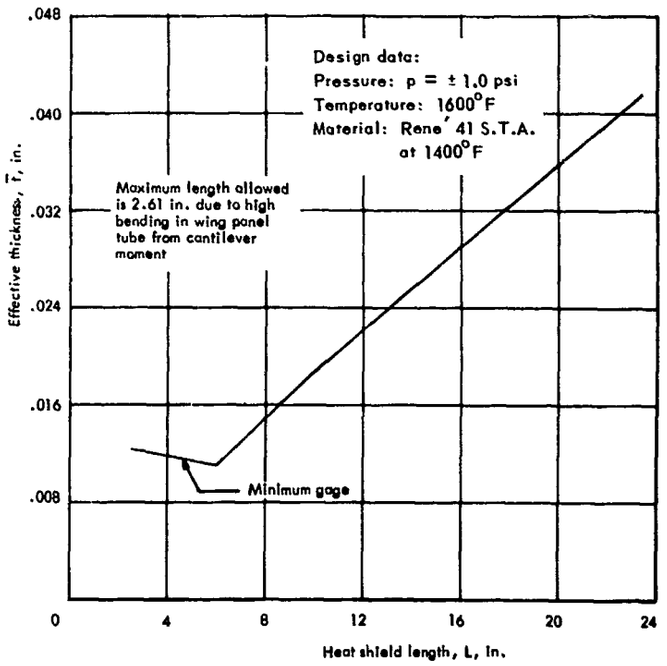

Figure 20-24. Length vs $\bar{t}$ for cantilevered modular heat shield

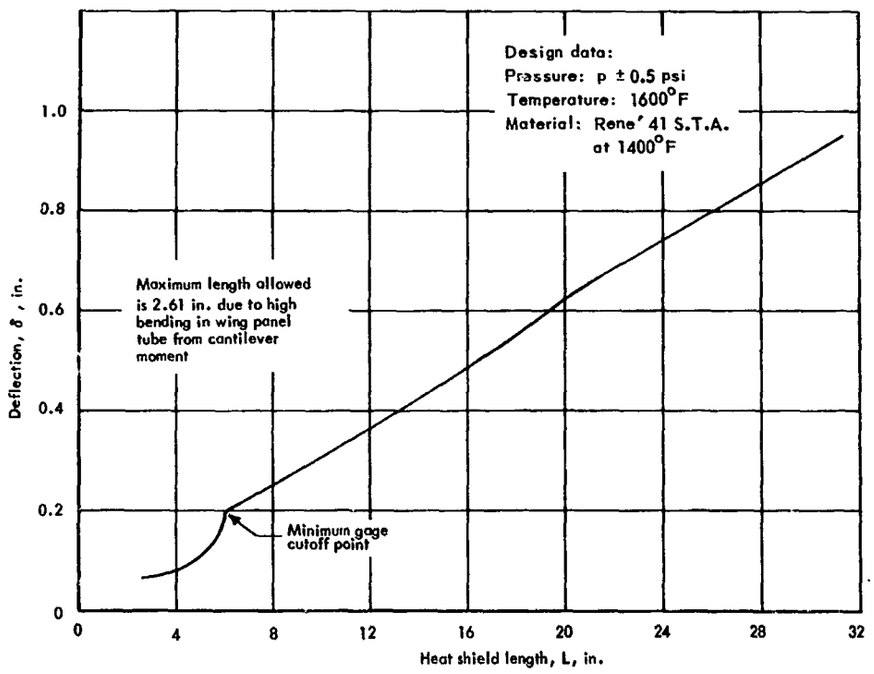

Figure 20-25. Length vs δ for cantilevered modular heat shield

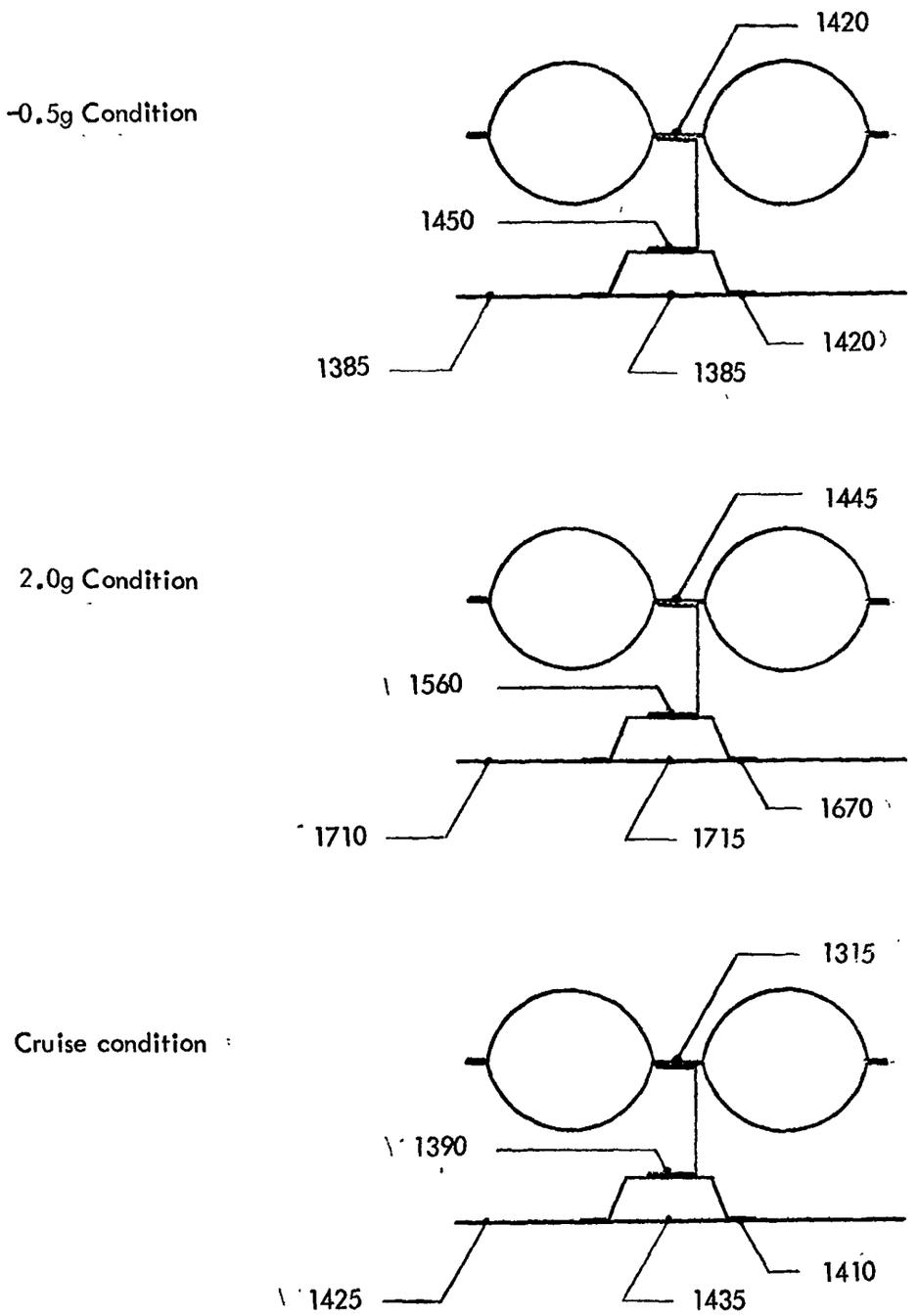

Note: Temperatures (°F) at FS 2366, BL 270, lower surface of semi-monocoque primary structure, with upper and lower shields, no insulation

Figure 20-26. Temperatures at lower surface attachment point for corrugated heat shield with hat sections and clip supports

Section 21

LEADING EDGE WEIGHT ANALYSIS

by

C. C. Richie

CONTENTS

TABLES

ILLUSTRATIONS

SYMBOLS

A	Cross section area
D	Ductility
E	Modulus of elasticity
F_{tu}	Ultimate tensile strength
G	Shear modulus
g	Gravitational acceleration
K	Number of stress levels considered
K_Q	Fatigue quality index
l	Length
M	Material constant used in equation 21-1
N_f	Cyclic life
N_i	Number of loading cycles to failure at the i^{th} stress level
n_i	Number of loading cycles applied at the i^{th} stress level
p	Pressure
q	Shear flow
R.A.	Reduction in area
T	Temperature
t	Thickness
$\bar{t}$	Equivalent panel thickness
U	Strain energy
z	Material constant used in equation 21-1
α	Linear coefficient of thermal expansion

γ Material constant used in equation 21-2

ΔT Temperature difference

$\Delta\epsilon$ Total strain range

$\Delta\sigma$ Stress range corresponding to total strain range ($\Delta\epsilon$)

ϵ Strain

σ Stress

Subscripts

el Denotes elastic value

f Denotes final value

o Denotes initial value

p Denotes plastic value

Section 21

LEADING-EDGE WEIGHT ANALYSIS

The leading-edge analysis consisted of a parametric thermal analysis, selection of the leading candidate material, structural evaluation of the candidate arrangements for the segmented and continuous concepts, design, and weight data.

Plasma-jet test results (presented in section 4) indicated that although the porous tantalum metal concept results in improvements by a factor of 2 over previously tested concepts, a sheetmetal concept with an oxidation-resistant coating showed marked improvement and therefore satisfies better the leading-edge oxidation-protection requirement. The coated sheetmetal concept was selected for detailed evaluation.

The leading-edge pressures used for the investigation are presented in table 21-1 and the design pressures, which are based on the net difference between internal and aerodynamic pressures, are shown in table 21-2. The leading edge pressure variation during maneuver is presented in figure 21-1.

PARAMETRIC THERMAL ANALYSIS AND MATERIAL SELECTION

On the basis of radiation equilibrium temperatures, the tantalum alloy Ta-10W was originally considered the leading candidate. However, a two-dimensional thermal analysis, the lower curve in figure 21-2, indicated lower temperatures which would allow use of the superalloy TD NiCr as presented in detail later in the discussion. Figure 21-2 is a plot of temperature versus material thickness for Ta-10W (tantalum alloy), Cb-752 (columbium alloy), and TD NiCr (dispersion-strengthened alloy). Initially, only internal radiation effects were evaluated for a hot load carrying leading edge (no insulation at the Rene' 41 leading edge spar). Later, conduction and internal radiation effects were determined using TD NiCr and an insulated concept (insulation at the Rene' 41 leading edge spar).

The transient-temperature analysis of figure 21-2 indicates that a maximum of 2200°F is achieved by increasing the leading-edge thickness to about 0.125 in., thus permitting the use of TD NiCr. TD NiCr does not require an oxidation-resistant coating. The details of this selection are presented in the following discussion.

A preliminary thermal analysis of the wing leading edge was conducted for three structural arrangements, which include two hot load carrying concepts (with and without a leading edge spar) and an insulated concept. Three leading edge materials were considered: preoxidized TD NiCr, silicide coated Ta-10W, and silicide coated Cb-752. Temperatures determined for the stagnation line on the leading edge and for the attachment points of the leading edge section

to the supporting structure are shown in tables 21-3, 21-4, and 21-5 for the +2.0-g condition. These temperatures were used to determine thermal strains for the various material arrangements at the maximum dynamic pressure condition. A material thickness of 0.12 inch at the radius was assumed, and radiation was the only mode of heat transfer accounted for within the structure. Table 21-3 shows temperatures for the hot load carrying concept without a leading edge spar (figure 21-2) for Ta-10W and for TD NiCr. Table 21-4 presents temperatures for the hot load carrying concept with a leading edge spar (fig. 21-4). For this concept, the nose beam and the panels immediately behind it were TD NiCr, with the leading edge shown for Ta-10W, TD NiCr, and Cb-752. Temperatures for the insulated concept (fig. 21-5) are presented in table 21-8 for Ta-10W and Cb-752. The leading edge spar in this case was protected by insulation and was assumed to be made from René 41.

Temperatures shown in Tables 21-3 and 21-4 for TD NiCr at the stagnation line are representative of temperature accounting for radiation, lateral conduction, and an emissivity of 0.75 (Section 5). The effect of lateral conduction at locations other than the stagnation line is much smaller because temperature gradients along the structure become insignificant behind the leading edge radius. The emittance value determined by test for TD NiCr was used in a later analysis of the insulated leading edge concept.

The results of the preliminary analysis of the hot load carrying concept are summarized to show the difference in peak temperature due to material and thickness at the leading edge radius. Figure 21-1 shows peak temperatures at the leading edge stagnation line for the three materials and a range of material thickness. Results for TD NiCr are presented for surface emittances of 0.75 and 0.90. The temperature increase of 95°F for the lower emittance is fairly constant over the range of material thickness shown (0.04 to 0.20 inch). A change in emittance from 0.80 to 0.70 for Ta-10W results in a 65°F increase in peak temperature. As the structure at the leading edge becomes thinner, heat capacity effects diminish and peak temperatures vary inversely with surface emittance, regardless of material.

Tables 21-6, 21-7, and 21-8 show results of the thermal analysis of the insulated leading edge concept for TD NiCr, with material thicknesses at the radius of 0.125, 0.375 and 0.625 inch, respectively. Temperatures are shown at three flight conditions for three locations on the radius (including the stagnation line) and for the supporting structure behind the radius. Conduction was included in the analysis, and the 0.75 emittance was used for TD NiCr. The leading edge section immediately behind the radius was assumed flat with an equivalent mass thickness ($\bar{t}_{FLAT}$) of either 0.03 or 0.06 inch.

Thickness of the section connecting the radius with the flat section is double t_{FLAT}. Peak temperatures at the stagnation line, T(4), are not more than 2200°F for any of the concepts shown. The effect of increasing material thickness at the radius is minor for the flat sections of the leading edge, where temperatures at all flight conditions change by less than 30°F as material thickness is increased from 0.125 to 0.625 inch. At the radius, temperatures are reduced by 50° to 100°F for the same thickness increase. Temperature gradient through the material at the stagnation line (temperature difference T(4) to T(9)) is a maximum of 65°F at the 2.0g condition for the 0.625-inch thickness. Differences at the stagnation line for the other flight conditions and material thicknesses are under 50°F. Differences through other locations on the radius, T(3) to T(8) and T(5) to T(10), are under 25°F for the three material thicknesses at any flight condition.

EVALUATION OF CANDIDATE LEADING EDGE CONCEPTS

Continuous Concept

The continuous leading edge concepts consist of relatively long segments that are attached to adjacent structure by sealed, nonslip joints. Cross sections of the four structural arrangements used in the continuous leading edge concepts evaluation are shown in figures 21-3, 21-4, 21-5, and 21-6.

From the preceding parametric thermal analysis data involving four structural arrangements, three materials and thicknesses ranging from 0.03 to 0.625 inch (the resulting eight variation of the continuous leading edge concept given in table 21-9) were further evaluated. Included in the evaluation were:

Analysis of thermal strains

Reusability requirements (refurbishment)

a. depth of oxide penetration

b. coating life

c. low cycle fatigue

Analysis of local buckling

Thermal strains were obtained based on a plane strain analysis (section 7, case three, bending about one axis) of the entire vehicle cross-section for each leading edge concept. Idealizing the leading edge and vehicle cross-section by discrete elements, the actual values of coefficient of expansion (α), elastic modulus (E), and temperature (T = 80°F) were used at each node point. Results of the plane strain analysis are shown in tables 21-3, 21-4, 21-5, and 21-10. The plane strain results indicate that the failure mode for the coated refractory metal systems (i.e., Ta-10W, Cb-752) is tension, due to the lower $\alpha\Delta T$ (i.e., product of the coefficient of thermal expansion and

corresponding temperature of the refractory metal) in comparison with the adjacent Rene 41 structure and its associated thermophysical properties. For the superalloy (TD NiCr) leading edge, compression is the failure criteria due to the higher $\alpha\Delta T$ of the TD NiCr in comparison to the Rene 41 structure and its $\alpha\Delta T$.

Reusability requirements were evaluated as follows. For TD NiCr, depth of oxide penetration was based on data taken from figure 4-18 of section 4. For coated Ta-10W, coating life data of section 5 were used. Low cycle fatigue data are presented later.

To analyze local buckling of the leading edge, the following procedure was used. Using the elastic thermal strain from a plane strain analysis, the corresponding stress level is obtained from the stress-strain curve for the given temperature. The compressive buckling stress for the curved leading edge nose is obtained using cylinder buckling theory from reference 21-1. Buckling allowables for the stiffened leading edge flats are based on orthotropic plate theory from reference 21-2.

A summary of results for the continuous leading edge concepts is presented in table 21-11 with the exception of weight and low cycle fatigue data which are presented later.

For the tension critical coated refractory metal concepts, the local buckling problem is eliminated; however, other problems exist. Coating life for the Cb-752 concepts is 500 hours at cruise conditions (stagnation temp 2300°F and p = 1.00 psi). This coating life is based on a compilation of test data for 1-hour time cycles at pressures less than one atmosphere, see section 4, fig. 4-19. Another reference, 21-3, reports a coating life for the cruise condition environment of approximately 200 hours; these data represent a more stringent environment of 1-hour time cycles at a pressure of one atmosphere. It can be seen from either of these references that the columbium coating life is much less than the required coating life of 4460 hours. To repair the coating of a refractory metal leading edge, the component must be removed and recoated. No other practical means exists at present for repairing the damaged disilicide coating. Also, to prevent eutectic reaction at the interface between the coated refractory metals and the adjacent Rene 41 structure, ceramic spacers are required. Thus, because of the unsatisfactory reusability evaluation, the coated refractory metal leading edge concepts were excluded from further consideration.

For the compression critical TD NiCr leading edge, the hot load carrying concepts, I-A-2 and I-B-2, proved unsatisfactory because of local buckling. However, further increase in thickness and corresponding reduction in temperature and thermal gradient were pursued. This approach led to the insulated concept, II-B-1, which possesses adequate buckling strength. Local buckling is precluded in the curved nose section because of the thickness and, in the flats, corrugations relieve the compressive stresses. Also, maximum oxide penetration for the TD NiCr concepts, based on stagnation point temperatures and a vehicle life of 10 000 hours, is less than 2 mils. Thus, the insulated concept was

selected as the best continuous leading edge concept and was further evaluated as indicated in the material on low cycle fatigue.

Segmented Leading Edge Concept

The segmented leading edge evaluation matrix is shown in table 21-12. Three concepts involving different nose and flat thicknesses were evaluated. A typical cross section is shown in figure 21-7. The superalloy, TD NiCr, was selected as the leading candidate material for reasons given in the preceding discussion.

Evaluation procedure for the segmented leading edge is identical with that for the continuous leading edge. Results of this evaluation are shown in table 21-13 with the exception of low cycle fatigue and weight data which are presented in subsequent sections.

Thermal strains were obtained based on a plane-strain analysis (section 7, case two, bending about two axes). To accommodate thermal expansion and bowing, the leading edge segment was attached to adjacent wing structure in the manner of a simply supported beam. Thus, the segment is free to expand in a direction parallel to the leading edge and is free to deflect in the plane and normal to the plane of the main wing structure. A parametric analysis of thermal deflections is shown in table 21-14. A summary of thermal strains from the plane strain analysis is shown in tables 21-15, 21-16, and 21-17. Before the plane-strain data can be used for the evaluation of low cycle fatigue, it is necessary to account for end effects which will be considered next.

To account for secondary thermal stress (or strain) near the stress free end of the segmented leading edge, the procedure presented in reference 21-4 was used. In this procedure, a self-equilibrating force group is applied to the end of the structure to liquidate the elementary stresses (section 7, case one, bending about two axes and axial loading) and so satisfy the boundary conditions for stress. The rate of decay of this force group is determined by a minimum energy principle. The problem is made as simple as possible by assuming that the temperature distribution over a cross-section does not vary along the length of the leading edge segment and that the segment contains closely spaced rigid ribs. The notations and sign conventions of figure 21-8 apply.

The force in any discrete element is assumed to be the product of a function of the cross section times a function of x

$$(\sigma A)_{x,j} = (\sigma A)_j \phi(x)$$

The distribution of $(\sigma A)_j$ is given by the elementary analysis.

The shear flow around the section is

$$q_{x,j} = q_j \frac{d}{dx}\left[\phi(x)\right]$$

where q_j is the shear flow determined from an elementary analysis in which the assumption is made that

$$\frac{\Delta(\sigma A)_{x,j}}{\Delta x} = (\sigma A)_j$$

The decay function $\phi(x)$ can be determined from the principle of minimum complementary energy. The total strain energy can be expressed in terms of ϕ as follows:

$$U = \frac{1}{2}\sum_j \left(\frac{\sigma^2 A}{E}\right)_j \int_0^\ell \phi^2 dx + \frac{1}{2}\sum_j \left(\frac{q^2 b}{Gt}\right)_j \int_0^\ell \left(\frac{d\phi}{dx}\right)^2 dx$$

The variation of the strain energy is then determined and set equal to zero; the result is

$$\delta U = \int_0^\ell \left[\phi \sum_j \left(\frac{\sigma^2 A}{E}\right)_j - \frac{d^2\phi}{dx^2}\sum_j \left(\frac{q^2 b}{Gt}\right)_j\right] \delta\phi \, dx + \sum_j \left(\frac{q^2 b}{Gt}\right)_j \left[\frac{d\phi}{dx}\,\delta\phi\right]_0^\ell = 0$$

The strain energy is a minimum if ϕ satisfies the following differential equation:

$$\frac{d^2\phi}{dx^2} - K^2\phi = 0$$

where

$$K^2 = \frac{\sum_j \left(\frac{\sigma^2 A}{E}\right)_j}{\sum_j \left(\frac{q^2 b}{Gt}\right)_j}$$

With the coordinate system of figure 21-8 and a segment of length 2ℓ, the following solution of the differential equations satisfies the boundary conditions of $\frac{d\phi}{dx} = 0$ when $x = 0$ and $\phi = 1$ when $x = \ell$:

$$\phi = \frac{\cosh Kx}{\cosh K\ell}$$

The reduction in thermal strain at the center of the leading edge segment is shown in figure 21-9 for concept I-A-1 of table 21-12. These results show that thermal stresses for short segments are considerably different from those predicted by elementary theory. Experimental evidence supporting this conclusion is given in reference 21-5 based on tests of ring stiffened cylinders.

The least weight insulated concept, I-A-1 of table 21-12 was selected as the best segmented leading concept and was further evaluated as indicated in the section on low cycle fatigue.

Low Cycle Fatigue

The method of analysis presented in this section is based on the Manson theory of low cycle fatigue (ref. 21-6). While it is recognized that this method of analysis is not precise, it will yield reasonable estimates of cyclic life based on very limited data. In this method, the relation between total strain and cyclic life is separated into plastic and elastic components which can be represented as straight lines on log paper. Relations for the slopes and intercepts of these lines are obtained by correlation with test data for a relatively large number of materials.

The relation between plastic strain and cyclic life N_f is related to the plastic strain per cycle ϵ_p by a power law in the form

$$\epsilon_f = M N_f^{z} \tag{21-1}$$

where M and z are material constants.

The relation between elastic strain and cyclic life is:

$$\epsilon_{el} = \frac{G}{E} N_f^{\gamma} \tag{21-2}$$

where ϵ_{el} is the elastic-strain range per cycle corresponding to the cyclic life N_f, E is the elastic modulus, and G and γ are other material constants.

The relation between total strain range and cyclic life is

$$\Delta\epsilon = \epsilon_p + \epsilon_{el} \tag{21-3}$$

$$= \epsilon_p + \frac{\Delta\sigma}{E}$$

$$= M N_f^{z} + \frac{G}{E} N_f^{\gamma}$$

where $\Delta\sigma$ is the stress range corresponding to the total strain range $\Delta\epsilon$.

Tensile ductility (in this discussion, plastic strain is taken as the "true" or "logarithmic" value, based on measurement of reduction in area in the tensile test) is given as:

$$D = \ln \frac{A_o}{A_f} = - \ln (1 - R.A.) \tag{21-4}$$

where D is the ductility, A_o and A_f are the initial and final areas of the fracture cross section in the tensile test, and R.A. is the conventional reduction in area = $(A_o - A_f)/A_o$.

Tensile fracture stress is determined by dividing the load just prior to fracture by the area measured just after fracture. An approximate relation for the fracture stress is

$$\sigma_f \approx \sigma_u (1 + D) \tag{21-5}$$

where σ_u is the ultimate tensile stress.

The correlation between plastic strain at life of 10 cycles and ductility is

$$(\epsilon_p)_{10} = 1/4\ D^{3/4} \tag{21-6}$$

The correlation of stress range at 10^5 cycles with ultimate tensile strength is

$$\frac{(\Delta\sigma)_{10^5}}{E} = 0.90\ \frac{\sigma_u}{E} \tag{21-7}$$

The correlation of stress range at 1/4 cycle with fracture stress is

$$(\Delta\epsilon_{el})_{1/4} = \frac{\Delta\sigma}{E}\ 1/4 = 2.5\ \frac{\sigma_f}{E} \tag{21-8}$$

The correlation of elastic and plastic strain components at 10^4 cycles is

$$(\epsilon_p)_{10^4} = \frac{0.0132 - (\Delta\epsilon_{el})_{10^4}}{1.91} \tag{21-9}$$

Relations between total strain and cyclic life involving ductility, ultimate tensile strength, and fracture stress are presented as follows: The two lines constituting elastic and plastic components of strain range can be determined by using relations involved in equations (21-1) through (21-9). The two components then yield the total strain range in terms of cyclic life and properties determined from the uniaxial tensile test. These relations for M, z, G and γ in terms of D, σ_u, and σ_f are given as follows:

$$\epsilon = \epsilon_{el} + \epsilon_p = \frac{G}{E} N_f^{\gamma} + M N_f^{z} \tag{21-10}$$

where

$$G = \frac{9}{4}\sigma_u\left(\frac{\sigma_f}{u}\right)^{0.9} \tag{21-11}$$

$$\gamma = -0.083 - 0.166 \log\left(\frac{\sigma_f}{\sigma_u}\right) \tag{21-12}$$

$$M = 0.827\ D\left[1 - 82\left(\frac{\sigma_u}{E}\right)\left(\frac{\sigma_t}{\sigma_u}\right)^{0.179}\right]^{-1/3} \tag{21-13}$$

$$z = -0.52 - 1/4 \log D + 1/3 \log\left[1 - 82\left(\frac{\sigma_u}{E}\right)\left(\frac{\sigma_f}{\sigma_u}\right)^{0.179}\right] \tag{21-14}$$

Comparisons of predicted total strain to measured total strain on a relatively large number of materials, show that the method can be made predominantly conservative by dividing the predicted strain by a scatter factor of 1.5.

The effect of mean strain is shown in figure 21-10 which indicates the situation which develops when the completely reversed stress exceeds the yield strength, (ref. 21-6.) A mean strain develops during the first cycle (or early cycles) and is followed by a repetitive cyclic-strain range $\Delta\epsilon$, of which ϵ_p is the plastic strain per cycle. Since the plastic strain is cyclic, the mean stress becomes equal to zero, the magnitude of the tensile stress equal to the compressive stress. Since σ represents the stress for one occurrence, it is evident that:

one cycle = 2 occurrences

The effect of complex loading is based on the Palmgren-Miner theory of linear cumulative fatigue damage (ref. 21-7). The basic equation is

$$\frac{n_1}{N_1} + \frac{n_2}{N_2} + \ldots + \frac{n_k}{N_k} = 1 \tag{21-15}$$

where

n_i = number of loading cycles applied at the i^{th} stress level

N_i = number of loading cycles to failure for the i^{th} stress level from the relevant constant life diagram

$\frac{n_i}{N_i}$ = cycle ratio

K = number of stress levels considered

Since the number of cycles n_1, n_2, . . ., at each stress level is known, the proportion α of the total life that will be consumed at each stress level can be determined. Thus, if N is the resultant life

$$n_1 = \alpha_1 N,\ n_2 = \alpha_2 N,\ \ldots,\ n_k = \alpha_k N$$

substitution in equation (21-15) gives

$$\frac{\alpha_1}{N_1} + \frac{\alpha_2}{N_2} + \ldots + \frac{\alpha_k}{N_k} = \frac{1}{N} \qquad (21\text{-}16)$$

This equation can be written (ref. 21-8)

$$N = \frac{1}{\frac{\alpha_1}{N_1} + \frac{\alpha_2}{N_2} + \ldots + \frac{\alpha_k}{N_k}} \qquad (21\text{-}17)$$

The relation between the total strain range and cyclic life of TD NiCr shown in figure 21-11 was obtained from computer program using equations (21-10 through (21-14). The figure shows that temperatures between 1600 to 2400°F have practically no influence on the low cycle fatigue of TD NiCr. This behavior indicates that the plastic component of the total strain range has a dominant effect on the low cycle fatigue strength of TD NiCr between 1 and 10^5 cycles. The plastic strain component depends on ductility, which is constant (R.A. = 5 percent) in the range between 1600 to 2400°F for TD NiCr.

The results of the low cycle fatigue evaluation for the selected continuous and segmented leading edge concepts are shown in table 21-18. A fatigue equality index, $K_Q = 2.0$, was applied to the limit elastic thermal strain. A nominal scatter factor of 1.5 was applied to the low cycle fatigue strain allowable. For the cumulative fatigue damage analysis, -0.5-g and 2.0-g conditions are assumed to occur for one of ten flights. Because of high thermal strains, the low cycle fatigue life of the continuous leading edge concept is only 12 flights. However, for a segment length of 20.0 inches (optimum length as discussed later), the thermal strains for the segmented leading edge concept were reduced to very low values. Thus, low cycle fatigue life for the segmented leading edge concept is very large, and far exceeds the required vehicle life of 8110 flights or 10 000 hours.

Selection of Leading Edge Geometry

Because of the high thermal strains of the continuous concept, the low-cycle fatigue life was below the acceptable level, thereby requiring early replacement. However, the maximum thermal strains at the nose of the segmented leading-edge segment are quite low, and fatigue life substantially exceeds the requirement of 8110 flights. Therefore, the length of the segmented leading edge was optimized by considering the weight, strength, performance, and aerodynamic heating. Since proportions of the segmented leading-edge cross-section (nose thickness of 0.125 inch and flat thickness of 0.030 inch) were selected to enable use of TD NiCr rather than coated refractory metal to minimize weight and thermal stresses, the optimum segment length was determined by holding cross-section dimensions constant and varying only the length.

Maximum stresses and deflections due to pressure occur on the lower surface of the leading edge segment at the aft edge support member. Attachment fittings are located at 20.7 percent of the segment length to minimize bending moments in the aft end of the leading edge segment. Maximum segment length based on ultimate strength is 20.0 inches. Based on the pressure loading for the +2.0-g condition, the maximum bending stress is 11 863 psi (ultimate). The corresponding temperature $T = 2000^{\circ}F$ and ultimate strength $F_{tu} = 12\ 000$ psi.

Performance evaluation of the segmented leading edge was based on fuel increments due to the expansion joint between segments, attachment screws, joint between leading edge segment and adjacent heat shields on wing panels, and overall deflection of the leading edge segment under thermal and pressure loading. For example, for a segment length of 20.0 inches, the maximum overall deflections (see fig. 21-12) on the upper and lower surfaces for the cruise condition were 0.022 inch (inward) and 0.120 inch (inward), respectively.

At the nose of the leading edge segment, the overall outward deflection was 0.053 inch. Difference in thermal expansion parallel to the leading edge for the +2.0-g and cruise conditions leaves a net gap between segments of 0.075 inch during cruise (not considering deformation of adjacent wing structure.)

As shown in figures 21-13 and 21-14, the optimum lengths of the leading-edge segments for the monocoque and semimonocoque concepts (based on minimum structural weight and drag penalty) were 20.0 inches and 22.5 inches, respectively. However, consideration of ultimate strength limits the semimonocoque segment length to 20.0 inches, and this length was selected. The drag penalty (fuel increment due to deflections, joints, and fasteners) shown is based on an equivalance between fuel and structure weight of 1.5 to 1.0, respectively. This ratio was determined from results of the vehicle-performance interaction evaluation. Since fewer attachment fittings are required, the weight of the leading-edge segment decreases with increasing segment length.

Additional aerodynamic heating occurs because of local changes in flow angle resulting from the segmented leading-edge distortions. For example, based on a leading edge segment length of 20.0 inches, forward deflection of the segmented leading edge stagnation line increases stagnation temperature by 15°F. Net inward deflection at the center of the lower surface aft edge of the segment due to pressure and thermal effects for the +2.0-g condition decreases the temperature 80°F. Corresponding net deflection of the extreme ends of the aft lower surface of the loading edge is outward relative to the wing reference surface, and the local temperature is increased 70°F.

SUMMARY OF DESIGN AND WEIGHT DATA

A summary of design and weight data for the selected continuous and segmented leading-edge concepts is shown in table 21-19. Because of the high thermal strains, the low cycle fatigue life of the continuous leading edge is very deficient (only 12 flights). The selected segment length of 20 inches leads to low strains and long life for the segmented leading edge. As shown, unit weights for the continuous and segmented leading edges are 8.31 lb/ft^2 and 4.89 lb/ft^2, respectively. The unit weights include insulation and the effects of oxidation.

The nose section of the continuous leading edge structures (figure 21-15) used in detailed analyses is machined from bar stock and the flats are formed from sheet and attached to the nose section with flush rivets. The nose assembly is attached to the main wing structure with brackets located between the heat-shield beads. The attachment brackets are spotwelded to the leading edge spar cap on one side and fastened to the removable leading edge assembly with screws on the other side. Sealed, nonslip, overlapping joints are provided between the leading edge and heat shield and also between the relatively long segments. Washout of the heat-shield corrugations, carried into the flats of the leading edge to relieve compressive thermal strains, are symmetrical about a median contour to minimize aerodynamic drag and local heating.

The integrally stiffened nose section of the segmented leading edge, shown in figure 21-16 is chem-milled from 0.125 inch sheet prior to forming. The removable leading edge is screw-attached to the main wing structure hinges. Overlapping joints are provided between the leading edge and heat shield and

also between adjoining segments. Experiments to determine the effect of hot air leakage through the lap joints are warranted. Heat-shield corrugations are washed out adjacent to the leading edge joint. This approach results in maximum uniformity and also reduces the cost of the leading edge.

The segmented leading edge was selected for final design primarily because it met the desired life requirements without refurbishment, assuming hot air leakage proves to be insignificant. Additionally, it was lower in weight than the continuous design, as shown in table 21-19.

The total weight of the leading edge for the entire wing is:

Primary structure	Leading edge weight, lb
Monocoque	1700
Semimonocoque	1956
Statically determinate	1956

REFERENCES

21-1 NASA Space Vehicle Design Criteria, Buckling of Thin-Walled Circular Cylinders, NASA SP-8007, September 1965.

21-2 Timoshenko, Stephen P.; and Gere, James M.: Theory of Elastic Stability, Second Ed., McGraw-Hill Book Co., Inc., 1961.

21-3 Personal Communication, L. Sama, Sylvania to J. W. Lewis, Lockheed-California Co., October 1967

21-4 Heldenfels, R. R.: The Effect of Nonuniform Temperature Distributions on the Stresses and Distortions of Stiffened-Shell Structures. NACA TN 2240, November 1950.

21-5 Anderson, M. S.; and Card, M. F.: Buckling of Ring-Stiffened Cylinders Under A Pure Bending Moment and A Nonuniform Temperature Distribution. NASA TN D-1513, November 1962.

21-6 Manson, S. S.: Thermal Stress and Low-Cycle Fatigure. McGraw Hill Book Company, 1966.

21-7 Lockheed-California Company, Structural Life-Assurance Manual, SLM No. 4, Methods of Fatigue Analysis.

21-8 Spotts, M. F.: Design For Expected Life. Product Engineering, 7 June 1965.

TABLE 21-1

LEADING EDGE PRESSURES

Area \ Load condition	Limit pressure, psi		
	-0.5g	2g	Cruise
Nose	2.25	3.25	0.93
Internal	0.30	0.35	0.10
Upper surface	0.20	0.08	0.02
Lower surface	0.0	0.88	0.54

TABLE 21-2

LEADING-EDGE DESIGN PRESSURES

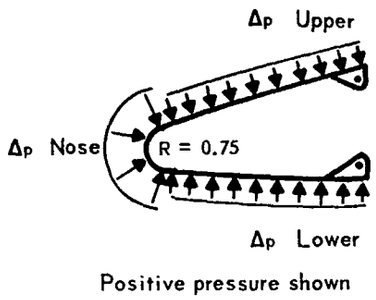

Positive pressure shown

Surface \ Condition	Limit Δp, psi		
	-0.5-g	2.0-g	Cruise
Δp Nose	1.95	2.9	0.83
Δp Upper	-0.1	-0.27	-0.08
Δp Lower	-0.3	0.53	0.44

TABLE 21-3

MONOCOQUE LEADING EDGE EVALUATION, CONTINUOUS HOT LOAD CARRYING CONCEPT WITHOUT LEADING EDGE SPAR, +2.0-g MANEUVER CONDITION

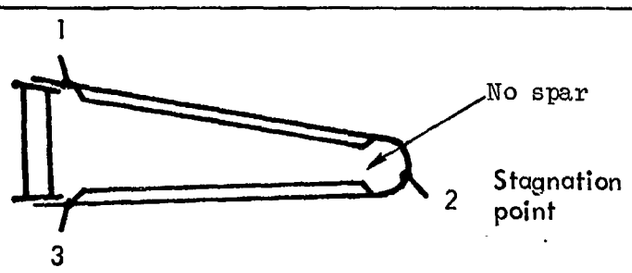

Node point	Material (a)	Mean linear thermal coefficient of expansion, $\alpha \times 10^{-6}$, in./in./^{o}F	Elastic modulus, E x 10^{6} psi	Temperature, ^{o}F	Limit elastic thermal stress, σ_t, ksi	Limit elastic thermal strain, ϵ_t, in./in.
1	Ta-10W	3.68 x 10^{-6}	20.2 x 10^{6}	1612	107	0.00530
2	Ta-10W	3.96	13.3	2304	28.6	0.00215
3	Ta-10W	3.76	18.9	1789	85.8	0.00454
1	TD NiCr	8.6	11.8	1575	-18.8	-0.00159
2	TD NiCr	8.72	5.6	2176	-39.1	-0.00699
3	TD NiCr	8.65	10.0	1715	-28.5	-0.00285

[a] Emissivity of TD NiCr assumed to be 0.9

TABLE 21-4

MONOCOQUE LEADING EDGE EVALUATION, CONTINUOUS HOT LOAD CARRYING CONCEPT INCLUDING LEADING EDGE SPAR, +2.0-g MANEUVER CONDITION

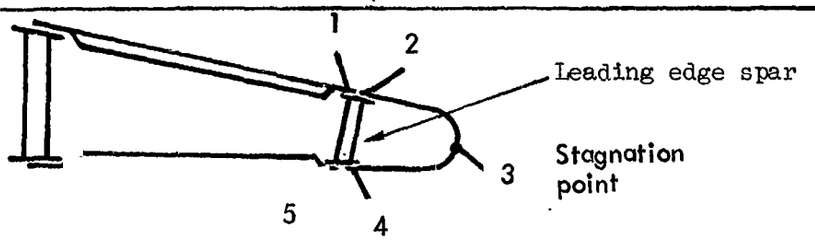

Node point	Material (a)	Mean linear thermal coefficient of expansion, $\alpha \times 10^{-6}$ in./in./^{o}F	Elastic modulus, E x 10^{6} psi	Temperature, ^{o}F	Limit elastic thermal stress, σ_t, ksi	Limit elastic thermal strain, e_t, ksi
1	TD NiCr	8.65 x 10^{-6}	10.0 x 10^{6}	1711	-29.8	-0.00298
2	Ta-10W	3.73	19.6	1711	98.8	0.00504
3	Ta-10W	3.97	13.2	2308	30.2	0.00229
4	Ta-10W	3.81	17.9	1888	76.1	0.00425
5	TD NiCr	8.65	8.0	1888	-36.0	-0.00450
1	Td NiCr	8.65	10.5	1682	-27.0	-0.00257
2	TD NiCr	8.65	10.5	1682	-27.0	-0.00257
3	TD NiCr	8.73	5.4	2207	-39.3	-0.00728
4	TD NiCr	8.65	8.4	1863	-34.7	-0.00413
5	TD NiCr	8.65	8.4	1863	-34.7	-0.00413
1	TD NiCr	8.65	10.2	1702	-29.1	-0.00285
2	Cb-752	4.33	12.1	1702	50.3	0.00416
3	Cb-752	4.53	10.4	2290	12.2	0.00117
4	Cb-752	4.40	11.9	1879	39.0	0.00328
5	TD NiCr	8.65	8.2	1879	-35.8	-0.00437

[a] Emissivity of TD NiCr assumed to be 0.9

TABLE 21-5

SPANWISE SEMIMONOCOQUE LEADING EDGE EVALUATION, CONTINUOUS HEAT SHIELDED AND INSULATED CONCEPT; NOSE THICKNESS = 0.12 IN., +2.0-g MANEUVER CONDITION

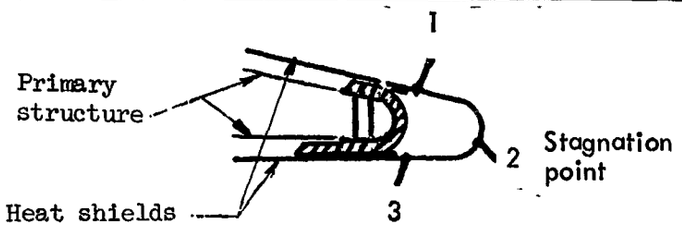

Node point	Material	Mean linear thermal coefficient of expansion, $\alpha \times 10^{-6}$ in./in./^{o}F	Elastic modulus, E x 10^{6} psi	Temperature, ^{o}F	Limit elastic thermal stress, σ_t, ksi	Limit elastic thermal strain, ϵ_t, in./in.
1	Ta-10W	3.70 x 10^{-6}	20.0 x 10^{6}	1654	88.2	0.00441
2	Ta-10W	3.98	12.0	2339	16.2	0.00125
3	Ta-10W	3.87	16.4	2025	44.5	0.00271
1	Cb-752	4.32	12.2	1648	42.1	0.00345
2	Cb-752	4.54	10.2	2311	0.978	0.0000959
3	Cb-752	4.44	11.7	2002	19.8	0.00169

TABLE 21-6

DETAIL TEMPERATURES FOR HEAT-SHIELDED AND INSULATED LEADING EDGE CONCEPT; NOSE THICKNESS = 0.125 IN.

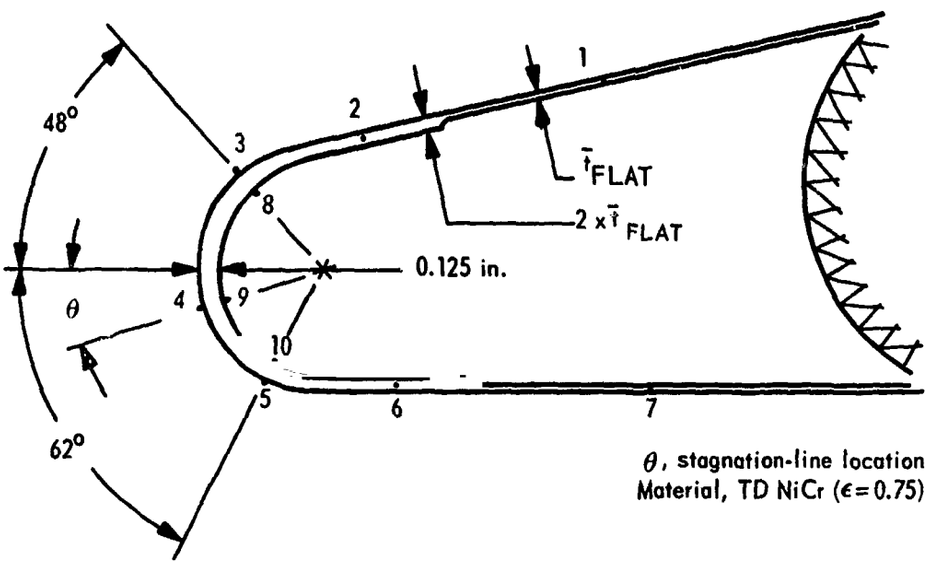

Thermal model of cross-section normal to leading-edge sweep

Temp location \ Condition	Temperature, °F					
	-0.5-g		+2.0-g		Cruise	
$\bar{t}$ FLAT, in.	0.03	0.06	0.03	0.06	0.03	0.06
T(1)	1925	1860	1795	1785	1340	1340
T(2)	1940	1890	1875	1865	1480	1495
T(3)	1975	1960	2005	1985	1625	1615
T(4)	2055	2045	2200	2190	1795	1790
T(5)	1920	1910	2135	2115	1770	1760
T(6)	1845	1860	2065	2015	1630	1645
T(7)	1765	1770	2025	1985	1515	1515
T(3) − T(8)	5	5	0	0	0	0
T(4) − T(9)	10	10	10	10	5	5
T(5) − T(10)	0	0	5	5	5	5

TABLE 21-7

DETAIL TEMPERATURES FOR HEAT-SHIELDED AND INSULATED LEADING EDGE CONCEPT; NOSE THICKNESS = 0.375 IN.

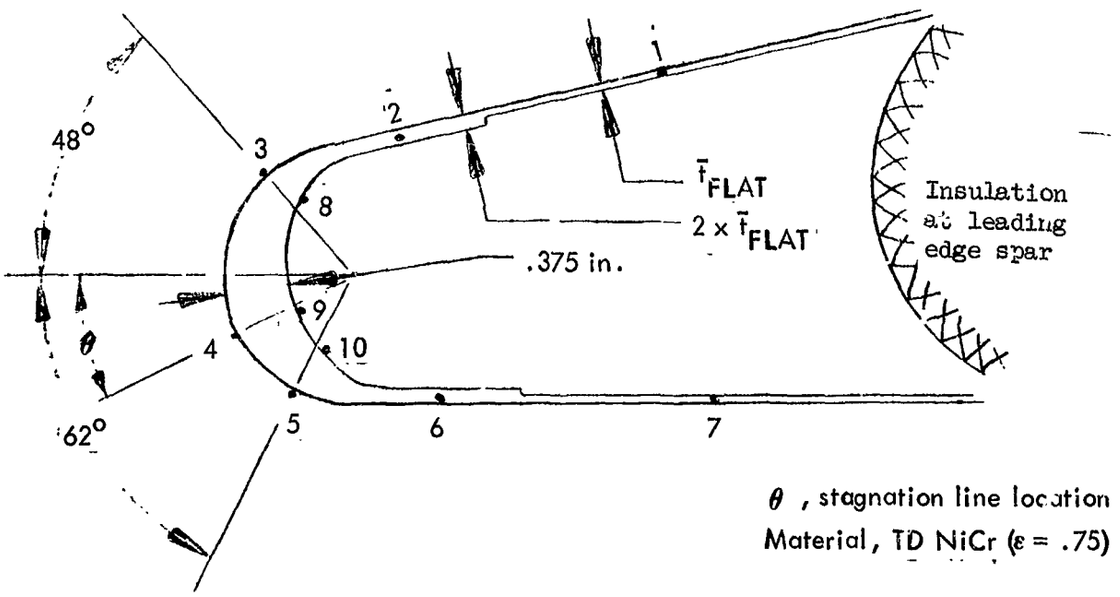

θ , stagnation line location

Material, TD NiCr (ε = .75)

Cross section normal to leading edge sweep

Condition / Temp location — $\bar{t}_{FLAT}$, in.	Temperature, °F					
	-0.5g		2.0g		Cruise	
	.03	.06	.03	.06	.03	.06
T(1)	1920	1855	1780	1775	1335	1335
T(2)	1935	1885	1860	1855	1495	1515
T(3)	1955	1940	1985	1970	1675	1660
T(4)	2000	1990	2100	2090	1770	1760
T(5)	1925	1915	2070	2055	1760	1750
T(6)	1840	1850	2045	2000	1630	1640
T(7)	1760	1765	2015	1975	1515	1515
T(3) - T(8)	10	5	0	0	-5	-5
T(4) - T(9)	25	25	40	40	20	20
T(5) - T(10)	-5	-5	15	15	5	5

TABLE 21-8

DETAIL TEMPERATURES FOR HEAT-SHIELDED AND INSULATED LEADING EDGE CONCEPT; NOSE THICKNESS = 0.625 IN.

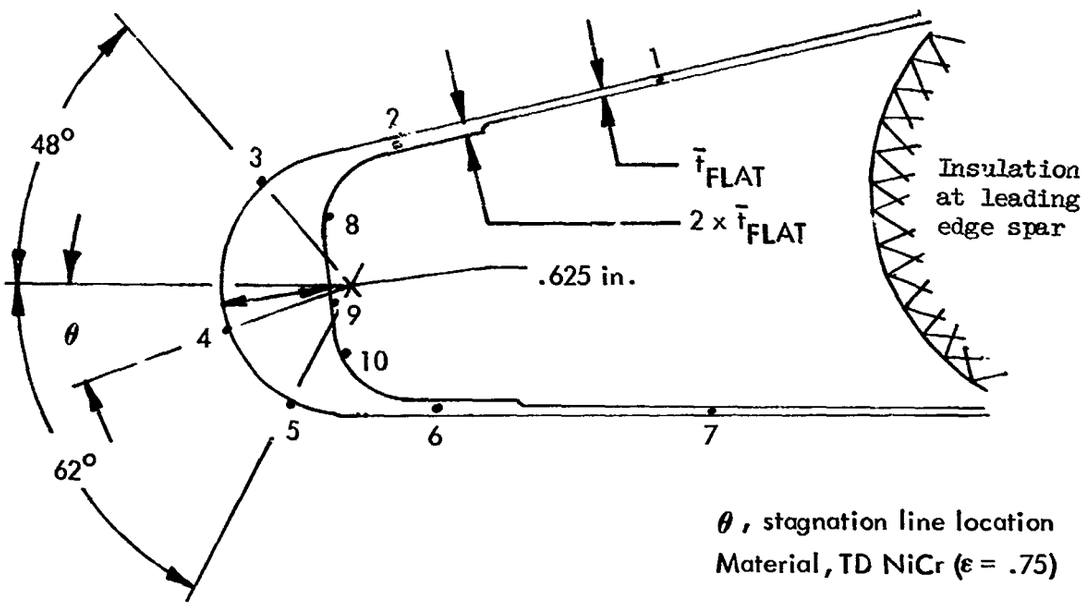

θ, stagnation line location

Material, TD NiCr (ε = .75)

Cross section normal to leading edge sweep

Temp location \ Condition	Temperature, °F					
	-0.5g		2.0g		Cruise	
$\bar{t}_{FLAT}$, in	.03	.06	.03	.06	.03	.06
T(1)	1920	1850	1775	1770	1335	1335
T(2)	1930	1875	1850	1845	1500	1520
T(3)	1940	1925	1965	1950	1690	1680
T(4)	1970	1965	2060	2050	1765	1755
T(5)	1910	1900	2035	2020	1755	1745
T(6)	1835	1840	2035	1990	1630	1640
T(7)	1755	1765	2015	1975	1515	1515
T(3) - T(8)	15	15	0	0	-10	-10
T(4) - T(9)	40	45	65	65	30	30
T(5) - T(10)	-5	-5	25	25	10	10

TABLE 21-9

CONTINUOUS LEADING EDGE EVALUATION MATRIX

I. Monocoque leading edge evaluation:
(Nose thickness = 0.12 in.; Flat thickness = 0.032 in.)

A. Hot load carrying concept without nose beam

1. Nose section material: Ta-10W
2. Nose section material: TD NiCr[a]

B. Hot load carrying concept with nose beam

1. Nose section material: Ta-10W
2. Nose section material: TD NiCr[a]
3. Nose section material: Cb-752

II. Spanwise semimonocoque leading edge evaluation:

A. Heat shielded and insulated concept
(Nose thickness = 0.06 in.; flat thickness = 0.06 in.)

1. Nose section material: Ta-10W
2. Nose section material: Cb-752

B. Heat shielded and insulated concept
(Nose thickness = 0.625 in.; flat thickness = 0.060 in.)

1. Nose section material: TD NiCr[b]

[a] Emissivity = 0.90

[b] Emissivity = 0.75

TABLE 21-10

SPANWISE SEMIMONOCOQUE LEADING EDGE EVALUATION, CONTINUOUS HEAT SHIELDED AND INSULATED CONCEPT; NOSE THICKNESS = 0.625 IN., FLAT THICKNESS = 0.060 IN.

Load condition	Node point	Material (a)	Mean linear thermal coefficient of expansion, $\alpha \times 10^{-6}$, in./in./°F	Elastic modulus E x 10^6, psi	Temperature, °F	Limit elastic thermal stress, σ_t, psi	Limit elastic thermal strain, ϵ_t, in./in.
0.5g	1	TD NiCr	8.66 x 10^{-6}	8.5 x 10^6	1850	0	- - - - -
	2		8.67	8.2	1876	-45,650	-.005566
	3		8.68	7.7	1926	-45,930	-.005965
	4		8.69	7.3	1964	-46,450	-.006363
	5		8.67	7.9	1900	-45,510	-.005761
	6		8.66	8.6	1842	-45,240	-.005260
	7		8.65	9.5	1763	0	- - - - -
2g	1		8.65	9.4	1770	0	- - - - -
	2		8.66	8.5	1845	-38,880	-.004574
	3		8.68	7.4	1950	-41,230	-.005572
	4		8.70	6.5	2050	-42,060	-.006470
	5		8.70	6.8	2020	-42,620	-.006268
	6		8.69	7.0	1989	-41,770	-.005967
	7		8.68	7.2	1973	0	- - - - -
Cruise	1		8.56	14.5	1335	0	- - - - -
	2		8.60	12.5	1520	-40,200	-.003216
	3		8.63	10.5	1680	-48,410	-.004610
	4		8.65	9.6	1757	-50,930	-.005305
	5		8.65	9.7	1745	-50,430	-.005199
	6		8.62	11.0	1640	-46,160	-.004197
	7	TD NiCr	8.60	12.5	1515	0	- - - - -

[a] Emissivity of TD NiCr = 0.75

TABLE 21-11

SUMMARY OF CONTINUOUS LEADING EDGE DATA

Item	Continuous leading edge concept							
	I-A-1	I-A-2	I-B-1	I-B-2	I-B-3	II-A-1	II-A-2	II-B-1
Main wing primary structure concept	Waffle	Waffle	Waffle	Waffle	Waffle	Tu' r	Tubular	Tubular
Nose area material	Ta-10W	TD NiCr[a]	Ta-10W	TD NiCr[a]	Cb-752	Ta-10W	Cb-7-2	TD NiCr[b]
Nose thickness, in.	0.12	0.12	0.12	0.12	0.12	0.06	0.06	0.625
Flat thickness, in.	0.032	0.032	0.032	0.032	0.032	0.06	0.06	0.06
Maximum temperature (stagnation point, 2g condition), °F	2304	2176	2308	2207	2290	2339	2311	2050
Maximum limit elastic thermal strain, ϵ_T, in./in.	0.00530	-0.00699	0.00504	-0.00728	0.00416	0.00441	0.00345	-0.00647
Maximum depth of oxidation, δ, in./side (stagnation point, 10 000 hr vehicle life)	--	0.00165	--	0.00165	--	--	--	0.00151
Coating life, hr	Not available	--	Not available	--	500	Not available	500	--
Local buckling	--	yes	--	yes	--	--	--	no

[a]Emissivity = 0.9

[b]Emissivity = 0.75

TABLE 21-12

SEGMENTED LEADING EDGE EVALUATION MATRIX

I. Spanwise semimonocoque leading edge evaluation:

A. Heat shielded and insulated concept
(nose section material: TD NiCr[a])

1. Nose thickness = 0.125 in.; flat thickness = 0.03 in.
2. Nose thickness = 0.125 in.; flat thickness = 0.06 in.
3. Nose thickness = 0.625 in.; flat thickness = 0.06 in.

[a]Emissivity = 0.75

TABLE 21-13

SUMMARY OF SEGMENTED LEADING EDGE DATA

Item	Segmented leading edge concept		
	I-A-1	I-A-2	I-A-3
Main wing primary structure concept	Tubular	Tubular	Tubular
Nose area material	TD NiCr[a]	TD NiCr[a]	TD NiCr[a]
Nose thickness, in.	0.125	0.125	0.625
Flat thickness, in.	0.030	0.060	0.060
Maximum temperature (stagnation point, 2g condition), ^{o}F	2200	2189	2050
Maximum limit elastic thermal strain, ε_T, in./in.	-0.00244	-0.002596	+0.001990
Maximum depth of oxidation, δ, in./side (stagnation point, 10 000 hr vehicle life)	0.00165	0.00165	0.00151
Coating life, hr	-	-	-
Local buckling margin of safety	0.025	0.025	High

[a]Emissivity = 0.75

TABLE 21-14

SUMMARY OF THERMAL DEFLECTIONS, SEGMENTED LEADING EDGE CONCEPT

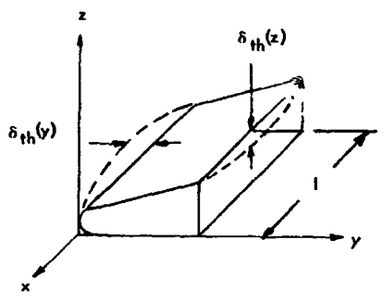

		Thermal deflection			
		t nose = .125 in., t flat = .03 in.,		t nose = .625 in., t flat = .06 in.	
Load condition	l, in.	δ_{th} (z), in.	δ_{th} (y), in.	δ_{th} (z), in.	δ_{th} (y), in.
-0.5g	10	.006	.007	.002	.006
	20	.026	.028	.009	.025
	30	.058	.063	.020	.057
2g	10	.016	.006	.013	.007
	20	.064	.037	.051	.028
	30	.144	.084	.115	.062
Cruise	10	.015	.013	.014	.014
	20	.058	.053	.056	.057
	30	.131	.119	.126	.129

TABLE 21-15

SPANWISE SEMIMONOCOQUE LEADING EDGE EVALUATION, SEGMENTED HEAT SHIELDED AND INSULATED CONCEPT; NOSE THICKNESS = 0.125 IN., FLAT THICKNESS = 0.03 IN.

Load condition	Node point	Material (a)	Mean linear thermal coefficient of expansion, $\alpha \times 10^{-6}$, in./in./°F	Elastic modulus E x 10^6, psi	Temperature, °F	Limit elastic thermal stress, σ_t, psi	Limit elastic thermal strain, ε_t, in./in.
-0.5g	1	TD NiCr	8.68 x 10^{-6}	7.7 x 10^6	1926	-2,693	-.000349
	2		8.68	7.5	1940	384	.000051
	3		8.69	7.2	1976	-2,231	-.000310
	4		8.70	6.5	2053	-12,199	-.001876
	5		8.67	7.7	1921	344	.000044
	6		8.66	8.5	1847	7,164	.000843
	7		8.65	9.5	1763	13,761	.001448
2g	1		8.65	9.1	1793	11,875	.001305
	2		8.67	8.2	1875	12,730	.001552
	3		8.69	6.9	2003	1,389	.000202
	4		8.73	5.5	2200	-13,422	-.002440
	5		8.71	5.9	2133	-4,614	-.000783
	6		8.70	6.4	2064	-171	-.000027
	7		8.70	6.7	2024	-3,212	-.000479
Cruise	1		8.56	14.5	1338	23,153	.001597
	2		8.59	12.9	1480	16,075	.001246
	3		8.62	11.1	1625	-2,036	-.000184
	4		8.66	9.1	1794	-20,795	-.002285
	5		8.65	9.4	1768	-14,797	-.001574
	6		8.62	11.0	1632	1,296	.000118
	7	TD NiCr	8.60	12.5	1514	7,260	.000581

[a]Emissivity of TD NiCr = 0.75.

TABLE 21-16

SPANWISE SEMIMONOCOQUE LEADING EDGE EVALUATION, SEGMENTED HEAT SHIELDED AND INSULATED CONCEPT; NOSE THICKNESS = 0.125 IN., FLAT THICKNESS = 0.06 IN.

Load condition	Node point	Material (a)	Mean linear thermal coefficient of Expansion, $\alpha \times 10^{-6}$, in./in./°F	Elastic modulus E x 10^6, psi	Temperature, °F	Limit elastic thermal stress, σ_t, psi	Limit elastic thermal strain, ϵ_t, in./in.
-0.5g	1	TD NiCr	8.66 x 10^{-6}	8.4 x 10^6	1859	-176	-.000021
	2		8.67	8.0	1889	1,744	.000218
	3		8.69	7.3	1961	-5,290	-.000725
	4		8.70	6.6	2046	-14,794	-.002242
	5		8.68	7.8	1912	-1,279	-.000164
	6		8.66	8.4	1858	3,038	.000362
	7		8.65	9.4	1772	9,368	.000997
2g	1		8.65	9.2	1784	10,245	.001113
	2		8.66	8.3	1867	9,624	.001160
	3		8.69	7.1	1986	-993	-.000140
	4		8.73	5.6	2189	-16,892	-.003017
	5		8.71	6.0	2114	-7,804	-.001301
	6		8.70	6.8	2015	-196	-.000029
	7		8.69	7.1	1983	-3,370	-.000474
Cruise	1		8.56	14.4	1339	21,281	.001478
	2		8.59	12.8	1494	8,945	.000699
	3		8.62	11.3	1615	-4,209	-.000373
	4		8.65	9.2	1789	-23,882	-.002596
	5		8.65	9.5	1759	-17,709	-.001864
	6		8.62	10.9	1643	-5,370	-.000493
	7	TD NiCr	8.60	12.5	1515	3,532	.000283

[a]Emissivity of TD NiCr = 0.75

TABLE 21-17

SPANWISE SEMIMONOCOQUE LEADING EDGE EVALUATION, SEGMENTED HEAT SHIELDED AND INSULATED CONCEPT; NOSE THICKNESS = 0.625 IN., FLAT THICKNESS = 0.06 IN.

Load condition	Node point	Material (a)	Mean linear thermal coefficient of expansion, $\alpha \times 10^{-6}$, in./in./°F	Elastic modulus E x 10^6, psi	Temperature, °F	Limit elastic thermal stress, σ_t, psi	Limit elastic thermal strain, ϵ_t, in./in.
-0.5g	1	TD NiCr	8.66 x 10^{-6}	8.5 x 10^6	1850	901	.000106
	2		8.67	8.2	1876	2,770	.000338
	3		8.68	7.7	1926	-2,175	-.000283
	4		8.69	7.3	1964	-7,376	-.001011
	5		8.67	7.9	1900	-158	-.000021
	6		8.66	8.6	1842	5,160	.000600
	7		8.65	9.5	1763	11,478	.001208
2g	1		8.65	9.4	1770	11,490	.001222
	2		8.66	8.5	1845	9,953	.001171
	3		8.68	7.4	1950	766	.000103
	4		8.70	6.5	2050	-7,712	-.001187
	5		8.70	6.8	2020	-1,722	-.000253
	6		8.69	7.0	1989	124	.000018
	7		8.68	7.2	1973	-3,612	-.000501
Cruise	1		8.56	14.5	1335	28,844	.001990
	2		8.60	12.5	1520	11,853	.000948
	3		8.63	10.5	1680	-6,441	-.000613
	4		8.65	9.6	1757	-13,255	-.001381
	5		8.65	9.7	1745	-8,089	-.000834
	6		8.62	11.0	1640	3,493	.000317
	7	TD NiCr	8.60	12.5	1515	9,718	.000778

[a]Emissivity of TD NiCr = 0.75

TABLE 21-18

LOW CYCLE FATIGUE EVALUATION FOR SELECTED LEADING EDGE CONCEPTS

Item		Scatter factor = 1.5	
		Continuous leading edge concept	Segmented leading edge concept
Main wing primary structure concept		S1b	S1b
Nose area material		TD NiCr	TD NiCr
Nose thickness, in.		0.625	0.125
Flat thickness, in.		0.060	0.030
Segment length, in.		-	20.0
Limit elastic thermal strain, ϵ_T, in./in.	-0.5g condition	-0.006363	-0.000616
	2g condition	-0.006470	-0.000850
	cruise condition	-0.005305	-0.000539
Leading edge life at ϵ_T, flights	-0.5g condition	8	15.0×10^5
	2g condition	6	2.4×10^5
	cruise condition	18	2.8×10^6
Total leading edge life, flights		12	11.9×10^5

[a] Including end effect

TABLE 21-19

LEADING-EDGE DESIGN AND WEIGHT DATA FOR SELECTED CONCEPTS

Item	Selected leading-edge concept	
	Continuous leading-edge concept	Segmented leading-edge concept
Nose area material	TD NiCr	TD NiCr
Nose thickness, in.	0.625	0.125
Flat thickness, in.	0.060	0.030
Segment length, in.	–	20.0
Maximum temperature, ^{o}F (stagnation point, +2-g condition)	2050	2200
Maximum limit elastic thermal strain, ϵ_T, in./in.	-0.00647	-0.000850
Maximum depth of oxidation, δ, in./side (stagnation point, 10,000-hr vehicle life)	0.00151	0.00165
Local buckling margin of safety	High	0.43
Low-cycle fatigue life, flights	12	11.9×10^5
Unit weight, lb/ft^2	8.31	4.89

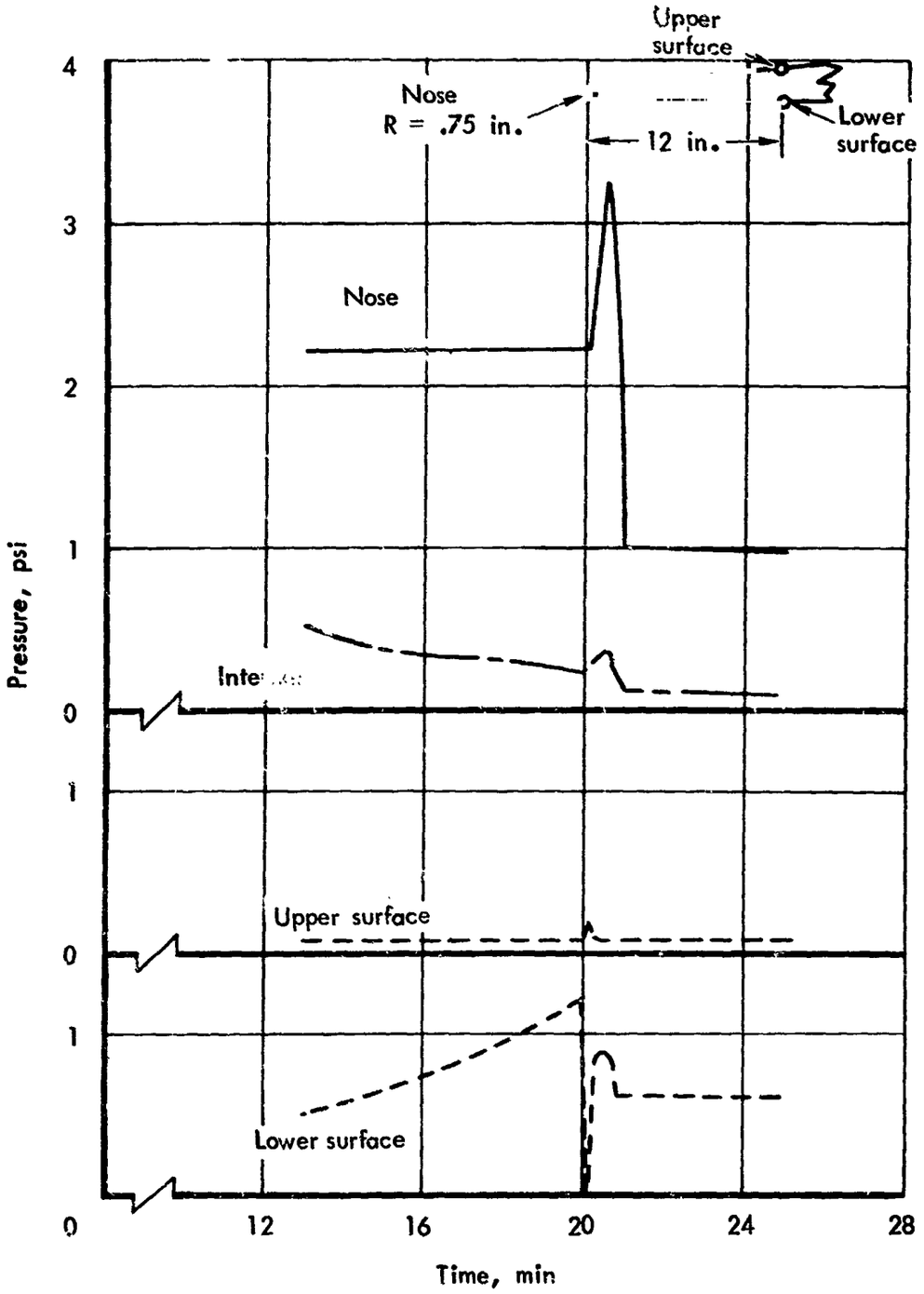

Figure 21-1. Wing leading edge pressure variations during maneuver

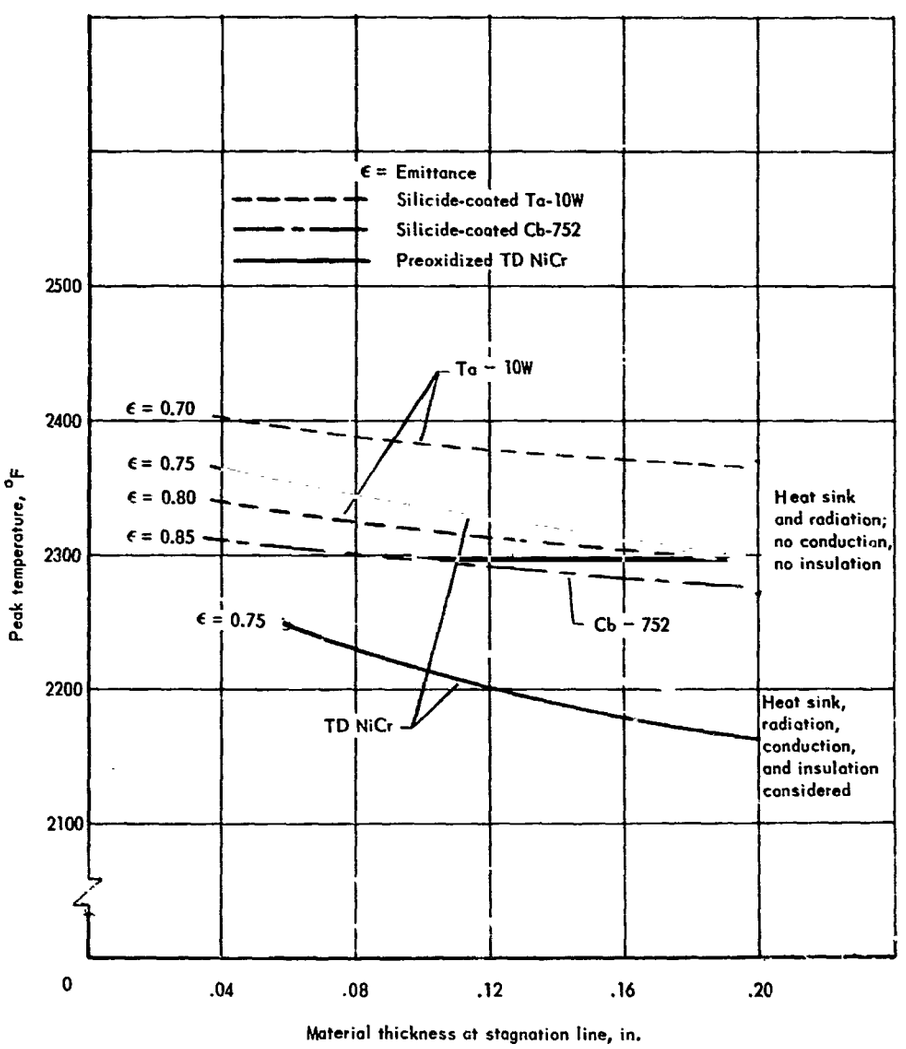

Figure 21-2. Peak temperature at leading edge stagnation line vs material thickness and emittance

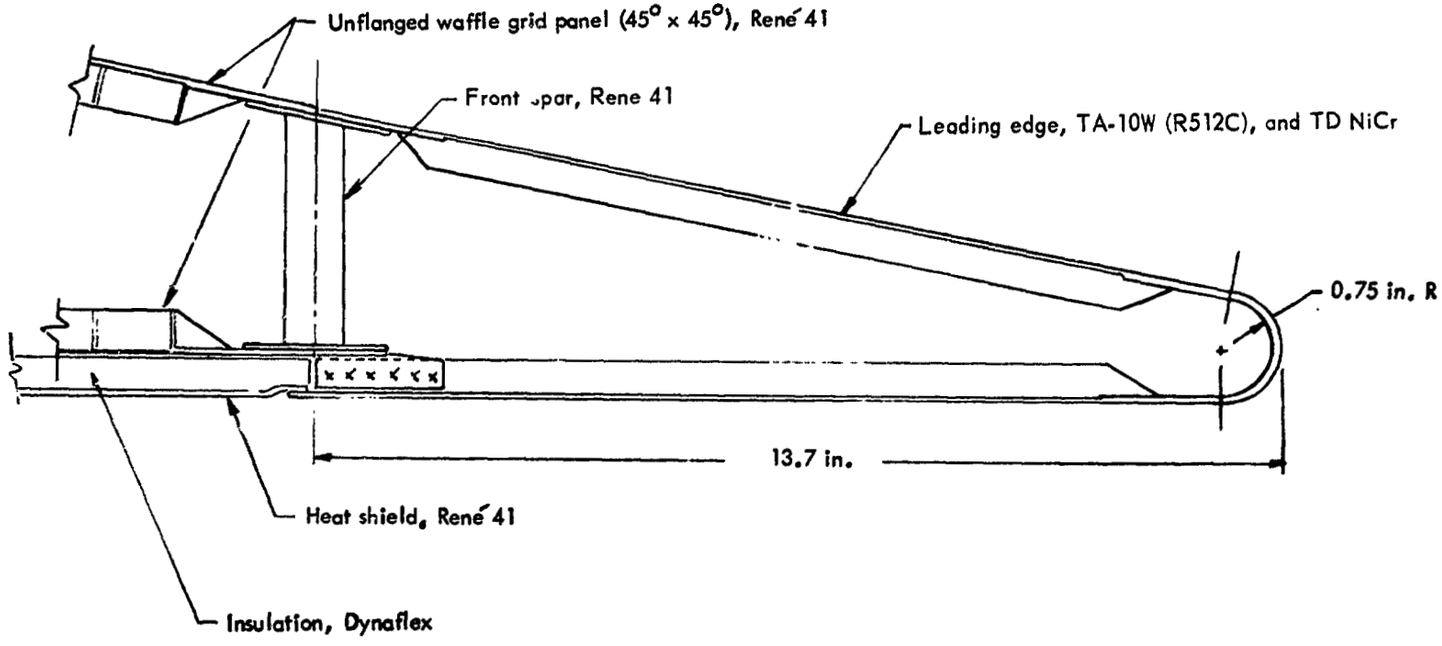

Figure 21-3. Monocoque leading edge evaluation, continuous hot load carrying concept, without leading edge spar

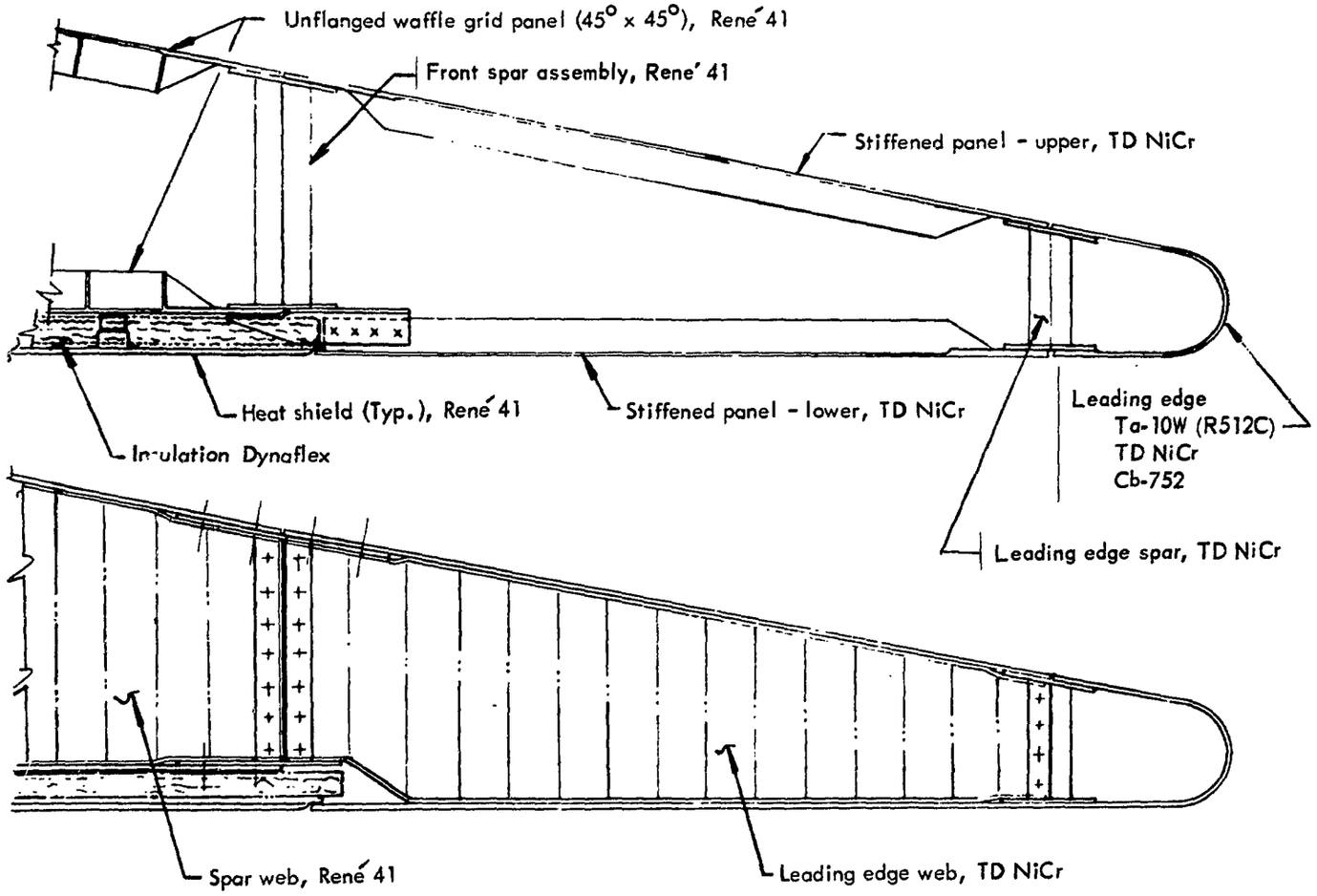

Figure 21-4. Monocoque leading edge evaluation, continuous hot load carrying concept, including leading edge spar

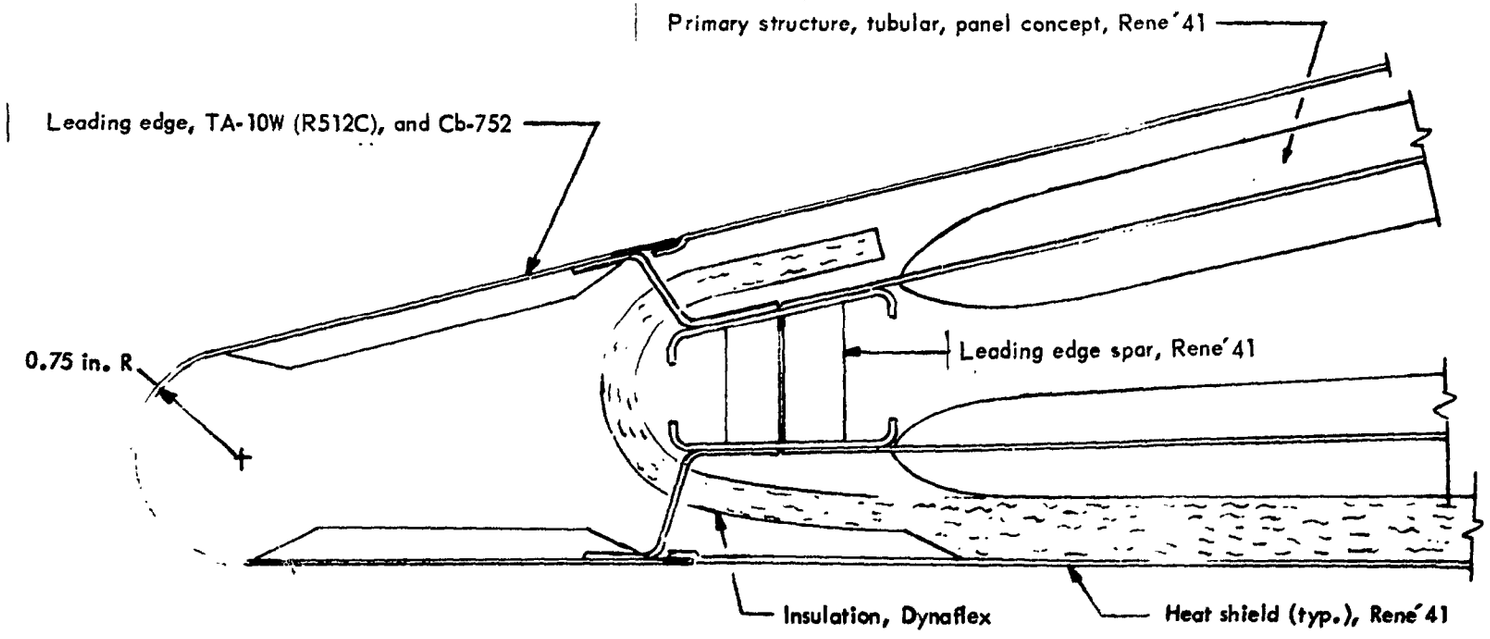

Figure 21-5. Spanwise semimonocoque leading edge evaluation, continuous heat shielded and insulated concept; leading edge

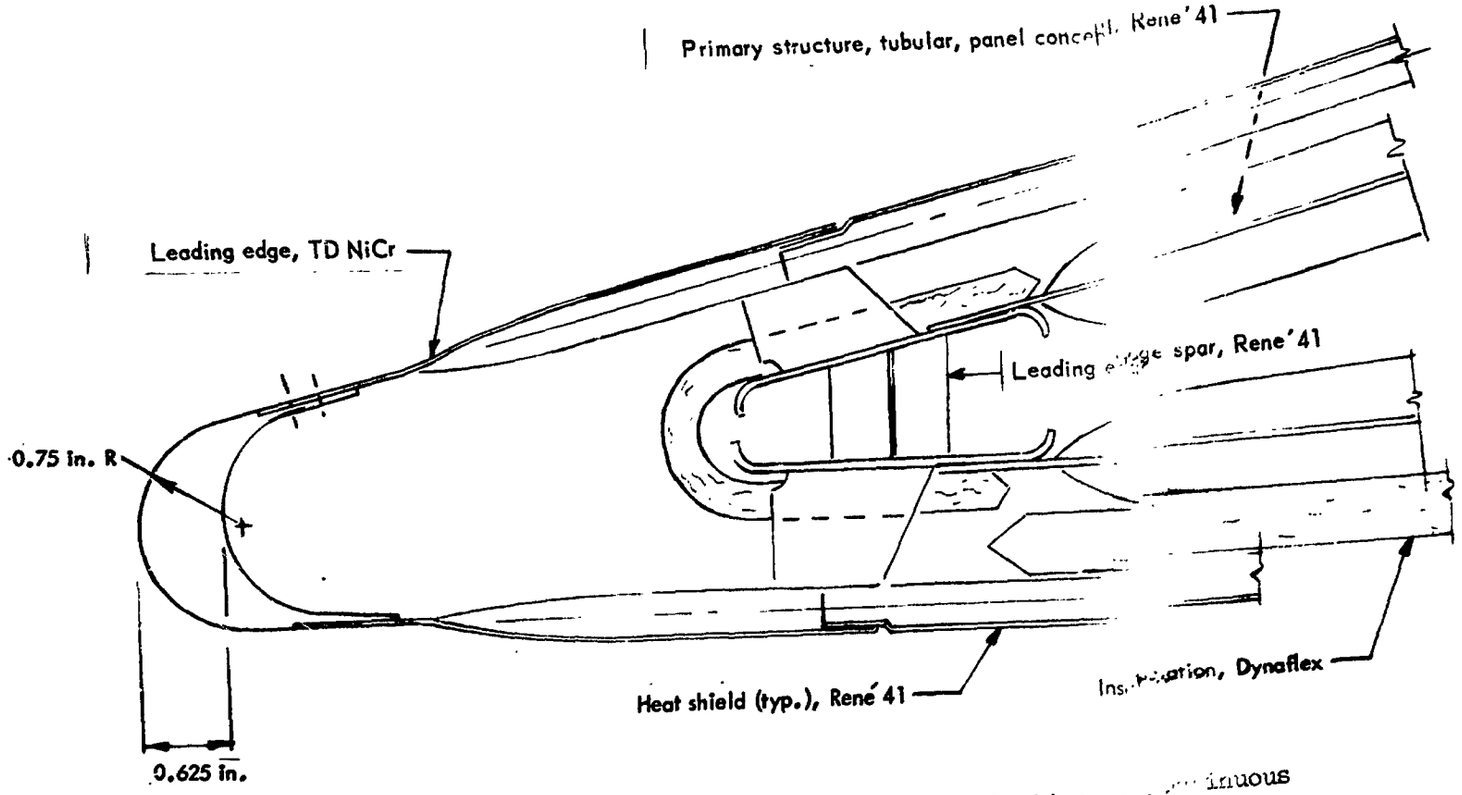

Figure 21-6. Spanwise semimonocoque lead edge evaluation, continuous heat shielded and insulated concept; leading edge thickness = 0.625 in., flat thickness 0.060 in.

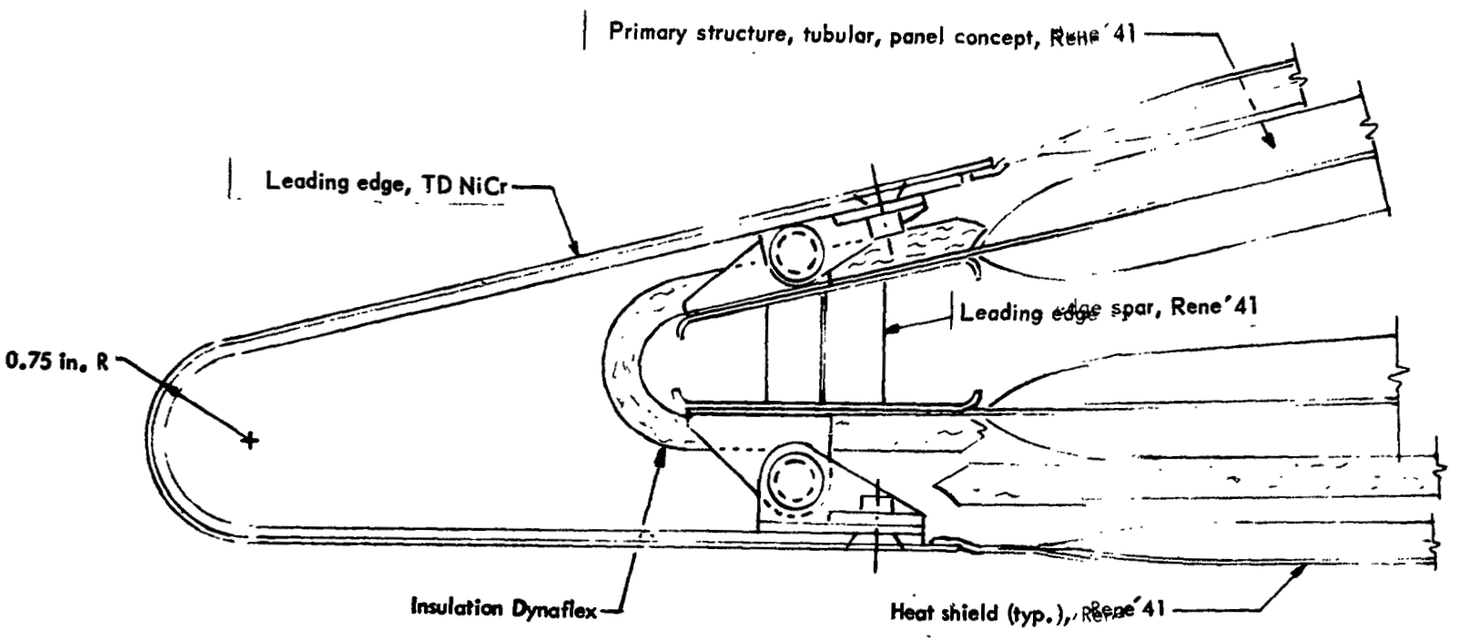

Figure 21-7. Spanwise semimonocoque leading edge evaluation, segmented heat shielded and insulated concept; leading edge thickness = 0.125 in.

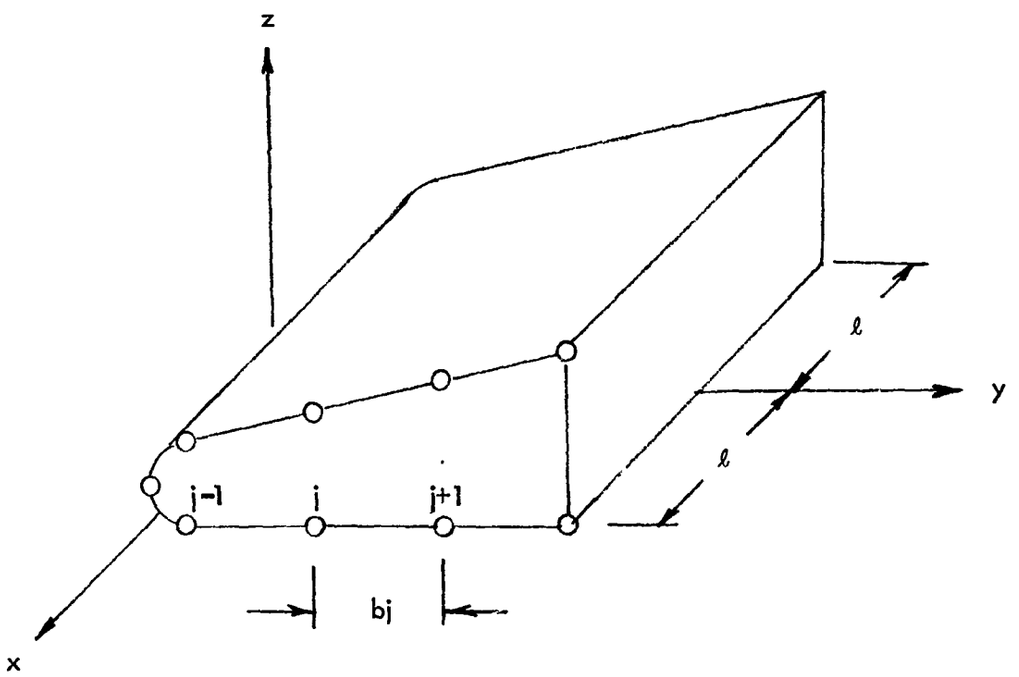

Figure 21-8. Sign conventions and notation used in analysis of the end effect for the segmented leading edge concept

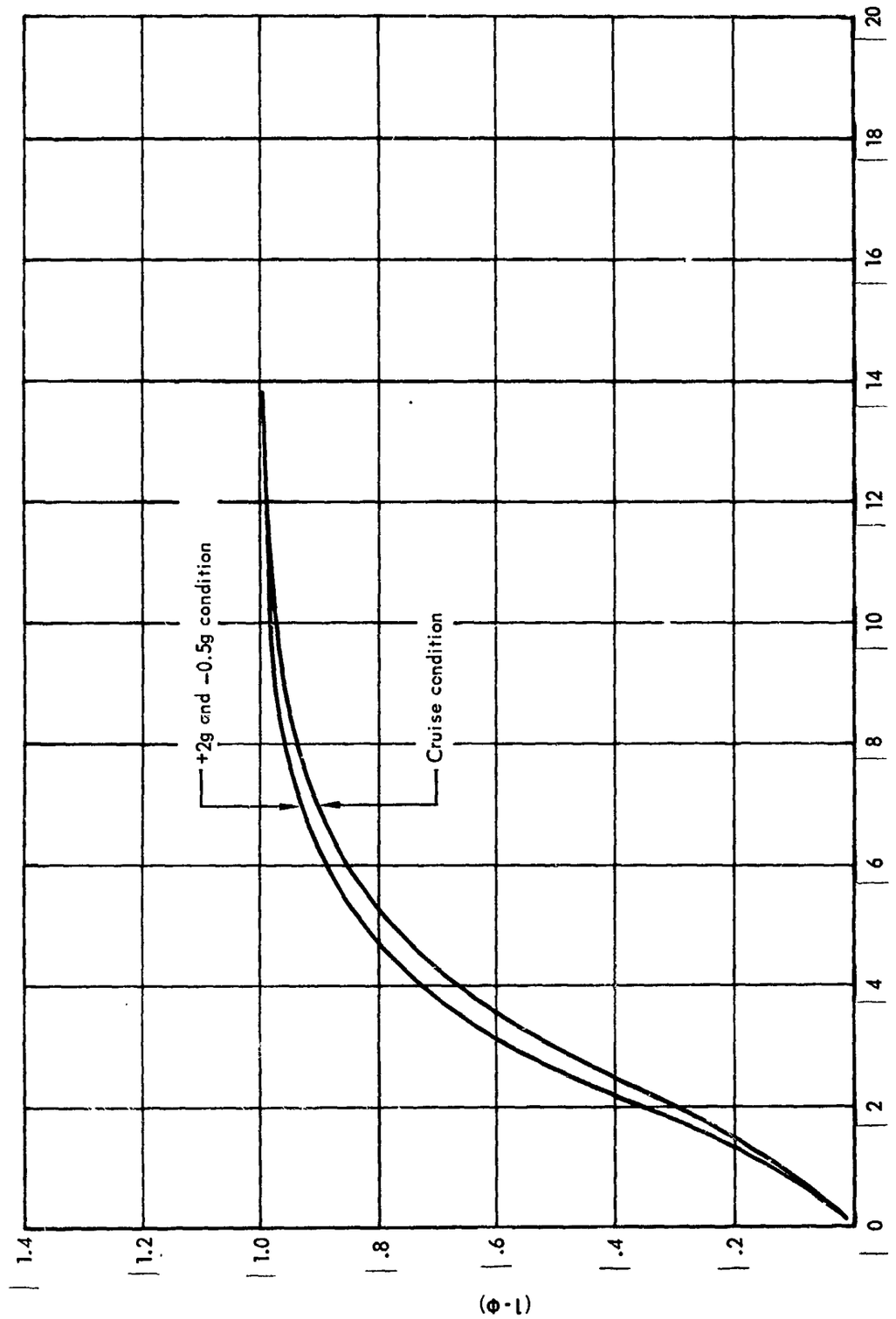

Figure 21-9. Thermal strain reduction factor at center of leading edge segment, segmented heat shielded and insulated concept

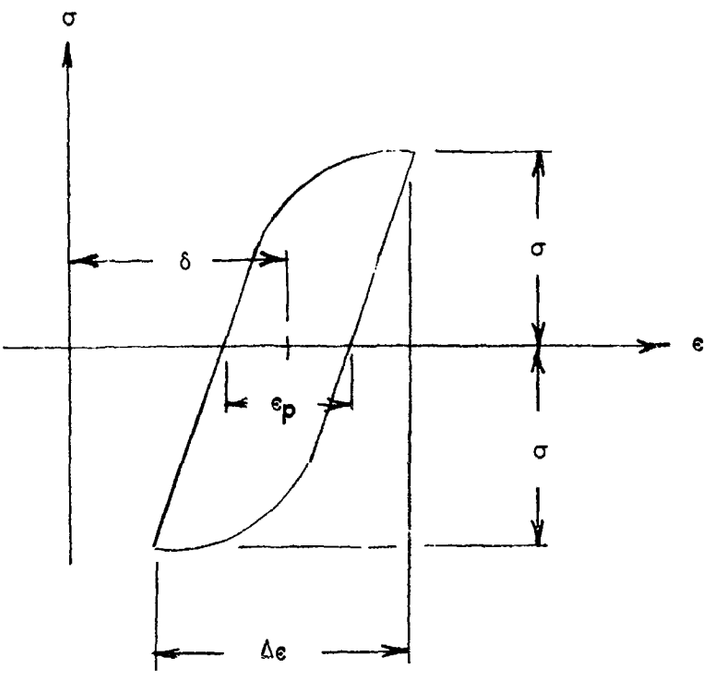

Figure 21-10. Cyclic stress and strain pattern involving zero mean stress and alternating plastic strain

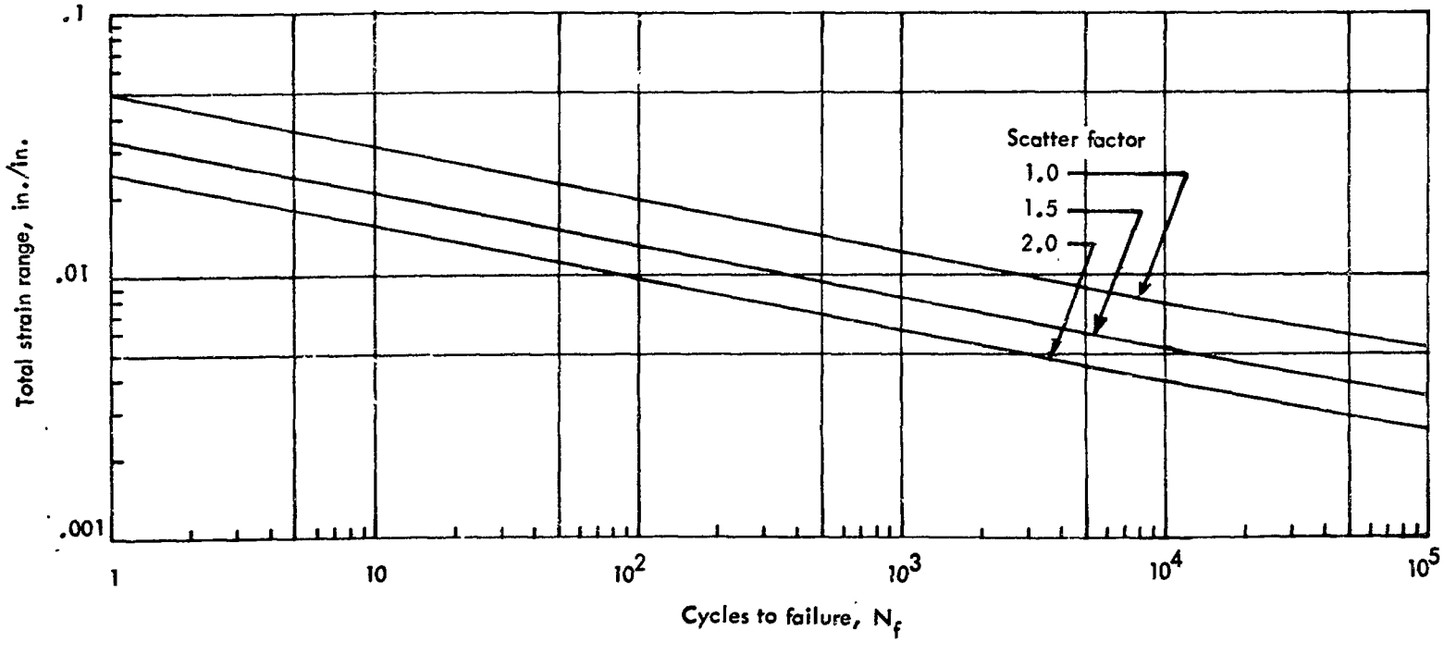

Figure 21-11. Relation between total strain range and cyclic life for TD NiCr

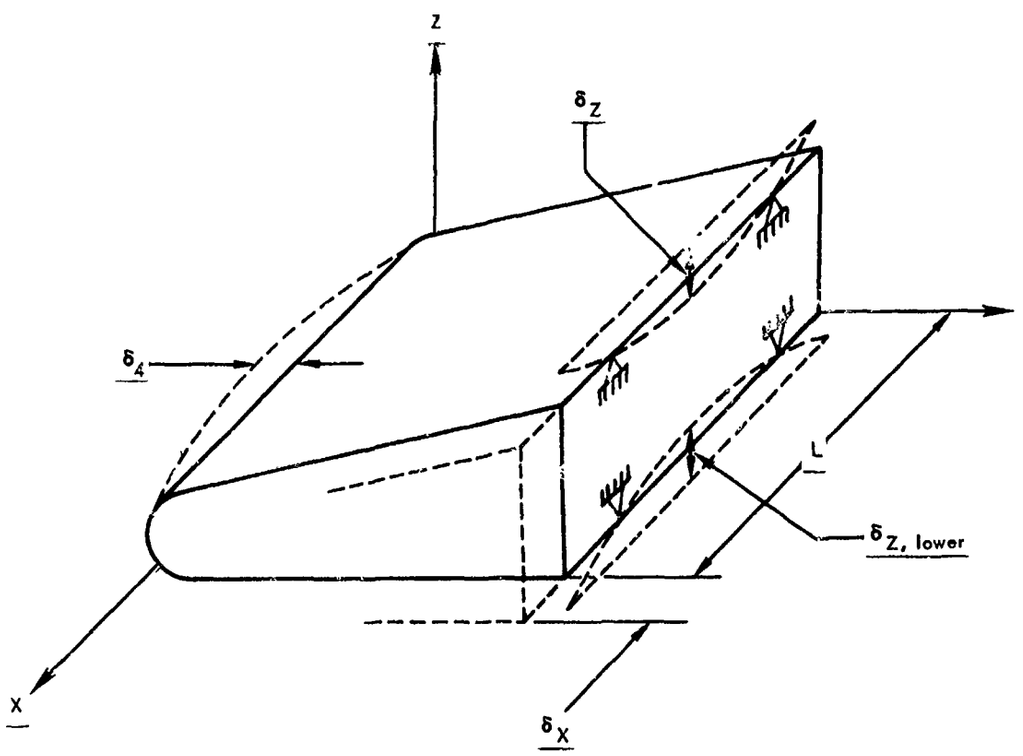

Figure 21-12. Deflection of segmented leading edge

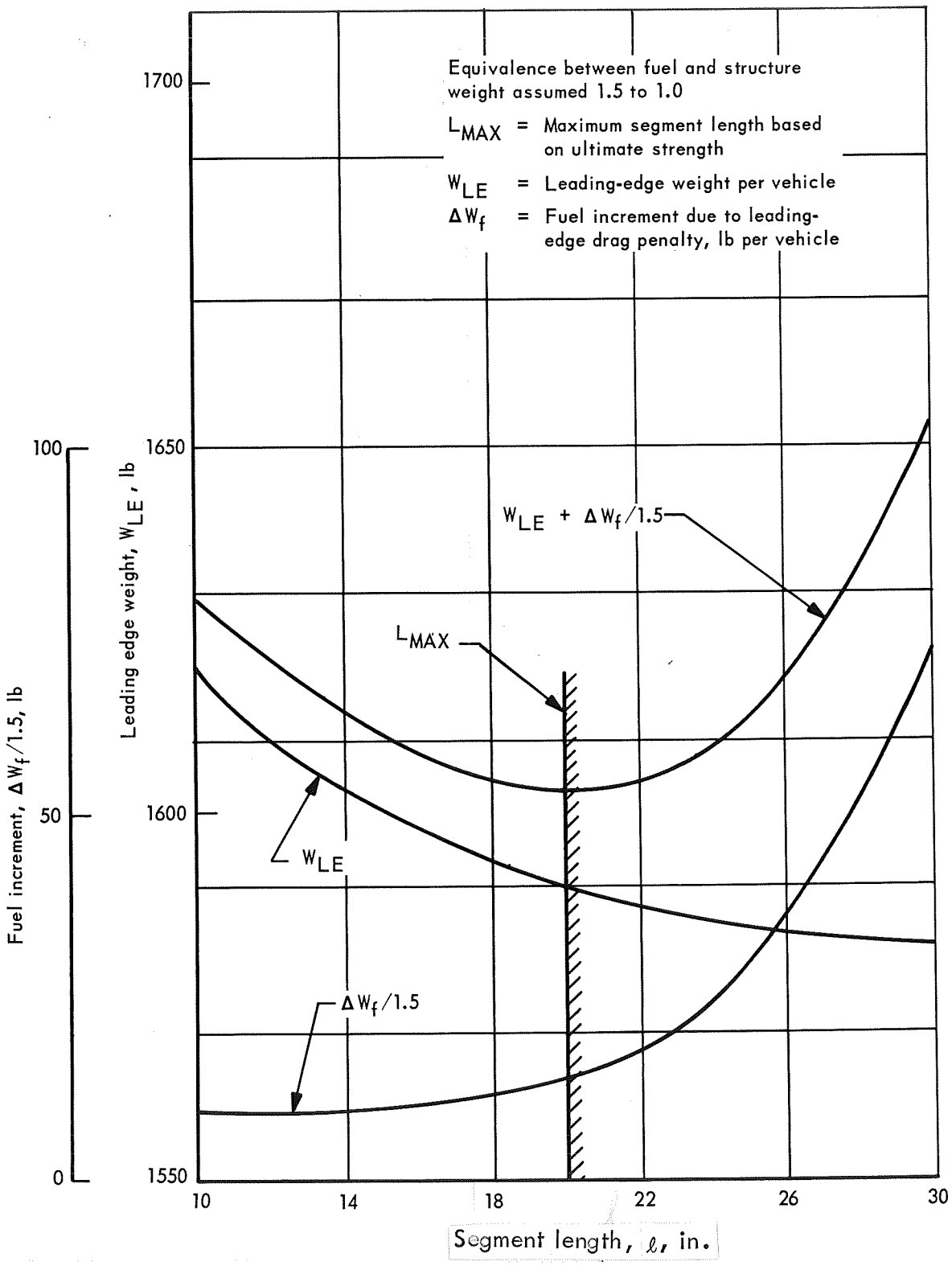

Figure 21-13. Optimum length of segmented leading edge for monocoque concept

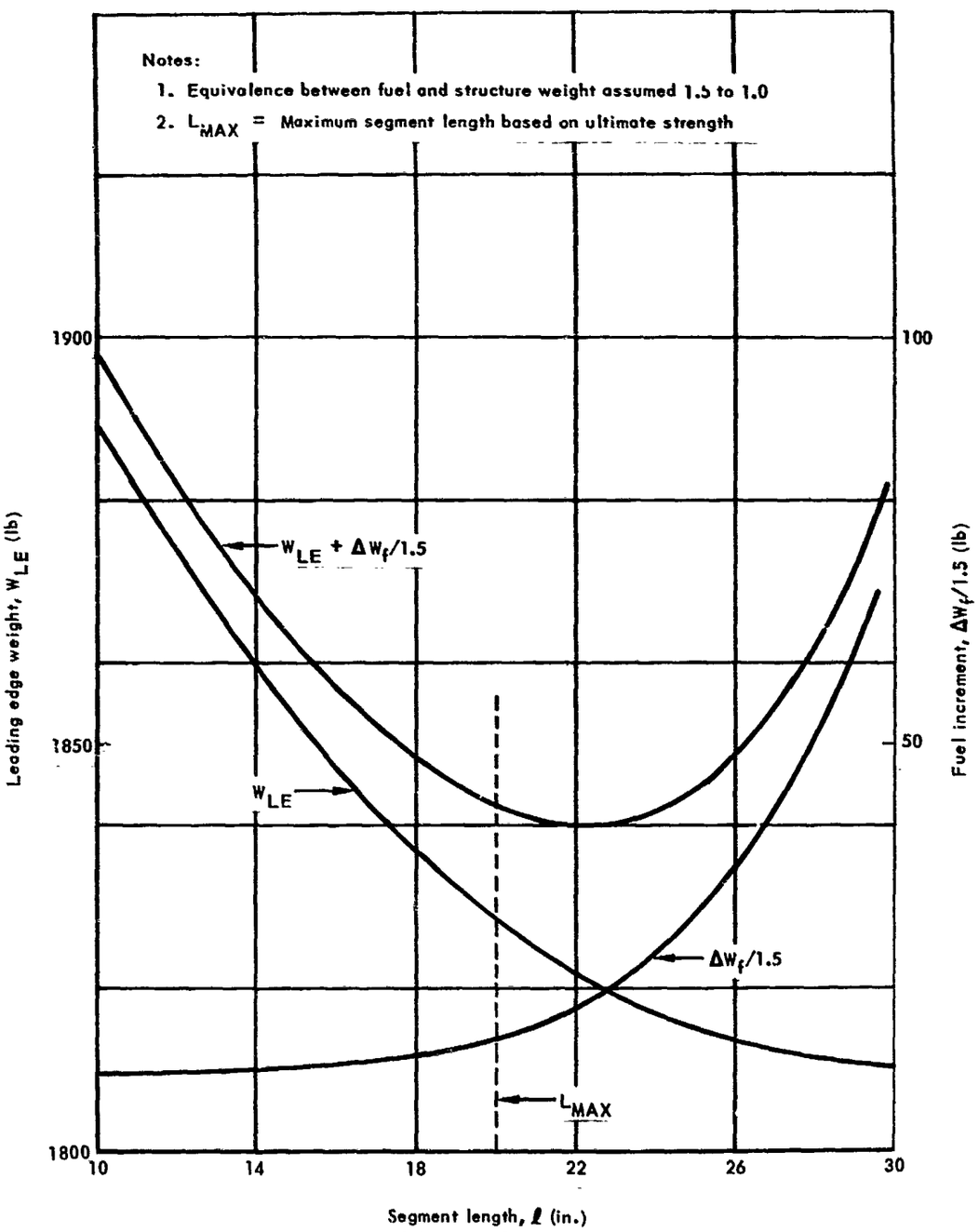

Figure 21-14. Optimum length of segmented leading edge, semimonocoque concept

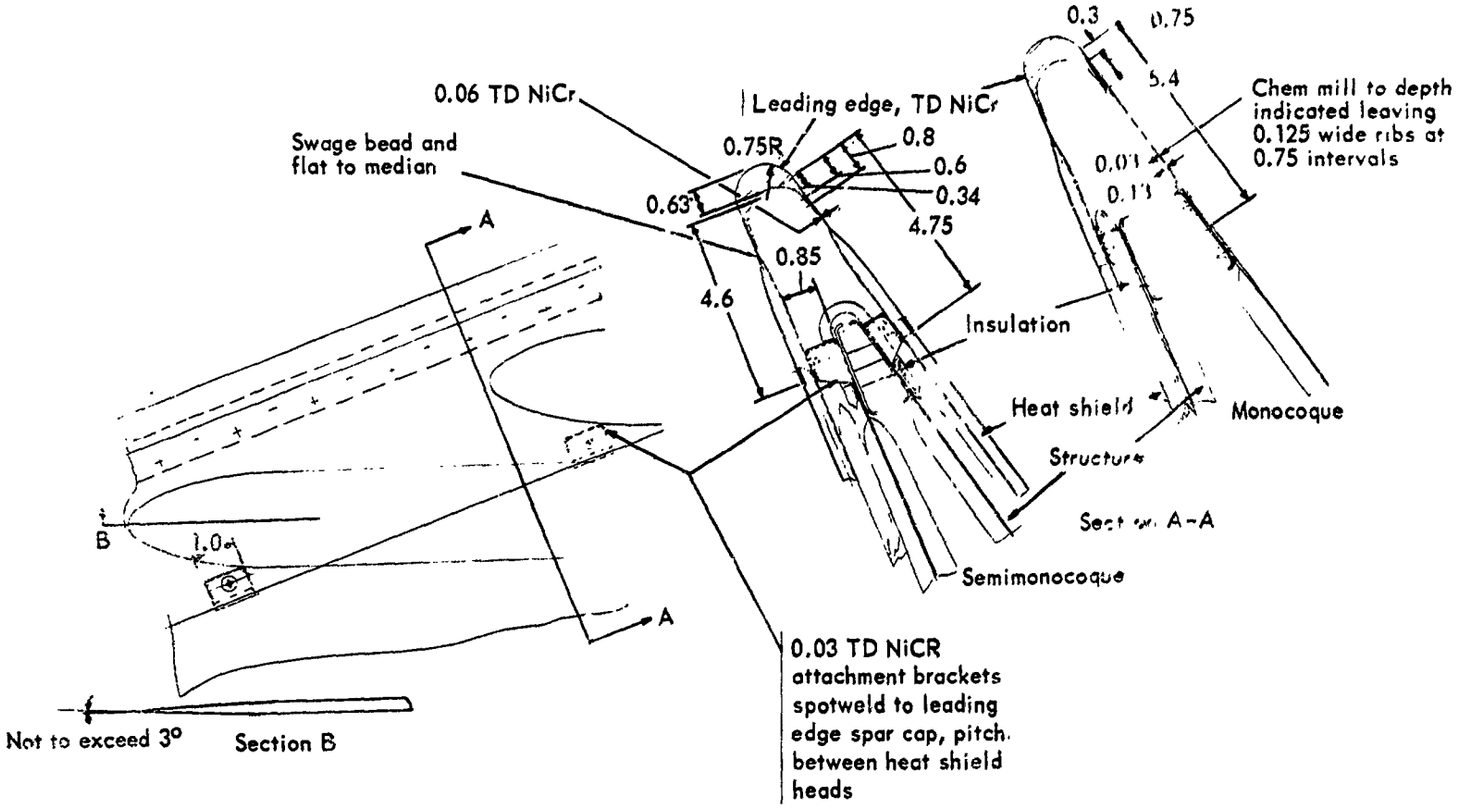

Figure 21-15. Leading edge nose section, continuous

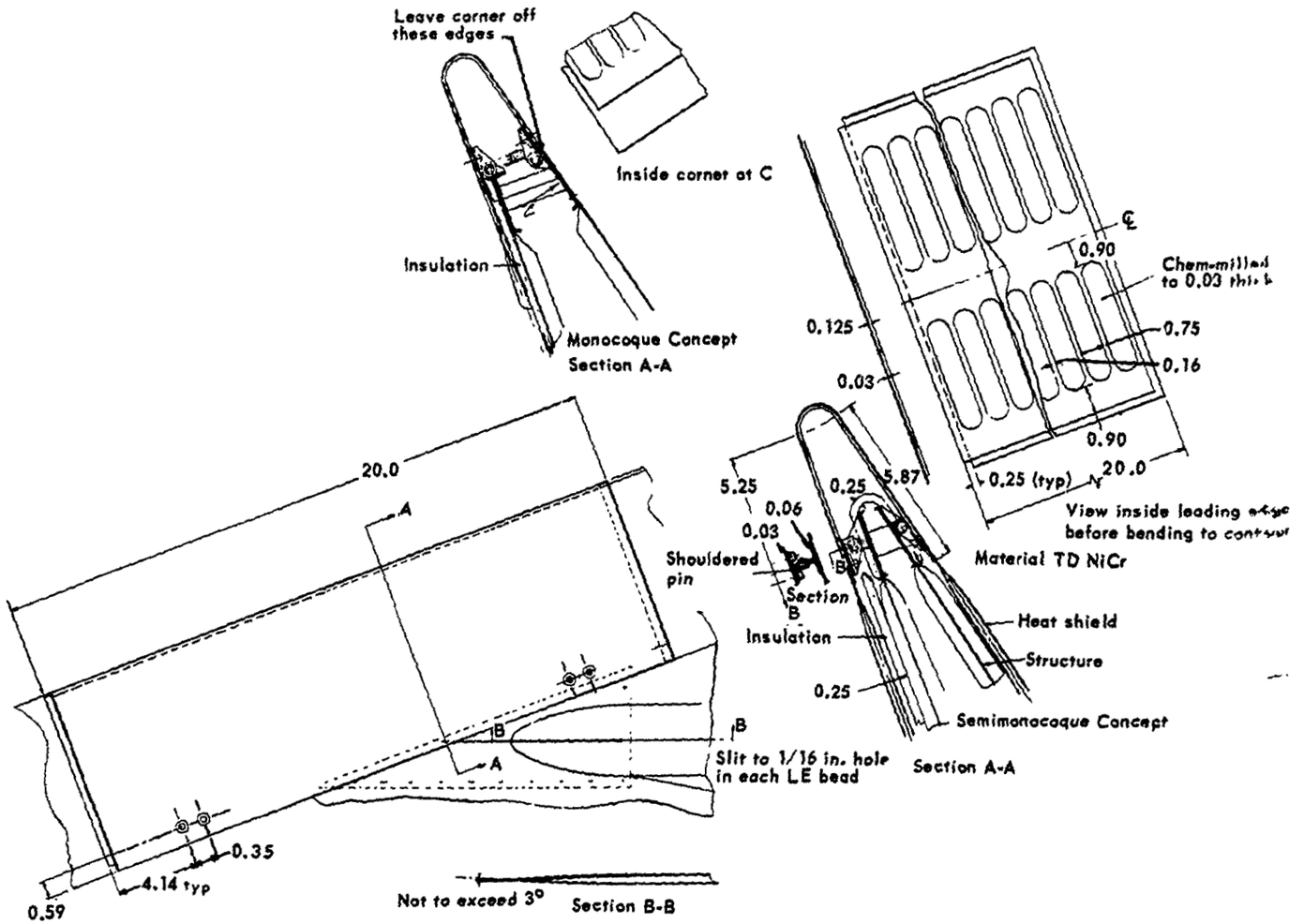

Figure 21-16. Segmented leading-edge

Section 22

TOTAL WING AND BASELINE VEHICLE WEIGHT ANALYSIS

by

I. F. Sakata, R. D. Mijares

CONTENTS

TABLES

ILLUSTRATIONS

SYMBOLS

A	Area
BL	Butt line
CMR	Fuel fraction designation used in vehicle weight and sizing program.
CWING	Wing weight coefficient used in vehicle weight and sizing program
FS	Fuselage station
f	Stress
g	Gravitational acceleration
L	Length
NOF	Nonoptimum factor for panels
P	Axial load in pounds
S	Wing planform area
t	Thickness
t	Equivalent thickness
W	Weight of total wing
W/S	Wing loading
w	Unit wing weight expressed in lb/ft^2

Section 22

TOTAL WING AND BASELINE VEHICLE WEIGHT ANALYSIS

Total wing weights for each of the six structural concepts were determined, as well as the component weights for the remaining portion of the baseline vehicle (550 000 pounds). These data were used as input for the interaction analysis of section 26.

Comprehensive analyses were conducted as presented in section 13, to determine final concept weights for the center area (centerline of vehicle to the intersection of the wing and fuselage), inboard area (intersection of the wing and fuselage to the wing one-third chordline), and outboard area (one-third chordline to the wing leading edge) of the selected wing section of figure 22-1.

To obtain the total wing weights for concept evaluation these unit weights (of the selected wing section) were related to the other areas of the wing by a multiplier. These multipliers were based on the analysis of the wing structural elements at selected locations using the internal loads data from the redundant analysis of each concept. The basic substructure arrangement (rib and spar spacing) was maintained identical to the study area, except for slight variation in the forward delta. In general, element weights were related to the detailed weight summary for each concept, with incremental changes determined through analysis of the structural elements (i.e., rib/spar caps, webs). The analyses were in sufficient depth to provide material to transmit the specified loads at acceptable stress levels. In areas where loads are small, minimum gage caps and panels are used. The panel requirements are determined through comparison with areas of similar loading and temperature.

The designated zones (A, B, and C) of the selected wing section are shown in figure 22-1. This designation was carried to the balance of the total wing, as indicated, using the same philosophy that was used for the detailed analysis area. By selection of the basic zones on the basis of common-type structures, a multiplier could readily be determined.

The zones include:

Location	Zone	General Type of Structure
Wing Center Section	A	Under-Fuselage
Wing Outboard Section	C	Heat Shielded or Insulated
Wing Inboard Section	B	Balance of Aft Delta (Basic Wing)
Wing Forward Section	D	Combined Under-Fuselage and Outboard Section of the Forward Delta
Trailing Edge	E	Elevon

REDUNDANT MODEL LOADS

To provide a rational basis for determining the total wing weight for each concept, the internal loads data from the redundant analysis were used. The aft wing loads for each concept is presented in figures 22-2 through 22-10. The lumped cap areas used as input to the redundant analyses are given with each figure for the spanwise and chordwise elements. To obtain the distributed in-plane loads and associated stresses, the extensional stiffness used for input to the redundant model is also presented for each concept. The incremental area required to bring the stress level to design values of the selected wing area is accomplished by direct ratio of the given value of extensional stiffness to the required value.

FORWARD DELTA WING STRUCTURE WEIGHTS

A weight summary for the wing forward delta structure is presented in table 22-1 and figure 22-11. Review of loads data and the requirements of similar structural areas indicates that minimum gage panels and substructure are adequate. Nonoptimum factors to account for panel edge-closeouts, attachments, and oxidation effects are determined from the selected wing section analysis. The unit weights vary between 4.12 and 6.11 psf between the minimum weight semimonocoque, spanwise beaded-skin concept, and the monocoque waffle concept, as indicated. These weights are used for determination of the total wing weight for each concept.

The basic type of structure varies as shown in figure 22-12. Formed sheet metal segments are used between Stations 790 and 1075; machined frame segments are assumed between Stations 1075 and 1345; and spanwise wing beams that extend under the fuselage with a fairing/heat shield structure is assumed from Station 1345 aft to Station 1932. The type of structure is assumed constant for all the concepts between Stations 790 and 1345. The average unit weight for this area is 3.51 psf or 3779 pounds, as previously shown in figure 22-11. This corresponds to a unit weight of 3.24 lbs/ft^2 for the forward area (487 square feet) and 3.73 psf for the aft area (590 square feet). The unit weight of the structure between Stations 1345 and 1932 varies with each concept. The

under-fuselage structure unit weight varies from 4.04 to 7.80 psf, and the outboard area varies between 5.20 to 7.79 psf.

Station 790 to 1075. - The chine is attached to the body structure by formed sheet metal bulkheads, as indicated in figure 22-13. The chine is assumed non-structural in this area with respect to body bending loads and transmits local pressure loads only. The skin is segmented to provide for thermal expansion.

Station 1075 to 1210. - Machined frame segments are used to attach the chine to the body structure and transmit the pressure loads to the body structure (fig. 22-13). The fuselage in this area is essentially a barrel-section with these frames externally attached. Sheet metal extensions are used to make up the remaining structure. Radial and tangential loads are introduced to the basic frame at the pinned attachment joint.

Station 1210 to 1375. - Machined frame segments with integral chine support elements are used in this area (fig. 22-13). Transition of the side shell from a circular shell (forward) to vertical panels is made in this region. The fitting at Station 1210 provides support for the resulting change in load paths and introduces an additional moment loading on the frame. A sheet metal structure is provided between the machined frame and the leading edge attachment points.

Station 1345 to Station 1932. - The wing (forward delta) in this region passes beneath the fuselage, as shown in figure 22-13. A separate fairing/heat shield is assumed on the lower surface as indicated. The basic arrangement is assumed similar to the study area. Minimum gage panels are used in all cases with associated non-optimum factors. The fuselage frames terminate at the wing-fuselage intersection; however, for bookkeeping purposes, the fairing weight is assumed to be contained in the fuselage unit weight; thus, the calculated wing unit weights are directly applicable for total wing weight determination.

AFT DELTA WING STRUCTURE WEIGHTS

Several areas of the aft delta wing structure were selected for analysis to determine unit weight changes required to transmit the applied loads at acceptable stress levels. Using the detailed weight-breakdown for each concept as the basis, the incremental weight changes determined were added to the basic values to obtain the unit weight of each area evaluated.

The center area (Zone A) weights increase aftward to accommodate the increase in spanwise shears and bending moments. No increase in the chordwise elemental weight is required, since the maximum loading in this direction occurs in the study area.

The inboard area (Zone B) weights also increase aftward to accommodate the increase in spanwise shears and bending moments. The combined effect of elevon forces (chordwise bending) and increased spanwise bending moments in the aft area

between FS 2800, and the control surfaces result in the highest unit weights on the total wing.

The outboard area (Zone C) wing weights are assumed to be constant for each concept except in the area of the elevons where the chordwise loads at BL 488 define these requirements. In addition, increase in the spanwise stiffness is required to transmit these loads inboard.

The elevons are assumed to weigh 10 psf for all concepts, with the calculated leading edge weights used with the appropriate concept.

The results of these analyses are presented in figures 22-14 through 22-16. The monocoque concept scaling relationships are presented in figure 22-14. The scaling relationship for the aft wing indicates that this concept results in the least weight change, since panel stiffening (i.e., waffle grid, honeycomb core) can be adjusted to accommodate the higher loading intensities without large weight changes. Since the weight changes for the waffle grid plate and honeycomb core sandwich were very similar (waffle slightly higher), the waffle concept scaling relationships were used for both concepts. For the semimonocoque, spanwise stiffened concepts and for the statically determinate, spanwise stiffened concept, the distribution factors were essentially the same (semimonocoque slightly higher). The wing of spanwise elements (i.e., panels and spars) were increased to transmit the higher inplane loads. The higher spanwise loads in the aft wing area are comparable to the chordwise (tubular) design data, and therefore were used for determination of the wing weights in that area. The chordwise concept requires an increase in spar weight to accommodate the increase in spanwise bending moments and shears. Since the maximum chordwise loads occur in the study area, panel designs are adequate to transmit the loads in this area.

TOTAL WING WEIGHTS FOR BASELINE VEHICLE

Total wing weights were determined for each concept, using the wing-section weights and the scaling relationships discussed previously. The wing average weights (psf) for the baseline (550 000 lb) vehicle, including elevon and leading-edge weights, are shown in table 22-2. The statically determinate concept incurs a fuselage weight penalty, over the other concepts, of 3 685 pounds. This is equivalent to a 0.365 psf of wing unit weight, based on the planform area, and must be added to the statically determinate weights to obtain a true weight comparison.

The results of the total wing-weight investigation provided the following ranking of structural concepts: semimonocoque spanwise beaded, semimonocoque spanwise tubular, monocoque honeycomb sandwich, statically determinate spanwise beaded, semimonocoque chordwise, and monocoque waffle. As indicated in table 22-2, the total wing weight of the honeycomb sandwich concept is lower than that for the statically determinate concept, which is a change from the wing investigation section analysis ranking discussed earlier. Honeycomb is lighter for the total wing because of better efficiency for the high biaxial load area of the aft wing.

BASELINE VEHICLE DATA

In addition to the wing weights, weights for all elements of the baseline vehicle were determined and used in the interaction analysis of section 26. Except for the statically determinate concept, which requires additional fuselage weight, identical weights were used for the remaining portion of the vehicle, for each structural concept.

Additional Fuselage Weight for Statically Determinate Concept

The statically determinate concept incurs a fuselage weight penalty over the other structural concepts for fuselage skin, decking (required to close out lower portion of fuselage), longitudinal stiffeners, and frame members.

The assumed baseline vehicle fuselage primary structure weight is 36 850 lb with an average mass distribution of 2.5 psf. This fuselage design uses bulkheads, rings, and longitudinal stiffened Rene' 41 panels with a panel t = 0.038 in. and conventional fuselage to wing attachments. The statically determinate fuselage has a weight of 3685 lb (10 percent) increase over the baseline vehicle fuselage weight, as shown below.

Item	Weight (lb)
Skin panels (corrugation-stiffened)	1646
Decking (beaded skin)	1340
Longitudinal stiffeners	200
Frame members	320
Contingency (5%) (Fittings, fasteners, etc.)	179
Total Weight Penalty	3685

The weight increase of the statically determinate fuselage was based on the redundant model loads (model elements and stresses are presented in figure 22-17 and table 22-3, respectively) and temperatures (table 22-4). Using these loads and temperatures, the increase in skin panel weight over the baseline vehicle, in which minimum gage (t = .038) corrugation stiffened panels were adequate, was determined using the wide column curve presented in figure 22-18.

To provide thermal protection for the tankage, fuselage decking was provided as shown in figure 22-19. This decking (beaded concept) is stiffened in the spanwise direction so that it is not strained with the fuselage body loads. Longitudinal stiffeners of I-beam configuration are provided to support the

decking and carry the longitudinal body loads. Figure 22-19 indicates the applicable planform area and support system (longitudinal stiffeners) for the fuselage deck. The same type of I-beam utilized for the longitudinal supports was used for connecting the frames at the lower portion of the fuselage.

VEHICLE WEIGHT AND SIZING

A weight sensitivity and vehicle sizing procedure (ref. 22-1) was used to synthesize and compute vehicle size and weight for the interaction analysis of section 26. While the procedure is used in the section 26 analysis, a summary of the primary variables and coefficients are given in table 22-5 of this section so that the baseline vehicle weight input requirements may be provided. Using the information of table 22-5, a sample calculation of weights for the baseline vehicle was performed and is shown in table 22-6, using the mass fraction data presented in section 1 (initially used for obtaining loads).

For the interaction analysis of section 26, all data of table 22-6 remains the same except for the wing weight, fuel fraction and weight, payload weight, and fuselage weight of the statically determinate concept. These inputs are presented in table 22-7 for each wing structural concept and for the three levels of reliability (low, nominal, and high). The statically determinate concept payloads of table 22-7 include the effect of the additional fuselage weight. The CWING values of table 22-7 are the wign weight coefficients used in the vehicle sizing procedure of reference 22-1, as presented in table 22-5.

A parametric investigation for the effect of scaling the baseline vehicle (wing loading $W/X = 66.8$ psf) was conducted and is shown in figure 22-20 for various wings (CWING), payloads and fuel fractions (CMR). The relationships between the coefficients CWING for the baseline vehicle weight can be determined from figure 22-20, as shown in the tabulation below.

CWING	Baseline vehicle wing weight - lb
0.006	48 420
0.008	64 560
0.010	80 700
0.012	96 840

The difference between scaling the wing using S (wing area) and $S^{1.5}$ versus $S^{1.4}$ is shown in figure 22-21. Typically, the monocoque concept has 20 percent of its structure proportional to S, which results in almost no difference. The semimonocoque concept may run to about 30 percent, which could result in a weight difference of only 3 percent. Therefore, the scaling factor of $S^{1.5}$ was used for the interaction evaluation of section 26.

REFERENCES

22-1 Jones, R.: Weight Synthesis and Sensitivity Programs, Lockheed-California Company, LR 21205, 1967.

TABLE 22-1

WING FORWARD DELTA WEIGHTS

Structure Concept	Monocoque				Semimonocoque						Statically Determinate	
	Biaxial				Spanwise				Chordwise		Spanwise	
	Waffle		Honeycomb		Tubular		Beaded		C. Beaded/Tubular		Beaded	
Zone (Figure 22-11)	3	4	3	4	3	4	3	4	3	4	3	4
1. Panels	0.1120	0.1180	0.0840	0.0830	0.0640	0.0660	0.0510	0.0550	0.0770	0.0810	0.0490	0.0550
2. $\bar{t}_u$, upper (in.)	0.045	0.045	0.034	0.032	0.026	0.026	0.020	0.020	0.026	0.029	0.020	0.020
3. $\bar{t}_e$, lower (in.)	0.045	0.045	0.034	0.032	0.026	0.026	0.020	0.020	0.026	0.029	0.020	0.020
4. NOF[a]	1.24	1.31	1.24	1.30	1.23	1.27	1.28	1.37	1.48	1.48	1.23	1.37
5. Caps - Rib/Spar	0.128	0.0135	0.0072	0.0072	0.0064	0.0063	0.0064	0.0063	0.0100	0.0095	0.0078	0.0084
6. Arib = Aspar ($in.^2$)	0.10	0.10	0.10	0.10	0.10	0.10	0.10	0.10	0.10	0.10	0.20[b]	0.20[b]
7. a, spar spac (in.)	45	45	90	90	90	90	90	90	30	30	90	90
8. b, rib spac (in.)	24	22.3	40	40	48	50	48	50	60	72	60	50
9. Webs-Rib/Spar (in.)	0.0568	0.0284	0.0263	0.0137	0.0239	0.0170	0.0239	0.0170	0.0491	0.0239	0.0363[b]	0.0242[b]
10. Heat shield/insul. (in.)	--	0.0214	---	0.0214	0.0130	0.0427	0.0130	0.0427	0.0143	0.0298	0.0131	0.0358
11. Total $\bar{t}$ (in.)	0.1816	0.1813	0.1175	0.1253	0.1073	0.1310	0.0943	0.1210	0.1504	0.1442	0.1062	0.1234
12. Total w (lb/ft)	7.80	7.79	5.05	5.38	4.61	5.62	4.04	5.20	6.46	6.20	4.56	5.30
13. Sn (ft^2)	960	693	980	693	980	693	980	693	980	693	980	693
14. Sn x w (lb)	7650	5400	4950	3730	4520	3890	3960	3600	6330	4300	4470	3670
15. Σ Sn W (aft) (lb)	13050		8680		8310		7560		10630		8140	
16. Σ Sn w (fwd) (lb)	3779		3779		3779		3779		3779		3779	
17. W (fwd delta) (lb)	16829		12459		12089		1339		14409		11919	
18. w (fwd delta)[c] (psia)	6.11		4.53		4.39		4.12		5.25		4.34	

a NOF = Non-optimum factor, includes closeout, fasteners, oxidation
b includes slip-joint assemblies
c S (fwd delta) = 2750 ft^2

TABLE 22-2

NOMINAL WING WEIGHTS FOR BASELINE AIRPLANE

Primary Structural Concept	Unit Weight						Weight							
	Zone					Lead. Edge	Zone					Lead Edge	Total Wing Weight	Total Wing Unit Weight
	A	B	C	D	E		A	B	C	D	E			
	(lb/ft^2)					(lb/ft)	(lb)							lb/ft^2
Monocoque, Unflanged Waffle	10.72	12.03	9.44	6.11	10.00	4.25	23 213	38 780	21 054	16 829	3210	1700	104 786	10.38
Monocoque, Honeycomb Sandwich	6.25	6.35	6.77	4.53	10.00	4.25	13 539	20 472	15 098	12 459	3210	1700	66 478	6.59
Semimono, Spanwise Tubular	4.82	5.61	5.70	4.39	10.00	4.89	13 421	22 853	12 408	12 089	3210	1956	65 937	6.53
Semimono, Spanwise Beaded	4.46	5.38	5.37	4.12	10.00	4.89	12 436	21 934	11 682	11 339	3210	1956	62 557	6.20
Semimono, Chordwise Stiffened	6.95	6.80	6.33	5.25	10.00	4.89	16 461	24 764	14 023	14 409	3210	1956	74 823	7.41
Statically[a] Determinate, Beaded	5.21	6.00	5.54	4.34	10.00	4.89	14 513	24 686	12 052	11 919	3210	1956	68 336	6.77

[a]Fuselage increment = 3685 lb.

TABLE 22-3

STATICALLY DETERMINATE FUSELAGE COMBINED STRESSES,
"ULTIMATE STRESSES," FLIGHT CONDITION ~ +2G

Fuselage station	Element no.	A ($in.^2$)	P_{comb} (lb)	f_{comb} (psi)
1700	16	2.26	+62 384	+27 600
	17	4.47	+122 953	+27 500
	18	3.29	-106 832	-32 470
	19	1.46	-78 585	-53 800
2058	26	2.26	+61 000	+26 960
	27	4.46	+180 000	+40 415
	28	3.29	-120 000	-36 450
	29	2.16	-121 000	-56 200
2320	51	2.38	+51 500	+21 580
	52	4.72	+198 000	+41 960
	53	3.70	-89 000	-23 970
	54	4.11	-161 000	-39 140
2412	61	2.39	+48 500	+20 249
	62	4.72	+180 000	+38 070
	63	3.78	-64 000	-16 929
	64	3.71	-164 000	-44 270

TABLE 22-4

FUSELAGE TEMPERATURE SUMMARY

Fuselage location	Temperature (°F)								
	FS 2058			FS 2320			FS 2580		
	-0.5G	+2.0G	(a) Cruise	-0.5G	+2.0G	(a) Cruise	-0.5G	+2.0G	(a) Cruise
Upper centerline	1146	1227	915	1140	1221	910	1135	1216	905
Horizontal tangency	1174	1243	926	1210	1279	960	1208	1279	958
Wing root	1289	1360	1028	1371	1441	1102	1301	1372	1040

(a) Average cruise temperature between t = 21.0 & t = 54.0 minutes

TABLE 22-5

PRIMARY VARIABLES AND COEFFICIENTS FOR WEIGHT/SIZING PROCEDURE

Item	Primary Variable	Coefficient
Aerodynamic Surfaces:		
Wing	Constant	500
Wing	$WG.^{6}SW.^{8}$	2.127 x cwing[(a)]
Vertical tail	SVT	8.530
Body group:		
Pressurized crew compartment	Constant	2000
Body structure	SBDY	2.2456[(b)]
Tankage structure	SBDY $(SPYE)^{1/2}$	0.081044
Induced environment protection:		
Thermal protection (tankage insulation)	SBDY	1.129
Launch, recovery, and docking:		
Landing gear	WG	0.030
Main propulsion:		
Main engine - airbreathing	Constant	-6132
Main engine - airbreathing	TTOT	0.146826
Air induction system	CSAP	201.3
Propellant distribution - fuel	TTOT	0.0098
Orientation controls, separation and ullage:		
Reaction control system	WG	0.0020
Aerodynamic control system	Constant	640
Aerodynamic control system	WG	0.010
Power conversion and distribution:		
Electrical	Constant	1400
Electrical	WG	0.0040
Hydraulic and pneumatic	WG	0.0050

Note: (a) varies with each wing structural concept,
cwing = 1.239 x wing weight
(b) The value is 2.4702 for statically determinate concept

TABLE 22-5

PRIMARY VARIABLES AND COEFFICIENTS FOR WEIGHT/SIZING PROCEDURE (Continued)

Item	Primary Variable	Coefficient
Guidance and navigation	Constant	1060
Instrumentation	Constant	1100
Communication	Constant	240
Environmental control:		
ECS - personnel	Constant	550
ECS - equipment	Constant	1180
Personnel provisions	Constant	2450
Crew station control and panels	Constant	200
Design reserve	ΣW_i	.020
Empty weight		Σ = WEMPT
Crew	NCREW(=3)	220
Payload (WPAY)	Input	--
Dry weight		Σ = WDRY
Residuals (unusable)	WFTOT	0.0050
Zero fuel weight		Σ = WZF
Reserve	WFTOT	0.050
Landing weight		Σ = WLW
Inflight Losses	SBDY	0.660
Loiter fuel	WLW	0.007455
Burnout weight		Σ = WIBO
Performance propellant	WFTOT - $\Sigma W_{misc\ fuel}$	
Liftoff Weight		Σ = WLO
Taxi fuel (WTF)	WG	0.00225
Run-up fuel	(WG - WTF)	0.00765
Maximum gross weight		Σ = WG

TABLE 22-5 – Concluded

PRIMARY VARIABLES AN. COEFFICIENTS FOR WEIGHT/SIZING PROCEDURE

Item	Primary Variable	Coefficient
Volume (VTOT = required):		
Available body (VBDY)	$SW^{3/2}$	0.096572
Fuel	WFTOT	0.23702
Crew compartment	Constant	500
Cargo compartment (Variable density)	VBDY-VTOT	
Equipment bay	WG	0.0050
Structure and insulation	SBDY	0.500
Miscellaneous	VTOT	0.0620
Area:		
Wing area (SW)	WG	0.0149705
Vertical tail (SVT)	SW	0.0995
Body cross-section (SPYE)	$(VBDY)^{2/3}$	0.1805
Inlet capture area (CSAP)	Constant	222
Body wetted area (SBDY)	$(VBDY)^{2/3}$	9.480
Total thrust (TTOT)	WG	0.510

TABLE 22-6

SAMPLE CALCULATION OF BASELINE VEHICLE DATA

VOLUMES (cu ft)		
Fuel - 220 000 (0.23702) =		52 144
Crew		500
Cargo - 72 088 to 68 073 =		4 015
Equipment - 550 000 (0.005) =		2 750
Structure and Insulation - 16 420 (0.50) =		8 210
Miscellaneous - 72 088 (0.062) =		4 469
	VTOT =	72 088
AREAS (sq ft):		
Wing - (550 000/66.7978) =		8 234
V.T. - 8234 (0.0995) =		818.8
Body C-S - $(72\,088)^{2/3}$ 0.1805 =		312.6
Inlet		222
Body Wet - $(72\,088)^{2.3}$ 9.48 =		16 420
WEIGHTS (lb):		
Wing - 500 + $(550\,000)^{0.6}$ $(8234)^{0.8}$ (0.01590729) =		60 500
Vertical Tail - (818.8) 8.54 =		6 990
Body and Insulation:		81 030
Crew Compartment	2 000	
Body Structure (16 420) 2.25 =	36 950	
Tankage (16 420) $(312.6)^{1/2}$ 0.081044 =	23 530	
Insulation (16 420) 1.13 =	18 550	
Landing Gear - (550 000) 0.030 =		16 500
Propulsion:		82 490
Main Engine - 550 000(0.510) 0.146826 - 6132 =	35 050	
Inlet - (222) 201.3 =	44 690	
Fuel System - 550 000 (0.510) 0.0098 =	2 750	

Note: a varies with each wing structural concept
f increases 3 685 lb for statically determinate concept

TABLE 22-6 – Concluded

SAMPLE CALCULATION OF BASELINE VEHICLE DATA

Orient. Controls - 640 + (550 000) 0.012 =		7 240
Power Conv/Dist - 1 400 + (550 000) 0.009 =		6 350
Miscellaneous System		6 780
Design Reserve (267 880) 0.02 =		5 360
	Empty Weight	273 240
Crew - 3 (220) =		660
Payload -		55 000[a]
Residuals - 220 000) 0.005 =		1 100
	Zero Fuel Weight	330 000
Reserve - (220 000) 0.05 =		11 000
	Landing Weight	341 000
Inflight Losses - (16 420) 0.66 =		10 840[a]
Loiter Fuel - (341 000) 0.007455 =		2 540[a]
	Burnout Weight	354 380
Performance Propellent - 220 000 - 29 050) =		190 950[a]
	Liftoff Weight	545 330
Taxi Fuel - (550 000) 0.00225 =		1 240
Run-Up Fuel - (550 000 - 1240) 0.00765 =		3 430
	Maximum Gross Weight	550 000

TABLE 22-7

INPUT DATA FOR INTERACTION ANALYSIS
(Baseline Vehicle - 550 000 pounds)

Primary Structure Concept	Reliability Level	CWING (1239×10^{-7} x Wing Weight)	CMR (Fuel Fraction)	WPAY (Payload)
Monocoque	Low	0.01191		19 412
Unflanged	Normal	0.01298	0.399398	10 714
Waffle	High	0.01389		3 427
Monocoque	L	0.00805		50 545
Honeycomb	N	0.00824	0.399824	49 023
Sandwich	H	0.00848		47 044
Semimono,	L	0.00782		52 430
Spanwise	N	0.00817	0.399504	49 563
Tubular	H	0.00860		46 126
Semimono,	L	0.007275		56 791
Spanwise	N	0.007752	0.399518	52 943
Beaded	H	0.008268		48 778
Semimono,	L	0.008545		46 544
Chordwise	N	0.009272	0.402624	40 677
Tubular	H	0.009752		36 802
Statically	L	0.008000		47 250
Determinate,	N	0.008468	0.399873	43 477
Beaded	H	0.008887		40 094

[a]Includes the effect of increased body weight.
For nominal reliability (47162 - 3685) = 43 477 lb.

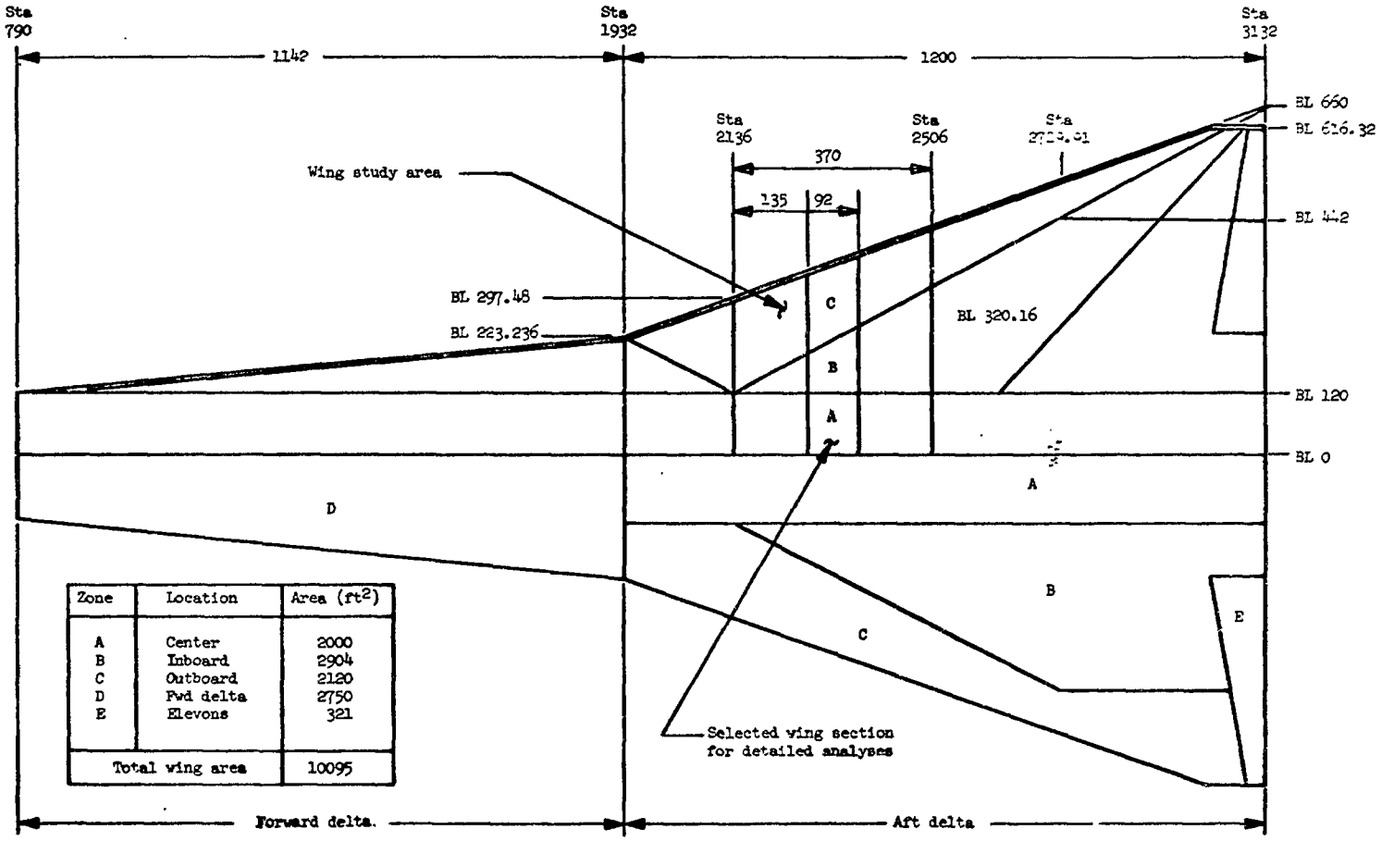

Zone	Location	Area (ft^2)
A	Center	2000
B	Inboard	2904
C	Outboard	2120
D	Fwd delta	2750
E	Elevons	321
Total wing area		10095

Figure 22-1. Wing geometry – baseline airplane

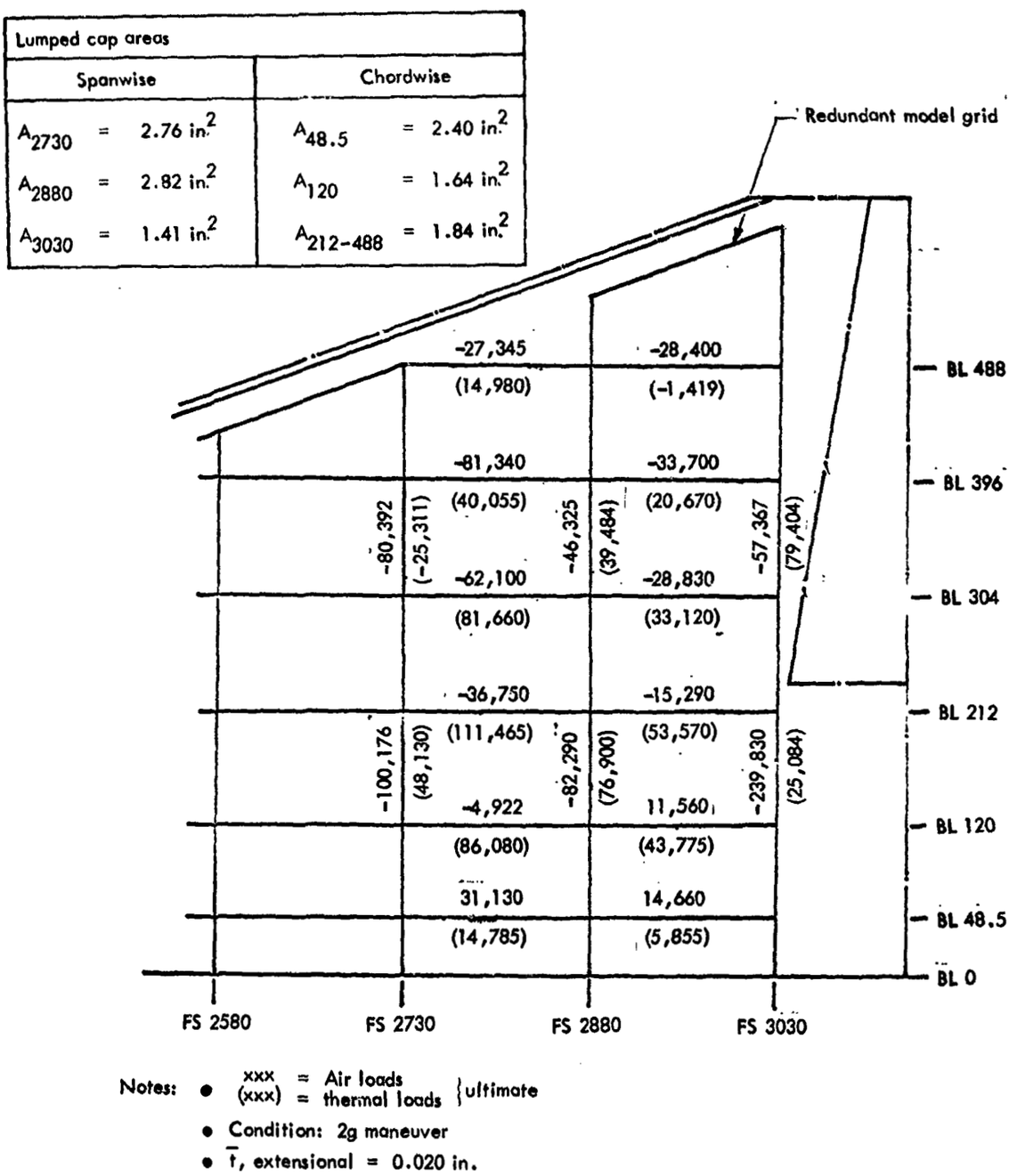

Figure 22-2. Redundant model loads – monocoque waffle concept (upper)

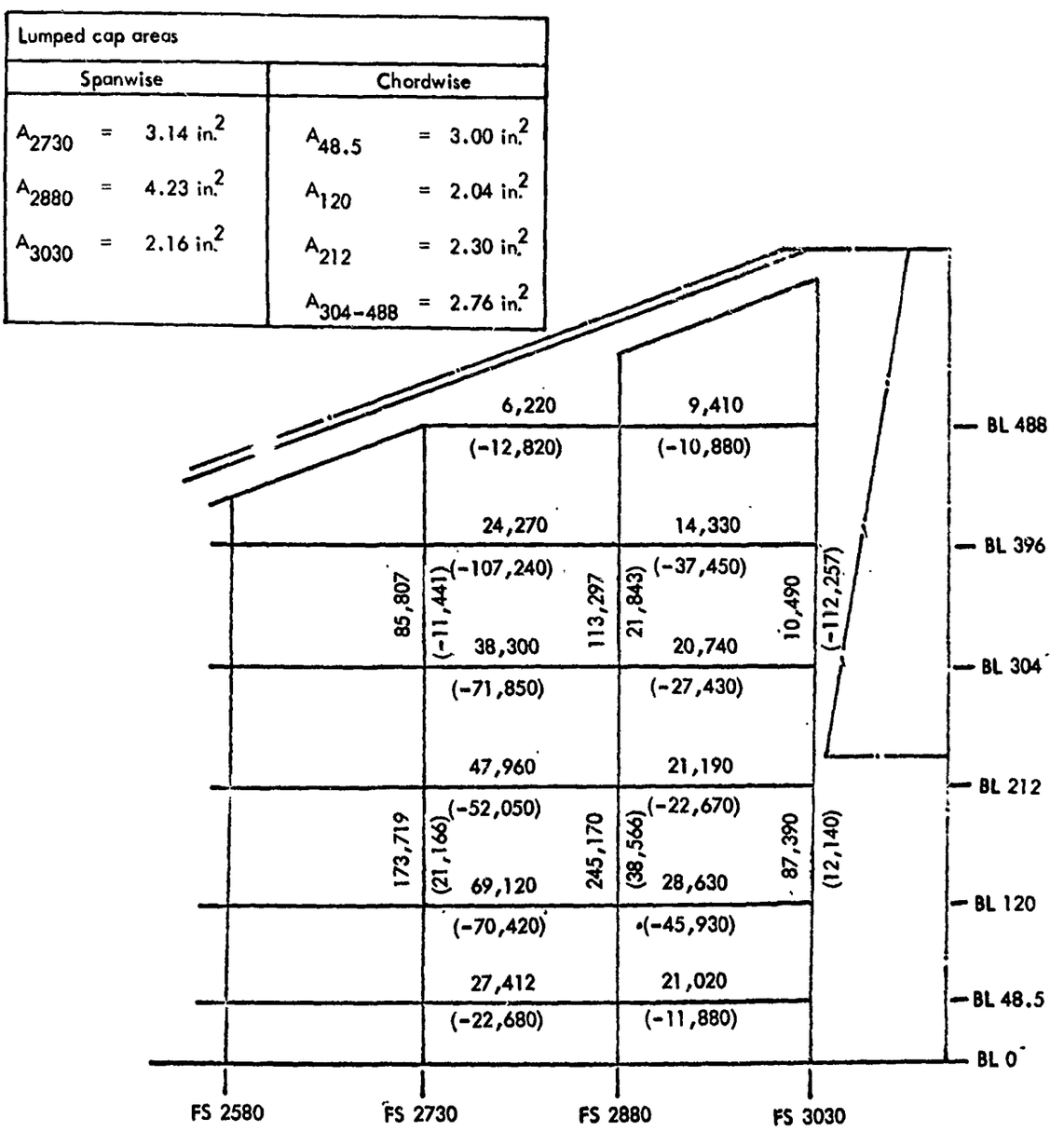

Notes:
- xxx = Air loads; (xxx) = thermal loads } ultimate
- Condition: 2g maneuver
- $\bar{t}$, extensional = 0.025-0.030 in.

Figure 22-3. Redundant model loads – monocoque waffle concept (lower)

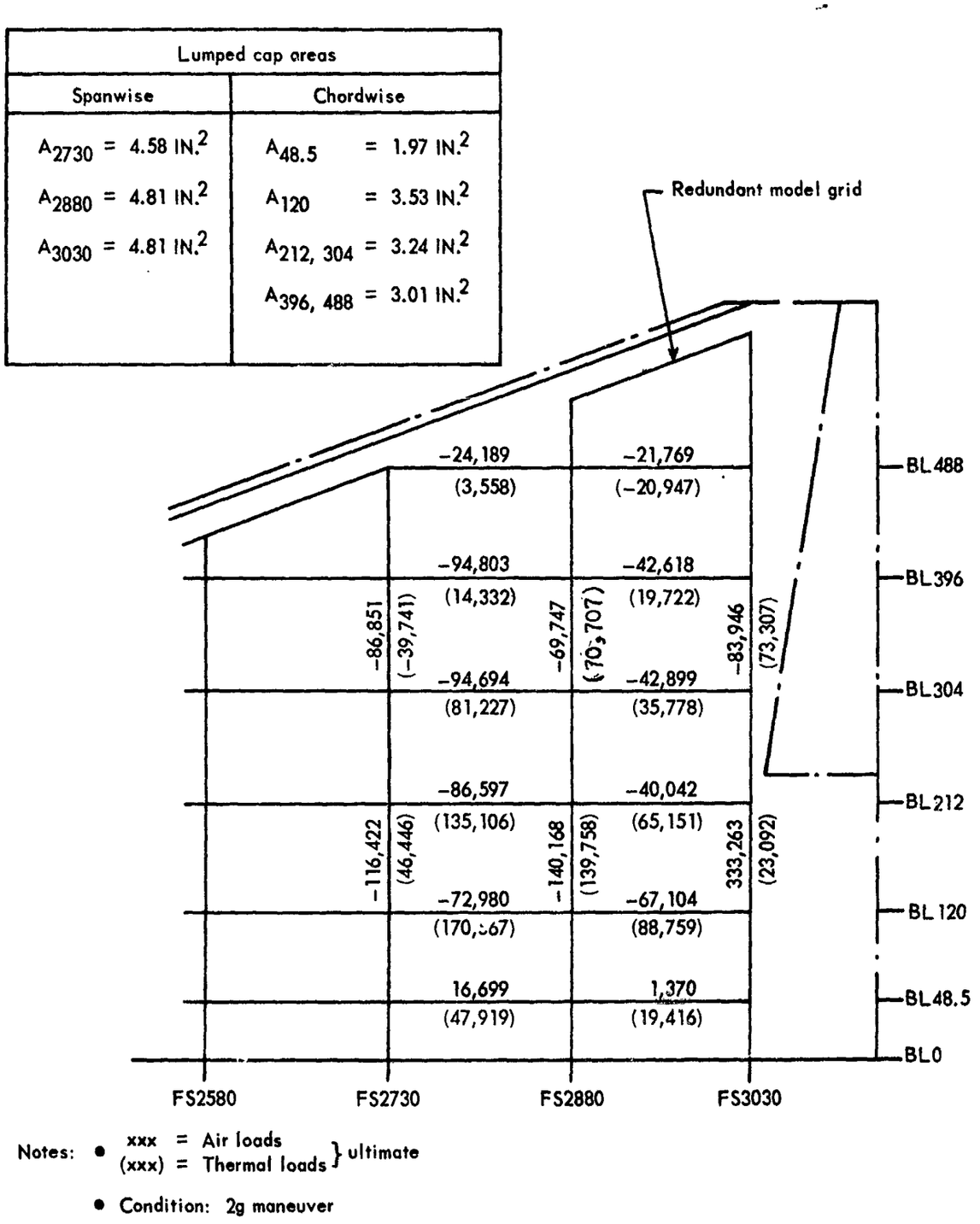

Figure 22-4. Redundant model loads - monocoque honeycomb concept (upper)

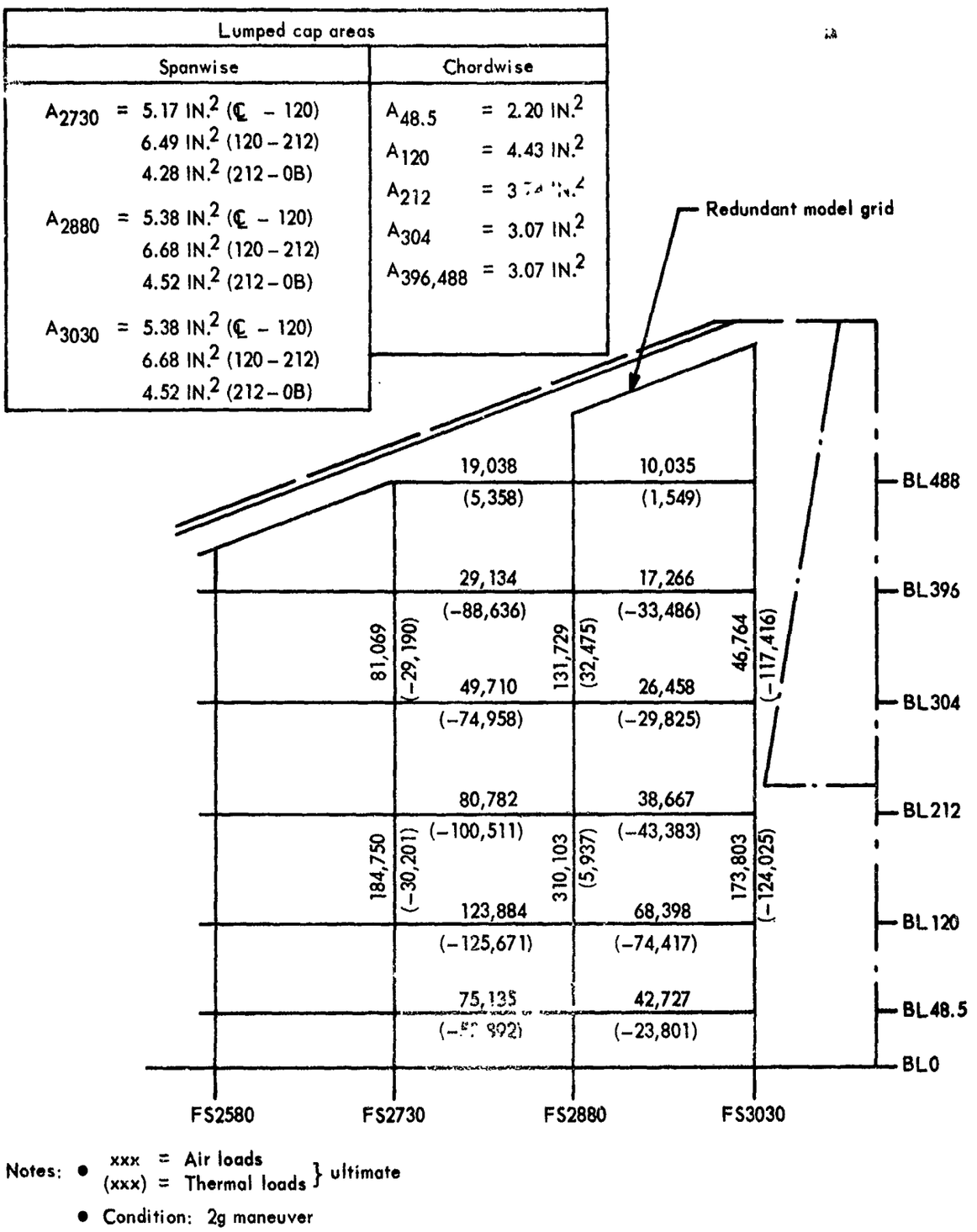

Figure 22-5. Redundant model loads - monocoque honeycomb concept (lower)

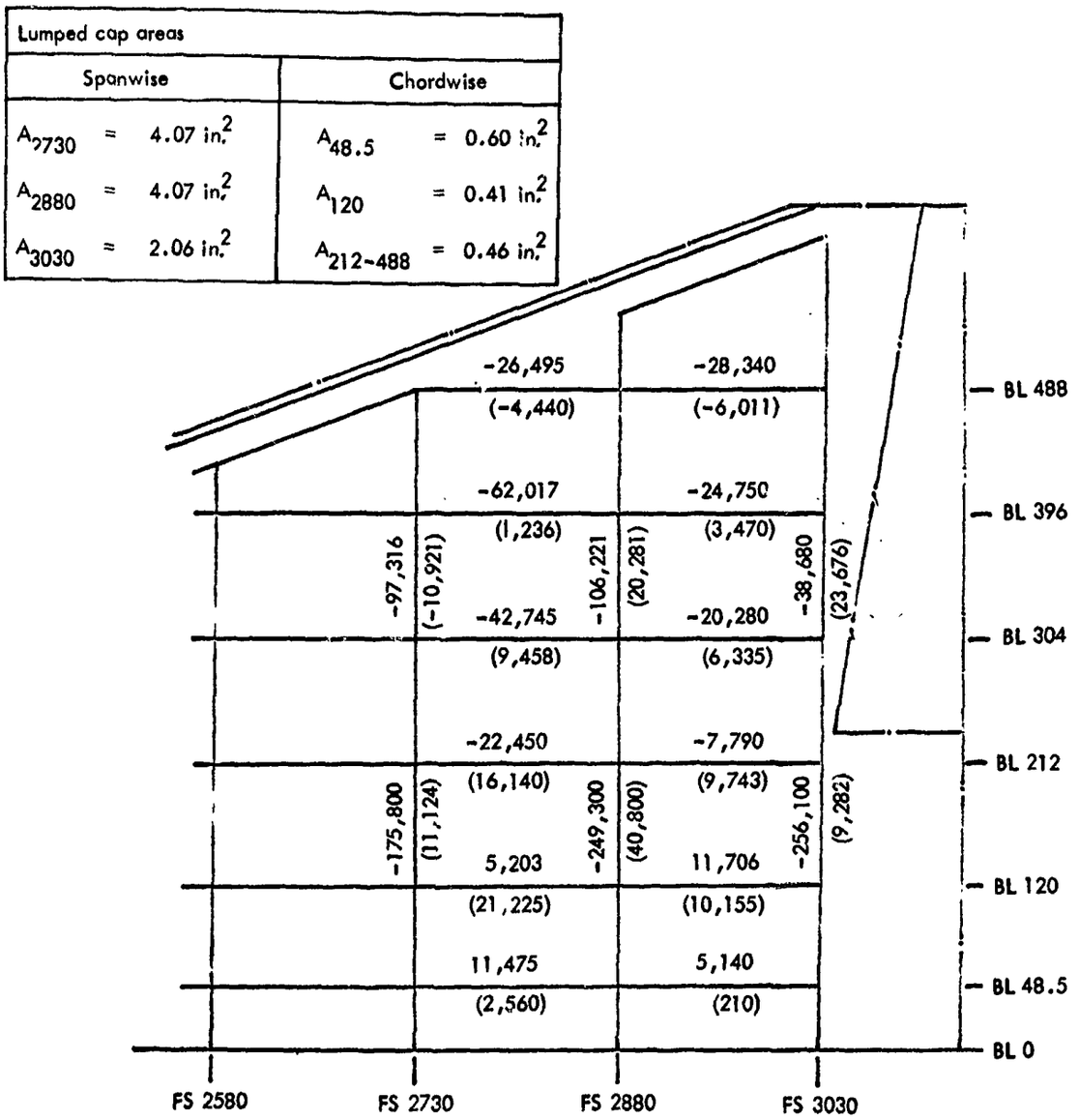

Notes:
- xxx = Air loads; (xxx) = thermal loads } ultimate
- Condition: 2g maneuver
- $\bar{t}_{span}$ = 0.028 in, $\bar{t}_{chord}$ = 0.005 in.

Figure 22-6. Redundant model loads – semimonocoque spanwise concept (upper)

Lumped cap areas	
Spanwise	Chordwise
$A_{2730} = 4.07\ in.^2$	$A_{48.5} = 0.60\ in.^2$
$A_{2880} = 4.07\ in.^2$	$A_{120} = 0.41\ in.^2$
$A_{3030} = 2.06\ in.^2$	$A_{212-488} = 0.46\ in.^2$

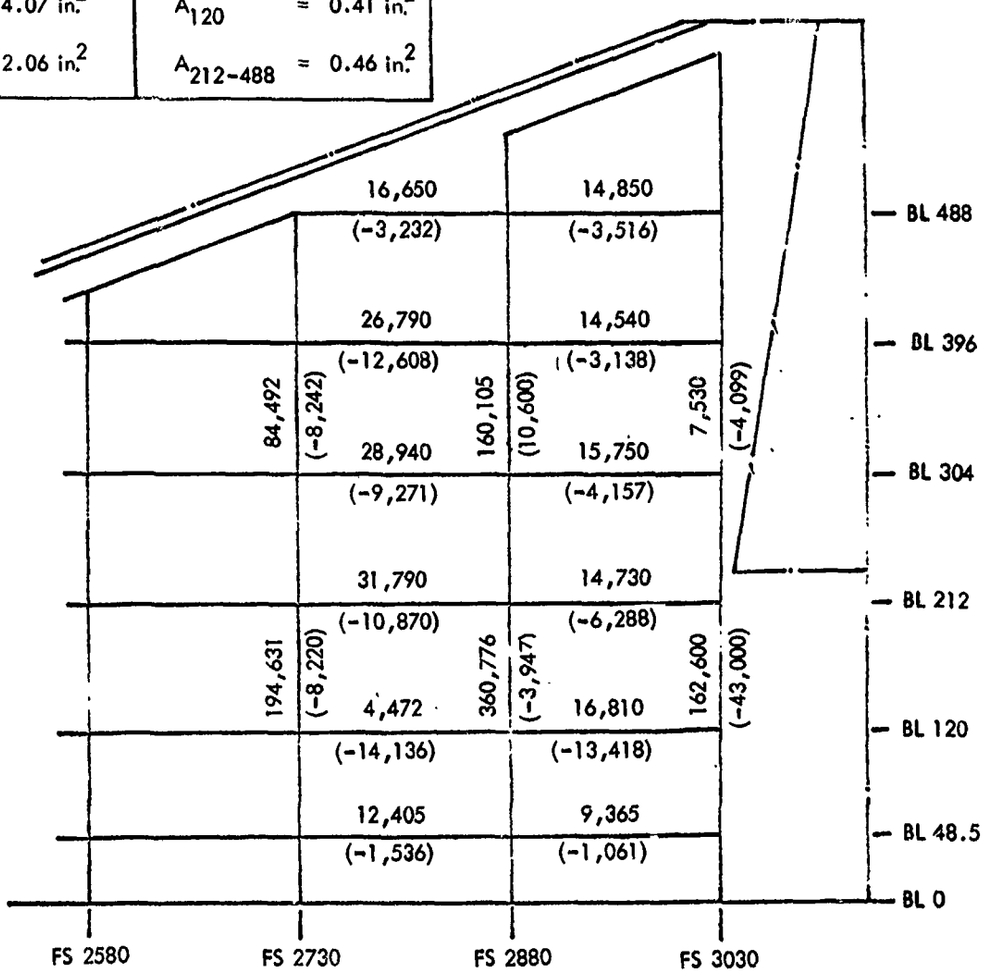

Notes:
- xxx = Air loads, (xxx) = thermal loads } ultimate
- Condition: 2g maneuver
- $\bar{t}_{span} = 0.028\ in.^2$, $\bar{t}_{chord} = 0.005 in.$

Figure 22-7. Redundant model loads – semimonocoque spanwise concept (lower)

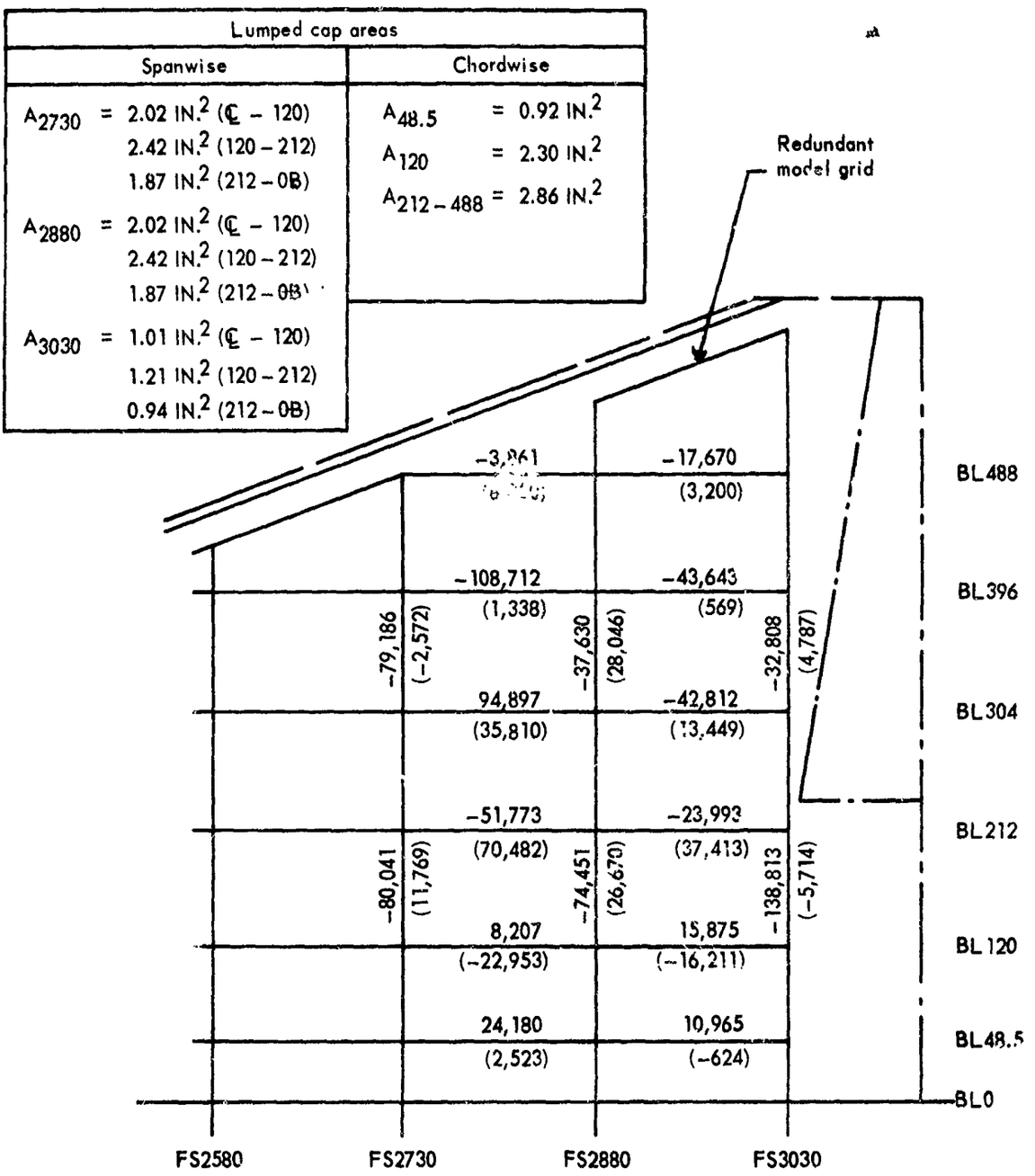

Notes: • xxx = Air loads
(xxx) = Thermal loads } ultimate

• Condition: 2g maneuver

Figure 22-8. Redundant model loads - semimonocoque chordwise concept (upper)

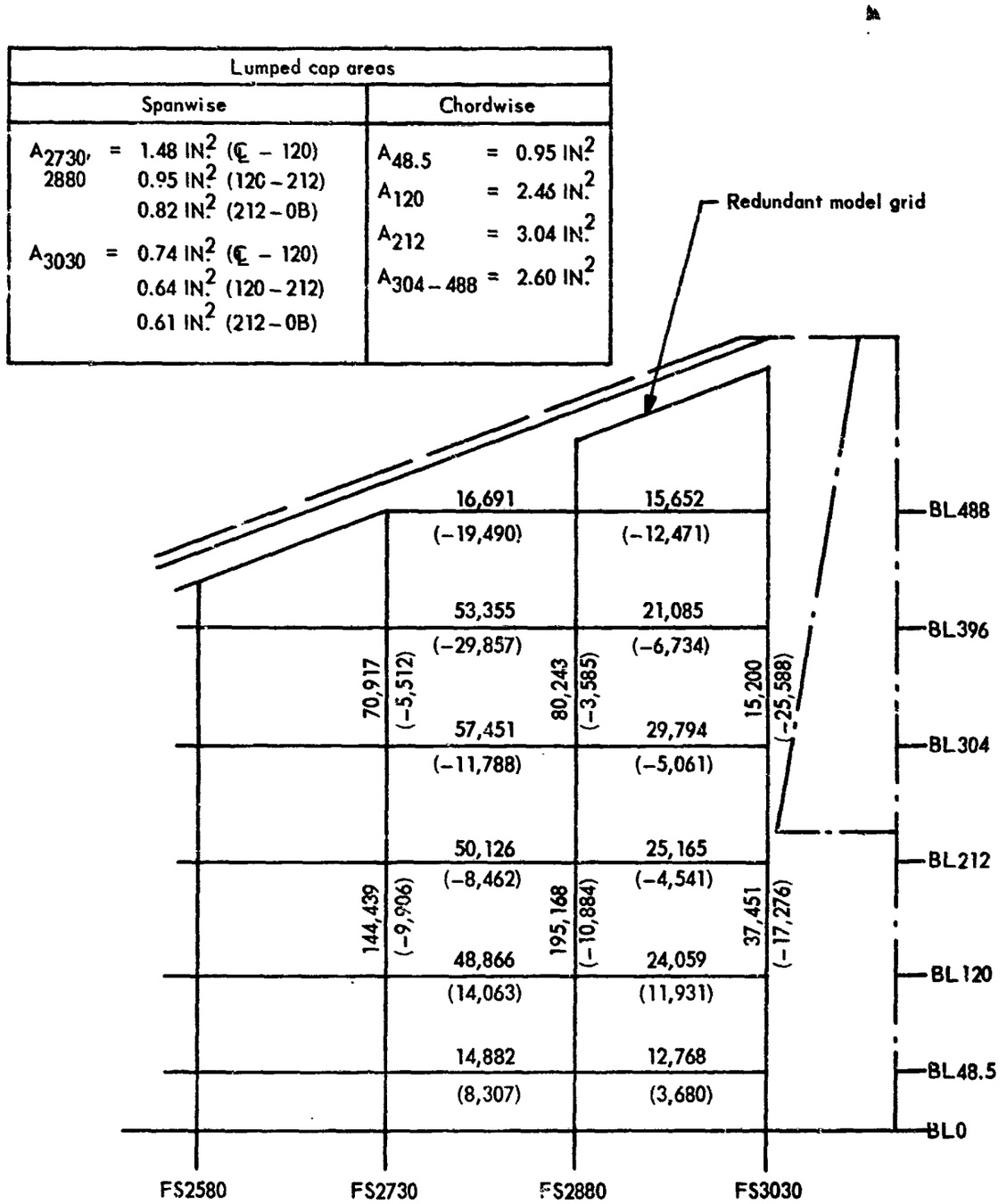

Figure 22-9. Redundant model loads - semimonocoque chordwise concept (lower)

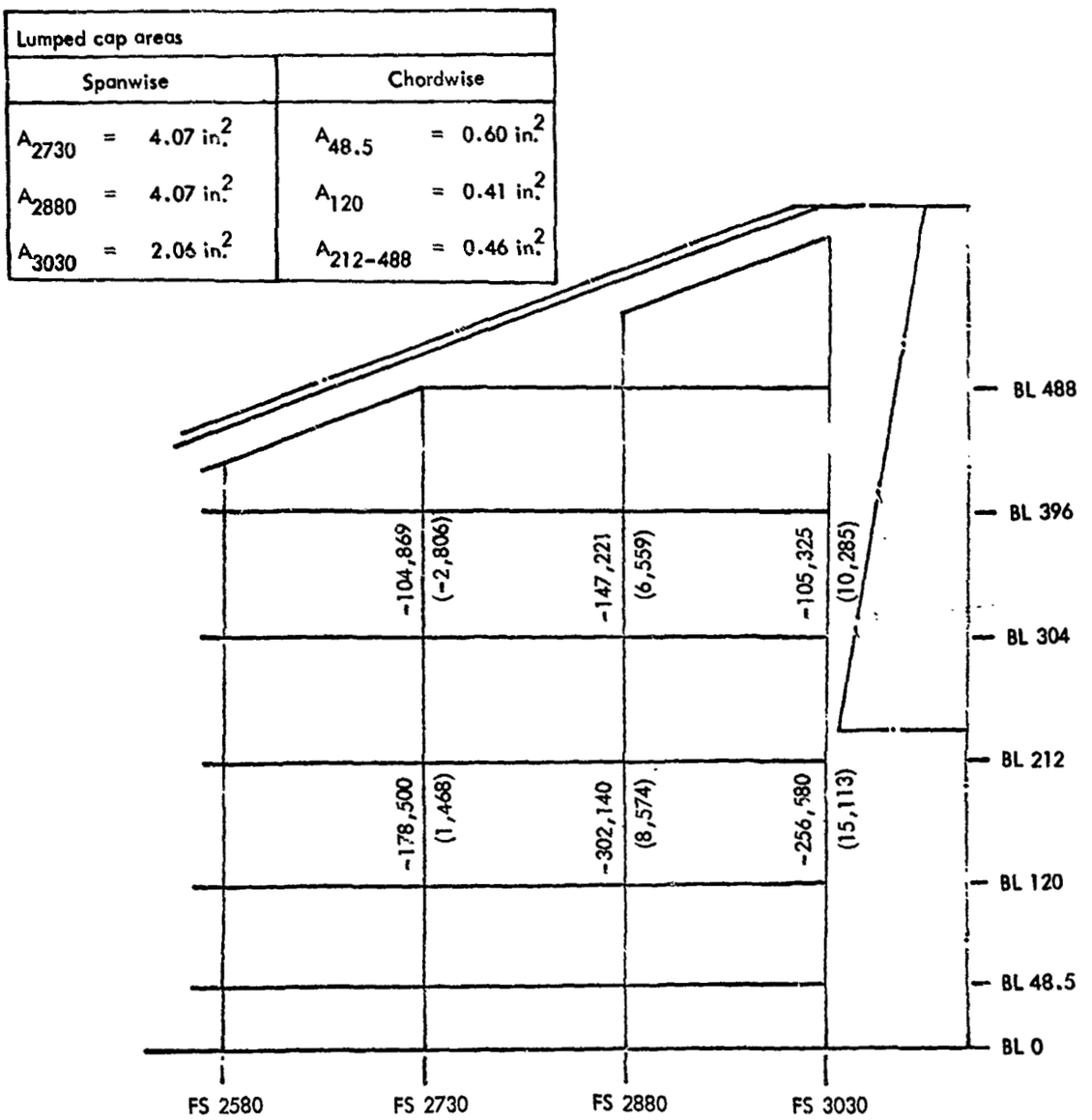

Notes:
- xxx = Air loads, (xxx) = thermal loads } ultimate
- Condition: 2g maneuver
- Upper surface shown, lower surface is opposite sign

Figure 22-10. Redundant model loads – statically determinate concept (upper and lower)

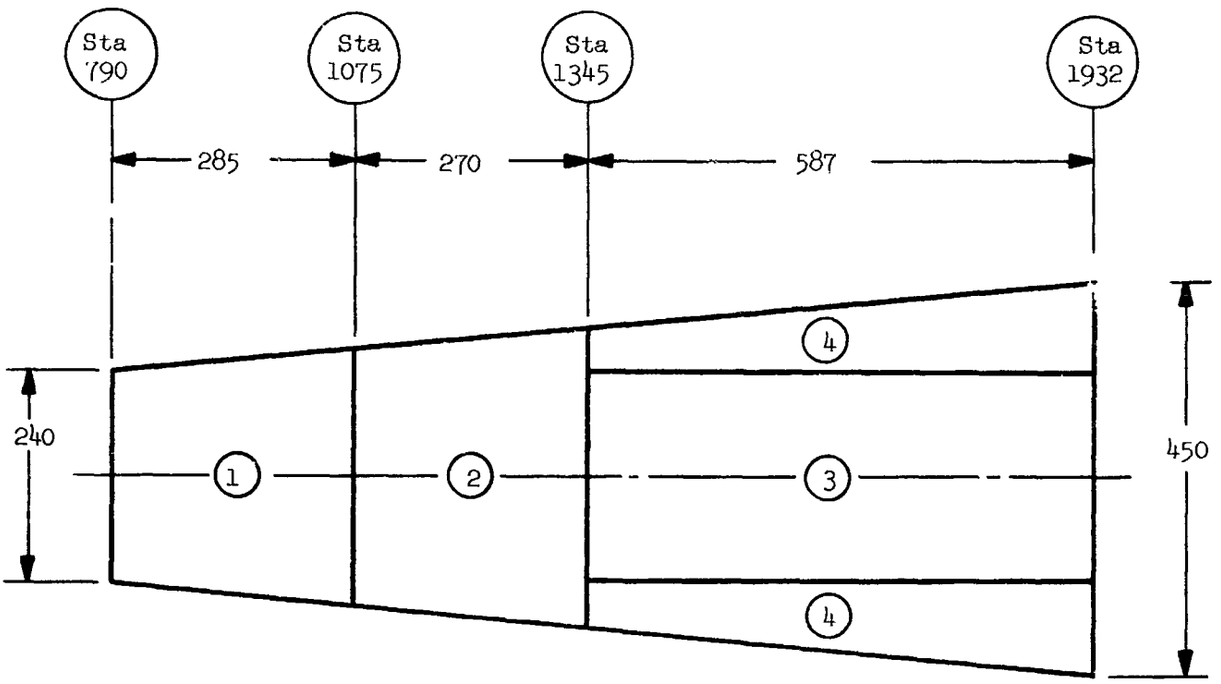

Zone	S_n (ft^2)	w_n (psf)	w_{aver} (psf)	W (lb)	Remarks
1	487	3.24	3.51	3779	Assume constant for all concepts
2	590	3.73			
3	980	–	–	–	Varies as indicated on Table 22-1
4	693	–	–	–	
Σ	2750	–	–	–	Refer to table 22-1 for weight variation

Figure 22-11. Forward delta geometry and weights

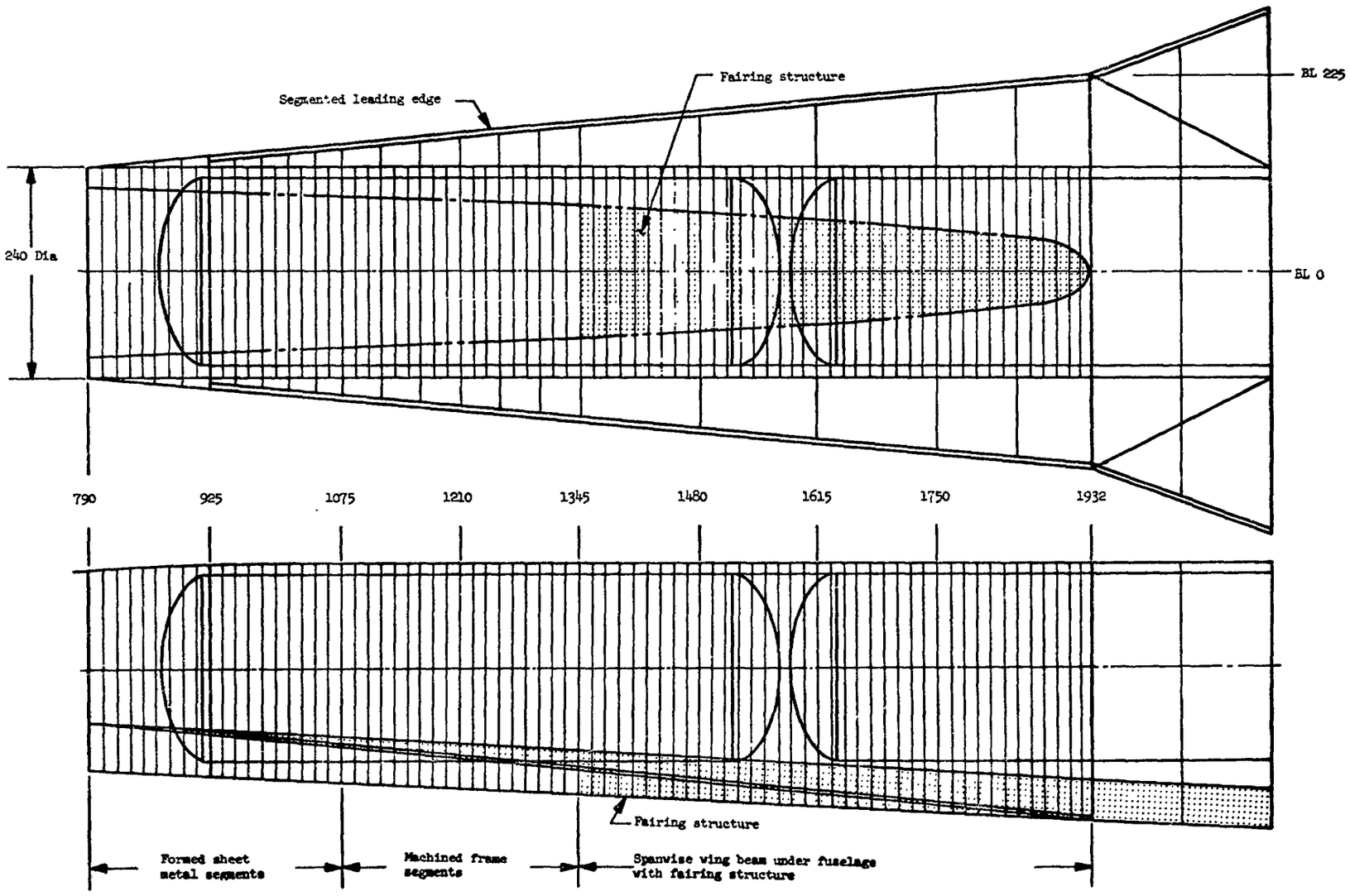

Figure 22-12. Wing forward – delta structure

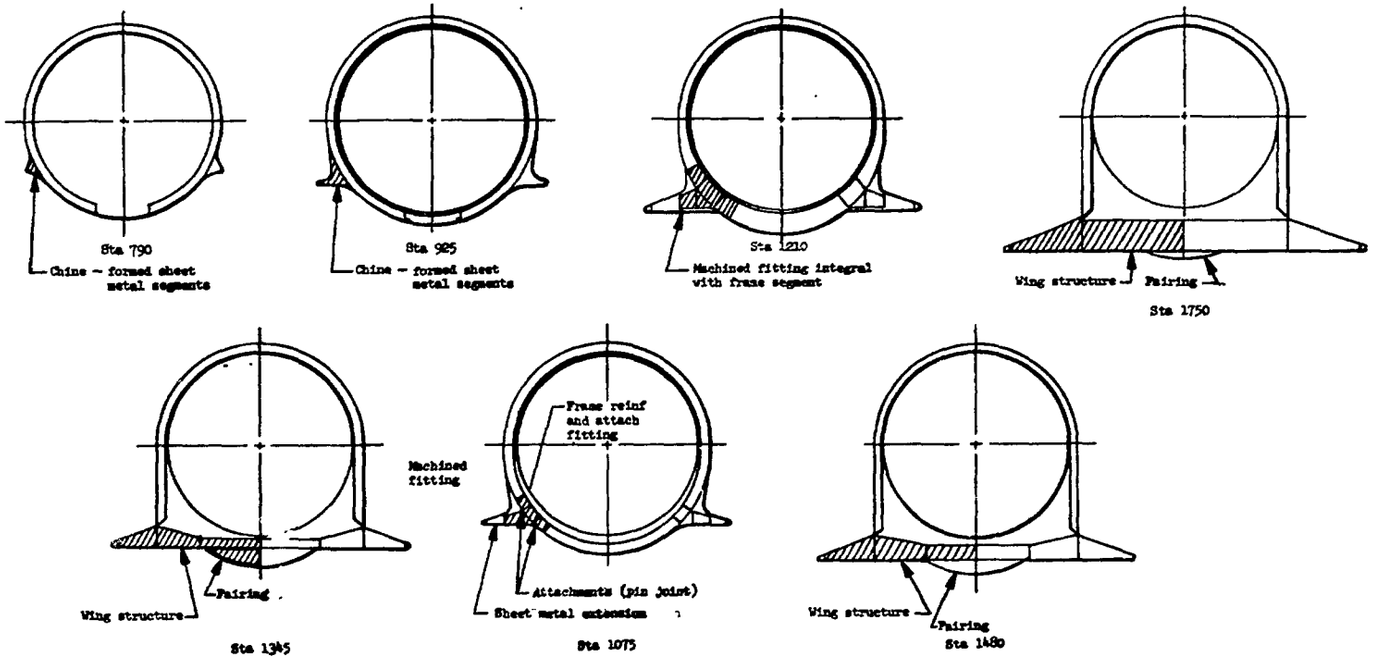

Figure 22-13. Forward delta structure at various fuselage stations

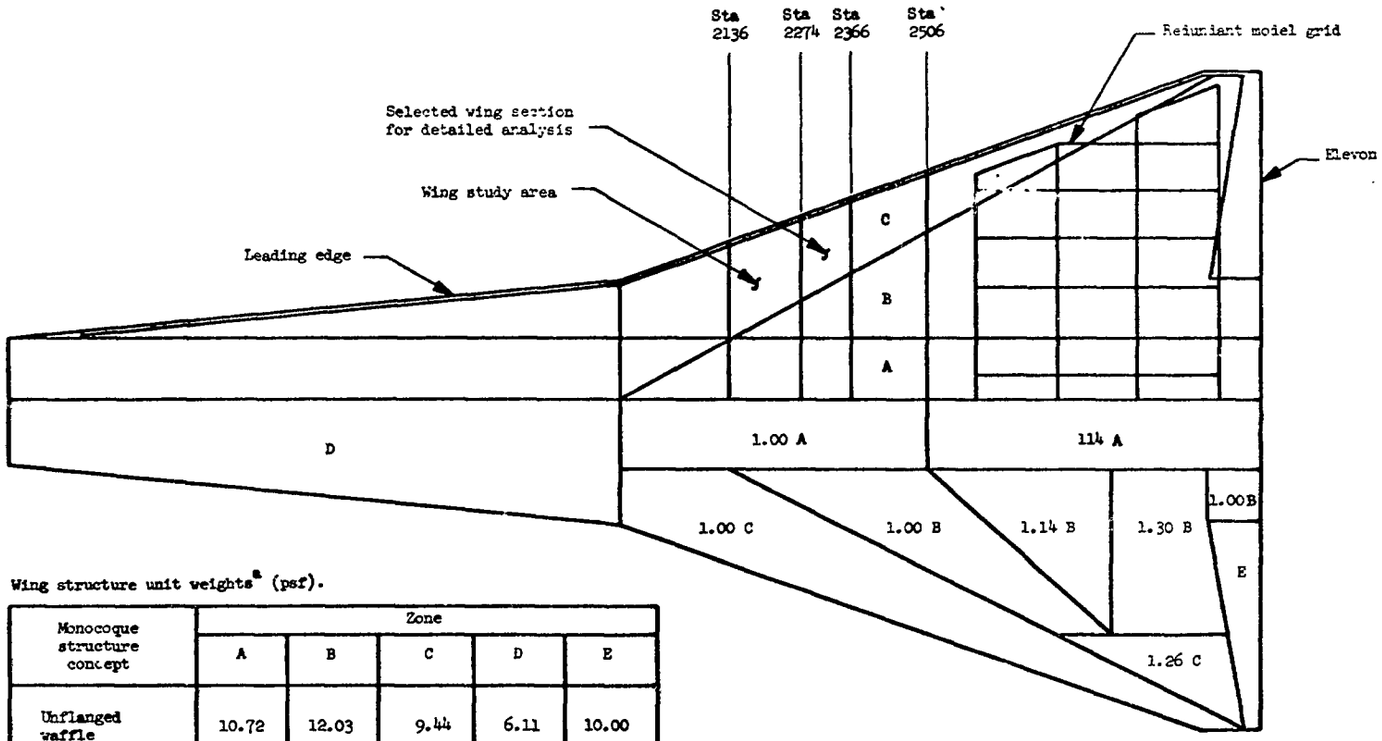

Wing structure unit weights[a] (psf).

Monocoque structure concept	Zone				
	A	B	C	D	E
Unflanged waffle	10.72	12.03	9.44	6.11	10.00
Honeycomb-core sandwich	6.25	6.35	6.77	4.53	10.00

[a] Nominal

Figure 22-14. Wing scaling factors – monocoque concepts

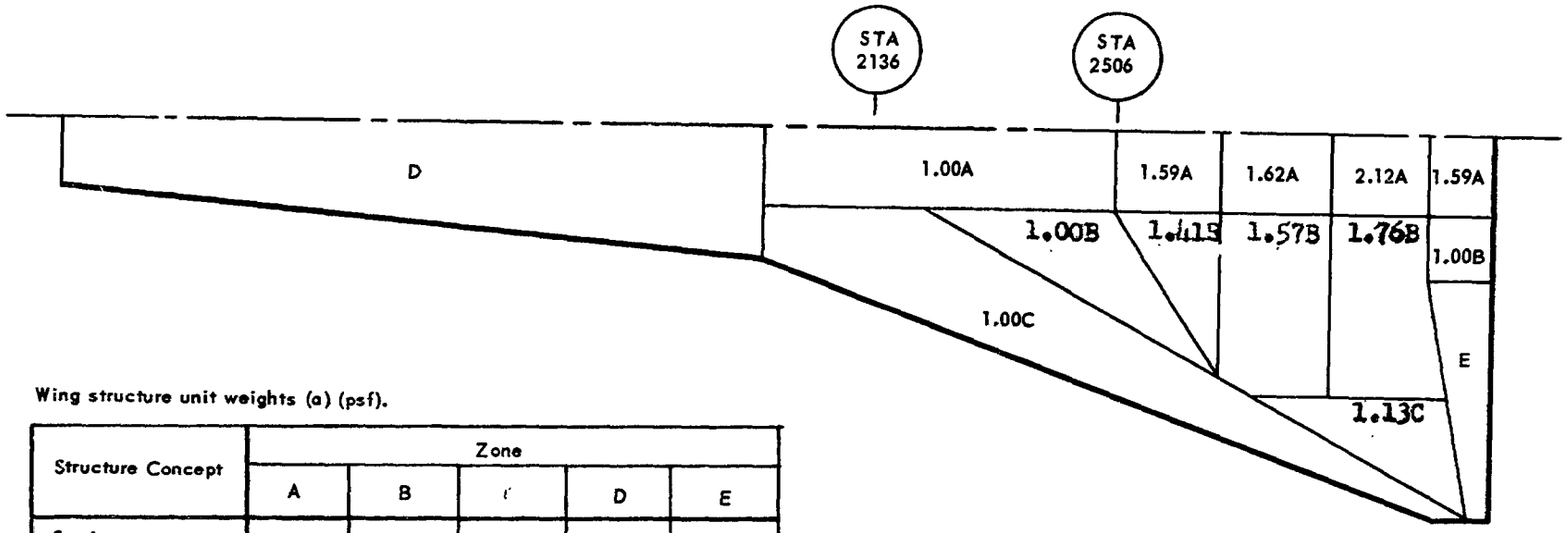

Wing structure unit weights (a) (psf).

Structure Concept	Zone				
	A	B	C	D	E
Semimonocoque tubular	4.82	5.61	5.70	4.39	10.00
Semimonocoque beaded	4.46	5.38	5.37	4.12	10.00
Statically determinate	5.21	6.00	5.54	4.34	10.00

a Nominal

Figure 22-15. Wing scaling factors - spanwise stiffened concepts

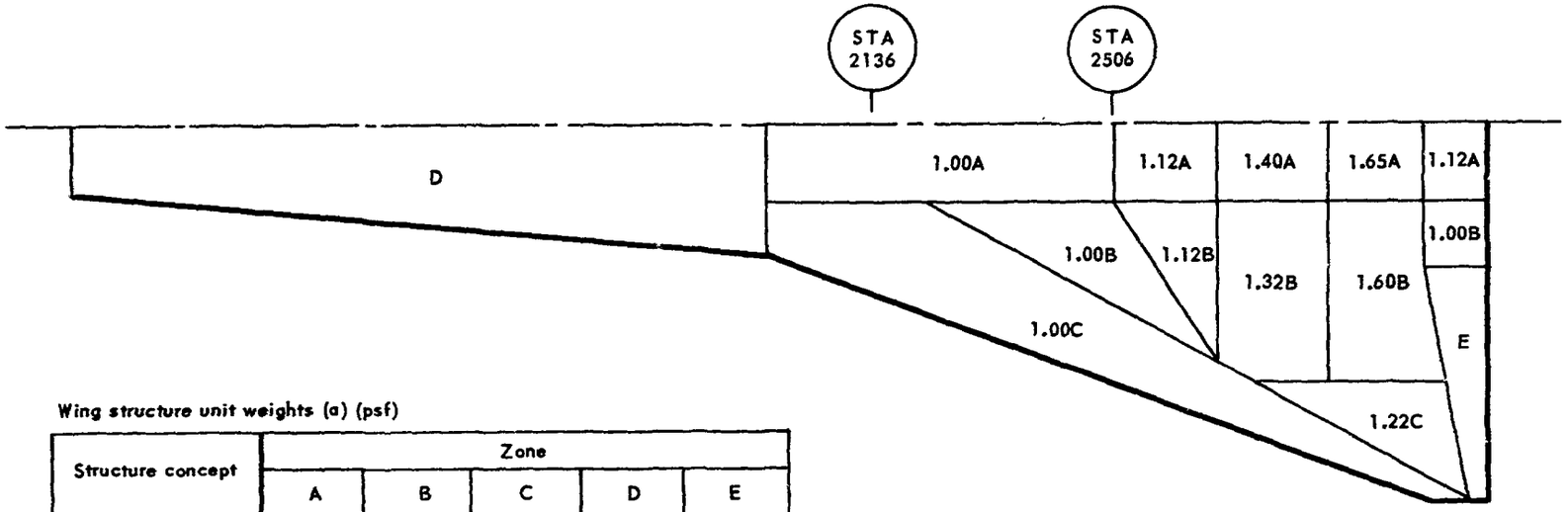

Wing structure unit weights (a) (psf)

Structure concept	Zone				
	A	B	C	D	E
Semimonocoque chordwise	6.95	6.80	6.33	5.25	10.00

[a]Nominal

Figure 22-16. Wing scaling factors - chordwise stiffened concept

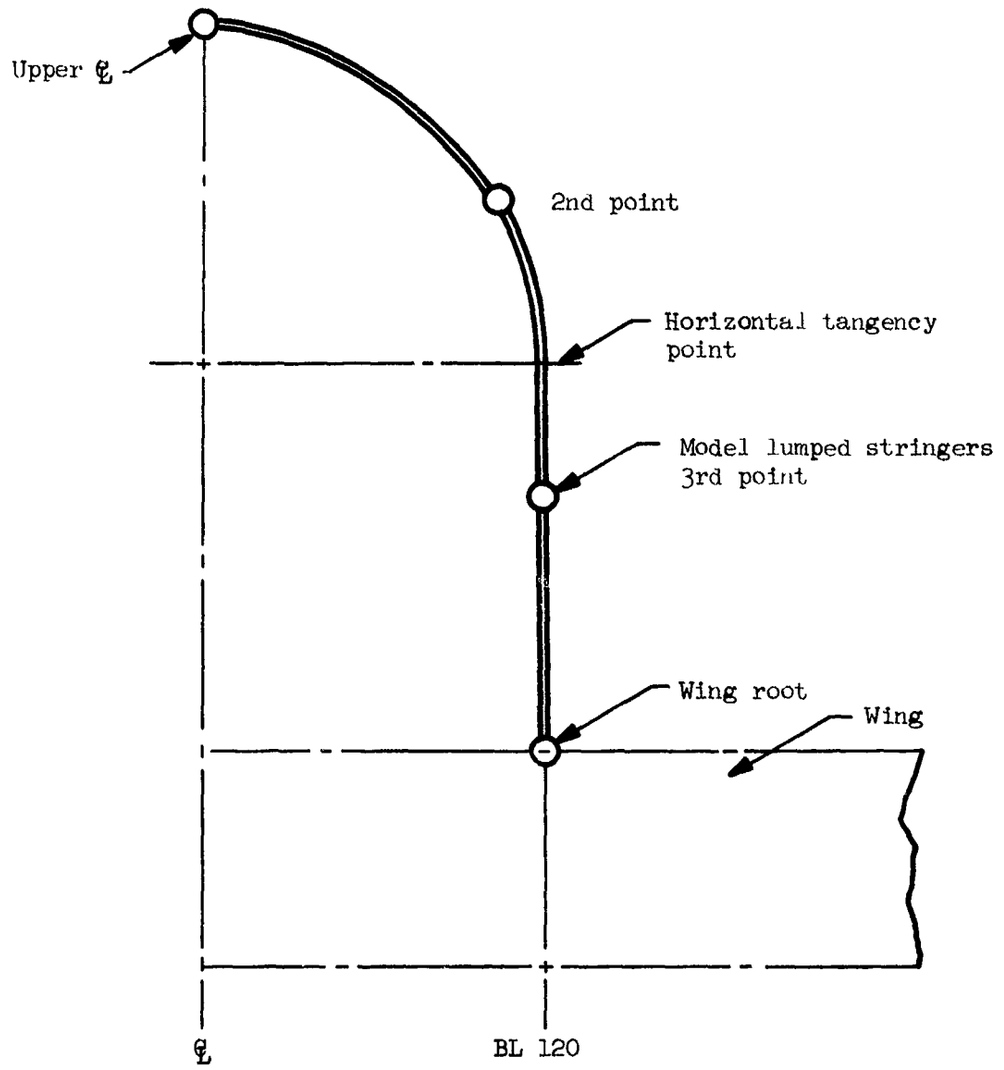

Model element numbers

Location	FS 1700	FS 2058	FS 2320	FS 2472
Upper ℄	16	26	51	61
2nd point	17	27	52	62
3rd point	18	28	53	63
Wing root	19	29	54	64

Figure 22-17. Redundant model idealized fuselage

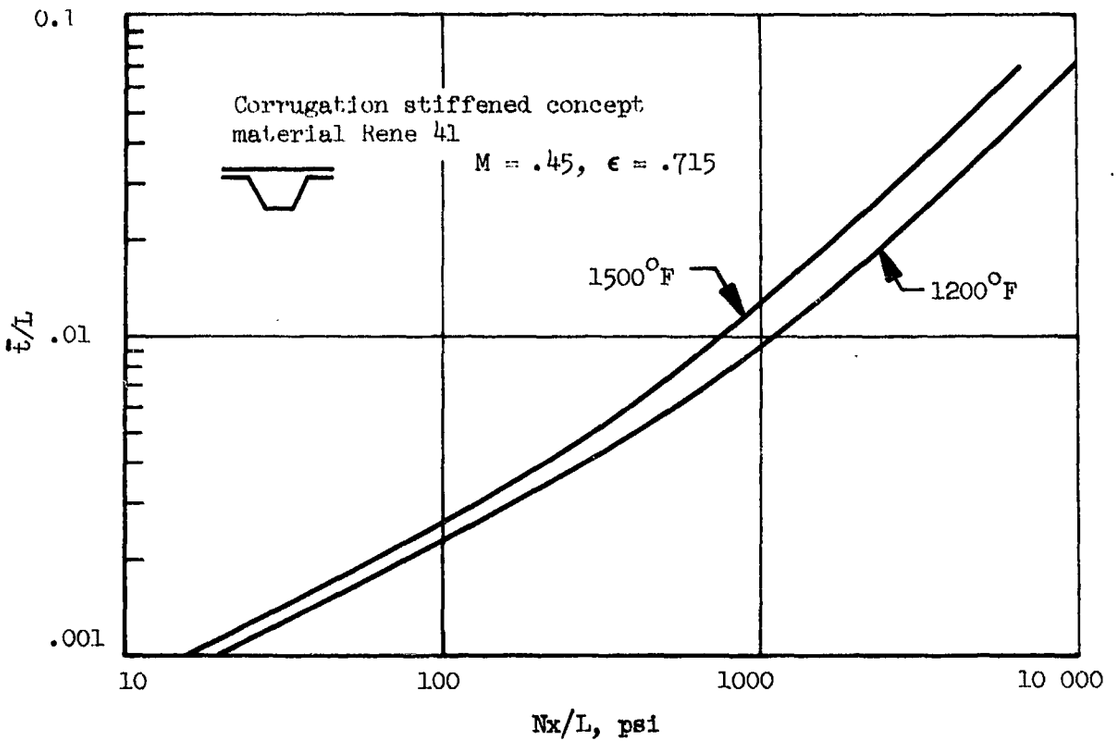

Figure 2-18. Wide column curve for sizing fuselage skin panels, statically determinate concept

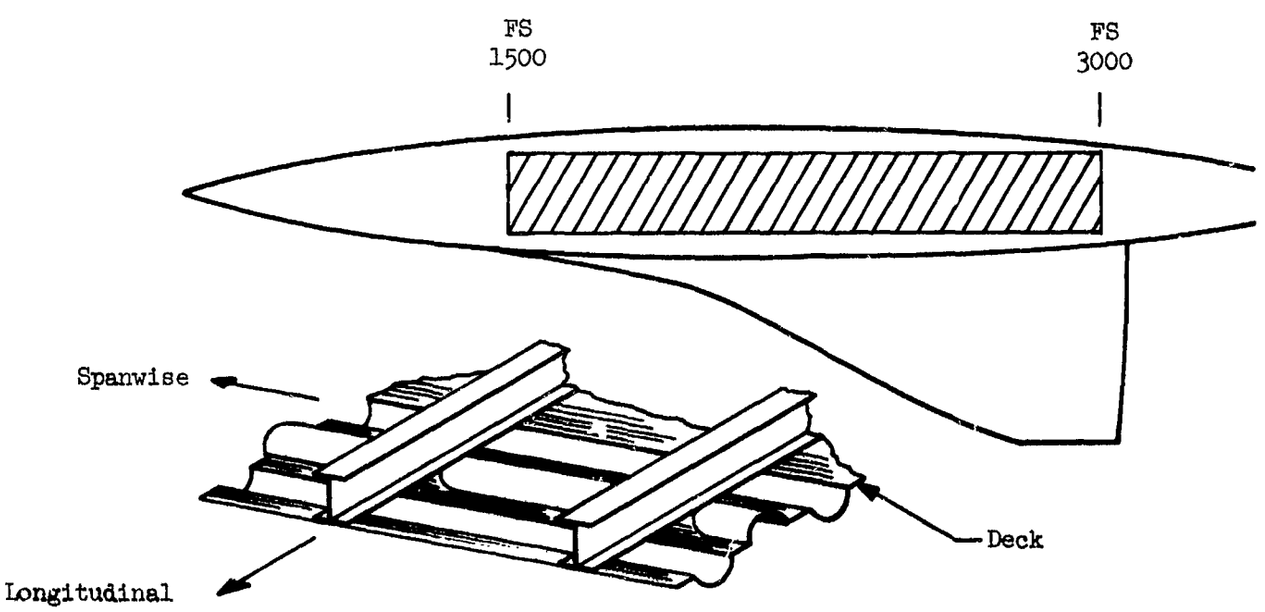

Figure 22-19. Decking and longitudinal stiffeners required for statically determinate concept

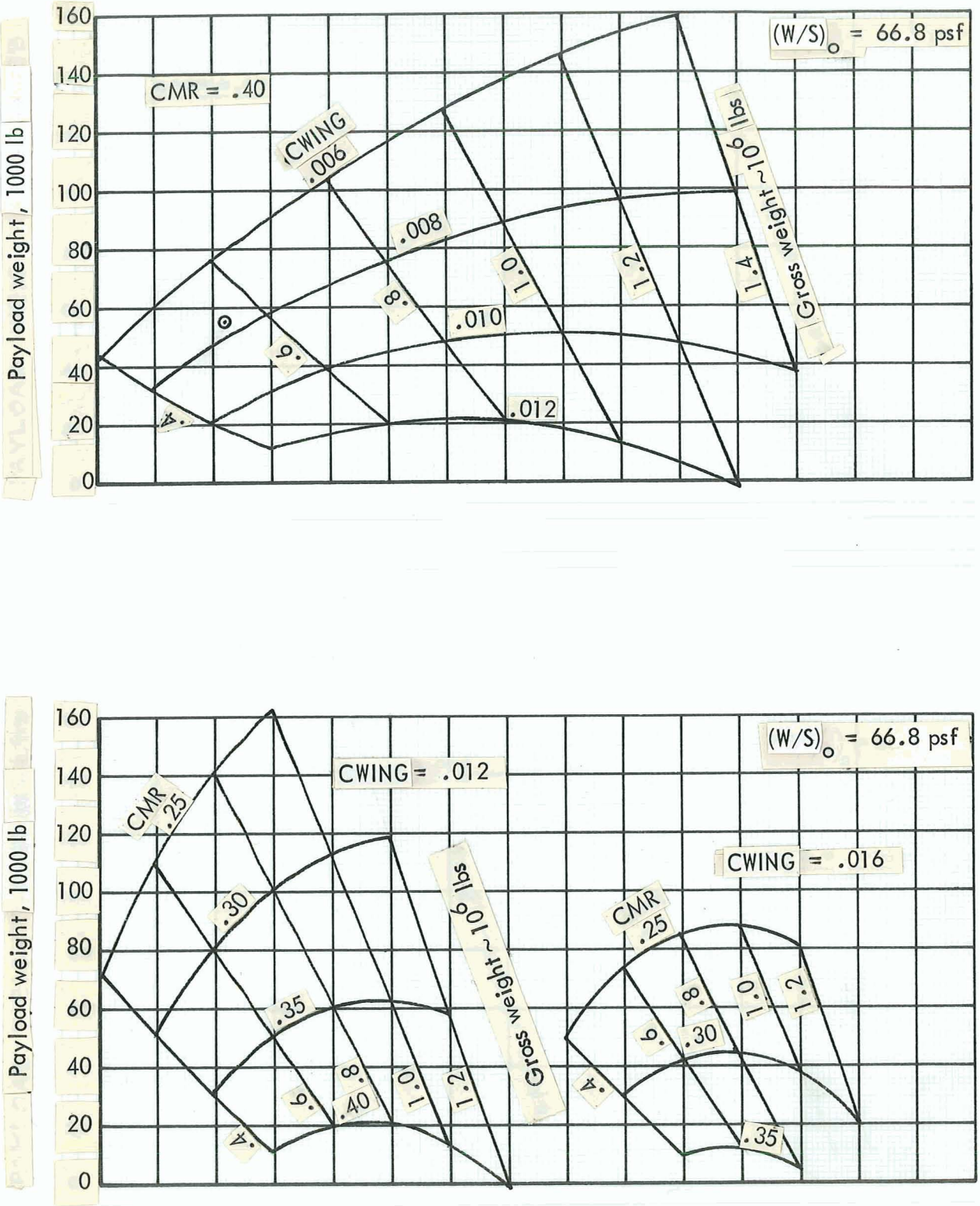

Figure 22-20. Vehicle scaling

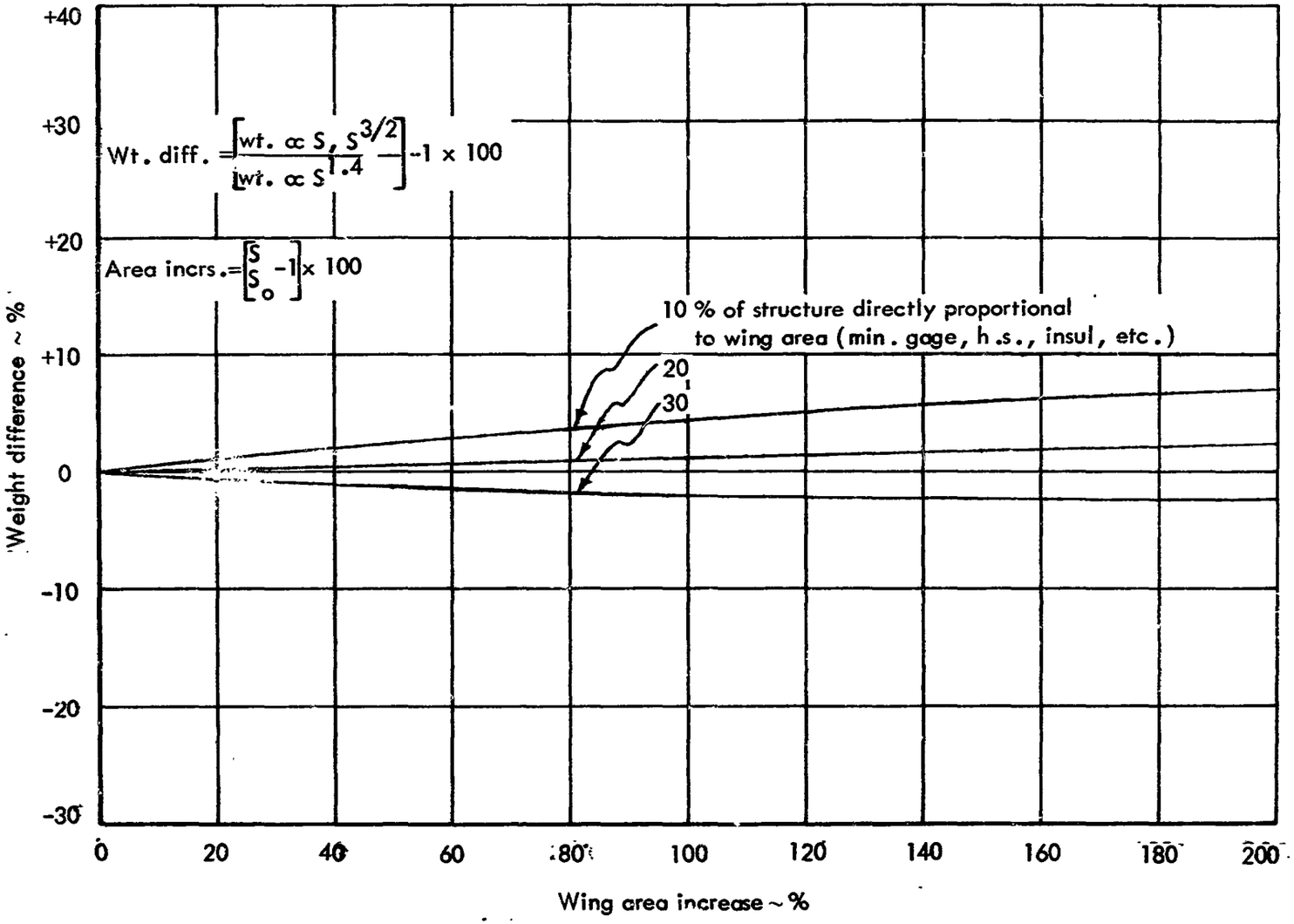

Figure 22-21. Wing scaling comparison